University of Alberta

Dehydration-melting of MORB-composition amphibolites at 7-22.5 kbar and 775-1050°C: constraints on phase relations, metamorphic facies transitions and origin of Archean TTG magmas

by

Rajeev Kumar Sasidharan Nair ©

A thesis submitted to the Faculty of Graduate Studies and Research
in partial fulfillment of the requirements for the degree of

Doctor of Philosophy

Department of Earth and Atmospheric Sciences

Edmonton, Alberta
Fall 2008

Library and
Archives Canada

Published Heritage
Branch

395 Wellington Street
Ottawa ON K1A 0N4
Canada

Bibliothèque et
Archives Canada

Direction du
Patrimoine de l'édition

395, rue Wellington
Ottawa ON K1A 0N4
Canada

Your file Votre référence
ISBN: 978-0-494-46419-9
Our file Notre référence
ISBN: 978-0-494-46419-9

NOTICE:
The author has granted a non-exclusive license allowing Library and Archives Canada to reproduce, publish, archive, preserve, conserve, communicate to the public by telecommunication or on the Internet, loan, distribute and sell theses worldwide, for commercial or non-commercial purposes, in microform, paper, electronic and/or any other formats.

The author retains copyright ownership and moral rights in this thesis. Neither the thesis nor substantial extracts from it may be printed or otherwise reproduced without the author's permission.

AVIS:
L'auteur a accordé une licence non exclusive permettant à la Bibliothèque et Archives Canada de reproduire, publier, archiver, sauvegarder, conserver, transmettre au public par télécommunication ou par l'Internet, prêter, distribuer et vendre des thèses partout dans le monde, à des fins commerciales ou autres, sur support microforme, papier, électronique et/ou autres formats.

L'auteur conserve la propriété du droit d'auteur et des droits moraux qui protège cette thèse. Ni la thèse ni des extraits substantiels de celle-ci ne doivent être imprimés ou autrement reproduits sans son autorisation.

In compliance with the Canadian Privacy Act some supporting forms may have been removed from this thesis.

While these forms may be included in the document page count, their removal does not represent any loss of content from the thesis.

Conformément à la loi canadienne sur la protection de la vie privée, quelques formulaires secondaires ont été enlevés de cette thèse.

Bien que ces formulaires aient inclus dans la pagination, il n'y aura aucun contenu manquant.

Canada

To my family

Abstract

Long duration dehydration-melting experiments were conducted on two amphibolites with compositions similar to mid-ocean-ridge basalts. The experiments were done using a piston cylinder apparatus in the pressure-temperature range 775-1050°C and 7-22.5 kbar. The amphibolites underwent dehydration melting at temperatures above 800°C through hornblende breakdown reactions: Hornblende + Plagioclase + Quartz = Clinopyroxene ± Orthopyroxene + Melt and Hornblende + Plagioclase + Quartz = Garnet + Clinopyroxene + Melt. The onset of melting in both amphibolites is at temperatures above the water-saturated solidus of basaltic rocks. The residual assemblage produced by these melting reactions corresponds to a low-P (7-10 kbar) orthopyroxene-bearing granulite and a high-P (>10 kbar) orthopyroxene-free garnet granulite. Tight experimental brackets and phase reversal experiments indicate that the low-P amphibolite-granulite transition occurs at temperatures >850°C whereas the high-P garnet-granulite assemblage forms at temperatures >825°C. At pressures above 17.5 kbar, plagioclase disappears from the assemblage and the residue becomes eclogitic. The transformation from garnet granulite to eclogite is characterized by decreases in the abundance of hornblende and plagioclase and an increase in the garnet/clinopyroxene ratio. Between 10-22.5 kbar the proportion of garnet in the residue is linearly correlated with pressure and the amount of garnet controls the density of the residue.

The melts produced in the experiments are felsic (SiO_2 58-73 wt%; Al_2O_3 ~15-23 wt.%; K_2O 1-5 wt.%, Na_2O/K_2O >1) and similar in composition to the Tonalite-Trondhjemite-Granodiorite (TTG) rocks that dominate many Archean cratons. Trace-element modelling using La and Yb as representative rare-earth-elements indicate that characteristic early Archean TTG signatures (<1 ppm Yb, La/Yb >15) requires the presence of ~ 20 wt. % garnet in the melt residue, which is only achieved at pressures above 15 kbar (>48 km depth). This depth constraint is inconsistent with early crust evolution models that posit melting at the base of oceanic plateaus or oceanic crust to produce TTGs. Models involving melting of subducted oceanic crust are more consistent with the depth constraint. However, operation of subduction process in the Archean is considered problematic. A new model of subduction initiation by lateral compositional contrasts between converging oceanic plateau and normal thickness oceanic lithosphere is developed to explain the origin of early Archean TTG and by inference that of the first continental nuclei.

Acknowledgements

This project was one of the most challenging tasks that I ever undertook in my life. Like many that have treaded this path before, there were many hurdles along the way, which at times seemed quite insurmountable. Overcoming some of these indecisive moments were made possible by some incredible people who were there to support me through these years. First and foremost among them is my supervisor Dr. Tom Chacko. Tom has supported me financially and intellectually for many years. I can honestly say that he taught me everything I know at this point. He has been incredibly patient with me over the years and encouraged me even when I led myself to explore some tangential aspects of the research project. I have not come across a more thoughtful person in my life. I could not have asked for any more support from him and he has been a great source of inspiration.

I would like to thank Dr. Robert Luth for his advice as a member of my supervisory committee and for being a great mentor for me at University of Alberta. He treated me like his own student and has also shown great interest in my future career. I am so grateful for the support he provided in the lab and for providing a prime office space in the lab, which I have been holding hostage for many years now. I would also like to thank Dr.Thomas Stachel for serving as a member of my supervisory committee and his encouragement through the years. I would also like to thank Dr. Dana Johnston (University of Oregon), Dr. Chris Herd and Dr. Martyn Unsworth for serving in the final examination committee, Dr. Sarah Gleeson for efficiently chairing the defense examination, and Dr. Robert Creaser and Dr. Alex Meldrum for serving in my candidacy examination committee.

Many other faculty members in the Department in the Earth and Atmospheric Sciences have been a constant source of support for me. In particular, I would like to thank the encouragement and support of Dr. Karlis Muehlenbachs who has also graciously supported many other graduate students in need in our department. Dr. Larry Heaman and Dr. Robert Creaser are thanked for informal discussions and for all the invites to mingle with the radiogenic isotope research group.

Dr. Sergei Matveev is thanked for all his help in using the electron microprobe. Don Resultay and Mark Labbe provided invaluable support in the thin section lab and Diane Caird helped me with finding and coordinating things in the experimental petrology lab.

I would like to thank the Department of Earth and Atmospheric Sciences for providing the opportunity to gain valuable teaching experience as a sessional instructor and as a teaching assistant. George Braybrook is thanked for training me on the SEM and for giving me a part-time job that helped me immensely.

Numerous friends helped make my stay in Edmonton a comfortable one and have supported me through many difficult times. It is impossible to name all of them here but I would particularly like to thank Sunil & Stacey Barran, Arees Rauf, Ryan & Lia Morelli, Russel Hartlaub, Trevor MacHattie, Will Hobbs, Natalie Zabcic, Sarah Gleeson, Joyce Harris and the Seethram's for all their support.

Finally, I would like to acknowledge three special people who made incredible sacrifices for me. My mother and sisters had to part with my company for many years when I moved to Edmonton. I am so thankful for their support through the years. This accomplishment is really for the three of them.

Table of Contents

Page

Chapter 1: Introduction and scope of this study

The origin of continental crust 1

Basaltic protoliths 4

Metabasaltic phase equilibria and scope of present study 5

Chapter 2: Dehydration melting of MORB-type amphibolites: constraints on the solidus and high-grade metamorphic facies transitions

Introduction 22

Previous studies and scope of the present study 24

Starting materials 31

Experimental procedure 33

Analytical techniques 35

Attainment of equilibrium 36

Redox conditions 40

Results

- Description of run products 43
- Phase stability and compositions 46
- Phase proportions 54

Melting reactions

- Fluid-absent solidus 55
- Reaction modelling 57

Discussion

- Petrological Applications 62
  - High-grade metamorphism of mafic rocks 62
    - Amphibolite-intermediate-P Granulite transition 63
    - Amphibolite/Granulite-Garnet-granulite transition 65

Problem of lower temperature garnet-cpx amphibolites 70
Garnet-granulite-Eclogite transition 74
Partial melt compositions and conditions of TTG genesis 77

Chapter3: Garnet growth during dehydration melting of MORB-composition amphibolites: implications for partial melts and restites

Introduction 145
Previous constraints on garnet stability in metabasalts 148

Results

  Criteria for phase stability 151
  Phase relationships 152
  Garnet growth textures 153
  Controls on garnet growth 154
  Garnet mode 158
  Garnet compositions 159
  Ti in Garnet 160
  Restite density 162

Discussion

  Implications for slab melts 163
  Implications for restite delamination 166

Chapter 4: Constraints on the origin of early-Archean TTG magmas and conjectures on Archean geodynamics and implications for the origin of crust-mantle systems

Introduction 194
Constraints on Archean TTG formation 196

Discussion

  Experimental constraints on garnet stability 198

Implications for tectonic models 199
A modified subduction model 201
Implications of the new model for crust-mantle evolution in Archean 207
Conclusions 210

Chapter 5: Conclusions and scope for future research

Dehydration-melting of MORB-derived amphibolites 232
Metamorphic facies transitions in MORB-derived metabasalts 233
Generation of Archean TTG magmas 236
Tectonic setting of early Archean TTGs and origin of continental nuclei 238
Future work 240

Appendix A: Electron microprobe analyses of experimental phases 250
Appendix B: Melt correction procedure 312
Appendix C: Mass balance using Singular Value Decomposition 317
Appendix D: Reprint of Geology paper co-authored by Dr. Thomas Chacko 328

List of Tables

Table 1.1: Composition of Mid-Ocean Ridge Basalts 19

Table 1.2: Comparison of starting materials 20

Table 2.1: Composition of starting materials 95

Table 2.2: Comparison of starting materials with mid-ocean ridge basalts 96

Table 2.3: Experimental conditions and run products 97

Table 2.4: Composition of hornblende 99

Table 2.5: Composition of clinopyroxene 101

Table 2.6: Composition of orthopyroxene 102

Table 2.7: Composition of garnet 102

Table 2.8: Composition of plagioclase 105

Table 2.9: Composition of glass 107

Table 2.10: Composition of magnetite 108

Table 2.11: Modal proportion of experimental phases 109

Table 2.12: Reaction coefficients from singular value decomposition 110

Table 2.13: Modal mass balance of melting reactions 111

Table 3.1: Calculated end-member composition of garnet 180

List of Figures

Figure 1.1: Comparison of starting materials with mid-ocean ridge basalts 21
Figure 2.1: Previous constraints on dehydration-melting solidus of metabasalts 112
Figure 2.2: Previous constraints on granulite, garnet-granulite and eclogite in metabasalts 113
Figure 2.3: Plot of experimental temperatures with those determined by Grt-Cpx thermometry 114
Figure 2.4: Calculated oxygen fugacity as a function of experimental temperature 116
Figure 2.5: Phase assemblage in experimental run products 117
Figure 2.6: Composition of amphiboles in Leake's diagram 118
Figure 2.7: Variation of Mg# in experimental amphiboles 119
Figure 2.8: Tetrahedral Al in experimental amphiboles 120
Figure 2.9: Wo-En-Fs diagram showing clinopyroxene compositions 121
Figure 2.10: Clinopyroxene compositions in Morimoto diagram 122
Figure 2.11: Variation of Al_2O_3 content of orthopyroxene with temperature 123
Figure 2.12: Garnet ternary diagram 124
Figure 2.13: Harker diagram for experimental melt compositions 125
Figure 2.14: Experimental melt compositions in normative feldspar diagram 127
Figure 2.15: K_2O-CaO-Na_2O ternary plot of melt compositions 128
Figure 2.16: Molar $Al_2O_3/(Na_2O+K_2O)$ vs $Al_2O_3/(CaO+Na_2O+K_2O)$ of melts 129
Figure 2.17: Variation of major/minor elements in melts with temperature 130
Figure 2.18: Plot of TiO_2+FeO+MgO in melts with temperature 134
Figure 2.19: Dehydration-melting phase relations of KAP and 3VG 135
Figure 2.20: Na_2O+K_2O-CaO vs SiO_2 (wt.%) of experimental melts 136
Figure 2.21: FeO/(FeO+MgO) vs SiO_2 (wt.%) of experimental melts 137
Figure 2.22: MgO and SiO_2 content of experimental melts compared with previous studies 138
Figure 2.23: Al_2O_3 and SiO_2 content of experimental melts compared with previous studies 139
Figure 2.24: K_2O and Na_2O content of experimental melts 140
Figure 2.25: Normative quartz-albite-orthoclase ternary plot of experimental melts 141
Figure 2.26: Na_2O/K_2O vs alumina saturation index of experimental melts 142
Figure 2.27: K_2O (wt.%) vs molar K/(K+Ca) of experimental melts 143
Figure 2.28: Na_2O-K_2O-CaO ternary comparing melts with those from previous studies 144
Figure 3.1: Phase relations of KAP and 3VG amphibolite 181
Figure 3.2: Backscattered images showing garnet growth textures 182
Figure 3.3: Backscatterd images showing distribution of garnet in experimental charges 183

Figure 3.4: Schematic diagram showing aspects of garnet growth by diffusion control and interface control 184
Figure 3.5: Radius rate plots for garnet growth in three KAP experiments 185
Figure 3.6: Variation of modal abundance of garnet with pressure 186
Figure 3.7: Variation of modal abundance of garnet as a function of experimental duration 187
Figure 3.8: TiO_2 vs FeO (wt.%) content of garnets 188
Figure 3.9: Distribution of TiO_2 between garnet and melt 189
Figure 3.10: Variation in the density of residual assemblage with P-T conditions 190
Figure 3.11: Variation in the density of restite as a function of garnet proportion 191
Figure 3.12: Variation of melt TiO_2 content as a function of temperature 192
Figure 3.13: Exsolved rutile in garnet from lower crustal xenoliths 193
Figure 4.1: Variation in Yb and La/Yb ratio of melt as a function of garnet mode in the residue 226
Figure 4.2: P-T diagram showing phase relations of amphibolite and garnet proportion contours 227
Figure 4.3: Model of Archean subduction and TTG formation 228
Figure 4.4: Effect of age of oceanic plateau on the thickness of mantle wedge 229
Figure 4.5: Secular variation of Mg# of TTG magmas (after Martin and Moyen, 2002) 230

CHAPTER 1: Introduction and scope of this study

Earth is unique among rocky planets in having a bimodal-composition crust; a basalt dominated oceanic crust and a more compositionally varied and evolved continental crust. Whereas basaltic crust is known to occur in other planetary bodies, the existence of a felsic crust similar to Earth's continental crust has not yet been discovered in other planets. Continental crust, despite constituting <1 % of the mass of the Earth, is a major geochemical reservoir accounting for a substantial proportion of many incompatible elements, including K, U, Th and La. Unlike oceanic crust, continental crust is heterogeneous in composition at many scales of observation. The origin and evolution of continental crust is fundamental to understanding the evolution of the Earth system. Two aspects of continental crust evolution have been actively debated since the advent of plate tectonic theory: (1) the process and the tectonic setting of its formation and, (2) the timing and growth (evolution) of this crust to its present state (Moorbath, 1977; McLennan and Taylor, 1983; Armstrong, 1981; 1991). Our understanding of the evolution of Earth and other planetary bodies hinge on how well we understand these aspects of continental crust formation.

The origin of continental crust

It is well known that Earth's silicate mantle represents the ultimate reservoir from which all of its crust was derived. Direct formation of juvenile crust from this reservoir occurs by partial melting of mantle peridotite, primarily through pressure release (decompression) melting. This is manifested today at specific settings on Earth; basaltic magmatism at mid-ocean ridges, formation of basalts and its differentiates in subduction zones and, predominantly basaltic and rare komatiitic magmatism in hotspot/plume settings. Thus, the net addition of juvenile material to the crust has been in the form of basaltic magmas throughout Earth's history. Although additions to the crust in the form of Mg-rich komatiitic basaltic and komatiitic magmas may have been important in the early Earth, the existing Archean rock record suggests that such magmas were volumetrically subordinate to basaltic magmas. Except for a relatively minor volume of differentiation products of basaltic magmas in subduction zones and hot spot/plume settings, large volumes of felsic igneous rocks characteristic of continental crust are not generated in any of the settings in which basaltic magmas are formed. However, exposed sections of continental crust in Archean cratons are composed of predominantly (up to 70 %) felsic crust, belonging to Tonalite-Trondhjemite-Granodiorite (TTG) group of igneous rocks (Moyen and Stevens, 2006). TTGs, representing the earliest coherent fragments of continental crust (Bowring and Williams, 1999) and a significant proportion of juvenile material added to continental crust between 4.0 and 2.5 Ga (Martin et al., 2005), mark a fundamental step in the formation and evolution of continental crust. Experimental studies of mantle peridotite compositions have shown that TTG magmas could not be direct partial melts from peridotitic source rocks. Two fundamental observations indicate that large volumes of TTG-type rocks in Archean cratons are not the direct differentiation products of mantle-derived magmas: (1) the paucity of a significant proportion of intermediate composition rocks in the Archean record that would be expected to result from a normal differentiation process and, (2) the absence of complimentary cumulate rocks to TTGs in the Archean rock record (Smithies, 2000; Condie, 2005). The origin of

TTGs through partial melting of basaltic crust was proposed in order to explain the large volumes of TTGs in the Archean record (e.g. Barker and Arth, 1976; Martin, 1987). Subsequently, experimental studies demonstrated that melts, comparable in major element chemistry to TTGs, can be generated by melting rocks of basaltic composition (e.g. Johnston, 1986; Beard and Lofgren, 1991; Rapp et al., 1991; Rushmer, 1991; Winther and Newton, 1991; Springer and Seck, 1997). Two aspects of the partial melting process are important in understanding the origin of Archean TTGs: (1) the pressure-temperature conditions at which partial melting occurs and, (2) the tectonic settings at which these conditions might be acheived. Despite the wide range of conditions and starting materials studied, discrepancy in some major-and minor-element compositions (e.g. Mg, Ni, Cr) between TTGs and experimentally generated melts exists (Sen and Dunn, 1994; Springer and Seck, 1997). Modification of pristine TTG melts through interaction with the overlying mantle wedge in subduction zones has been proposed to resolve these differences (Rapp et al., 1999; Martin and Moyen, 2002). Such a process requires a subduction zone tectonic setting for TTG formation. However, the occurrence of plate tectonics and subduction processes in the Archean is not accepted by some (Hamilton, 1998; Bleeker, 2002; Bedard, 2006) and a direct connection between TTG magmas and slab melts (adakites) is questioned by others (Smithies, 2000; Condie, 2005). Accurate knowledge of the metamorphic evolution of basaltic rocks and their phase relations during partial melting may help better define the conditions of TTG formation and place constraints on the tectonic settings of their formation and by implication that of continental crust. Further, in a plate tectonic regime, recycling of oceanic crust in subduction zones is an integral part of the crustal evolution process.

Knowledge of the pressure-temperature conditions at which metamorphic facies transformations occur in basaltic crust is important to understand the material evolution in subduction zones. Basaltic composition rocks are also thought to be common in the lower parts of continental crust (Rushmer, 1991) and are reworked during continental collision or subduction events. Thus knowledge of the phase relations of metabasalts is important to improve our understanding of crustal evolutionary processes in different tectonic settings.

Basaltic protoliths

Because phase relations in metamorphosed basalts are in part controlled by the bulk composition of the basaltic protolith, it is important to address the chemical variability in basaltic rocks. Six major types of basalts have been recognized based on tectonic setting: (a) mid-ocean ridge basalts (MORB), (b) back-arc basin basalt (BARB), (c) oceanic-plateau basalt (OPB), (d) ocean-island basalt (OIB), (e) island-arc/continental-arc basalts (IAB), and (f) continental-flood basalt (CFB). The chemical and mineralogical variability in these basalts are interpreted as reflecting the differing degrees of partial melting of a homogenous mantle source followed by variable degree of differentiation (Grove and Kinzler, 1992).

Mid-ocean ridges have a global strike length of approximately 65,000 km and represent the most voluminous site of basalt magma production in modern day Earth (~5 to 20 km^3 of magma produced per year) (BVTP, p. 133). Arguably, mid-ocean ridge type settings were also the sites of basalt magma production in the early Earth, although the evidence for their existence remains fragmentary (Furnes et al., 2007) given the transient nature of oceanic crust through geologic time. Nevertheless, MORBs represent the most abundant rock type constituting the oceanic crust today and are likely to have dominated oceanic crust in the early Earth as well. The maximum age of oceanic crust today is only 180 Ma, reflecting the continuous recycling of MORB crust into the mantle by subduction processes. If MORB production has occurred through most of Earth's history, recycling processes have continuously modified this primary crustal entity and have played an important part in the evolution of the planet's crust, especially its continental crust. Therefore, knowledge of metamorphic phase equilibria in MORB-type bulk compositions is important for understanding the material evolution of Earth's crust. MORBs are typically olivine tholeiites with remarkably uniform major-element composition (Table 1.1) although minor variations are observed in the abundance of incompatible major elements like K and Ti. Tholeiitic basalts also represent the most abundant volcanic rock type in the Archean (Arndt et al., 1997). Arndt et al. (1997) showed that Archean tholeiites overlap modern MORB's in major-element chemistry but exhibit higher SiO_2, FeO and lower TiO_2 contents than the MORB range (Figure 1.1). Thus, olivine tholeiitic bulk compositions are ideal protolith material to study the metamorphic evolution of oceanic crust.

Metabasaltic phase equilibria and scope of present study

On the basis of his work in the Orijarvi region of Southern Finland, Eskola (1914, 1915) noted a predictable relationship between mineral assemblage and bulk rock composition and thereby developed the concept of metamorphic facies. Eskola (1920) recognized five original metamorphic facies (greenschist, amphibolite, hornfels, sanidinite, and eclogite) in mafic rocks to which he later added three more facies (granulite, epidote-amphibolite, glaucophane schist) (Eskola, 1939). Since then the usefulness of characteristic facies assemblages in mafic rocks in defining the relative physical conditions (especially temperature and pressure) of metamorphism has been widely recognized (e.g., Glassley and Sorenson, 1980; Harley, 1985; Harley, 1998). With the advent of internally consistent thermodynamic data sets (e.g., Powell and Holland, 1988; Berman, 1988) it has been possible to model phase equilibria in mafic rocks and place constraints on the temperature and pressure of equilibration. However, key reactions involving amphibole and melt are inadequately modelled by internally consistent thermodynamic data sets due to the complex nature of amphibole solid solutions and uncertainties in the thermodynamic data for felsic melts (e.g. Pattison, 2003). Direct determination of the location of key reactions and documentation of mineral compositional variations across these reaction boundaries through targeted experiments on specific bulk compositions is an important step towards quantifying the P-T conditions of metamorphism as well as for refining the thermodynamic data set for complex phases.

Phase relations of metabasalts under both H_2O-saturated and H_2O-deficient conditions have been investigated in experimental studies. Many of these studies investigated subsolidus phase relations in metabasaltic compositions at H_2O saturated conditions (Spear, 1981; Moody et al., 1983; Poli, 1993; Ernst and Liu, 1998). The focus of these subsolidus experimental investigations varied from determining amphibole stability (Spear, 1981) to characterization of greenschist- to amphibolite (Moody et al.,

1983) and amphibolite- to eclogite-facies (Poli, 1993) transitions. These studies provide important information for understanding the low-medium grade metamorphic evolution of basaltic rocks. At higher temperatures mafic rocks develop granulite-facies mineral assemblages. High-grade metabasaltic rocks have recently received considerable attention due to the extreme conditions of crustal metamorphism recorded by these rocks (e.g. Indares and Martignole, 2003; O'Brien and Rotzler, 2003; Pattison, 2003). At granulite-facies conditions, rocks are well above the water-saturated solidus for basalts and undergo partial melting if water is available. In crust lacking a free fluid phase, this is generally achieved by the breakdown of hydrous phases like hornblende. This process, variably referred to as dehydration-melting (Brown and Fyfe, 1970; Thompson, 1982), fluid-absent melting (Vielzeuf and Montel, 1994), or vapor-absent melting (Rutter and Wyllie, 1988), is a dominant intra-crustal differentiation process fractionating source rocks into a fusible granitic (*sensu lato*) melt and a refractory residual assemblage. Dehydration melting processes have been invoked to explain migmatitization at upper amphibolite to granulite facies conditions (e.g. Waters, 1988; Percival, 1983; Harley, 1985; Hartel and Pattison, 1996). Understanding the phase relations during dehydration melting is important for understanding the metamorphic facies transitions and conditions of partial melting in metabasaltic rocks. Unlike subsolidus phase relations that can be modelled with some accuracy by internally consistent thermodynamic data sets, targeted dehydration melting experiments on relevant bulk compositions remain the most accurate means of studying specific metabasalt equilibria.

A number of studies have investigated the dehydration melting phase equilibria of metabasalts using amphibolites of varying compositions (see Table 1.2 for summary).

The starting materials for these experiments varied in their bulk composition, amphibole compositions and relative proportions of amphibole and plagioclase. Whereas many studies sought to provide constraints on the fluid-absent (dehydration-melting) solidus (Wolf and Wyllie, 1994; Lopez and Castro, 2001), others investigated the viability of producing TTG or adakitic melts from amphibolitic sources (Rapp et al., 1991; Sen and Dunn, 1994, Springer and Seck, 1997). Despite the wide range of bulk compositions and experimental conditions studied, there is considerable uncertainty in the position of key phase boundaries during dehydration melting of metabasalts. In particular, there is a paucity of experimental data at temperatures close to the dehydration melting solidus. The position of key metamorphic facies transitions in metabasalts at conditions close to the solidus are commonly deduced by extrapolation of higher temperature experimental data. The use of such extrapolated phase boundary constraints may yield erroneous results and ultimately lead to unrealistic petrological models. The present study reports the findings of dehydration melting experiments on two basaltic bulk compositions in the P-T range 775-1050 °C, 7-22.5 kbar.

The primary objective of the present study is to provide better constraints on the dehydration melting phase equilibria of metabasalts at high temperatures and pressures characteristic of subducted oceanic crust and of the middle and lower crust in collisional orogens. In particular, the study aims to resolve uncertainties in our understanding of metabasaltic phase equilibria in MORB-type bulk compositions including the position and topology of the dehydration-melting solidus, conditions of garnet and plagioclase stability, the amphibolite to granulite transition, and the amphibolite/granulite to eclogite transition. The study provides data on phase relations of two MORB-type amphibolites over a wider range of P-T conditions than previously determined on any one starting composition. More specifically, the study provides critical experimental data at conditions close to the initiation of dehydration melting in metabasalts. The study, therefore, compliments many previous dehydration melting studies on amphibolitic bulk compositions that were largely conducted at temperatures >950 °C. The results of the present experiments provide important information on the phase transitions that occur at temperatures corresponding to the initial stages of dehydration melting of MORB-type metabasalts and on the nature of melts generated at these conditions.

The results of this study are presented in the following three chapters:

Chapter 2 outlines the details of the starting materials, experimental and analytical procedures and also presents the new phase equilibrium results. The data are discussed in conjunction with those from previous studies to place better constraints on the dehydration melting solidus. The results are also applied to understand the pressure dependent metamorphic facies transitions in metabasalts.

Chapter 3 provides details of garnet growth during dehydration melting of metabasalts. The growth of garnet in metabasaltic bulk compositions is a key petrologic constraint in that garnet significantly influences the HREE budget of magmas (Barker and Arth, 1976; Martin, 1986) and also strongly influences the density of the residual assemblage (Green and Ringwood, 1967; Wolf, 1992; Wolf and Wyllie, 1993; Komiya et al., 2002). Garnet compositional data, textural and growth characteristics in metabasalts are used to place constraints on the conditions required for forming HREE-depleted, TTG-type magmas and in turn to evaluate the viability of tectonic models that have been proposed for early Earth (Zegers and van Keken, 2001; van Thienen et al., 2004; Lustrino, 2005; Bedard, 2006).

Chapter 4 outlines a new tectonic model for the origin of Archean TTG magmas. TTG magma suites have been variably interpreted as products of basalt melting in subduction zones (Martin, 1986; Foley et al., 2002), or in the root zones of thick oceanic or oceanic plateau crust (Atherton and Petford, 1993; Zegers and van Keken, 2001; Condie, 2005; Bedard, 2006). There is also considerable ambiguity in the P-T conditions of melting and the residual phase assemblage that equilibrated with a TTG melt (Foley et al., 2002; 2003; Rapp et al., 2003). I show how equilibrium constraints derived from experiments are inconsistent with previously proposed lower crustal melting models (Zegers and van Keken, 2001; Bedard, 2006) for the origin of TTGs. I then propose a model for how subduction processes may have initiated in a hotter Archean Earth and produced widespread TTG magmatism. The model is compatible with many observations in the Archean rock record including the temporal and spatial association between TTGs and abundant mafic/ultramafic magmatism, the roughly coeval origin of Archean cratonic crust and its associated mantle lithosphere, and the crustal oxygen isotope signatures of Archean TTG magmas.

Chapter 5 is a summary of the key petrological and geodynamic constraints derived from the results of this study and also outline the scope of future research.

References:

Armstrong, R.L. (1981) Radiogenic Isotopes: The case for crustal recycling on a near-steady-state no-continental-growth Earth. Philosophical Transactions of the Royal Society of London A, 301, 443-472.

Armstrong, R.L. (1991) The persistent myth of crustal growth. Australian Journal of Earth Sciences, 38, 613-630.

Arndt, N.T., Albarede, F. and Nisbet, E.G. (1997) Mafic and Ultramafic magmatism. In: de Wit, M.J. and Ashwal, L.D. (eds.) Greenstone Belts. Oxford Science Publications, 233-254.

Atherton, M.P. and Petford, N. (1993) Generation of sodium-rich magmas from newly underplated basaltic crust. Nature, 362, 144-146.

Barker, F. and Arth, J.G. (1976) Generation of trondhjemetic-tonalitic liquids and Archean bimodal trondhjemite-basalt suites. Geology, 4, 596-600.

Beard, J.S. and Lofgren, G.E. (1991) Dehydration and water-saturated melting of basaltic and andesitic greenstones and amphibolites at 1, 3, and 6.9 kbar. Journal of Petrology, 32, 365-401.

Bedard, J.H. (2006) A catalytic delamination-driven model for coupled genesis of Archaean crust and sub-continental lithospheric mantle. Geochimica et Cosmochimica Acta, 70, 1188-1214.

Berman, R.G. (1988) Internally consistent thermodynamic data for minerals in the system Na_2O-K_2O-CaO-MgO-FeO-Fe_2O_3-Al_2O_3-SiO_2-TiO_2-H_2O-CO_2. Journal of Petrology, 29, 445-522.

Bleeker, W. (2002) Archean tectonics: a review, with illustrations from the Slave craton. Geological Society of London Special Publication, 199, 151-181.

Bowring, S.A. and Williams, I.S. (1999) Priscoan (4.00-4.03 Ga) orthogneisses from norwestern Canada. Combinations to Mineralogy and Petrology, 134, 3-16.

Brown, G.C. and Fyfe, W.S. (1970) The production of granitic melts during ultrametamorphism. Contributions to Mineralogy and Petrology, 28, 310-318.

BVTP (1981) Basaltic Volcanism on Terrestrial Planets. Pergamon Press Inc., New York, 1286 p.

Carswell, D.A. (1990) Eclogites and the eclogite facies: definitions and classification. Carswell, D. A. (ed.) Eclogite Facies Rocks, Chapman & Hall, New York, 1-13.

Clemens, J.D. and Vielzeuf, D. (1987) Constraints on melting and magma production in the crust. Earth and Planetary Science Letters, 86, 287-306.

Condie, K.C. (2005) TTGs and adakites: are they both slab melts? Lithos, 80, 33-44.

Ernst, W.G. and Liu, J. (1998) Experimental phase-equilibrium study of Al- and Ti-contents of calcic amphibole in MORB- A semi quantitative thermobarometer. American Mineralogist, 83, 952-969.

Eskola, P. (1914) On the petrology of the Orijarvi region in southwestern Finland. Bulletin of Comm. Geol. Finlande, 40.

Eskola, P. (1915) On the relations between the chemical and mineralogical composition in the metamorphic rocks of the Orijarvi region. Bull. Comm. Geol. Finlande, 44.

Eskola, P. (1939) Die metamorphen Gesteine. In: Barth, T.F.W., Correns, C.W. and Eskola, P. (eds.) Die Entstehung der Gesteine. Julius Springer, Berlin. 263-407.

Foley, S.F., Tiepolo, M. and Vannuci, R. (2002) Growth of continental crust in subduction zones controlled by melting of amphibolite. Nature, 417, 837-840.

Foley, S.F., Buhre, S. and Jacob, D.E. (2003) Evolution of Archean crust by delamination and shallow subduction. Nature, 421, 249-252.

Furnes, H., de Wit, M., Staudigel, H., Rosing, M. and Muehlenbachs, K. (2007) A vestige of the Earth's oldest ophiolites. Science, 315, 1704-1707.

Glassley, W.E. and Sorensen, K. (1980) Constant P-T amphibolite to granulite facies transition in Agto (West Greenland) metadolerites: implications and applications. Journal of Petrology, 21, 69-105.

Grove, T.L. and Kinzler, R.J. (1992) Fractionation of mid-ocean ridge basalt. In: Morgan, J.P., Blackman, D.K. and Stintin, J.M. (eds.) Mantle flow and melt generation at mid-ocean ridges. Geophysical Monograph, 71, American Geophysical Union, 281-310.

Hamilton, W.B. (1998) Archean tectonics and magmatism were not products of plate tectonics. Precambrian Research, 91, 143-179.

Harley, S.L. (1985) Garnet-orthopyroxene bearing granulites from Enderby land, Antarctica: metamorphic pressure-temperature-time evolution of the Archean Napier Complex. Journal of Petrology, 26, 819-856.

Harley, S.L. (1998) On the occurrence and the characterization of ultrahigh-temperature crustal metamorphism. In: Treloar, P.J. and O'Brien, P.J. (eds.) What drives metamorphism and metamorphic reactions? Geological Society of London, Special Publication, 138, 81-107.

Indares, A.D. and Martignole, J. (2003) Towards the upper limits of the granulite facies. Journal of Metamorphic Geology, 21, 1-2.

Johnston, A.D. (1986) Anhydrous P-T phase relations of near-primary high-alumina basalt from the South Sandwich Islands: Implications for the origin of island arcs and tonalite-trondhjemite series rocks. Contributions to Mineralogy and Petrology, 92, 368-382.

Kay, R.W. and Kay, S.M. (1991) Creation and destruction of lower continental crust. Geol. Rundsch., 80, 259-272.

Komiya, T., Hayashi, M., Maruyama, S. and Yurimoto, H. (2002) Intermediate-P/T type Archean metamorphism of the Isua supracrustal belt: implications for secular change of geothermal gradients at subduction zones and for Archean plate tectonics. American Journal of Science, 302, 806-826.

Lustrino, M. (2005) How the delamination and detachment of lower crust can influence basaltic magmatism. Earth Science Reviews, 72, 21-38.

Martin, H. (1986) Effect of steeper Archean geothermal gradient on geochemistry of subduction-zone magmas. Geology, 14, 753-756.

Martin, H. and Moyen, J.-F. (2002) Secular changes in TTG composition as markers of the progressive cooling of the earth. Geology, 30, 319-322.

Martin, H., Smithies, R.H., Rapp, R., Moyen, J.-F. and Champion, D. (2005) An overview of adakite, tonalite-trondhjemite-granodiorite (TTG), and sanukitoid: relationships and some implications for crustal evolution. Lithos, 79, 1-24.

McLennan, S.M. and Taylor, S.R. (1983) Continental freeboard, sedimentation rates and growth of continental crust. Nature, 306, 169-172.

Moody, J.B., Meyer, D. and Jenkins, J.E. (1983) Experimental characterization of the greenschist/amphibolite boundary in mafic systems. American Journal of Science, 283, 48-92.

Moorbath, S. (1977) Ages, isotopes and evolution of the Precambrian continental crust. Chemical Geology, 20, 151-187.

Moyen, J.-F. and Stevens, G. (2006) Experimental constraints on TTG petrogenesis: Implications for Archean Geodynamics. In: Benn, K., Mareschal, J-C. and Condie, K.C. (eds.) Archean Geodynamics and Environments. Geophysical Monograph, 164, 149-175.

O'Brien, P.J. and Rotzler, J. (2003) High-pressure granulites: formation, recovery of peak conditions and implications for tectonics. 21, 3-20.

Pattison, D.R.M. (2003) Petrogenetic significance of orthopyroxene-free garnet + clinopyroxene + plagioclase ± quartz-bearing metabasites with respect to the amphibolite and granulite facies. Journal of Metamorphic Geology, 21, 21-34.

Percival, J.A. (1983) High-grade metamorphism in the Chapleau-Foleyet area, Ontario. American Mineralogist, 68, 667-686.

Poli, S. (1993) The amphibolite-eclogite transformation: An experimental study on basalt. American Journal of Science, 293, 1061-1107.

Powell, R. and Holland, T.J.B. (1988) An internally consistent thermodynamic data set with uncertainties and correlations: 3. Application methods, a worked example and a computer program. Journal of Metamorphic Geology, 6, 173-204.

Rapp, R.P., Watson, E.B. and Miller, C.F. (1991) Partial melting of amohibolite/eclogite and the origin of Archean trondhjemites and tonalites. Precambrian Research, 51, 1-25.

Rapp, R.P., Shimizu, N., Norman, M.D. and Applegate, G.S. (1999) Reaction between slab-derived melts and peridotite in the mantle wedge: experimental constraints at 3.8 GPa. Chemical Geology, 160, 335-356.

Rapp, R., Shimizu, N. and Norman, M.D. (2003) Growth of early continental crust by partial melting of eclogite. Nature, 425, 605-609.

Rudnick, R.L. (1995) Making continental crust. Nature, 378, 571-578.

Rushmer, T. (1991) Partial melting of two amphibolites: contrasting experimental results under fluid-absent conditions. Contributions to Mineralogy and Petrology, 107, 41-59.

Rushmer, T. (1993) Experimental high-pressure granulites: some applications to natural mafic xenolith suites and Archean granulite terranes. Geology, 21, 411-414.

Rutter, M.J. and Wyllie, P.J. (1988) Melting of vapour-absent tonalite at 10 kbar to simulate dehydration-melting in the deep crust. Nature, 331, 159-160.

Smithies, R.H. (2000) The Archean tonalite-trondhjemite-granodiorite (TTG) series is not an analogue of Cenozoic adakite. Earth and Planetary Science Letters, 182, 115-125.

Spear, F.S. (1981) An experimental study of hornblende stability and compositional variability in amphibolite. American Journal of Science, 281, 697-734.

Taylor, S.R. and McLennan, S.M. (1985) The Continental Crust: its composition and evolution. Blackwell, Oxford.

Thompson, A.B. (1982) Dehydration melting of pelitic rocks and the generation of H_2O-undersaturated granitic liquids. American Journal of Science, 282, 1567-1595.

van Thienen, P., van den Berg, A.P. and Vlaar, N.J. (2004) Production and recycling of oceanic crust in the early Earth. Tectonophysics, 386, 41-65.

Vielzeuf, D. and Montel, J.M. (1994) Partial melting of metagreywackes. Part I. Fluid-absent experiments and phase relationships. Contributions to Mineralogy and Petrology, 117, 375-393.

Waters, D.J. (1988) Partial melting and the formation of granulite facies assemblages in Namaqualand, South Africa. Journal of Metamorphic Geology, 6, 387-404.

Winther, T.K. and Newton, R.C. (1991) Experimental melting of hydrous low-K tholeiite: evidence on the origin of Archaean cratons. Bulletin of Geological Society of Denmark., 39, 213-228.

Wolf, M.B. and Wyllie, P.J. (1993) Garnet growth during amphibolite anatexis: implications of a garnetiferous restite. The Journal of Geology, 101, 357-373.

Wolf, M.B. and Wyllie, P.J. (1994) Dehydration-melting of amphibolite at 10 kbar: the effects of temperature and time. Contributions to Mineralogy and Petrology, 115, 369-383.

Wyllie, P.J., Wolf, M.B. and van der Laan, S.R. (1997). Conditions of formation of tonalites and trondhjemites: Magmatic sources and products. In: de Wit, M. and Ashwal, L.D. (eds.) Greenstone belts. Oxford Monographs on geology and geophysics 35, 256-266.

Zegers, T.E. and van Keken, P.E. (2001) Middle Archean continent formation by crustal delamination. Geology, 29, 1083-1086.

Table1.1: Average composition of unaltered Mid-Ocean Ridge Basalts (MORB). Data from PETDB database.

	MORB-IR		**MORB-EPR**		**MORB-MAR**		**AVERAGE MORB**	
n	652	1σ	3816	1σ	3090	1σ		1σ
Wt.%								
SiO_2	50.77	0.74	50.59	0.96	50.77	0.85	50.58	0.62
TiO_2	1.59	0.47	1.80	0.39	1.39	0.33	1.45	0.30
Al_2O_3	15.64	0.91	14.57	0.86	15.36	0.65	15.45	0.75
FeO^T	9.41	1.27	10.83	1.33	9.62	0.81	9.98	1.02
MnO	0.17	0.05	0.20	0.04	0.17	0.04	-	-
MgO	7.46	0.92	7.17	1.27	7.76	0.81	7.95	0.71
CaO	10.99	0.83	11.42	0.91	11.70	0.78	11.56	0.60
Na_2O	3.02	0.46	2.80	0.30	2.55	0.38	2.71	0.38
K_2O	0.21	0.22	0.16	0.12	0.19	0.19	0.18	0.15
P_2O_5	0.18	0.08	0.18	0.06	0.15	0.06	0.15	0.05
Total	99.45		99.73		99.66		99.86	

Table 1.2: Comparison of composition of starting materials and conditions investigated in dehydration melting studies of metabasaltic rocks.

Study†	Starting Material*	TAS classification	P-T range investigated	Quartz present?	Whole Rock		
					K_2O (wt.%)	Mg#	TiO_2 (wt.%)
Beard and Lofgren, 1991	amphibolite	basalt	1-7 kbar; 850-1000 °C	yes	0.16	0.44	1.74
Rapp et al., 1991; Rapp and Watson, 1995	alkali basalt	trachybasalt	8-32 kbar; 1000-1150 °C	no	0.82	0.51	1.18
	high-Al basalt	basalt	8-32 kbar; 1000-1150 °C	yes	0.21	0.51	2.06
	low-K tholeiite	basalt	8-32 kbar; 1000-1150 °C	yes	0.08	0.58	0.72
	low-K greenstone	basalt	8-32 kbar; 1000-1150 °C	no	0.19	0.47	1.19
Rushmer, 1991	alkali basalt	basalt	8 kbar; 950-1000 °C	yes	0.44	0.59	1.27
	island arc tholeiite	basalt	8 kbar; 950 °C	yes	0.26	0.61	1.00
Sen and Dunn, 1994	amphibolite	basalt	15 and 20 kbar; 850-1150 °C	yes	0.80	0.53	1.22
Wolf and Wyllie, 1994	amphibolite	basalt	10 kbar; 750-1000 °C	no	0.10	0.69	0.40
Patino Douce and Beard, 1995	amphibolite	andesite	3-15 kbar; 840-1000 °C	yes	0.70	0.60	1.70
Springer and Seck, 1997	mafic granulite	basalt	2-15 kbar; 1050-1200 °C	no	0.17	0.49	2.02
Skjerlie and Patino Douce, 2002	eclogite	basalt	10-32 kbar; 800-1150 °C	yes	0.14	0.71	0.76
Lopez and Castro, 2001	amphibolite	basalt	4-14 kbar; 725-950 °C	no	0.09	0.53	1.61
3VG, present study	amphibolite	basalt	7-22.5 kbar, 775-1050 °C	yes	0.88	0.54	1.09
KAP, present study	amphibolite	basalt	7-22.5 kbar, 775-1050 °C	yes	0.77	0.47	0.80

†- only dehydration melting studies reported; * - starting composition as described in the original paper.

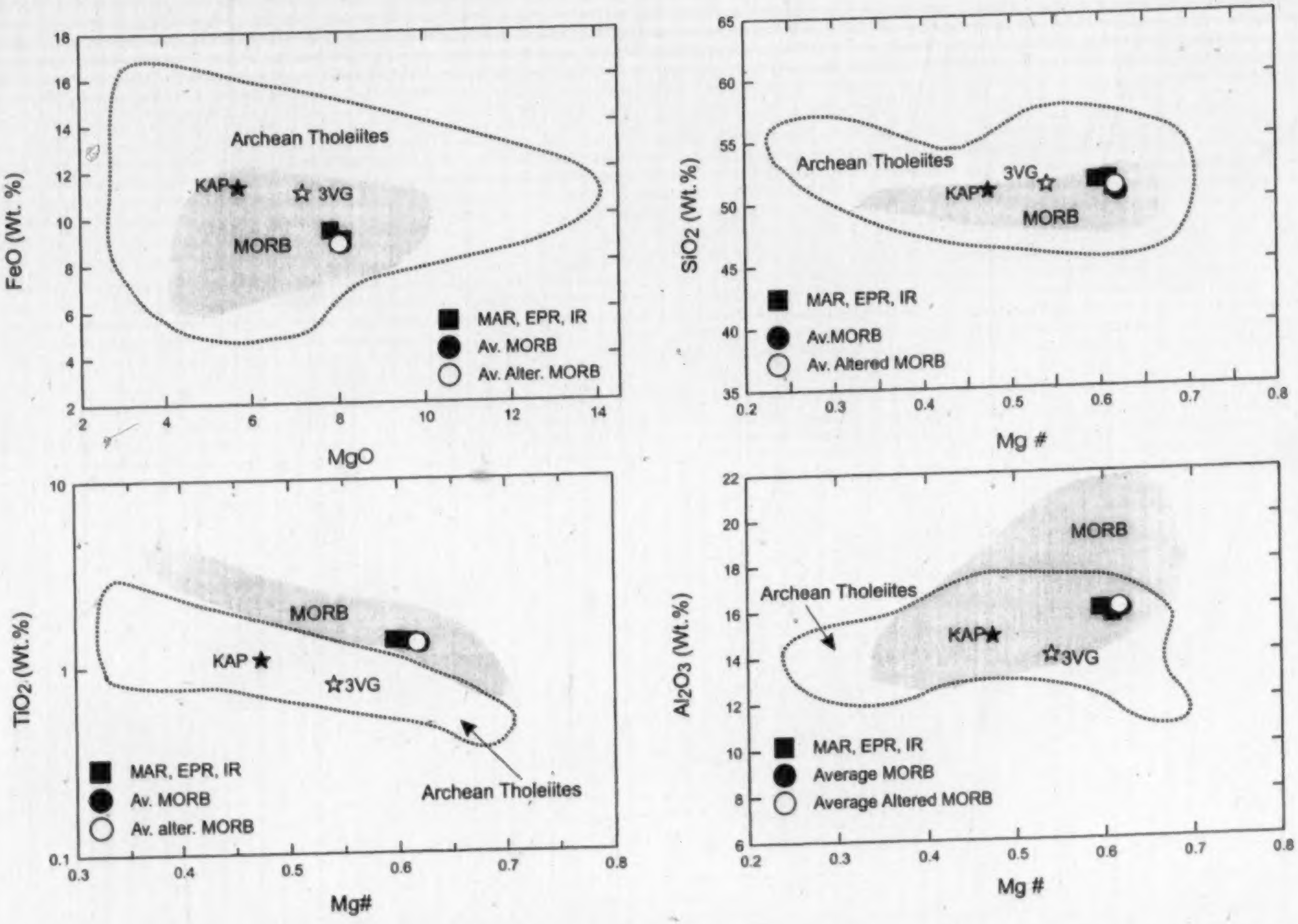

Figure 1.1: Composition of the starting materials compared with mid-ocean ridge basalts (MORB) and Archean tholeiites. Fields for Archean tholeiites and MORB's from Arndt et al., 1997. Composition of different MORB's taken from PETDB database.

CHAPTER 2: Dehydration melting of MORB-type amphibolites: constraints on the solidus and high-grade metamorphic facies transitions

INTRODUCTION

At any stage in Earth's history the net flux of material from mantle to crust occurred through the production and eruption of basaltic magmas. Basaltic rocks, formed at such diverse settings as mid-ocean ridges, subduction zones, oceanic plateaus, and within-plate settings, are subjected to tectono-metamorphic processes that ultimately control the material evolution of Earth's crust. Basaltic magmas, their differentiates and metamorphosed equivalents, are the ultimate protoliths from which continental crust was derived. Understanding the evolution of metabasaltic rocks is therefore fundamental to understanding the evolution of continental crust.

Large volumes of basalt magma erupt in modern-day mid-ocean ridge settings and this may have been true for much of Earth's history. These settings also serve to hydrate the basalt protoliths through interactions between the erupted basalts and sea water. Hydrated mid-ocean ridge basalts (MORB), therefore, represent a common protolith involved in the petrological evolution of Earth's crust. Knowledge of the phases and phase compositional relationships in these metabasalts is necessary for understanding the growth of continental crust as well as material balance during crust-mantle recycling processes. MORB composition basalts are subjected to progressive metamorphism during tectonic burial, in zones of continent-continent collision or more commonly through subduction processes. Mineralogical changes in basaltic rocks accompanying changes in temperature and pressure led to the formulation of the metamorphic facies concept (Eskola, 1920). Although facies boundaries and names are based on mineralogical changes in mafic (basaltic) bulk composition, mafic rocks have proved less definitive in terms of defining facies transitions at moderate-to high-temperature conditions due to the presence of high variance assemblages when compared to rocks of pelitic and semi-pelitic bulk composition. Quantitative evaluation of intensive parameters of metamorphism requires information about the changes in phase assemblage, and in the case of solid solution minerals, changes in the phase composition. At high grades of metamorphism, the behavior of complex solid solutions like hornblende and silicate melt, which are at present inadequately modelled by available thermodynamic data, require phase relations in representative bulk compositions be studied directly using an experimental approach. Study of phase compositional relationships from such experiments is also critical for improving the thermodynamic data available for these phases.

This paper presents results of new dehydration melting experiments conducted on two MORB-type amphibolites. One of the main objectives of the present study was to understand phase relations of typical MORB-type amphibolites at a wider range of conditions than has been investigated on any single bulk composition previously. Experimental conditions investigated in this study spanned from subsolidus temperatures to temperatures above hornblende stability and from pressures below the stability of garnet to pressures above the stability limit of plagioclase. The results provide important constraints on the dehydration melting solidus as well as on the pressure dependent metamorphic facies transitions in these bulk compositions at supersolidus conditions. Finally, melt compositional data along with phase relations of the melt residue are used to place constraints on the conditions of formation of tonalite-trondhjemite-granodiorite (TTG) type magmas derived by partial melting of metabasaltic bulk compositions.

Previous studies and scope of present study

The phase relations of metabasites have been investigated in many studies (Green and Ringwood, 1967; Essene et al., 1970; Hansen, 1981; Ellis and Thompson, 1986; Beard and Lofgren, 1991; Rushmer, 1991; Rapp et al., 1991; Winther and Newton, 1991; Wolf and Wyllie, 1994; Sen and Dunn, 1994; Patino Douce and Beard, 1995; Rapp and Watson, 1995; Liu et al., 1996; Springer and Seck, 1997; Ernst and Liu, 1998; Lopez and Castro, 2001). Starting materials used in these studies include synthetic oxide powder mixtures (Hansen, 1981), mechanically mixed natural minerals (Patino Douce and Beard, 1995), glasses prepared from natural basaltic rocks (Green and Ringwood, 1967), and natural rock powders (Rushmer, 1991; Sen and Dunn, 1994; Wolf and Wyllie, 1994; Lopez and Castro, 2001). Experimental investigations on natural rock powders predominantly used amphibolites, thought to be representative of metamorphosed fragments of ancient oceanic crust. Many experimental studies investigating basaltic phase equilibria were conducted in the presence of varying amounts of H_2O (Essene et al., 1970; Ellis and Thompson, 1986; Winther and Newton, 1991; Liu et al., 1996; Springer and Seck, 1997; Ernst and Liu, 1998). Although phase relations observed in H_2O-present experiments may be applicable to the uppermost part of oceanic crust during subduction or during fluid influx during metamorphism and useful in defining minimum conditions of crustal anatexis, fluid-absent conditions are thought to prevail in the lower crust (Clemens and Vielzeuf, 1987). Under such conditions melting occurs at temperatures corresponding to the breakdown of hydrous phases considerably above the water-saturated solidus, a process variably referred to as fluid-absent melting, vapour-absent melting or dehydration melting (Brown and Fyfe, 1970; Thompson, 1982). Dehydration-melting equilibria are thought to reflect more accurately phase relations in mafic rocks when they are incorporated into active tectonic regimes such as continent-continent collision or subduction zones. A dehydration-melting process has been invoked in many studies to explain migmatites commonly observed in high-grade terranes (e.g. Hartel and Pattison, 1996; Kar et al., 2003).

A number of studies investigated the dehydration melting phase equilibria of metabasalts that varied in bulk composition, amphibole composition and in relative proportions of amphibole and plagioclase (summarized in Table 1.2). Some of these experimental studies had quartz in the starting material (Beard and Lofgren, 1991; Rushmer, 1991; 1993; Sen and Dunn, 1994; Patino Douce and Beard, 1995) whereas others did not (Wolf and Wyllie, 1991; Springer and Seck, 1997; Lopez and Castro, 2001). Many studies sought to provide constraints on the fluid-absent (dehydration-melting) solidus (Wolf and Wyllie, 1994; Lopez and Castro, 2001), whereas others investigated the viability of producing TTG or adakitic melts from amphibolitic sources (Rapp et al., 1991; Sen and Dunn, 1994, Springer and Seck, 1997). Winther and Newton (1991) investigated partial melting behavior of low-K metabasalts, but the experiments were not fluid-absent. Given below is a summary of the experimental constraints provided by previous studies.

Beard and Lofgren (1991) investigated the dehydration melting behavior of natural metabasaltic rocks previously metamorphosed at greenschist to hornblende-hornfels facies conditions at 1, 3 and 6.9 kbar at temperatures between 850-1000 °C. The dehydration melting solidus was not bracketed in any of the starting compositions as melt was present even in the lowest temperature experiments. The restite assemblage in these experiments consisted of plagioclase + orthopyroxene + clinopyroxene + magnetite ± ilmenite. The melt compositions ranged from granodioritic to tonalitic.

Rushmer's (1991) dehydration melting experiments on a tholeiitic and an alkali basalt composition at 8 kbar showed that the dehydration melting solidus temperature for tholeiitic basalt is lower than that of alkali basalt. Rushmer (1991) attributed this to the presence of hydrous phases like biotite and cummingtonite in the starting tholeiitic composition. Rushmer's (1993) subsequent experiments on the alkali basalt composition at 12-18 kbar showed that garnet appeared in this bulk composition above 12 kbar and that the restite assemblage at high pressures (garnet-granulite) resembles many lower crustal xenoliths.

Wolf and Wyllie (1994) conducted a series of dehydration melting experiments on a natural high Ca-amphibolite (14.3 wt. % CaO) at 10 kbar in the temperature range 750-1000 °C. They reported the presence of melt at 750 °C, the lowest temperature experiment in their study. Garnet appeared as a phase between 850 and 1000 °C. Garnet was absent above and below this temperature window and garnet abundance was reported to decrease between 875 and 900 °C. Wolf and Wyllie (1994) attributed the absence of garnet in their experiments at temperatures below 850 °C to nucleation difficulties and argued that garnet is in fact stable at these conditions. Melt compositions generated correspond to tonalites but with much higher Al_2O_3 and CaO contents when compared to natural tonalites, reflecting the Ca-and Al-rich bulk composition of the starting material.

Sen and Dunn (1994) presented dehydration melting data on a natural amphibolite at 15 and 20 kbar in the temperature range 850-1150 °C. The solidus reaction was not bracketed in this study, but was inferred to have a negative slope and to lie on the low temperature side of the lowest temperature experiments (850 and 800 °C at 15 and 20 kbar, respectively) between 15 and 20 kbar in order for the observed phase relations to be consistent with that of Wolf and Wyllie (1994) at 10 kbar (Figures 2.1 and 2.2). The residual assemblage was garnet bearing at all conditions and plagioclase was present in all 15 kbar experiments up to 975 °C and only present in the 800 °C experiment at 20 kbar. Amphibole was absent at temperatures above 900 °C at 20 kbar. Partial melts generated in the experiments were similar in composition to adakitic magmas but for lower MgO and CaO contents of the experimental melts.

Springer and Seck (1997) reported dehydration melting systematics of a metabasalt of quartz tholeiite composition at temperatures above 1000 °C. Their reported solidus above 1000 °C is inconsistent with the lower temperature solidus reported in other studies. Details of the experimental phase relations near 1000 °C were not given and hence cannot be evaluated.

Lopez and Castro (2001) provided constraints on the fluid-absent solidus for a MORB-type amphibolite between 4 and 14 kbar. They showed that below pressures where garnet is stable, the fluid-absent solidus is located at a higher temperature than at pressures above garnet stability. The lower temperature solidus at higher pressures was influenced by the breakdown of hydrous phases like epidote. Importantly, however, they argued that the solidus is located at a temperature 150 °C higher than the water-saturated solidus.

The minimum conditions required for dehydration melting of amphibolites were outlined by Wolf and Wyllie (1994). They argued that dehydration melting at pressures above garnet stability could begin at temperatures as low as those of the water-saturated solidus. The reasoning behind this argument was that the amphibole breakdown process responsible for garnet production would also release some water, which in turn would cause melting at temperatures above the water-saturated solidus. While this reasoning appears sound, there is no clear evidence experimentally for melting at such low temperatures. Wolf and Wyllie's (1994) reported solidus is characterized by three segments with distinct P-T slopes (Figure 2.1): a lower pressure near-vertical segment where garnet is not a stable phase, a near-horizontal positively sloped segment where garnet joins the residual phase assemblage and, a higher pressure steeply sloped segment above garnet-in that is coincident with the water-saturated solidus. The solidus, therefore, has an 'S' shape that has never been mapped in experimental studies (Moyen and Stevens, 2006). Vielzeuf and Schmidt (2001) argued against the positive slope for the middle segment of 'S'-shaped solidus based on thermodynamic considerations. As pointed out by Vielzeuf and Schmidt (2001) the arguments for a positive slope of this segment is based on one experiment with large uncertainties in the estimated melt proportion. Thus, despite the wide range of bulk compositions and P-T conditions that has been investigated, there is considerable uncertainty regarding the position of dehydration melting solidus of metabasalts. This is partly due to the lack of adequate experimental data at low (<900 °C) temperatures. Even when experimental brackets for solidus reactions are available, the data were obtained over a limited pressure range requiring inference of the position of solidus by connecting data points from multiple studies conducted on different bulk compositions (e.g. Wolf and Wyllie, 1994; Sen and Dunn, 1994). Despite these limitations, Wolf and Wyllie's (1994) solidus is widely used in petrological models (e.g. Rapp, 1997; Zegers and van Keken, 2001).

There is also considerable uncertainty in the position of key phase boundaries such as the garnet-in and plagioclase-out boundaries. The importance of these phase boundaries is that they also represent facies boundaries in mafic rocks. The lowest pressure at which garnet becomes stable during dehydration melting demarcates a (sub)-facies transition in metabasaltic rocks (de Waard, 1965; Hansen, 1981; Pattison, 2003). Specifically, it demarcates orthopyroxene-bearing intermediate-P granulites from high-P orthopyroxene-free garnet-clinopyroxene granulites (Green and Ringwood, 1966; 1967; O'Brien and Rotzler, 2003; Pattison, 2003) (Figure 2.2). Green and Ringwood (1967) provided experimental constraints on the location of this boundary through crystallization experiments on different basalt composition glasses. Phase identification in Green and Ringwood's (1967) study was done by optical microscopy of grain mounts and x-ray diffraction which may have introduced some uncertainties in constraining phase equilibrium boundaries. Despite the general agreement between the different studies, none of the studies were specifically designed to constrain this boundary in natural metabasaltic rocks. Green and Ringwood's (1967) experimental data are also limited to temperatures above 1000 °C requiring extrapolation to lower temperature region near the solidus of common amphibolitic rocks.

At higher pressures (and moderate to high temperatures), the disappearance of plagioclase defines the granulite to eclogite transition in metabasalts (Carswell, 1990; Oh and Liou, 1998; O'Brien and Rotzler, 2003). Thus, opx-free garnet-cpx granulite assemblages form a paragenetic link between intermediate-P granulites and higher-P eclogites (Pattison, 2003; Indares and Martignole, 2003). Eclogite formation in metabasaltic rocks is proposed to play a key role in a number of processes including slab pull during subduction (Cloos, 1993), subduction zone seismicity (Peacock and Wang, 1999), lower crustal delamination (Kay and Kay, 1991; Zegers and van Keken, 2001; Lustrino, 2005) and the genesis of TTG magmas (Zegers and van Keken, 2001; Rapp et al., 2003). Accordingly, accurate knowledge of the P-T conditions of eclogite stability is central to a better understanding of these processes. Green and Ringwood's (1967) glass crystallization experimental results remain the most commonly used constraint for the granulite-eclogite boundary and is widely used in many tectonic models (Cloos, 1993; Zegers and van Keken, 2001) and in proposed petrogenetic grids (Oh and Liou, 1998). As with the garnet-in boundary at lower pressure, Green and Ringwood's (1967) data on plagioclase stability is limited to temperatures >1000 °C and requires relatively long extrapolation to lower temperatures.

Knowledge of the P-T conditions of garnet and plagioclase stability in metabasalts is also important for modelling the trace-element composition of melts that can be generated from metabasaltic source rocks. It has been shown that melts comparable to TTGs in major-element composition can be produced by partial melting of metabasaltic rocks under fluid-absent conditions (Johnston, 1986; Rapp et al., 1991; Springer and Seck, 1997). However, the rare-earth-element (REE) compositions of

Archean TTGs, characterized by highly fractionated REE patterns with strong depletion in Heavy Rare Earth Elements (HREE), is thought to reflect a garnet-bearing residuum. The HREE content of melt is primarily controlled by the proportion of garnet in the partial melting residue (Nair and Chacko, 2005; Moyen and Stevens, 2006). Documenting variations in the modal proportions of restite phases, in particular garnet, with changing pressure and temperature is therefore critical for placing constraints on conditions of generation of Archean TTG's.

This chapter discusses the results of new dehydration melting experiments conducted on two high-grade metabasaltic rocks and addresses the existing uncertainties in (a) the dehydration melting solidus in MORB-type metabasalts, (b) the stability fields of garnet and plagioclase in MORB-type metabasalts and, (c) the conditions for generating HREE depleted Archean TTG magmas.

Starting materials

The starting materials for the experiments were two natural high-metamorphic-grade amphibolites from Three Valley Gap, British Columbia and the Kapuskasing Structural Zone, Ontario. In both these terranes prograde transition from amphibolite to granulite is documented in bulk compositions similar to the starting materials or in interlayered lithologies of different bulk composition (Nyman et al., 1995; Hartel and Pattison, 1996). The mineral assemblages in the starting materials equilibrated at P-T conditions close to those of the amphibolite-granulite transition. Published P-T estimates from Kapuskasing and Three Valley Gap indicate metamorphic conditions of 9 kbar and 685-735 °C (Percival, 1983) and 7.5-9 kbar and 720-820°C (Nyman et al., 1995), respectively. These temperature estimates are also corroborated by widespread migmatisation in both areas indicating temperatures above the water-saturated solidus for amphibolites (e.g. Nyman et al., 1995; Hartel and Pattison, 1996). Hartel and Pattison (1996) argued on the basis of experimental data that Percival's (1983) P-T estimate for the Kapuskasing rocks significantly underestimated peak metamorphic conditions. They suggested that peak conditions were 10-11 kbar, 800-850 °C. Regardless of the exact P-T conditions of equilibration, field relationships indicate that the rocks experienced near granulite-facies temperatures. Nair and Chacko (2002) argued that use of starting materials that were metamorphosed to near solidus temperatures are ideal for investigating dehydration melting processes in that mineral compositions in such rocks closely approximate those of natural samples undergoing incipient melting. Reaction boundaries determined using these starting materials provide more accurate constraints than those obtained from chemically simple end-member systems or natural rocks that have equilibrated at conditions far from the reactions of interest. Use of latter starting materials may result in spurious phase relations that have limited petrological applicability.

The bulk rock and mineralogical composition of the starting materials are given in Table 2.1. Both starting materials contain the mineral assemblage hornblende-plagioclase-quartz-clinopyroxene-garnet, with hornblende and plagioclase constituting >85 vol. % of the rock. Accessory titanite and ilmenite were also present in these samples. The major-element compositions of the starting materials are very similar to average MORB glass except for the slightly lower TiO_2 and Al_2O_3 and significantly higher K_2O content. The Al_2O_3 content of the KAP starting material is within one standard deviation of the MORB average whereas that of the 3VG starting material is 1.3 wt. % lower. The TiO_2 contents of both starting materials are within 2 standard deviations of average mid-ocean ridge basaltic glass (Table 2.2). The major-element compositions of the starting materials are also similar to the MORB-derived amphibolites reported by Castro et al. (1996). Many of these amphibolites also show TiO_2 depletion and K_2O enrichment relative to fresh MORB glass.

Average MORB is olivine normative. CIPW norm calculations assuming $Fe^{3+}/\Sigma Fe = 0.15$ (Christie et al., 1986) indicate both starting materials to be slightly olivine normative (Table 2.2). Oceanic crust becomes oxidized through seawater and hydrothermal alteration and within the first 10-20 Ma of its evolution attains an average $Fe^{3+}/\Sigma Fe$ of 0.45 ± 0.15 (Bach and Edwards, 2003). Norm calculations performed at this post-alteration $Fe^{3+}/\Sigma Fe$ value would characterize the starting materials as quartz normative.

Experimental Procedure

All experiments were conducted on powdered starting materials under nominally fluid-absent conditions in an end-loaded piston-cylinder apparatus in the C.M. Scarfe Experimental Petrology Laboratory at the University of Alberta. Small (~2cm^3) pieces of the starting amphibolites were crushed in a tungsten carbide shatter box. The resulting powder was then hand ground in acetone to an average grain size of 5-10 um using an agate mortar. The powdered material was stored in an oven at 110 °C for several days before loading into the experimental capsules. Gold tubings (2 mm outer diameter) was used to make the capsules. The open end of the loaded capsule was crimped and kept in an oven at 110 °C for at least 10 hours before it was welded shut. The sealed capsules were placed inside a pressure cell consisting of a tapered graphite furnace (Kushiro, 1976) sheathed on the outside by a Pyrex glass sleeve which in turn was enclosed within an outer NaCl pressure sleeve. Space between the ceramic inner parts of the furnace and the capsule was filled with very finely ground Pyrex powder. The NaCl outer sleeve was fired at 300-350 °C for ~1 hr before use in the experiments. The 1.91 cm (3/4 inch) sample assembly was jacketed with Pb foil to minimize friction between the assembly and pressure vessel.

The pressures reported are nominal hydraulic pressures measured with a Heise bourdon tube gauge and converted to sample pressure using a theoretically calculated amplification factor. The P-T position of the reaction grossular + quartz = wollastonite + anorthite (Windom and Boettcher, 1976; Mattioli and Bishop, 1984) was used to evaluate the correspondence of calculated pressure with true sample pressure. These calibration experiments indicated that no pressure correction is required and the reported pressures are considered to be accurate within 0.5 kbar. Temperatures were measured using W5Re-W26Re thermocouples relative to an Omega electronic ice point. Temperature during the experiments was controlled by a Eurotherm 818 digital temperature controller which regulated the temperature to within ±10 °C of the desired set point.

Two different pressure ramping procedures were used for the experiments. For experiments up to 12.5 kbar, the samples were cold pressurized to 2-3 kbar above the desired pressure, and the temperature then manually increased to the target experimental temperature over a 10-15 min period. The final experimental conditions were always attained by a release of pressure (hot, piston-out technique). At pressures ≥15 kbar, it was found advantageous to use a 'hot piston-in' technique whereby samples after initial cold pressurization (to a value <3-5 kbar of the desired pressure) were first heated to temperature high enough to soften the sample assembly before advancing the piston to achieve the target pressure. Temperature was then manually adjusted to the desired set point and set to be controlled by the Eurotherm controller. The heating step usually lasted about 10 minutes.

Phase reversal experiments were attempted by conducting two-stage experiments in which stage 1 corresponds to conditions at which a phase was previously documented to be stable and stage 2 to conditions at which the phase is believed to be unstable. A successful reversal experiment involves the disappearance of phases grown in at the first stage and growth of phases that indicate a reversal in the direction of reaction. Phase reversal experiments were attempted for bracketing phase appearances as a function of both temperature and pressure. Successful phase reversal temperature brackets were obtained for opx-in and garnet-in boundaries. The large volume of the furnace assembly permitted the use of two capsules in each experiment, one containing KAP and the other the 3VG starting material. The capsules were weighed before and after each experiment and those with any tear and/or weight loss >0.1 mg were discarded. Further details of the experimental procedures are given in Nair (2000) and Nair and Chacko (2002).

Analytical Techniques

Successful experimental run products were mounted in epoxy and analyzed using energy-dispersive (EDS) and wavelength-dispersive (WDS) modes using a JEOL 8900 electron microprobe at the University of Alberta. WDS analyses on crystalline phases were performed at an accelerating voltage of 15 kV, a beam current of 15 nA, and a beam diameter between 1 and 3 μm. Natural mineral standards were used for all WDS measurements. X-ray counts were converted to concentrations by means of the ZAF correction routine using JEOL software.

A slightly different analytical procedure was used for WDS analyses of quenched melt pockets (glass). Glass was analyzed with an accelerating voltage of 15 kV, a beam current of 5 nA, and beam diameter varying from <1 μm (fully focused beam) to 15 μm. Whenever possible a large beam size was used to minimize alkali volatilization but this was precluded in some cases by the small size of the melt pockets. Na and K were analyzed first during WDS analyses and counting time for Na was limited to 10 s. The count rate decay of Na at these analytical conditions was found to be a function of the beam diameter. The melt analyses were corrected for Na-loss using a correction factor that was determined based on the observed variations in Na as a function of beam size (see appendix B for details).

Attainment of equilibrium

The ubiquitous presence of relict minerals from the starting materials in the run products warranted a careful assessment of degree of equilibration in the present experiments.

Experimental duration

Duration of the present experiments varied from 2 days at temperatures ≥1000 °C and up to 5 weeks at lower temperatures. To the best of my knowledge, these are the longest duration experiments that have been conducted on metabasaltic starting materials at fluid-absent conditions.

Homogeneity of crystal growths and systematic variations in phase compositions

Many experimental studies have shown that equilibrium is generally not achieved on the scale of the entire experimental charge in experiments with natural rock powders (Skjerlie and Johnston, 1996; Skjerlie and Patino Douce, 2002). There were several indications of non-equilibrium between the seeds in the starting materials and the phase components that grew during the experiments. This is clearly evident for garnets in KAP experiments, which showed distinct cores whose compositions were indistinguishable from the garnet seeds in the starting material. However, the composition of the garnet overgrowths is remarkably uniform both within and between the newly formed grains. This suggests that while intra-crystalline diffusion was slow, the growth of phases was not limited by this process. Growth occurred relatively fast, perhaps promoted by diffusion of components through intergranular melt channels. The homogeneity of overgrowths along with their regular compositional variation with pressure and temperature suggest that growth of new garnet took place under near equilibrium conditions. Systematic mineral and melt compositional variations (see below) indicates that the system was reactive and that phase compositions were approaching equilibrium at the conditions of the experiment.

Application of geothermometers

Partitioning of Fe^{2+} and Mg between co-existing garnet and clinopyroxene is a function of temperature and to a lesser extent pressure. The temperature dependence of Fe^{2+} and Mg between garnet and clinopyroxene has been calibrated into a geothermometer (e.g. Raheim and Green, 1974; Ellis and Green, 1979; Pattison and Newton 1989; Ai, 1994; Krogh, 1988; Krogh-Ravna, 2000; Nakamura, 2006). Although, these calibrations yield somewhat different temperatures (Green and Adam, 1991; Nakamura and Hirajima, 2005) when applied to natural rocks or experimental data, they are nonetheless useful for assessing the extent of equilibration in experimental run products in which garnet and clinopyroxene co-exist. I used compositional data of co-existing garnet and clinopyroxene from the run products to calculate temperatures using the calibrations by Ellis and Green (1979), Krogh (1988), Krogh-Ravna (2000), Nakamura (2006), and using TWQ software v.2.34 (Berman, 1991). Temperatures were calculated using the average analyzed composition of garnet and clinopyroxene from the run products and assuming that Fe is entirely in the ferrous state in both phases. In the experimental products in which garnet and/or cpx were zoned, the average rim compositions of the zoned phase were used in the calculation.

The calculated temperatures (Figure 2.3) deviate somewhat from the experimental temperatures indicating either that compositional equilibrium was not fully achieved in my experiments or that one or more of the thermometer calibrations are in error. The error bars in the calculated temperatures (Figure 2.3) correspond to 1σ compositional uncertainty in Fe/Mg ratio of clinopyroxene. The discrepancy between calculated and experimental temperatures is not surprising as the presence of zoning (in the form of relict cores in some garnet and cpx) is suggestive of a solution-precipitation mechanism which does not necessarily produce equilibrium compositions (Pattison, 1994). There are indications, however, that the measured compositions were close to equilibrium compositions. Firstly, the calculated temperatures are mostly within 50° C of experimental temperatures. In particular, there is excellent agreement between calculated temperatures using TWQ and experimental temperatures at low temperatures. The correspondence of calculated temperatures using recent calibrations of Krogh-Ravna (2000) and Nakamura (2006) is also satisfactory. Secondly, there is a clear positive correlation between calculated temperatures and experimental temperature (Figure 2.3). This indicates that the phases were reactive during the experiments and that the K_d for Fe-Mg partitioning changes systematically with temperature.

Phase reversal experiments

Successful phase reversal is regarded as a rigorous demonstration of equilibrium in phase equilibrium experiments (Holloway and Wood, 1988; Pattison, 1994; Aranovich and Newton, 1998). In the present study phase reversal brackets were achieved at 7 kbar for orthopyroxene and at 12.5 kbar for garnet. This involved performing two-stage experiments, initially at P-T conditions where opx/garnet was deemed stable from previous experiments and then lowering the temperatures (while keeping the pressure constant). The criterion for successful reversal is the absence of opx/garnet in the run product after the two-stage experiment. At 7 kbar, the first appearance of opx was reversed between 900 and 850 °C and between 900 and 825 °C in the KAP and 3VG bulk compositions, respectively. In both starting materials the presence of garnet was reversed between 850 and 775 °C at 12.5 kbar. As far as I am aware, this is the first documentation of successful phase reversals in dehydration melting experiments in amphibolites. I argue, based on these successful phase reversals, that equilibrium was achieved in my experiments in terms of phase stability relations.

Redox Conditions

No external oxygen fugacity (fO_2) buffers were used in these experiments. It is well known that the stability of Fe-bearing minerals is affected by the prevailing fO_2 conditions (e.g. Moody et al., 1983). The following discussion outlines the constraints that I have on the prevailing fO_2 conditions in the present experiments.

Comparative oxygen barometry

It has been argued that in piston-cylinder experiments, the nature of the pressure cell assembly imposes a certain fO_2 on the sample (Patino Douce and Beard, 1995). Some previous experimental studies suggest that NaCl-graphite pressure cells impose a fO_2 that is one to two log units below the quartz-fayalite-magnetite (QFM) buffer (Patino Douce and Beard 1995, 1996; Nair and Chacko 2002). However, Liu et al. (1996) reported fO_2 conditions 0.2-0.3 log units higher than QFM in their experiments employing a NaCl pressure medium. In general, however, fO_2 during experiments using similar cell assemblies are close to that defined by the QFM buffer which is somewhat lower than the fO_2 conditions in the upper part of a subducting oceanic crust.

Qualitative estimates of fO_2 during the experiments can also be obtained from the stability relations of minor Fe-, Ti-bearing phases (Spear, 1981; Moody et al., 1983;

Schmidt and Thompson, 1996). Moody et al. (1983) argued that in mafic systems, titanite (sphene), ilmenite and magnetite are characteristic of fO_2 conditions near that of the QFM and Ni-NiO buffers. In the present study the minor Fe-Ti phases observed were titanite, ilmenite, magnetite (ulvospinel), rutile and pyrrhotite. In general titanite was observed at lower temperatures and ilmenite/magnetite at higher temperatures, although the latter two minerals do not coesist in any of the experimental charges (Table 2.3). Rutile is only present in trace amounts and is restricted to pressures above 17.5 kbar and pyrrhotite at pressures above 20 kbar. It is interesting to note that the relative stability fields of the minor Fe-Ti phases except pyrrhotite in this study are similar to those observed from hydrous experiments with basalt similar to the present starting materials (Ernst and Liu, 1998). The latter experiments were externally buffered at QFM conditions. Despite the anhydrous nature of the present experiments, these comparable results may indicate fO_2 conditions near the QFM buffer.

Calculated oxygen fugacity

A quantitative estimate of fO_2 was obtained using the equilibrium:

$$2Fe_3O_4 + 6SiO_2 = 3Fe_2Si_2O_6 + O_2$$

in five experimental charges (3VG3, 3VG14, 3VG26, 3VG27 and KAP 22) that contained co-existing magnetite and orthopyroxene. Of these, the 3VG experiments were conducted at 7 kbar and the KAP experiment at 10 kbar. None of the other experiments contained phase assemblages amenable to the calculation of fO_2. Because quartz was not a stable phase in the experiments from which oxygen fugacity estimates were made, calculations were done for SiO_2 activity values of 1 and 0.8. Calculations were performed using the QUIIF program (Anderson et al., 1993). The calculated fO_2 values are plotted in Figure 2.4 in relation to some common petrologic buffer reactions (hematite-magnetite (HM), quartz-fayalite-magnetite (QFM) and nickel-bunsenite (Ni-NiO)). The calculated fO_2 values range between QFM + 1.3 and QFM + 1.9 log units for calculations done assuming $a\text{SiO}_2 = 1$ (Figure 2.4). This represents a maximum value for fO_2 in these experiments. The fO_2 values determined using $a\text{SiO}_2 = 0.8$ are about 0.6 log units below the estimates using $a\text{SiO}_2 = 1$ (Figure 2.4). These estimates are very similar to fO_2 values reported from the dehydration melting experiments on amphibolites by Beard and Lofgren (1991). Sen and Dunn (1994) calculated fO_2 from the Fe^{3+}/Fe^{2+} ratio of quenched melt from an experiment in which their starting amphibolite was completely molten. Their reported fO_2 value (QFM -0.5 log units) is ~ 2-2.5 log units below that estimated in the present experiments. The experiment from which Sen and Dunn (1994) calculated the fO_2 value was done using a Pt-C capsule and may have imposed lower fO_2 conditions during the experiment (Holloway et al., 1992). The oxygen fugacity values reported by most previous dehydration melting studies on amphibolite bulk compositions using Au capsules were between HM and QFM buffers (e.g. Beard and Lofgren, 1991; Rushmer, 1991; Wolf and Wyllie, 1994), consistent with the fO_2 estimates from the present experiments. Beard and Patino Douce (1995) argued that fO_2 values during experiments tend to be buffered by the experimental assembly due the small volume of the sample used in experiments. Interestingly, however, the fO_2 estimates from amphibolite dehydration-melting experiments are 2-3 log units higher than fO_2 estimates from dehydration melting experiments on pelitic and semi-pelitic bulk compositions conducted using Au capsules (e.g. Patino Douce and Beard, 1995; Nair and Chacko, 2002). The reason for this difference is unclear, but may be related to the higher total Fe content and higher Fe^{3+}/Fe^{2+} of the starting mafic compositions relative to the pelitic starting materials used in experiments. It is also possible that minor amounts of graphite that may have been present in the semi-pelitic starting materials (e.g. Nair, 2000; Nair and Chacko, 2002) limited the maximum fO_2 conditions in those experiments to below that of the QFM buffer.

RESULTS

A summary of the experimental conditions and the observed phase assemblage in both bulk compositions studied is presented in Table 2.3 and Figure 2.5.

Description of run products

7 kbar

A melt phase could not be identified in the lowest temperature experiments (825 °C) in KAP, but a trace amount of melt was observed in the 3VG bulk composition. A trace amount of clinopyroxene was, however, present in both KAP and 3VG compositions at 825 °C. I consider these to be relict cpx seeds from the starting material as microprobe analyses showed them to have compositions indistinguishable from the starting cpx. Quenched melt was positively identified at 850 °C in both KAP and 3VG experiments. Garnet was absent in the 7 kbar experiments and none of the garnet seeds survived the duration of the experiments. Phase relations in both starting materials are characterized by two distinct temperature dependent mineral assemblages, hbl-plag-cpx-melt and hbl-plag-cpx-opx-melt, the former representing the lower temperature assemblage. Relict quartz was observed at temperatures below 875 °C. The proportions of hbl and plag decrease with temperature and those of cpx and opx increase with temperature. Hornblende is stable to 950 °C in both compositions.

10 kbar

The phase relations of the 10 kbar 3VG experiments are very similar to those at 7 kbar, except for the presence of garnet at 850 °C. At temperatures above 850 °C, opx is stable in this bulk composition. Quartz is present as a relict phase up to 900 °C. Modal variation patterns of all other phases remain the same. Trace amounts of hornblende persisted to 1000 °C.

In the KAP experiments, garnet was positively identified in the temperature range 800-900 °C. Garnets in the 800 °C experiments are, however, compositionally similar to the garnet seeds and lack neoblastic growth textures. Thus, I consider this experiment to be outside the garnet stability field. Garnet disappeared from the assemblage at temperatures above 900 °C. Unlike 3VG, garnets do not co-exist with orthopyroxene in this bulk composition. Relict quartz was observed at temperatures below 850 °C.

12.5 kbar

Opx is absent from the KAP experiments but is present in 3VG experiments at 900 and 950 °C. The abundance of garnet and cpx in the Hbl-Plag-Grt-Cpx±Opx assemblage is greater than at 10 kbar.

15 kbar

Opx is absent from both starting compositions in the temperature range investigated. A marked increase in the abundance of garnet is observed at temperatures above 900 °C. The individual garnet crystals are also significantly larger and exhibit well developed poikilitic habit at temperatures >850 °C. Significantly larger melt pockets can be observed randomly distributed between the garnet crystals at these conditions.

17.5 kbar

Garnet becomes a dominant residual phase in both bulk compositions. The abundance of plagioclase is markedly lower than in the lower pressure experiments. Rutile rather than ilmenite becomes the titaniferous phase compared to lower pressure experiments.

20 kbar

Plagioclase is significantly less abundant than in lower P experiments and is in fact absent from the 3VG composition at 900 °C. Garnet is more abundant than in the lower pressure runs. Hornblende only occurs in trace amounts and was absent from the 900 °C experiment in both the KAP and 3VG experiments..

22.5 kbar

The residual assemblage is truly eclogitic, except in the 850 °C experiment with KAP which contains trace amounts of plagioclase. Phengite was observed at 850 °C in both bulk compositions. Hornblende is absent from all 22.5 kbar experiments.

Phase stability and compositions

Hornblende

Hornblende is a residual phase in the experimental run products and, when present, coexists with plagioclase. Above the solidus, the modal abundance of hornblende decreases with temperature. Hornblende has both an upper temperature and an upper pressure stability limit in the bulk compositions studied. At 7 kbar it disappears from both bulk compositions between 950 and 1000 °C and also disappears from both bulk compositions at pressures greater than 20 kbar.

Amphibole compositions are given in Table 2.4. Amphibole structural formulae were calculated following Leake et al. (1997) assuming 23 O atoms per formula unit and having the general form $A_{0\text{-}1}B_2C_5T_8O_{22}(OH)_2$, where A, B, C and T refer to the 10-12 fold coordinated site, six to eight fold coordinated sites, octahedral sites, and tetrahedral sites, respectively. Even though minor amounts of Cl and possibly F were present in the amphiboles, these were ignored during structural formula calculations. Cation site assignment followed the scheme of Leake et al. (1997) and in the order T, C, B and A so that the following criteria were met: Tetrahedral occupancy = 8.00, octahedral occupancy = 5.00, B-site occupancy = 2.00, and A-site occupancy = 0-1.00. Fe^{3+}/Fe^{2+} ratios were calculated by normalizing to 13 total cations (excluding Ca, Na, and K). The differences in amphibole composition between the KAP and 3VG experiments reflect bulk compositional differences of the starting materials. In 3VG experiments, amphiboles are pargasitic in composition whereas in KAP experiments they range in composition from ferro-pargasite to pargasite (Figure 2.6). At the same experimental conditions, 3VG hornblende has a higher Mg-number than that of KAP. Stoichiometric constraints result in covariance of Mg-number with Si in both bulk compositions with Mg-number generally increasing with decreasing Si (Figure 2.6). Although the variation is irregular, Mg-number in amphibole increases with temperature (Figure 2.7). Al^{IV} increases with Mg, whereas Al^{VI} decreases marginally with increasing Mg. The incorporation of Al in the tetrahedral site involves coupled substitutions of Al, Fe^{3+}, and Ti on the octahedral site and Na on the A-site. This is evident in a plot of Al^{IV} versus Na (A-site) + 2Ti(VI) + Al(VI) + Fe^{3+}(VI), which exhibits a reasonably good correlation (Figure 2.8). However, lack of correlation between these cations (Na, Fe^{3+}, Ti) and Al^{1V}(not shown) and the variation of A-site occupancy at relatively constant Al^{1V} indicate that the substitution involves complex permutations of edenite (□(A) + Si = Na(A) + Al(IV)), Tschermakite (2Si(IV) + 2Mg(VI) = 2Al(IV) + 2 Al(VI)), ferri-tschermakite (2Si(IV) + 2Mg(VI) = 2Al(IV) + 2Fe^{3+}(VI)) and Ti-tschermakite (2Si(IV) + Mg(VI) = 2 Al(IV) + Ti (VI)) substitution mechanisms, with increasing edenite-type substitution and decreasing tschermakite-type substitution at higher temperatures.

Clinopyroxene.

Clinopyroxene (cpx) is a product phase in all the experiments that exceeded the fluid-absent solidus of the starting materials. In some of the sub-solidus experiments it occurred as a relict phase. In the super-solidus experiments, relict and neoblastic cpx could be distinguished on the basis of its chemical composition and textural relationship with other phases. Newly grown cpx occurs as prismatic crystals, commonly with small inclusions of quenched melt and/or amphibole. During the experiments, Cpx preferentially nucleated and grew along the margins of hornblende. Cpx in 17.5 and 20 kbar experiments exhibits distinct zoning with Ca-rich and Al-poor cores. Cpx also occurs as inclusions in garnet in experiments that produced abundant garnet. These cpx inclusions have compositions similar to the cpx crystals in the matrix and are, therefore, interpreted as products of fluid-absent melting reactions that were poikilitically enclosed by the faster growing garnet crystals.

Cpx exhibits distinct compositional changes with pressure and temperature (Table 2.5). The starting cpx, which is diopsidic in composition, becomes more augitic with increasing temperature/degree of partial melting at pressures <17.5 kbar (Figure 2.9). At pressures >17.5 kbar, the pyroxenes become distinctly more omphacitic in composition (Figure 2.10). This transition from quadrilateral augitic to omphacitic cpx in 3VG coincides with the disappearance of plagioclase from the residue and hence also marks the transition from garnet-cpx granulite to eclogite. In the KAP composition, the transition to omphacitic pyroxene is accompanied by a significant decrease in abundance of plagioclase in the residue. The jadeite component in cpx ranges from 3 to 31 mole percent. Cpx with >20% jadeite component (omphacite) only occurs at pressures >20 kbar. The Ca-Tschermak component remains relatively constant or marginally increases with pressure. The most distinct compositional variation with temperature is an increase in Al_2O_3 content, which corresponds to an increase in Ca-Tschermak component. Increasing temperature also produces a decrease in jadeite component of the omphacitic pyroxenes at pressures above 17.5 kbar.

Orthopyroxene

Orthopyroxene is a product phase at pressures <12.5 kbar. It occurs as long prismatic crystals, commonly with a spongy or skeletal habit. In the 7 kbar experiments opx coexists with cpx in both the 3VG and KAP compositions. In the 3VG experiments, opx coexist with garnet at 12.5 kbar at 950 and 1000 °C and at 850 °C at 10 kbar. Opx is absent from all KAP experiments done at pressures above 7 kbar.

Orthopyroxene compositions are presented in Table 2.6. In 3VG, the enstatite mole fraction in orthopyroxene ranges from 0.51- 0.57 with enstatite component increasing with temperature. In the KAP experiments, the enstatite component ranges from 0.54-0.64 and increases with pressure. In both bulk compositions, the enstatite component marginally decreases with pressure. Mg-number in opx is less than that in hornblende in all experiments where they coexist. Mg-number in opx is less than the coexisting cpx except in the 1000 °C experiment at 7 kbar on KAP where both phases have an X_{Mg} of 0.64. The Al_2O_3 content of opx increases with temperature and pressure (Figure 2.11).

Garnet

Garnet is present both as a relict and as a neoblastic phase in experimental run products that equilibrated at pressures above 10 kbar. Neoblastic garnets occur in two textural modes: as overgrowths on pre-existing garnet seeds and as homogeneously nucleated garnets. The former can easily be distinguished in backscattered electron images due to compositional differences between the seeds (outlining the core of the garnet crystals) and overgrowths. This compositional/textural feature was used as a criterion for establishing the stability field of garnet in these bulk compositions. In run products that were interpreted to have equilibrated in the stability field of garnet, the grains showed unequivocal presence of overgrowths. Further, garnet seeds that persisted in some of the experiments outside of the garnet stability field exhibited resorbed margins and lacked euhedral grain outlines that characterize overgrowths and neoblastic garnets. Garnet compositions are given in Table 2.8. Garnet in both bulk compositions are almandine rich (44-56 mole %) with pyrope content varying from 10-32 mole % (Figure 2.12). Grossular content ranges from 20-31 mole %. The garnets are also characterized by high Ti contents (0.65-1.58 wt. %). The compositions of garnets are discussed in more detail in chapter 3.

Plagioclase

Plagioclase is a residual phase in many experiments. It is a reactant during dehydration melting and its abundance decreases with temperature and pressure. Plagioclase abundance decreases significantly at temperatures above 1000 °C. Plagioclase disappears from the residual assemblage at pressures > 17.5 kbar. Plagioclase compositions are given in Table 2.8. The plagioclase crystals generally exhibit homogenous chemical compositions and reflect the composition of the starting plagioclase in KAP and 3VG. Plagioclase in KAP is more albitic than those in 3VG at comparable experimental conditions. The composition of plagioclase does not show simple correlations with pressure or temperature in both bulk compositions, which is likely due to the complex relationship between plagioclase compositions and the abundance of other Ca- or Na-bearing phases in the experimental charges. In general, however, there is a tendency for the anorthite content to decrease with pressure and increase with temperature (see Table 2.8). The orthoclase component in plag is always less than the 0.5 mole percent.

Oxides

Oxide phases were observed in only a few experimental charges. The abundance and stability of these phases in the present experiments were likely reduced by the low TiO_2 content of the starting materials. Magnetite (ulvospinel solid solution) and traces of ilmenite and rutile were the phases observed in the experimental run products. None of these oxide phases were found together in the same experiment. Magnetite was the most common oxide phase present in the experiments and occurred in some lower pressure experiments. Table 2.10 shows the composition of magnetites analyzed. Rutile and ilmenite crystals occurred as trace phases in some experiments and their small grain size precluded quantitative chemical analyses of these phases. Rutile was only observed at P $\geq$17.5 kbar.

Phengite

Phengite was observed at 22.5 kbar and 850 °C in both KAP and 3VG. This is consistent with the stability field of phengite reported by Skejerlie and Patino Douce (2002). Phengite was not analyzed quantitatively.

Titanite

Titanite was observed in a few experiments with both KAP and 3VG. Titanite in general is restricted to low temperatures (<900 °C) and low-moderate pressures. This is consistent with the observation that titanite replaces rutile in eclogites retrograded to amphibolite-facies conditions (e.g. Storey et al., 2003)

Melt

Varying amounts of glass (quenched melt) is present in experimental run products in which P-T conditions exceeded the fluid-absent melting solidus. Glass is difficult to distinguish from plagioclase on BSE images because the two phases have similar mean atomic numbers. However, melt pools generally exhibit a negative polishing relief and commonly impinge on the grain boundaries of crystalline phases with a low re-entrant angle. At low degrees of melting, melt occurs as thin isolated pockets at grain boundary intersections. In run products that have undergone moderate degrees of melting, melt forms a network of grain boundary films. In many run products quenched melt was found segregated along the edges of the capsule material. In run products that contain high proportions of garnet, melt pockets preferentially occur near garnet crystals, likely reflecting a strain shadow effect of the garnet crystals.

Table 2.9 shows the major element composition of melt pockets that were large enough to permit WDS analyses. The reported melt compositions are given on an anhydrous basis and were corrected for Na loss as a function of the electron beam diameter used during the analysis (details of correction procedure given in Appendix B). Figure 2.13 shows Harker-type variation diagrams of the measured melt compositions, which show similar patterns for melts produced from both 3VG and KAP bulk compositions. In a normative feldspar classification diagram melts span the compositional range granite-tonalite-trondhjemite-granodiorite for both starting materials

(Figure 2.14). Most of the melts fall near the triple junction between the fields of trondhjemite-granodiorite-granite. In a K_2O-CaO-Na_2O ternary plot the melt compositions mainly fall in the tonalite-granodiorite fields with two analyses from the 3VG experiments falling in the quartz-monzonite field (Figure 2.15). The melt compositions are predominantly peraluminous but a few are metaluminous (Figure 2.16). The silica content of the melt ranges from 58-73 wt. % on an H_2O-free basis. The least siliceous melts (<60 wt.% SiO_2) occur in the lower pressure experiments. This is consistent with melts coexisting with a SiO_2-rich residual assemblage containing abundant plagioclase ± orthopyroxene below 12.5 kbar. The decrease in plagioclase and increase in garnet in the residual assemblage at higher pressures buffer the SiO_2 content of the coexiting melt to high SiO_2 values. In general, the SiO_2 contents of melts decrease with increasing temperature (Figure 2.17) with the decrease more pronounced above 950 °C, when quartz is not a stable phase in the residue. The higher silica content of melts produced at temperatures below 950 °C reflects progress of melting reactions in which quartz is a dominant reactant. At temperatures above 950 °C, the melting reaction involves hornblende + plagioclase, which produces melts with lower SiO_2 contents. The Al_2O_3 content of melt does not vary systematically with temperature but generally decreases with increasing pressure (Figure 2.17). Al_2O_3 contents of melts range 14.8-22.9 wt.% and 14.7-20 wt. % in the KAP and 3VG experiments, respectively, with the majority of the melt analyses showing more than 15 wt.% Al_2O_3. TiO_2 and FeO contents of the melts are positively correlated with temperature at all pressures (Figure 2.17). However, there is no distinct variation of melt TiO_2 content with pressure, whereas FeO contents of the melts decreases with pressure. MgO contents of melt also vary positively with temperature, although the variations are more subtle than in the case of Ti and Fe. The total ferromagnesian component ($FeO+MgO+TiO_2$) of melt is positively correlated with temperature and negatively correlated with pressure (Figure 2.18). CaO in general seems to increase with temperature, but a few experiments deviates from this general trend (Figure 2.17). K_2O content of melt ranges between 1.1-5.4 wt. % in 3VG and between 1.9 and 4.3 wt. % in KAP. K_2O content generally decreases with temperature although some experiments deviate from this trend in both bulk compositions. The high K_2O content of low-temperature melts indicates the strongly incompatible behavior of K during dehydration melting. The generally higher K_2O content of the melts in this study compared to many previous metabasalt melting experiments reflects the K-rich nature of the starting materials compared to N-MORB composition.

Phase Proportions

Knowledge of phase proportions provides information on the nature of reactions operative during dehydration melting and also on the evolution of residual assemblage. Phase proportions were determined in this study using a combination of mass balance involving analyzed mineral compositions and grayscale thresholding of backscattered electron (BSE) images using the software ImageJ (Rasband, 1997-2005). Compositional X-ray maps of selected elements were used in some cases to help distinguish between phases that were sometimes difficult to differentiate by grayscale thresholding of BSE images only. The calculated phase proportions are given in Table 2.11. The uncertainties on the modal proportions vary for different phases but are typically <5% (absolute error) for phases other than garnet and melt. For garnet proportions, the uncertainty is typically <2% (absolute error) because grayscale values for garnet in the experiments do not overlap with other phases reducing the uncertainty in its modal estimate. The uncertainty in the reported proportions of the melt phase is likely larger than those for other phases as the proportion of melt was largely determined by mass balance. In general, the uncertainties in the modal proportions of phases at high pressures are much less than stated above because of the limited number of phases observed in the high-pressure run products.

Melting Reactions

Fluid-absent solidus

A key petrological constraint in understanding magma generation and the evolution of metamorphic assemblages is the onset of melting. Only a few of the many dehydration melting experimental studies have sought to provide constraints on the fluid-absent solidus (Beard and Lofgren, 1991; Rushmer, 1991; Wolf and Wyllie, 1994; Sen and Dunn, 1994; Lopez and Castro, 2001) and still fewer studies provide experimental brackets for the solidus reaction at more than one pressure (Lopez and Castro, 2001).

Solidus conditions compiled by Wolf and Wyllie (1993; 1994) (Figure 2.1) are widely used in petrological models involving metabasaltic lithologies (e.g. Rapp, 1998; Wyllie et al., 1998; Zegers and van Keken, 2001). Wolf and Wyllie (1994) assumed that water is available for melting at pressures above 10 kbar through hornblende breakdown and that this breakdown process allows melting to occur at temperatures as low as the water-saturated solidus of metabasalts. Wolf and Wyllie (1994) argued that temperature conditions near the solidus are not accessible to experimental investigations due to nucleation difficulties of phases such as garnet. They suggested that even though garnet did not nucleate in dehydration melting experiments at temperatures below 850 °C, it was in fact stable to temperatures as low as those of the water-saturated solidus. This resulted in the proposal of an 'S-shaped' solidus (Figure 2.1) that is widely used for petrological modelling of the evolution of metabasalts. However, as recently pointed out by Martin and Moyen (2006), this S-shaped solidus has not been mapped experimentally.

In the present study, experimental brackets for the fluid-absent solidus were obtained in the pressure range 7-15 kbar for both starting materials. The position of the solidus inferred from these experiments is shown in Figure 2.19. At 7 kbar, the solidus is located between 825 and 850 °C in the KAP experiments, whereas the lowest temperature experiment with the 3VG composition yielded a trace amount of melt at 825 °C. At pressures above garnet stability (~10 kbar) the solidus has a negative dP/dT slope for both starting materials. At pressures >12 kbar, the solidus of the KAP composition is slightly lower than that of 3VG. In general, the solidus is located at a higher temperature between 10 and 15 kbar in the present experiments, compared to that of Lopez and Castro (2001).

My results indicate a backbend in the solidus to lower temperatures when garnet joins the residual assemblage, generally consistent with the findings of previous workers (Wolf and Wyllie, 1994; Lopez and Castro, 2001). However, the positively sloped segment of the solidus inferred by Wolf and Wyllie at the transition from the opx to the garnet stability field in metabasalts is not corroborated by the new experimental results. The results are consistent with a negative slope for the solidus within the garnet stability field as reported by Lopez and Castro (2001). The present results also do not support the argument by Wolf and Wyllie (1994) that the fluid-absent solidus should bend back to intersect the water-saturated basalt solidus at pressures where garnet is a stable residual phase. Instead, fluid-absent melting involving hornblende-bearing assemblages occurs at temperatures 100-150 °C above the water-saturated solidus in the pressure range 10-15 kbar. Melting at temperatures between these two solidi would only occur if water is made available through breakdown of hydrous phases other than hornblende or of hornblende with a chemical composition significantly different than that present in the starting materials of my experiments.

Phase proportions in the experiments are consistent with solidus reactions of the form

Below 10 kbar,

Hornblende + Plagioclase + Quartz = Orthopyroxene + Clinopyroxene + Melt --------(1)

and above 10 kbar,

Hornblende + Plagioclase + Quartz = Garnet + Clinopyroxene + Melt -------------------(2)

The inferred reactions are similar to those deduced in many previous dehydration melting studies on amphibolites.

Reaction Modelling

Precise information regarding melting reactions is important in understanding many aspects of amphibolite melting including the controls on the melting process and the evolution of the restitic assemblage. Variations in the modal abundance of phases in the experimental products are commonly used to infer the melting reactions involved.

Quantification of these melting reactions requires mass balance analysis of experimental charges. I attempted to quantify the melting reactions by modelling initial stages of partial melting by constructing a mass balance between phases present in the starting materials and the experimental run products. Melt compositional data were generally not available for low temperatures (<900°C) because of the small dimensions of the melt pools. Modelling of reactions was done for the experimental products at 900 °C between 10-22.5 kbar. Due to the lack of adequate phase compositional data (particularly of melt) at 900 °C, melting reactions at 7 kbar were modelled using phase compositional data from the 950 °C experiment. I used a singular valued decomposition (SVD) method (Fisher, 1989) for mass balancing and determination of the reaction space. The technique involves analyzing the null (reaction) space of a rank deficient 'model' matrix of the original phase compositions to examine possible reaction relationships between the phases considered. More details of the matrix analyses are provided in Appendix C. Computations were done using the software C-space®, which allows algebraic analyses of compositional relations in multi-component chemical systems (Torres-Roldan et al., 2000).

Mass balance analyses were done in the chemical system Si-Ti-Al-Fe-Mg-Mn-Ca-Na-K which accounts for over 98 % of the oxygen-free composition of the rock. All the components were given equal weights in the SVD analyses. H was not included in the mass balance due to lack of precise information on the H_2O contents of the melt and hornblende. Fe was considered to be in the ferrous state for all the phases, including melt. Other elements (e.g. Cr, F, Cl) are present in negligible amounts in some of the phases but were ignored for the mass balance procedure. The mineral phases considered for mass balance are hornblende, plagioclase, orthopyroxene, clinopyroxene, garnet, quartz and quenched melt. Together these phases account for >98 % of the experimental run products. Phases that were present in trace quantities in some experimental products (e.g. titanite, ilmenite, and magnetite) were not considered for mass balance. Measured oxide compositions of the phases were recast into cations, normalized to the total oxygen in one formula unit of the phase. For the melt phase, compositions were recast assuming 10 oxygens per formula unit following the method of Hartel and Pattison (1996). Quartz was assumed to be pure. Hornblende and plagioclase compositions in the starting materials were used for SVD analyses rather than the composition of these phases in the experiment. This was done with the aim of understanding the melting systematics at the beginning of melting when metabasaltic protoliths undergo dehydration melting. Thus the reactions presented represent mass balance between the starting assemblage (of the starting materials) and the observed product phases in the experiments. The stoichiometric coefficients of reactions determined by mass balance are given in Table 2.12. It should be noted, however, that the modelled mass balance may not accurately represent the stoichiometry of solidus reaction, as modelling was not done using phase compositions at the solidus. The conditions at which reactions are modelled are 100 °C or more above the dehydration melting solidus for the bulk compositions studied. The modelled mass balances, therefore likely represent a time integrated model of dehydration melting reactions in the bulk compositions studied. Nevertheless, the determined reaction coefficients are useful for evaluating the nature of melting reactions and control on melt reactions at the initial stages of dehydration melting of the bulk compositions studied.

The model reactions presented in Table 2.12 are in agreement with the reactions 1 and 2 (see above) determined from variations in phase proportions in the experimental products. It is important to note, however, that the modelled reaction coefficients are not equivalent to the modal proportions of phases in the respective experimental run products. Reaction coefficients and modes will only converge to the same value if all the reactants are available in the starting materials in the exact proportions in which they participate in the melting reaction. In all other cases, observed modes represent a measure of the reaction progress and are controlled by the availability of (one or more) reactant phases.

At all pressures investigated, quartz is the reactant with the largest stoichiometric coefficient. The relatively low abundance of quartz in metabasaltic rocks at high grades, therefore, means that reaction progress and melt productivity at near solidus conditions is limited by the availability of quartz. This appears to be a general feature during high-grade metamorphism and anatexis of amphibolites (e.g. Hartel and Pattison, 1996). Hartel and Pattison identified the abundance of quartz as the primary control on reaction progress in their modelling of dehydration-melting of granulites in Kapuskasing Structure Zone, Ontario. Once quartz reacts out of the assemblage the melt reaction may switch to one involving hornblende and plagioclase. I am unable to evaluate the stoichiometry of this higher temperature reaction (hbl + plag = cpx ± opx ± garnet +melt) from the available data.

The reaction stoichiometries given in Table 2.12 in general, account well for the observed modal variation of phases observed in experiments in which partial melting occurred. Although relatively large stoichiometric coefficients for melt among product phases imply high melt productivity during amphibolite melting, the actual amount of melt produced in the 900°C experiments is considerably smaller due to the presence of residual hornblende and plagioclase. This may be attributed to a number of factors including, deviation of modal abundance of reactants in protoliths from the modelled reactions resulting in insufficient reaction progress or due to non-modal melting. Clearly, the stoichiometric coefficients of reactants in the modelled reactions differ from modal abundance of these phases in the starting materials. Therefore, reaction progress in the present experiments is limited by the relative proportion of the reactant phases present in the starting materials. As reaction progress appears to be controlled at initial stages of amphibolite melting by the availability of quartz, it is convenient to normalize the reaction coefficients to unit mole of reacting quartz (see Table 2.12). As pressure increases, the mole fraction of hornblende and plagioclase that reacts with quartz increases. This corresponds with an increase in mole fraction of garnet and cpx produced by melting at higher pressures. Table 2.13 shows the mass balance converted to modal proportions of phases using molar volumes of phases calculated using formulations for compressibilities and thermal expansivities given by Berman and Aranovich (1996). For solid solutions molar volume was calculated using linear interpolation between the end members. The ratio of hornblende to quartz consumed by the melting reactions increases from 1.5-2 at pressures below 15 kbar to ~5 at pressures above 17.5 kbar. This is consistent with decreasing proportions of hornblende and plagioclase with increasing pressure (at constant temperature) in the residue. The similarity in the modal mineralogical composition of the two starting materials enables us to make inferences about the relative melt productivity as a function of bulk compositional differences of the starting materials. Modal mass balance suggests that at the initial stages of melting (when quartz is present), the melt productivity of the KAP composition is greater than that of the 3VG composition. I attribute this observation to the higher Fe/Mg of the KAP starting material and in turn the KAP amphibole, which likely breaks down at lower temperature than the more magnesian 3VG amphibole. Therefore, for a given amount of quartz, melt production would be greater in Fe-rich amphibolites. Hartel and Pattison (1996) arrived at the same conclusion from studying the modal and compositional variations in the migmatitic mafic granulites of Kapuskasing Structural Zone. However, once quartz is exhausted or in quartz-absent amphibolites other compositional factors such as the composition of the feldspars may play a role in the melt productivity of amphibolites at initial stages of dehydration melting.

DISCUSSION

Petrological Applications

High-grade metamorphism of mafic rocks

A major goal of metamorphic petrology is to generate internally consistent databases for minerals, which can then be used to model the metamorphic evolution of different rock types. Accurate knowledge of mineralogical and compositional changes that can be related to changes in intensive variables of metamorphic systems is fundamental to achieving this goal. In mafic rocks, this is hampered by some inherent difficulties arising from (a) the presence of a complex solid solution phase, amphibole, which has proved to be difficult to model thermodynamically and, (b) lack of mineralogical changes over a sufficiently narrow temperature interval that can be compared with mineralogical zones in other bulk compositions (Yardley, 1989). A common practice to overcome these difficulties is to study experimentally representative mafic compositions and apply the results directly to natural occurrences. A few studies have thus shed information on subsolidus evolution of metabasic rocks (e.g. Moody et al., 1983; Poli, 1993). The present experimental results are directly applicable to the high-grade metamorphic evolution of hydrated MORB-type basaltic rocks under fluid-absent conditions. The experimental phase relations are discussed below in the context of important facies transitions that occur in mafic rocks during high grade metamorphism.

Amphibolite - Intermediate-P granulite transition

The co-existence of orthopyroxene + clinopyroxene in metabasaltic bulk compositions is considered to be the diagnostic assemblage of the granulite-facies (e.g. Eskola, 1914; Pattison, 2003). Orthopyroxene + clinopyroxene + plagioclase assemblages have been documented in many regional granulite-facies terranes and have been variously described as mafic granulite, two-pyroxene granulite or pyroxene granulite (Srikantappa, 1996; Yamamoto and Yoshino, 1998; Kar et al., 2003). The assemblage has also been noted in some lower crustal xenoliths (Rushmer, 1993). It has been inferred from thermobarometric studies in spatially associated metapelitic rocks that opx-cpx-plag assemblage is stabilized at low to moderate pressures (3-10 kbar).

Previous studies have shown that orthopyroxene becomes stable in metabasaltic bulk compositions at temperatures slightly above the dehydration melting solidus at low to moderate pressures. Beard and Lofgren (1989) provided experimental brackets for the appearance of opx in the pressure range 1-7 kbar. Lopez and Castro (2000) bracketed opx-in at 6 kbar between 850 and 900 °C. Lopez and Castro (2000) also documented the occurrence of opx at temperature >900 °C at 10 kbar, although no low temperature bracket was provided. Experiments on quartz-rich amphibolites gave different results with opx appearing as a product of dehydration melting at the solidus between 3-15 kbar (Patino Douce and Beard, 1995). In these experiments, opx coexist with garnet at 12 and 15 kbar at temperatures above the solidus (Patino Douce and Beard, 1995).

In my experiments, Opx-in was bracketed between 825 and 850 °C in 3VG and between 875 and 900 °C in KAP at 7 kbar. The appearance of opx was reversed at 7 kbar in two-stage experiments in both the 3VG and KAP compositions. Specifically, the two-stage reversal experiments were conducted between 900 and 825 °C in 3VG and between 900 and 850 °C in KAP. In both cases, opx that had grown in the high-temperature stage of the experiment was completely consumed in the low-temperature stage. At 10 kbar, opx did not form in any of the experiments with the KAP composition, but was stable at temperatures >850 °C in the 3VG experiments. The 3VG composition also has a narrow pressure interval between ~10-12.5 kbar where opx and garnet occur together.

These present results are consistent with previous experiments and indicate that temperatures >850 °C are required to stabilize opx in metabasaltic rocks under fluid-absent conditions. My experiments, however, tightly constrain the position of this reaction with tight experimental brackets and reversals. Also, my results suggest that opx forms at slightly lower temperatures in Mg-rich bulk compositions (3VG). These compositions also expand opx stability to higher pressures, allowing for the coexistence of garnet and opx. This pressure interval in which garnet-opx-cpx granulites are stable is transitional between lower pressure, garnet-free two-pyroxene granulites and higher pressure, opx-free garnet-cpx granulites. The range of pressures over which this transitional assemblage will be stable is determined by bulk compositional factors, being larger in Mg- and Si-rich metabasalts. In typical MORB-type metabasaltic rocks (olivine tholeiites), the occurrence of coexisting garnet and opx would be limited to a narrow pressure interval and, therefore, if occurring would be diagnostic of P-T conditions of metamorphism.

Amphibolite/Granulite - Garnet-granulite transition

While a coexisting opx + cpx + plag in metabasaltic rocks is definitive of granulite facies, the status of opx-free garnet + cpx assemblages has been debated in recent studies (Pattison, 2003). De Waard (1965) classified the former assemblage as 'orthopyroxene-plagioclase subfacies' and the latter as 'clinopyroxene-almandine subfacies' of granulite facies. The two assemblages were linked through the pressure sensitive equilibrium orthopyroxene + plagioclase = garnet + clinopyroxene + quartz with orthopyroxene stable on the low pressure side and garnet on the high pressure side. Accurate determination of the conditions at which these assemblages become stable is important to understand the tectono-metamorphic history of high-grade terranes. Early experimental investigation by Green and Ringwood (1967) confirmed that garnet-clinopyroxene assemblages form a paragenetic link between lower pressure granulite and higher pressure eclogite facies. An experimental study by Hansen (1981) on the end-member system $CaO-MgO-Al_2O_3-SiO_2$ bracketed the garnet-in boundary between 13.4 and 14 kbar at 900 ^{o}C with the garnet-in curve having a positive P-T slope of 8.5 bar/K.

Green and Ringwood (1967) conducted experiments on different basaltic composition glasses at temperatures >1000 °C and addressed the role of bulk composition in the appearance of garnet. The Green and Ringwood results (1967) remain the most widely applied experimental data for metabasaltic phase equilibria, particularly for garnet-granulite and eclogite formation. However, their experiments were conducted at temperatures of ≥ 1000 °C and therefore require long down-temperature extrapolation to be generally applicable to naturally occurring garnet-cpx assemblages, which mostly form at temperatures <900 °C (O'Brien and Rotzler, 2003). Another problematic aspect of the Green and Ringwood (1967) experiments is that they involved crystallization of basaltic glasses. Glasses crystallize rapidly but do not necessarily produce mineral assemblages that reflect the true equilibrium assemblage for that P-T condition (e.g. Pattison, 1994). In addition to the glass crystallization experiments, many amphibolite dehydration melting experiments using natural or synthetic rock powders have documented the occurrence of garnet at 10 kbar and higher pressures (Rushmer, 1993; Wolf and Wyllie, 1994; Sen and Dunn, 1994 etc.). However, none of these studies systematically investigated the stability of garnet during amphibolite melting. In particular, these experimental studies did not provide low temperature brackets. The present results, therefore, provide better constraints on the stability of garnet-bearing assemblages during dehydration melting of amphibolites.

The lowest pressure at which garnet is stable in the present experiments is 10 kbar, which is consistent with the results of many previous studies. In the more Mg-rich 3VG starting material, garnet is stable at 10 kbar only at 850 °C and becomes a significant part of the residual assemblage only at pressures > 12.5 kbar. In the KAP bulk composition, garnet is stable at temperatures above 800 °C at 10 kbar and in all experiments conducted at higher pressures. An attempt to reverse the appearance of garnet in two-stage experiments at different pressures was not successful. In a two-stage isothermal experiment (950 °C and 15-10 kbar), first in the stability field of garnet and subsequently quenched in the opx stability field, opx failed to nucleate and garnet persisted as a metastable phase. I attribute this result to the lack of free quartz after the completion of the initial reaction phase, which produces a quartz- and opx-free garnet + cpx assemblage. Lack of quartz as a reactant inhibited the down-pressure reaction garnet + cpx + quartz = opx + plagioclase during the second stage of the attempted reversal experiment. This reasoning is supported by the results of a two-stage experiment in which the starting material was seeded with a layer of quartz on top. The run product after the two stage experiment (initially held in the garnet stability field and subsequently in opx stability field) showed the presence of opx crystals near the quartz layer. Away from the quartz layer, the residual assemblage was dominated by garnet + cpx. This two-stage experiment also demonstrates the effect of silica saturation on opx stability. Opx is stabilized relative to garnet in silica-saturated bulk compositions compared to silica-under-saturated basalts (Green and Ringwood, 1967). It has been suggested that a garnet-cpx assemblage in silica-saturated rocks is diagnostic of high-pressure granulite facies (Green and Ringwood, 1967). In silica-saturated metabasalts the lowest pressure at which garnet is stabilized is a function of the Fe/Mg of the basaltic protolith (Green and Ringwood, 1967). Garnet is stabilized at relatively lower pressures in Fe-rich bulk compositions. The lowest pressure at which garnet is stable in the Fe-rich KAP composition (10 kbar) can be taken as the lower pressure limit for stabilizing garnet-cpx granulites in MORB-derived metabasalts. Thus the transition from medium-pressure cpx-opx granulite to high-pressure garnet-cpx granulite occurs along a transitional boundary that has a shallow positive P-T slope.

My experimental results also provide constraints on the lowest temperatures at which garnet is stabilized in MORB-type amphibolites during dehydration melting. Pattison (2003) evaluated the utility of opx-free garnet-cpx assemblages in defining a minimum temperature of formation. He concluded that many experimental studies indicated similar temperatures of formation (~850 °C) for opx-free garnet-granulite and lower pressure opx-bearing granulites. Wolf and Wyllie (1994), however, argued that near solidus portions of the amphibolite dehydration melting process are not amenable to experimental investigations due to nucleation difficulties involving garnet. They suggested that at temperatures <850 °C garnet fails to nucleate in experimental studies and that if equilibrium were to be achieved garnet would be stable at temperatures as low as the H_2O-saturated solidus for metabasalts. Winther and Newton (1991), Sen and Dunn (1994), and Lopez and Castro (2001) reported garnet-in at temperatures well above (>100 °C higher) the water-saturated solidus of basalt. Sen and Dunn had garnet seeds in the starting materials, which would have avoided nucleation difficulties. Their lowest temperature experiments (800 and 850 °C at 20 and 15 kbar, respectively) had garnet but no low temperature brackets for the appearance of garnet were provided. They reported a negative slope for the garnet-in curve in order to be consistent with the results of Wolf and Wyllie (1994) at 10 kbar.

Results of the present study are useful in addressing the low-temperature stability of garnet in metabasalts for two reasons. First, the long duration of my experiments compared to previous studies have facilitated a closer approach to phase equilibrium. Second, the presence of garnet in the starting material (hereafter called seeds) have avoided nucleation difficulties involving this phase. The phase relations observed in the present experiments indicate that a minimum temperature of ~800-825 °C is required to stabilize garnet (Figure 2.19) during dehydration melting of amphibolites of MORB composition. These results are consistent with the 800-850 °C bracket for garnet appearance obtained in previous studies at 12 kbar (Lopez and Castro, 2001), and at 10 kbar (Wolf and Wyllie, 1994). However, the results of the present study are better constrained by successful phase reversal experiments in which the appearance of garnet was reversed. The lack of garnet (even seeds) in the reversal experiments and the lowest temperature experiments conducted at 10 and 15 kbar suggests that the absence of garnet is not due to nucleation difficulties, but the result of its instability at these conditions. Importantly a lowest temperature limit of 800 °C for garnet stability in metabasalts compares favorably with temperature estimates in the range of 750-850 °C obtained from high-pressure granulite-facies assemblages using Fe-Mg exchange thermometers (Pattison, 2003; O'Brien and Rotzler, 2003). The lowest temperature estimates from natural high-pressure granulites are, however, about 50 °C lower than the experimental constraint, which may reflect post-peak Fe-Mg resetting of the Fe-Mg exchange equilibria used in calculating the temperature. Importantly, the low temperature constraint is similar to, but slightly less than, the temperature required for stabilizing opx at intermediate pressures during dehydration melting of metabasalts. The present results do not support the hypothesis that garnet forms through dehydration melting of amphibolites at temperatures as low as the H_2O saturated basalt solidus (Wolf and Wyllie, 1994).

Problem of lower temperature garnet-cpx amphibolites

The present experimental data indicate that, in MORB-type metabasalts, opx-free garnet + cpx assemblages develop at temperatures > 800 °C between 10 and 15 kbar. This is only slightly less than the temperatures required to stabilize intermediate pressure (< 10 kbar) two-pyroxene granulites and is consistent with thermobarometric data from natural high pressure granulites (Pattison, 2003; O'Brien and Rotzler, 2003). However, the use of opx-free garnet + cpx assemblages as low temperature indicators of metamorphism is complicated by the occurrence of the same assemblage at lower temperature (620-700°C) amphibolite facies conditions (Pattison, 2003). Two such documented occurrences are Pelona Schist in southern California (Graham and Powell, 1984) and Mica Creek in British Columbia (Ghent et al., 1983). Pattison (2003) considered the possibility that the discrepancy between experimental predicted temperatures and that recorded in these terranes arise from (a) Fe-Mg resetting of the exchange reactions, (b) influx of low a_{H2O} fluids during metamorphism, or (c) possible temperature overstepping of the relevant reaction in dehydration melting experiments. Significant Fe-Mg resetting was ruled out for these amphibolite facies occurrences. Thermodynamic modelling suggests that low a_{H2O} imposed by influx of fluids may result in the development of the assemblage at low temperatures (Pattison, 2003). However, a source for the low a_{H2O} fluids is not apparent in these terranes (Pattison, 2003). The third possibility that experimental results overstep the relevant reaction cannot be fully tested given the dependence of reactions on bulk compositional differences. The lowest temperature at which opx-free garnet + cpx assemblages are stable in the present study (800-825 °C) is slightly lower than previously reported experimental brackets (>850 °C). Given the long duration of the present experiments and tight experimental brackets, I argue that these temperatures represent the minimum temperatures at which opx-free garnet + cpx assemblages are stabilized in MORB-type bulk compositions during dehydration melting.

Pattison (2003) argued that development of opx-free garnet + cpx assemblages at amphibolite-facies conditions is controlled by mineral compositional factors. He suggested that Fe-rich mineral compositions, Ca-rich garnet and, Ti-poor hornblende lead to subsolidus breakdown of amphibole to form garnet + cpx assemblages. The higher temperature estimate for stabilizing garnet + cpx derived from the experiments may be the result of using pargastic amphiboles in the starting materials. Pattison (2003) also used pargasitic end member amphiboles in calculating the phase equilibria. In Fe- and Ca-rich bulk compositions, pargasitic amphibole may be an inappropriate model for understanding phase equilibria involving amphiboles at lower temperatures. I suggest that the occurrence of opx- free garnet + cpx assemblages at P-T conditions equivalent to amphibolite facies may have been the result of breakdown of ferro-actinolitic hornblende in relatively Fe- and Ca-rich metabasalts. This reaction can be written as

$$2(Ca_2Fe_5Si_8O_{22}(OH)_2)_{\text{in Hbl}} + 3(CaAl_2Si_2O_8)_{\text{in Plag}} = (Ca_3Al_2Si_3O_{12})_{\text{in Garnet}} + 2(Fe_3Al_2Si_3O_{12})_{\text{in Garnet}} + 4(CaFeSi_2O_6)_{\text{in Cpx}} + 5\,SiO_2 + 2(H_2O)_{\text{in melt/vapor}} \text{ ------------------ } (3)$$

There have been very few studies done on the stability and thermodynamic properties of actinolitic amphiboles and thus the exact location of the equilibrium (3) in P-T space is unknown. Therefore, it is unclear if reaction 3 is a subsolidus dehydration reaction or a supersolidus dehydration melting reaction. A recent experimental investigation on the stability of end member ferro-actinolite indicates that it is stable up to mid-amphibolite facies (Jenkins and Bozhilov, 2003). Amphibole compositions from many low- to mid-amphibolite facies terranes also suggest that actinolitic amphiboles are common (Raase, 1974; Begin and Carmichael, 1992). A first order conclusion that can be drawn from these observations is that ferro-actinolitic hornblende is probably stable up to mid-amphibolite facies conditions. If reaction 3 is responsible for the development of garnet + cpx assemblage in amphibolite-facies metabasalts, some constraints can be placed on the P-T position of this reaction from mineral isograd relations in these localities. At Mica Creek, for example, the garnet + cpx isograd in mafic rocks occurs between the sillimanite-in and K-feldspar-in isograds in interlayered metapelites (Ghent et al., 1983). Whereas the interlayered metapelitic layers show migmatization, the mafic rocks show no evidence of melting (Pattison, 2003). Therefore, reaction 3 must occur at a temperature within the sillimanite stability field but below the water-saturated basalt solidus. So a combination of the requirement of Fe-rich bulk compositions and a restricted P-T interval at which the proposed ferro-actinolite break down reaction occurs may explain the rarity of garnet + cpx assemblages at amphibolite-facies conditions. That these assemblages develop at low temperatures only in Fe-rich bulk compositions are supported by the Fe-rich nature of hornblende, garnet and clinopyroxene in Mica Creek and Pelona Schist relative to those in granulite-facies occurrences (Pattison, 2003).

Importantly, the ferro-actinolite breakdown reaction occurs at lower temperatures than the equivalent breakdown reaction for pargasitic amphiboles

$$2\,(\mathrm{NaCa_2Mg_4AlSi_6Al_2O_{22}(OH)_2})_{\text{in Hbl}} + (\mathrm{CaAl_2Si_2O_8})_{\text{in Plag}} + 5\,\mathrm{SiO_2} = 2\,(\mathrm{Mg_3Al_2Si_3O_{12}})_{\text{in Garnet}} + 2\,(\mathrm{Ca_3Al_2Si_3O_{12}})_{\text{in Garnet}} + 2\,(\mathrm{CaMgSi_2O_6})_{\text{in Cpx}} + 2\,(\mathrm{NaAlSi_3O_8})_{\text{in Plag}} + 2\,(\mathrm{H_2O})_{\text{in melt}} \text{ --------------- } (4)$$

Reaction (4) is analogous to reaction (2), which corresponds to the transition from amphibolite to high-P garnet-granulite facies. One important difference between reaction (3) and (4) is that quartz is a reactant in (4) while it is produced during reaction (3). This might be important in the progress of dehydration melting and extent of migmatization in metabasalts. The importance of quartz in the progress of dehydration melting of amphibolite was discussed by Hartel and Pattison (1996) in the genesis of mafic granulites in Kapuskasing Structural Zone, Ontario. These authors argued that the primary control on the extent of dehydration melting in the mafic granulites was the abundance of quartz in the protolith due to its low modal abundance in mafic rocks. In MORB-type basalts (olivine tholeiites), quartz is produced during subsequent metamorphic evolution. The amount of quartz available at the onset of dehydration melting is dependent upon the progress of quartz-producing subsolidus reactions. In Fe-rich metabasalts, operation of reaction 3 will make more quartz available for dehydration melting solidus reaction 4 to progress. Metabasaltic rocks, whose bulk compositions favor sequential progress of reaction 3 and 4, would experience a larger degree of melting (or higher reaction progress) at the onset of melting than rocks in which reaction 3 is inhibited. Bulk compositional factors that favor this outcome include high Fe/Mg and Ca/Na ratios of basaltic protoliths. This is consistent with Hartel and Pattison's (1996) observation that in Kapuskasing Structure Zone, mafic granulites exhibiting the greatest extent of (dehydration melting) reaction progress are those with the highest Fe/Mg ratio. Hartel and Pattison inferred that the high Fe/Mg layers had higher modal quartz content, as quartz is a limiting reactant during dehydration melting. I suggest that the larger amount of quartz in the high Fe/Mg lithologies may have originated through reaction 3 during prograde evolution at amphibolite-facies conditions. Thus, in Fe-rich metbasaltic rocks granulite-facies garnet + cpx assemblages may represent two stages of garnet growth- an initial (subsolidus?) growth at amphibolite facies and a subsequent super-solidus granulite facies overprint. Lack of experimental data on the stability of ferro-actinolitic hornblende prohibits defining a lower temperature limit for amphibolite-facies garnet + cpx assemblages. Careful examination of textural patterns and compositional zoning in garnet may be required to elucidate the different stages of garnet growth in high-P mafic granulites. At present, compositional differences of the constituent minerals (along with P-T data if available) of garnet + cpx assemblages and presence or absence of migmatitic textures remain the only criterion to distinguish amphibolite-facies occurrences from those at granulite-facies conditions. However, the position of reaction 2 determined in this study provides a lower temperature limit for formation of the garnet + cpx assemblage through dehydration melting. The similarity in the estimated temperatures of reaction 2 to those required to form opx + cpx assemblages ('classic' granulites) at lower pressures, suggest that position of reaction 2 could be used to define the high pressure amphibolite-granulite-facies boundary.

Garnet-granulite - Eclogite transition

At the highest pressures of metamorphism recorded in natural metabasaltic rocks, the mineral assemblage consists dominantly of garnet and cpx and is characterized by the absence of plagioclase. This assemblage *sensu stricto* defines the eclogite facies in metabasalts (Green and Ringwood, 1967). At high-temperature conditions the transformation of metabasaltic rocks to eclogite-facies assemblages occurs through the high-pressure granulite facies described in the previous section. Specifically, the transition to eclogite facies is defined by the disappearance of plagioclase and is accompanied by physicochemical changes that affect the density of the rock. This transition has, therefore, been proposed to play key role in a number of geodynamic processes including subduction (Cloos, 1993), lower crustal delamination (Zegers and van Keken, 2001), and magma genesis (Rapp et al., 2003). The density increase accompanying transformation of basaltic rocks to eclogite is believed to be the origin of slab pull forces and delamination processes require eclogite formation to produce gravitational instabilities. Knowledge of the depth at which the eclogite transformation occurs is critical to understanding and evaluating these geological processes.

Green and Ringwood's (1967) glass crystallization experiments on two quartz-tholeiite compositions is the first study to investigate in detail the basalt-eclogite transition in mafic rocks. They bracketed plagioclase-out between 17 and 18 kbar and between 19 and 20 kbar at 1000 and 1100 °C, respectively. Due to lack of experimental data at lower temperatures, Green and Ringwood (1967) extrapolated their high temperature plagioclase-out curve to lower temperatures using the average P-T gradient determined for this curve in their study on two quartz tholeiite bulk compositions. From this they concluded that eclogite or high-P granulite rather than gabbro is stable throughout large regions of continental crust. Extrapolation of their experimental data to near (dehydration-melting) solidus conditions (~800 °C) indicate that eclogite can be stabilized in metabasaltic rocks at pressures as low as 12.5 kbar.

The results of the present experiments at 800 °C and 12.5 kbar indicate that amphibolite rather than eclogite is the stable form of metabasalt. A true eclogitic phase assemblage was not observed in any of the 800 °C experiments in the present study. Plagioclase-out was bracketed between 850 and 950°C in the present study. At 850°C, plagioclase out was bracketed between 20 and 22.5 kbar in the KAP composition. At 850°C, in the 3VG composition, trace amounts of plagioclase were observed at 22.5 kbar complicating the trajectory of the plagioclase-out curve. There is no indication, however, that this experiment is unreliable. In the 3VG bulk composition, plagioclase is stable up to 17.5 and 20 kbar at 900 and 950°C respectively. In the KAP composition, plagioclase is stable up to 20 kbar at 900 and 950°C. The apparent higher pressure stability of plagioclase in KAP may be due to the slightly higher Na_2O content of the KAP starting material and the consequent higher albite content of KAP plagioclase. The present results indicate that the slope of plagioclase-out boundary has a much shallower P-T slope than suggested by Green and Ringwood (1967). Extrapolation of Green and Ringwood's (1967) plagioclase-out curve to near-solidus conditions results in significant underestimation of the pressure necessary to form eclogite. Using such extrapolations in constructing petrogenetic grids (e.g. Oh and Liou, 1998) leads to the erroneous inference that eclogite is stable throughout large regions of continental crust. The present results show that a minimum pressure of 18 kbar is required to stabilize eclogite in MORB-type bulk compositions during dehydration melting (Figure 2.19). This limits eclogite formation to the base of tectonically thickened continental crust or subduction zones.

The new constraints are more consistent with thermobarometric data from high-pressure mafic granulite occurrences (O'Brien and Rotzler, 2003). Many of these high-pressure rocks would be expected to have eclogite-facies assemblages if previously reported constraints on gabbro-eclogite transition in quartz-tholeiite compositions (Green and Ringwood, 1967) are used to infer the facies boundary. This inconsistency is avoided if the present results are used to constrain the granulite-eclogite transition boundary in metabasalts.

Partial melt compositions and conditions of TTG genesis

Silica-rich partial melts generated during experimental melting of mafic rocks are important in understanding not only the conditions of magma genesis at lower crustal to upper mantle depths, but also in understanding the geochemical signatures of magmas generated at these conditions. The results of present experiments can be used to refine our understanding of mineral/melt equilibria during partial melting of MORB-type metabasalts under fluid-absent conditions, a commonly envisaged physical environment at lower crustal/upper mantle depths. Precambrian continental felsic magmas exhibit a secular trend from a low-K tonalite-trondhjemite series characteristic of early- to mid-Archean to a relatively K-rich granodiorite-granite magma series that is more common in the late-Archean and Proterozoic time.

Metaluminous to peraluminous silica-rich melts produced in this study are broadly similar to those reported in previous dehydration melting studies on basaltic bulk compositions. The major-element systematics of the melts generated share many characteristics of Archean TTG rocks. Melt compositions produced are rhyolitic to trachyandesitic in composition, with relatively silica-poor andesitic melts restricted to the lower pressure, higher temperature experiments (<12.5 kbar). The higher silica content of the melts above 12.5 kbar reflects the increasing abundance of garnet and decreasing abundance of plagioclase in the residual assemblage that is in equilibrium with the melt. Melts are predominantly alkalic-calc to calc-alkalic in a Na_2O+K_2O-CaO vs SiO_2 plot, with some analyses falling in the alkalic field (Figure 2.20). The CaO content of melts is at the lower end of the range reported for TTGs.

Melt compositions range from ferroan to magnesian and have FeO/(FeO+MgO) values that overlap with Archean tonalites for melts with SiO_2 content >65 wt. % (Figure 2.21). Archean TTG compositions, however, extend to much lower FeO/(FeO+ MgO) values than shown by experimental melts. This difference appears to be typical for experimental melts with >65 wt. % SiO_2 from metabasaltic rocks, which shows MgO contents that are at the lower end of the range observed in TTGs (Figure 2.22). The higher MgO content and Mg# of some Archean TTGs is attributed to the interaction of TTG melts with peridotitic rocks during ascent from their source regions to emplacement levels (Martin and Moyen, 2002). However, this interaction also results in a decrease in the SiO_2 content of the melts (Rapp et al., 1999). The presence of some high silica TTGs (>65 wt.% SiO_2) with higher Mg# than partial melts generated in experimental studies suggest that more Mg-rich protoliths (komatiitic basalts) than used in experimental dehydration melting studies including the present study may have been important in the generation of these granitoids.

The Al_2O_3 content of the melts are somewhat higher than the range observed in TTGs (Figure 2.23). This result is generally similar to the experimental melts with SiO_2 >60 wt. % reported from previous dehydration melting studies on amphibolites (Rapp and Watson, 1995; Sen & Dunn, 1994; Springer and Seck, 1997). Barker and Arth (1976) used a cut off value of 15 wt. % Al_2O_3 to distinguish two groups of TTG granitoids, a high Al_2O_3 type and low Al_2O_3 type. The melt compositions produced in the present study are more comparable to the high Al_2O_3 type (Figure 2.23). Martin (1994) argued that most Archean TTGs belong to the high-Al_2O_3 group. There has been some discussion on the influence of residual assemblage on the Al_2O_3 content of melts. Rapp et al. (1991) attributed plagioclase abundance in the melt residue as the primary control on Al_2O_3 content of the melt. They argued that melts become progressively Al-rich with increasing pressure because of decreasing plagioclase in the melt residue. In contrast, the lowest Al_2O_3 melts were observed in the higher pressure experiments of this study. The critical factor controlling the Al_2O_3 content of the melt is the bulk Al_2O_3 content of the restite mineral assemblage, which is higher in the high-pressure experiments due to the presence of abundant garnet and high-Al clinopyroxene in the residue. The Al_2O_3 contents of these high-pressure melts are more comparable to TTGs. The present results indicate that if Archean high-Al_2O_3 TTGs are pristine melts derived from hydrated metabasalts, they must have formed at pressures >15 kbar as melts generated at lower pressures have much higher Al_2O_3 content than that reported for average Archean TTG. Alternatively, lower-pressure melts may have been modified to lower Al_2O_3 contents through interaction with the surrounding rocks during ascent or by plagioclase fractionation to produce TTGs. A lower-pressure origin for Archean (especially early Archean) TTGs is also not supported by the highly fractionated REE pattern and depletion in HREEs of these rocks, which suggest origin of the TTG magmas at greater depths (where abundant garnet causes these REE signatures). The relatively high Sr content and the lack of negative Eu anomalies in TTGs argue against significant plagioclase fractionation after magma generation.

One notable difference in the composition of melts generated in this study compared to Archean TTGs is in the relatively higher K_2O content of the experimental melts (Figure 2.24). The high potassium content of the present starting materials relative to unaltered MORB and starting materials used in many previous studies resulted in production of melts whose normative feldspar compositions straddle between the trondhjemite, granodiorite and granite fields (Figure 2.14). The K_2O content of melts generated in this study are among the highest reported for partial melts generated from metabasalts. This is reflected in a normative Qtz-Ab-Or plot of the experimental melts (Figure 2.25). With the exception of two melt analyses from the 3VG bulk compositions, these melts have Na_2O/K_2O ratio >1, consistent with tonalitic-granodioritic melts produced from previous metabasalt melting experiments (Figure 2.26). The melts produced in the present experiments, however, in general have lower Na_2O/K_2O ratio than those produced in previous dehydration melting experiments. Na_2O/K_2O ratios of melts produced during dehydration melting appear to be a function of K-content of the starting basaltic source as well as the temperature of melting. High K-content of starting materials and lower melt fractions (corresponding to lower melting temperatures) result in lower melt Na_2O/K_2O ratios. The K_2O content of the starting materials (0.7 wt. % for KAP and 0.8 wt. % for 3VG) correspond to K-enriched basalts. Although, fresh MORB magmas typically have low K_2O, the K_2O content of basalts are commonly enriched during hydrothermal alteration (Zhou and Fyfe, 1989; Alt and Teagle, 2003). Thus, many MORB-derived amphibolites have elevated K_2O contents similar to the starting materials used in this study. Moderate to high K_2O content is also a common feature of basalts produced in subduction-related magmatic arcs (Sisson et al., 2005). Partial melting of amphibolites derived from these relatively K-rich lithologies result in the production of magmas that are more potassic than tonalitic-trondhjemitic magmas generated from low-K basaltic sources (Sisson et al., 2005). Thus the altered metbasaltic source rocks for Archean TTG's may have had lower K_2O contents than the starting materials used in my study. A K_2O vs K/(K+Ca) plot (Figure 2.27) shows that melts generated from the KAP and 3VG compositions correspond to moderately potassic granodiorites. Winther (1996) argued that partial melting of Archean tholeiites cannot produce granodioritic melts. In contrast, the present results indicate that moderately K-rich tholeiites can in fact generate magmas of this composition. Generation of large granodiorite batholiths is commonly attributed to a hybridization process through interaction of mafic magma with pre-existing felsic (tonalitic) crust (Moyen et al., 2001; Lopez et al., 2005). The present results, however, suggests that granodiorite melts could be generated directly from moderately K-rich tholeiitic basalts (Figure 2.28) without resorting to melt interaction processes. Partial melting of moderate- to high-K amphibolites derived from arc basalts could generate granodiorite to granitic magmas. These processes may have been more common in the late Archean and Phanerozoic when subduction systems were widespread and a significant volume of island arc materials were incorporated during accretionary processes.

References

Ai, Y. (1994) A revision of the garnet-clinopyroxene Fe2+-Mg exchange geothermometer. Contributions to Mineralogy and Petrology, 115, 467-473.

Alt, J.C. and Teagle, D.A.H. (2003) Hydrothermal alteration of upper oceanic crust formed at a fast-spreading ridge: mineral, chemical, and isotopic evidence from ODP site 801. Chemical Geology, 201, 191-211.

Andersen, D.J., Lindsley, D.H. and Davidson, P.M. (1993) QUIIF: a Pascal program to assess equilibria among Fe-Mg-Mn-Ti oxides, pyroxenes, olivine and quartz. Computers and Geosciences, 19, 1333-1350.

Aranovich, L.Y. and Newton, R.C. (1998) Reversed determination of the reaction: Phlogopite + quartz = enstatite + potassium feldspar + H_2O in the ranges 750-875 °C abd 2-12 kbar at low H_2O activity with concentrated KCl solutions. American Mineralogist, 83, 193-204.

Bach, W. and Edwards,K.J. (2003) Iron and sulfide oxidation within the basaltic ocean crust: Implications for chemolithoautotrophic microbial biomass production. Geochemica et Cosmochimica Acta, 67, 3871-3887.

Bach, W., Peucker-Ehrenbrink, B., Hart, S.R., and Blustajn, J.S. (2003) Geochemistry of hydrothermally altered oceanic crust: DSDP/ODP Hole 504B – Implications for seawater-crust exchange budgets and Sr-and Pb-isotopic evolution of the mantle. Geochemistry, Geophysics, Geosystems, 4, 8904.

Beard, J.S. and Lofgren, G.E. (1991). Dehydration melting and water-saturated melting of basaltic and andesitic greenstones and amphibolites at 1,3, and 6.9 kb. Journal of Petrology, 32, 365-401.

Berman, R.G. (1991) Thermobarometry using multiequilibrium calculations: a new technique with petrologic applications. Canadian Mineralogist, 29, 833-855.

Berman, R.G. and Aranovich, L. Ya (1996) Optimized standard state solution properties of minerals 1. Model calibration for olivine, orthopyroxene, cordierite, garnet, and ilmenite in the system FeO-MgO-CaO-Al_2O_3-TiO_2-SiO_2. Contributions to Mineralogy and Petrology, 126, 1-24.

Brown, G.C. and Fyfe, W.S. (1970) The production of granitic melts during ultrametamorphism. Journal of Petrology, 28, 310-318.

Cameron, E.M., Cogulu, E.H. and Stirling, J. (1993) Mobilization of gold in the deep crust: evidence from mafic intrusions in the Bamble belt, Norway. Lithos, 30, 151-166.

Castro A., Fernandez, C., De La Rosa J.D., Moreno-ventas, I. and Rogers, G. (1996). Significance of MORB-derived amphibolites from Aracena Metamorphic Belt, Southwest Spain. Journal of Petrology, 37, 235-260.

Christie, D.M., Carmichael, I.S.E. and Langmuir, C.H. (1986) Oxidation states of mid-ocean ridge basalt glasses. Earth and Planetary Science Letters, 79, 397-411.

Clemens, J.D. and Vielzeuf, D. (1987) Constraints on melting and magma production in the crust. Earth and Planetary Science Letters, 86, 287-306.

Cloos, M. (1993) Lithospheric buoyancy and collisional orogenesis: subduction of oceanic plateaus, continental margins, island arcs, spreading ridges, and sea mounts. Geological Society of America Bulletin, 105, 715-737.

Eskola, P. (1920) The mineral facies of rocks. Norsk. Geol. Tidsskr., 6, 143-194.

Ellis, D.J. and Green, D.H. (1979) An experimental study of the effect of Ca upon garnet-clinopyroxene Fe-Mg exchange equilibria. Contributions to Mineralogy and Petrology, 71, 13-22.

Ellis, D.J. and Thompson, A.B. (1986) Subsolidus and partial melting reactions in the quartz-excess $CaO + MgO + Al_2O_3 + SiO_2 + H_2O$ system under water-excess and water-deficient conditions to 10 kb: some implications for the origin of peraluminous melts from mafic rocks. Journal of Petrology, 27, 91-121.

Ernst, W.G. and Liu, J. (1998) Experimental phase-equilibrium study of Al- and Ti-contents of calcic amphibole in MORB- A semiquantitative thermobarometer. American Mineralogist, 83, 952-969.

Essene, E.J., Hensen, B.J., and Green, D.H. (1970) Experimental study of amphibolite and eclogite stability. Physics of Earth and Planetary Interiors, 3, 378-384.

Fisher, G.W. (1989) Matrix analysis of metamorphic mineral assemblages and reactions. Contributions to Mineralogy and Petrology, 102, 69-77.

Frost, B.R., Barnes, C.G., Collins, W.J., Arculus, R.J., Ellis, D.J. and Frost, C.D. (2001) A geochemical classification for granitic rocks. Journal of Petrology, 42, 2033-2048.

Green, D.H. and Ringwood, A.E. (1967) An experimental investigation of the gabbro to eclogite transformation and its petrological applications. Geochimica et Cosmochimica Acta, 31, 767-833.

Green, D.H. and Adam, J. (1991) Assessment of the garnet-clinopyroxene Fe-Mg exchange thermometer using new experimental data. Journal of Metamorphic Geology, 9, 341-347.

Hansen, B., (1981) The transition from pyroxene granulite facies to garnet clinopyroxene granulite facies. Experiments in the system CaO-MgO-Al_2O_3-SiO_2. Contributions to Mineralogy and Petrology, 76, 234-242.

Harlov, D.E. (2000) Apparent pyrrhotite-chalcopyrite solid solutions in charnockites: the Shevaroy Hills Massif, Tamil Nadu, S. India and the Bamble Sector, SE Norway. Mineralogical Magazine, 64, 853-865.

Harlov, D.E., Newton, R.C., Hansen, E.C. and Janardhan, A.S. (1997) Oxide and sulphide minerals in highly oxidized, Rb-depleted, Archean granulites of the Shevaroy Hills Massif, South India: oxidation states and the role of metamorphic fluids. Journal of Metamorphic Geology, 15, 701-717.

Hartel, T.H.D. and Pattison, D.R.M. (1996) Genesis of the Kapuskasing (Ontario) migmatitic mafic granulites by dehydration melting of amphibolite: the importance of quartz to reaction progress. Journal of Metamorphic Petrology, 14, 591-611.

Holloway, J.R. and Wood, B.J. (1988) Simulating the Earth: Experimental geochemistry, Unwin Hyman, Boston, Massachussets, 196 p.

Indares, A.D. and Martignole, J. (2003) Towards the upper limits of granulite facies. Journal of Metamorphic Geology, 21, 1-2.

Itaya, T., Brothers, R.N. and Black, P.M. (1985) Sulfides, oxides and sphene in high-pressure schists from New Caledonia. Contributions to Mineralogy and Petrology, 91, 151-151.

Johnston, A.D. (1986) Anhydrous P-T phase relations of near-primary high-alumina basalt from the South Sandwich Islands: Implications for the origin of island arcs and tonalite-trondhjemite series rocks. Contributions to Mineralogy and Petrology, 92, 368-382.

Kar, R., Bhattacharya, S. and Sheraton, J.W. (2003) Hornblende-dehydration melting in mafic rocks and the link between massif-type charnockite and associated granulites, Eastern Ghats Granulite Belt, India. Contributions to Mineralogy and Petrology, 145, 707-729.

Kelley, K.A., Plank, T., Ludden, J. and Staudigel, H. (2003) Composition of altered oceanic crust at ODP sites 801 and 1149. Geochemistry, Geophysics, Geosystems, 4,8910.

Krogh, E.J. (1988) The garnet-clinopyroxene Fe-Mg geothermometer- a reinterpretation of existing experimental data. Contributions to Mineralogy and Petrology, 99, 44-48.

Krogh-Ravna, E. (2000) The garnet-clinopyroxene Fe^{2+}-Mg geothermometer: an updated calibration. Journal of Metamorphic Geology, 18, 211-219.

Kushiro, I. (1976) A new furnace assembly with a small temperature gradient in solid-media, high-pressure apparatus. Carnegie Institution of Washington Yearbook, 68, 231-233.

Lambert, I.B. and Wyllie, P.J. (1972) Melting of gabbro (quartz eclogite) with excess water to 35 kilobars, with geological applications. Journal of Geology, 80, 693-708.

Leake, B.E. and 21 others (1997) Nomenclature of amphiboles: report of the Subcommittee on amphiboles of the International Mineralogical Association, Commission on New Minerals and Mineral Names. Canadian Mineralogist, 35, 219-246.

Liu, J., Bohlen, S.R. and Ernst, W.G. (1996). Stability of hydrous phases in subducting oceanic crust. Earth and Planetary Science Letters, 143, 161-171.

Lopez, S. and Castro, A. (2001) Determination of the fluid-absent solidus and supersolidus phase relationships of MORB-derived amphibolites in the range 4-14 kbar. American Mineralogist, 86, 1396-1403.

Lopez, S., Castro, A. and Garcia-Casco, A. (2005) Production of granodiorite melt by interaction between hydrous mafic magma and tonalitic crust. Experimental constraints and implications for the generation of Archaean TTG complexes. Lithos, 79, 229-250.

Luhr, J.F. (1990) Experimental phase relations of water- and sulfur-saturated arc magmas and the 1982 eruptions of EL Chichon volcano. Journal of Petrology, 31, 1071-1114.

Lustrino, M. (2005) How the delamination and detachment of lower crust can influence basaltic magmatism. Earth Science Reviews, 72-21-38.

Martin, H. (1987) Petrogenesis of Archaean tondhjemites, tonalites and granodiorites from Eastern Finland: Major and trace elements geochemistry. Journal of Petrology, 28, 921-953.

Martin, H. and Moyen, J.-F. (2002) Secular changes in TTG composition as markers of the progressive cooling of the Earth. Geology, 30, 319-322.

Mattioli, G.S. and Bishop, F.C. (1984) Experimental investigation of the chromium-aluminum mixing parameter in garnet. Geochimica et Cosmochimica Acta, 48, 1367-1371.

Moody, J.B., Meyer, D. and Jenkins, J.E. (1983) Experimental characterization of the greenschist/amphibolite boundary in mafic systems. American Journal of Science, 283, 48-92.

Moyen, J.-F., Martin, H. and Jayananda, M. (2001) Multi-element geochemical modelling of crust-mantle interactions during late-Archean crustal growth: the Closepet granite (South India). Precambrian Research, 112, 87-105.

Moyen, J.-F. and Stevens, G. (2006) Experimental constraints on TTG petrogenesis: Implications for Archean Geodynamics. In: Benn, K., Mareschal, J-C. and Condie, K.C. (eds.) Archean Geodynamics and Environments. Geophysical Monograph, 164, 149-175.

Nair, R. (2000) Fluid-absent melting of high-grade semi-pelites: P-T constraints on orthopyroxene formation and implications for granulite genesis. Unpublished M.Sc. Thesis. University of Alberta, Canada, p 87.

Nair, R. and Chacko, T. (2002) Fluid-absent melting of high-grade semi-pelites: P-T constraints on orthopyroxene formation and implications for granulite genesis. Journal of Petrology, 43, 2121-2142.

Nakamura, D. (2006) A new formulation of garnet-clinopyroxene thermometer using large number of experimental data with graphite capsules. 19th general meeting of the International Mineralogical Association, Kobe, Japan (July, 2006), Programs with Abstract, p. 102.

Nakamura, D. and Hirajima, T. (2005) Experimental evaluation of garnet-clinopyroxene geothermometry as applied to eclogites. Contributions to Mineralogy and Petrology, 150, 581-588.

Nyman, M.W., Pattison, D.R.M. and Ghent, E.D. (1995) Melt extraction during formation of K-feldspar + sillimanite migmatites, west of Revelstoke, British Columbia. Journal of Petrology, 36, 351-372.

O'Brien, P.J. and Rotzler, J. (2003) High-pressure granulites: formation, recovery of peak conditions and implications for tectonics. Journal of Metamorphic Geology, 21, 3-20.

Oh, C.W. & Liou, J.G. (1998) A petrogenetic grid for eclogite and related facies under high-pressure metamorphism. The Island Arc, 7, 36-51.

Patiño Douce, A.E. and Beard, J.S. (1995) Dehydration-melting of biotite gneiss and quartz amphibolite from 3 to 15 kbar. Journal of Petrology, 36, 707-738.

Patiño Douce, A.E. and Beard, J.S. (1996) Effects of P, f(O)2 and Mg/Fe ration on dehydration melting of model metagraywackes. Journal of Petrology, 37, 999-1024.

Pattison, D.R.M. (1994) Are reversed Fe-Mg exchange and solid solution experiments really reversed? American Mineralogist, 79, 938-950.

Pattison, D.R.M. (2003) Petrogenetic significance of orthopyroxene-free garnet + clinopyroxene + plagioclase-bearing metabasites with respect to the amphibolite and granulite facies. Journal of Metamorphic Geology, 21, 21-31.

Pattison, D.R.M. and Newton, R.C. (1989) Reversed experimental calibration of the garnet-clinopyroxene Fe-Mg exchange thermometer. Contributions to Mineralogy and Petrology, 101, 87-103.

Peacock, S.M. and Wang, K. (1999) Seismic consequences of warm versus cool subduction zone metamorphism: Examples from northeast and southwest Japan. Science, 286, 937-939.

Percival, J.A. (1983) High-grade metamorphism in the Chapeau-Foleyet area, Ontario. American Mineralogist, 68, 667-686.

Poli, S. (1993) The amphibolite-eclogite transformation: an experimental study on basalt. American Journal of Science, 293, 1061-1107.

Raheim, A. and Green, D.H. (1974) Experimental determination of the temperature and pressure dependence of the Fe-Mg partition coefficient for coexisting garnet and clinopyroxene. Contributions to Mineralogy and Petrology, 48, 179-203.

Rapp, R.P. (1997) Heterogenous source regions for Archean granitoids: experimental and geochemical evidence. In: de Wit, M. and Ashwal, L.D. (eds.) Greenstone belts. Oxford Monographs on geology and geophysics 35, 267-279.

Rapp, R.P., Watson, E.B., and Miller, C.F. (1991) Partial melting of amphibolite/eclogite and the origin of Archean trondhjemites and tonalites. Precambrian Research, 51, 1-25.

Rapp, R.P., and Watson, E.B. (1995) Dehydration melting of metabasalt at 8-32 kbar: implications for continental growth and crust-mantle recycling. Journal of Petrology, 36, 891-931.

Rapp, R.P., Shimizu, N. and Norman, M.D. (2003) Growth of early continental crust by partial melting of eclogite. Nature, 425, 605-609.

Rapp, R.P., Shimizu, N., Norman, M.D. and Applegate, G.S. (1999) Reaction between slab-derived melts and peridotite in the mantle wedge: experimental constraints at 3.8 GPa. Chemical Geology, 160, 335-356.

Rasband, W.S. (1997-2005) ImageJ, U. S. National Institutes of Health, Bethesda, Maryland, USA, http://rsb.info.nih.gov/ij/.

Rushmer, T. (1991) Partial melting of two contrasting amphibolites: contrasting experimental results under fluid-absent conditions. Contributions to Mineralogy and Petrology, 107, 41-59.

Sen, C. and Dunn, T. (1994) Dehydration melting of a basaltic composition amphibolite at 1.5 and 2.0 GPa: implications for the origin of adakites. Contributions to Mineralogy and Petrology, 117, 394-409.

Schmidt, M.W. and Thompson, A.B. (1996). Epidote in calc-alkaline magmas: an experimental study of stability, phase relationships, and the role of epidote in magmatic evolution. American Mineralogist 81, 462-474.

Sengupta, P. , Raith, M.M. and Datta, A. (2004) Stability of fluorite and titanite in a calc-silicate rock from Vizianagram area, Eastern Ghats Belt, India. J. Met. Geol, 22, 345-359.

Sisson, T.W., Ratajeski, K., Hankins, W.B. and Glazner, A.F. (2005) Voluminous granitic magmas from common basaltic sources. Contributions to Mineralogy and Petrology, 148, 635-661.

Skjerlie, K.P. and Johnston, A.D. (1993) Vapor-absent melting at 10 kbar of biotite- and amphibole-bearing tonalitic gneiss: implications for the generation of A-type granites. Geology, 20, 263-266.

Skjerlie, K.P. and Patino Douce, A.D. (2002) The fluid-absent partial melting of a zoisite-bearing quartz eclogite from 1.0 to 3.2 GPa; implications for melting in thickened continental crust and for subduction-zone processes. Journal of Petrology, 43, 291-314.

Spear, F.S. (1981) An experimental study of hornblende stability and compositional variability in amphibolite. American Journal of Science, 281, 697-734.

Springer, W. and Seck, H.A. (1997) Partial fusion of basic granulite at 5 to 15 kbar: implications for the origin of TTG magmas. Contributions to Mineralogy and Petrology, 127, 30-45.

Storey, C.D., Brewer, T.S, and Parrish, R.R. (2003) Grenvillian age decompression of eclogites in the Glenelg-Attadale Inlier, NW Scotland. Geophysical Research Abstracts, v. 5, 06080.

Thompson, A.B. (1982) Dehydration melting of pelitic rocks and the generation of H2O-undersaturated granitic liquids. American Journal of Science, 282, 1567-1595.

Torres-Roldan, R.L., Garcia-Casco, A. and Garcia-Sanchez, P.A. (2000) CSpace: An integrated workplace for the graphical and algebraic analysis of phase assemblages on 32-bit Wintel platforms. Computers and Geosciences, 26, 779-793.

Vielzeuf, D. and Schmidt, M.W. (2001) Melting relations in hydrous systems revisited: application to metapelites, metagreywackes and metabasalts. Contribution to Mineralogy and Petrology, 141, 251-267.

De Waard, D. (1965) The occurrence of garnet in the granulite facies terrane of the Adirondack Highlands. Journaly of Petrology, 6, 165-191.

Wones, D.R. (1989) Significance of the assemblage titanite+magnetite+quartz in granitic rocks. American Mineralogist, 74, 744-749.

Windom, K.E. and Boettcher, A.L. (1976) The effect of reduced activity of anorthite on the reaction grossular + quartz = anorthite + wollastonite: a model for plagioclase in the earth's lower crust and upper mantle. American Mineralogist, 61, 889-896.

Winther, K.T. (1996) An experimentally based model for the origin of tonalitic and trondhjemitic melts. Chemical Geology, 127, 43-59.

Winther, K.T. and Newton, R.C. (1991) Experimental melting of hydrous low-K tholeiite: evidence on the origin of Archaean cratons. Bulletin of Geological Society of Denmark, 39, 213-228.

Wolf, M.B. and Wyllie, P.J. (1993) Amphibolite dehydration-melting: sorting out the solidus. In: Prichard, H.M., Alabaster, T., Harris, N.B.W. & Neary, C.R. (eds.) Magmatic Processes and Plate Tectonics, Geological Society of London, Special Publication 76, 405-416.

Wolf, M.B. and Wyllie, P.J. (1994) Dehydration-melting of amphibolite at 10 kbar: the effects of temperature and time. Contributions to Mineralogy and Petrology, 44, 151-179.

Wones, D.R. (1989) Significance of the assemblage titanite + magnetite + quartz in granitic rocks. American Mineralogist, 74, 744-749.

Wyllie, P.J., Wolfe, M.B. and van der Laan, S.R. (1997). Conditions of formation of tonalites and trondhjemites: Magmatic sources and products. In: de Wit, M. and Ashwal, L.D. (eds.) Greenstone belts. Oxford Monographs on geology and geophysics 35, 256-266.

Yamamoto, H. and Yoshino, T. (1998) Superposition of replacements in the mafic granulites of the Jijal complex of the Kohistan arc, northern Pakistan: dehydration and rehydration within deep arc crust. Lithos 43, 219-234.

Yardley, B.W. (1989) An introduction to metamorphic petrology. Longman Earth Science Series. P 248.

Zegers, T.E. and van Keken, P.E. (2001) Middle Archean continental formation by crustal delamination. Geology, 29, 1083-1086.

Table 2.1: Composition of starting materials used in the experiments.

Wt.%	SiO_2	TiO_2	Al_2O_3	FeO^T	MnO	MgO	CaO	Na_2O	K_2O	Total	Mode*	Mg#
Kapuskasing (KAP)												
Hornblende	42.28	1.81	12.53	17.82	0.28	9.23	10.95	1.12	1.12	97.14	55	0.48
Plagioclase	58.19	0.00	26.19	0.03	0.01	0.00	7.98	7.00	0.25	99.65	35	
Garnet	37.56	0.04	20.72	26.02	2.86	2.99	9.69	0.02	n.a.	99.90	1	0.17
Clinopyroxene	50.87	0.27	2.68	11.89	0.38	10.94	21.97	0.68	0.03	99.71	4	0.62
Quartz											6	
Three Valley Gap (3VG)												
Hornblende	43.14	2.17	12.28	14.76	0.12	11.01	11.11	1.50	1.48	97.57	53	0.57
Plagioclase	56.60	0.00	27.25	0.09	0.01	0.00	9.42	6.21	0.40	99.98	35	
Garnet	37.97	0.05	21.46	26.21	1.17	5.77	7.24	0.02	n.a.	99.89	<1	0.28
Clinopyroxene	52.08	0.15	2.10	11.05	0.24	12.80	21.12	0.50	0.03	100.07	5	0.67
Quartz											7	
Bulk composition (wt.%)												
KAP^+	51.44	1.09	15.01	11.44	0.24	5.79	11.22	3.00	0.77	100.00		0.47
$3VG^+$	51.95	0.80	14.14	11.18	0.18	7.29	11.06	2.52	0.88	100.00		0.54
MORB	50.58	1.45	15.45	9.98	n.a	7.95	11.56	2.71	0.18	99.86		0.59
	(0.62)	(0.30)	(0.75)	(1.02)	-	(0.71)	(0.60)	(0.38)	(0.15)			

*- mode estimated from thin sections of the rocks from the starting materials was taken; Mg# = Mg/(Mg+Fe) molar; n.a.- not available

+- XRF anyalses recalculated to 100; MORB data from PETDB database; numbers in brackets are 1 sigma std. deviation of oxide (wt.%) for MORB.

Table 2.2: Comparison of starting materials with mid-ocean ridge basalts. MORB data from PETDB database.

	MORB-IR		**MORB-EPR**		**MORB-MAR**		**AVERAGE**		**KAP†**	**3VG†**	**MORB-derived amphibolite***
n	652	1σ	3816	1σ	3090	1σ	**MORB**	1σ			
Wt.%											
SiO_2	50.77	0.74	50.59	0.96	50.77	0.85	50.58	0.62	51.40	51.92	50.73
TiO_2	1.59	0.47	1.80	0.39	1.39	0.33	1.45	0.30	1.09	0.80	1.20
Al_2O_3	15.64	0.91	14.57	0.86	15.36	0.65	15.45	0.75	14.99	14.13	16.91
FeO^T	9.41	1.27	10.83	1.33	9.62	0.81	9.98	1.02	11.43	11.17	8.40
MnO	0.17	0.05	0.20	0.04	0.17	0.04	-	-	0.24	0.18	0.18
MgO	7.46	0.92	7.17	1.27	7.76	0.81	7.95	0.71	5.78	7.28	7.43
CaO	10.99	0.83	11.42	0.91	11.70	0.78	11.56	0.60	11.21	11.05	11.90
Na_2O	3.02	0.46	2.80	0.30	2.55	0.38	2.71	0.38	2.99	2.52	2.91
K_2O	0.21	0.22	0.16	0.12	0.19	0.19	0.18	0.15	0.77	0.88	0.19
P_2O_5	0.18	0.08	0.18	0.06	0.15	0.06	0.15	0.05	0.09	0.06	0.14
Total	99.45		99.73		99.66		99.86		100.00	100.00	100.00
NORM											
Quartz	0		0		0		0		0	0	0
Orthoclase	1.24		0.95		1.12		1.06		4.55	5.20	1.06
Albite	25.55		23.69		21.58		22.93		25.30	21.32	24.62
Anorthite	28.50		26.71		29.90		29.46		25.21	24.64	32.55
Nepheline	0		0		0		0		0	0	0
Diopside	20.41		23.77		22.32		22.10		24.93	24.70	20.73
Hypersthene	11.49		13.46		15.49		11.72		6.73	14.23	10.86
Olivine	8.81		7.30		6.26		9.63		11.00	8.24	5.48
Magnetite	0.00		0		0.00		0		0	0	1.97
Ilmenite	3.02		3.42		2.64		2.75		2.07	1.52	2.28
Apatite	0.42		0.42		0.35		0.35		0.21	0.14	0.33

n= no of analyses; *†- given on an anhydrous basis; *-MORB derived amphibolite data from Castro et al., 1996 renormalized to 100%.*
IR- Indian Ridge; EPR- East Pacific Ridge, MAR- Mid-Atlantic Ridge.

Table 2.3: Experimental conditions and run products.

Run No.	P (kbar)	T (°C)	Duration (hours)	Phase Assemblage
Three Valley Gap(3VG)				
3VG-12	7	825	672	Hbl, Plag, (Cpx), Qtz, (Melt)
3VG-01	7	850	336	Hbl, Plag, Cpx, Opx, Qtz, Melt
3VG-27	7	875	336	Hbl, Plag, (Cpx),Opx, Melt, Mag
3VG-03	7	900	336	Hbl, Plag, Cpx, Opx, Melt, Mag
3VG-26	7	950	168	Hbl, Plag, Cpx, Opx, Melt, Mag
3VG-14	7	1000	72	Cpx, Opx, Plag, Melt, Mag
3VG-24*	7	900	192	
		825	144	Cpx, Hbl, Plag, Melt
3VG-32a*	7	900	288	
		850	624	Cpx, Hbl, Plag, Opx, Melt, Mag
3VG-32b*	7	900	288	
		850	624	Cpx, Hbl, Plag, Opx, Melt, Apat, Mag
3VG-11	10	775	720	Hbl, Plag, (Cpx), Qtz, Melt, Ttn
3VG-10	10	800	504	Hbl, Plag, (Cpx), Qtz, Melt
3VG-06	10	850	504	Hbl, Plag, Cpx, Opx, (Grt), Qtz, Melt
3VG-05	10	900	504	Hbl, Plag, Cpx, Opx, Qtz, Melt
3VG-04	10	950	168	Hbl, Plag, Cpx, Opx, Melt
3VG-22	10	1000	48	(Hbl), Plag, Cpx, Opx, Melt
3VG-19	12.5	800	1056	Hbl, Plag, (Cpx), Qtz
3VG-16	12.5	850	336	Hbl,Plag, Cpx, Grt, Qtz, Melt
3VG-15	12.5	900	336	Hbl, Plag, Cpx, (Grt), Melt
3VG-20	12.5	950	192	Hbl, Plag, Cpx, Grt, Opx, Melt
3VG-18	12.5	1000	96	Cpx, Grt, Opx, Plag, Melt
3VG-25*	12.5	850	168	
		775	504	Cpx,Hbl, Plag, Melt?
3VG-21	15	775	552	Hbl, Plag, Cpx, Qtz, Sph, Melt
3VG-28	15	800	240	Hbl, Plag, Cpx, Qtz, Melt, Ttn, Ap
3VG-29	15	825	720	Hbl, Plag, Cpx, Grt, Qtz, Melt
3VG-08	15	900	336	Hbl, Plag, Cpx, Grt, Qtz, Melt
3VG-07	15	950	240	Cpx, Plag, Grt, Qtz, Melt
3VG-09	15	1050	72	Cpx, (Plag), Grt, Melt
3VG-39	17.5	850	456	Cpx,Hbl, Grt, Plag, Qtz, Melt?
3VG-34	17.5	900	312	Cpx,Hbl, Grt, Plag, Melt, Rut
3VG-35	17.5	950	264	Cpx,Hbl, Grt, Plag, Melt, Rut
3VG-40	17.5	950	192	Cpx,Hbl, Grt, Plag, Melt, Rut
3VG-42	17.5	1050	48	Cpx, Hbl, Grt, Melt
3VG-36	20	850	480	Cpx, Hbl, Grt, Qtz, Plag, (Melt), Pyr
3VG-31	20	900	240	Cpx, Grt, Melt, Apat, Rut
3VG-44	20	900	48	Grt,Cpx, (Plag), (Qtz) Melt, Rut
3VG-41	20	950	168	Cpx, Grt, Plag, Melt, Pyr
3VG-43	22.5	850	1008	Grt, Cpx,Qtz,Plag, Pheng,Melt
3VG-38	22.5	900	336	Cpx, Grt,(Qtz), Melt, Pyr
3VG-45	22.5	950	144	Grt, Cpx,(Qtz),Melt,Rut
3VG-46	22.5	1000	72	Grt,Cpx,Melt, Pyr

Run No.	P (kbar)	T (°C)	Duration (hours)	Phase Assemblage
Kapuskasing(KAP)				
KAP-12	7	825	672	Hbl, Plag, (Cpx), Qtz
KAP-01	7	850	336	Hbl, Plag, Cpx, Qtz, Melt
KAP-27	7	875	312	Hbl, Plag, Cpx, Melt, Mag, Ap,Py
KAP-03	7	900	336	Hbl, Plag, Cpx, Opx, Melt
KAP-02	7	950	168	Hbl, Plag, Cpx, Opx, Melt, Mag
KAP-14	7	1000	72	Cpx, Opx, Plag, Melt
KAP-24*	7	900	192	
		825	144	Hbl, Cpx, Plag,Qtz, Melt
KAP-30*	7	900	144	
		850	552	Hbl, Cpx, Plag, Qtz, Melt, Mag
KAP-11	10	775	720	Hbl, Plag, (Cpx), Plag, Qtz, (Melt)
KAP-10	10	800	504	Hbl, Plag, Cpx, Grt, Plag, Qtz, Melt
KAP-06	10	850	504	Hbl, Plag, Cpx, Grt, Plag, Melt
KAP-05	10	900	504	Hbl, Plag, Cpx, Grt, Plag, Melt
KAP-04	10	950	168	Hbl, Plag, Cpx, (Grt), Plag, Melt
KAP-22	10	1000	48	Hbl, Plag, Cpx, Plag, Melt,Mag
KAP-19	12.5	800	1056	Hbl, Plag, (Cpx), Grt, Qtz
KAP-16	12.5	850	336	Hbl, Plag, Cpx, Grt, Qtz, Melt
KAP-15	12.5	900	336	Hbl, Plag, Cpx, Grt, Melt
KAP-20	12.5	950	192	Hbl, Plag, Cpx, Grt, Apat, Melt
KAP-18	12.5	1000	96	Cpx, Grt, Plag, Melt
KAP-25*	12.5	850	168	
		775	504	Hbl, (cpx), Plag, Melt?
KAP-21	15	775	552	Hbl, Plag, Cpx, Ttn, Qtz
KAP-28	15	800	240	Hbl, Plag, Cpx, Grt, Melt,Ilm
KAP-29	15	825	720	Hbl, Plag, Cpx, Grt, Melt
KAP-08	15	900	336	Hbl, Plag, Cpx, Grt, Melt
KAP-07	15	950	240	Hbl, Plag, Cpx, Grt, Melt
KAP-09	15	1050	72	Hbl, Plag, Cpx, Grt, Melt
KAP-39	17.5	850	456	Hbl, Cpx, Plag, Grt, Qtz, Melt, Rut
KAP-34	17.5	900	312	Cpx, Hbl?, Grt, Plag, Melt, Pyr, Apat
KAP-35	17.5	950	264	Cpx, Plag, Grt, Melt, Pyr
KAP-40	17.5	950	192	Cpx, Plag, Grt, Melt, Rut
KAP-42	17.5	1050	48	Cpx, Plag, Grt, Melt
KAP-36	20	850	480	Hbl, Cpx, Grt, Plag, (Qtz), (Melt)
KAP-31	20	900	240	Grt,Cpx, Plag, Melt
KAP-44	20	900	48	Grt,Cpx, Plag, Melt,Rut, Pyr
KAP-41	20	950	168	Hbl, Cpx, Grt, Plag, Melt, Rut
KAP-43	22.5	850	1008	Grt, Cpx, (Qtz),Pheng, Melt, Rut
KAP-38	22.5	900	336	Grt, Cpx, (Qtz), Melt
KAP-45	22.5	950	144	Grt, Cpx,(Qtz), Melt
KAP-46	22.5	1000	72	Grt, Cpx, (Plag), Melt,Pyr

Abbreviations after Kretz (1983); Brackets indicate the presence of trace amount of an . otherwise common phase in the experiments; ru, ilm, Ttn and pyr are present only in trace amounts.

*-indicates a two stage experiment.

Table 2.4: Average composition of hornblende in the experiments.

Run No.	[illegible]		[illegible]		[illegible]		[illegible]		[illegible]		[illegible]		[illegible]		[illegible]		[illegible]		[illegible]		[illegible]		[illegible]		[illegible]		[illegible]		[illegible]		[illegible]		[illegible]		[illegible]		[illegible]		[illegible]		[illegible]		[illegible]	
P (kbar)	7		7		7		7		7		10		10		10		10		10		10		12.5		12.5		12.5		12.5		12.5		15		15		15		15		15		17.5	
T (°C)	[illegible]		[illegible]		[illegible]		[illegible]		[illegible]		[illegible]		[illegible]		[illegible]		[illegible]		[illegible]		[illegible]		[illegible]		[illegible]		[illegible]		[illegible]		[illegible]		[illegible]		[illegible]		[illegible]		[illegible]		[illegible]		[illegible]	
n	[illegible]	1σ	[illegible]	1σ	[illegible]	1σ	[illegible]	1σ	[illegible]	1σ	[illegible]	1σ	[illegible]	1σ	[illegible]	1σ	[illegible]	1σ	[illegible]	1σ	[illegible]	1σ	[illegible]	1σ	[illegible]	1σ	[illegible]	1σ	[illegible]	1σ	[illegible]	1σ	[illegible]	1σ	[illegible]	1σ	[illegible]	1σ	[illegible]	1σ	[illegible]	1σ	[illegible]	1σ
Oxides (wt%)																																												
SiO_2	[illegible]	[illegible]	[illegible]	[illegible]	[illegible]	[illegible]	[illegible]	[illegible]	[illegible]	[illegible]	[illegible]	[illegible]	[illegible]	[illegible]	[illegible]	[illegible]	[illegible]	[illegible]	[illegible]	[illegible]	[illegible]	[illegible]	[illegible]	[illegible]	[illegible]	[illegible]	[illegible]	[illegible]	[illegible]	[illegible]	[illegible]	[illegible]	[illegible]	[illegible]	[illegible]	[illegible]	[illegible]	[illegible]	[illegible]	[illegible]	[illegible]	[illegible]	[illegible]	[illegible]
TiO_2	[illegible]	[illegible]	[illegible]	[illegible]	[illegible]	[illegible]	[illegible]	[illegible]	[illegible]	[illegible]	[illegible]	[illegible]	[illegible]	[illegible]	[illegible]	[illegible]	[illegible]	[illegible]	[illegible]	[illegible]	[illegible]	[illegible]	[illegible]	[illegible]	[illegible]	[illegible]	[illegible]	[illegible]	[illegible]	[illegible]	[illegible]	[illegible]	[illegible]	[illegible]	[illegible]	[illegible]	[illegible]	[illegible]	[illegible]	[illegible]	[illegible]	[illegible]	[illegible]	[illegible]
Al_2O_3	[illegible]	[illegible]	[illegible]	[illegible]	[illegible]	[illegible]	[illegible]	[illegible]	[illegible]	[illegible]	[illegible]	[illegible]	[illegible]	[illegible]	[illegible]	[illegible]	[illegible]	[illegible]	[illegible]	[illegible]	[illegible]	[illegible]	[illegible]	[illegible]	[illegible]	[illegible]	[illegible]	[illegible]	[illegible]	[illegible]	[illegible]	[illegible]	[illegible]	[illegible]	[illegible]	[illegible]	[illegible]	[illegible]	[illegible]	[illegible]	[illegible]	[illegible]	[illegible]	[illegible]
Cr_2O_3	[illegible]	[illegible]	[illegible]	[illegible]	[illegible]	[illegible]	0	[illegible]	[illegible]	[illegible]	[illegible]	[illegible]	[illegible]	[illegible]	[illegible]	[illegible]	[illegible]	[illegible]	[illegible]	[illegible]	[illegible]	[illegible]	[illegible]	[illegible]	[illegible]	[illegible]	[illegible]	[illegible]	[illegible]	[illegible]	[illegible]	[illegible]	[illegible]	[illegible]	[illegible]	[illegible]	[illegible]	[illegible]	[illegible]	[illegible]	[illegible]	[illegible]	[illegible]	[illegible]
FeO^*	[illegible]	[illegible]	[illegible]	[illegible]	[illegible]	[illegible]	[illegible]	[illegible]	[illegible]	[illegible]	[illegible]	[illegible]	[illegible]	[illegible]	[illegible]	[illegible]	[illegible]	[illegible]	[illegible]	[illegible]	[illegible]	[illegible]	[illegible]	[illegible]	[illegible]	[illegible]	[illegible]	[illegible]	[illegible]	[illegible]	[illegible]	[illegible]	[illegible]	[illegible]	[illegible]	[illegible]	[illegible]	[illegible]	[illegible]	[illegible]	[illegible]	[illegible]	[illegible]	[illegible]
MnO	[illegible]	[illegible]	[illegible]	[illegible]	[illegible]	[illegible]	[illegible]	[illegible]	[illegible]	[illegible]	[illegible]	[illegible]	[illegible]	[illegible]	[illegible]	[illegible]	[illegible]	[illegible]	[illegible]	[illegible]	[illegible]	[illegible]	[illegible]	[illegible]	[illegible]	[illegible]	[illegible]	[illegible]	[illegible]	[illegible]	[illegible]	[illegible]	[illegible]	[illegible]	[illegible]	[illegible]	[illegible]	[illegible]	[illegible]	[illegible]	[illegible]	[illegible]	[illegible]	[illegible]
MgO	[illegible]	[illegible]	[illegible]	[illegible]	[illegible]	[illegible]	[illegible]	[illegible]	[illegible]	[illegible]	[illegible]	[illegible]	[illegible]	[illegible]	[illegible]	[illegible]	[illegible]	[illegible]	[illegible]	[illegible]	[illegible]	[illegible]	[illegible]	[illegible]	[illegible]	[illegible]	[illegible]	[illegible]	[illegible]	[illegible]	[illegible]	[illegible]	[illegible]	[illegible]	[illegible]	[illegible]	[illegible]	[illegible]	[illegible]	[illegible]	[illegible]	[illegible]	[illegible]	[illegible]
CaO	[illegible]	[illegible]	[illegible]	[illegible]	[illegible]	[illegible]	[illegible]	[illegible]	[illegible]	[illegible]	[illegible]	[illegible]	[illegible]	[illegible]	[illegible]	[illegible]	[illegible]	[illegible]	[illegible]	[illegible]	[illegible]	[illegible]	[illegible]	[illegible]	[illegible]	[illegible]	[illegible]	[illegible]	[illegible]	[illegible]	[illegible]	[illegible]	[illegible]	[illegible]	[illegible]	[illegible]	[illegible]	[illegible]	[illegible]	[illegible]	[illegible]	[illegible]	[illegible]	[illegible]
Na_2O	[illegible]	[illegible]	[illegible]	[illegible]	[illegible]	[illegible]	[illegible]	[illegible]	[illegible]	[illegible]	[illegible]	[illegible]	[illegible]	[illegible]	[illegible]	[illegible]	[illegible]	[illegible]	[illegible]	[illegible]	[illegible]	[illegible]	[illegible]	[illegible]	[illegible]	[illegible]	[illegible]	[illegible]	[illegible]	[illegible]	[illegible]	[illegible]	[illegible]	[illegible]	[illegible]	[illegible]	[illegible]	[illegible]	[illegible]	[illegible]	[illegible]	[illegible]	[illegible]	[illegible]
K_2O	[illegible]	[illegible]	[illegible]	[illegible]	[illegible]	[illegible]	[illegible]	[illegible]	[illegible]	[illegible]	[illegible]	[illegible]	[illegible]	[illegible]	[illegible]	[illegible]	[illegible]	[illegible]	[illegible]	[illegible]	[illegible]	[illegible]	[illegible]	[illegible]	[illegible]	[illegible]	[illegible]	[illegible]	[illegible]	[illegible]	[illegible]	[illegible]	[illegible]	[illegible]	[illegible]	[illegible]	[illegible]	[illegible]	[illegible]	[illegible]	[illegible]	[illegible]	[illegible]	[illegible]
F	n.d.		0	n.d.	n.d.	-	0	-	n.d.	n.d.	0	[illegible]	0	[illegible]	0	[illegible]	0	[illegible]	0	[illegible]	[illegible]	[illegible]	[illegible]	[illegible]	[illegible]	[illegible]	[illegible]	[illegible]	n.d.	n.d.	[illegible]	[illegible]	[illegible]	[illegible]	n.d.	n.d.	[illegible]	[illegible]	[illegible]	n.d.	0	[illegible]	n.d.	n.d.
Cl	n.d.		[illegible]	[illegible]	n.d.	-	[illegible]	[illegible]	n.d.	n.d.	[illegible]	[illegible]	[illegible]	[illegible]	[illegible]	[illegible]	[illegible]	[illegible]	[illegible]	[illegible]	[illegible]	[illegible]	[illegible]	[illegible]	[illegible]	[illegible]	[illegible]	n.d.	[illegible]	[illegible]	n.d.	n.d.	[illegible]	[illegible]	[illegible]	[illegible]	n.d.	n.d.	[illegible]	[illegible]	[illegible]	[illegible]	n.d.	n.d.
Total	[illegible]		[illegible]		[illegible]		[illegible]		[illegible]		[illegible]		[illegible]		[illegible]		[illegible]		[illegible]		[illegible]		[illegible]		[illegible]		[illegible]		[illegible]		[illegible]		[illegible]		[illegible]		[illegible]		[illegible]		[illegible]		[illegible]	
Cations (23 O)																																												
Si	[illegible]		[illegible]		[illegible]		[illegible]		[illegible]		[illegible]		[illegible]		[illegible]		[illegible]		[illegible]		[illegible]		[illegible]		[illegible]		[illegible]		[illegible]		[illegible]		[illegible]		[illegible]		[illegible]		[illegible]		[illegible]		[illegible]	
Al(iv)	[illegible]		[illegible]		[illegible]		[illegible]		[illegible]		[illegible]		[illegible]		[illegible]		[illegible]		[illegible]		[illegible]		[illegible]		[illegible]		[illegible]		[illegible]		[illegible]		[illegible]		[illegible]		[illegible]		[illegible]		[illegible]		[illegible]	
Al(vi)	[illegible]		[illegible]		[illegible]		[illegible]		[illegible]		[illegible]		[illegible]		[illegible]		[illegible]		[illegible]		[illegible]		[illegible]		[illegible]		[illegible]		[illegible]		[illegible]		[illegible]		[illegible]		[illegible]		[illegible]		[illegible]		[illegible]	
Fe(III)	[illegible]		[illegible]		[illegible]		[illegible]		[illegible]		[illegible]		[illegible]		[illegible]		[illegible]		[illegible]		[illegible]		[illegible]		[illegible]		[illegible]		[illegible]		[illegible]		[illegible]		[illegible]		[illegible]		[illegible]		[illegible]		[illegible]	
Ti	[illegible]		[illegible]		[illegible]		[illegible]		[illegible]		[illegible]		[illegible]		[illegible]		[illegible]		[illegible]		[illegible]		[illegible]		[illegible]		[illegible]		[illegible]		[illegible]		[illegible]		[illegible]		[illegible]		[illegible]		[illegible]		[illegible]	
~~Cr~~	[illegible]		[illegible]		[illegible]		[illegible]		[illegible]		[illegible]		[illegible]		[illegible]		[illegible]		[illegible]		[illegible]		[illegible]		[illegible]		[illegible]		[illegible]		[illegible]		[illegible]		[illegible]		[illegible]		[illegible]		[illegible]		[illegible]	
Fe(II)	[illegible]		[illegible]		[illegible]		[illegible]		[illegible]		[illegible]		[illegible]		[illegible]		[illegible]		[illegible]		[illegible]		[illegible]		[illegible]		[illegible]		[illegible]		[illegible]		[illegible]		[illegible]		[illegible]		[illegible]		[illegible]		[illegible]	
Mn	[illegible]		[illegible]		[illegible]		[illegible]		[illegible]		[illegible]		[illegible]		[illegible]		[illegible]		[illegible]		[illegible]		[illegible]		[illegible]		[illegible]		[illegible]		[illegible]		[illegible]		[illegible]		[illegible]		[illegible]		[illegible]		[illegible]	
Mg	[illegible]		[illegible]		[illegible]		[illegible]		[illegible]		[illegible]		[illegible]		[illegible]		[illegible]		[illegible]		[illegible]		[illegible]		[illegible]		[illegible]		[illegible]		[illegible]		[illegible]		[illegible]		[illegible]		[illegible]		[illegible]		[illegible]	
Ca	[illegible]		[illegible]		[illegible]		[illegible]		[illegible]		[illegible]		[illegible]		[illegible]		[illegible]		[illegible]		[illegible]		[illegible]		[illegible]		[illegible]		[illegible]		[illegible]		[illegible]		[illegible]		[illegible]		[illegible]		[illegible]		[illegible]	
Na	[illegible]		[illegible]		[illegible]		[illegible]		[illegible]		[illegible]		[illegible]		[illegible]		[illegible]		[illegible]		[illegible]		[illegible]		[illegible]		[illegible]		[illegible]		[illegible]		[illegible]		[illegible]		[illegible]		[illegible]		[illegible]		[illegible]	
K	[illegible]		[illegible]		[illegible]		[illegible]		[illegible]		[illegible]		[illegible]		[illegible]		[illegible]		[illegible]		[illegible]		[illegible]		[illegible]		[illegible]		[illegible]		[illegible]		[illegible]		[illegible]		[illegible]		[illegible]		[illegible]		[illegible]	
Na(M4)	[illegible]		[illegible]		[illegible]		[illegible]		[illegible]		[illegible]		[illegible]		[illegible]		[illegible]		[illegible]		[illegible]		[illegible]		[illegible]		[illegible]		[illegible]		[illegible]		[illegible]		[illegible]		[illegible]		[illegible]		[illegible]		[illegible]	
Na (A)	[illegible]		[illegible]		[illegible]		[illegible]		[illegible]		[illegible]		[illegible]		[illegible]		[illegible]		[illegible]		[illegible]		[illegible]		[illegible]		[illegible]		[illegible]		[illegible]		[illegible]		[illegible]		[illegible]		[illegible]		[illegible]		[illegible]	
A-site	[illegible]		[illegible]		[illegible]		[illegible]		[illegible]		[illegible]		[illegible]		[illegible]		[illegible]		[illegible]		[illegible]		[illegible]		[illegible]		[illegible]		[illegible]		[illegible]		[illegible]		[illegible]		[illegible]		[illegible]		[illegible]		[illegible]	
Total	[illegible]		[illegible]		[illegible]		[illegible]		[illegible]		[illegible]		[illegible]		[illegible]		[illegible]		[illegible]		[illegible]		[illegible]		[illegible]		[illegible]		[illegible]		[illegible]		[illegible]		[illegible]		[illegible]		[illegible]		[illegible]		[illegible]	
X_{Mg}	[illegible]		[illegible]		[illegible]		[illegible]		[illegible]		[illegible]		[illegible]		[illegible]		[illegible]		[illegible]		[illegible]		[illegible]		[illegible]		[illegible]		[illegible]		[illegible]		[illegible]		[illegible]		[illegible]		[illegible]		[illegible]		[illegible]	

Table 2.4: Hornblende compositions contd…

Run No.	KAP-1		KAP-37		KAP-3		KAP-9		KAP-11		KAP-13		KAP-6		KAP-5		KAP-4		KAP-22		KAP-19		KAP-16		KAP-15		KAP-20		KAP-18		KAP-21		KAP-28		KAP-25		KAP-8		KAP-7		KAP-30	
P (kbar)	7		7		7		7		10		10		10		10		10		10		12.5		12.5		12.5		12.5		12.5		15		15		15		15		15		17.5	
T (°C)	880		875		900		950		775		800		850		900		950		1000		800		850		900		950		1000		775		800		825		900		950		850	
n	25	1σ	14	1σ	24	1σ	25	1σ	28	1σ	24	1σ	55	1σ	41	1σ	43	1σ	19	1σ	12	1σ	19	1σ	10	1σ	18	1σ	21	1σ	18	1σ	30	1σ	12	1σ	18	1σ	9	1σ	10	1σ
Oxides (Wt.%)																																										
SiO_2	41.55	0.42	41.65	0.73	41.82	0.45	40.96	0.68	41.61	0.33	41.6	0.56	42.37	0.71	41.81	0.79	41.41	0.96	41.22	0.73	42.35	0.42	41.16	0.88	42.27	0.49	41.82	0.79	41.49	0.66	42.19	0.62	42.12	0.54	42.48	0.49	41.3	0.56	41.46	0.45	42.57	0.35
TiO_2	1.86	0.12	1.79	0.16	1.94	0.16	2.09	0.45	1.9	0.28	1.77	0.20	1.77	0.18	1.85	0.25	1.77	0.29	2.13	0.99	1.73	0.19	1.86	0.14	1.77	0.27	2.03	0.29	2.25	0.46	1.81	0.16	1.85	0.23	1.86	0.13	1.81	0.16	2.34	0.34	1.87	0.15
Al_2O_3	12.70	0.36	13.22	0.74	12.8	0.35	12.71	0.09	12.76	0.43	11.97	0.59	12.69	0.42	13.26	0.62	12.86	0.43	13.33	1.01	12.88	0.41	13.16	0.90	12.82	0.35	12.82	0.50	13.07	0.74	13.16	0.72	13.26	0.87	12.71	0.39	12.73	0.55	13.21	0.15	12.93	0.30
Cr_2O_3	0.03	0.01	0.05	0.01	0.03	0.01	0.04	0.01	0.03	0.02	0.03	0.02	0.06	0.02	0.05	0.03	0.06	0.02	0.05	0.02	0.04	0.01	0.08	0.02	0.05	0.02	0.05	0.02	0.06	0.02	0.05	0.02	0.06	0.02	0.05	0.01	0.04	0.01	0.08	0.02	0.04	0.01
FeO^T	18.19	0.44	18.19	0.81	17.09	0.61	17.74	0.78	18.23	0.46	18.05	0.44	18.21	0.57	18.30	0.50	18.21	0.56	17.92	0.62	17.99	0.36	18.22	0.40	17.85	0.47	17.10	0.88	17.45	0.65	17.82	0.53	17.98	0.59	17.36	0.68	17.09	0.64	16.99	0.33	17.84	0.81
MnO	0.26	0.03	0.26	0.03	0.25	0.03	0.24	0.04	0.35	0.05	0.26	0.03	0.23	0.02	0.22	0.04	0.22	0.03	0.23	0.03	0.23	0.03	0.24	0.03	0.19	0.04	0.20	0.05	0.19	0.03	0.24	0.03	0.22	0.04	0.19	0.05	0.23	0.04	0.03	0.03	0.22	0.05
MgO	8.60	0.33	8.73	0.43	9.41	0.46	8.79	0.46	8.53	0.28	8.78	0.35	8.86	0.55	8.88	0.98	8.48	0.09	9.18	0.39	8.70	0.28	8.88	0.45	9.15	0.26	9.15	0.36	9.25	0.29	8.71	0.31	8.79	0.37	9.05	0.31	8.71	0.42	9.33	0.34	8.38	0.46
CaO	11.68	0.11	11.75	0.15	11.86	0.22	11.5	0.32	11.74	0.16	12.11	0.17	11.13	0.23	11.21	0.17	10.88	0.36	11.32	0.96	11.43	0.16	11.82	0.13	11.66	0.24	11.71	0.37	11.64	0.84	11.94	0.25	11.88	0.16	11.38	0.19	11.53	0.21	11.32	0.26	11.88	0.21
Na_2O	1.63	0.09	2.46	0.57	1.77	0.13	2.75	0.51	1.8	0.14	1.57	0.09	1.69	0.06	1.67	0.10	2.22	0.38	1.88	0.27	1.74	0.10	1.71	0.08	2.02	0.15	2.00	0.24	2.26	0.30	1.72	0.10	1.73	0.13	1.94	0.11	1.91	0.21	2.41	0.16	1.94	0.28
K2O	1.12	0.05	0.16	0.03	1.07	0.07	1.05	0.16	1.15	0.06	1.05	0.07	1.08	0.10	1.20	0.17	1.13	0.11	0.14	0.03	1.13	0.12	0.14	0.03	0.16	0.02	0.13	0.03	0.13	0.03	0.15	0.02	0.16	0.03	1.08	0.06	1.1	0.07	1.12	0.04	1.15	0.07
F	0.00	0.00	0	0.00	0	0.00	0	0.00	0	0.00	0	0.00	0.00	0.00	0.00	0.00	0	0.00	0	0.00	n.d.	n.d.	0	0.00	0	0.00	0	0.00	0	0.00	0	0.00	0	0.00	0	n.d.	0	0.00	0.21	0.01	n.a.	n.d.
Cl	0.03	0.02	0.03	0.02	0.02	0.01	0.02	0.01	0.02	0.01	0.03	0.01	0.02	0.01	0.03	0.01	0.02	0.01	0.03	0.02	n.d.	n.d.	0.03	0.02	0.03	0.02	0.03	0.02	0.03	0.02	0.03	0.02	0.03	0.02	0	n.d.	0.02	0.01	0.03	0.02	n.a.	n.d.
Total																																										
Cations (23 O)																																										
Si	6.252		6.236		6.243		6.214		6.262		6.327		6.294		6.216		6.260		6.129		6.323		6.187		6.274		6.267		6.187		6.290		6.258		6.343		6.267		6.197		6.373	
Al(iv)	1.748		1.764		1.757		1.786		1.738		1.673		1.706		1.784		1.740		1.871		1.677		1.813		1.726		1.733		1.813		1.710		1.742		1.657		1.733		1.803		1.627	
Al(vi)	0.504		0.557		0.455		0.487		0.531		0.472		0.516		0.539		0.551		0.464		0.589		0.519		0.533		0.546		0.483		0.602		0.579		0.580		0.544		0.524		0.654	
Fe(III)	0.342		0.312		0.400		0.086		0.268		0.180		0.557		0.591		0.388		0.721		0.319		0.538		0.477		0.389		0.414		0.357		0.440		0.247		0.247		0.209		0.026	
Ti	0.222		0.201		0.217		0.238		0.216		0.202		0.198		0.184		0.201		0.238		0.194		0.209		0.198		0.229		0.253		0.202		0.208		0.208		0.207		0.263		0.211	
Cr	0.004		0.006		0.004		0.005		0.004		0.004		0.007		0.006		0.007		0.006		0.005		0.006		0.006		0.006		0.007		0.006		0.007		0.006		0.005		0.007		0.005	
Fe(II)	1.947		1.953		1.743		2.165		2.012		2.116		1.706		1.684		1.914		1.506		1.927		1.752		1.739		1.761		1.762		1.865		1.794		1.921		1.986		1.914		2.208	
Mn	0.033		0.032		0.032		0.031		0.032		0.033		0.029		0.028		0.028		0.029		0.029		0.030		0.024		0.025		0.024		0.031		0.028		0.024		0.030		0.004		0.028	
Mg	1.949		1.938		2.089		1.989		1.918		1.993		1.989		1.969		1.911		2.035		1.937		1.946		2.024		2.043		2.057		1.937		1.946		2.015		1.970		2.079		1.870	
Ca	1.883		1.875		1.843		1.869		1.897		1.973		1.771		1.785		1.762		1.803		1.828		1.903		1.852		1.880		1.860		1.906		1.888		1.821		1.874		1.813		1.870	
Na	0.475		0.707		0.511		0.809		0.466		0.463		0.484		0.481		0.651		0.572		0.504		0.488		0.581		0.580		0.660		0.496		0.498		0.562		0.562		0.698		0.563	
K	0.215		0.030		0.203		0.203		0.221		0.204		0.205		0.228		0.218		0.027		0.215		0.027		0.030		0.025		0.024		0.029		0.030		0.206		0.213		0.214		0.220	
Na(M4)	0.117		0.125		0.155		0.131		0.103		0.027		0.229		0.215		0.238		0.197		0.172		0.097		0.148		0.120		0.140		0.092		0.112		0.179		0.126		0.187		0.130	
Na (A)	0.358		0.582		0.356		0.678		0.365		0.436		0.255		0.267		0.413		0.376		0.332		0.401		0.433		0.459		0.520		0.404		0.386		0.382		0.436		0.511		0.433	
A-site	0.573		0.612		0.559		0.881		0.587		0.640		0.460		0.494		0.630		0.402		0.547		0.428		0.463		0.484		0.544		0.433		0.415		0.588		0.649		0.724		0.653	
Total	15.573		15.612		15.559		15.881		15.587		15.640		15.460		15.494		15.630		15.402		15.547		15.428		15.463		15.484		15.544		15.433		15.415		15.588		15.649		15.724		15.653	
X_{Mg}	0.50		0.50		0.55		0.48		0.49		0.49		0.54		0.54		0.50		0.57		0.50		0.53		0.54		0.53		0.54		0.51		0.52		0.51		0.50		0.52		0.46	

n.a.-not analyzed.

Table 2.5: Average compositions of clinopyroxene in experiments.

Run No.	SVG-13		SVG-1		SVG-37		SVG-28		SVG-14		SVG-11		SVG-16	
P (kbar)	7		7		7		7		7		10		10	
T (° C)	835		850		875		950		1000		775		800	
n	10	1σ	15	1σ	14	1σ	15	1σ	10	1σ	7	1σ	8	1σ
Oxide (Wt.%)														
SiO_2	52.00	0.29	51.94	0.28	52.14	0.25	51.37	0.30	50.80	0.82	52.12	0.27	51.07	0.77
TiO_2	0.13	0.04	0.15	0.04	0.09	0.03	0.24	0.09	0.60	0.25	0.10	0.03	0.11	0.04
Al_2O_3	1.89	0.30	1.96	0.32	1.90	0.33	2.34	0.41	3.72	0.88	2.34	0.17	1.84	0.75
Cr_2O_3	0.01	0.01	0.00	0.00	0.06	0.06	0.02	0.04	0.02	0.01	0.00	0.00	0.00	0.00
FeO^T	11.12	0.06	11.28	0.29	11.73	0.40	12.85	0.74	12.45	1.01	11.44	0.14	11.23	0.63
MnO	0.33	0.05	0.32	0.03	0.31	0.05	0.32	0.03	0.30	0.08	0.30	0.03	0.34	0.02
MgO	12.05	0.30	12.43	0.21	12.29	0.22	12.34	0.27	13.18	0.80	11.71	0.07	12.21	0.28
CaO	21.90	0.83	21.21	0.43	21.31	0.40	20.16	1.58	18.74	2.02	21.03	0.30	21.30	1.48
Na_2O	0.43	0.09	0.38	0.07	0.44	0.06	0.43	0.06	0.46	0.04	0.40	0.04	0.33	0.14
Total	99.91		99.65		100.36		99.6		100.23		99.83		98.49	
Cations (6 O)														
Si	1.942		1.951		1.950		1.945		1.909		1.967		1.960	
Ti	0.004		0.004		0.002		0.007		0.014		0.003		0.003	
Al	0.082		0.087		0.080		0.104		0.164		0.104		0.086	
Cr	0.000		0.000		0.002		0.001		0.001		0.000		0.000	
Fe2+	0.351		0.358		0.360		0.390		0.391		0.361		0.355	
Mn	0.011		0.010		0.010		0.010		0.010		0.010		0.011	
Mg	0.678		0.700		0.686		0.697		0.737		0.659		0.689	
Ca	0.889		0.858		0.856		0.818		0.753		0.853		0.863	
Na	0.031		0.028		0.032		0.033		0.033		0.030		0.030	
Total	4.000		4.000		4.000		4.011		4.011		3.993		4.000	

Run No.	SVG-4		SVG-3		SVG-4		SVG-15		SVG-13		SVG-18		SVG-18	
P (kbar)	10		10		10		12.5		12.5		12.5		12.5	
T (° C)	850		900		950		800		850		900		1000	
n	3	1σ	4	1σ	3	1σ	2	1σ	15	1σ	10	1σ	28	1σ
Oxide (Wt.%)														
SiO_2	51.92	0.10	51.90	0.09	51.84	0.23	52.40	0.21	51.85	0.33	51.84	0.30	49.79	1.41
TiO_2	0.13	0.03	0.21	0.10	0.13	0.08	0.11	0.00	0.16	0.03	0.12	0.07	0.85	0.28
Al_2O_3	2.04	0.17	2.50	0.55	2.62	0.84	2.41	0.11	2.30	0.09	1.94	0.77	6.29	1.80
Cr_2O_3	0.02	0.03	12.22	0.01	0.01	0.01	0.02	0.01	0.01	0.01	0.00	0.01	0.01	0.01
FeO^T	11.14	0.20	0.31	0.06	11.80	0.96	11.78	0.01	11.06	0.01	11.21	0.03	13.00	1.32
MnO	0.32	0.01	12.16	0.03	0.32	0.05	0.33	0.00	0.34	0.02	0.34	0.04	0.23	0.07
MgO	12.47	0.06	19.95	0.27	11.80	0.10	12.11	0.12	12.20	0.29	12.38	0.30	11.80	0.35
CaO	21.16	0.17	0.43	1.10	20.01	1.09	20.80	0.12	21.13	0.87	21.30	1.14	17.79	2.23
Na_2O	0.46	0.06	0.01	0.07	0.83	0.11	0.40	0.00	0.46	0.10	0.42	0.17	0.77	0.25
Total	99.68		99.75		99.53		100.54		100.2		99.99		99.25	
Cations (6 O)														
Si	1.960		1.900		1.933		1.951		1.940		1.960		1.885	
Ti	0.004		0.006		0.004		0.003		0.005		0.000		0.010	
Al	0.091		0.110		0.112		0.106		0.105		0.086		0.236	
Cr	0.001		0.384		0.000		0.001		0.000		0.000		0.000	
Fe2+	0.352		0.009		0.364		0.368		0.364		0.354		0.412	
Mn	0.010		0.377		0.010		0.010		0.011		0.011		0.007	
Mg	0.702		1.089		0.675		0.676		0.686		0.690		0.677	
Ca	0.857		0.017		0.847		0.830		0.851		0.864		0.720	
Na	0.033		0.001		0.039		0.036		0.034		0.031		0.057	
Total	4.008		3.983		4.000		4.000		4.009		4.008		4.009	

Run No.	SVG-35		SVG-6		SVG-7		SVG-5		SVG-34-r		SVG-33	
P (kbar)	15		15		15		15		17.5		17.5	
T (° C)	835		900		950		1050		950		900	
n	6	1σ	7	1σ	10	1σ	23	1σ	10	1σ	10	1σ
Oxide (Wt.%)												
SiO_2	52.30	0.28	51.48	0.20	51.22	0.47	49.87	0.85	51.42	0.87	50.81	0.78
TiO_2	0.12	0.03	0.14	0.06	0.70	0.20	0.83	0.14	0.62	0.08	0.80	0.14
Al_2O_3	2.02	0.01	2.28	0.05	5.65	1.17	7.48	1.34	8.43	0.92	8.75	0.87
Cr_2O_3	0.01	0.01	0.01	0.02	0.00	0.01	0.01	0.01	0.02	0.01	0.01	0.01
FeO^T	11.14	0.04	11.55	0.85	10.27	0.45	11.13	0.95	8.94	0.70	9.11	0.78
MnO	0.30	0.02	0.32	0.06	0.14	0.05	0.16	0.00	0.09	0.03	0.09	0.02
MgO	12.30	0.49	12.28	0.21	12.10	0.20	11.08	0.37	10.83	0.23	10.44	0.28
CaO	21.64	0.01	20.34	0.70	18.01	0.77	17.54	1.40	16.82	0.30	17.80	0.08
Na_2O	0.42	0.07	0.46	0.08	1.22	0.25	1.07	0.16	2.42	0.29	2.28	0.21
Total	100.28		98.81		100.01		99.78		99.80		100.28	
Cations (6 O)												
Si	1.963		1.960		1.900		1.860		1.890		1.871	
Ti	0.003		0.004		0.020		0.018		0.017		0.022	
Al	0.090		0.102		0.247		0.329		0.368		0.378	
Cr	0.000		0.000		0.000		0.000		0.001		0.000	
Fe2+	0.300		0.368		0.316		0.347		0.294		0.280	
Mn	0.011		0.010		0.004		0.005		0.005		0.003	
Mg	0.691		0.605		0.670		0.600		0.579		0.572	
Ca	0.880		0.830		0.749		0.701		0.664		0.706	
Na	0.031		0.034		0.088		0.077		0.173		0.163	
Total	4.004		4.003		3.990		3.987		3.981		3.999	

Run No.	SVG-44		SVG-41		SVG-43		SVG-34-r		SVG-45		SVG-46	
P (kbar)	20		20		22.5		22.5		22.5		22.5	
T (° C)	900		850		850		900		950		1000	
n	18	1σ	9	1σ	10	1σ	9	1σ	18	1σ	11	1σ
Oxide (Wt.%)												
SiO_2	51.81	0.66	51.83	0.65	52.86	0.54	52.96	0.80	52.83	0.80	52.50	0.56
TiO_2	0.72	0.11	0.82	0.20	0.45	0.06	0.52	0.10	0.55	0.13	0.63	0.10
Al_2O_3	11.60	0.62	10.20	0.66	10.79	1.05	11.34	1.68	9.81	0.83	9.55	0.79
Cr_2O_3	0.01	0.01	0.01	0.01	0.02	0.01	0.01	0.01	0.01	0.01	0.01	0.01
FeO^T	7.77	0.43	8.10	0.36	7.13	0.39	7.26	0.28	7.5	0.29	8.42	0.33
MnO	0.06	0.02	0.09	0.02	0.07	0.04	0.1	0.03	0.09	0.05	0.13	0.03
MgO	9.16	0.31	9.91	0.22	8.94	0.52	8.87	0.63	9.36	0.31	10.20	0.29
CaO	10.29	0.38	10.80	0.05	15.90	0.43	14.5	0.86	16.47	0.63	16.05	0.44
Na_2O	3.8	0.35	3.27	0.20	4.37	0.25	3.96	0.19	3.55	0.15	2.96	0.16
Total	100.32		101.23		100.01		99.05		100.27		100.06	
Cations (6 O)												
Si	1.877		1.878		1.900		1.920		1.920		1.891	
Ti	0.020		0.022		0.012		0.014		0.015		0.017	
Al	0.490		0.438		0.460		0.480		0.419		0.409	
Cr	0.000		0.000		0.001		0.000		0.000		0.000	
Fe2+	0.235		0.246		0.210		0.220		0.227		0.260	
Mn	0.000		0.003		0.002		0.003		0.003		0.004	
Mg	0.404		0.534		0.481		0.485		0.506		0.550	
Ca	0.560		0.663		0.618		0.563		0.640		0.630	
Na	0.267		0.229		0.300		0.290		0.250		0.213	
Total	3.994		3.990		4.003		3.985		3.980		3.989	

Run No.	KAP-13		KAP-1		KAP-37		KAP-28		KAP-14		KAP-15		KAP-6	
P (kbar)	7		7		7		7		7		10		10	
T (° C)	835		850		875		950		1000		830		830	
n	3	1σ	10	1σ	15	1σ	22	1σ	10	1σ	21	1σ	22	1σ
Oxide (Wt.%)														
SiO_2	51.24	0.84	50.80	0.40	52.14	0.61	51.1	0.24	50.47	0.36	51.41	0.8	51.24	0.38
TiO_2	0.34	0.21	0.27	0.04	0.2	0.10	0.29	0.10	0.62	0.08	0.34	0.1	0.2	0.07
Al_2O_3	2.57	0.60	2.75	0.33	2.36	0.65	2.93	0.61	4.42	0.43	2.45	0.5	2.46	0.47
Cr_2O_3	0.05	0.02	0.04	0.02	0.07	0.07	0.07	0.10	0.02	0.01	0.02	0	0.03	0.01
FeO^T	11.82	0.33	12.34	0.40	12.38	0.70	12.7	0.71	13.00	0.44	11.66	0.8	11.8	0.65
MnO	0.36	0.07	0.33	0.03	0.34	0.07	0.36	0.06	0.42	0.02	0.35	0	0.32	0.03
MgO	11.21	0.33	10.8	0.20	11.36	0.87	11.4	0.48	12.78	0.87	10.82	0.6	10.74	0.40
CaO	21.16	1.29	21.46	0.44	21.19	1.29	20.6	1.44	17.96	0.75	21.79	0.8	22.05	0.44
Na_2O	1.16	0.01	0.88	0.06	0.96	0.43	0.81	0.16	0.81	0.04	0.81	0.1	0.66	0.08
Total	99.91		99.17		100.6		100.26		100.23		99.34		99.5	
Cations (6 O)														
Si	1.942		1.940		1.966		1.932		1.890		1.957		1.951	
Ti	0.010		0.008		0.006		0.008		0.016		0.007		0.006	
Al	0.115		0.124		0.100		0.131		0.196		0.110		0.110	
Cr	0.001		0.001		0.002		0.002		0.001		0.001		0.001	
Fe2+	0.375		0.391		0.386		0.402		0.409		0.371		0.376	
Mn	0.012		0.011		0.011		0.012		0.013		0.011		0.010	
Mg	0.633		0.600		0.636		0.643		0.710		0.614		0.610	
Ca	0.859		0.880		0.850		0.835		0.723		0.889		0.900	
Na	0.087		0.060		0.070		0.060		0.057		0.049		0.049	
Total	4.033		4.036		4.020		4.023		4.007		4.004		4.012	

Run No.	KAP-19		KAP-16		KAP-18		KAP-13		KAP-29		KAP-30		KAP-8	
P (kbar)	12.5		12.5		12.5		12.5		15		15		15	
T (° C)	900		830		900		1000		850		835		~900	
n	4	1σ	15	1σ	14	1σ	20	1σ	8	1σ	7	1σ	9	1σ
Oxide (Wt.%)														
SiO_2	51.71	0.58	51.03	0.08	51.14	0.85	49.83	1.96	51.44	0.24	50.67	0.85	50.34	0.37
TiO_2	0.21	0.05	0.24	0.06	0.3	0.15	0.87	0.42	0.2	0.06	0.28	0.19	0.00	0.08
Al_2O_3	2.18	0.41	3.03	1.12	2.91	0.94	5.4	2.33	2.63	0.33	3.44	1.85	6.01	0.40
Cr_2O_3	0.02	0.02	0.02	0.01	0.03	0.01	0.04	0.02	0	0.00	0.06	0.01	0.00	0.01
FeO^T	11.5	0.36	11.06	0.80	11.8	0.70	12.80	0.96	12.4	0.46	11.71	0.86	11.01	0.40
MnO	0.04	0.05	0.34	0.04	0.30	0.08	0.28	0.07	0.31	0.04	0.2	0.07	0.11	0.01
MgO	11.15	0.39	11.17	0.63	11.42	0.47	10.8	0.46	10.83	0.36	10.71	0.80	10.0	0.28
CaO	22.47	0.28	21.86	0.87	21.83	1.20	19.83	1.81	21.56	0.30	21.53	1.23	19.2	0.37
Na_2O	0.6	0.04	0.6	0.14	0.64	0.09	0.95	0.25	0.64	0.06	0.79	0.25	1.03	0.11
Total	99.96		99.44		100.15		99.89		99.96		99.75		99.58	
Cations (6 O)														
Si	1.957		1.940		1.932		1.878		1.950		1.929		1.891	
Ti	0.006		0.007		0.009		0.019		0.006		0.010		0.016	
Al	0.097		0.113		0.130		0.241		0.117		0.154		0.262	
Cr	0.001		0.001		0.001		0.001		0.000		0.001		0.001	
Fe2+	0.364		0.371		0.376		0.408		0.393		0.371		0.348	
Mn	0.001		0.011		0.009		0.009		0.010		0.010		0.003	
Mg	0.630		0.634		0.643		0.583		0.612		0.605		0.610	
Ca	0.911		0.892		0.871		0.787		0.874		0.878		0.773	
Na	0.044		0.044		0.047		0.070		0.047		0.058		0.111	
Total	4.010		4.016		4.016		4.017		4.009		4.013		4.016	

Run No.	KAP-7		KAP-9		KAP-33		KAP-35		KAP-44		KAP-41	
P (kbar)	15		15		17.5		20		20		20	
T (° C)	950		1050		900		850		900		850	
n	12	1σ	12	1σ	18	1σ	20	1σ	13	1σ	4	1σ
Oxide (Wt.%)												
SiO_2	48.72	0.81	47.17	0.87	50.05	0.73	50.26	0.87	51.3	0.83	50.61	0.43
TiO_2	0.96	0.17	1.25	0.14	0.94	0.10	0.69	0.12	0.73	0.12	0.85	0.06
Al_2O_3	7.28	0.71	9.00	0.82	8.49	0.73	10.05	0.64	11.09	0.96	10.23	0.20
Cr_2O_3	0.03	0.02	0.04	0.01	0.00	0.02	0.06	0.00	0.00	0.02	0.04	0.01
FeO^T	10.86	0.37	12.28	0.80	10.75	0.67	8.51	0.65	9.2	0.62	8.83	0.18
MnO	0.1	0.01	0.17	0.06	0.13	0.03	0.07	0.06	0.09	0.01	0.1	0.02
MgO	10.42	0.27	9.85	0.35	9.19	0.20	8.61	0.36	8.69	0.46	8.83	0.24
CaO	18.73	0.24	17.08	0.78	17.96	0.64	15.90	0.54	15.71	0.60	17.15	0.36
Na_2O	1.85	0.11	1.24	0.12	2.33	0.10	4.13	0.29	3.77	0.37	3.3	0.09
Total	99.67		98.58		100.29		100.26		100.7		99.94	
Cations (6 O)												
Si	1.804		1.780		1.874		1.920		1.870		1.860	
Ti	0.027		0.036		0.026		0.019		0.020		0.024	
Al	0.322		0.438		0.371		0.432		0.470		0.449	
Cr	0.001		0.001		0.001		0.002		0.001		0.001	
Fe2+	0.340		0.380		0.330		0.266		0.280		0.276	
Mn	0.003		0.006		0.004		0.002		0.003		0.003	
Mg	0.583		0.560		0.503		0.469		0.466		0.475	
Ca	0.783		0.713		0.714		0.633		0.613		0.676	
Na	0.113		0.094		0.167		0.282		0.266		0.236	
Total	4.004		4.014		3.990		4.025		4.000		4.008	

Run No.	KAP-43		KAP-38		KAP-48		KAP-49	
P (kbar)	22.5		22.5		22.5		22.5	
T (° C)	850		900		950		1000	
n	10	1σ	5	1σ	14	1σ	19	1σ
Oxide (Wt.%)								
SiO_2	52.26	0.66	51.22	0.83	51.96	0.87	50.87	0.86
TiO_2	0.67	0.17	1.06	0.62	0.70	0.20	1.06	0.22
Al_2O_3	13.1	1.10	13.1	0.95	12.14	1.20	11.8	1.07
Cr_2O_3	0.03	0.02	0.05	0.03	0.04	0.02	0.04	0.02
FeO^T	7.06	0.36	8.20	0.57	7.90	0.55	8.21	0.85
MnO	0.06	0.02	0.06	0.04	0.09	0.03	0.1	0.03
MgO	7.07	0.39	7	0.61	7.42	0.64	8.29	0.48
CaO	14.8	0.83	14.72	0.73	16.70	0.83	16.06	1.00
Na_2O	5.2	0.31	4.46	0.22	4.22	0.17	3.06	0.30
Total	100.63		100.06		100.41		100.7	
Cations (6 O)								
Si	1.887		1.884		1.880		1.865	
Ti	0.018		0.029		0.021		0.030	
Al	0.556		0.562		0.518		0.507	
Cr	0.001		0.001		0.001		0.001	
Fe2+	0.220		0.255		0.242		0.261	
Mn	0.002		0.003		0.003		0.003	
Mg	0.380		0.380		0.401		0.451	
Ca	0.584		0.574		0.614		0.626	
Na	0.353		0.314		0.297		0.251	
Total	3.990		3.992		3.960		3.987	

Table 2.6: Average compositions of orthopyroxene in the experiments.

Run No.	3VG-1		3VG-27		3VG-3		3VG-26		3VG-14		3VG-6		3VG-5		3VG-4		3VG-23		3VG-22		3VG-20		3VG-18		KAP-3		KAP-14		KAP-22	
P (kbar)	7		7		7		7		7		10		10		10		12.5-10		10		12.5		12.5		7		7		10	
T (°C)	850		875		900		950		1000		850		900		950		950		1000		950		1000		900		1000		1000	
n	10	1σ	1	1σ	17	1σ	26	1σ	14	1σ	8	1σ	32	1σ	12	1σ	17	1σ	26	1σ	13	1σ	5	1σ	23	1σ	8	1σ	4	1σ
SiO_2	49.5	0.25	50.27	-	49.33	0.37	50.54	0.48	49.55	0.27	50.96	0.66	50.34	0.39	49.00	0.54	50.27	0.55	49.68	0.37	49.59	0.39	48.22	0.66	50.59	0.64	51.64	0.71	49.06	0.10
TiO_2	0.16	0.06	0.22	-	0.3	0.16	0.21	0.06	0.41	0.03	0.11	0.07	0.23	0.04	0.26	0.04	0.22	0.04	0.34	0.05	0.26	0.04	0.35	0.06	0.31	0.13	0.34	0.05	0.33	0.03
Al_2O_3	2.28	0.38	1.51	-	3.23	0.30	3.28	0.39	4.41	0.54	2.42	1.24	3.36	0.45	3.79	0.63	4.83	0.67	5.22	0.65	4.85	0.48	6.07	0.68	3.45	0.61	3.74	0.34	5.60	0.17
Cr_2O_3	0.01	0.01	0.01	-	0.02	0.02	0.02	0.04	0.01	0.01	0.01	0.01	0.01	0.01	0.01	0.02	0.02	0.05	0.03	0.05	0.03	0.04	0.01	0.01	0.01	0.01	0.01	0.00	0.05	0.06
FeO^T	27.65	0.89	28.55	-	25.96	0.86	25.4	0.63	23.15	0.60	28.45	0.94	27.80	0.38	27.59	0.57	25.45	0.37	24.74	0.33	26.04	0.57	24.21	0.09	24.09	0.75	20.93	0.01	25.55	0.63
MnO	0.55	0.05	0.54	-	0.41	0.02	0.43	0.03	0.34	0.02	0.65	0.09	0.45	0.08	0.41	0.03	0.35	0.03	0.35	0.02	0.39	0.03	0.25	0.02	0.65	0.05	0.59	0.62	0.51	0.04
MgO	17.02	0.41	16.95	-	18.12	0.70	18.12	0.43	19.57	0.20	16.36	0.74	16.65	0.26	16.32	0.30	17.2	0.39	17.53	0.32	16.73	0.38	18.19	0.40	18.62	0.72	21.15	0.78	16.75	0.07
CaO	1.90	0.65	1.93	-	1.90	0.53	1.89	0.25	2.28	0.70	1.57	0.66	1.66	0.35	1.99	0.59	1.72	0.18	1.98	0.30	1.97	0.75	1.70	0.12	2.07	1.14	1.82	0.14	2.06	0.79
Na_2O	n.a	-	n.a	-	n.a	-	0.06	0.03	n.d.	-	0.1	0.12	0.06	0.03	n.a	-	0.09	0.03	0.09	0.04	0.1	0.05	n.a	-	0.10	0.11	0.06	0.03	0.09	0.04
K_2O	n.a	-	n.a	-	n.a	-	0.04	0.06	n.d.	-	0.05	0.04	0.04	0.02	n.a	-	0.03	0.02	0.03	0.02	0.03	0.02	n.a	-	0.06	0.08	0.01	0.01	0.03	0.01
Total	99.07		99.98		99.27		100.01		99.72		100.68		100.69		99.37		99.98		99.99		99.99		99.00		99.95		100.29		100.03	
Cations (6O)																														
Si	1.925		1.943		1.898		1.920		1.872		1.949		1.920		1.897		1.906		1.881		1.890		1.842		1.915		1.913		1.867	
Ti	0.005		0.006		0.009		0.006		0.012		0.003		0.007		0.008		0.006		0.010		0.007		0.010		0.009		0.009		0.009	
Al	0.104		0.069		0.146		0.147		0.196		0.109		0.151		0.173		0.207		0.233		0.218		0.273		0.154		0.163		0.251	
Cr	0.000		0.000		0.001		0.001		0.000		0.000		0.000		0.000		0.001		0.001		0.001		0.000		0.000		0.000		0.002	
Fe^{2+}	0.899		0.923		0.835		0.807		0.731		0.910		0.889		0.893		0.807		0.783		0.830		0.773		0.762		0.648		0.813	
Mn	0.018		0.018		0.013		0.014		0.011		0.021		0.015		0.013		0.011		0.011		0.013		0.008		0.021		0.019		0.016	
Mg	0.967		0.977		1.039		1.026		1.102		0.933		0.947		0.942		0.972		0.990		0.951		1.036		1.051		1.188		0.950	
Ca	0.079		0.080		0.078		0.077		0.092		0.064		0.068		0.083		0.070		0.080		0.080		0.070		0.084		0.072		0.084	
Na	n.d.		n.d.		n.d.		0.006		n.d.		0.007		0.004		n.d.		0.007		0.007		0.007		n.d.		0.007		0.004		0.007	
K	n.d.		n.d.		n.d.		0.002		n.d.		0.002		0.002		n.d.		0.001		0.001		0.001		n.d.		0.003		0.000		0.001	
Total	4.018		4.016		4.020		3.997		4.018		3.989		3.996		4.009		3.980		3.989		3.990		4.012		3.996		3.993		3.994	

n.a.-not analyzed; n.d.-not determined

Table 2.7: Average compositions of garnet in experiments.

Run No.	3VG-16		3VG-15		3VG-25		3VG-18		3VG-28		3VG-6		3VG-7		3VG-9		3VG-39		3VG-34	
P (kbar)	12.5		12.5		12.5		12.5		15		15		15		15		17.5		17.5	
T (°C)	850		900		950		1000		825		900		950		1000		850		950	
n	7	1σ	5	1σ	9	1σ	10	1σ	12	1σ	4	1σ	20	1σ	8	1σ	10	1σ	20	1σ
SiO_2	38.78	0.43	38.70	0.25	38.68	0.45	38.32	0.17	38.31	0.25	38.90	0.23	39.00	0.31	38.65	0.24	38.49	0.33	38.67	0.37
TiO_2	0.64	0.07	1.10	0.13	0.85	0.28	1.10	0.12	0.62	0.11	1.13	0.12	1.51	0.16	1.29	0.47	0.71	0.11	1.18	0.26
Al_2O_3	21.20	0.36	21.25	0.14	20.90	0.44	21.38	0.10	21.40	0.23	20.74	0.16	20.73	0.32	21.03	0.42	21.42	0.24	21.29	0.31
Cr_2O_3	n.d.	n.d.	n.d.	n.d.	n.d.	-	n.d.	-	n.d.	-	0	-	0.01	0.01	0.02	0.01	n.d.	-	n.d.	-
FeO^T	24.78	0.43	24.21	0.31	24.75	0.33	22.67	0.18	23.41	0.41	23.67	0.20	22.55	0.48	20.77	0.43	22.07	0.33	21.82	0.37
MnO	1.38	0.08	0.70	0.05	0.83	0.04	0.48	0.04	1.51	0.09	0.62	0.16	0.46	0.07	0.42	0.09	0.75	0.08	0.32	0.08
MgO	5.19	0.36	6.57	0.20	7.00	0.33	8.46	0.25	4.14	0.15	6.30	0.70	7.83	0.38	8.34	0.16	5.82	0.25	8.06	0.27
CaO	8.64	0.41	7.83	0.23	7.56	0.53	7.57	0.20	10.83	0.43	8.59	0.68	8.90	0.32	8.63	0.35	11.32	0.45	8.24	0.42
Na_2O	0.06	0.03	n.d.		0.06	0.04	0.04	0.02	0.06	0.06	0.07	0.01	0.10	0.03	0.06	0.01	0.07	0.03	n.d.	-
Total	100.85		100.43		100.69		100.01		100.37		99.82		99.99		99.20		100.35		99.61	
Cations (12 O)																				
Si	3.003		2.987		2.981		2.944		2.981		2.993		2.986		2.975		2.972		2.972	
Ti	0.037		0.064		0.049		0.064		0.036		0.066		0.087		0.075		0.041		0.068	
Al	1.936		1.927		1.904		1.936		1.971		1.900		1.877		1.908		1.949		1.928	
Fe2+	1.606		1.569		1.595		1.456		1.523		1.539		1.448		1.337		1.425		1.402	
Mn	0.091		0.046		0.054		0.031		0.100		0.041		0.030		0.027		0.049		0.021	
Mg	0.599		0.754		0.804		0.968		0.480		0.730		0.874		0.957		0.635		0.927	
Ca	0.717		0.648		0.624		0.623		0.903		0.716		0.698		0.712		0.936		0.678	
Na	0.009		0.009		0.009		0.006		0.009		0.011		0.015		0.007		0.010		n.d.	
Cr	n.d.		n.d.		n.d.		n.d.		n.d.		0.000		0.001		0.001		n.d.		n.d.	
Total	7.997		7.991		8.022		8.028		8.002		7.996		7.986		7.999		8.018		7.996	
X_{pyrope}	0.20		0.25		0.26		0.31		0.16		0.24		0.29		0.32		0.21		0.31	
$X_{grossular}$	0.24		0.21		0.20		0.20		0.30		0.24		0.22		0.23		0.31		0.22	
$X_{almandine}$	0.53		0.52		0.52		0.47		0.51		0.51		0.48		0.44		0.47		0.46	
$X_{spessartine}$	0.03		0.02		0.02		0.01		0.03		0.01		0.01		0.01		0.02		0.01	

Run No.	3VG-35		3VG-40		3VG-36		3VG-31		3VG-44		3VG-41		3VG-43		3VG-38		3VG-45		3VG-46	
P (kbar)	17.5		17.5		20		20		20		20		22.5		22.5		22.5		22.5	
T (°C)	850		900		850		900		900		950		850		900		950		1000	
n	25	1σ	10	1σ	10	1σ	16	1σ	21	1σ	16	1σ	11	1σ	11	1σ	20	1σ	20	1σ
SiO_2	37.99	0.25	38.73	0.34	38.57	0.30	38.53	0.39	39.32	0.73	38.87	0.27	38.11	0.29	38.05	0.33	38.71	0.29	38.97	0.26
TiO_2	1.38	0.22	1.56	0.11	0.78	0.14	1.16	0.15	1.14	0.20	1.28	0.17	0.98	0.14	1.35	0.13	1.28	0.14	1.30	0.12
Al_2O_3	21.00	0.33	21.47	0.40	21.79	0.25	21.42	0.35	21.15	0.08	21.7	0.28	21.86	0.21	21.68	0.27	21.43	0.03	21.17	0.04
Cr_2O_3	n.d.	-	n.d.	-	n.d.	-	n.d.	-	n.d.	-	n.d.	-	n.d.	-	n.d.	-	n.d.	-	n.d.	-
FeO^T	22.08	0.45	22.20	0.44	22.05	0.27	21.37	0.32	21.62	0.71	21.32	0.48	22.1	0.71	21.43	0.83	21.48	0.63	21.44	0.50
MnO	0.37	0.03	0.37	0.03	0.46	0.05	0.29	0.03	0.33	0.08	0.34	0.02	0.34	0.09	0.28	0.04	0.32	0.20	0.36	0.23
MgO	7.85	0.42	7.80	0.23	6.09	0.34	7.80	0.83	7.65	0.83	7.98	0.29	7.21	0.71	7.79	0.65	7.23	0.90	7.57	0.30
CaO	8.05	0.37	8.12	0.33	10.42	0.48	8.53	0.83	8.86	0.09	8.82	0.66	9.37	0.37	8.65	0.53	9.39	0.62	8.70	0.09
Na_2O	n.d.	-	0.13	0.04	0.13	0.03	n.d.	-	0.20	0.15	0.12	0.06	0.13	0.04	0.14	0.02	0.15	0.05	0.16	0.04
Total	98.71		100.40		100.28		99.21		100.28		100.41		101.08		100.17		99.98		100.03	
Cations (12 O)																				
Si	2.955		2.968		2.967		2.969		3.002		2.980		2.971		2.953		2.970		2.982	
Ti	0.081		0.091		0.045		0.068		0.066		0.072		0.066		0.078		0.074		0.075	
Al	1.925		1.932		1.975		1.945		1.902		1.948		1.957		1.952		1.937		1.909	
Fe2+	1.435		1.416		1.418		1.377		1.380		1.358		1.404		1.388		1.377		1.372	
Mn	0.024		0.024		0.029		0.019		0.021		0.022		0.022		0.018		0.021		0.023	
Mg	0.911		0.898		0.698		0.906		0.870		0.906		0.816		0.887		0.827		0.898	
Ca	0.671		0.664		0.858		0.704		0.726		0.720		0.762		0.724		0.772		0.718	
Na	n.d.		n.d.		0.019		n.d.		0.030		0.018		0.019		0.021		0.022		0.023	
Cr	n.d.		n.d.		n.d.		n.d.		n.d.		n.d.		n.d.		n.d.		n.d.		n.d.	
Total	8.002		7.995		8.010		7.990		7.997		8.003		8.006		8.003		7.999		8.000	
X_{pyrope}	0.30		0.30		0.23		0.30		0.29		0.30		0.27		0.30		0.28		0.30	
$X_{grossular}$	0.22		0.22		0.29		0.23		0.24		0.24		0.25		0.24		0.26		0.24	
$X_{almandine}$	0.47		0.47		0.47		0.46		0.46		0.45		0.47		0.46		0.46		0.46	
$X_{spessartine}$	0.01		0.01		0.01		0.01		0.01		0.01		0.01		0.01		0.01		0.01	

Table 2.7: Garnet compositions contd...

Run No.	KAP-4		KAP-16		KAP-15		KAP-33		KAP-18	
P (kbar)	10		12.5		12.5		12.5		12.5	
T (° C)	900		850		900		950		1000	
n	7	1σ	15	1σ	10	1σ	14	1σ	32	1σ
SiO_2	38.09	0.22	37.10	0.42	37.67	0.23	38.24	0.30	37.77	0.39
TiO_2	0.65	0.18	0.94	0.16	1.10	0.12	0.81	0.09	1.06	0.26
Al_2O_3	21.14	0.15	19.97	0.40	20.14	0.29	20.99	0.30	19.72	0.63
Cr_2O_3	n.d.	n.d.	0.04	0.02	0.04	0.02	n.d.	n.d.	0.05	0.03
FeO^T	25.85	0.33	24.39	0.31	24.96	0.31	24.72	0.23	23.73	0.29
MnO	1.35	0.17	1.26	0.31	0.84	0.17	0.83	0.11	0.73	0.06
MgO	4.98	0.33	4.17	0.16	5.10	0.14	6.39	0.25	7.19	0.66
CaO	8.23	0.47	9.27	0.81	8.03	0.49	8.24	0.37	7.67	0.71
Na_2O	0.06	0.02	0.07	0.06	0.09	0.02	0.06	0.06	0.06	0.02
Total	101.24		97.21		98.12		100.26		98.00	
Cations (12 O)										
Si	3.011		2.995		2.999		2.986		2.981	
Ti	0.038		0.057		0.066		0.047		0.065	
Al	1.924		1.900		1.889		1.920		1.840	
Fe2+	1.699		1.646		1.661		1.605		1.571	
Mn	0.090		0.086		0.057		0.055		0.049	
Mg	0.573		0.502		0.616		0.730		0.849	
Ca	0.681		0.802		0.685		0.685		0.651	
Na	0.007		0.011		0.013		0.009		0.009	
Cr			0.003		0.002				0.003	
Total	7.992		8.002		7.992		8.039		8.026	
X_{pyrope}	0.19		0.17		0.20		0.24		0.27	
$X_{grossular}$	0.23		0.26		0.23		0.22		0.21	
$X_{almandine}$	0.56		0.54		0.55		0.52		0.50	
$X_{spessartine}$	0.03		0.03		0.02		0.02		0.02	

Run No.	KAP-8		KAP-7		KAP-5		KAP-34		KAP-35	
P (kbar)	15		15		15		17.5		17.5	
T (° C)	900		950		1050		900		950	
n	4	1σ	20	1σ	25	1σ	10	1σ	13	1σ
SiO_2	38.12	0.15	38.48	0.18	37.87	0.37	38.62	0.20	37.91	0.24
TiO_2	1.25	0.03	1.48	0.17	1.34	0.26	1.39	0.16	1.56	0.26
Al_2O_3	20.16	0.16	20.09	0.29	20.04	0.46	20.71	0.23	20.16	0.49
Cr_2O_3	0.07	0.02	0.03	0.02	0.04	0.02	n.d.	n.d.	n.d.	n.d.
FeO^T	23.81	0.09	23.70	0.36	22.40	0.40	23.98	0.30	23.52	0.40
MnO	0.68	0.18	0.62	0.06	0.54	0.04	0.59	0.16	0.48	0.07
MgO	5.89	0.34	6.47	0.18	7.54	0.26	6.33	0.30	6.55	0.20
CaO	8.85	0.26	8.96	0.36	8.47	0.39	9.31	0.37	8.94	0.43
Na_2O	0.10	0.02	0.08	0.02	0.14	0.07	0.16	0.05	n.d.	
Total	98.95		99.88		98.47		100.56		99.12	
Cations (12 O)										
Si	2.986		2.992		2.971		2.972		2.969	
Ti	0.074		0.086		0.079		0.081		0.092	
Al	1.860		1.840		1.853		1.883		1.861	
Fe2+	1.564		1.541		1.476		1.521		1.540	
Mn	0.045		0.041		0.036		0.038		0.032	
Mg	0.690		0.750		0.882		0.726		0.765	
Ca	0.745		0.746		0.712		0.770		0.750	
Na	0.015		0.012		0.021		0.024			
Cr	0.004		0.002		0.002					
Total	8.002		8.008		8.033		8.017		8.009	
X_{pyrope}	0.23		0.24		0.29		0.24		0.25	
$X_{grossular}$	0.24		0.24		0.23		0.25		0.24	
$X_{almandine}$	0.51		0.50		0.48		0.50		0.50	
$X_{spessartine}$	0.01		0.01		0.01		0.01		0.01	

Run No.	KAP-40		KAP-42		KAP-38		KAP-44		KAP-41	
P (kbar)	17.5		17.5		20		20		20	
T (° C)	950		1000		850		900		950	
n	11	1σ	11	1σ	10	1σ	19	1σ	10	1σ
SiO_2	38.70	0.23	38.09	0.39	38.74	0.37	38.761	0.66	38.94	0.21
TiO_2	1.47	0.14	1.33	0.23	1.04	0.17	1.228	0.13	1.57	0.16
Al_2O_3	20.26	0.27	20.74	0.39	21.00	0.15	20.336	0.23	20.54	0.51
Cr_2O_3	n.d.	n.d.	n.d.	n.d.	n.d.	n.d.	n.d.	n.d.	n.d.	n.d.
FeO^T	23.70	0.33	22.61	0.46	23.10	0.56	22.662	0.66	23.46	0.26
MnO	0.59	0.11	0.60	0.02	0.55	0.17	0.572	0.32	0.48	0.06
MgO	6.93	0.23	7.34	0.16	8.14	0.49	8.136	0.56	6.64	0.27
CaO	8.74	0.44	9.03	0.31	10.73	0.89	9.606	0.61	8.86	0.61
Na_2O	0.11	0.03	0.08	0.03	0.15	0.04	0.221	0.11	0.12	0.03
Total	100.66		100.82		100.54		99.76		100.71	
Cations (12 O)										
Si	2.990		2.982		2.991		3.000		2.994	
Ti	0.085		0.076		0.060		0.072		0.091	
Al	1.839		1.889		1.919		1.860		1.860	
Fe2+	1.532		1.480		1.491		1.466		1.507	
Mn	0.038		0.039		0.036		0.038		0.031	
Mg	0.796		0.837		0.892		0.710		0.783	
Ca	0.721		0.740		0.888		0.799		0.729	
Na	0.016		0.012		0.022		0.033		0.018	
Cr										
Total	8.016		8.013		8.000		8.008		8.004	
X_{pyrope}	0.26		0.27		0.20		0.23		0.26	
$X_{grossular}$	0.23		0.24		0.30		0.26		0.24	
$X_{almandine}$	0.50		0.47		0.50		0.49		0.49	
$X_{spessartine}$	0.01		0.01		0.01		0.01		0.01	

Run No.	KAP-43		KAP-38		KAP-45		KAP-46	
P (kbar)	22.5		22.5		22.5		22.5	
T (° C)	850		900		950		1000	
n	11	1σ	9	1σ	14	1σ	17	1σ
SiO_2	39.04	0.32	38.63	0.22	38.90	0.35	38.891	0.63
TiO_2	1.06	0.14	1.29	0.13	1.35	0.30	1.295	0.34
Al_2O_3	21.29	0.18	21.09	0.36	20.78	0.07	20.76	0.08
Cr_2O_3	n.d.	n.d.	n.d.	n.d.	n.d.	n.d.	n.d.	n.d.
FeO^T	22.66	0.72	22.65	0.22	22.12	0.88	22.074	0.73
MnO	0.52	0.16	0.53	0.16	0.44	0.34	0.406	0.37
MgO	8.82	0.44	8.21	0.46	8.51	0.31	8.172	0.27
CaO	10.76	0.98	9.96	0.61	9.92	0.88	10.057	0.76
Na_2O	0.16	0.05	0.13	0.06	0.17	0.06	0.216	0.09
Total	100.81		100.40		100.60		99.87	
Cations (12 O)								
Si	2.993		2.989		2.992		3.003	
Ti	0.061		0.075		0.073		0.075	
Al	1.924		1.914		1.889		1.889	
Fe2+	1.446		1.459		1.427		1.425	
Mn	0.034		0.035		0.029		0.026	
Mg	0.831		0.713		0.748		0.710	
Ca	0.884		0.834		0.820		0.832	
Na	0.022		0.019		0.036		0.032	
Cr								
Total	7.999		8.009		8.004		7.994	
X_{pyrope}	0.21		0.24		0.25		0.24	
$X_{grossular}$	0.29		0.27		0.27		0.28	
$X_{almandine}$	0.48		0.48		0.47		0.48	
$X_{spessartine}$	0.01		0.01		0.01		0.01	

Table 2.8: Average compositions of plagioclase in the experiments.

Run No.	3VG-12		3VG-1		3VG-27		3VG-3		3VG-28		3VG-14		3VG-11		3VG-10		3VG-6		3VG-5	
P (kbar)	7		7		7		7		7		7		10		10		10		10	
T (°C)	825		850		875		900		950		1000		775		800		850		900	
n	20	1σ	18	1σ	20	1σ	25	1σ	20	1σ	13	1σ	16	1σ	18	1σ	38	1σ	35	1σ
Oxide Wt.%																				
SiO_2	56.64	0.28	56.64	0.62	57.16	0.33	56.53	0.81	56.23	1.00	53.44	0.48	57.05	0.57	57.11	0.30	57.19	0.33	56.62	0.46
TiO_2	0.01	0.02	0.01	0.01	0.01	0.02	0.01	0.01	0.01	0.02	0.02	0.03	0.00	0.01	0.01	0.01	0.01	0.02	0.02	0.02
Al_2O_3	27.45	0.21	27.27	0.45	27.27	0.20	27.15	0.40	27.66	0.56	28.46	0.57	27.10	0.34	27.12	0.29	27.00	0.41	27.18	0.31
FeO^T	0.62	0.06	0.59	0.12	0.52	0.04	0.52	0.10	0.53	0.08	0.77	0.12	0.52	0.07	0.52	0.05	0.53	0.16	0.52	0.11
MnO	0.01	0.01	0.01	0.01	0.01	0.01	0.01	0.01	0.01	0.01	0.02	0.01	0.01	0.01	0.01	0.01	0.01	0.01	0.01	0.01
MgO	0.00	n.d.	0.00	n.d.	0.00	n.d.	0.01	0.01	0.00	n.d.	0.00	n.d.	0.00	n.d.	0.00	n.d.	0.06	0.12	0.03	0.06
CaO	9.55	0.19	9.60	0.35	9.08	0.20	9.33	0.38	9.48	0.69	12.35	0.38	9.53	0.19	9.33	0.29	9.20	0.24	9.36	0.37
Na_2O	5.80	0.17	5.65	0.21	6.30	0.14	5.76	0.25	5.96	0.40	4.38	0.18	5.88	0.16	5.93	0.17	5.74	0.14	5.84	0.19
K_2O	0.67	0.10	0.56	0.09	0.40	0.02	0.25	0.06	0.38	0.05	0.30	0.09	0.46	0.06	0.45	0.08	0.59	0.14	0.45	0.03
Total	100.88		100.31		100.75		99.56		100.24		100.73		100.95		100.46		100.33		100.02	
Cations (8 O)																				
Si	2.538		2.544		2.564		2.551		2.527		2.411		2.555		2.558		2.564		2.548	
Ti	0.000		0.000		0.000		0.000		0.000		0.001		0.000		0.000		0.000		0.001	
Al	1.450		1.444		1.436		1.444		1.465		1.507		1.430		1.431		1.426		1.442	
Fe	0.018		0.022		0.019		0.020		0.020		0.029		0.019		0.019		0.020		0.020	
Mn	0.000		0.000		0.000		0.000		0.000		0.001		0.000		0.000		0.000		0.000	
Mg	0.000		0.000		0.000		0.001		0.000		0.000		0.000		0.000		0.004		0.002	
Ca	0.459		0.462		0.436		0.451		0.456		0.597		0.457		0.446		0.442		0.451	
Na	0.504		0.492		0.546		0.504		0.518		0.383		0.510		0.515		0.499		0.509	
K	0.038		0.032		0.023		0.014		0.022		0.017		0.026		0.026		0.034		0.026	
Total	5.008		4.999		5.012		4.985		5.010		5.005		4.999		4.997		4.989		4.996	
X_{albite}	0.50		0.50		0.54		0.52		0.52		0.38		0.51		0.52		0.51		0.52	
$X_{anorthite}$	0.46		0.47		0.43		0.47		0.46		0.60		0.46		0.45		0.45		0.46	
$X_{orthoclase}$	0.04		0.03		0.02		0.01		0.02		0.02		0.03		0.03		0.03		0.03	

Run No.	3VG-4		3VG-22		3VG-19		3VG-18		3VG-29		3VG-8		3VG-7		3VG-9		3VG-35		3VG-41	
P (kbar)	10		10		12.5		12.5		15		15		15		15		17.5		20	
T (°C)	950		1000		800		850		825		900		950		1050		950		950	
n	28	1σ	21	1σ	17	1σ	11	1σ	19	1σ	16	1σ	37	1σ	19	1σ	19	1σ	11	1σ
Oxide Wt.%																				
SiO_2	57.25	0.36	56.66	0.98	57.07	0.51	57.28	0.31	57.70	0.42	57.11	0.44	57.28	0.33	57.20	0.84	56.96	0.23	57.75	0.69
TiO_2	0.02	0.02	0.02	0.04	0.01	0.02	0.02	0.03	0.00	0.01	0.01	0.02	0.01	0.01	0.03	0.02	0.01	0.01	0.00	0.00
Al_2O_3	27.08	0.29	27.94	0.66	26.92	0.39	27.25	0.32	26.97	0.34	27.51	0.43	27.30	0.34	26.92	0.88	27.56	0.17	27.52	0.33
FeO^T	0.51	0.06	0.56	0.07	0.52	0.06	0.50	0.07	0.51	0.11	0.48	0.06	0.44	0.05	0.52	0.11	0.41	0.04	0.37	0.04
MnO	0.01	0.01	0.01	0.01	0.00	0.00	0.01	0.01	0.01	0.01	0.01	0.01	0.01	0.01	0.01	0.01	0.01	0.01	0.01	0.01
MgO	0.01	0.01	n.d	n.d.	0.00	n.d.	n.d	n.d.	n.d.	n.d.	0.00	n.d.	0.02	0.04	0.09	0.12	0.00	n.d.	0.00	n.d.
CaO	8.69	0.19	10.01	0.77	9.31	0.35	9.38	0.19	9.00	0.27	8.90	0.33	9.01	0.20	8.61	0.64	9.21	0.18	9.08	0.22
Na_2O	6.35	0.17	5.69	0.38	5.95	0.15	5.99	0.10	6.10	0.16	6.39	0.19	6.09	0.13	6.02	0.34	6.28	0.14	6.30	0.12
K_2O	0.46	0.05	0.43	0.07	0.41	0.05	0.44	0.04	0.39	0.08	0.41	0.05	0.41	0.04	0.39	0.08	0.38	0.03	0.40	0.08
Total	100.38		101.31		100.20		100.85		100.77		100.81		100.54		99.79		100.81		101.44	
Cations (8 O)																				
Si	2.564		2.522		2.562		2.555		2.573		2.549		2.560		2.572		2.544		2.569	
Ti	0.001		0.001		0.000		0.001		0.000		0.000		0.000		0.001		0.000		0.000	
Al	1.429		1.466		1.424		1.433		1.417		1.447		1.438		1.427		1.450		1.437	
Fe	0.019		0.021		0.020		0.019		0.019		0.018		0.016		0.019		0.015		0.014	
Mn	0.000		0.000		0.000		0.000		0.000		0.000		0.000		0.000		0.000		0.000	
Mg	0.001		0.000		0.000		0.000		0.000		0.000		0.001		0.006		0.000		0.000	
Ca	0.417		0.477		0.448		0.448		0.434		0.426		0.431		0.416		0.440		0.431	
Na	0.552		0.490		0.518		0.518		0.527		0.553		0.528		0.526		0.543		0.541	
K	0.027		0.024		0.024		0.025		0.022		0.023		0.023		0.022		0.020		0.023	
Total	5.010		5.002		4.996		4.999		4.993		5.016		4.997		4.987		5.013		5.006	
X_{albite}	0.55		0.49		0.52		0.52		0.54		0.55		0.54		0.55		0.54		0.54	
$X_{anorthite}$	0.42		0.48		0.45		0.45		0.44		0.42		0.44		0.43		0.44		0.43	
$X_{orthoclase}$	0.03		0.02		0.02		0.02		0.02		0.02		0.02		0.02		0.02		0.02	

Table 2.8: Plagioclase compositions...

Run No.	KAP-13		KAP-1		KAP-27		KAP-3		KAP-2		KAP-14	
P (kbar)	7		7		7		7		7		7	
T (°C)	825		850		875		900		950		1000	
n	35	1σ	29	1σ	14	1σ	39	1σ	34	1σ	17	1σ
Oxide Wt.%												
SiO_2	58.85	0.44	58.09	0.36	58.78	0.44	57.78	0.73	58.10	0.86	57.70	1.12
TiO_2	0.01	0.02	0.03	0.03	0.02	0.03	0.01	0.01	0.02	0.02	0.02	0.05
Al_2O_3	26.35	0.46	26.40	0.29	26.34	0.47	26.30	0.30	26.10	0.18	27.00	0.09
FeO^T	0.01	0.09	0.44	0.07	0.07	0.25	0.33	0.11	0.44	0.08	0.03	0.29
MnO	0.01	0.01	0.02	0.01	0.02	0.02	0.01	0.01	0.01	0.01	0.01	0.01
MgO	0.00	n.d.	0.02	0.05	0.03	n.d.	0.03	0.01	0.01	0.01	0.03	n.d.
CaO	7.74	0.35	8.20	0.11	7.20	0.40	8.20	0.48	7.74	0.33	8.70	0.83
Na_2O	7.03	0.18	6.86	0.17	7.06	0.15	6.41	0.38	7.08	0.16	6.39	0.83
K_2O	0.35	0.03	0.36	0.13	0.26	0.05	0.45	0.04	0.35	0.05	0.41	0.10
Total	100.66		101.10		100.47		99.61		99.96		100.83	
cations (8 O)												
Si	2.614		2.613		2.613		2.587		2.609		2.575	
Ti	0.000		0.001		0.001		0.000		0.001		0.001	
Al	1.379		1.378		1.370		1.385		1.384		1.418	
Fe	0.010		0.016		0.001		0.003		0.016		0.000	
Mn	0.000		0.001		0.001		0.000		0.000		0.000	
Mg	0.000		0.001		0.000		0.001		0.000		0.000	
Ca	0.370		0.389		0.378		0.390		0.373		0.410	
Na	0.607		0.574		0.606		0.553		0.616		0.552	
K	0.020		0.020		0.015		0.026		0.014		0.023	
Total	5.000		4.996		5.011		4.986		5.013		4.984	
X_{albite}	0.61		0.58		0.61		0.57		0.61		0.56	
$X_{anorthite}$	0.37		0.40		0.38		0.41		0.37		0.42	
$X_{orthoclase}$	0.02		0.02		0.01		0.03		0.01		0.02	

Run No.	KAP-11		KAP-10		KAP-6		KAP-5		KAP-4	
P (kbar)	10		10		10		10		10	
T (°C)	775		800		850		900		950	
n	14	1σ	18	1σ	28	1σ	31	1σ	32	1σ
Oxide Wt.%										
SiO_2	58.53	0.30	58.33	0.87	58.26	0.52	58.40	0.59	58.53	0.25
TiO_2	0.00	0.01	0.01	0.02	0.01	0.02	0.01	0.02	0.01	0.01
Al_2O_3	26.46	0.26	26.64	0.58	26.35	0.21	26.41	0.20	26.20	0.18
FeO^T	0.50	0.10	0.53	0.05	0.50	0.13	0.50	0.08	0.48	0.08
MnO	0.01	0.01	0.01	0.01	0.01	0.01	0.00	0.01	0.01	0.01
MgO	0.03	n.d.	0.00	n.d.	0.02	0.04	0.01	0.02	0.01	0.02
CaO	8.34	0.30	8.27	0.30	8.17	0.14	8.23	0.35	7.65	0.23
Na_2O	6.54	0.18	6.65	0.12	6.87	0.19	6.38	0.32	6.93	0.21
K_2O	0.44	0.12	0.38	0.09	0.34	0.11	0.37	0.06	0.38	0.10
Total	100.87		100.81		100.32		100.33		100.06	
cations (8 O)										
Si	2.605		2.596		2.604		2.607		2.611	
Ti	0.000		0.000		0.000		0.000		0.000	
Al	1.388		1.387		1.386		1.390		1.387	
Fe	0.018		0.019		0.019		0.018		0.018	
Mn	0.001		0.001		0.000		0.001		0.000	
Mg	0.000		0.000		0.002		0.001		0.001	
Ca	0.387		0.394		0.391		0.393		0.367	
Na	0.564		0.574		0.578		0.552		0.601	
K	0.025		0.021		0.019		0.021		0.021	
Total	4.996		5.000		5.000		4.984		5.006	
X_{albite}	0.57		0.58		0.59		0.57		0.61	
$X_{anorthite}$	0.40		0.40		0.40		0.41		0.37	
$X_{orthoclase}$	0.03		0.02		0.02		0.02		0.02	

Run No.	KAP-19		KAP-16		KAP-18		KAP-28		KAP-29		KAP-8	
P (kbar)	12.5		12.5		12.5		15		15		15	
T (°C)	800		850		1000		800		825		900	
n	18	1σ	19	1σ	16	1σ	20	1σ	18	1σ	18	1σ
Oxide Wt.%												
SiO_2	58.27	0.37	58.14	0.40	57.98	0.39	58.43	0.33	58.04	0.48	58.30	0.40
TiO_2	0.01	0.01	0.01	0.02	0.01	0.02	0.01	0.02	0.02	0.02	0.01	0.03
Al_2O_3	26.32	0.30	26.05	0.30	26.14	0.24	26.40	0.24	25.90	0.48	26.33	0.23
FeO^T	0.50	0.04	0.50	0.05	0.59	0.11	0.48	0.05	0.54	0.20	0.51	0.08
MnO	0.01	0.01	0.02	0.01	0.00	0.01	0.01	0.01	0.01	0.01	0.01	0.01
MgO	0.00	n.d.	0.06	n.d.	0.00	n.d.	0.00	n.d.	0.06	n.d.	0.01	n.d.
CaO	8.10	0.20	8.15	0.28	8.31	0.25	8.22	0.22	7.90	0.20	8.06	0.24
Na_2O	6.80	0.14	6.58	0.15	6.45	0.14	6.86	0.16	6.87	0.18	6.86	0.17
K_2O	0.35	0.06	0.33	0.05	0.38	0.03	0.32	0.05	0.34	0.08	0.36	0.03
Total	100.34		99.76		99.45		100.72		99.83		100.29	
cations (8 O)												
Si	2.596		2.612		2.599		2.602		2.614		2.600	
Ti	0.000		0.000		0.000		0.000		0.001		0.000	
Al	1.387		1.379		1.381		1.386		1.377		1.386	
Fe	0.019		0.020		0.022		0.018		0.000		0.018	
Mn	0.000		0.001		0.001		0.000		0.000		0.001	
Mg	0.000		0.000		0.000		0.000		0.003		0.001	
Ca	0.393		0.391		0.403		0.392		0.384		0.385	
Na	0.573		0.571		0.565		0.592		0.602		0.570	
K	0.020		0.019		0.021		0.012		0.020		0.021	
Total	4.990		4.993		4.999		5.005		4.990		4.997	
X_{albite}	0.58		0.59		0.57		0.60		0.59		0.59	
$X_{anorthite}$	0.40		0.40		0.41		0.39		0.38		0.39	
$X_{orthoclase}$	0.02		0.02		0.02		0.01		0.02		0.02	

Run No.	KAP-7		KAP-9		KAP-48		KAP-44		KAP-46	
P (kbar)	15		15		17.5		20		22.5	
T (°C)	950		1050		950		900		1000	
n	34	1σ	41	1σ	20	1σ	18	1σ	8	1σ
Oxide Wt.%										
SiO_2	58.62	0.51	58.66	0.53	58.37	0.84	58.21	0.28	58.45	0.26
TiO_2	0.02	0.02	0.02	0.02	0.01	0.02	0.01	0.03	0.01	0.03
Al_2O_3	26.34	0.63	26.15	0.40	25.94	0.66	26.86	0.20	26.60	0.19
FeO^T	0.50	0.09	0.50	0.09	0.46	0.04	0.47	0.04	0.38	0.06
MnO	0.01	0.01	0.01	0.01	0.01	0.01	0.01	0.01	0.01	0.01
MgO	0.04	0.05	0.05	0.05	0.00	n.d.	0.03	n.d.	0.30	n.d.
CaO	7.90	0.30	7.96	0.37	7.78	0.60	7.81	0.22	8.18	0.10
Na_2O	6.53	0.25	6.80	0.24	6.76	0.35	6.98	0.15	6.82	0.08
K_2O	0.40	0.08	0.41	0.04	0.37	0.08	0.30	0.12	0.32	0.09
Total	99.95		99.61		99.71		100.53		100.70	
cations (8 O)										
Si	2.583		2.613		2.631		2.596		2.600	
Ti	0.001		0.001		0.000		0.000		0.000	
Al	1.408		1.367		1.373		1.401		1.385	
Fe	0.019		0.021		0.017		0.017		0.010	
Mn	0.000		0.000		0.001		0.000		0.001	
Mg	0.003		0.003		0.000		0.000		0.000	
Ca	0.386		0.380		0.375		0.378		0.390	
Na	0.601		0.576		0.589		0.600		0.588	
K	0.023		0.023		0.021		0.017		0.018	
Total	5.000		4.993		4.987		5.012		5.000	
X_{albite}	0.60		0.59		0.60		0.60		0.59	
$X_{anorthite}$	0.38		0.38		0.39		0.38		0.39	
$X_{orthoclase}$	0.02		0.02		0.02		0.02		0.02	

Table 2.9: Glass (quenched melt) compositions (normalized to 100% anhydrous).

Run.No.	3VG28		3VG14		3VG05		3VG04		3VG22		3VG15		3VG20	
P (kbar)	7		7		10		10		10		12.5		12.5	
T (°C)	950		1000		900		950		1000		900		950	
n	6	1σ	6	1σ	4	1σ	9	1σ	4	1σ	4	1σ	8	1σ
SiO_2	65.30	0.70	61.44	1.11	73.34	2.34	68.38	0.29	59.87	0.52	64.83	0.73	68.24	0.36
TiO_2	0.42	0.08	0.72	0.09	0.19	0.05	0.28	0.06	0.80	0.10	0.14	0.04	0.32	0.05
Al_2O_3	18.27	0.88	17.82	1.08	14.69	0.84	16.97	0.32	18.81	2.41	20.00	0.33	17.23	0.86
FeO	5.13	0.19	5.20	0.23	2.07	0.04	2.76	0.08	8.41	0.90	2.80	0.23	3.15	0.22
MnO	0.09	0.04	0.12	0.03	0.07	0.03	0.04	0.03	0.08	0.04	0.06	0.02	0.04	0.04
MgO	0.82	0.07	1.70	0.71	0.34	0.05	0.36	0.06	0.99	0.82	0.27	0.05	0.44	0.11
CaO	2.17	0.33	5.41	1.21	2.31	0.16	1.43	0.16	5.47	1.13	0.65	0.06	2.59	0.43
Na_2O^*	5.40	0.32	5.23	0.53	3.37	0.15	5.27	0.15	6.06	0.79	6.99	1.10	4.94	0.44
K_2O	2.25	0.16	2.48	0.25	3.50	0.16	4.39	0.26	2.61	0.50	4.32	0.44	2.94	0.21
Cl	0.17	0.03	0.11	0.02	0.11	0.02	0.13	0.02	0.10	0.02	0.15	0.04	0.11	0.03
Analytical Total	92.64		96.46		93.34		94.82		94.27		90.19		93.37	
Mg #	0.22		0.37		0.22		0.19		0.25		0.15		0.20	
A/CNK	1.30		0.96		1.10		1.05		0.94		1.15		1.15	

Run.No.	3VG18		3VG08		3VG07		3VG09		3VG34		3VG35		3VG40	
P (kbar)	12.5		15		15		15		17.5		17.5		17.5	
T (°C)	1000		900		950		1050		900		950		950	
n	10	1σ	8	1σ	6	1σ	6	1σ	11	1σ	6	1σ	10	1σ
SiO_2	63.62	0.28	70.86	1.88	69.43	0.47	64.11	0.22	71.57	0.73	69.44	0.68	70.07	0.20
TiO_2	0.78	0.07	0.37	0.19	0.45	0.02	0.73	0.06	0.31	0.02	0.44	0.04	0.43	0.02
Al_2O_3	17.98	0.15	15.67	0.99	16.79	0.50	18.06	0.21	16.10	0.23	16.49	0.40	16.49	0.13
FeO	4.60	0.09	1.96	0.76	2.13	0.08	4.40	0.21	1.56	0.09	1.96	0.23	2.05	0.15
MnO	0.04	0.04	0.03	0.02	0.05	0.02	0.06	0.03	0.02	0.02	0.03	0.02	0.03	0.03
MgO	0.91	0.08	0.75	0.67	0.43	0.11	0.82	0.12	0.29	0.05	0.54	0.48	0.34	0.06
CaO	3.29	0.15	2.12	0.31	2.00	0.20	3.45	0.16	1.44	0.32	2.15	0.94	1.77	0.06
Na_2O^*	6.23	0.19	4.59	0.33	5.37	0.42	6.06	0.17	4.81	0.46	5.66	0.12	5.50	0.13
K_2O	2.90	0.08	3.51	0.72	3.20	0.13	2.22	0.06	3.75	0.07	3.15	0.13	3.11	0.07
Cl	0.10	0.02	0.13	0.03	0.15	0.02	0.08	0.03	0.16	0.04	0.14	0.02	0.21	0.04
Analytical Total	94.91		93.38		93.42		96.09		93.55		94.43		94.06	
Mg #	0.26		0.41		0.26		0.25		0.24		0.33		0.23	
A/CNK	0.99		1.06		1.10		1.08		1.11		1.04		1.10	

Run.No.	3VG42		3VG31		3VG44		3VG41		3VG38		3VG45		3VG48	
P (kbar)	17.5		20		20		20		22.5		22.5		22.5	
T (°C)	1000		900		900		950		900		950		1000	
n	16	1σ	10	1σ	11	1σ	11	1σ	12	1σ	8	1σ	6	
SiO_2	68.04	0.39	71.36	0.28	73.83	0.48	70.81	0.27	72.17	0.49	73.07	0.49	71.89	
TiO_2	0.87	0.06	0.30	0.03	0.23	0.04	0.33	0.04	0.26	0.10	0.34	0.03	0.51	
Al_2O_3	17.45	0.13	15.75	0.12	16.03	0.26	15.61	0.14	15.43	0.12	15.11	0.10	15.39	
FeO	3.66	0.14	1.20	0.08	1.26	0.11	1.39	0.06	1.10	0.08	1.42	0.10	1.66	
MnO	0.03	0.02	0.03	0.02	0.02	0.02	0.02	0.03	0.03	0.02	0.03	0.03	0.02	
MgO	0.75	0.08	0.26	0.10	0.27	0.03	0.27	0.03	0.23	0.06	0.25	0.04	0.33	
CaO	1.65	0.10	1.10	0.26	2.94	0.06	1.36	0.06	1.06	0.08	1.31	0.06	1.53	
Na_2O^*	4.66	0.11	5.66	0.16	3.97	0.11	5.95	0.15	3.96	0.24	4.33	0.16	5.17	
K_2O	2.93	0.03	3.86	0.06	1.13	0.07	3.89	0.06	5.43	0.16	3.92	0.13	3.30	
Cl	0.16	0.03	0.13	0.02	0.22	0.03	0.17	0.02	0.36	0.04	0.21	0.02	0.17	
Analytical Total	93.34		91.73		89.98		93.16		91.23		93.95		94.13	
Mg #	0.27		0.28		0.28		0.26		0.27		0.24		0.26	
A/CNK	1.30		0.99		1.42		0.97		1.00		1.08		1.06	

Run.No.	KAP02		KAP14		KAP05		KAP04		KAP22		KAP15		KAP20	
P (kbar)	7		7		10		10		10		12.5		12.5	
T (°C)	950		1000		900		950		1000		900		950	
n	6	1σ	5	1σ	10	1σ	7	1σ	7	1σ	10	1σ	6	1σ
SiO_2	58.77	0.15	61.45	0.18	72.61	0.96	68.59	0.20	59.47	1.26	69.03	1.07	68.73	0.63
TiO_2	0.28	0.06	0.92	0.08	0.22	0.03	0.29	0.01	0.95	0.09	0.37	0.04	0.49	0.02
Al_2O_3	22.90	0.19	17.54	0.31	14.78	0.30	20.36	0.12	18.86	0.58	16.76	0.34	17.22	0.17
FeO	5.03	0.21	5.13	0.26	2.17	0.15	3.71	0.12	7.71	0.82	2.31	0.13	3.38	0.14
MnO	0.14	0.04	0.15	0.03	0.05	0.03	0.08	0.04	0.15	0.04	0.03	0.03	0.04	0.04
MgO	0.46	0.06	1.59	0.12	0.32	0.03	0.34	0.01	1.01	0.33	0.42	0.05	0.56	0.08
CaO	1.86	0.07	4.78	0.16	2.36	0.06	1.36	0.05	5.55	0.39	2.78	0.05	3.21	0.24
Na_2O^*	7.89	0.31	5.51	0.36	4.17	0.19	6.84	0.26	4.54	0.41	5.32	0.14	3.86	0.39
K_2O	2.80	0.11	2.80	0.59	3.26	0.07	4.38	0.05	1.82	0.16	2.83	0.04	2.44	0.14
Cl	0.07	0.04	0.13	0.02	0.03	0.02	0.08	0.04	0.04	0.02	0.04	0.02	0.06	0.01
Analytical Total	98.76		96.72		92.00		96.42		93.15		89.84		90.77	
Mg #	0.14		0.36		0.21		0.14		0.19		0.25		0.23	
A/CNK	1.32		0.94		1.04		0.90		1.11		1.06		1.27	

Run.No.	KAP18		KAP08		KAP09		KAP34		KAP35		KAP40		KAP42	
P (kbar)	12.5		15		15		17.5		17.5		17.5		17.5	
T (°C)	1000		900		1050		900		950		950		1000	
n	8	1σ	4	1σ	10	1σ	9	1σ	6	1σ	16	1σ	9	1σ
SiO_2	62.47	0.37	67.10	2.88	60.24	0.66	72.18	0.72	69.86	0.70	69.35	1.46	63.77	0.51
TiO_2	0.69	0.05	0.80	0.37	1.15	0.06	0.30	0.05	0.45	0.04	0.46	0.07	1.01	0.07
Al_2O_3	18.39	0.30	16.31	0.43	18.41	0.29	15.87	0.26	16.41	0.40	16.73	0.67	17.82	0.46
FeO	5.58	0.27	2.86	1.06	5.76	0.25	1.58	0.21	2.23	0.44	2.06	0.26	4.53	0.18
MnO	0.10	0.03	0.08	0.02	0.05	0.04	0.04	0.02	0.06	0.03	0.03	0.02	0.06	0.04
MgO	0.79	0.17	1.07	1.10	0.78	0.14	0.32	0.25	0.47	0.29	0.49	0.43	0.65	0.25
CaO	3.04	0.22	2.93	1.84	3.41	0.33	1.82	0.14	2.28	0.14	2.54	0.27	3.27	0.13
Na_2O^*	6.50	0.31	5.57	0.11	7.50	0.29	4.86	0.15	5.23	0.06	5.32	0.84	6.83	0.19
K_2O	2.40	0.30	3.42	0.27	2.84	0.25	3.16	0.82	2.81	0.71	2.87	1.11	2.36	0.97
Cl	0.04	0.04	0.07	0.01	0.06	0.02	0.10	0.03	0.08	0.04	0.09	0.03	0.07	0.04
Analytical Total	95.30		91.70		94.18		92.28		93.70		93.29		97.01	
Mg #	0.20		0.40		0.19		0.27		0.27		0.30		0.20	
A/CNK	1.08		0.95		0.96		1.14		1.11		1.08		1.01	

Run.No.	KAP36		KAP31		KAP44		KAP41		KAP43		KAP38		KAP45		KAP48	
P (kbar)	20		20		20		20		22.5		22.5		22.5		22.5	
T (°C)	850		900		900		950		850		900		950		1000	
n	7	1σ	10	1σ	7	1σ	10	1σ	5	1σ	16	1σ	9	1σ	19	1σ
SiO_2	73.00	0.23	71.89	0.32	72.63	0.40	71.93	0.71	73.91	0.57	71.11	0.84	73.16	0.35	71.21	0.23
TiO_2	0.19	0.02	0.33	0.04	0.27	0.02	0.36	0.06	0.13	0.02	0.27	0.04	0.34	0.04	0.49	0.03
Al_2O_3	16.09	0.17	16.60	0.18	16.10	0.17	16.04	0.37	15.96	0.14	15.98	0.27	15.70	0.25	15.66	0.12
FeO	1.01	0.06	1.33	0.06	1.13	0.07	1.54	0.06	1.04	0.08	1.09	0.16	1.37	0.07	1.64	0.11
MnO	0.03	0.02	0.03	0.03	0.02	0.03	0.02	0.03	0.01	0.01	0.02	0.02	0.02	0.02	0.03	0.03
MgO	0.17	0.04	0.19	0.03	0.20	0.07	0.20	0.04	0.24	0.10	0.27	0.32	0.17	0.03	0.30	0.02
CaO	1.30	0.07	1.36	0.11	1.66	0.08	1.71	0.07	1.67	0.08	1.65	0.77	1.54	0.06	1.92	0.10
Na_2O^*	4.19	0.17	5.19	0.33	4.39	0.39	5.21	0.21	3.84	0.45	5.29	0.16	4.22	0.35	5.40	0.82
K_2O	3.89	0.16	3.01	0.14	3.51	0.25	2.88	0.06	2.86	0.23	4.22	0.34	3.31	0.06	3.18	0.03
Cl	0.14	0.03	0.08	0.02	0.10	0.04	0.08	0.03	0.24	0.08	0.11	0.01	0.09	0.02	0.07	0.03
Analytical Total	90.66		91.27		92.40		93.02		87.46		91.63		92.82		96.32	
Mg #	0.23		0.20		0.24		0.19		0.29		0.30		0.18		0.25	
A/CNK	1.17		1.20		1.16		1.13		1.30		0.98		1.20		1.02	

Na_2O (wt. %) corrected for Na loss except for KAP02 where the uncorrected analysis is reported.

Std deviations reported are for uncorrected analyses.

Table 2.10: Magnetite compositions.

Run. No.	3VG-27		3VG-3		3VG-26		3VG-14		KAP30		KAP-22	
P (kbar)	7		7		7		7		7		10	
T(°C)	875		900		950		1000		900-850		1000	
n	10	1σ	17	1σ	18	1σ	1	1σ	1	1σ	9	1σ
Oxide Wt.%												
SiO_2	1.53	1.45	0.94	0.92	0.81	0.98	0.60	-	0.97	-	3.67	2.84
TiO_2	6.17	4.37	10.17	0.24	7.79	0.48	7.28	-	3.68	-	12.43	0.76
Al_2O_3	2.10	0.51	3.71	0.21	4.27	0.43	5.04	-	2.52	-	7.70	0.62
Cr_2O_3	0.01	0.01	0.09	0.08	0.04	0.02	0.05	-	0.10	-	0.58	0.07
FeO	35.89	2.82	38.54	0.92	36.23	1.21	33.44	-	32.95	-	44.19	3.25
Fe_2O_3	50.26		41.55		46.30		47.94		55.66		25.54	
MnO	0.38	0.13	0.26	0.02	0.25	0.02	0.28	-	0.45	-	0.29	0.03
MgO	1.46	0.32	1.71	0.31	1.92	0.20	3.33	-	1.41	-	2.08	0.24
CaO	0.16	0.16	0.32	0.09	0.34	0.28	-	-		-	0.64	0.70
Total	97.97		97.28		97.93		97.94		97.75		97.12	
Cations (4O)												
Si	0.058		0.036		0.030		0.022		0.037		0.134	
Ti	0.176		0.289		0.220		0.202		0.105		0.342	
Al	0.094		0.165		0.189		0.219		0.113		0.332	
Cr	0.000		0.002		0.001		0.001		0.002		0.011	
Fe^{3+}	1.437		1.182		1.310		1.332		1.599		0.700	
Fe^{2+}	1.139		1.220		1.135		1.032		1.048		1.353	
Mn	0.012		0.008		0.008		0.009		0.015		0.009	
Mg	0.083		0.096		0.107		0.183		0.080		0.114	
Sum	3.000		2.999		3.000		3.000		2.999		2.994	

Fe^{3+} determined by stoichiometry.

Table 2.11: Modal proportion of phases estimated using a combination of grayscale thresholding of backscattered electron images and massbalance.

3VG P (kbar) T (°C)	7 825	7 900	7 950	7 1000	10 850	10 900	10 1000	12.5 850	12.5 900	12.5 950	12.5 1000	15 900	15 950	17.5 850	17.5 900	17.5 950	17.5 1050	20 850	20 900	20 950	22.5 900	22.5 950	22.5 1000
Residue (wt.%)																							
Garnet	0.0	0.0	0.0	0.0	0.0	0.0	0.0	2.5	0.3	4.7	8.4	21.2	25.1	8.5	31.3	33.2	28.3	14.3	33.8	34.1	30.1	33.6	36.1
Cpx	6.4	14.2	37.6	39.8	11.6	16.9	42.0	17.6	32.9	32.0	50.0	33.4	37.7	24.0	56.4	57.7	71.7	85.7	66.2	65.9	69.9	66.4	63.9
Plag	36.2	48.7	35.8	35.3	27.7	34.1	37.4	21.9	34.9	20.1	18.2	26.1	18.2	13.3	7.0	5.3	0	0	0	0	0	0	0
Hornblende	52.9	26.9	17.0	21.6	49.2	40.7	20.6	53.2	31.9	37.6	18.8	19.3	19.0	49.6	5.3	3.8	0	0	0	0	0	0	0
Opx	0.0	10.3	9.6	3.2	6.2	8.3	0.0	0.0	0.0	5.6	4.5	0.0	0	0	0	0	0	0	0	0	0	0	0
Quartz	4.5	0.0	0.0	0.0	5.3	0.0	0.0	4.8	0.0	0.0	0.0	0.0	0	4.6	0	0	0	0	0	0	0	0	0
Total (*Residue*)	100	100	100	100	100	100	100	100	100	100	100	100	100	100	100	100	100	100	100	100	100	100	100
Melt Fraction (wt)	0	0.08	0.17	0.28	0.04	0.05	0.25	0.10	0.08	0.20	0.25	0.12	0.22	0.10	0.35	0.28	0.36	0.19	0.26	0.27	0.24	0.26	0.28

KAP P (kbar) T (°C)	7 850	7 900	7 950	7 1000	10 850	10 900	10 950	10 1000	12.5 850	12.5 900	12.5 950	12.5 1000	15 900	15 950	15 1050	17.5 850	17.5 900	17.5 950	17.5 1050	20 850	20 900	20 950	22.5 900	22.5 950	22.5 1000
Residue (wt.%)																									
Garnet	0	0	0	0	2.2	3.7	0	0	5.3	3.7	12.7	8.8	18.1	21.7	16.7	20.4	28.3	27.3	24.6	30.2	34.1	26.9	32.0	31.8	33.9
Cpx	9.6	21.9	30.3	47.6	14.7	20.4	32.9	42.9	17.4	20.4	27.1	50.7	33.8	32.6	70.8	26.1	43.7	45.2	67.1	55.2	60.6	57.2	68.0	68.2	61.7
Plag	30.6	35.9	37.9	44.1	26.2	25.9	30.2	32.9	25.6	25.9	25.8	23.7	29.0	22.1	12.5	17.9	15.2	15.4	8.3	14.6	5.2	11.1	0	0	4.4
Hornblende	54.3	34.9	27.2	0	54.1	50.0	36.9	24.2	47.9	50.0	34.4	16.8	19.1	23.7	0	29.1	12.9	12.1	0	0	0	4.8	0	0	0
Opx	0	7.3	4.6	8.4	0	0	0	0	0	0	0	0	0	0	0	0	0	0	0	0	0	0	0	0	0
Quartz	5.5	0	0	0	2.8	0	0	0	3.8	0	0	0	0	0	0	6.5	0	0	0	0	0	0	0	0	0
Total (*Residue*)	100.0	100.0	100.0	100.0	100.0	100.0	100.0	100.0	100.0	100.0	100.0	100.0	100.0	100.0	100.0	100.0	100.0	100.0	100.0	100.0	100.0	100.0	100.0	100.0	100.0
Melt Fraction (wt)	0.04	0.11	0.24	0.22	0.05	0.14	0.13	0.20	0.10	0.16	0.19	0.23	0.18	0.14	0.35	0.09	0.26	0.18	0.32	0.13	0.26	0.20	0.28	0.24	0.24

Table 2.12: Reaction coefficents for dehydration melting reactions determined by mass balance using singular value decomposition.

	per unit weight of reactants								per unit weight of quartz reacted							
3VG	Hbl	Plag	Qtz		Grt	Cpx	Opx	Melt	Hbl	Plag	Qtz		Grt	Cpx	Opx	Melt
7kbar	0.11	0.14	0.75	=	-	0.27	0.06	0.32	0.15	0.18	1.00	=	-	0.36	0.09	0.43
10kbar	0.11	0.03	0.86	=	-	0.22	0.13	0.25	0.13	0.03	1.00	=	-	0.26	0.15	0.29
12.5 kbar	0.16	0.22	0.62	=	0.10	0.39	-	0.31	0.25	0.34	1.00	=	0.16	0.62	-	0.49
15 kbar	0.09	0.17	0.74	=	0.05	0.22	-	0.30	0.12	0.22	1.00	=	0.07	0.29	-	0.40
17.5 kbar	0.16	0.23	0.61	=	0.12	0.45	-	0.26	0.26	0.36	1.00	=	0.19	0.72	-	0.42
20 kbar	0.14	0.27	0.59	=	0.10	0.46	-	0.25	0.23	0.46	1.00	=	0.18	0.77	-	0.41
22.5 kbar	0.20	0.30	0.50	=	0.18	0.64	-	0.20	0.40	0.59	1.00	=	0.35	1.28	-	0.40
KAP																
7kbar*	0.07	0.29	0.64	=	-	0.13	0.02	0.44	0.11	0.45	1.00	=	-	0.21	0.03	0.68
10kbar	0.07	0.18	0.75	=	0.05	0.15	-	0.31	0.09	0.24	1.00	=	0.06	0.20	-	0.41
12.5 kbar	0.10	0.24	0.66	=	0.08	0.21	-	0.34	0.16	0.37	1.00	=	0.13	0.32	-	0.52
15 kbar	0.19	0.27	0.54	=	0.18	0.35	-	0.33	0.35	0.50	1.00	=	0.33	0.65	-	0.62
17.5 kbar	0.14	0.26	0.60	=	0.13	0.30	-	0.30	0.22	0.44	1.00	=	0.22	0.49	-	0.49
20 kbar	0.16	0.31	0.53	=	0.16	0.44	-	0.27	0.31	0.59	1.00	=	0.31	0.84	-	0.51
22.5 kbar	0.20	0.41	0.39	=	0.21	0.58	-	0.26	0.50	1.05	1.00	=	0.53	1.48	-	0.66

Mass balance estimated for the 900 °C experiment in all cases except at 7 kbar, where mass balance was analysed for 950 °C experiments.

* melt composition for mass balance from the 1000 °C experiment.

Table 2.13: Modal mass balance calculated by converting reaction coefficients from Table 2.12.

	modal mass balance (per unit volume of quartz reacted)							
3VG								
	Hbl	**Plag**	**Qtz**		**Grt**	**Cpx**	**Opx**	**Melt**
7kbar	1.76	0.79	1.00	=	-	1.03	0.12	2.34
10kbar	1.57	0.13	1.00	=	-	0.74	0.21	1.58
12.5 kbar	3.00	1.49	1.00	=	0.83	1.81	-	2.71
15 kbar	1.45	0.96	1.00	=	0.37	0.84	-	2.23
17.5 kbar	3.09	1.57	1.00	=	0.99	2.10	-	2.34
20 kbar	2.70	1.96	1.00	=	0.90	2.22	-	2.30
22.5 kbar	4.72	2.53	1.00	=	1.78	3.69	-	2.21
KAP								
7kbar	1.29	1.95	1.00	=	-	0.60	0.04	3.76
10kbar	1.08	1.04	1.00	=	0.33	0.58	-	2.26
12.5 kbar	1.87	1.58	1.00	=	0.65	0.91	-	2.86
15 kbar	4.14	2.14	1.00	=	1.69	1.88	-	3.42
17.5 kbar	2.65	1.87	1.00	=	1.13	1.43	-	2.75
20 kbar	3.71	2.54	1.00	=	1.59	2.43	-	2.86
22.5 kbar	5.92	4.49	1.00	=	2.72	4.27	-	3.70

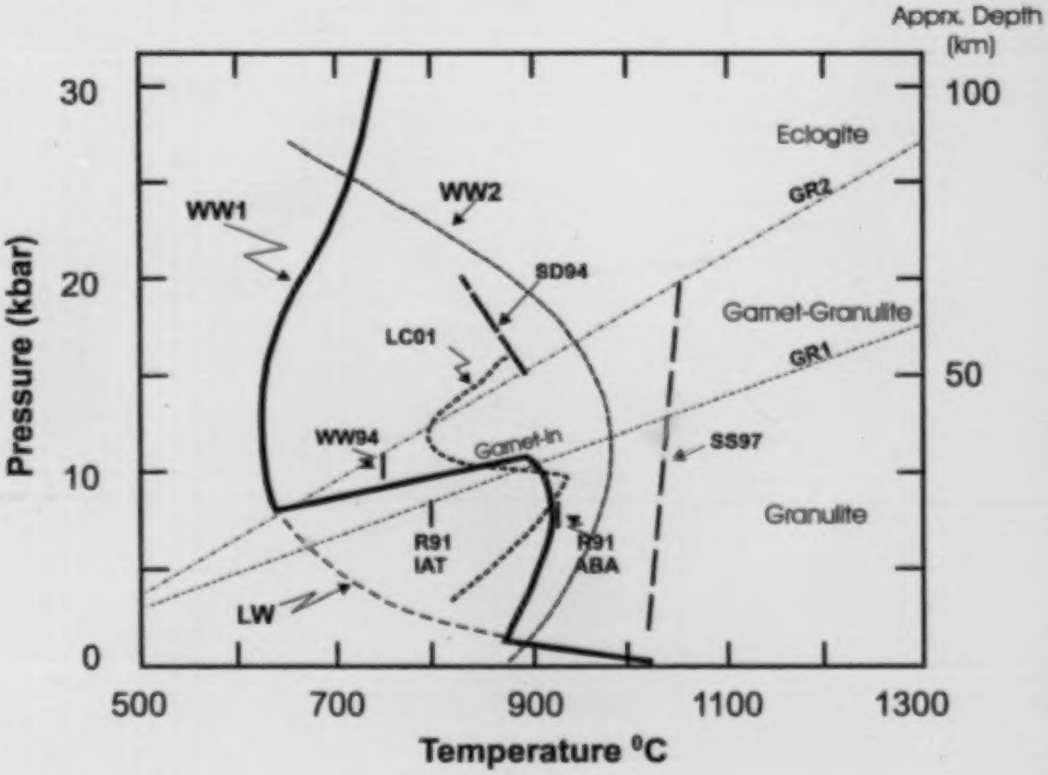

Figure 2.1: P-T diagram showing experimental constraints on dehydration melting solidus of metabasalts. The solid S-shaped curve labelled WW1 is considered the minimum conditions of dehydration melting of metabasalts (after Wolf and Wyllie, 1993). Other solidus curves shown are: R91- Rushmer(1991), ABA- alkali basalt, IAT- island-arc tholeiite; WW94- Wolf and Wyllie (1994); SD94- Sen and Dunn (1994); SS97- Springer and Seck (1997); LC01- Lopez and Castro (2001). Other curves shown on the figure are LW- water-saturated solidus of basalts (Lambert and Wyllie, 1972); WW2- amphibole-out curve (Wolf and Wyllie, 1993); GR1, GR2 - garnet-in and plagioclase-out on quartz-tholeiites, respectively (Green and Ringwood, 1967)

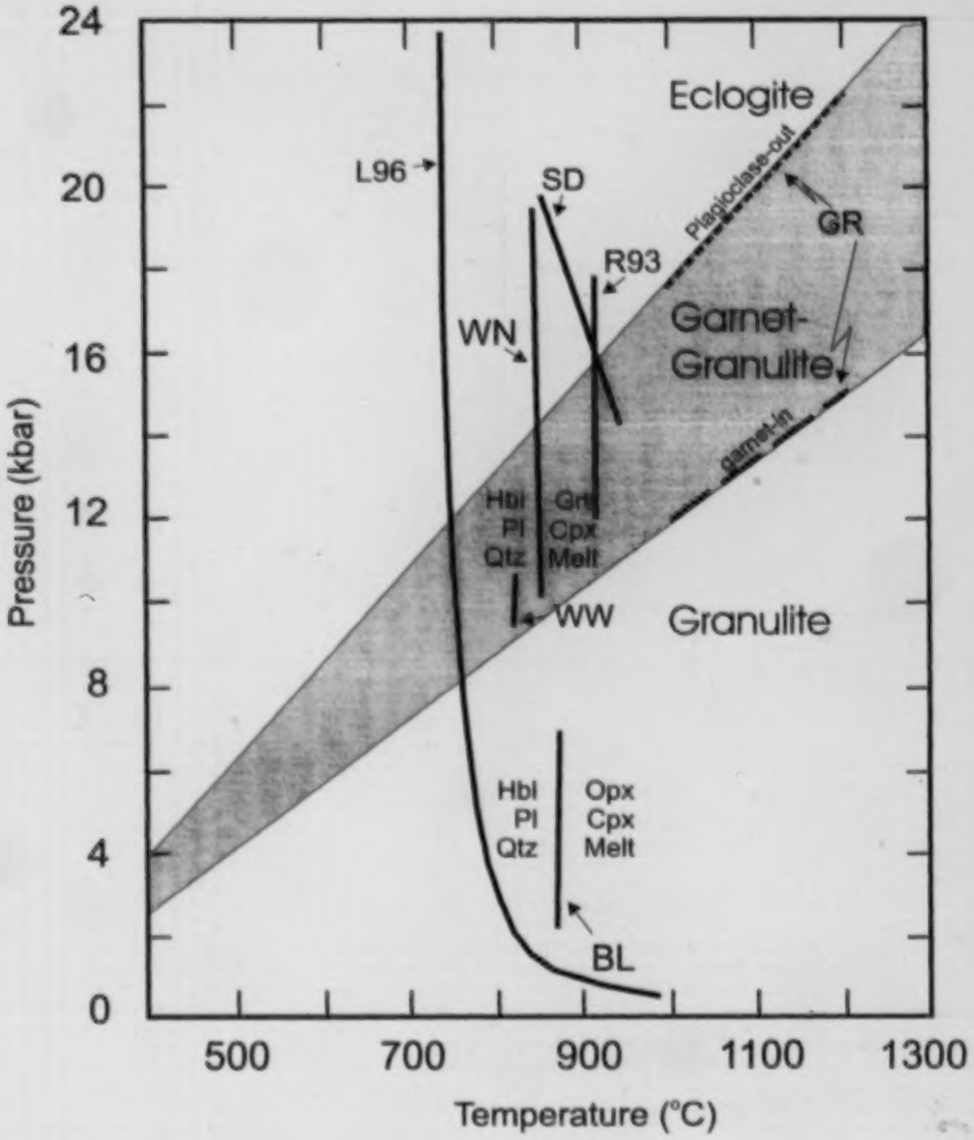

Figure 2.2: Experimental constraints on the stability of granulite, garnet-granulte and eclogite facies mineral assemblages during metamorphism of amphibolites (after Pattison, 2003). GR-Green and Ringwood (1967); BL-Beard and Lofgren (1991); WN-Winther and Newton (1991); R93- Rushmer (1993); WW-Wolf and Wyllie (1994); SD-Sen and Dunn (1994); L96- wet basalt solidus, Liu et al. (1996). Fields for granulite, garnet-granulite and eclogite drawn after Green and Ringwood (1967). Generic reactions stabilizing granulite and garnet-granulite during prograde metamorphism of amphibolites are also shown.

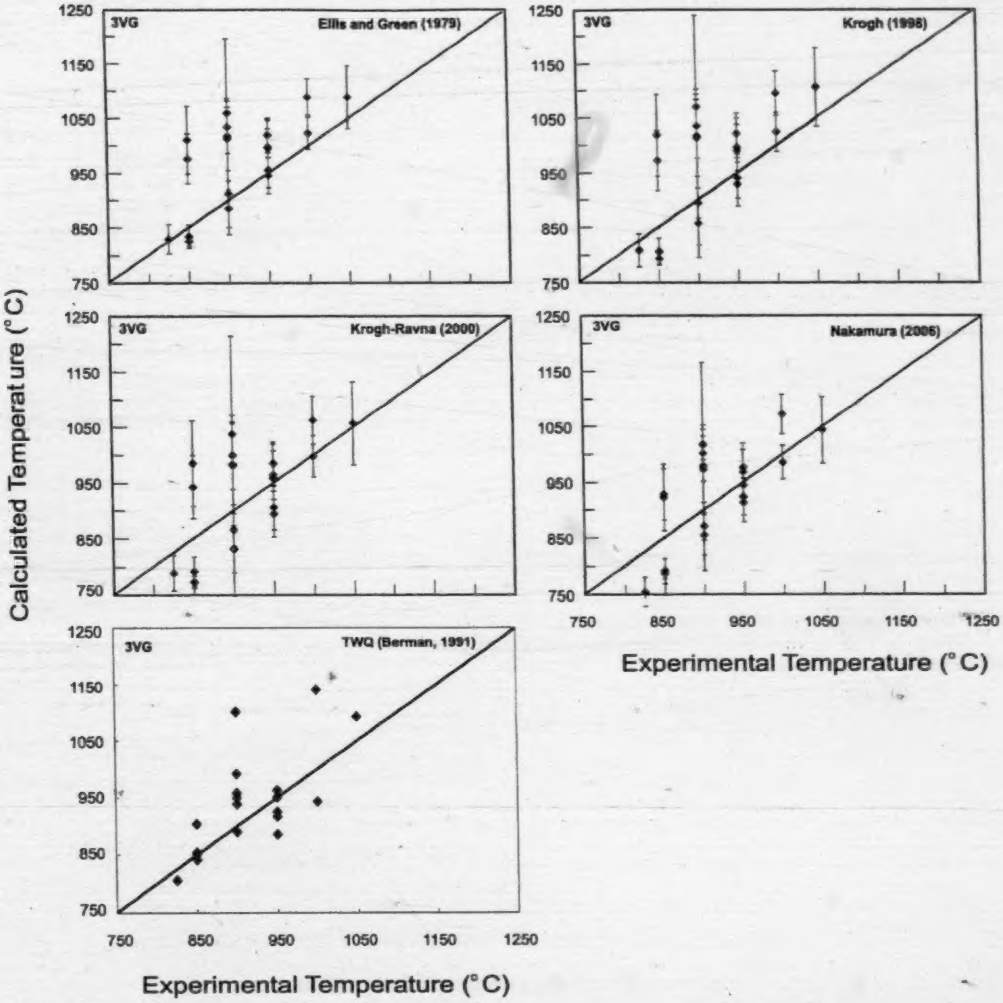

Figure 2.3: Calculated temperatures using different Fe/Mg exchange calibrations between garnet and clinopyroxene plotted against experimental temperatures for 3VG composition. The error bars (not shown for TWQ results) represent the range in calculated temperatures by propagating 1-sigma analytical uncertainty in the Fe/Mg composition of clinopyroxene. The straight line indicates 1:1 correspondence between calculated and experimental temperatures.

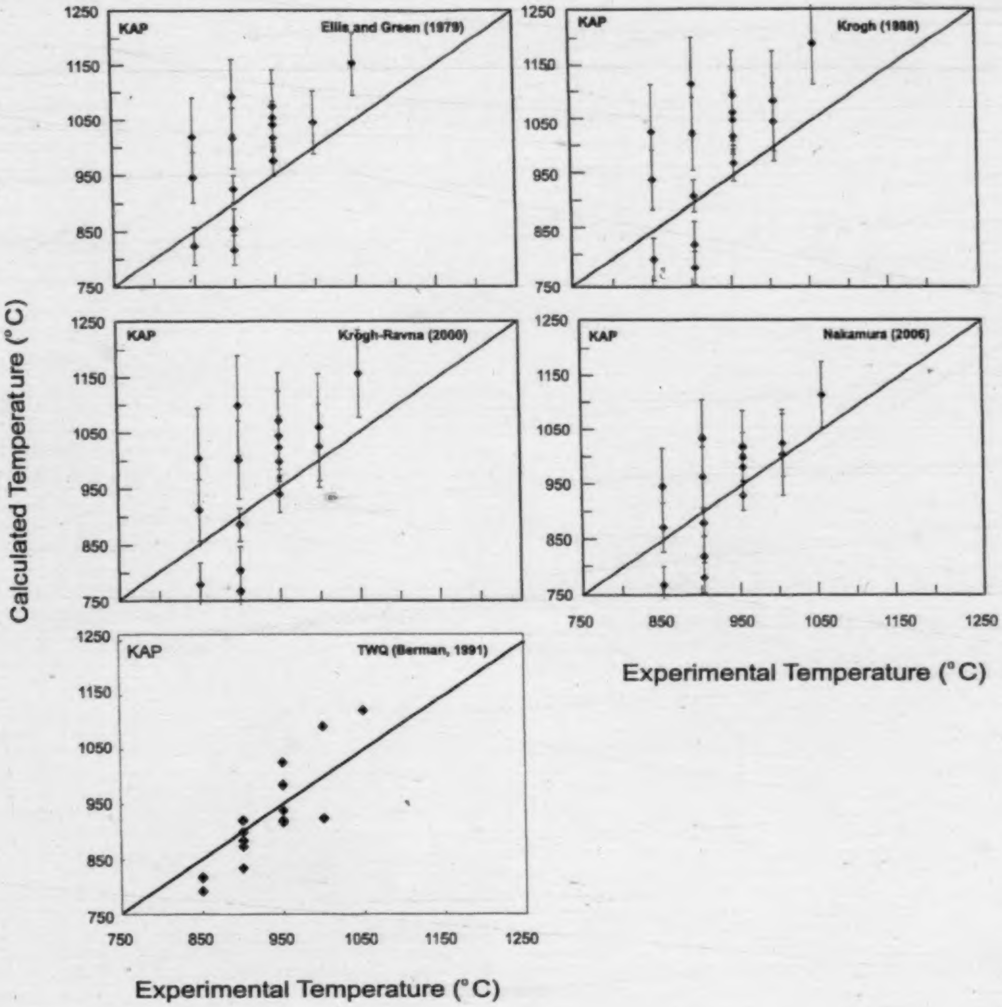

Figure 2.3(contd..): Calculated temperatures using different Fe/Mg exchange calibrations between garnet and clinopyroxene plotted against experimental temperatures for KAP composition. The error bars (not shown for TWQ results) represent the range in calculated temperatures by propagating 1-sigma analytical uncertainty in the Fe/Mg composition of clinopyroxene. The straight line indicates 1:1 correspondence between calculated and experimental temperatures.

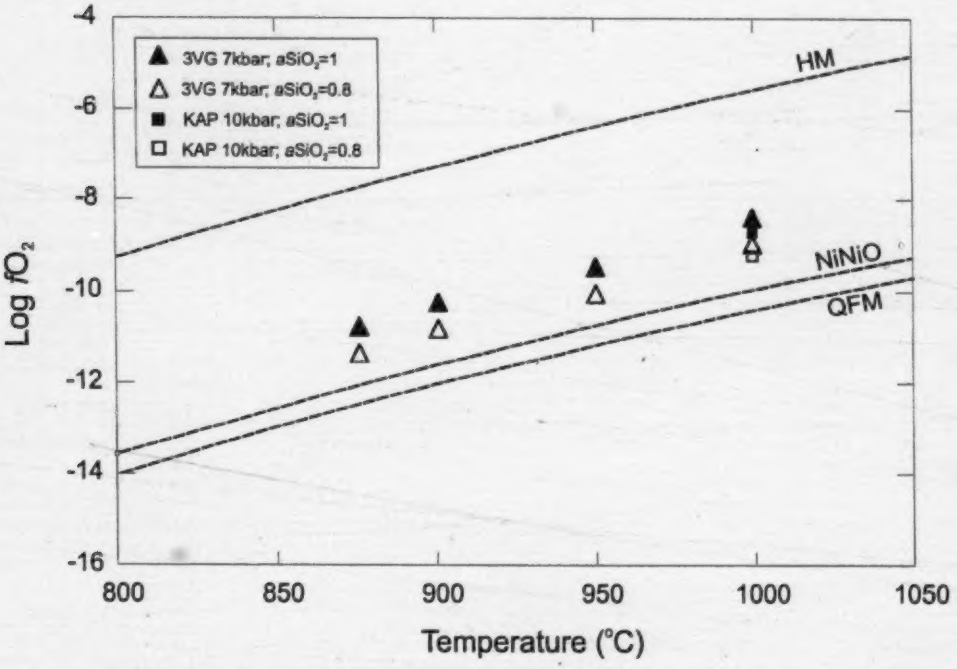

Figure 2.4: Calculated fO_2 values from coexisting magnetite and orthopyroxene composition in the experiments using the equilibrium $2Fe_3O_4 + 6SiO_2 = 3Fe_2Si_2O_6 + O_2$ for two estimates of SiO_2 activity: closed symbols $aSiO_2$=1 and open symbols $aSiO_2$=0.8 Dashed curves shows the position of different buffer reactions. HM- hematite-magnetite buffer; NiNiO- nickel-nickel oxide buffer; QFM- quartz-fayalite-magnetite buffer. Buffer curves calculated from Lindsley (1976).

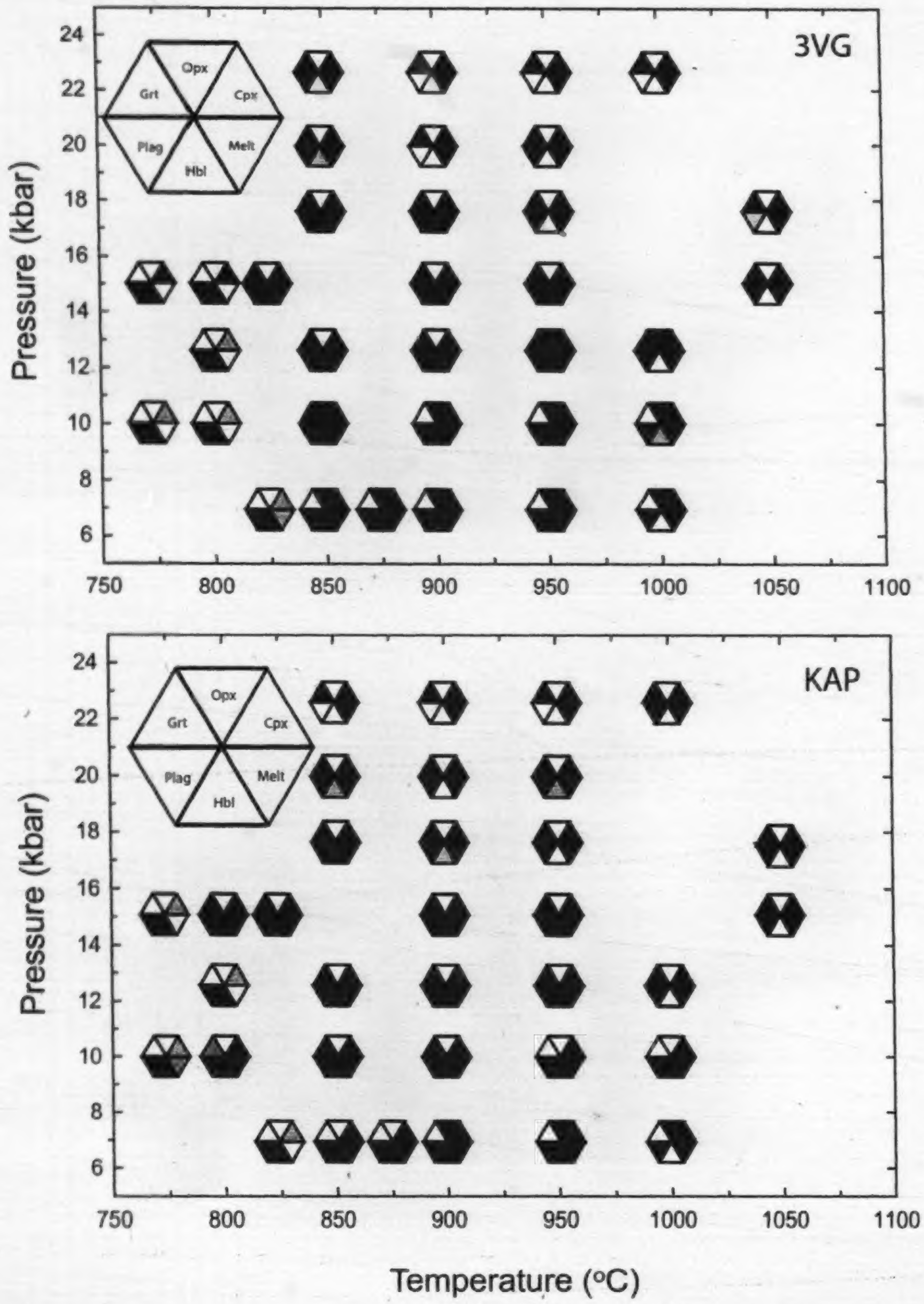

Figure 2.5: Phase assemblage observed in the experimental run products. A filled symbol indicates the presence of the phase and an open symbol indicate absence of the phase. Lightly shaded symbols indicate the presence of trace amount of the phase. Stability relations of quartz is not shown. Quartz is present in all experiments up to 850 °C except at 20 kbar where only trace amounts of quartz was present. Trace amount of quartz were also observed in 22.5 kbar experiments up to 950 °C.

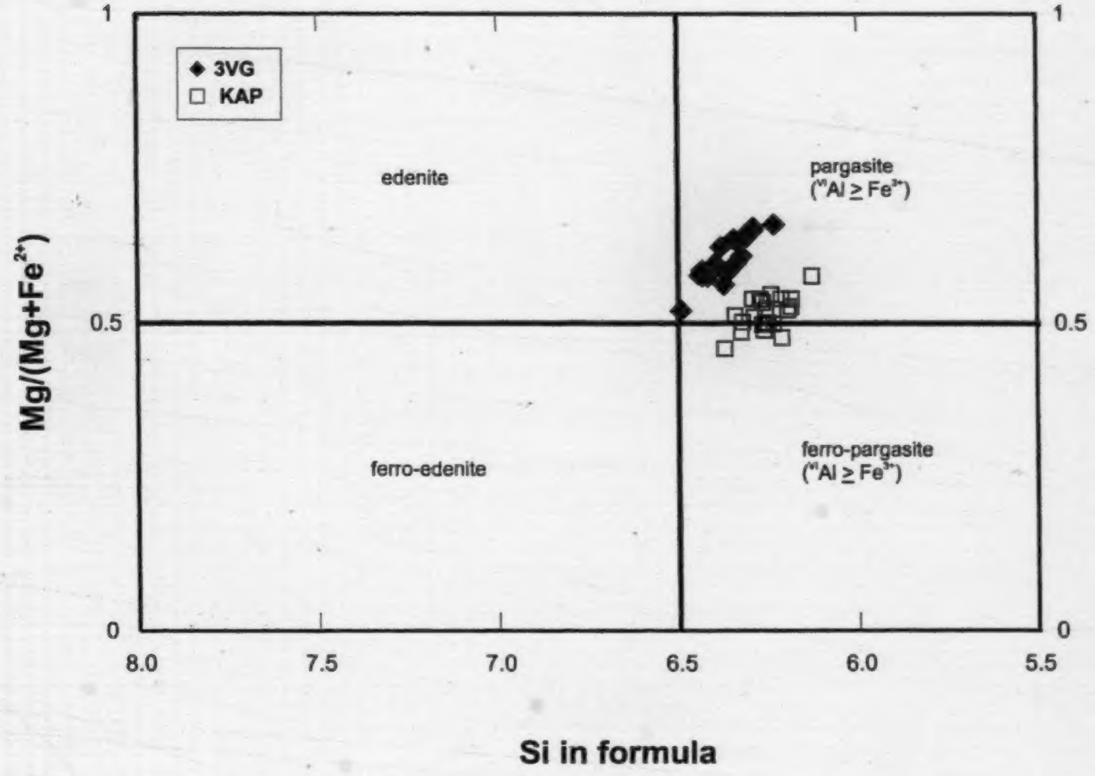

Figure 2.6: Experimental amphiboles plotted after the nomenclature of Leake (1997).

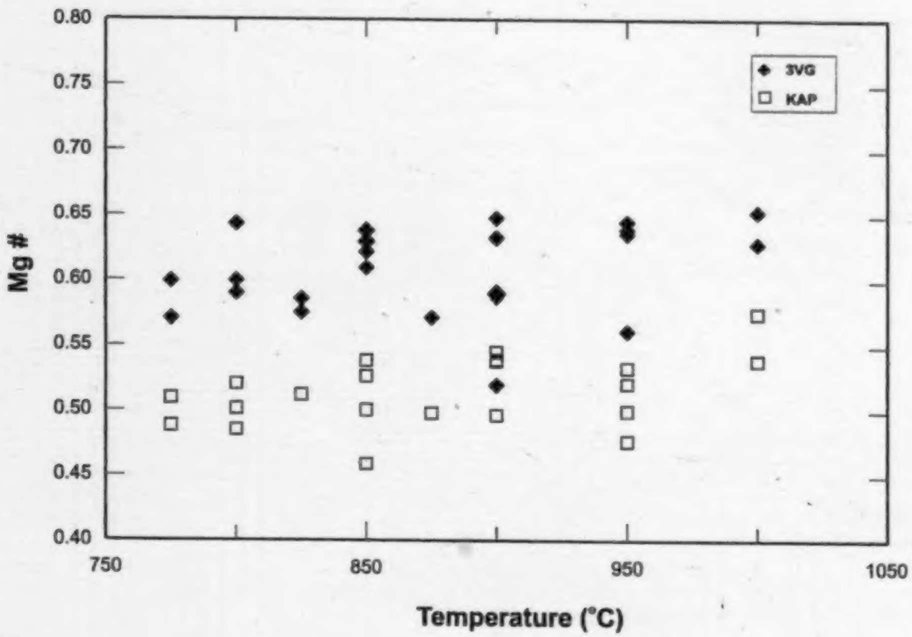

Figure 2.7: Variation of Mg# (Mg/Mg+Fe) of experimental amphiboles.

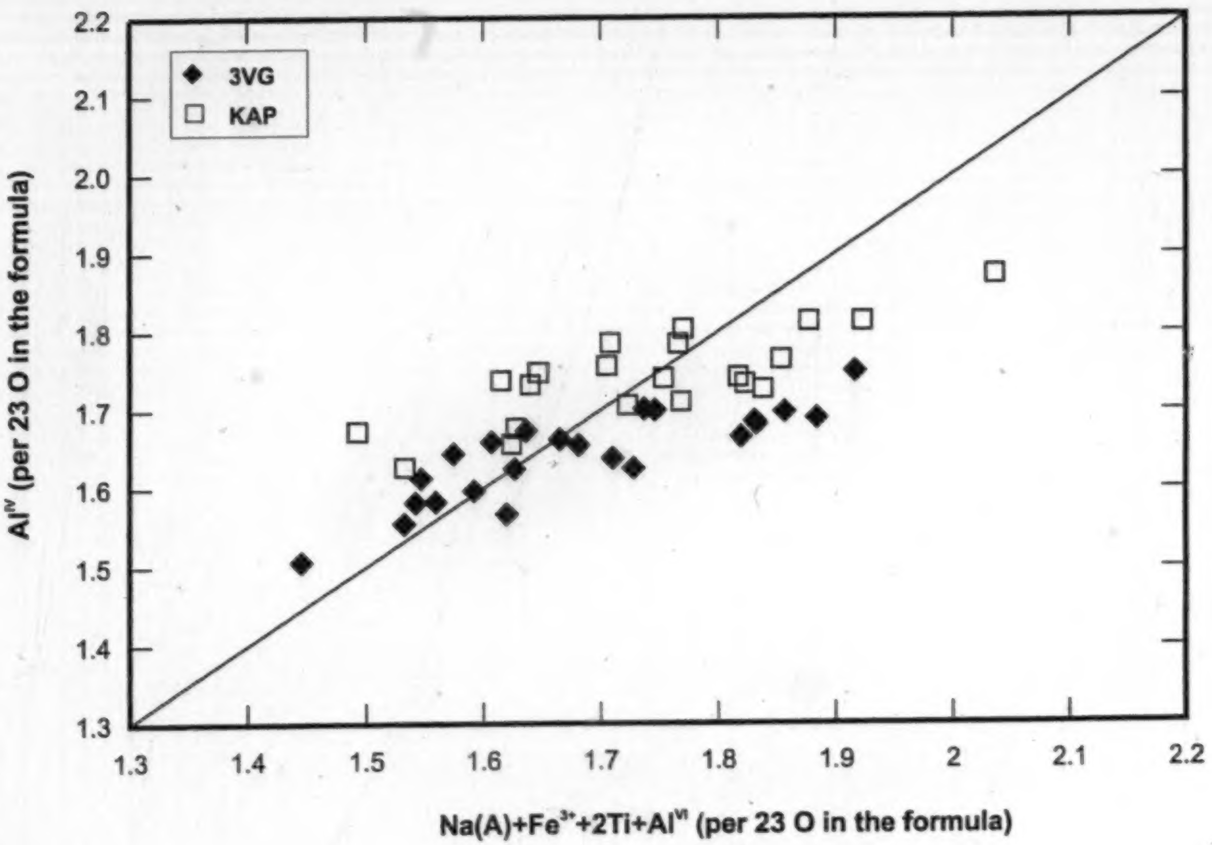

Figure 2.8: Variation of tetrahedral Al (Al^{IV}) in experimental amphiboles with Na (in A site)+Fe^{3+}+Ti+octahedral Al (Al^{VI}).

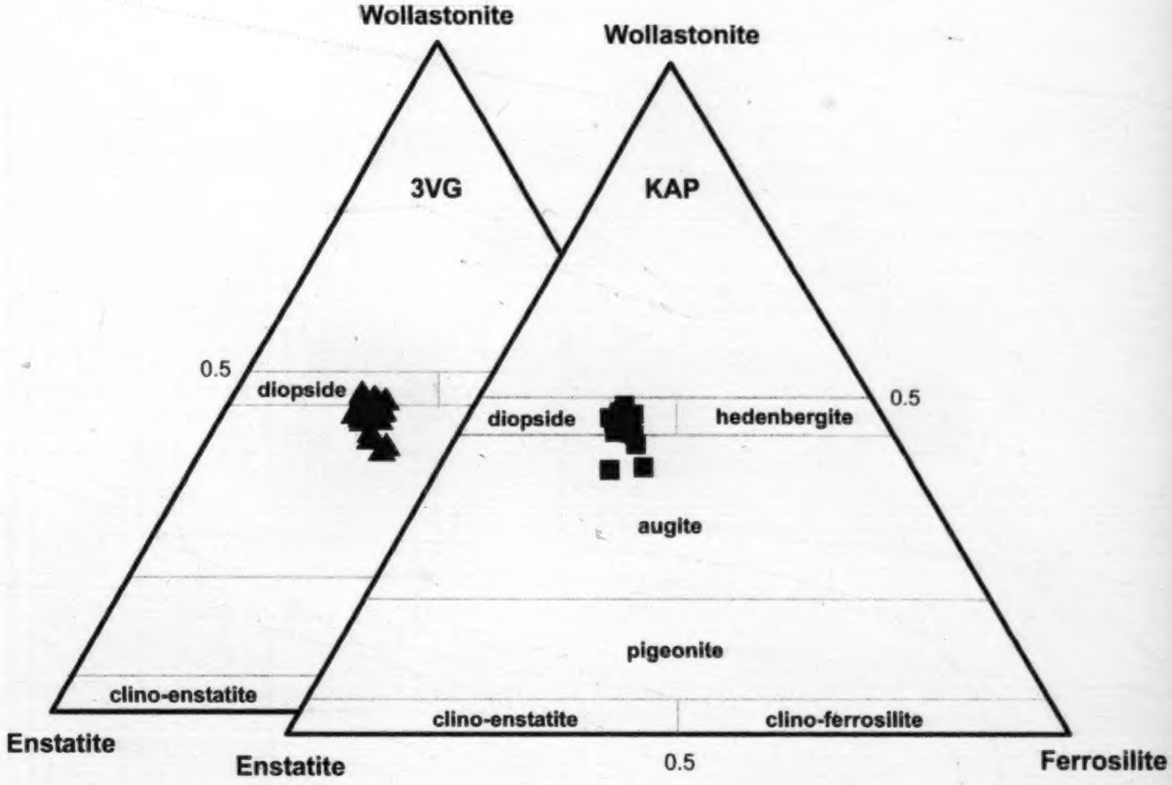

Figure 2..9: Wo-En-Fs ternary diagram showing clinopyroxene compositions.

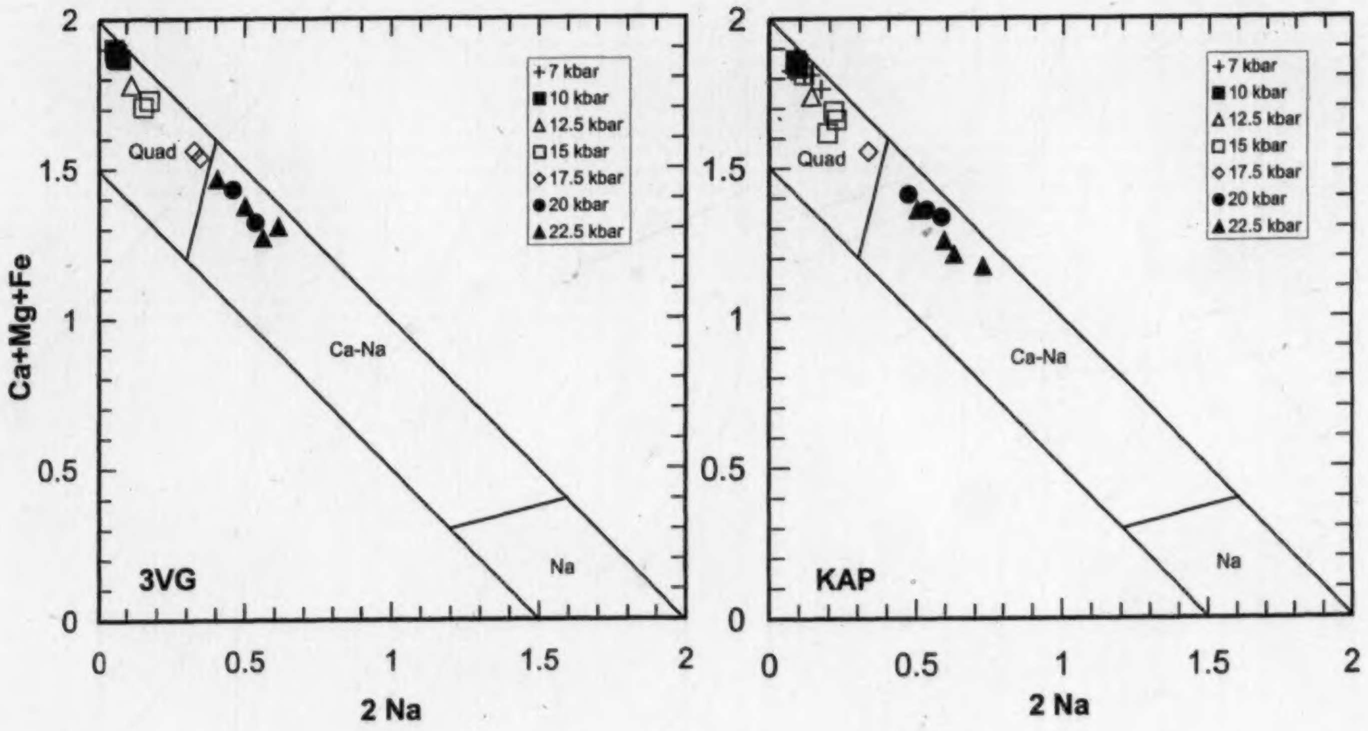

Figure 2.10: Pyroxene compositions plotted as a function of quadrilateral pyroxene components (Ca+Mg+Fe2+) and Jadeite component (2Na) (diagram after Morimoto (1988)).

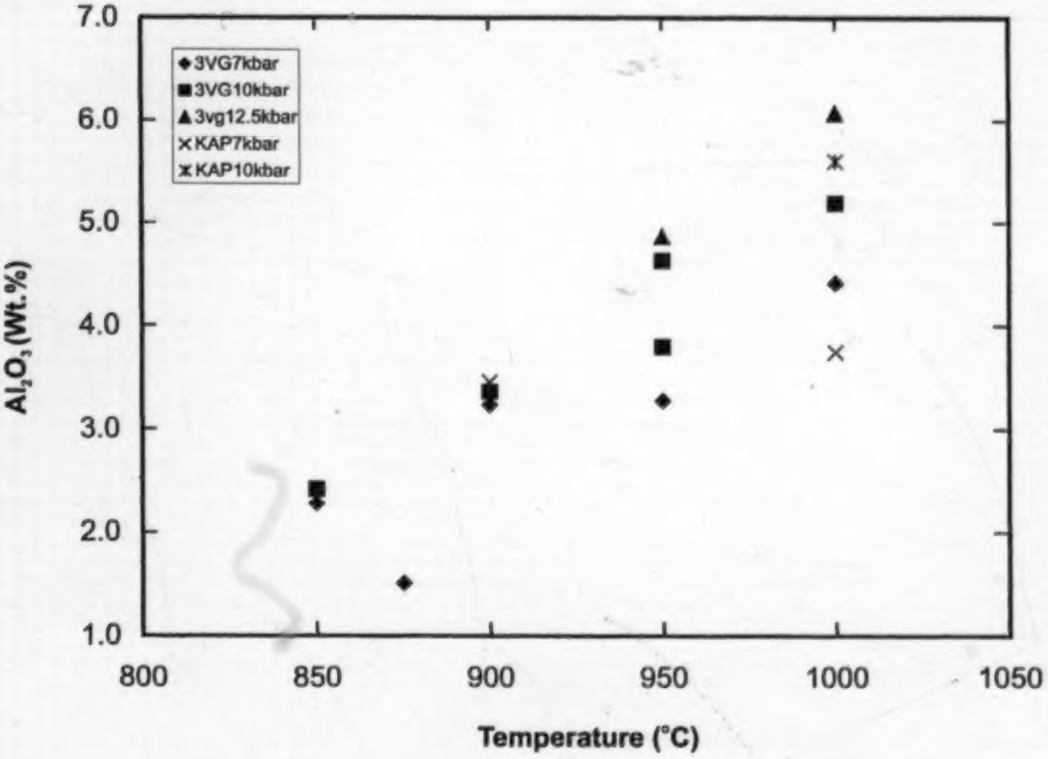

Figure 2.11: Variation of Al_2O_3 with temperature in orthopyroxene.

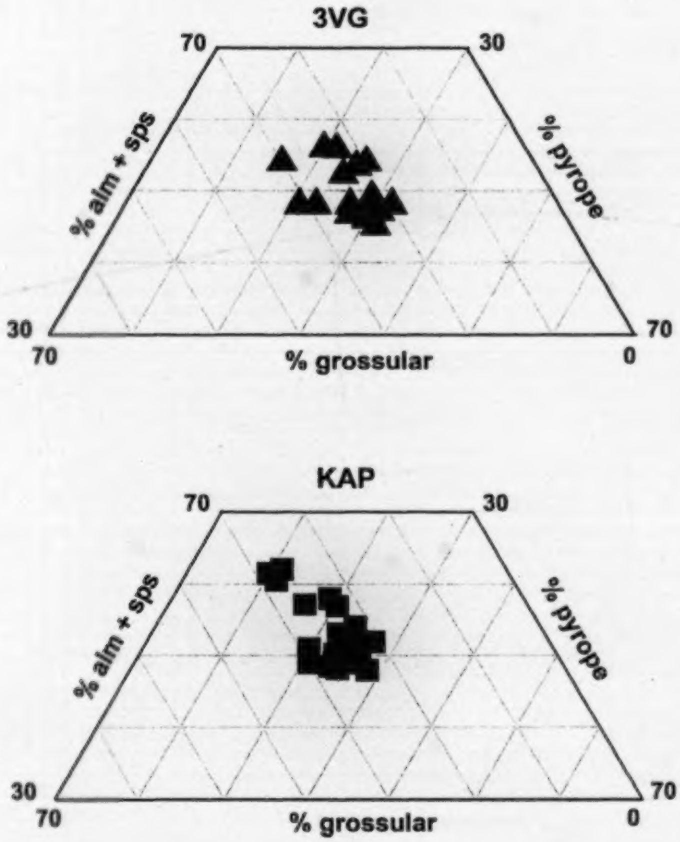

Figure 2.12: Garnet compositions plotted in an end member ternary diagram.

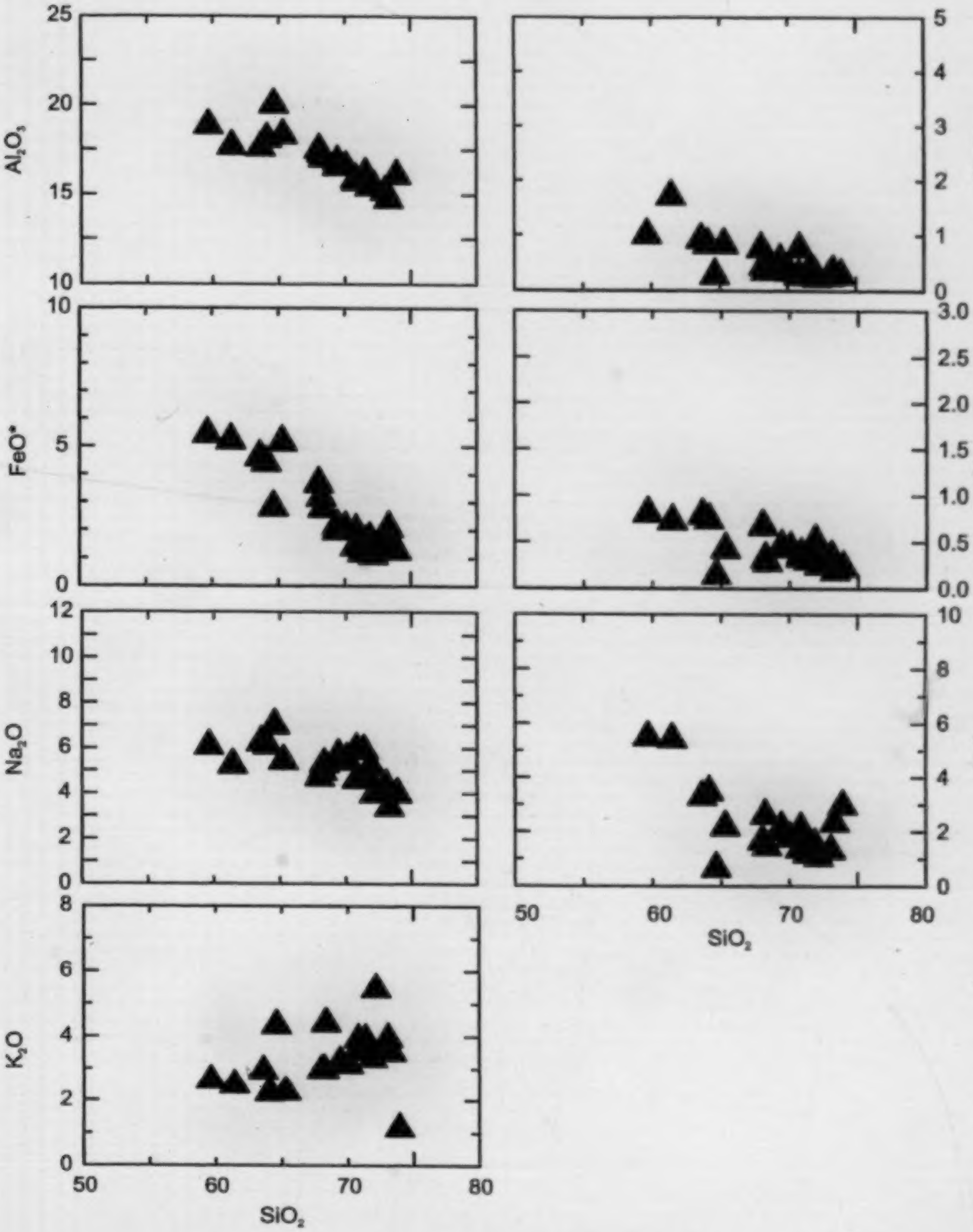

Figure 2.13: Harker variation diagram for 3VG melt compositions.

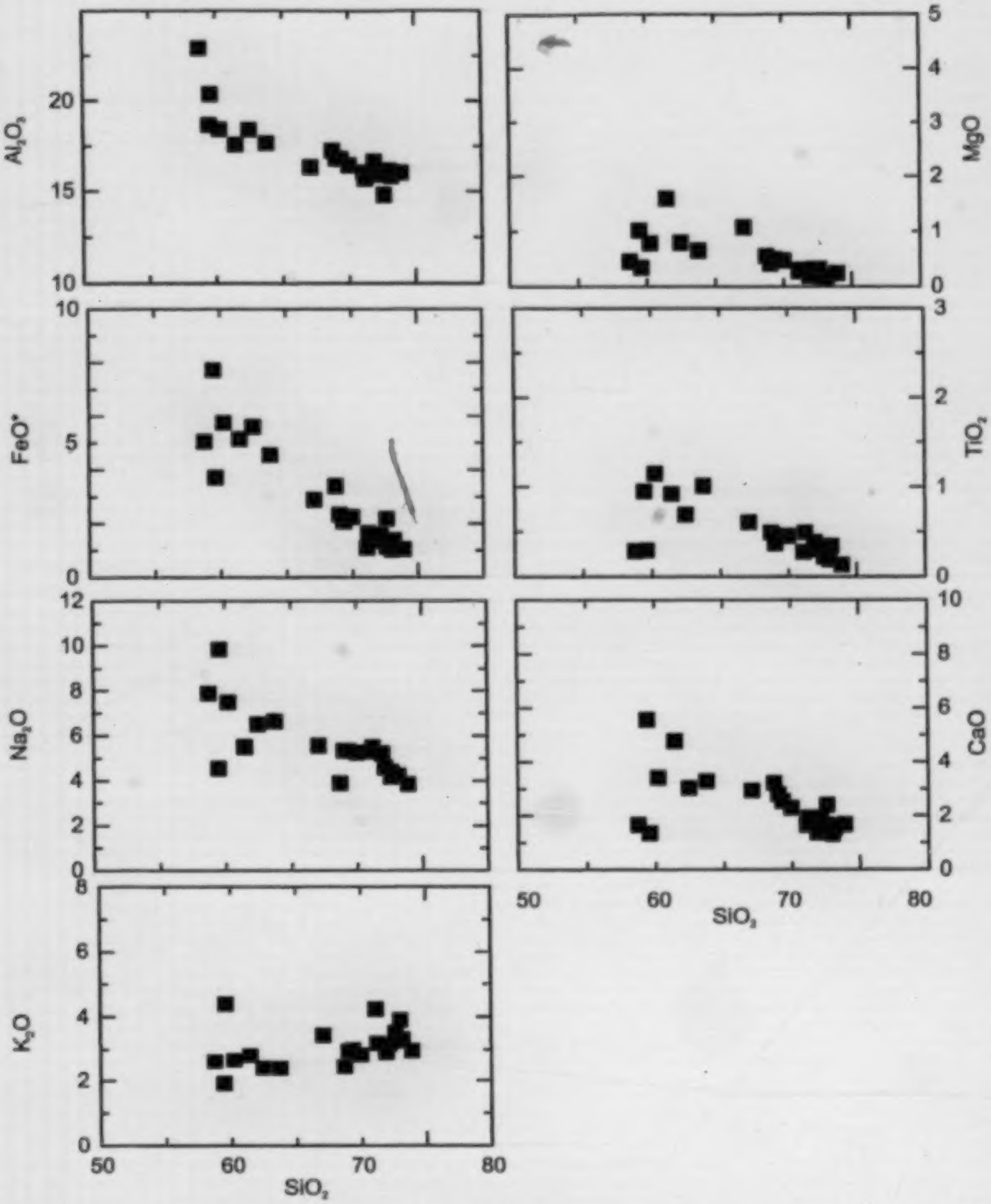

Figure 2.13 contd.: Harker diagrams for KAP melt compositions.

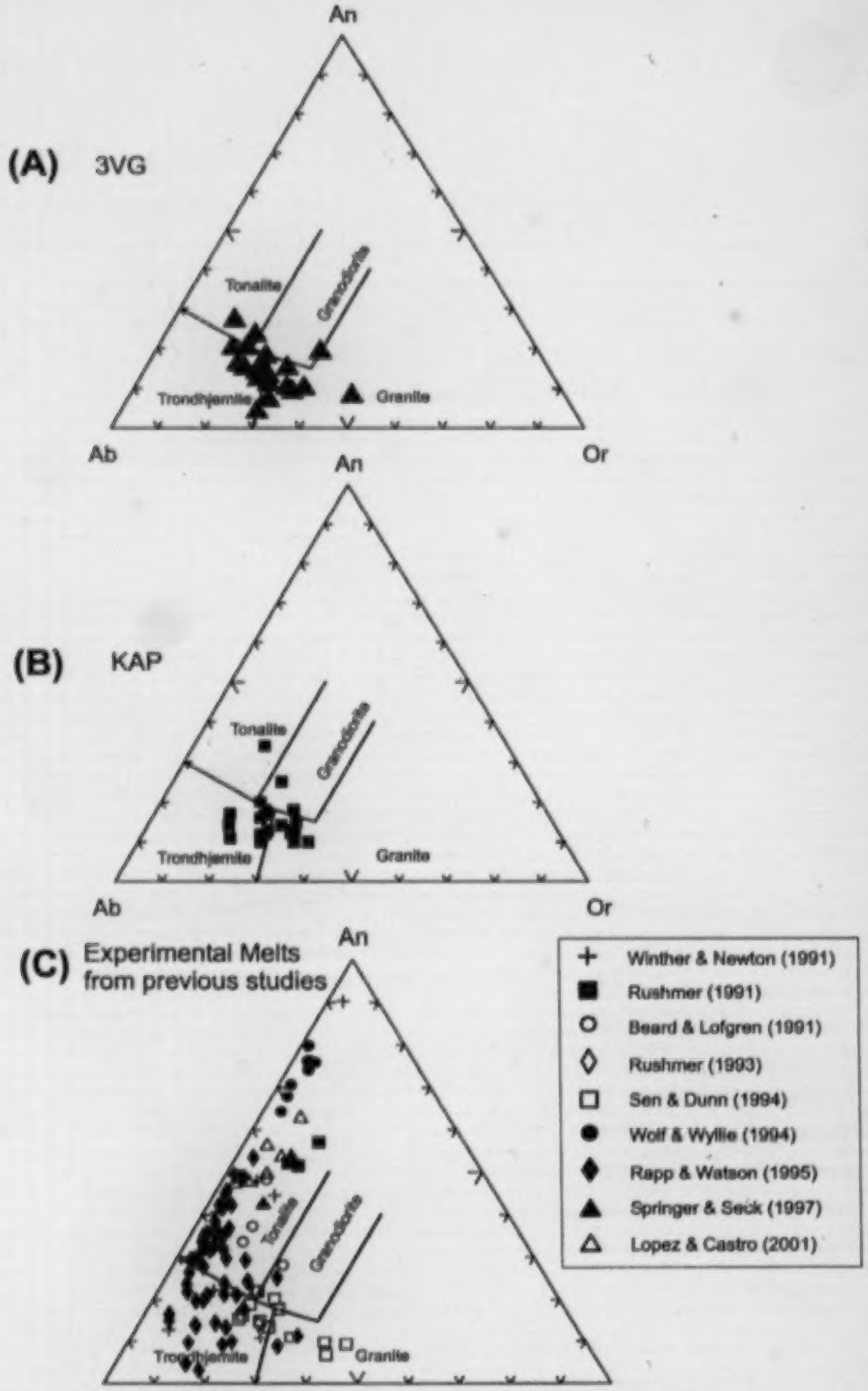

Figure 2.14: Composition of partial melts plotted on a normative feldspar diagram (Barker,1979). (A) 3VG, (B) KAP, (C) previous dehydration melting experiments on metbasalts. WN91, Winther and Newton (1991); R91, Rushmer (1991); BL91, Beard and Lofgren (1991), SD94, Sen and Dunn (1994); WW94, Wolf and Wyllie; RW95, Rapp and Watson (1995); SS97, Springer and Seck (1997); LC01, Lopez and Castro (2001).

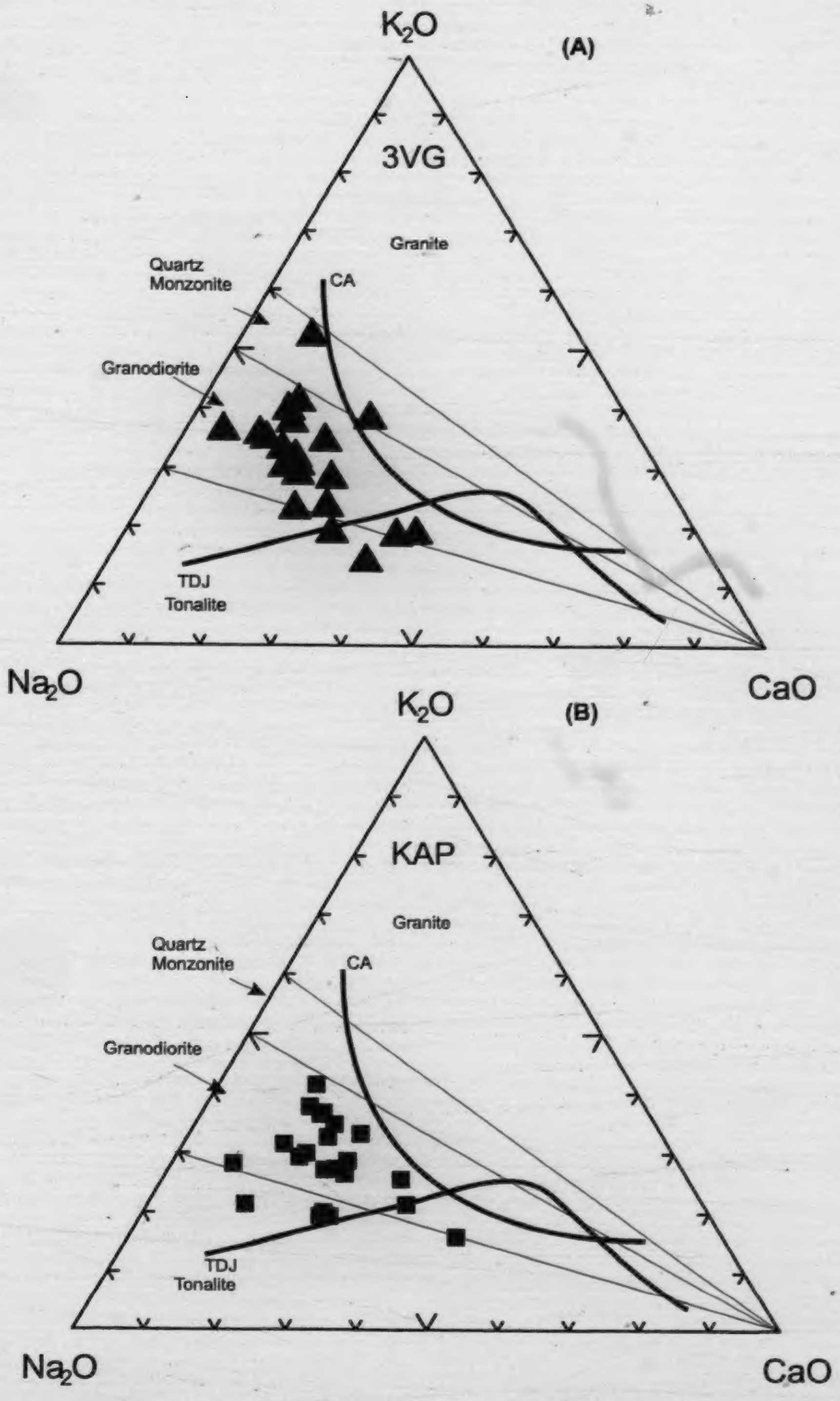

Figure 2.15: K_2O-CaO-Na_2O ternary plot of melt compositions: (A) 3VG, (B) KAP. Curves labelled CA and TDJ represents calc-alkaline and trondhjemite trends, respectively.

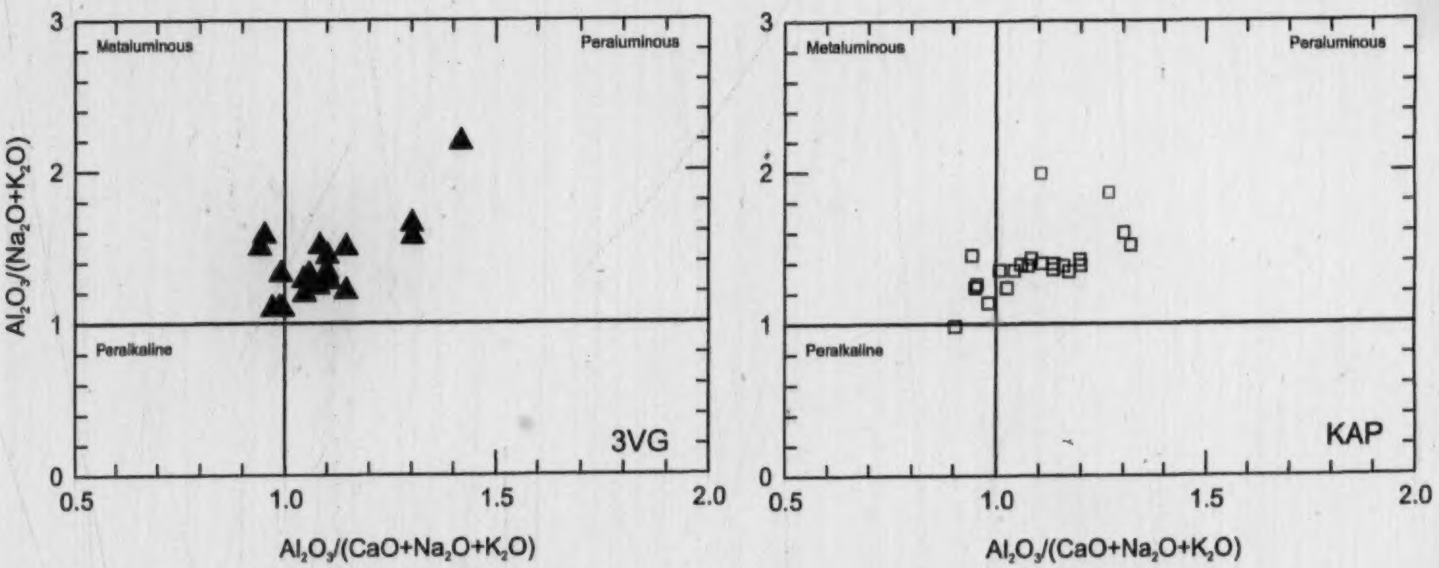

Figure 2.16: Experimental melt compositions plotted as a function of molar $Al_2O_3/(Na_2O+K_2O)$ and ASI ($Al_2O_3/(CaO+Na_2O+K_2O)$).

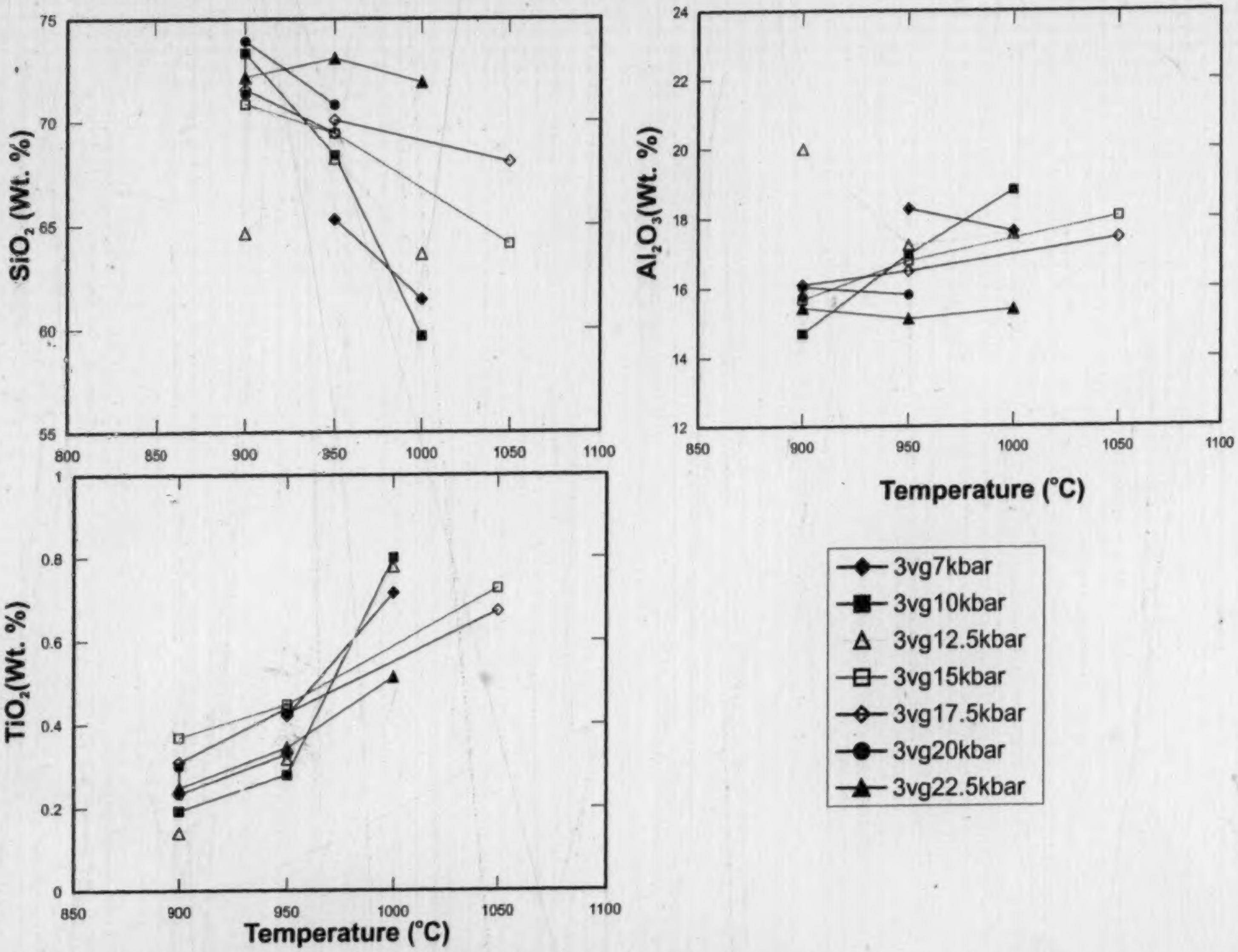

Figure 2.17: Variation of melt compositions with temperature.

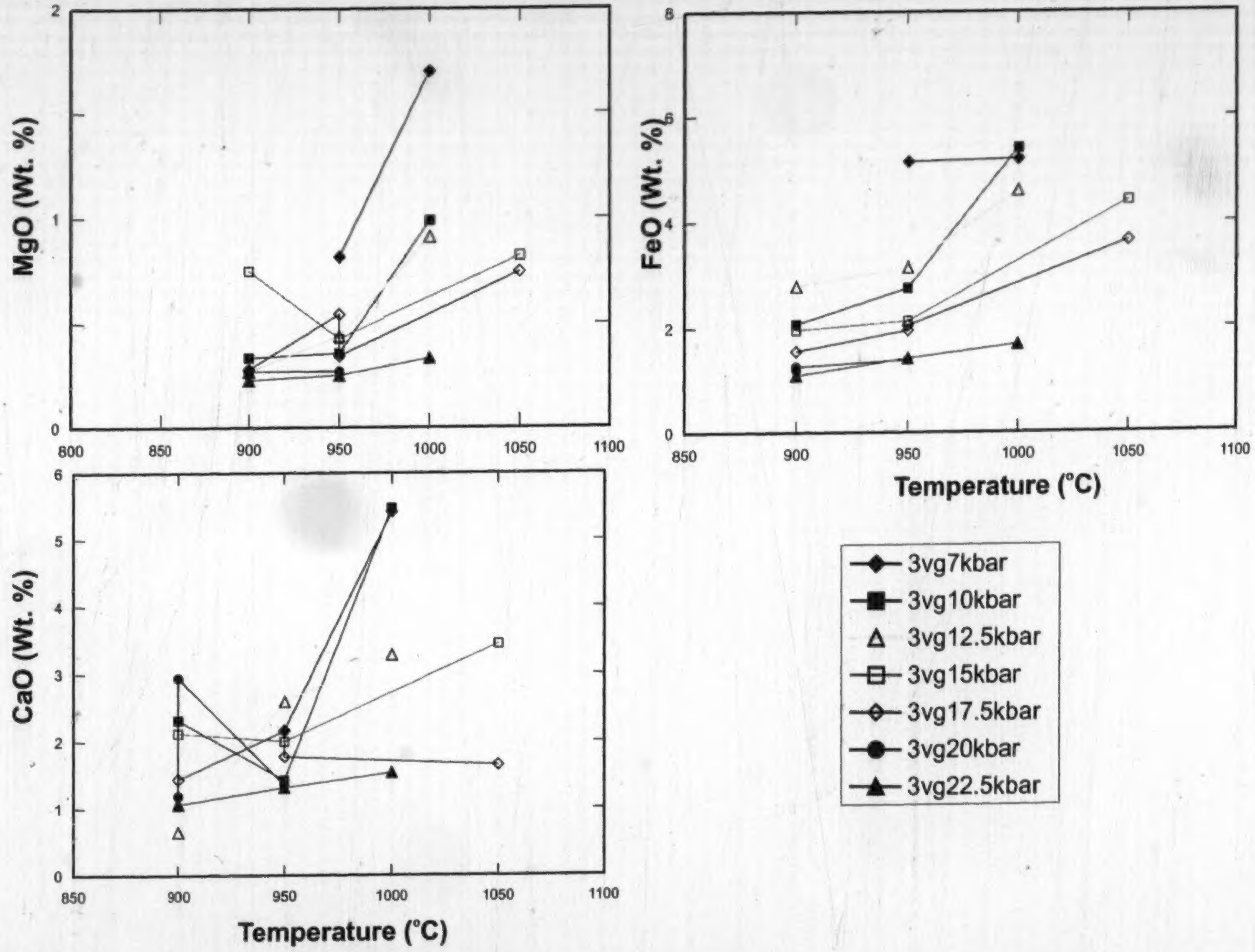

Figure 2.17: Variation of melt compositions with temperature.

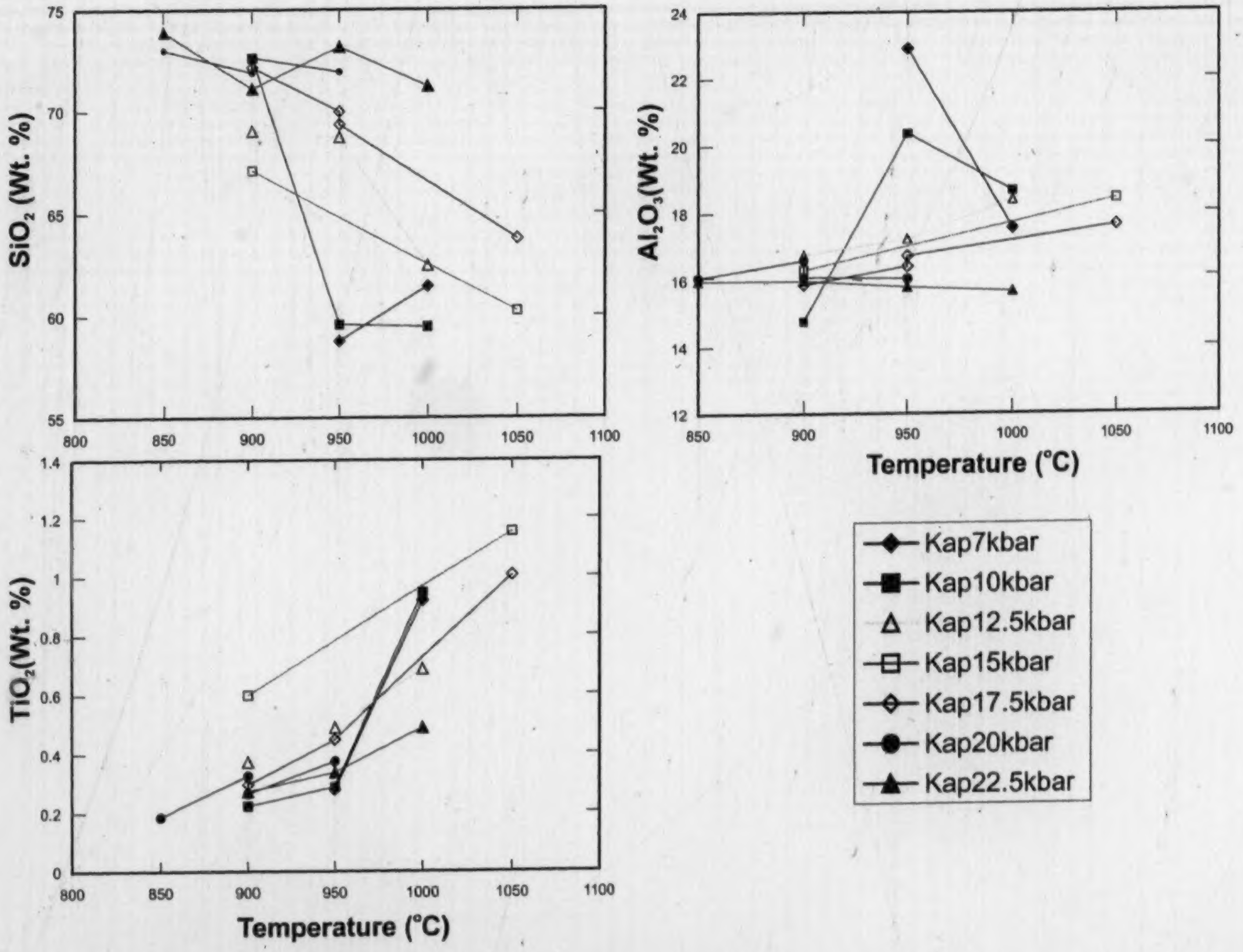

Figure 2.17: Variation of melt compositions with temperature.

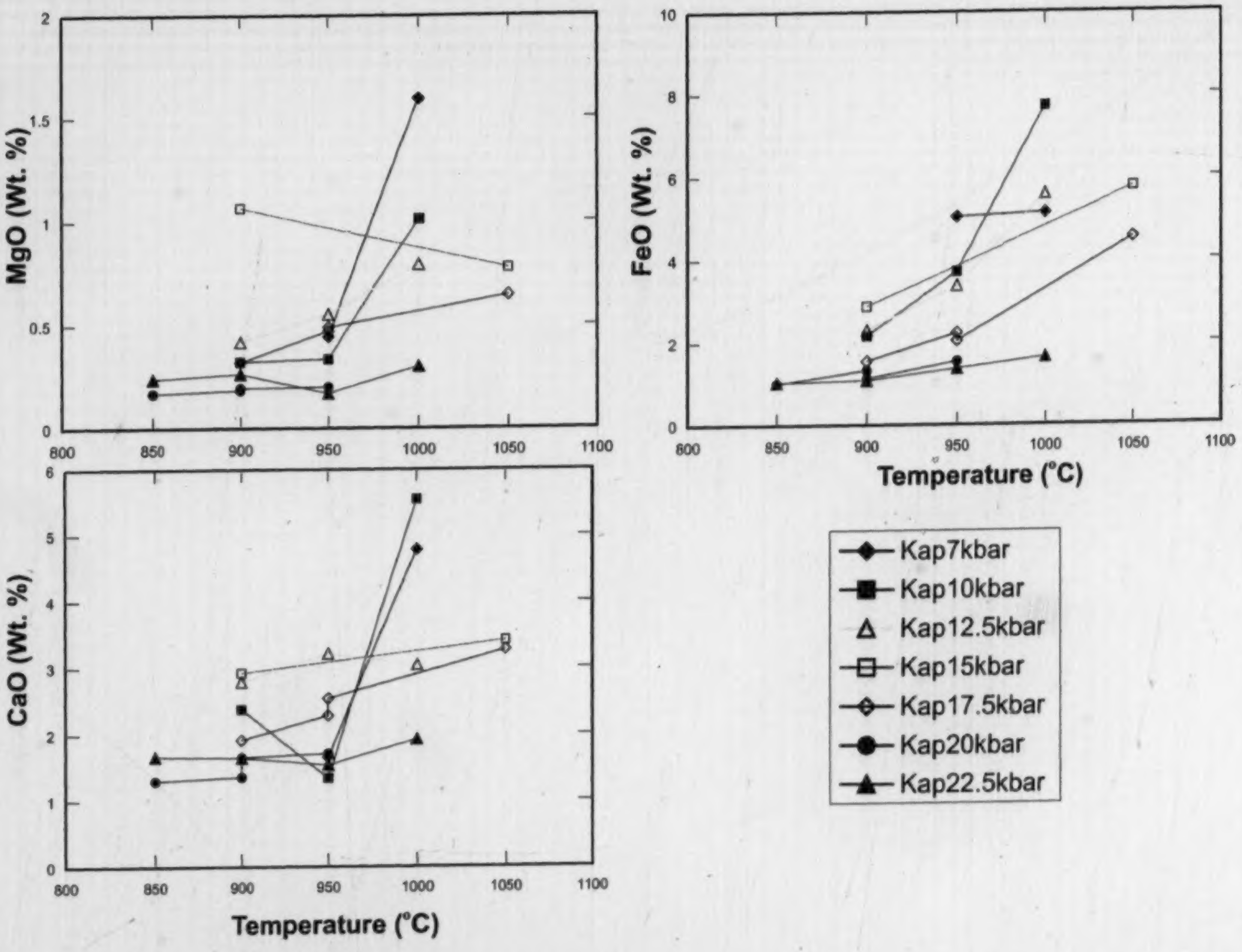

Figure 2.17: Variation of melt compositions with temperature.

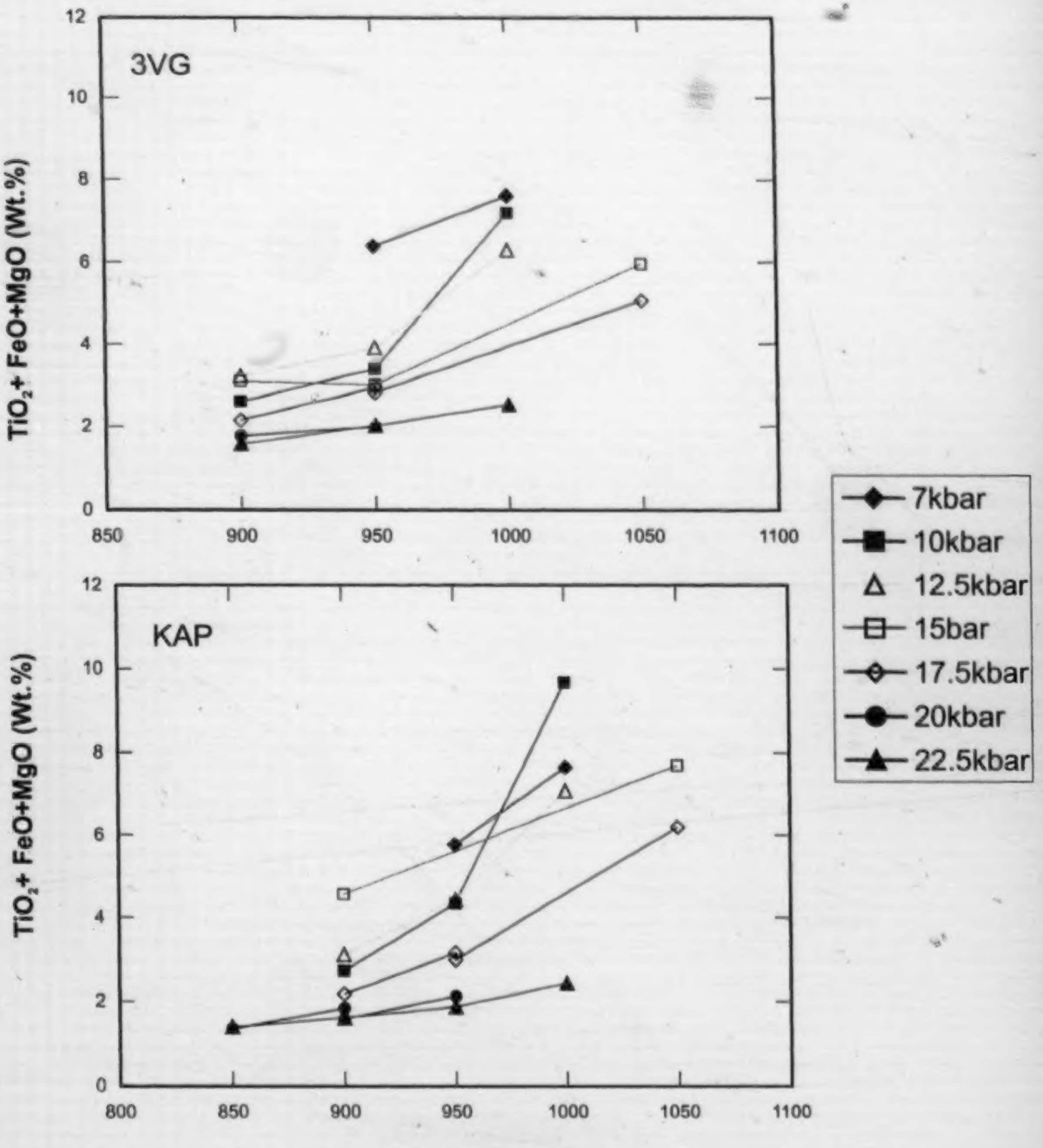

Figure 2.18: Plot of TiO2+FeO + MgO (wt%) in melt vs experimental temperatue.

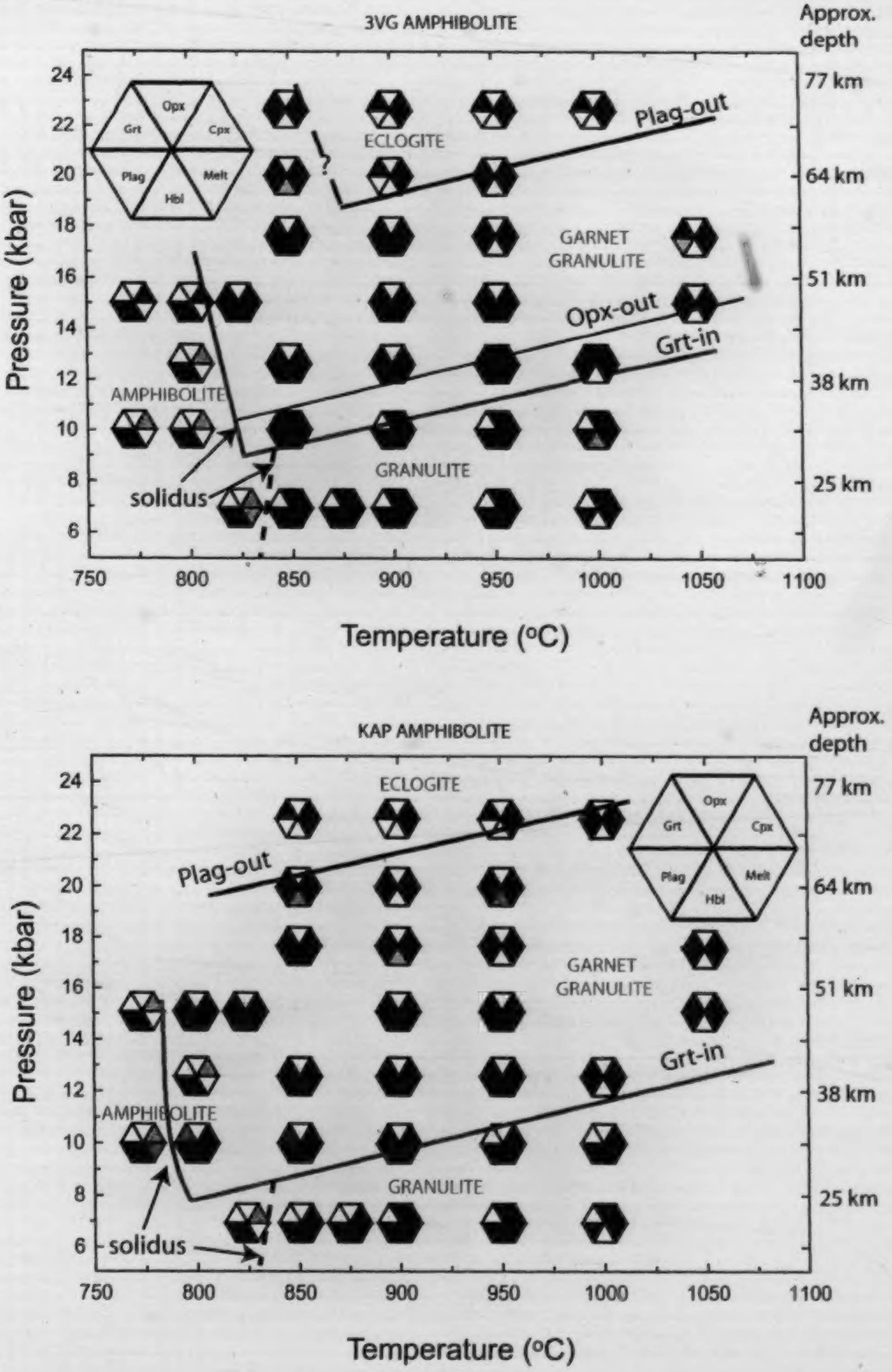

Figure 2.19: Dehydration melting phase relations of KAP and 3VG amphibolites with inferred phase boundaries.

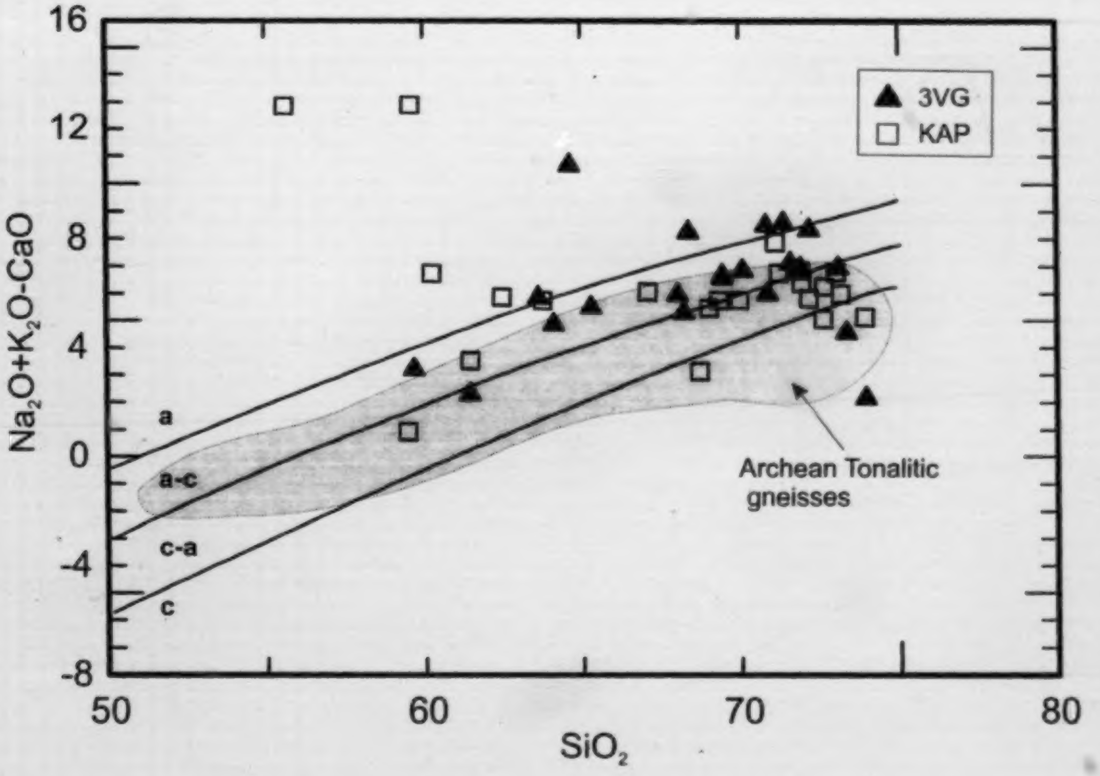

Figure 2.20: Na_2O+ K_2O-CaO vs SiO_2 (wt. %) of experimental melts. a-alkalic; a-c, alkalic-calc; c-a, calc-alkalic; c, calcic. Field for Archean tonalitic gneisses from Frost et al. (2001).

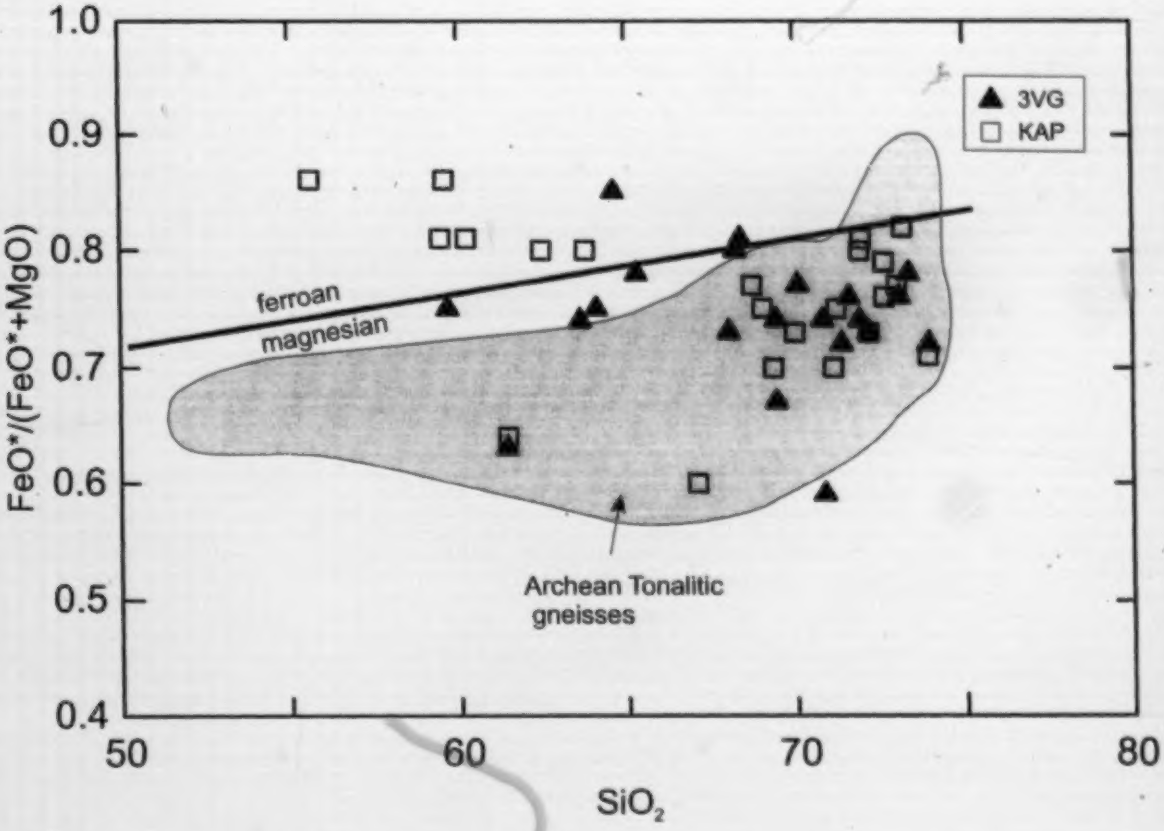

Figure 2.21: FeO*/(FeO*+MgO) (molar) vs. SiO$_2$ (wt.%) of experimental melts. Field for Archean tonalitic gneisses from Frost et al. (2001). FeO*, total Fe measured as FeO.

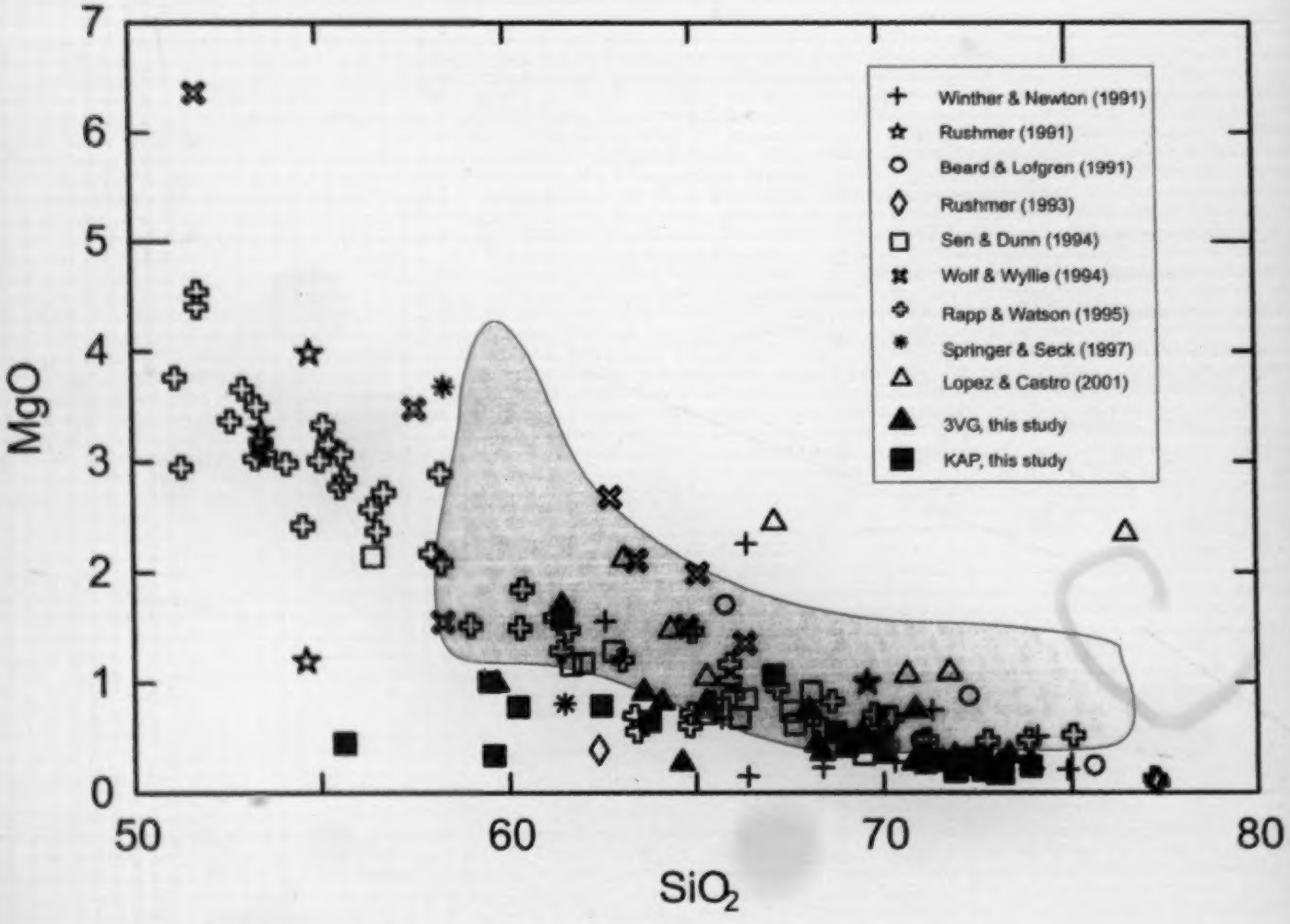

Figure 2.22: MgO content (wt. %) of experimental melts produced in this study with those from previous metabasalt melting experiments. The shaded field represents the range of values for TTGs (from Sen and Dunn, 1994).

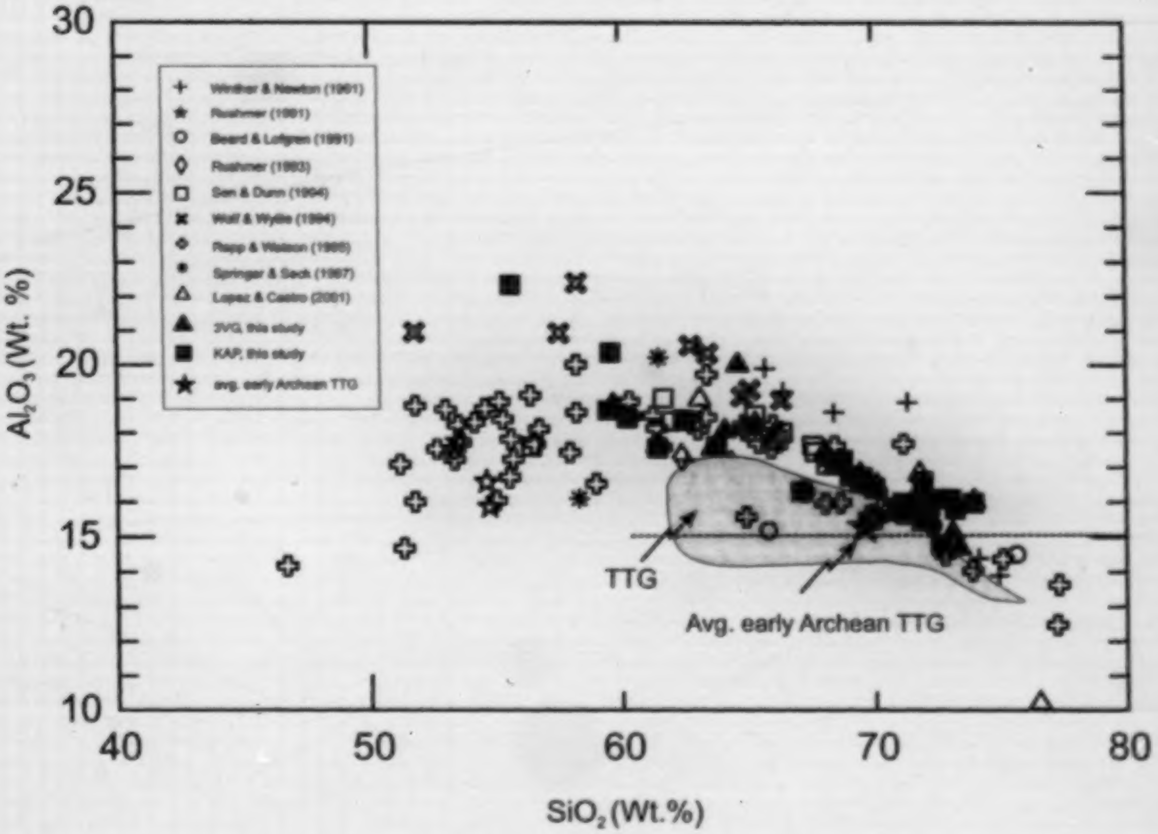

Figure 2.23: Al_2O_3 vs SiO_2 of partial melts compared with partial melts from previous experiments; dashed line separates High-Al TTGs from Low-Al TTGs (Barker and Arth, 1976); TTG field from Springer and Seck (1997); average early Archean TTG from Martin et. Al. (2005).

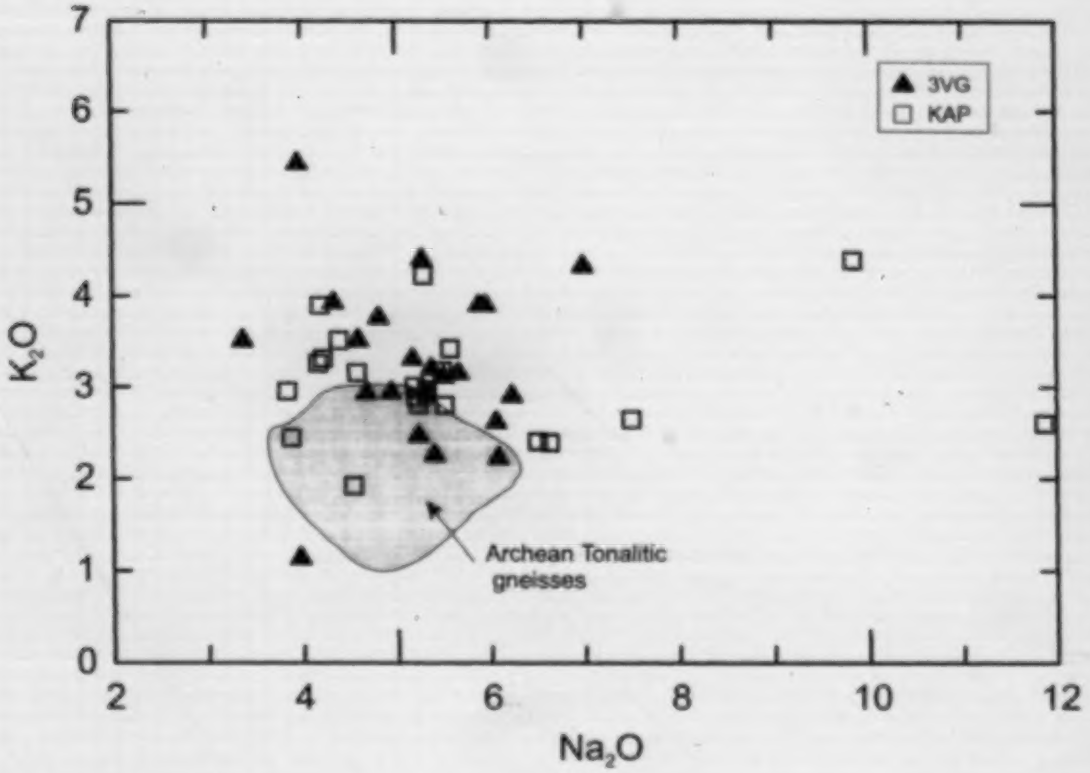

Figure 2.24: K_2O vs Na_2O (wt. %) of experimental melts. Field for Archean tonalitic gneisses from Frost et al. (2001).

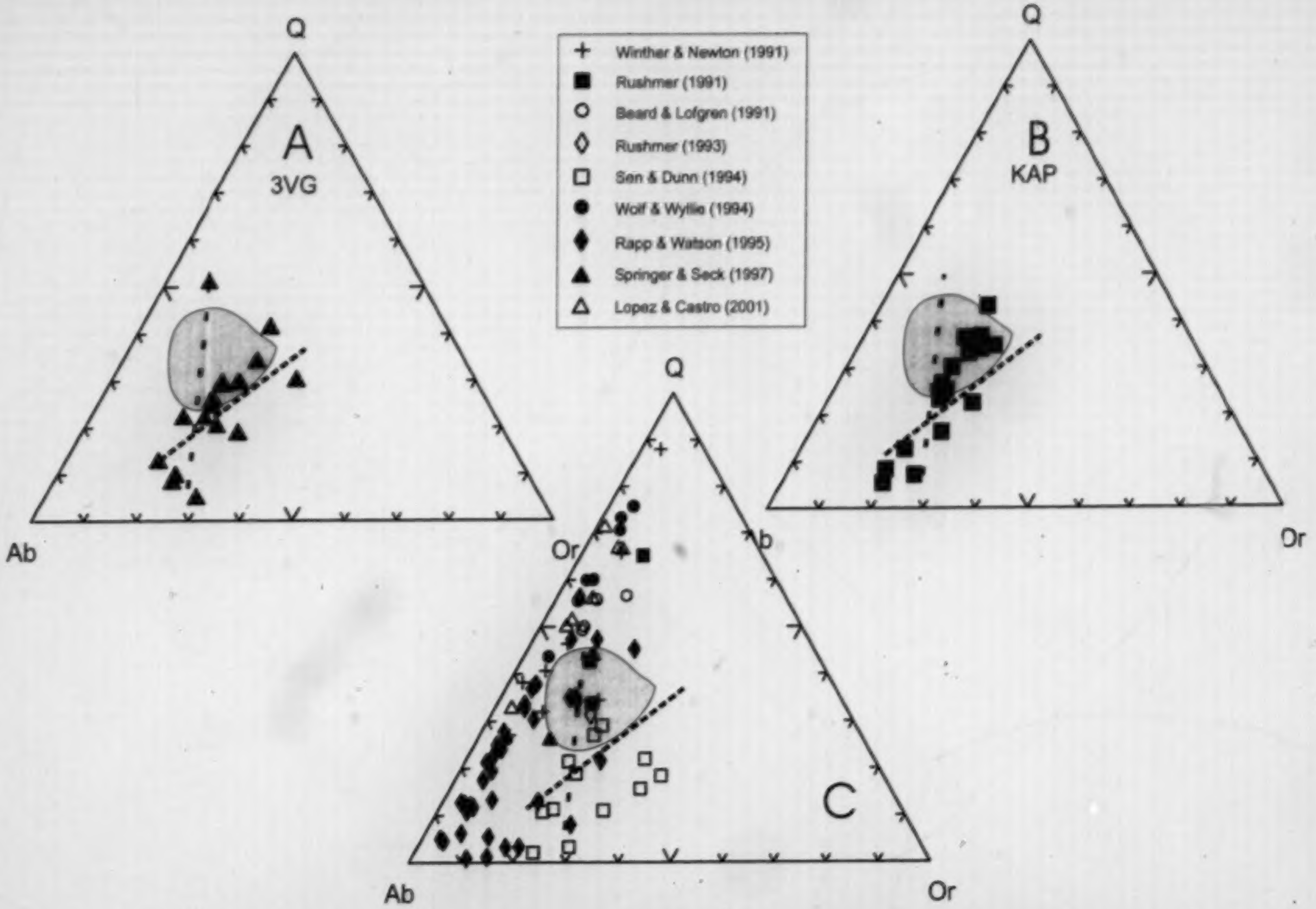

Figure 2.25: Normative Quartz (Q)-Albite (Ab)-Orthoclase (Or) ternary plot of experimental melts (A) 3VG, (B) KAP, and (C) melts from previous studies. The shaded field represents TTG (Martin, 1987). The dashed line represents calc-alkaline trend (Martin, 1987).

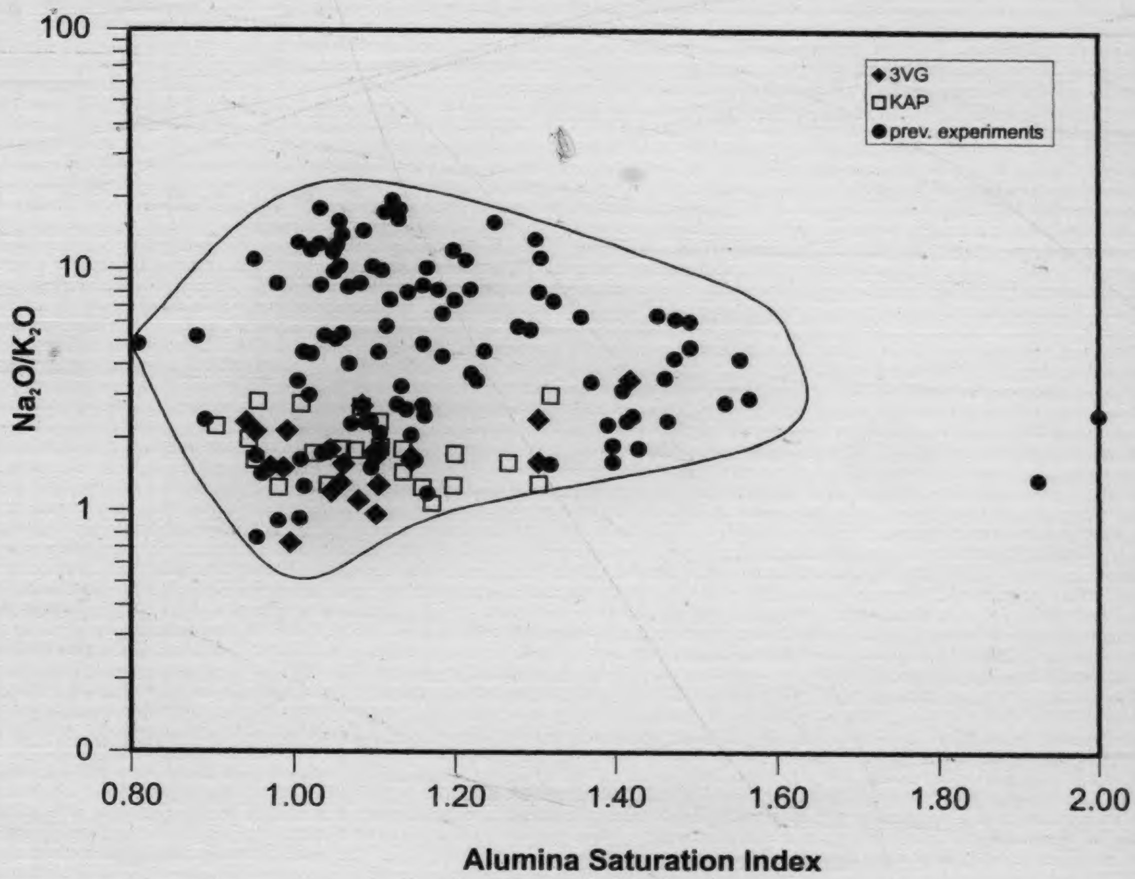

Figure 2.26: Na_2O/K_2O vs ASI for experimental melts compared with those from previous experiments.

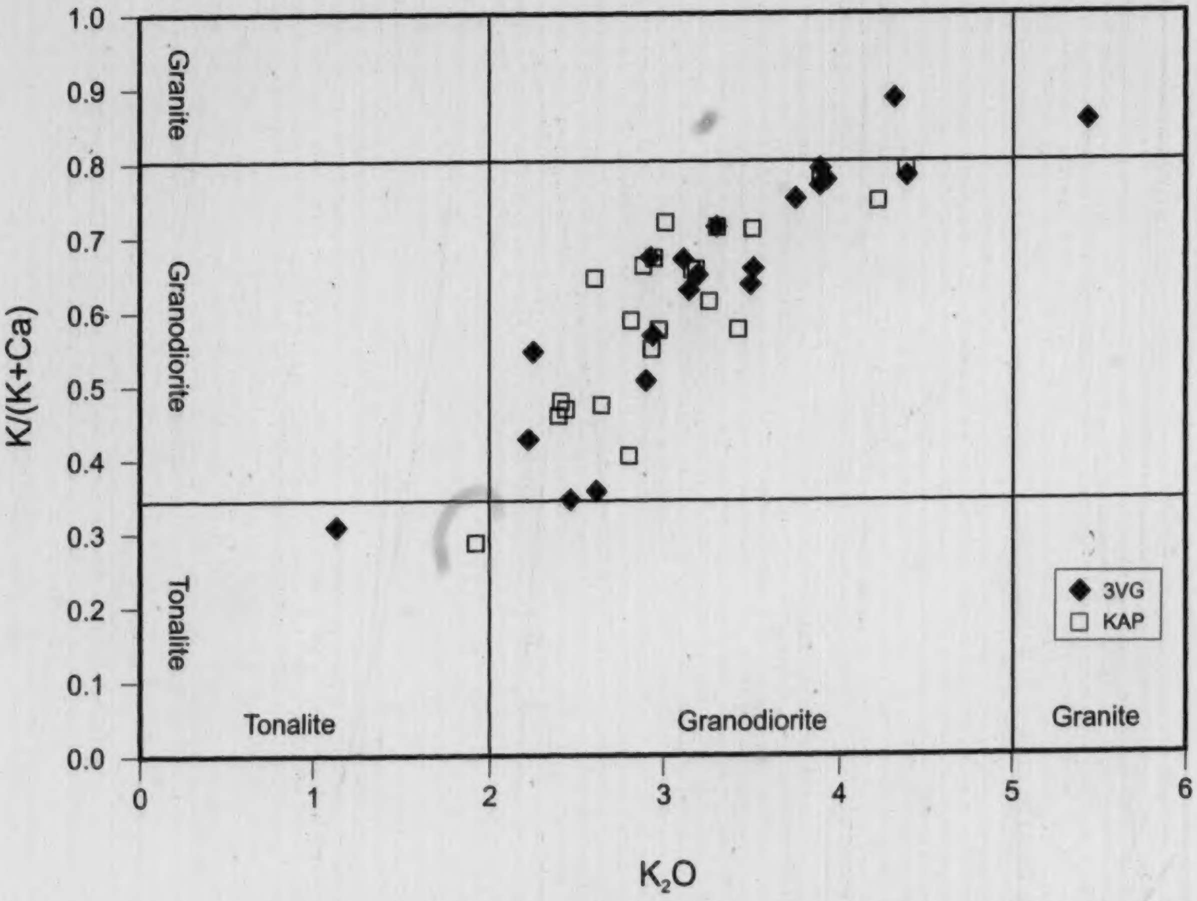

Figure 2.27: K$_2$O (Wt.%) Vs. K/(K+Ca) (molar) of experimental melts. Fields are after Lopez et al. (2005).

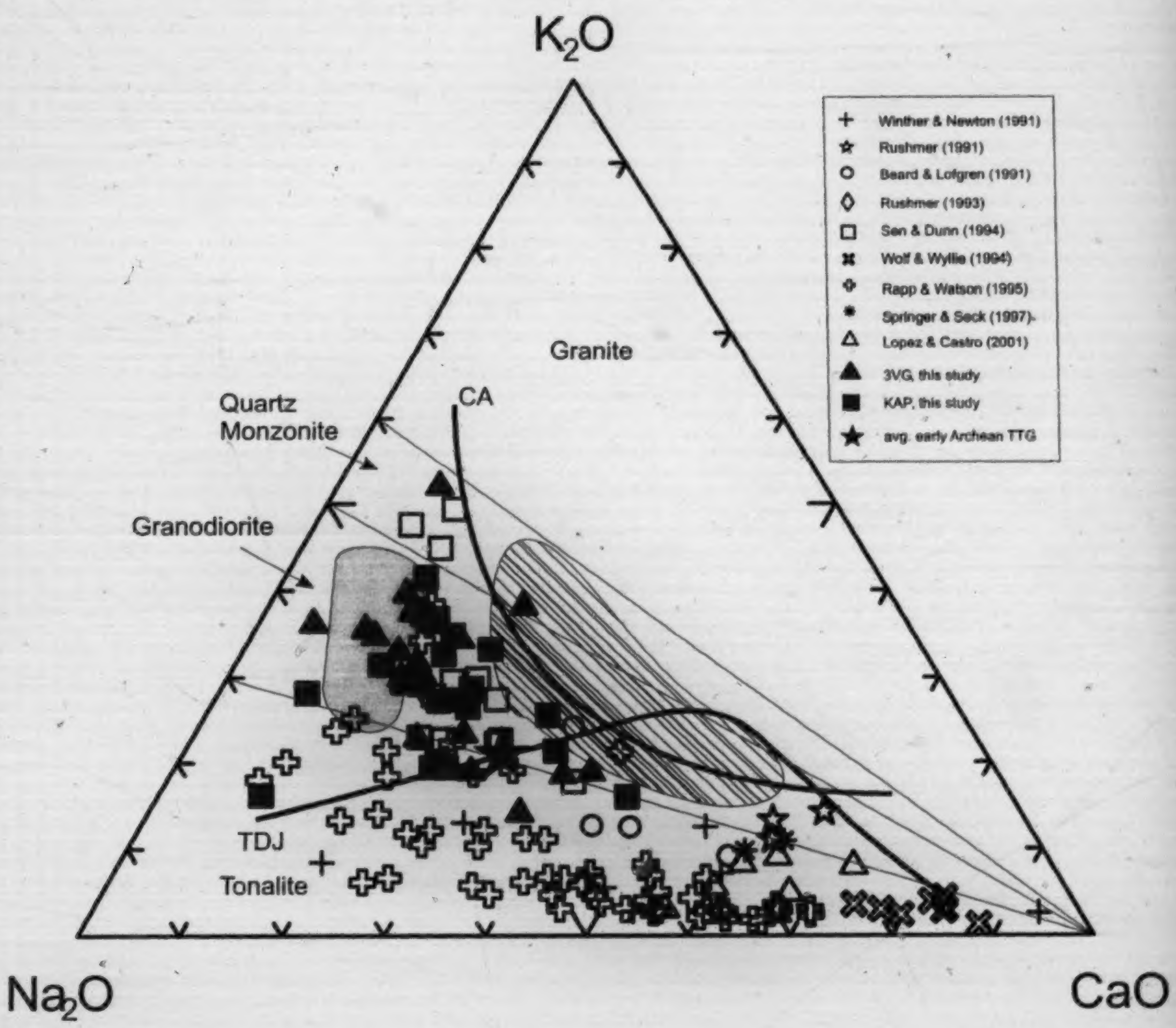

Figure 2.28: Na_2O-K_2O-CaO (wt.%) ternary showing composition of experimental melts. Shaded area represent hybrid K-richmelts produced by interaction of mafic magma with tonalite (Lopez et al., 2005). Hatched area represent the field of late Archean Closepet granite (Jayananda et al., 1996). Average early Archean TTG from Martin et al. (2005); CA, TDJ represent classic calc-alkaline and trondhjemetic trends, respectively (Barker and Arth, 1976).

Chapter 3: Garnet growth during dehydration melting of MORB-composition amphibolites: implications for partial melts and restites

INTRODUCTION

The growth of garnet in metabasaltic bulk compositions plays a key role in petrologic and geodynamic processes. In a petrological context, the presence of garnet in the crystalline residue is considered a pre-requisite for the generation of felsic magmas with strong heavy rare-earth-element (HREE) depletion (and highly fractionated REE patterns) from basaltic protoliths (Barker and Arth, 1976; Jahn et al., 1981). Source regions of Archean Tonalite-Trondhjemite-Granodiorite (TTG) and Phanerozoic adakitic magmas are believed to have satisfied this requirement (Martin 1986; Drummond and Defant, 1990). During metamorphism of basaltic rocks the appearance of garnet demarcates low- and intermediate-pressure 'two-pyroxene granulites' from high-pressure 'garnet-granulites' (DeWaard 1965; Green and Ringwood, 1967; Pattison 2003). Garnet-bearing, opx-absent assemblages form a paragenetic link between intermediate pressure granulites and high-pressure eclogites (Hansen, 1981; Pattison, 2003). In a geodynamic context, the high density of garnet-bearing assemblages is thought to play a key role in crustal recycling processes. Subduction of oceanic crust at active continental margin or island arc settings represents the primary mode of material transfer from crust to mantle in a plate tectonic framework. Increase in density of oceanic crust through stabilization of garnet-bearing assemblages contributes to the slab pull, which is considered an important driving force for subduction (Forsyth and Uyeda, 1975). An alternative crustal recycling process termed delamination (Kay and Kay, 1991) also requires stabilization of dense metamorphic assemblages in the lower crust. In this process, the increase in density of lower crust causes delamination of the lower crust along with the mantle lithosphere (Kay and Kay, 1991) or foundering of lower crust through the mantle lithosphere (Vlaar et al., 1994). Wolf and Wyllie (1993) argued that separation of melt from a garnet-rich high-density residue during dehydration melting in amphibolites could lead to the foundering of this residue through the underlying mantle. Such lower crustal delamination processes have recently been invoked to explain the origin of continental crust in the early Archean (Zegers and van Keken, 2001; Bedard, 2006). Wolf and Wyllie (1993) suggested that foundering of metabasaltic lower crust may occur in crust with thickness <40 km. This depth constraint is incorporated in many delamination models (e.g. Zegers and van Keken, 2001). In these models the delaminating lower crust is commonly considered to be in the eclogite facies. However, the results of many dehydration melting experiments indicate that plagioclase is a stable phase in metabasaltic rocks at these conditions and, therefore, the residual assemblage does not strictly correspond to an eclogite. The new experimental results presented in Chapter 2 also indicate that the residue of dehydration melting in MORB-type compositions become eclogitic only at depths >55 km. While this may appear to be a trivial semantic difference, it is important to evaluate the depths at which the phase assemblage attains sufficiently high density to effect delamination of lower crust. As will be shown in this chapter, the density of a mafic metamorphic assemblage can be linearly correlated with the abundance of garnet in the residue. Knowledge of garnet stability relations and its growth during metamorphism of metabasaltic lithologies will help us better understand lower crustal petrological and geodynamic processes.

Under fluid-absent conditions, garnet formation in high-grade metabasites is attributed to the following reactions (e.g. Pattison, 2003):

Hornblende + Plagioclase ± Quartz =

Garnet + Clinopyroxene ± Fe-Ti oxides + Melt----(1)

Orthopyroxene + Plagioclase =

Garnet + Clinopyroxene + Quartz--------------------(2)

Reaction 2 is pressure sensitive and marks the transition between 'two-pyroxene' granulites and garnet-cpx granulites. Reaction 1 marks the prograde break down of hornblende at pressures above reaction 2. The location of reaction 1 in MORB-type bulk compositions provides a temperature constraint for high-pressure amphibolite-granulite transition under fluid absent conditions. However, practical applicability of reaction 1 as a lower temperature indicator of amphibolite-granulite transition is hampered by the occurrence of garnet + cpx assemblages at amphibolite-facies conditions (Bucher and Frey, 1994; Pattison, 2003). At present, there are no accurate criteria with which to distinguish amphibolite- and granulite-facies garnet + cpx assemblages. One possible solution is to use widespread migmatitic fabric in conjunction with mineralogy as indicative of granulite-facies (Pattison 2003). At amphibolite-facies conditions migmatization requires excess water and, therefore, would be restricted to the vicinity of shear zones that may act as conduits for the influx of H_2O-rich fluids. In contrast, migmatization at granulite-facies conditions is widely believed to be a fluid-absent process proceeding through melting reactions involving hydrous minerals. The origin of leucosomes in many granulite-facies metabasites had been interpreted as resulting from dehydration melting involving hornblende breakdown reactions (e.g. Hartel and Pattison, 1996). Provided the above conditions apply, a temperature minimum for the amphibolite-granulite transition can be determined by tightly constraining the position of reaction 1.

The size, spatial distribution and compositional zoning in garnet has been used to infer mechanisms of porphyroblasts growth in metamorphic rocks (Kretz, 1974; Carlson, 1989; Carlson et al., 1995; Daniel and Spear, 1999; Spiess et al., 2001). Such studies are vital to our understanding of the kinetics of metamorphic reactions as well as the textural evolution of metamorphic rocks. These studies have addressed the relative importance of diffusion-controlled growth versus interface-controlled growth during porphyroblasts formation in metamorphic rocks. The study of garnet growth textures under controlled experimental conditions is a necessary complement to these studies on natural rocks in order to understand the mechanisms of crystal growth during metamorphism. However, very few experimental studies have described the textural aspects of garnet growth in sufficient detail. Here, I use textural aspects of garnet growth in the experiments and radius-rate calculations to show the importance of interface-controlled growth of garnet porphyroblasts.

In this paper, I also assess the role of garnet in controlling the HREE budget during dehydration melting and high-field-strength element (HFSE) depletion in the crust and its implications for crust-mantle geodynamic processes in Archean.

Previous constraints on garnet stability in metabasalts

Many studies have sought to provide broad constraints on the garnet stability field in metabasites under varying pH_2O conditions (Holloway and Burnham, 1972, Beard and Lofgren, 1989; 1991; Rushmer, 1991; Rapp et al., 1991; Winther and Newton, 1991; Wolf and Wyllie, 1994; Sen and Dunn, 1994; Lopez et al., 2001). My focus here is to constrain garnet stability relations in tectonically buried or subducted MORB-type rocks in a hot geothermal gradient that may have existed in the Archean. Under these conditions, pore water from the rocks would be driven off at shallow depths (Bjornerud and Austrheim, 2004) and the water available for high-grade metamorphic reactions would be stored primarily in hydrous phases like hornblende. Melt production at temperatures below the dry solidus for MORB will occur through dehydration-melting reactions. In this paper, I investigate garnet stability relations during dehydration-melting of hornblende-bearing MORB-type rocks. At fluid-absent conditions garnet is stabilized through reactions analogous to reaction 1 above.

There is considerable ambiguity in the temperature location of reaction 1 reported in different experimental studies (Pattison, 2003). While this partly reflects the varying bulk compositions used in the experiments, tight experimental brackets over a range of pressures are not available from these studies. However, these studies have confirmed that in a variety of basaltic bulk compositions garnet formation is restricted to pressures above 10 kbar (Beard and Lofgren, 1991; Rushmer 1991; Wolf and Wyllie, 1994; Lopez and Castro, 2001). This is consistent with phase relations in glass crystallization experiments on different basaltic compositions (Green and Ringwood, 1967). Of the dehydration melting studies, only Lopez and Castro (2001) provided pressure brackets for the appearance of garnet near the solidus. Winther and Newton (1991) conducted experiments in the presence of varying amounts of H_2O, with one set of experiments containing 0.78% H_2O, the results of which are used for the present discussion. They reported a near isothermal topology for reaction 1 around 850 °C in the pressure interval 5–21 kbar in their experiments on an average Archean tholeiite. However, the position of the reaction in P-T space was not tightly bracketed. Lopez and Castro (2001) bracketed the appearance of garnet between 800 and 850 °C at 12 kbar. Sen and Dunn (1994) conducted dehydration melting experiments on a natural amphibolite at 15 and 20 kbar. They did not provide a bracket for garnet appearance, but reported a negative slope for reaction 1 in order to be consistent with the phase relations of Wolf and Wyllie (1994) at 10 kbar. Patino Douce and Beard (1995) reported a positive slope for the garnet-producing melting reaction in the pressure interval 12-15 kbar in experiments with a synthetic quartz-amphibolite. Orthopyroxene was reported as a product of the garnet-producing reaction in the entire pressure range investigated. However, the starting composition of Patino Douce and Beard (1995) is not typical of MORB-derived amphibolites.

Winther and Newton (1991), Sen and Dunn (1994), and Lopez and Castro (2001) reported garnet-in at temperatures well above (>100 °C higher) the water-saturated solidus of basalt. However, Wolf and Wyllie (1993) argued that garnet could be stabilized in metabasaltic rocks at temperatures as low as the water-saturated solidus of basalts. They argued that nucleation difficulties at temperatures below 850 °C prevented the growth of garnet in many experimental investigations. Sen and Dunn (1994) had garnet in their starting material, which should have avoided nucleation difficulties during the experiments. Their lowest temperature experiment at 800 °C (20 kbar) contained garnet, but cannot be used to substantiate the argument of Wolf and Wyllie (1994) as no experiments were done at temperatures close to the water-saturated solidus.

Here, I present results of dehydration melting experiments on two MORB-type amphibolites at conditions that span most of the hornblende breakdown interval. The present experiments were conducted for longer duration (see Table 2.3) than previous studies and in the presence of minor amounts of garnet in the starting material, which offsets possible nucleation difficulties involving garnet. When nucleation difficulties are overcome, garnet grows rapidly relative to other crystalline phases during amphibolite dehydration melting (Wolfe and Wyllie, 1993). The presence of garnet seeds in the starting material should, therefore, enable growth of garnet at conditions where it is thermodynamically stable. Thus, I argue that garnet stability relations presented here are better constrained than in previous studies.

RESULTS

Criteria for phase stability

Due to the presence of minor amounts of some product phases (garnet, cpx) in the starting materials, several criteria were used to assess phase stability at the experimental conditions. These include, (a) an increase in modal abundance of a phase relative to the starting proportions, (b) textural evidence indicating reaction relationship between different phases (e.g. inclusion of clinopyroxene within garnet (both products of amphibolite dehydration melting) due to relative differences in the growth kinetics), (c) presence of overgrowths on phase seeds, and (d) distinct changes in the composition of a phase compared with the starting compositions. Applying these criteria, metastable persistence of some seeds was noted in many low temperature experiments. The phase stability relations discussed in this paper are based on mineral growth criteria discussed above rather than mineral appearance.

Phase relationships

Experimental results indicate a lower pressure limit of 10 kbar for garnet stability at the temperature range investigated (Figure 3.1). This result is consistent with the findings of previous experimental studies (Sen and Dunn, 1994; Lopez and Castro, 2001). Garnet appearance was bracketed in the 3VG experiments to between 800 and 850 °C in the pressure range 10-15 kbar. Within this pressure interval garnet formation is attributed to the reaction Hbl + Plag + qtz = grt + cpx ± opx + melt. This reaction has a steep negative dP/dT slope. Garnet appearance was bracketed at 12.5 kbar between 850 and 775 °C. In the KAP experiment, garnet appearance was bracketed between 800 and 850 °C at 10 and 12.5 kbar and between 775 and 800 °C at 15 kbar. Orthopyroxene coexist with garnet in 3VG in the pressure interval 10-12.5 kbar. In experiments with the more Fe-rich KAP composition, orthopyroxene and garnet do not coexist in any of the experiments. Absence of garnet in the lowest temperature experiments on both KAP and 3VG cannot be attributed to nucleation difficulties, as many growth sites were available in the form of garnet seeds in the starting materials. Accordingly, I attribute the lack of garnet below 850 °C (and below 800 °C for KAP at 15 kbar) to its thermodynamic instability. This is supported by the complete absence of garnet in the low temperature experiments, suggesting that the garnet seeds were consumed by reaction during the experiments.

Garnet growth textures

Garnet occurs as two morphologic types in the experimental run products - as overgrowths on garnet seeds and as discrete grains (neoblasts) that nucleated during the experiments (Figure 3.2 A-D). The former type is easily recognized by the presence of a rim that is compositionally distinguishable from that of the starting garnet core. Remnant garnet seeds were present as cores in almost all the experiments with the KAP starting material. Garnet crystals are typically poikiloblastic, incorporating other phases during its growth. These inclusions (most commonly clinopyroxene and hornblende) are distinct textural features of neoblastic garnets and overgrowths. The cores, representing relict garnet seeds, are devoid of any inclusions (Figure 3.2 A). The compositions of pyroxene inclusions in garnets are identical to pyroxenes in the matrix that grew during the experimental conditions. This indicates that the growth rate of pyroxene crystals was slow relative to that of the adjacent garnet crystals, which grew at a faster rate to poikilitically enclose the pyroxenes. The hornblende inclusions appear to be relics of the starting hornblende.

Despite the anhedral nature of the garnet seeds, the overgrowths developed euhedral, equant crystal boundaries. Melt pockets commonly fringe garnet crystals and are easily identified by their distinctive dihedral angles with crystalline phases (Figure 3.2 C). At experimental conditions where less garnet is produced (<900 °C, <15 kbar), melt is generally segregated around the capsule walls. In experiments where abundant garnet is present, quenched melt is disseminated in pockets around the garnets (Figure 3.2) suggesting that the presence of garnet crystals serve as collection sites for melt.

Another feature of garnet growth in these experiments is the apparent difference in the number of garnet nuclei in the two starting materials. Although the amounts of garnet produced were similar in both bulk compositions, growth occurred on a larger number of nuclei in KAP than in 3VG. Interestingly, 3VG garnets are on average much larger than the KAP garnets at the same experimental conditions (Figure 3.3). I attribute this grain size difference to differences in availability of garnet seeds. More specifically, the lower number of garnet nuclei in 3VG resulted in the growth of larger grains on those fewer nuclei. Importantly, the proportions of garnet in both bulk compositions follow a similar correlation with pressure (see below).

Controls on garnet growth

Growth of porphyroblasts in metamorphic rocks is believed to occur by diffusion of components through an intergranular fluid phase (Carlson, 1989). In the present experiments, at super-solidus conditions, a silica-rich melt is present as the intergranular fluid phase and facilitates transport of ions to growth sites. Given homogenous melt distribution within the charge, the growth of porphyroblasts like garnet during the experiments is controlled by the diffusion rate of elements through the melt (diffusion control) and/or by the rate of incorporation of these materials at the garnet interface (interface control). During diffusion controlled growth, individual garnet crystals tap elements from a diffusional domain that may or may not overlap with diffusional domains of other crystals (Figure 3.4). Overlap of diffusional domains will result in competition for materials and limited growth of crystals within that domain. Therefore, during diffusion controlled crystal growth, isolated crystals are expected to grow larger than crystals that are clustered together or closely spaced. Also, nucleation of new crystals would be limited to areas outside the diffusional domain of pre-existing crystals. This results in a non-random distribution of crystals (Daniel and Spear, 1999). During interface controlled growth, pre-existing crystals do not inhibit nucleation of new crystals in its vicinity. A more random distribution as well as clustering of crystals would be expected in this case. Also, due to lack of competition for growth ingredients, crystal sizes are not influenced by the distance to next nearest neighbor, which for interface controlled growth is much less than that for diffusion-controlled growth (Figure 3.4).

Random distribution of garnet crystals in the current experiments (Figure 3.3 A&B) is suggestive of an interface-controlled growth mechanism. No correlation between the size of the crystals and its distance to the next nearest neighbor was observed in the experimental charges. Crystals that occurs in clusters were found to be as large as isolated crystals indicating that diffusional processes were not rate limiting. In many higher temperature experiments, growth domains of individual garnet crystals impinged to form grain aggregates (Figure 3.2D). Grain aggregation has been documented to be a common growth feature in natural garnet porphyroblasts (Daniel and Spear, 1998). A higher degree of grain aggregation was observed in the 3VG than in the KAP experiments. This could be the result of larger average size of garnet crystals and growth addition to relatively fewer and closely spaced nuclei in 3VG. During diffusion-controlled growth, inhibition of crystal nucleation within the diffusional domain of pre-existing crystals would, in general, lead to less aggregation of these crystals with neoblasts (Figure 3.4). The common occurrence of growth impingement between neoblasts and overgrowths (on seeds) in the present experiments indicate that nucleation of new crystals was independent of the locations of pre-existing crystals, a feature of interface-controlled growth.

The radius-rate method (Kretz, 1974; Daniel and Spear, 1999) has been applied to understand the growth mechanisms in natural garnets. In this method, compositional zoning profiles in garnets are utilized to calculate the relative growth rate. This is done by calculating the radial distance between two compositional contours for a pair of garnets and dividing this distance in the smaller garnet by the distance in the larger garnet. This parameter, normalized Δr, is a measure of amount of material added to garnet over a compositional interval. A plot of Δr vs. normalized radius (defined as the ratio of the radius of the small garnet measured from the centre to the midpoint of the two compositional contours to a similar measurement in the large garnet) is a radius-rate curve, the shape of which varies for diffusion controlled growth and interface controlled growth (Figure 3.5). Diffusion-controlled growth is characterized by a concave upward profile signifying faster growth for smaller crystals. In contrast, interface-controlled growth is characterized by a radius rate curve showing a normalized rate equal to unity signifying identical radial increments for crystals, regardless of their size.

Although compositional zoning of garnet did not occur during the present experiments, the lack of compositional equilibrium between the garnet seeds and overgrowths provide us with two distinct compositional domains that can be used for radius-rate calculations. Calculations were made by modifying the method employed by Daniel and Spear (1999). Radius rate plots were calculated from BSE images for three

KAP samples in the following manner. KAP samples were chosen because of the ease with which compositional difference between the seed and overgrowths could be detected on BSE images. From the BSE image the area of a garnet seed was measured by counting the pixels by grayscale thresholding (using NIH Image software, Rasband, 1997-2005) and a corresponding radius (r_1) calculated from a circle with an area equal to the measured area. A similar procedure was carried out for the garnet overgrowth on that seed and a corresponding overgrowth radius calculated (r_2). The difference between the two measurements (r_2-r_1) is a function of the growth rate of garnet during the experiments. The average of the sum of two measurements also gives the average radius (R) for the garnet crystal. This procedure was repeated for five garnet crystals of varying sizes from the same experiment. Only crystals without obvious growth impingement were chosen for measurements. Radius-rate plots were then made by plotting normalized Δr $((r_2-r_1)_{\mathrm{small\ grain}}/(r_2-r_1)_{\mathrm{large\ grain}})$ against normalized radius $((r_2+r_1)/2)_{\mathrm{small\ grain}}/((r_2+r_1)/2)_{\mathrm{large\ grain}})$ for a pair of garnets. The largest uncertainty in this method is introduced by measuring crystals that are cut off-centre which could lead to a higher or lower calculated Δr values if the concerned crystal is small or large, respectively. Another uncertainty in the calculated radius of the overgrowths is imposed by the presence of mineral inclusions within the overgrown domain. The effect of this in radius rate calculations was reduced by visually selecting crystals with similar inclusion density for area measurements.

Radius rate plots for the different KAP samples reflect a similar trend (Figure 3.5). The radius rate data for these samples are relatively flat or show a slight linear trend. The majority of the points have normalized Δr <1, suggesting that growth was either faster for the large crystal or that the measurements were done on large crystals that were sectioned off-centre. Although most of the radius rate values are less than one, they are close to unity as would be expected for interface-controlled growth. In general, the radius rate data do not exhibit any significant upward curvature as would be expected with diffusion-controlled growth. Diffusion-controlled growth predicts higher Δr for lower normalized radii (implying that smaller crystals grow proportionately faster), which is not borne out by the radius rate measurements on garnets in the present experiments.

Garnet mode

The estimated modal abundances of phases are given in Table 2.11. Figure 3.6 shows the variation in the modal abundance (as volume percent of the product phases) of garnet as a function of pressure. The influence of experimental duration on the modal abundance of garnet was assessed at 17.5 kbar and 20 kbar at 950 and 900 °C, respectively. The largest discrepancy in garnet abundance is in the 20 kbar (900 °C) experiments where garnet is 7% more abundant in the 240 hour experiment than in the 48 hour experiment (Figure 3.7). This difference is outside the typical uncertainties in the modal abundance estimate of garnet in these experiments. The difference in garnet abundance in 192 and 264 hour experiments at 17.5 kbar is minor. I concur with the observation of Wolfe and Wyllie (1993) that phase abundances approach equilibrium in experiments over 4 days duration. On the basis of the longer duration of my experiments compared to those of previous studies, I argue that the garnet abundances reported here are likely closer to the equilibrium value. Garnet abundance is positively correlated with pressure (at temperature >850 °C, r^2 = 0.88 and 0.93 for 3VG and KAP, respectively). Above 850 °C, increase in garnet abundance with pressure follows a similar pattern for both bulk compositions (1.7 vol.%/kbar for KAP and 1.6 vol.%/kbar for 3VG) (Figure 3.6). There seems to be a weak positive correlation between garnet abundance and temperature (at constant pressure), but the variation is within the uncertainty of the garnet mode estimate.

Garnet compositions

The average compositions of garnets from the experimental run products are reported in Table 2.8. The garnet compositions reflect bulk compositional differences between the two starting materials, with those from 3VG showing generally higher MgO and lower FeO and CaO contents than the KAP garnets at the same experimental conditions. Garnets are almandine rich (47- 56 mole % for KAP and 44 – 53 mol% for 3VG) with very low Cr_2O_3 (< 0.06 wt.% Cr_2O_3). Pyrope content varies from 10 – 27 mole % in the KAP experiments and 16 - 32 mole % in 3VG experiments. Grossular content of garnets is very similar in both bulk compositions generally varying between 20 and 31 mole %.

3VG

The Mg-number of garnet varies between 0.24-0.42 and increases with temperature and more subtly with pressure at the experimental conditions investigated. Garnets in run products with textural evidence for growth are characterized by higher Mg-number, MgO, TiO_2 and lower FeO and MnO contents than the starting garnet.

These geochemical features were used as criteria for new garnet growth in the experiments. In general, MnO content decreases with increasing temperature. The grossular content varies between 20 and 31 mole % and decreases with increasing temperature.

KAP

The Mg-number of garnet varies between 0.23-0.38 and increases with temperature and subtly with pressure. As with 3VG, garnets have higher MgO, TiO_2 and lower FeO and MnO contents than the starting garnets. In contrast to the 3VG experiments, many garnets are zoned in the KAP experiments with the core having compositions similar to the starting garnet. Grossular content ranges between 0.21 and 0.29 mole % and does not show any appreciable variation with pressure or temperature.

Ti in Garnet

Moderate to high Ti contents observed in the experimental garnets (0.65-1.57 wt. % TiO_2 in KAP and 0.62-1.58 wt. % TiO_2 in 3VG) is a characteristic of, but not unique to, the present experiments. A compilation of experimental garnet compositions from previous metabasalt melting experiments also reveals moderate to high Ti concentrations in garnets (Figure 3.8). None of the garnets in the present study and only 5 of 78 garnet analyses from previous experiments have TiO_2 contents < 0.5 wt. %. The compilation is mostly from dehydration melting experiments but also include a few water-undersaturated melting experiments (experiments with free water but in quantities insufficient to saturate the melt phase at the P-T conditions investigated) on metabasalts.

I suggest that in the temperature range 850-1200 °C, TiO_2 content >0.5 wt. % is a characteristic feature of garnets produced by hornblende dehydration melting reactions. This is true for metabasaltic rocks with a range of Fe/Mg ratios and bulk TiO_2 contents. Although there is considerable scatter in the data, the TiO_2 content of garnet appears to be weakly correlated with temperature and pressure in my experiments (Table 2.8). In general, TiO_2 in garnet increases with temperature up to 1000 °C. Above this temperature, Ti content drops marginally reflecting a change in the partitioning of Ti at these conditions. At constant temperature, Ti in garnet increases marginally with pressure.

Tetravalent Ti occupies the octahedral site in garnet, requiring charge compensation in the structure (Meagher, 1980). A number of charge compensating substitutions mechanisms have been proposed for incorporating Ti in the octahedral site of garnet. These include substitution of monovalent cations in the dodecahedral site (NaTi garnet), Fe^{3+} in the tetrahedral site (schorlomite) (Chakhmouradian & McCammon, 2005), Mg in the octahedral site (Mg-morimotoite), Al in the tetrahedral site (Al-schorlomite), Fe^{2+} in the octahedral site (morimotoite), and Fe^{2+} in both octahedral and dodecahedral site (Fe-morimotoite) (Meagher, 1980; Petermann et al., 2003). The relative importance of these substitution mechanisms was evaluated by recalculating the garnet analyses into end members using the calculation scheme of Locock (2008)(Table 3.1). This scheme assumes 8 cations and 12 oxygens with no vacancies and uses charge balance constraints to evaluate the proportions of ferric and ferrous iron in the garnet. It also assigns Ti in garnet to six endmembers on the basis of charge balance, reflecting the six substitution mechanisms listed above. All of the above mentioned substitution mechanisms, except Fe-morimotoite and schorlomite substitutions, can be invoked to explain the high Ti content in the garnets from the present study. Na_2O was not measured for all the garnets from my experiments. However, available data indicate that substitutions involving NaTi garnet and Mg-Morimotoite appear to be minimal. Al-schorlomite and morimotoite components seem to be the main charge balancing substitutions accompanying incorporation of Ti into the garnet structure in my experiments.

Figure 3.9 is a plot of the distribution coefficient (K_d) of TiO_2 between garnet and liquid in experiments for which compositional data are available. At melt TiO_2 <1 wt. %, K_d values are >1 indicating that Ti is preferentially partitioned into garnet during dehydration melting of metabasaltic compositions. A review of available data indicate that melt TiO_2 contents exceed 1 wt. % only at temperatures above 1000 °C. In the present study only two of the measured melt compositions (both at 1050 °C) had TiO_2 content >1 wt. %. The garnet-melt TiO_2 distribution coefficient is >1 for all available garnet-melt compositions.

Restite Density

I calculated the density of the residue of partial melting using measured mineral compositions and abundances and mineral molar volume, compressibilities and thermal expansivities given by Berman and Aranovich (1996). For solid solutions like garnet, plagioclase, clinopyroxene and orthopyroxene, mineral density was calculated as a linear interpolation between those of the end members. The calculated restite density as a function of pressure is shown in Figure 3.10. For a pressure increase from 10 to 22.5

kbar, there is near-linear increase in density of the restite for both bulk compositions. Within this pressure range density of the restite increases from 2.96 to 3.47 g/cm^3 for the 3VG composition and 3.00 to 3.45 g/cm^3 for the KAP composition. The increase in density of the restitic assemblage with pressure is directly correlated with the proportion of garnet in the residue (Figure 3.11).

DISCUSSION

Implications for slab melts

Experimental melt compositional data indicate that melt TiO_2 contents are below 1 wt. % at temperatures below 1000 °C (Figure 3.12). Experimental data on TiO_2 solubility in silicate melts indicate that this is a function of temperature, melt composition and, to a lesser extent, pressure (Ryerson and Watson, 1987). Above 1000 °C, melt TiO_2 contents exceed 1 wt. %. Purported slab melts such as high-SiO_2 adakites and Archean TTG's are characterized by TiO_2 content < 1 % (Martin et al, 2005). Many of these magmas are characterized by a negative Ti anomaly in primitive-mantle normalized trace-element diagrams. Garnet compositional data from our experiments indicate that this mineral can sequester significant Ti in its structure and contribute to the low TiO_2 contents and negative Ti anomalies of slab-derived magmas. If these magmas were generated at temperatures above 1000 °C, they must have undergone fractionation of Ti-rich phases during transport to their emplacement level.

The high TiO_2 content observed in garnets of dehydration melting experiments have important geochemical and petrological implications. Continental crust and depleted mantle have subchondritic Nb/La, Nb/Ta and Ti/Zr ratios (Rudnick et al., 2000). This mass imbalance in Nb, Ta and Ti between continental crust and depleted mantle, its presumed complementary reservoir, has been attributed to the presence of rutile in refractory eclogites that are sequestered within deeper levels of the Earth's mantle (Rudnick et al., 2000). The basis of this conclusion is the sporadic occurrence of rutile in eclogite xenoliths, its high K_d values for Nb and Ta during partial melting, and a deficit in the Ti budget of calculated bulk compositions using modal abundance and compositions of garnet and omphacite in eclogite xenoliths (Rudnick et al., 2000). The Ti content of eclogitic garnets in these calculations was generally assumed to be <0.5 wt. %. The observed deficit in Ti in the mass balance calculations was translated to an estimate of rutile abundance assuming no preference of other phases for Ti. On the basis of higher TiO_2 content of garnets presented here and reported in previous studies, I suggest that the Ti deficiency and in turn the calculated rutile abundances may have been overestimated in these computations. My results show that in low-Ti amphibolites, garnet can be an important repository for Ti (and possibly other HFSE) during metamorphism of metabasaltic rocks and that Ti behaves compatibly during partial melting of metabasalts in the garnet stability field.

Although experimental data suggest high TiO_2 (>0.5 %) to be a common feature of residual garnets during dehydration melting of amphibolites, available garnet compositional data from natural high-pressure granulite and eclogite-facies rocks show relatively low TiO_2 contents (Figure 3.8). The rarity of high Ti-garnets in natural high-pressure granulite and eclogite samples may indicate that a Ti-rich phase is exsolved from garnet during cooling or exhumation of these rocks. The presence of numerous rutile and ilmenite inclusions in garnet in many eclogite and other lower crustal mafic xenoliths has been attributed to such an exsolution process (Hills and Haggerty, 1989; Zhang et al., 2003). Many such inclusions in the form of crystallographically oriented rutile needles have been noted in eclogite and clinopyroxenite xenoliths (Hills and Haggerty, 1989; Figure 3.13) and in exhumed ultra-high pressure terranes (Zhang et al., 2003). Other studies have reported randomly oriented rutile inclusions in garnets from eclogite xenoliths (Usui et al., 2006). Avoidance of rutile inclusions and lamellae during microprobe analyses of garnet (a routine spot selection criterion during microprobe work) may have resulted in the measurement of garnet TiO_2 contents that are reflective of post-exhumation rather than peak metamorphic conditions. If this is true, re-integration of exsolved rutile lamellae with matrix garnet composition is required to obtain the TiO_2 content of garnet at peak metamorphic conditions.

Garnet-melt trace element partitioning data are used extensively in trace-element modelling of partial melts generated from mafic and ultramafic source rocks (e.g. Hirschman and Stolper, 1996; Moyen et al., 2006). The high TiO_2 content of garnet has implications for partitioning of trace elements between garnet and co-existing melt (Petermann et al., 2003; Dwarzski et al., 2006). Garnet-melt partitioning data indicate that Ti behaves compatibly to at least 1000 °C. A number of charge compensating substitutions accompany substitution of Ti into the garnet structure as described above. Incorporation of highly charged trace elements (e.g. Th, U, HFSE, REE) in garnet during melting is achieved through substitution schemes analogous to the Ti-substitution mechanisms (Petermann et al., 2003). The presence of high Ti content in garnet may limit the charge compensating mechanisms available for incorporating other highly charged trace elements. Garnet-melt partition coefficients for highly charged trace elements are, therefore, lower for Ti-rich garnets than for Ti-poor garnets (Petermann et al., 2003). The Ti-effect may counteract the effect of other cations on the trace element partitioning behavior of garnet. For example, van Westrenen et al. (2001) showed that eclogitic garnets with more than 19 mol % Ca have higher partition coefficients for many HFSE than garnets with less Ca. The residual garnets of the present study have > 19 mol % Ca, similar to garnets from many high pressure granulite and eclogitic assemblages. However, the high Ti of garnet in the present study may offset the effect of Ca on HFSE partitioning. Klimm et al. (2008) did not find any difference in the partitioning behavior of highly charged cations in Ti-free and Ti-bearing garnet. The partitioning behavior observed in the experiments of Klimm et al. (2008) may have been caused by the relatively high grossular content of garnets in their study. A systematic study of the contrasting effects of Ti and Ca on the trace-element partitioning behavior of garnets is required to fully understand the garnet signatures that likely result from partial melting of MORB-derived mafic rocks in the garnet stability field.

Implications for restite delamination

Kay and Kay (1991) advocated delamination of lower crust as a crustal recycling mechanism. This process has been purported to take place in areas of thickened continental crust (Bird, 1979; Ducea and Saleeby, 1996; Zandt et al., 2004) and oceanic plateaus (Zegers and van Keken, 2001; Bedard, 2006). Delamination, as originally proposed, involves the sinking of lower crust and mantle components of the lithosphere into asthenosphere (Kay and Kay, 1991; Lustrino, 2005). More recently a different mode of delamination has been proposed in which the formation of high density assemblages in mafic lower crust lead to Rayleigh-Taylor instabilities causing the lower crust to sink into the mantle (Zegers and Van Keken, 2001). Such a delamination process has been proposed to be the dominant mode of crustal recycling before the onset of modern-style plate tectonic process in the late Archean (Vlaar et al., 1994; van Thienen et al., 2004a, 2004b; Bedard, 2006). Implicit in the delamination models is the requirement that restite density exceeds 3.3 g/cm^3, the density of the underlying mantle (Ringwood and Green, 1966). This density increase is largely attributed to the formation of a dense eclogite-facies assemblage in the mafic lower crust (Zegers and van Keken, 2001; van Thienen et al., 2004b).

My calculations show that restite density, which is directly proportional to the amount of garnet in the residue, only exceeds the density of the underlying mantle at pressures above ~17.5 kbar (Figure 3.9), which corresponds to a depth of ~55 km. This depth corresponds to the transition of the restite assemblage from garnet-granulite to eclogite-facies. For two reasons, this depth estimate is likely to represent a minimum value. Firstly, the calculated restite density assumes complete segregation of melt from the residue, which is likely never achieved in nature. Textural observations in the experimental charges indicate that presence of abundant garnet provides pockets where melt could collect without being removed. Unless active deformation forces melt out of these pockets, the effective density of the restite would be lowered by the presence of disseminated melt pockets. Secondly, the lower parts of oceanic crust would be composed of cumulates with higher Mg/Fe than the differentiated rocks at upper levels of the crust (Farnetani et al., 1996; Foley et al., 2003). If this were the case, the depth requirement for generating the necessary amount of garnet would be > 55 km, given the positive correlation between the lower pressure limit of garnet stability and the Mg-number of the basalt protolith (Green and Ringwood, 1967; Foley et al., 2003). A 55 km thickness estimate of crust required for effecting delamination is considerably greater than the average thickness of continental or oceanic crust. It is important to note that this thickness requirement is also larger than the thickness estimates for Archean oceanic crust using parameterized mantle melting models (McKenzie and Bickle, 1988; Vlaar and van den Berg; 1991). Thus crustal thickening by tectonic or magmatic processes is a prerequisite to delamination. Oceanic Plateaus with crustal thickness larger than normal oceanic crust have been suggested as possible locales for delamination of lower crust (e.g. Zegers and van Keken, 2001). Modern-day oceanic plateau sequences are thought to have been generated above anomalously hot mantle. The thickness of the crust in the Ontong Java plateau, the world's largest oceanic plateau is ~35 km (Gladczenko et al., 1997), much less than the thickness required to stabilize an eclogitic mineral assemblage. Delamination processes in the Archean as envisaged in the models of Zegers and van Keken (2001) and Bedard (2006) could not have been a viable geodynamic process unless unusually thick (>50 km thick) oceanic plateaus were produced in the Archean. Without evidence for the existence of such anomalously thick plateaus, lower crustal delamination models cannot be considered a viable alternative to plate tectonic processes in the Archean. The minimum thickness (55 km) necessary to effect delamination of lower crust thus appears to require a crustal thickening event, which is most easily achieved in a plate tectonic setting at convergent plate margins. Some delamination models for the Archean invoke multiple delamination events as a mechanism to generate the large volumes of felsic magmas observed in the Archean geologic record (Bedard, 2006). Multiple delamination of lower crust requires repeated thickening of the crust (after initial and subsequent delamination events) to >50-55 km. The difficulty of attaining the requisite thickness for even a single delamination event raises serious questions about the viability of multiple delamination events in Archean.

References:

Barker, F. and Arth, J.G. (1976) Generation of tondhjemitic-tonalitic liquids and Archean bimodal trondhjemite-basalt suites. Geology, 4, 596-600.

Beard, J.S. and Lofgren, G.E. (1989) Effect of water on the composition of partial melts of greenstone and amphibolite. Science, 244, 195-197.

Beard, J.S. and Lofgren, G.E. (1991) Dehydration melting and water-saturated melting of basaltic and andesitic greenstones and amphibolites at 1, 3, and 6.9 kbar. Journal of Petrology, 32, 365-401.

Bedard, J.H. (2006) A catalytic delamination-driven model for coupled genesis of Archean crust and sub-continental lithospheric mantle. Geochimica et Cosmochimica Acta, 70, 1188-1214.

Begin, N.J. and Carmichael, D.M. (1992) Textural and compositional relationships of Ca-amphiboles in metabasites of the Cape Smith Belt, Northern Quebec: implications for a miscibility gap at medium pressure. Journal of Petrology, 33, 1317-1343.

Berman, R.G. and Aranovich, L. Ya (1996) Optimized standard state solution properties of minerals 1. Model calibration for olivine, orthopyroxene, cordierite, garnet, and ilmenite in the system FeO-MgO-CaO-Al2O3-TiO2-SiO2. Contributions to Mineralogy and Petrology, 126, 1-24.

Bjornerud, M.G. and Austrheim, H. (2004) Inhibited eclogite formation: The key to the rapid growth of strong and buoyant Archean continental crust. Geology, 32, 765-768.

Bucher, K. and Frey, M. (1994) Petrogenesis of metamorphic rocks. Berlin. Springer-Verlag.

Carlson, W.D. (1989) The significance of intergranular diffusion to the mechanisms and kinetics of porphyroblasts crystallization. Contributions to Mineralogy and Petrology, 103, 1-24.

Carlson, W.D., Denison, C. and Ketcham, R.A. (1995) Controls on the nucleation and growth of porphyroblasts: kinetics from natural textures and numerical models. Geological Journal, 30, 207-225.

Carswell, D.A. and O'Brien, P.J. (1993) Thermobaraometry and geotectonic significances of high-pressure granulites: examples from the Moldanubian Zone of the Bohemian Massif in Lower Austria. Journal of Petrology, 34, 427-459.

Chakhmouradian, A.R. and McCammon, C.A. (2005) Schorlomite: a discussion of the crystal chemistry, formula, and inter-species boundaries. Physics and Chemistry of Minerals, 32, 277-289.

Clarke, G.L., Klepeis, K.A. & Daczko, N.R. (2000) Cretaceous high-P granulites at Milford Sound, New Zealand: metamorphic history and emplacement in a convergent margin setting. Journal of Metamorphic Geology, 18, 359-374.

Daniel, C.G. and Spear, F.S. (1999) The clustered nucleation and growth processes of garnet in regional metamorphic rocks from the north-west Connecticut, USA. Journal of Metamorphic Geology, 17, 503-520.

Drummond, M.S. and Defant, M.J. (1990) A model for trondhjemite-tonalite-dacite genesis and crustal growth via slab melting: Archean to modern comparisons. Journal of Geophysical Research, 95, 21503-21521.

Dwarzki, R.E., Draper, D.S., Shearer, C.K. and Agee, C.B. (2006) Experimental insights on crystal chemistry of high-Ti garnets from garnet-melt partitioning of rare-earth and high-field strength elements. American Mineralogist, 91, 1536-1546.

Ducea, M.N. and Saleeby, J.B. (1996) Buoyancy sources for a large, unrooted mountain range, the Sierra Nevada California: evidence from xenolith thermobaormetry. Journal of Geophysical Research, 101, 8229-8244.

Ernst, W.G. (1966) Synthesis and stability relations of ferrotremolite. American Journal of Science, 264, 36-65.

Ernst, W.G. and Liu, J. (1998) Experimental phase-equilibrium study of Al- and Ti-contents of calcic amphibole in MORB- A semiquantitative thermobarometer. American Mineralogist, 83, 952-969.

Farnetani, C.G., Richards, M.A. and Ghiorso, M.S. (1996) Petrological models of magma evolution and deep crustal structure beneath hotspots and flood basalt provinces. Earth and Planetary Science Letters, 143, 81-94.

Foley, S.F., Buhre, S. and Jacob, D.E. (2003) Evolution of Archean crust by delamination and shallow subduction. Nature, 421, 249-252.

Forsyth, D. and Uyeda, S. (1975) Relative importance of driving forces of plate motion. Geophysical Journal of Royal Astronomical Society, 43, 163-200.

Ghent, E.D., Stout, M.Z. and Raeside, R.P. (1983) Plagioclase-clinopyroxene-garnet-quartz equilibria and the geobarometry and geothermometry of garnet amphibolites from Mica Creek, British Columbia. Canadian Journal of Earth Sciences, 20, 699-706.

Gladczenko, T.D., Coffin, M.F. and Eldholm, O. (1997) Crustal structure of the Ontong Java Plateau: Modeling of new gravity and existing seismic data. Journal of Geophysical Research, 102, 22711-22729.

Graham, C.M. and Powell, R. (1984) A garnet-hornblende geothermometer: Calibration, testing, and application to the Pelona Schist, southern California. Journal of Metamorphic Geology, 2, 13-31.

Green, D.H. and Ringwood, A.E. (1967) An investigation of the gabbro to eclogite transformation and its petrological applications. Geochimica et Cosmochimica Acta, 31, 767-833.

Hansen, B. (1981) The transition from pyroxene granulite facies to garnet clinopyroxene granulite facies. Experiments in the system $CaO-MgO-Al_2O_3-SiO_2$. Contributions to Mineralogy and Petrology, 76, 234-242.

Hartel, T.H.D. and Pattison, D.R.M. (1996) Genesis of Kapuskasing (Ontario) migmatitic mafic granulites by dehydration melting of amphibolite: the importance of quartz to reaction progress. Journal of Metamorphic Geology, 14, 591-611.

Hellner, E. and Schurmann, K. (1966) Stability of metamorphic amphiboles: the tremolite-ferro-actinolite series. Journal of Geology, 74, 322-331.

Hills,D.V. and Haggerty, S.E. (1989) Petrochemistry of eclogites from the Koidu Kimberlite Complex, Sierra Leone. Contributions to Mineralogy and Petrology, 103, 397-422.

Hirschman, M.M. and Stolper, E.M. (1996) A possible role for garnet pyroxenite in the origin of the 'garnet signature' in MORB. Contributions to Mineralogy and Petrology, 124, 185-208.

Holloway, J.R. and Burnham, C.W. (1972) Melting relations of basalt with equilibrium water pressure less than total pressure. Journal of Petrology, 13, 1-29.

Holtta, R., Huhma,H., Manttari,I., Peltonen, P. and Juhanoja, J. (2000) Petrology and geochemistry of mafic granutite xenoliths from the Lahtojoki kimberlite pipe, eastern Finlan. Lithos, 51, 109-133.

Jahn, B-, M., Glikson, A.Y., Peucat, J.J., and Hickman, A.H. (1981) REE geochemistry and isotopic data of Archean silicic volcanics and granitoids from the Pilbara Block, Western Australia: implications for the early crustal evolution. Geochimica et Cosmochimica Acta, 45, 1633-1652.

Jenkins, D.M. and Bozhilov, K.N. (2005) Stability and thermodynamic properties of ferro-actinolite: a re-investigation. American Journal of Science, 303, 723-752.

Kay, R.W. and Kay, S.-M (1991) Creation and destruction of lower continental crust. Geologische Rundschau, 80, 259-278.

Klein, M., Stosch, H.-G. and Seck, A. (1997) Partitioning of high field-strength and rare-earth elements between amphibole and quartz dioritic to tonalitic melts: An experimental study. Chemical Geology, 138, 257-271.

Klein, M., Stosch, H.-G., Seck, A. and Shimizu, N. (2000) Experimental partitioning of high field strength and rare earth elements between clinopyroxene and garnet in andesitic to tonalitic systems. Geochimica et Cosmochimica Acta, 64, 99-115.

Kretz, R. (1974) Some models for the rate of crystallization of garnet in metamorphic rocks. Lithos, 7, 123-131.

Lockock, A.J. (2008) An Excel program to reset analyses of garnet into end-member components, and a synopsis of the crystal chemistry of natural silicate garnets. Computers & Geosciences, Doi:10.1016/j.cageo.2007.12.013

Lopez, S. and Castro, A. (2001) Determination of the fluid-absent solidus and supersolidus phase relationships of MORB-derived amphibolites in the range of 4-14 kbar. American Mineralogist, 86, 1396-1403.

Martin,H. (1986) Effect of steeper Archean geothermal gradient on geochemistry of subduction-zone magmas. Geology, 14, 753-756.

Martin, H., Smithies, R.H., Rapp, R., Moyen, J.-F. and Campion, D. (2005) An overview of adakite, tonalite-trondhjemite-granodiorite(TTG), and sanukitoid: relationships and some implications for crustal evolution. Lithos, 79, 1-24.

McKenzie, D. and Bickle, M.J. (1988) The volume and composition of melt generated by extension of the lithosphere. Journal of Petrology, 29, 625-679.

Meagher, E.P. (1980) Silicate garnets. In: Ribbe, P.H. (ed.) Orthosilicates. Review of Mineralogy, 5, 25-66.

Moyen, J.-F and Stevens, G. (2006) Experimental constraints on TTG petrogenesis: Implications for Archean geodynamics. In: Condie, K.C. and Benn, K. (eds.) Archean Geodynamics and Enviroments. Geophysical monograph, 164, 149-175.

Nair, R. and Chacko,T. (2002) Fluid-absent melting of high-grade semi-pelites: P-T constraints on orthopyroxene formation and implications for granulite genesis. Journal of Petrology, 43, 2121-2142.

Nyman, M.W., Pattison, D.R.M. and Ghent, E.D. (1995) Melt extraction during formation of K-feldspar + sillimanite migmatites, west of Revelstoke, British Columbia. Journal of Petrology, 36, 351-372.

Patino Douce, A.E. and Beard, J.S. (1995) Dehydration-melting of biotite gneiss and quartz amphibolite from 3 to 15 kbar. Journal of Petrology, 36, 707-738.

Pattison, D.R.M. (2003) Petrogenetic significance of orthopyroxene-free garnet+clinopyroxene+plagioclase±quartz-bearing metabasites with respect to the amphibolite and granulite facies.

Percival, J (1983) High-grade metamorphism in the Chapleau-Foleyet area Ontario. American Mineralogist, 68, 667-686.

Petermann, M., Hirschmann, M.M., Hametner, K., Gunther, D. and Schmidt, M.W. (2004) Experimental determination of trace element partitioning between garnet and silica-rich liquid during anhydrous partial melting of MORB-like eclogite. Geochemisty, Geophysics, Geosystems, 5, Paper number 2003GC000638.

Raase, P. (1974) Al and Ti contents of hornblende, indicators of pressure and temperature of regional metamorphism. Contributions to Mineralogy and Petrology, 45, 231-236.

Rapp, R.P., Watson, E.B. and Miller, C.F. (1991) Partial melting of amphibolite/eclogite and the origin of Archean trondhjemites and tonalites. Precambrian Research, 51, 1-25.

Rapp, R.P. and Watson, E.B. (1995) Dehydration melting of metabasalt at 8-32 kbar: implications for continental growth and crust-mantle recycling. Journal of Petrology, 36, 891-931.

Rudnick, R.L., Barth, M., Horn, I. and McDonough, W.F. (2000) Rutile-bearing refractory Eclogites: missing link between continents and depleted mantle. Nature, 287, 278-281.

Rasband, W.S. (1997-2005) ImageJ, U. S. National Institutes of Health, Bethesda, Maryland, USA, http://rsb.info.nih.gov/ij/.

Rushmer, T. (1991) Partial melting of two amphibolites: contrasting experimental results under fluid-absent conditions. Contributions to Mineralogy and Petrology, 107, 41-59.

Ryerson, F.J. and Watson, E.B. (1987) Rutile saturation in magmas: implications for Ti-Nb-Ta depletion in island-arc basalts. Earth and Planetary Science Letters, 86, 225-239.

Sen, C. and Dunn, T. (1994) Dehydration melting of a basaltic composition amphibolite at 1.5 and 2.0 GPa: implications for the origin of adakites. Contributions to Mineralogy and Petrology, 117, 394-409.

Spiess, R., Peruzzo, L., Prior, D.J. and Wheeler, J. (2001) Development of garnet porphyroblasts by multiple nucleation, coalescence and boundary misrorientation-driven rotations. Journal of Metamorphic Geology, 19, 269-290.

Springer, W. and Seck, H.A. (1997) Partial fusion of basic granulites at 5 to 15 kbar: implications for the origin of TTG magmas. Contributions to Mineralogy and Petrology, 127, 30-45.

Stosch, H.-G., Ionov, G.A., Puchtel, I.S., Galer, S.J.G. and Sharpouri, A. (1995) Lower crustal xenoliths from Mongolia and their bearing on the nature of the deep crust beneath central Asia. Lithos, 36, 227-242.

Tinkham, D.K. and Ghent, E.D. (2004) Modelling the effects of H2O activity and bulk-rock H_2O content on the developments of clinopyroxene-bearing garnet amphibolite assemblages at Mica Creek, British Columbia.

Usui, T., Nakamura, E. and Helmstaedt, H. (2006) Petrology and geochemistry of eclogite xenoliths from the Colorado Plateau: implications for the evolution of subducted oceanic crust. Journal of Petrology, 47, 929-964.

van Thienen, P., van den Berg, A.P. and Vlaar, N.J. (2004a) Production and recycling of oceanic crust in the early Earth. Tectonophysics, 386, 41-65.

van Thienen, P., van den Berg, A.P. and Vlaar, N.J. (2004b) On the formation of continental silicic melts in thermochemical mantle convection models: implications for early Earth. Tectonophysics, 394, 111-124.

van Westrenen, W., Blundy, J.D. and Wood, B.J. (2001) High field strength element/rare earth element fractionation during partial melting in the presence of garnet: implications for identification of mantle heterogeneities. Geochemistry, Geophysics, Geosystems, 2, paper number 2000GC000133.

Vlaar, N.J. and van den Berg, A.P. (1991) Continental evolution and archeo-sea levels. In: Sabadini, R., Lambeck, K., Boschi, E. (eds.) Glacial isostasy, Sealevel and Mantle Rheology. Kluwer Dordrecht, Netherlands.

Vlaar, N.J., van Keken, P.E. and van den Berg, A.P. (1994) Cooling of the Earth in the Archean: consequences of pressure-release melting in a hotter mantle. Earth and Planetary Science Letters, 121, 1-18.

de Waard, D. (1965) The occurrence of garnet in granulite facies terrane of the Adirondack Highlands. Journal of Petrology, 6, 165-191.

Winther, K.T. and Newton, R.C. (1991) Experimental melting of hydrous low-K tholeiite: evidence on the origin of Archaean cratons. Bulletin of Geological Society of Denmark, 39, 213-228.

Wolf, M.B. and Wyllie, P.J. (1993) Garnet growth during amphibolite anatexis: implications of a garnetiferous restite. Journal of geology, 101, 357-373.

Wolf, M.B. and Wyllie, P.J. (1994) Dehydration-melting of amphibolite at 10 kbar: the effects of temperature and time. Contributions to Mineralogy and Petrology, 115, 369-383.

Zandt, G., Gilbert, H., Owens, T.J., Ducea, M., Saleeby, J. and Jones, C.H. (2004) Active foundering of a continental arc root beneath the southern Sierra Nevada in California. Nature, 431, 41-46.

Zegers, T.E. and van Keken, P.E. (2001) Middle Archean continental formation by crustal delamination. Geology, 29, 1083-1086.

Zhang,R.Y., Zhai, S.M., Fei, Y.W. and Liou, J.G. (2003) Titanium solubility in coexisting garnet and clinopyroxene at very high pressure: the significance of exsolved rutile in garnet. Earth and Planetary Science Letters, 216, 591-601.

Table 3.1: End member compositions of garnet in the experiements calculated using the scheme of Lockock (2008).

Run No.	3VG-16	3VG-20	3VG-15	3VG-18	3VG-29	3VG-8	3VG-7	3VG-9	3VG-39	3VG-34	3VG-35	3VG-40	3VG-36	3VG-31	3VG-44	3VG-41	3VG-43	3VG-38	3VG-45	3VG-46
P (kbar)	12.5	12.5	12.5	12.5	15	15	15	15	17.5	17.5	17.5	17.5	20	20	20	20	22.5	22.5	22.5	22.5
T (°C)	850	950	900	1000	825	900	950	1050	850	900	950	850	850	900	900	950	850	900	950	1000
n	7	9	5	10	12	4	30	8	10	20	25	10	10	18	21	16	11	11	20	20
Endmember																				
Schorlomit	-	0.013	0.005	0.032	0.010	0.003	-	0.012	0.018	0.014	0.023	0.018	0.019	0.017	-	0.021	0.016	0.024	0.015	0.009
Morimotoi	0.019	0.013	0.017	-	0.007	0.038	0.030	0.041	-	0.030	0.035	0.010	-	0.015	0.026	0.013	0.004	0.009	0.019	0.034
NaTi garn	0.005	0.005	0.005	-	0.005	0.005	0.008	0.004	0.003	-	-	-	0.004	0.010	0.015	0.009	0.010	0.010	0.011	0.011
Morimotoi.	0.004	-	-	-	-	-	0.001	-	-	-	-	-	-	-	0.003	-	-	-	-	-
Uvarovite	-	-	-	-	-	-	0.000	0.001	-	-	-	-	-	-	-	-	-	-	-	-
Spessartin	0.030	0.018	0.015	0.010	0.033	0.014	0.010	0.009	0.016	0.007	0.008	0.008	0.010	0.006	0.007	0.007	0.007	0.006	0.007	0.008
Pyrope	0.199	0.287	0.252	0.322	0.160	0.244	0.291	0.319	0.211	0.309	0.304	0.300	0.232	0.302	0.289	0.302	0.272	0.296	0.278	0.299
Almandine	0.529	0.504	0.515	0.456	0.503	0.501	0.474	0.432	0.456	0.458	0.465	0.470	0.462	0.451	0.452	0.445	0.460	0.450	0.453	0.446
Grossular	0.210	0.147	0.178	0.143	0.279	0.190	0.165	0.181	0.271	0.177	0.163	0.171	0.264	0.195	0.204	0.199	0.222	0.200	0.218	0.193
Andradite	-	0.033	-	0.032	0.004	-	-	-	0.022	-	0.003	-	0.002	0.004	-	0.004	0.009	0.005	-	0.000

Run No.	KAP-5	KAP-16	KAP-15	KAP-20	KAP-18	KAP-8	KAP-7	KAP-9	KAP-34	KAP-35	KAP-40	KAP-42	KAP-36	KAP-44	KAP-41	KAP-43	KAP-38	KAP-45	KAP-46
P (kbar)	10	12.5	12.5	12.5	12.5	15	15	15	17.5	17.5	17.5	17.5	20	20	20	22.5	22.5	22.5	22.5
T (°C)	900	850	900	950	1000	900	950	1050	900	950	850	1050	850	900	950	850	900	950	1000
n	7	15	10	14	32	4	20	25	10	13	11	11	10	19	10	11	9	14	17
Endmember																			
Schorlomit	-	0.008	-	0.021	0.010	0.004	0.006	0.007	0.017	0.017	0.009	0.012	0.004	-	0.009	0.003	0.017	0.005	-
Morimotoi	0.008	0.032	0.034	-	0.038	0.050	0.061	0.038	0.022	0.058	0.050	0.041	0.029	0.038	0.055	0.020	0.021	0.038	0.024
NaTi garn	0.003	0.005	0.007	0.002	0.004	0.008	0.006	0.010	0.012	-	0.008	0.006	0.011	0.017	0.009	0.011	0.010	0.013	0.016
Morimotoi.	0.014	-	0.002	-	-	-	-	-	-	-	-	-	-	-	-	-	-	-	0.005
Uvarovite	-	0.001	0.001	-	0.002	0.001	0.001	0.002	-	-	-	-	-	-	-	-	-	-	-
Spessartin	0.030	0.030	0.019	0.018	0.016	0.016	0.014	0.012	0.013	0.011	0.013	0.013	0.012	0.013	0.010	0.011	0.012	0.010	0.009
Pyrope	0.187	0.167	0.205	0.246	0.282	0.229	0.250	0.293	0.242	0.255	0.265	0.279	0.197	0.229	0.261	0.210	0.238	0.249	0.235
Almandine	0.554	0.533	0.543	0.504	0.483	0.499	0.484	0.445	0.481	0.485	0.477	0.459	0.487	0.476	0.480	0.476	0.470	0.459	0.468
Grossular	0.193	0.217	0.179	0.168	0.126	0.177	0.166	0.156	0.186	0.162	0.154	0.172	0.259	0.212	0.170	0.262	0.220	0.221	0.234
Andradite	-	0.008	-	0.038	0.040	0.015	0.012	0.039	0.026	0.013	0.024	0.020	0.000	0.010	0.006	-	0.013	0.005	-

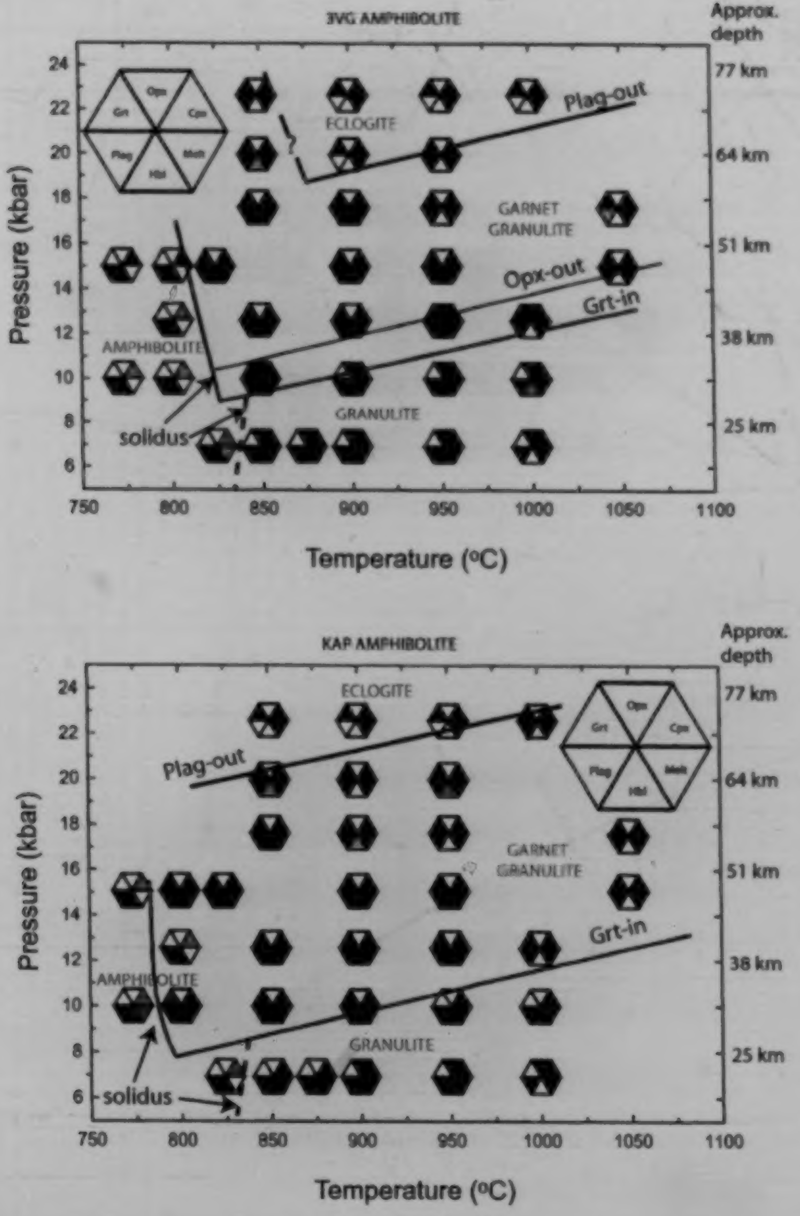

Figure 3.1: P-T phase diagram of 3VG and KAP amphibolites. Garnet-in and plagioclase out boundaries indicating stabilization of garnet-granulite and eclogite-facies assemblages, respectively, are shown. Note the region in the 3VG phase diagram where both garnet and orthopyroxene coexist.

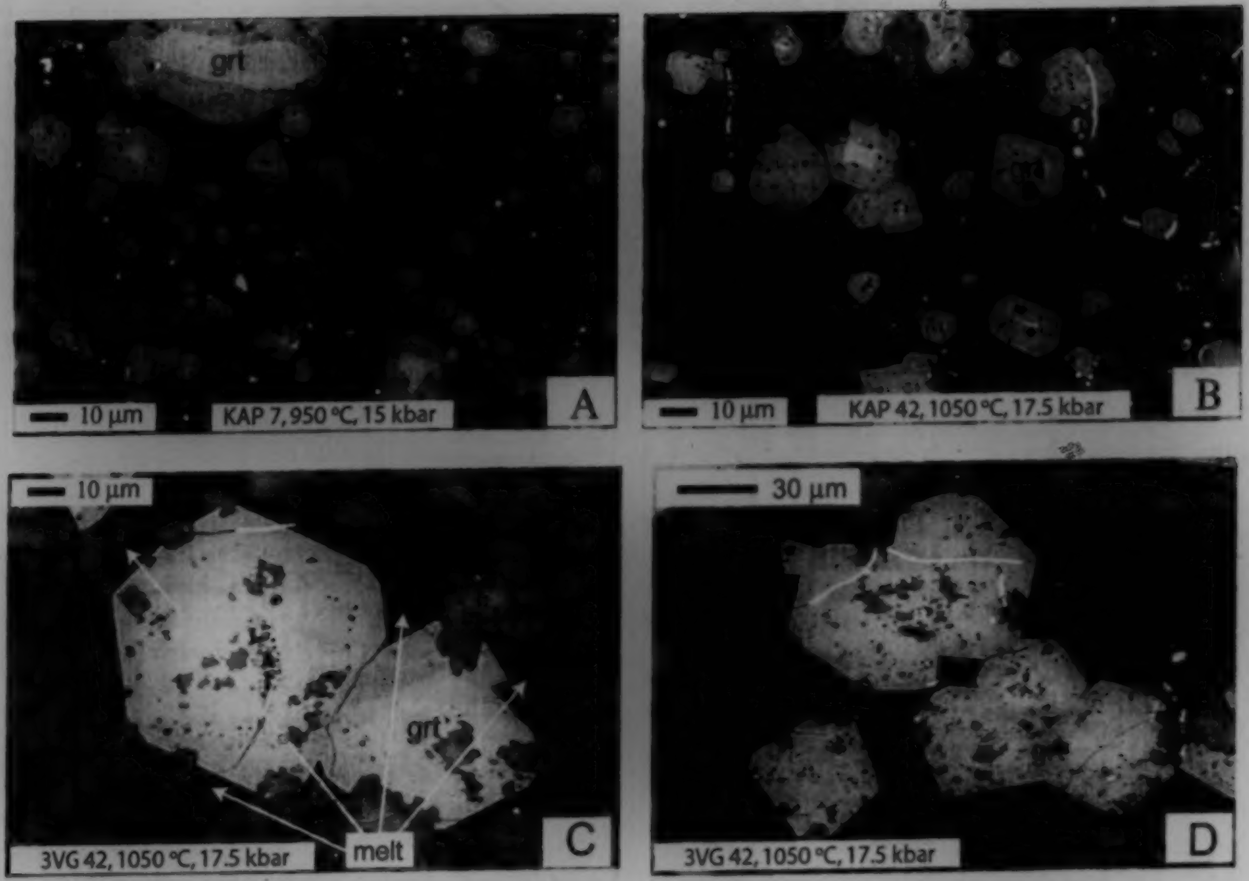
grt
10 µm
KAP 7, 950 °C, 15 kbar
A
10 µm
KAP 42, 1050 °C, 17.5 kbar
B
10 µm
grt
melt
3VG 42, 1050 °C, 17.5 kbar
C
30 µm
3VG 42, 1050 °C, 17.5 kbar
D

Figure 3.2: BSE images showing garnet growth textures during dehydration melting of amphibolites. (A) KAP sample showing neoblastic overgrowth on garnet seeds. Note the compositional contrast between the overgrowth and the seed (core). Also note the abundant mineral inclusions (dark spots) in the overgrowth domain of the crystals. (B) KAP sample showing garnet neoblasts and overgrowths. (C) Neoblastic garnet crystals showing melt distribution along grain boundaries. (D) 3VG sample showing aggregation of garnet neoblasts during growth.

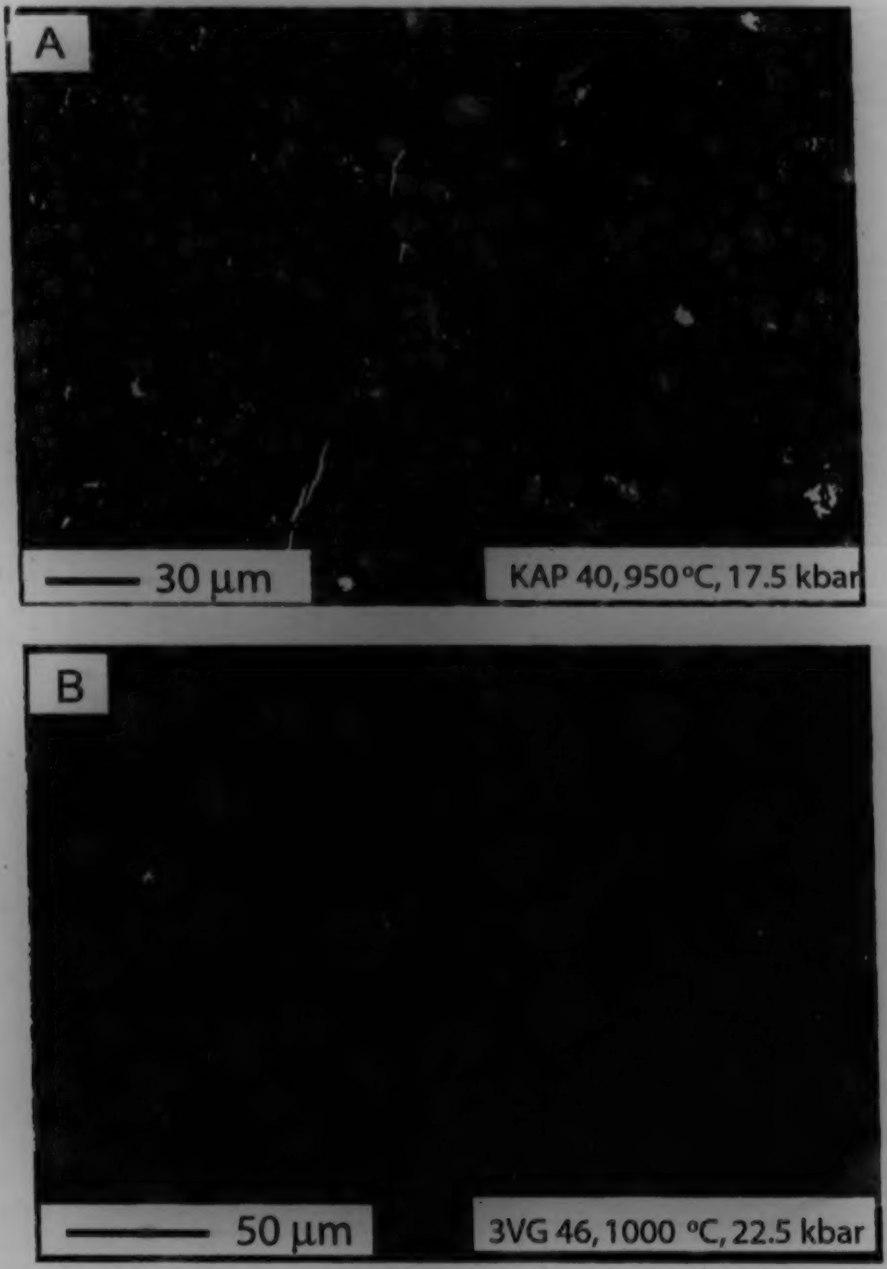
A
30 µm
KAP 40, 950 °C, 17.5 kbar
B
50 µm
3VG 46, 1000 °C, 22.5 kbar

Figure 3.3: BSE images showing typical random distribution of garnet crystals in the experiments. (A) KAP (B) 3VG. KAP garnets grew on a relatively larger number of nuclei (seeds) than 3VG. Growth on a limited number of nuclei in 3VG resulted in the formation of larger crystals.

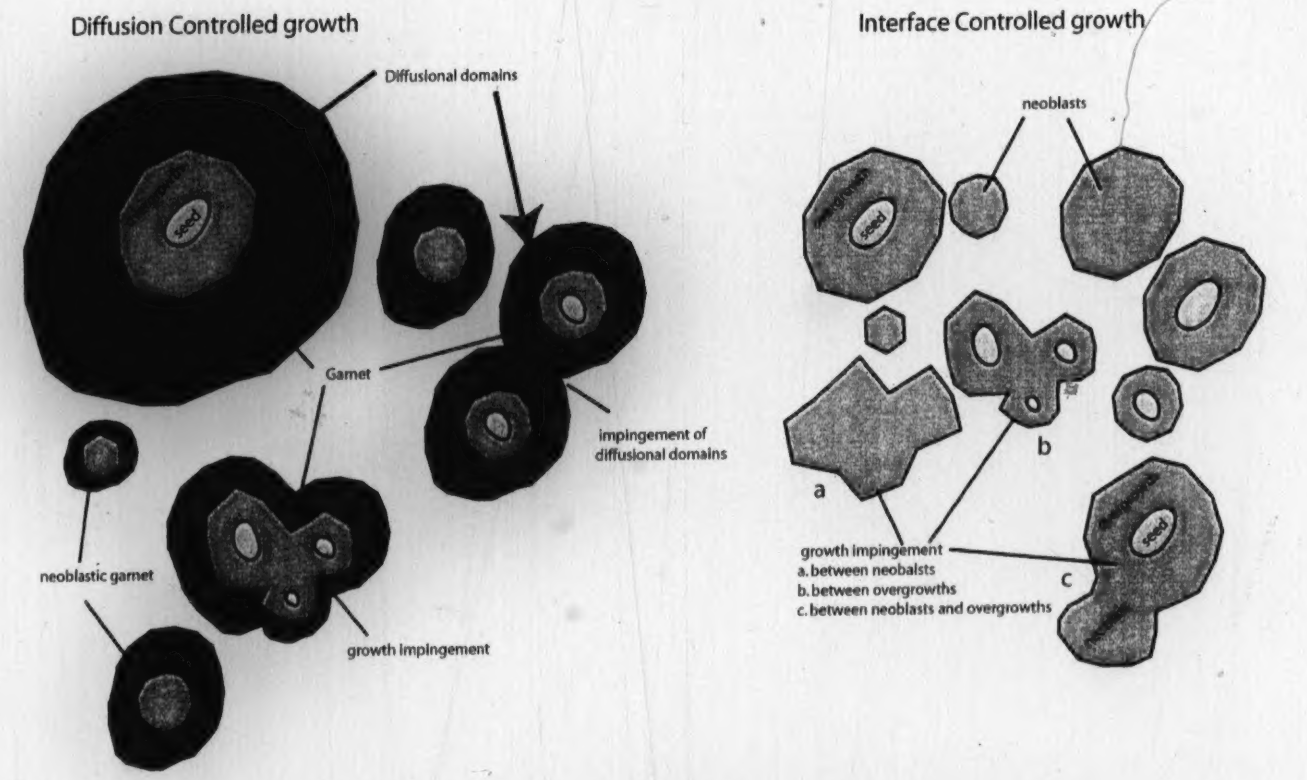
Diffusion Controlled growth
Diffusional domains
seed
overgrowth
Garnet
impingement of diffusional domains
neoblastic garnet
growth impingement
Interface Controlled growth
neoblasts
seed
overgrowth
a
b
c
growth impingement
a. between neobalsts
b. between overgrowths
c. between neoblasts and overgrowths

Figure 3.4: Schematic diagram showing predicted aspects of diffusion-controlled and interface-controlled growth of garnet during the experiment. During diffusion-controlled growth, the establishment of diffusional gradient around a garnet crystal inhibits nucleation of new crystals near within its diffusional domain. This leads to non-random distribution of garnet crystals as well as greater nearest-neighbour distances during crystallization. Interface controlled growth results in random distribution of garnet crystals. Also, during diffusion controlled growth impingement of growth domains is restricted and limited to the seeds. Lack of nucleation barriers near pre-existing crystals results in more occurrences of growth impingement in the case of interface-controlled growth.

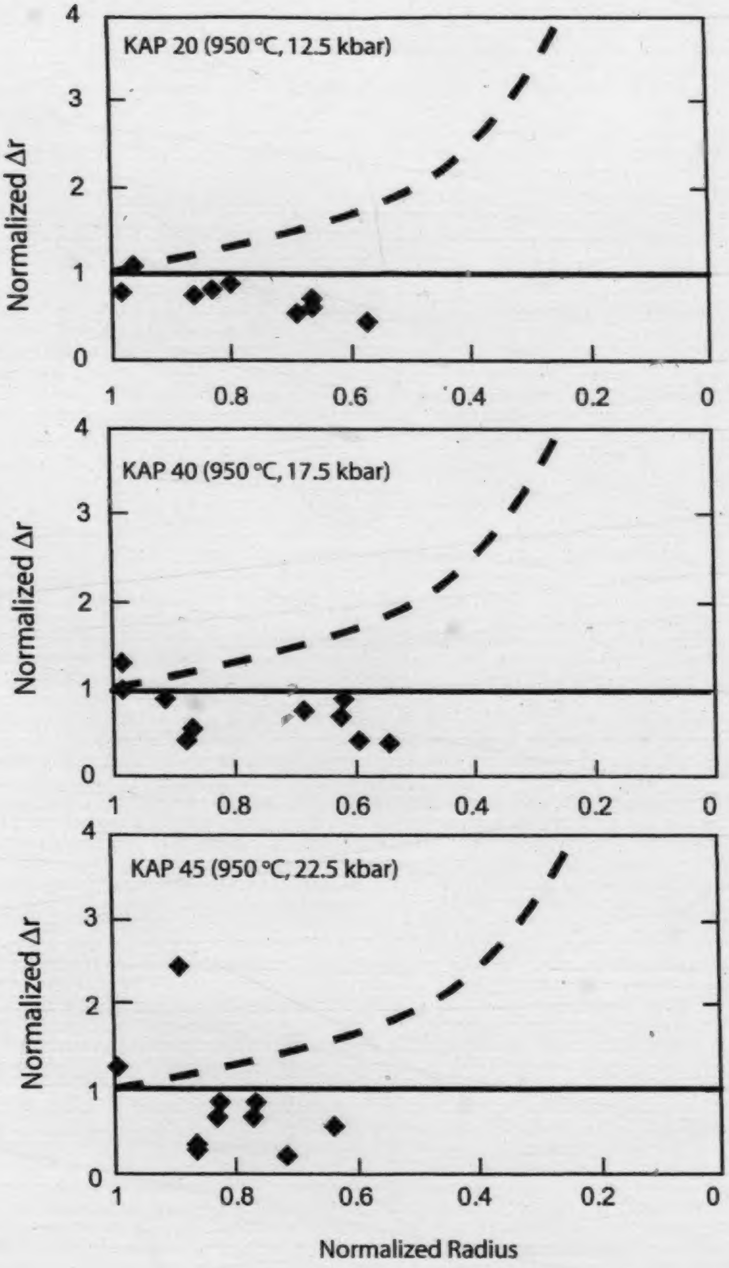

Figure 3.5: Radius rate plots for garnet growth in three KAP experiments. The dashed curve corresponds to diffusion-controlled growth and the solid line to endmember interface-controlled growth. The relatively linear pattern of the data and normalized Δr values closer to unity (except for one garnet in KAP 45) indicate an interface control on garnet growth during the experiments.

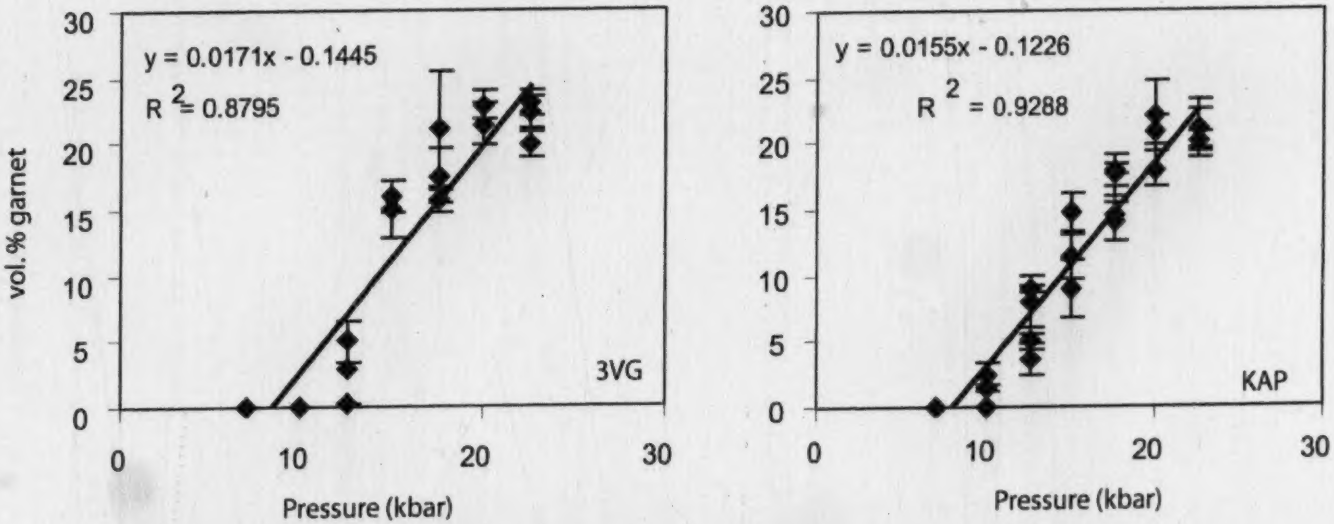

Figure 3.6.: Garnet abundance (vol.%) with pressure. Data includes garnet abundance in the temperature range 850-1050 °C, except for 3VG where regression was done for abundance data between 900 and 1050 °C.
Inclusion of garnet abundance data at 850 °C for 3VG show a similar trend but at much lower garnet abundace at respective pressure, indicating that garnet growth occurs predominantly at temperarutes >850 °C. Error bars represent 1σ standard deviation of garnet abundance estimates from differnt BSE images of an experimental run.

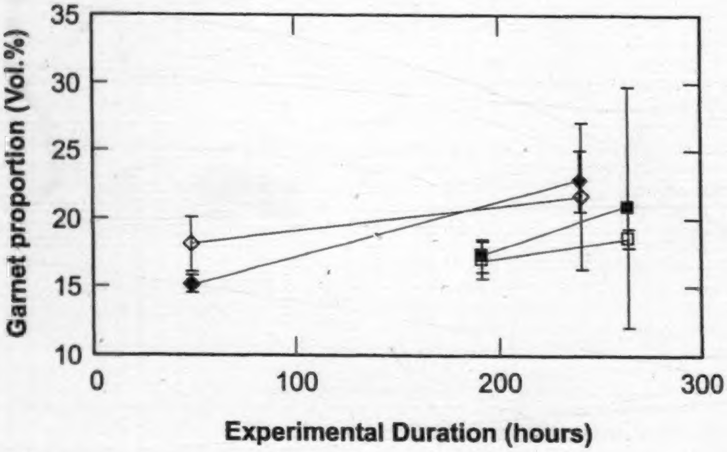

Figure 3.7: Variation in the proportion of garnet as a function of duration of the experiment. Diamonds-experiments at 20 kbar, 900°C; Squares- experiments at 17.5 kbar, 950°C; closed symbols-3VG experiments; open symbol-KAP experiments. Error bars represent 2-sigma standard deviation of garnet modal estimates.

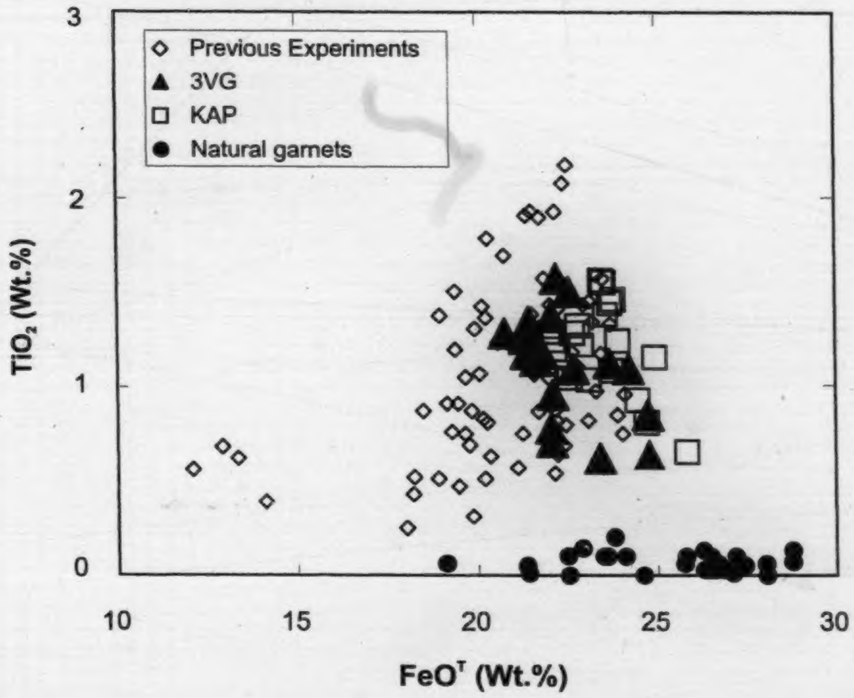

Figure 3.8: Plot of TiO$_2$ vs FeO^T in experimental garnets. Also shown are garnet compositions from natural amphibolitesand granulites for comparison. The natural garnets have low TiO$_2$ content and many from the amphibolite localities have high FeO^T content. Previous experimental data from: Winther and Newton (1991); Sen and Dunn (1994); Patino Douce and Beard (1995); Rapp and Watson (1995); Springer and Seck (1997); Ernst and Liou (1998); Lopez and Castro (2001). Natural garnet data from Ghent et al.(1993); Percival (1983); Graham and Powell (1984); Carswell and O'Brien (1993); Stosch et al.(1995);Hartel and Pattison (1996); Clarke et al. (2000); Cook et al. (2000); Holtta et al. (2000).

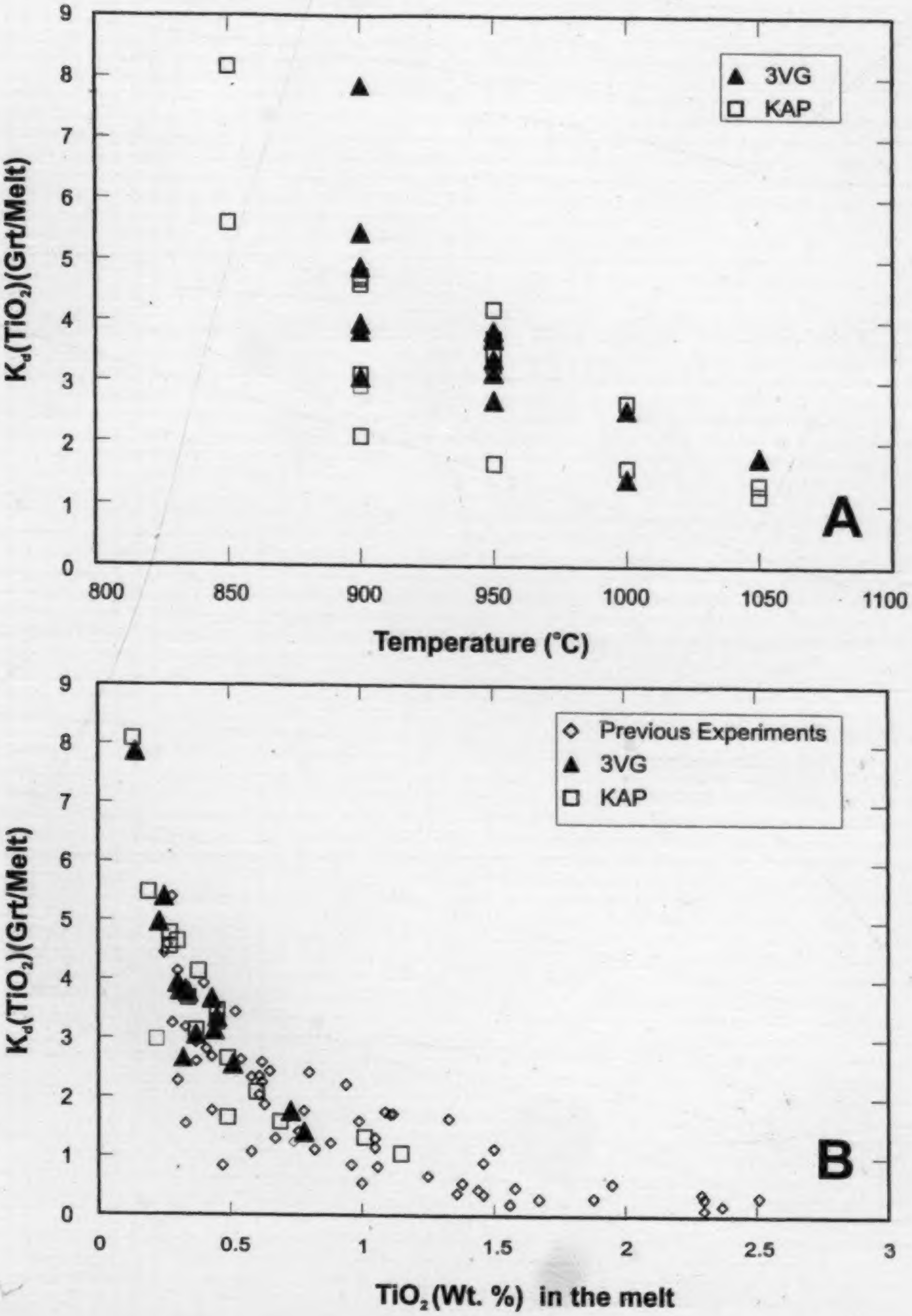

Figure 3.9: (A) Distribution of TiO_2 between garnet and melt as a function of temperature. garnet/melt Kd's are >1 and decreases with increasing temperature. (B) Variation of garnet/melt Kd for Ti as a function of TiO_2 content of melt. Sources of previous experimental data same as in figure 3.8.

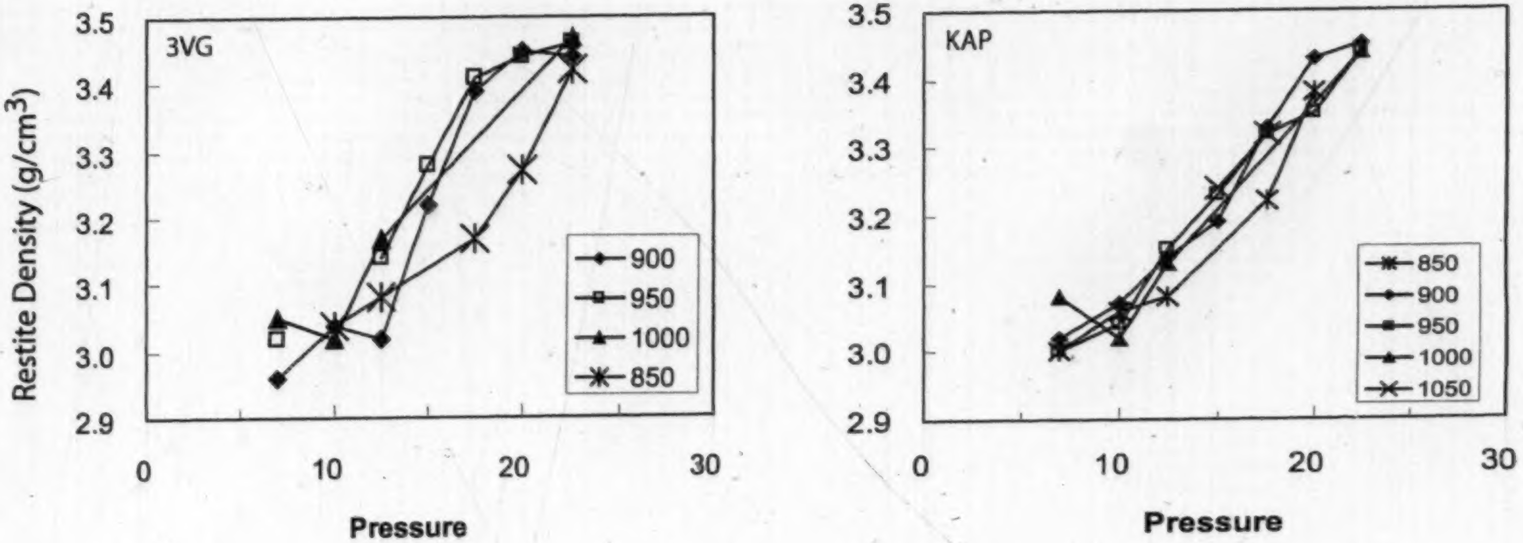

Figure 3.10: Calculated density of restite as a function of pressure for experiments at different temperatures.

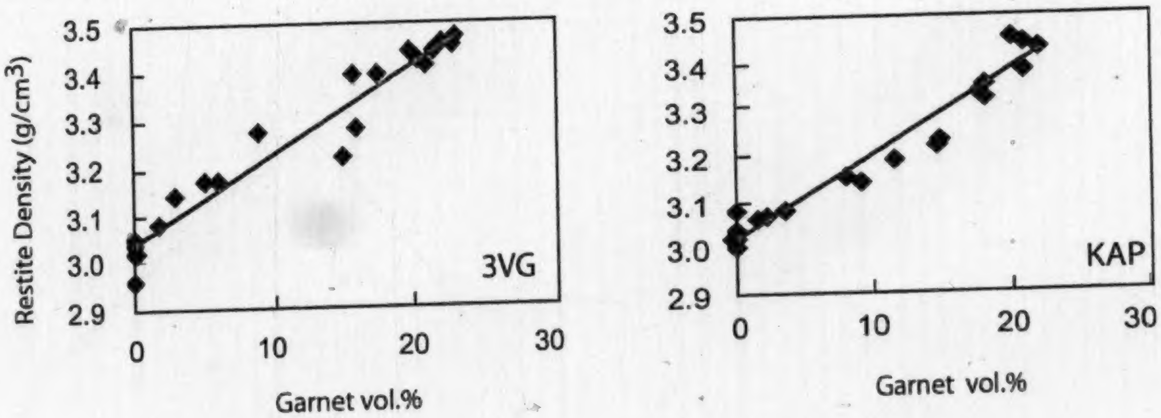

Figure 3. 11:Plot of restite density (g/cm^3) versus garnet abundance (vol. %) in the experimental charge.

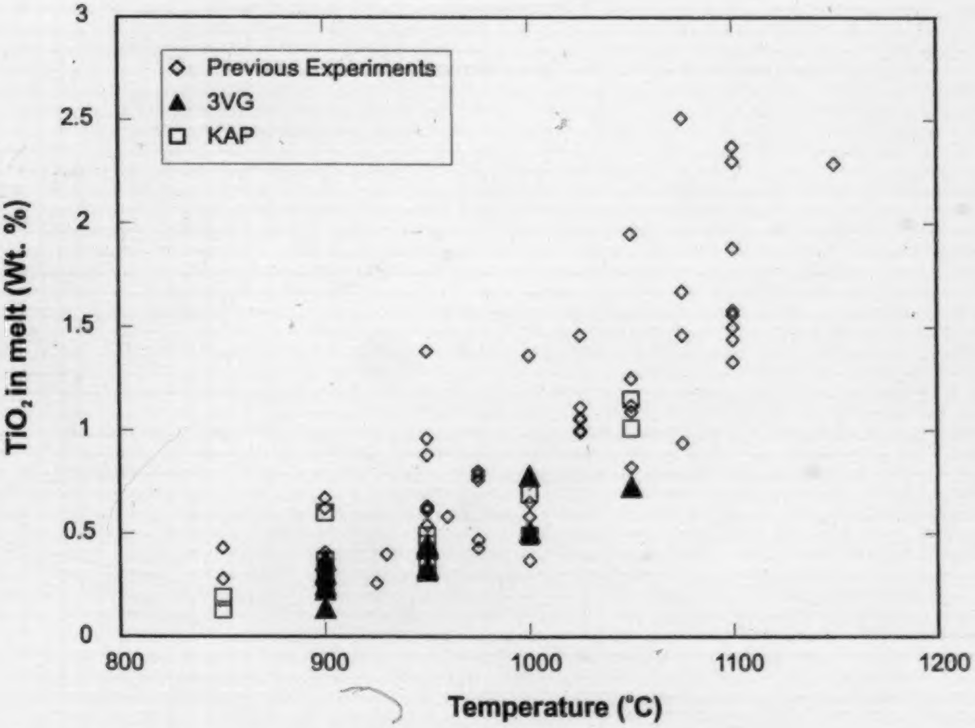

Figure 3.12: Plot of melt TiO_2 content as a function of temperature. Shown also are data from previous metabasalt melting experiments (sources same as in figure 3.7).

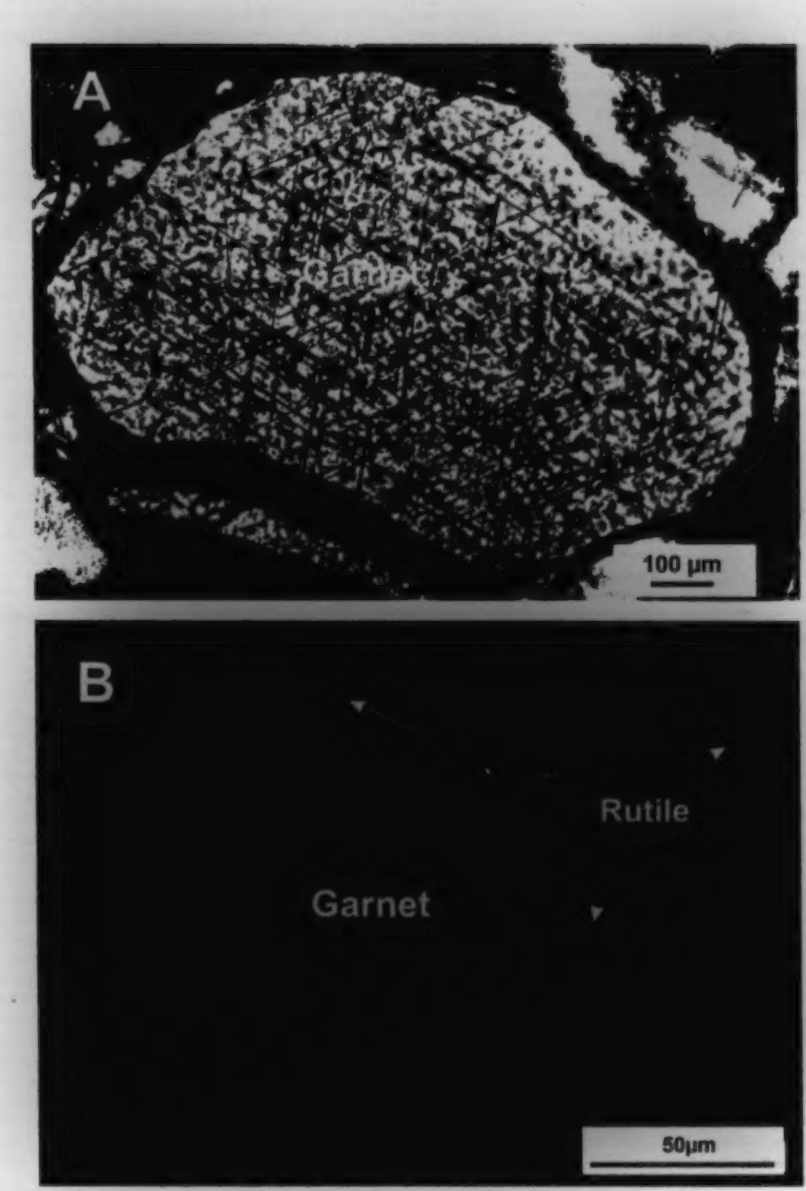

Figure 3.13: Photomicrographs (in plane polarized light) showing exsolved rutile lamellae in garnets from lower crustal xenoliths of Diavik kimberlite pipe . Note the crystallographically controlled orientation of rutile lamellae in figure A. Figure B shows the rod shape of rutile lamellae. Such lamellae are common in garnets of eclogite xenoliths and exhumed high-pressure terranes.

Chapter 4: Constraints on the origin of early-Archean TTG magmas and conjectures on Archean geodynamics and implications for the origin of crust-mantle systems

(A version of this chapter co-authored by Dr. Thomas Chacko has been published in Geology, a reprint of which is attached in Appendix D)

INTRODUCTION

Archean Tonalite-Trondhjemite-Granodiorite (TTG) magma suites represent the oldest coherent pieces of felsic continental crust (Bowring and Williams, 1999). Plutonic rocks of TTG composition, together with tholeiitic and komatiitic volcanics, form the dominant magmatic suite in Archean cratons. Understanding the origin of these magma suites and their spatial and temporal relationship to each other is important in understanding the origin of continental crust and in evaluating the geodynamic processes that were operative in the early Archean.

Many petrologically diverse processes have been proposed for the origin of TTG type rocks. These include (a) fractional crystallization of basaltic magmas (Arth et al., 1978), (b) Sodium metasomatism of granitic precursors (Drummond et al., 1986; Fiannacca et al., 2005), (c) direct melting of mantle (Moorbath, 1975) and, (d) partial melting of diverse lithologies including greywackes (Arth and Hanson, 1975), eclogites (Arth and Hanson, 1972; Rapp et al., 2003), amphibolites (Barker and Arth, 1976; Martin, 1986; Foley et al., 2002), basalts (Johnston, 2986) and tonalites (Johnston and Wyllie, 1988). Processes a-c are unlikely to have been responsible for the large volume of TTGs found in Archean terranes. The paucity of intermediate composition rocks and cumulate rocks in the Archean plutonic record render fractional crystallization processes in TTG formation less favourable. Metasomatic processes may have been locally important but are unlikely to have affected large volumes of crust. Moreover, such processes require the presence of granitic precursors (Fiannacca et al., 2005), and are therefore, not viable as an explanation for earliest TTG formation. Partial melting of unaltered mantle peridotites yield mafic magmas and not TTGs (e.g. Jaques and Green, 1980; Hirose and Kushiro, 1993; Walter, 1988). Only some late Archean high-Mg diorites (sanukitoids) could feasibly be explained by direct partial melting of a metasomatised mantle source (Evans and Hanson, 1997). The role of partial melting of metabasaltic rocks in generating Archean TTGs have received considerable attention due to the common spatial association of these two rock types, their geochemically complementary nature (e.g. Rollinson, 1997) and abundance of metabasaltic protoliths in Archean cratons.

Experimental and theoretical studies support the origin of TTG rocks through the partial melting of hydrated metabasaltic rocks (e.g. Rapp et al., 1991; Sen and Dunn, 1994; Springer and Seck, 1997; Martin et al., 2005). Understanding the conditions at which partial melting of metabasalt occurs has been the focus of many studies because of the potential of linking the melting process to specific tectonic environments. Highly fractionated REE patterns ($(La/Yb)_N$ = 15-100) and depletion in HREE (Yb < 1 ppm) of TTGs require generation of these magmas at depths where garnet and/or amphibole constitute a large proportion of the residue (Martin, 1986). A number of tectonic models have been proposed to satisfy this requirement, including melting of subducted oceanic crust (Martin, 1986; Foley et al., 2002), melting in the root zones of oceanic plateaus, or thick oceanic crust followed by delamination of eclogitized lower crust (Zegers and van Keken 2001; Condie, 2005; Bedard, 2006). All of the above tectonic settings are capable of generating magmas comparable to TTG in terms of their *major-element* compositions, making interpretation of the specific tectonic setting of formation of the first continental crust equivocal. Here, I consider some fundamental characteristics of Archean TTGs including their spatial relationship in granite-greenstone terrains, HREE depletion and oxygen isotope systematics and present new experimental data to argue that conditions envisaged in lower crustal melting and delamination models are inadequate in explaining early Archean TTG formation. I propose a modified subduction model for the origin of TTG that formed the first continental nuclei.

Constraints on Archean TTG formation

Any model of TTG formation should (a) account for the high proportion of TTG (up to > 60%) in many Archean cratons, (b) address the conditions required for generating the observed HREE depletion in early Archean TTG, (c) satisfy the requirement that hydrated basaltic rocks be present in the source region of TTG to produce significant quantities of melt at reasonable crustal temperatures (<1100°C) (Foley et al., 2002), and (d) explain the enriched $\delta^{18}O$ signatures of Archean TTGs indicative of low temperature hydrothermal alteration of basaltic protoliths (King et al., 1998; 2000; Bindeman et al., 2005).

Experimental studies have produced TTG-type melts by ~ 20 % partial melting of metabasaltic protoliths at temperatures >900°C (e.g. Rapp et al., 1991). The high proportion of TTG in many Archean cratons, therefore, requires a large volume of mafic composition rocks in the magma source region. The HREE depletion in TTG is generally attributed to the presence of garnet in the residue of TTG source rocks (Martin, 1986). I evaluated the amount of residual garnet that must be left behind in the source region to produce the observed HREE depletion in early Archean TTG by combining modal abundance data from experiments with published mineral/melt partition coefficients for REE (Springer and Seck, 1997; Klein et al., 1997; 2000). I used Yb as a representative element to assess the degree of HREE depletion in the melt and the La/Yb of the melt ratio as a monitor of the extent of REE fractionation during dehydration-melting of metabasalts. For the calculations, average Yb and La contents of 3.0 and 6.8 ppm and 0.78 and 32 ppm were used for MORB and early Archean TTG, respectively. The values for MORB are from the PETDB database (http://www.petdb.org) and the values for early Archean TTGs from Martin et al. (2005). Calculations indicate that for 20% partial melting of a MORB-composition source rock, at least 20 weight per cent garnet is required in the melt residue to generate the observed Yb depletion in average early Archean TTG (Figure 4.1). As shown in Chapter 3, garnet abundance in the residue during dehydration melting of metabasaltic rocks can be correlated with equilibration pressure. The equilibration pressure for stabilizing the required amount of garnet can then be converted to the depth at which TTG magmas are generated. Here, I use my new experimental constraints on garnet stability to address the depth requirements of source regions of early Archean TTG magmas. The discussion below is based specifically on the results of the 3VG experiments but essentially identical conclusions are reached with data from the KAP experiments.

DISCUSSION

Experimental constraints on garnet stability

In metabasaltic rocks, the appearance of garnet is in part controlled by the bulk composition of the protolith (Green and Ringwood, 1967; Foley et al., 2003). There is no consensus on the composition of Archean oceanic crust, which in most models is considered to be the source of TTG. However, the broad similarity of Archean tholeiitic sequences to normal modern-day MORB suggests that the two may not have been greatly different, at least for the volcanic components of the crust. Recent reports of pillow basalts and associated sheeted dykes from a proposed ophiolites sequence in the 3.8 Ga Isua supracrustal belt in Greenland have a MORB-like composition (Furnes et al., 2007). Although Archean basaltic volcanics may range to more Mg-rich compositions (Bickle et al., 1994; Foley et al., 2003), a first-order constraint on the depth requirements for TTG formation can be derived from garnet stability relations in MORB-type amphibolites.

My new experimental data indicate that garnet first becomes stable at ~10 kbar in MORB-type metabasalts, consistent with the results of previous experimental studies (e.g. Wolf and Wyllie, 1994). The proportion of garnet in the residue is directly correlated with pressure at which melting occurs (Table 2.11). Importantly, pressures greater than 15 kbar (> 48 km) are required to stabilize 20 wt.% garnet in the melt residue (Figure 4.2: Table 2.11). Most Archean high-Al TTGs are believed to have formed with little or no plagioclase in the residue (Martin et al., 2005) due to the high Sr/Y ratios exhibited by these rocks. My experimental data indicate that pressures >18 kbar are needed to form a plagioclase-free eclogite mineral assemblage (Figure 4.2). This corresponds to melting depths >58 km. Some petrologists (Bickle et al., 1994; Foley et al., 2003) argue that the Archean oceanic crust would have been more Mg-rich than typical MORBs. If this was the case, the depth requirement for granulite-eclogite transition and for generating the necessary garnet to produce strong HREE depletion in partial melts would further increase because of the inverse dependence of garnet stability/abundance on the Mg-number (Mg/(Mg+Fe)) of the protolith (Green and Ringwood, 1967: Foley et al., 2003). The estimated depth of 48 km, to stabilize 20 wt. % garnet in the melt residue in MORB-type compositions is, therefore, the minimum depth at which melting must occur to produce early Archean TTGs. This requirement for source regions of TTG magmas is consistent with conditions proposed for TTG formation by some recent studies based on trace element modelling (Moyen and Stevens, 2006; Xiong, 2006). The depth requirement is also consistent with the results of experimental phase relations of trondhjemites, which shows that pressures >13 kbar are required to stabilize garnet as a liquidus phase (Johnston and Wyllie, 1988; van der Laan and Wyllie, 1992).

Implications for tectonic models

The requirement of melt generation at depths >48 km has implications for all of the proposed mechanisms for early Archean TTG generation. Proposed delamination models are problematic due to the large crustal thickness necessary to transform mafic rocks to eclogite in order to induce the delamination process. Eclogite formation is a critical feature of all these models (Zegers and van Keken, 2001; Bedard, 2006).

Parameterized modelling of mantle melting indicates that even with a mantle potential temperature of 1500 °C, the resulting oceanic crust is unlikely to have been > 20 km thick (Vlaar and van den Berg, 1991). The base of such crust would not be in the eclogite stability field, or for that matter in the garnet stability field (~35 km or 10 kbar). As a consequence, melts generated in the lower parts of this crust would not have the HREE depletion observed in early Archean TTG. Some of the delamination models envisage thickening of the crust (to eclogite stability limits) through underplating of basaltic magma (Zegers and van Keken, 2001). Although such a process may help attain the depth requirement for generating strongly HREE-depleted TTG magmas, melt production in this case would occur in rocks that had never interacted with surface fluids. In contrast, the oxygen isotope compositions of zircons crystallized from TTG magmas suggest derivation from rocks that had a prior history of surface fluid-rock interaction (Bindeman et al., 2005).

Models invoking melting in the root zones of oceanic plateaus (e.g. Condie, 2005) have the same inadequacies as above in that oceanic plateaus thicker than 35 km are not known in the modern-day or ancient rock record. Moreover, root zones of oceanic plateaus are likely dominated by cumulates and other high-Mg derivatives (Foley et al., 2002) which would not be conducive to generating the required amount of garnet (at depths suggested by lower crustal melting models) for effecting HREE depletion in the melt. Indeed, the REE pattern of felsic magmas generated today in oceanic plateau settings are unlike those of Archean TTG (Martin and Sigmarsson, 2007).

Another problem with lower crustal melting and crustal delamination models for TTG formation is the limited melt productivity of lower crustal rocks at reasonable crustal temperatures (<1100 °C). Melt production in the basal sections of oceanic plateau type crust would be significantly less due to the high Mg-content and generally anhydrous nature of these rocks. Many Archean cratons, however, exhibit voluminous TTG magmatism. Advocates of delamination and lower crustal melting models have recognised this problem of low melt productivity and have invoked repeated delamination events (Bedard, 2006), unusually thick oceanic plateaus or crustal thickening post-dating TTG production (Zegers, 2004) in order to explain the discrepancy between TTG magma volume produced by delamination models and the observed volume of Archean TTG.

Models involving melting of subducted oceanic crust (Martin, 1986; Foley et al., 2002) are more consistent with the depth requirements for generating TTG. However, the role of subduction processes in the Archean has been disputed on physical grounds that plates could not attain the negative buoyancy required to initiate the subduction process (e.g. Vlaar et al., 1994). Below I present a modified subduction model that addresses these concerns.

A modified subduction model

Existing subduction models for the Archean argue that subduction occurred along a steeper geothermal gradient and that the average age of subducting lithosphere was significantly younger than in post-Archean times (Martin, 1986). Although it is intuitive that any subduction processes before the existence of continents would have to be intra-oceanic, how and why such subduction processes initiate remains uncertain. Notably, there is a problem involving subduction of thicker oceanic crust in the Archean. Here, I present a model that would account for the initiation of subduction and resultant TTG magmatism in the Archean.

There is a general consensus that the Archean Earth was hotter than at present, although the magnitude of the temperature difference is a matter of debate (Nisbet et al., 1993; Abbot et al., 1994; Pollack, 1997). Today, Earth's heat loss mechanisms involve cooling of the mantle through the production of plates at ocean ridges and intermittent plume activity (Davies, 1993). It is likely that the Archean Earth also supported both of these cooling mechanisms. Early Archean oceanic crust would therefore have comprised two entities; 'normal' oceanic crust, produced by mantle upwelling at divergent margins, and oceanic plateaus, produced by upwelling mantle plumes (Figure 4.3A). Both of these entities would have been positively buoyant relative to modern-day oceanic crust because of their large crustal thickness. However, a slight buoyancy contrast is established due to the greater thickness and slightly more Mg-rich nature of plateau crust, making it buoyant relative to 'normal' oceanic crust of the same age. A relatively larger buoyancy/density contrast exists between the plateau lithosphere and normal oceanic lithosphere owing to differences in the composition of lithospheric mantle in these two entities. Normal oceanic mantle lithosphere is less depleted than that of the plateau because of the smaller degree of melting experienced by the mantle in producing oceanic crust. The mantle source region of a plateau is highly depleted because of extraction of large volumes of tholeiitic and komatiitic magmas that form the plateau sequences. Density differences between the mantle residue after 'normal' oceanic crust and oceanic plateau formation were calculated based on the residual mineral modes and compositions from peridotite melting experiments (Walter, 1998). I calculated a minimum density contrast of 0.6%

based on melt residuum data at 30 kbar for melt fractions of 14 % and 37 % (Walter, 1998). This corresponds well with the 0.7 % density contrast calculated based on the differences in the composition of highly depleted fore-arc and less depleted abyssal peridotites (Niu et al., 2003). The net effect of oceanic plateau creation is a less dense residual mantle that rises buoyantly and underplates the plateau crust. Once underplated, this strongly depleted mantle (which I term "proto-mantle lithosphere" or PML) cools conductively to eventually become the plateau lithosphere. Cooling of the PML occurs at slower rate compared to oceanic mantle lithosphere because of its much larger thickness. The slower cooling of the PML is also affected by a decrease in thermal diffusivity due to the high initial temperature of the residuum.

The net result of these compositional, thermal and density differences between normal oceanic and oceanic plateau lithosphere is that a gravitational instability develops when the two are juxtaposed. This gravitational instability is enhanced if the formation age of the oceanic plateau is younger than the adjacent oceanic lithosphere. Convergence of normal oceanic lithosphere and oceanic plateaus could have been a common occurrence in the Archean because of the smaller size of the plates and the tendency for oceanic plateaus to form near the margins of plates (King and Anderson, 1995). This facilitates the subduction of relatively dense normal oceanic lithosphere under the plateau crust, through the depleted residuum (Figure 4.3B). A similar model for initiation of subduction was proposed recently for the Cenozoic-age Solomon arc (Niu et al., 2003). My model differs from this previous model in the location of the subducting plate. The Benioff plane in my model is located within the mantle residuum (PML) of the oceanic plateau rather than below this layer (Figure 4.3B). This is consistent with seismic profiles showing shallow dipping reflectors within the shallow mantle beneath some Archean cratons (Calvert et al., 1995). Analogue models of subduction zones have stressed the importance of density contrast between converging lithospheric plates in the initiation of the subduction process (Mart et al., 2005). Interestingly, these models also suggest that, given appropriate boundary conditions, the down-going plate can subduct at relatively shallow angle into the ductile lithospheric layer of the overriding plate (Mart et al., 2005). The location and angle of the subduction plane in this experiment is determined by the depth to the top of the ductile lithosphere. I propose that the depth at which PML of the oceanic plateau supports ductile deformation determines the top of the subduction plane. This depth is a function of the cooling history of the melt residuum after oceanic plateau extraction and, therefore, determined by the time interval between formation of the plateau and the initiation of subduction. Specifically, a short time interval leads to a hotter PML and in turn a shallower subduction plane. Variations in the age of plateaus at the onset of subduction, therefore, determine the thickness of lithospheric mantle wedge.

The zone of weakness for subduction initiation develops as ductile fault or shear zone arising from compressive stresses sustained between PML and the converging oceanic lithosphere. Despite the high initial viscosity of the PML, ductile deformation and slab penetration is enabled by shear localization near the boundaries of subducting lithosphere by viscous energy dissipation caused by shear heating (Costa et al., 2003; Kaus and Podladchikov, 2006) and possible viscosity reduction by dewatering (Hirth and Kohlstedt, 1996) of sediments at the top of the slab. Dewatering of sediments may also cause melting near the top margins of the descending lithosphere, which in turn may partition strain into these melt-rich zones (Holtzman et al., 2005; Regenauer-Lieb et al., 2001). This would lead to the development of localized shear zones, the formation of which appears to a necessary condition to initialize subduction processes (Regnauer-Lieb et al., 2001; Kaus and Podladchikov, 2006). The higher heat flow in the Archean, combined with the relatively young age of oceanic crust and shear heating during subduction would cause the hydrothermally altered portions of the subducting crust to melt and produce TTG-type magmas. Because of a thicker pillow lava section in Archean relative to present-day oceanic crust (Bickle et al., 1994; Kent et al., 1996) (Figure 3a), a larger thickness of Archean oceanic crust likely experienced hydration through interaction with seawater. In turn, this thick, hydrated pillow lava section would be capable of producing a larger volume of TTG magma than is possible by slab melting in the present day. Importantly, melting of the subducted slab under thick plateau crust would enable melting to occur at sufficient depth to generate >20 % garnet in the residue and strong HREE depletion in the TTG magma.

Archean TTGs, generally, have higher MgO/(FeO+MgO) (Mg#) than experimental melts from amphibolites. Interaction of slab melts with the mantle wedge has been proposed to account for the higher Mg-number of TTG relative to experimental melts from metabasalts (Rapp et al., 1999; Martin et al., 2005). Variation in the Mg# of TTG has been attributed to differing degrees of interaction with the mantle wedge (Smithies, 2000; Martin and Moyen, 2002; Smithies et al., 2003). A secular trend in Mg# of TTGs has been suggested, with increase in Mg# towards the late Archean (Martin and Moyen, 2002: Smithies et al., 2003) (Figure 4.4). This secular trend has been attributed to cooling of the Earth towards the end of Archean, where cooler geotherms results in melting of the oceanic crust at progressively greater depths (Martin and Moyen, 2002)

(Figure 4.5C). Thus, late Archean TTGs derived from subducted oceanic crust have to travel through a thicker mantle wedge resulting in more interaction and consequently higher Mg#. While this argument is petrologically sound, I offer another possible explanation for varying degrees of TTG-mantle interaction using the framework of the new proposed model. As argued above, the depth to the Benioff zone under an oceanic plateau controls the thickness of the mantle wedge. In turn my model predicts that this depth is a function of the age of oceanic plateau at the time of plateau-oceanic lithosphere convergence and subduction initiation (Figure 4.4 A&B). When the plateau is relatively young, localized shear zones that initiate the subduction process form at relatively shallower depths, resulting in relatively flat subduction under the plateau. The thickness of the lithospheric mantle wedge through which the slab melts have to be transported is as a consequence smaller. When the plateau is older, subduction of oceanic lithosphere occurs at a steeper angle which is determined by depth at which the thermal structure of the plateau permits development of ductile shear zones. The slab melts in this case have to travel through a much larger thickness of lithospheric mantle wedge. In the new model, varying degrees of TTG melt-mantle interaction is caused by variations in the age of oceanic plateau at the onset of subduction, as this determines the thickness of the lithospheric wedge through which TTG melts are transported to their emplacement levels. This might, in part, explain the relatively large spread in Mg# of TTGs of a given age that presumably were generated from oceanic crust under similar geothermal gradients (Figure 4.4). Alternatively, it is also possible that TTG production in the Archean may have involved melting of metabasaltic protoliths with differing Mg#. During late Archean times, however, the combined effect of lower geothermal gradient and older age of plateau lithosphere at the onset of subduction would have led to generally greater interaction of slab melts with the mantle wedge.

Another implication of the proposed influence of plateau age on the location of Benioff zones is that the slab dip in subduction zones is not only a function of the thermal regime and thickness of the subducting slab alone, but also on the thermal structure of the overriding plate. It is commonly believed that subduction of relatively thick and/or warm oceanic crust results in flat subduction (e.g. Cloos, 1993; Gutscher et al., 2000). The corollary to this argument is that thinner and older oceanic crust would subduct with a larger dip angle. Both these generalizations are not universally valid. There are many areas on Earth where relatively young oceanic crust undergoes deep subduction (e.g. Western Colombia (Pennington, 1981), South Central Chile (Gutscher et al., 2000), Mexico (Suarez et al., 1990). On the contrary, subduction of relatively older oceanic crust at the Peru trench (Gutscher et al., 1999) and under central Chile (Barazangi and Isacks, 1976) occurs along flat trajectories. These subduction 'anomalies' may be explained if the thermal structure of the hinterland plays a role in the location of Benioff Zone during subduction as suggested here. I argue that flat slab subduction of old (and cold) oceanic lithosphere can occur if the thermal structure of the hinterland facilitates development of shallow shear zones and low angle thrust faults, the necessary weak zones to initiate subduction. Similarly, flat subduction can also occur without having the subducting crust attain a certain critical thickness as commonly thought.

Implications of the new model for crust-mantle evolution in Archean

Although beyond the data presented in this thesis, the proposed subduction model has implications for the evolution of crust-mantle systems in the Archean and is briefly discussed in this section. It is now reasonably established that the origin and evolution of crust-mantle systems were coupled in many Archean cratons (Richardson et al., 1984; Moser et al., 2001; Davis et al., 2003). The oldest domains of continental crust are represented by granite-greenstone belt association in Archean cratons. One of the important features of the granite-greenstone architecture is the close spatial and temporal association between the felsic plutonic rocks of TTG composition and mafic/ultramafic lavas of tholeiitic-komatiitic compositions. While TTG rocks typically show arc geochemical signatures (Weaver and Tarney, 1981; Martin, 1999), the associated tholeiitic and komatiitic lavas have been shown to exhibit geochemical signatures indicative of a plume or hot spot source (e.g. Wyman and Hollings, 1998; Kerrich and Xie, 2002, Wyman and Kerrich, 2002, Sproule et al., 2002). Association of rock units in Archean cratons with these complimentary tectonic signatures is considered an Archean geodynamic paradox (Bedard, 2006). Whereas arcs are fingerprints of a plate tectonic mode of mantle convection, plume related magmatism attests to a mode of mantle convection that is considered independent of the plate framework (Campbell and Hill, 1988; Campbell and Griffiths, 1992; Davies, 1993). Attempts have, therefore, been made to explain the architecture of Archean granite-greenstone associations as a result of a single tectonic environment (Zegers and van Keken, 2001; Bedard, 2006). Models by Zegers and van Keken (2001) and Bedard (2006) attempt to explain continental crust formation in a plume setting through vertical tectonic processes. Bedard (2006) considers the arc geochemical signatures in felsic plutonic rocks of Archean cratons as spurious. In the new proposed model, I show how products of plume and plate mode of mantle convection could have interacted to produce the characteristic granite-greenstone association in Archean cratons. I have shown that subduction zones are the favoured sites for early Archean TTG formation and that subduction zones may have preferentially nucleated along the margins of plume-derived oceanic plateaus. The interaction of plate and plume modes of convection may have been more widespread in the Archean than during Phanerozoic. Therefore, I argue that it is unnecessary to consider these to two geodynamic regimes as mutually incompatible in the Archean.

Archean cratons are characterized by a thick sub-continental lithospheric mantle (SCLM) root, the presence of which is believed to be the root cause of tectonic stability of cratons through time (Abbot et al., 1997; O'Reilly et al., 2001). The process of SCLM formation is actively debated (Wyman and Kerrich, 2002; Davis et al., 2003; Griffin et al., 2003). Two end member models have been proposed for the origin of SCLM: (a) plume models which equate the SCLM to the residue of mantle melting (e.g. Wyman and Kerrich, 2002; Griffin et al., 2003) and (b) subduction-accretion models which attribute the formation of SCLM to subcretion of subducted lithosphere (Helmstaedt and Schulze, 1989). Studies of cratonic SCLM, much like their overlying crustal components, show evidence for the interaction of both plume and arc components during its evolution. The highly depleted nature of peridotite xenoliths from Archean cratons (Boyd, 1989) is consistent with it being the residuum of large degree mantle melting such as would be expected during the ascent of a mantle plume (Griffin et al., 1999; Herzberg, 1999; Wyman and Kerrich, 2002). In contrast many data from eclogitic xenoliths from cratonic SCLM suggest that they are remnants of subducted oceanic crust (Jacob et al., 1994;

Jacob and Foley, 1999). The proposed model adequately explains how cratonic SCLM could have acquired the signatures of both plume melting and subduction processes. In my model, the SCLM represents the residuum of oceanic plateau extraction (plume component) that has been modified by subduction processes along the margin of the oceanic plateau. The modification of the oceanic plateau residuum through subduction of oceanic lithosphere through the residuum causes the composition of peridotite xenoliths from SCLM to deviate from that of a modelled single stage plume melt residuum. During subduction, ascending melts and volatiles from the slab modifiy the mantle (wedge) under the cratons. Such slab-mantle interaction processes were proposed to explain the high Si content of Archean SCLM (Kelemen et al., 1998). Further melting of this re-enriched mantle may produce a residuum that is highly refractory. An important feature of the new model is that the formation of the SCLM is intimately linked to the formation and stabilization of the continental crust. This is consistent with the purported broadly coeval origin of crust and SCLM in Archean cratons (Richardson et al., 1984; Moser et al, 2000).

CONCLUSIONS

I have shown based on experimental data and REE modelling that depths >48 km are required to generate early Archean TTG. This depth constraint is inconsistent with early crust evolution models that posit melting at the base of oceanic plateaus or thick oceanic crust (15-40 km thickness) to explain the origin of early Archean continental crust. I argue that depths >45 km were likely not attained in the base of normal oceanic crust or oceanic plateau crust in the Archean. Experimental data also suggests that delamination of lower crust may not have been a viable crustal recycling mechanism in the Archean due to lack of sufficiently thick oceanic crust to form abundant eclogite.

Experimental constraints are consistent with a model of TTG formation by melting of subducted oceanic crust. I propose that subduction zones initiated in the Archean from gravitational instability of the oceanic lithosphere arising from chemical differences between converging oceanic plateau and normal oceanic lithosphere. In the Archean, buoyant oceanic plateau lithosphere may have provided the boundary conditions for nucleating subduction zones. In my model, the spatial and temporal association in Archean cratons of tholeiitic to komatiitic volcanics, thick lithospheric mantle roots and TTG-composition magmatic rocks is the result of two separate but linked processes, the formation of an oceanic plateau and its associated mantle root followed by initiation of subduction beneath the plateau and the generation of TTG magmas in the subducting oceanic crust. Oceanic plateaus served as the nuclei for Archean cratons as they represent the substrate on which TTG composition magmas were emplaced. This model successfully explains and contributes to the debate on many petrological and geodynamic issues concerning early crustal evolution including the origin of subduction systems, TTG magmas, TTG-mafic/ultramafic magma association, stabilization of continental crust as well as the broadly coeval formation of cratons and their lithospheric root.

References:

Abbot, D.H., Burgess, L., Longhi, J. and Smith, W.H.F. (1994) An empirical thermal history of the Earth's upper mantle. Journal of Geophysical Research, 99, 13835-13850.

Abbot, D.H., Drury, R. and Mooney, W.D. (1997) Continents as lithological icebergs: the importance of buoyant lithospheric roots. Earth and Planetary Science Letters, 149, 15-27.

Arth, J.G. and Hanson, G.N. (1972) Quartz diorite derived by partial melting of Eclogite or amphibolite at mantle depths. Contributions to Mineralogy and Petrology, 37, 161-174.

Arth, J.G., and Hanson, G.N. (1975) Geochemistry and origin of the early Precambrian crust of northeastern Minnesota. Geochimica et Cosmochimica Acta, 39, 325-362.

Arth, J.G., Barker, F., Peterman, Z.E. and Friedman, I. (1978) Geochemistry of the gabbro-diorite-tonalite-trondhjemite suite of southwest Finland and its implications for the origin of tonalitic and trondhjemitic magmas. Journal of Petrology, 19, 289-316.

Barazangi, M. and Isacks, B. (1976) Spatial distribution of earthquakes and subduction of the Nazca Plate beneath South America. Geology, 4, 686-692.

Barker, F. and Arth, J.G. (1976) Generation of trondhjemitic-tonalitic liquids and Archean bimodal trondhjemite basalt suites. Geology, 4, 596-600.

Bedard, J.H. (2006) A catalytic delamination-driven model for coupled genesis of Archean crust and sub-continental lithospheric mantle. Geochimica et Cosmochimica Acta, v. 70, p. 1188-1214.

Bindeman, I.N., Eiler, J.M., Yogodzinski, G.M., Tatsumi, Y., Stern, C.R., Grove, T.L., Portnyagin, M., Hoernle, K., and Danyushevsky, L.V. (2005) Oxygen isotope evidence for slab melting in modern and ancient subduction zones. Earth and Planetary Science Letters, v. 235, p. 480-496 .

Bickle, M.J. (1994) Implications of melting for stabilization of the lithosphere and heat loss in the Archean. Earth and Planetary Science Letters, v. 80, p. 314-324.

Bickle, M.J., Nisbet, E.G., and Martin, A. (1994) Archean greenstone belts are not oceanic crust. Journal of Gelogy,,v.102, p. 121-138 (1994).

Bowring, S.A. and Williams, I.S. (1999) Priscoan (4.00-4.03 Ga) orthogneisses from northwestern Canada. Contributions to Mineralogy and Petrology. 134, 3-16

Boyd, F.R. (1989) Composition and distinction between oceanic and cratonic lithosphere. Earth and Planetary Science Letters, 96, 15-26.

Calvert, A.J., Sawyer, E.W., Davis, W.J., and Ludden, J.N. (1995) Archaean subduction inferred from seismic images of a mantle suture in the Superior Province. Nature, v. 375, p. 670-674.

Campbell, I.H. and Griffiths, R.W. (1992) The changing nature of mantle hotspots through time: implications for the chemical evolution of the mantle. Journal of Geology, 92, 497-523.

Campbell, I.H. and Hill, R.I. (1988) A two-stage model for the formation of the granite-greenstone terrains of the Kalgoorlie-Norseman area, Western Australia. Earth and Planetary Science Letters, 90, 11-25.

Cloos, M. (1993) Lithospheric buoyancy and collisional orogenesis: Subduction of oceanic plateaus, continental margins, island arcs, spreading ridges, and seamounts. Geological Society of America Bulletin, 105, 715-737.

Costa, A., and Macedonio, G. (2003) Viscous heating in fluids with temperature dependant viscosity: implications for magma flows. Non-linear processes in Geophysics 10, 101-111 (2003).

Condie, K.C. (2005) TTGs and adakites: are they both slab melts? Lithos, v. 80, p. 33-44.

Davies, G.F. (1993) Conjectures on the thermal and tectonic evolution of the Earth. Lithos, v. 30, p. 281-289.

Davis, W.J., Jones, A.G., Bleeker, W. and Grutter, H. (2003) Lithosphere development in the Slave craton: a linked crustal and mantle perspective. Lithos, 71, 575-589.

Drummond, M.S., Ragland, P.C. and Wesolowski, D. (1986) An example of trondhjemite genesis by means of alkali metasomatism: Rockford Granite, Alabama Appalachians. Contributions to Mineralogy and Petrology, 93, 98-113.

Evan, O.C. and Hanson, G.N. (1997) Late-to post-kinematic Archean granitoids of the S.W. Superior province: derivation through direct mantle melting. In de Wit, M.J. and Ashwal, L.D. (eds.) Greenstone Belts. Oxford: Oxford University Press, pp. 280-295.

Fiannacca, P., Brotzu, P., Cirrincione, R., Mazzoleni, P. and Pezzino, A. (2005) Alkali metasomatism as a process for trondhjemite genesis: evidence from Aspromonte Unit, north-eastern Peloritani, Sicily. Mineralogy and Petrology, 84, 19-45.

Foley, S.F., Tiepolo, M., and Vannuci, R. (2002) Growth of continental crust in subduction zones controlled by melting of amphibolite. Nature, v. 417, p. 837-840.

Foley, S.F., Buhre, S., and Jacob, D.E. (2003) Evolution of the Archaean crust by delamination and shallow subduction. Nature 421, 249-252.

Furnes, H., de Witt, M., Staudigel, H., Rosing, M. and Muehlenbachs, K. (2007) A vestige of Earth's oldest ophiolites. Science, 315, 1704-1707.

Green, D.H., and Ringwood, A.E. (1967) An experimental investigation of the gabbro to eclogite transformation and its petrological applications. Geochimica et Cosmochimica Acta, v. 31, p. 767-833 .

Griffin, W.L., O'Reilly, S.Y. and Ryan, C.G. (1999) The composition and origin of sub-continental lithospheric mantle. In: Yingwei Fei, Bertka, C.M. and Mysen, B.O (eds.) Mantle Petrology: Field observations and high pressure experimentation: A tribute to Francis R. (Joe) Boyd. The Geochemical Society Special Publication, 6, 13-45.

Griffin, W.L., O'Reilly, S.Y., Abe, N., Aulbach, S., Davies, R.M., Pearson, N.J., Doyle, B.J. and Kivi, K. (2003) The origin and evolution of Archean lithospheric mantle. Precambrian Research, 127, 19-41.

Gutscher, M.-A., Olivet, J.-L., Aslanian, D., Maury, R. and Eissen, J.P. (1999) The 'lost Inca Plateau': Cause of flat subduction beneath Peru? Earth and Planetary Science Letters, 171, 335-341.

Gutscher, M.-A., Spakman, W. and Bijwaard, H. (2000) Geodynamics of flat subduction: Seismicity and tomographic constraints from the Andean margin. Tectonics, 19, 814-833.

Herzberg, C. (1999) Phase equilibrium constraints on the formation of cratonic mantle. In: Yingwei Fei, Bertka, C.M. and Mysen, B.O (eds.) Mantle Petrology: Field observations and high pressure experimentation: A tribute to Francis R. (Joe) Boyd. The Geochemical Society Special Publication, 6, 241-247.

Hirose, K. and Kushiro, I. (1993) Partial melting of dry peridotites at high pressures:determination of composition of melts segregated from peridotite using aggregates of diamond. Earth and Planetary Science Letters, 114, 477-489.

Hirth, G., and Kohlstedt, D.L. (1996) Water in the oceanic upper mantle:implications for rheology, melt extraction and evolution of the lithosphere. Earth and Planetary Science Letters, v. 144, p. 93-108.

Holtzman, B.K., Kohlstedt, D.L., and Morgan, J.P. (2005) Viscous energy dissipation and strain partitioning in partially molten rocks. Journal of Petrology, v. 46, p. 2569-2592.

Jacob, D.E. and Foley, S.F. (1999) Evidence for Archean ocean crust with low high field strength element signature from diamondiferous eclogite xenoliths. Lithos, 48, 317-336.

Jacob, D., Jagoutz, E., Lowry, D., Mattey, D. and Kudrjavtseva, G. (1994) Diamondiferous eclogites from Siberia: remnants of Archean oceanic crust. Geochimica et Cosmochimica Acta, 58, 5191-5207.

Jaques, A.L. and Green, D.H. (1980) Anhydrous melting of peridotite at 0-15 kb pressure and the genesis of tholeiitic basalts. Contributions to Mineralogy and Petrology, 73, 287-310.

Johnston, A.D. (1986) Anhydrous P-T phase relations of near-primary high-alumina basalt from the South Sandwich Islands: Implications for the origin of island arcs and tonalite-trondhjemite series rocks. Contributions to Mineralogy and Petrology, 92, 368-382.

Johnston, A.D. and Wyllie, P.J. (1988) Constraints on the origin of Archean trondhjemites based on phase relationships of Nuk gneiss with H_2O at 15 kbar. Contributions to Mineralogy and Petrology, 100, 35-46.

Kaus, B.J.P., and Podladchikov, Y.Y. (2006) Initiation of localized shear zones in viscoelastoplastic rocks. Journal of Geophysical Research, v. 111, p. 1-18 (2006).

Kelemen, P.B., Hart, S.R. and Bernstein, S. (1998) Silica enrichment in the continental upper mantle lithosphere via melt/rock reaction. Earth and Planetary Science Letters, 164, 387-406

Kent, R.W., Hardarson, B.S., Saunders, A.D., and Storey, M. (1996) Plateaux ancient and modern: Geochemical and sedimentological perspectives on Archean oceanic magmatism. Lithos, v. 37, p. 129-142.

Kerrich, R. and Xie, Q.L. (2002) Compositional recycling structure of an Archean super-plume: Nb-Th-U-LREE systematics of Archean komatiites and basalts revisited. Contribution to Mineralogy and Petrology, 142, 476-484.

King, E.M., Valley, J.W., Davis, D.W. and Edwards, G.R. (1998) Oxygen isotopic ratios of Archean plutonic zircons from granite-greenstone belts of the Superior province: indicator of magmatic source. Precambrian Research, 92, 365-387.

King, E.M., Valley, J.W. and Davis, D.W. (2000) Oxygen isotope evolution of volcanic rocks at the Sturgeon Lake volcanic complex, Ontario. Canadian Journal of Earth Sciences, 37, 39-50.

King, S.C., and Anderson, D.L. (1995) An alternative mechanism of flood basalt formation. Earth and Planetary Science Letters, v. 136, p. 269-279.

Klein, M., Stosch, H.-G., and Seck, A. (1997) Partitioning of high field-strength and rare-earth elements between amphibole and quartz dioritic to tonalitic melts: An experimental study. Chemical Geology, v. 138, p. 257-271.

Klein, M., Stosch, H.-G., Seck, A., and Shimizu, N. (2000) Experimental partitioning of high field strength and rare earth elements between clinopyroxene and garnet in andesitic to tonalitic systems. Geochimica et Cosmochimica Acta, v. 64, p. 99-115.

Mart, Y., Aharonov, E., Mulugeta, G., Ryan, W., Tentler, T., and Goren, L. (2005) Analogue modelling of the initiation of subduction. Geophysical Journal International, v. 160, p. 1081-1091.

Martin, E. and Sigmarsson, O. (2007) Crustal thermal state and origin of silicic magma in Iceland: the case of Torfajkull, Ljsufjll and Snfellsjkull volcanoes. Contributions to Mineralogy and Petrology, 153, 593-605.

Martin, H. (1986) Effect of steeper Archean geothermal gradient on geochemistry of subduction-zone magmas. Geology, v. 14, p. 753-756.

Martin, H. (1999) Adakitic magmas: modern analogues of Archean granitoids. Lithos, 46, 411-429.

Martin, H., and Moyen, J.-F. (2002) Secular changes in TTG composition as markers of progressive cooling of the Earth. Geology , v. 30, p. 319-322.

Martin, H., Smithies, R.H., Rapp, R., Moyen, J.-F., and Campion, D. (2005) An overview of adakite, tonalite-trondhjemite-granodiorite (TTG), and sanukitoid: relationships and some implications for crustal evolution. Lithos, v. 79, p. 1-24.

Moorbath, S. (1975) Evolution of Precambrican crust from strontium isotopic evidence. Nature, 254, 395-398.

Moser, D.E., Flowers, R.M. and Hart, R.J. (2001) Birth of the Kaapvaal tectosphere 3.08 billion years ago. Science, 291, 465-468.

Moyen, J.-F. and Stevens, G. (2006) Experimental constraints on TTG petrogenesis: implications for Archean geodynamics. In: Benn, K., Mareschal, J. and

Condie, K. (eds.) Archean geodynamics and environments. AGU geophysical monograph, 164, 149-175.

Nair, R., and Chacko, T. (2002) Fluid-absent melting of high-grade semi-pelites: P-T constraints on orthopyroxene formation and implications for granulite genesis, Journal of Petrology, v.43, p. 2121-2142.

Nisbet, E.G., Cheadle, M.J., Arndt, N.T. and Bickle, M.J. (1993) Constraining potential temperature of the Archean mantle: a review of the evidence from komatiites. Lithos, 30, 291-307.

Niu, Y., O'Hara, M.J., and Pearce, J.A. (2003) Initiation of subduction zones as a consequence of lateral compositional buoyancy contrast in the lithosphere: a petrologic perspective. Journal of Petrology, v. 44, p. 851-866.

O'Reilly, S.Y., Griffin, W.L., Poudjom, D.Y. and Morgan, P. (2001) Are lithospheres forever? Tracking changes in subcontinental lithospheric mantle through time. GSA Today, 11, 4-9.

Peacock, S.M. (2003) Thermal structure and metamorphic evolution of subducting slabs. In: Eiler, J.M. (ed.) Inside the Subduction Factory. Geophysical Monographs, 138, 7-22.

Peacock, S.M. and Wang, K. (1999) Seismic consequences of warm versus cold subduction metamorphism: Examples from Southwest and Northeast of Japan, 286, 937-939.

PETDB. (2006) Petrologic data base of the ocean floor. http://www.petdb.org/. Accessed June 2006.

Pollack, H.N. (1997) Thermal characteristics of the Archean. In: de Wit, M.J. and Ashwal, L.D. (eds.) Greenstone Belts. Oxford Science Publications, 223-232.

Rapp, R.P., Watson, E.B., and Miller, C.F. (1991) Partial melting of amphibolite/eclogite and the origin of Archean trondhjemites and tonalites. Precambrian Research, v. 51, p. 1-25.

Rapp, R.P., Shimizu, N., Norman, M.D., and Applegate, G.S. (1999) Reaction between slab-derived melts and peridotite in the mantle wedge: experimental constraints at 3.8 GPa. Chemical Geology, v. 160, p. 335-356.

Rapp,R.P., Shimizu, N. and Norman, M.D. (2003) Growth of early continental crust by partial melting of Eclogite. Nature, 425, 605-609.

Regenauer-Lieb, K., Yuen, D.A. and Branlund, J. (2001) The initiation of subduction: critically by addition of water? Science, 294, 578-580.

Richardson, S.H., Gurney, J.J., Erlank, A.K. and Harris, J.W. (1984) Origin of diamonds in old enriched mantle. Nature, 310, 198-202.

Rollinson, H. (1997) Eclogite xenoliths in west African kimberlites as residue from Archean granitoid crust formation, Nature, 389, 173-176.

Sen, C., and Dunn, T. (1994) Dehydration melting of a basaltic composition amphibolite at 1.5 and 2.0 GPa:implication for origin of adakites. Contributions to Mineralogy and Petrology, v. 117, p. 394-409.

Smithies, R.H. (2000) The Archean tonalite-trondhjemite-granodiorite (TTG) series is not an analogue of Cenozoic adakite. Earth and Planetary Science Letters, 182, 115-125.

Smithies, R.H., Champion, D.C. and Cassidy, K.F. (2003) Formation of Earth's early Archaean continental crust. Precambrian Research, 127, 89-101.

Springer, W., and Seck, H.A. (1997) Partial fusion of basic granulites at 5 to 15 kbar: implications for the origin of TTG magmas. Contributions to Mineralogy and Petrology, v. 127, p. 30-45.

Sproule, R.A., Lesher, C.M., Ayer, J.A., Thurston, P.C. and Herzberg, C.T. (2002) Spatial and temporal variations in the geochemistry of komatiites and komatiitic basalts in the Abitibi greenstone belt. Precambrian Research, 115, 153-186.

Suarez, G., Montfret, T., Wittlinger,G. and David, C. (1990) Geometry of subduction and depth of the seismogenic zone in the Guerro gap, Mexico, Nature, 345, 336-338.

van der Laan, S.R. and Wyllie, P.J. (1992) Constraints on Archean Trondhjemite genesis from hydrous crystallization experiments on Nuk gneiss at 10-17 kbar. Journal of Geology, 100, 57-68.

Vlaar, N.J., and van den Berg, A.P. (1991) Continental evolution and archeo-sea levels. In: Sabadini, R., Lambeck, K. Boschi, E. (Eds.) Glacial isostasy, Sealevel and Mantle Rheology. Kluwer Dordrecht .

Walter, M.J. (1998) Melting of garnet-peridotite and the origin of komatiite and depleted lithosphere. Journal of Petrology, v. 90, p. 29-60.

Weaver, B.L. and Tarney, J. (1981) Lewisian gneiss geochemistry and Archean crustal development models. Earth and Planetary Science Letters, 55, 171-180.

Wyman, D. and Kerrich, R. (2002) Formation of Archean continental lithospheric roots: the role of mantle plumes. Geology, 30, 543-546.

Wyman, D. and Hollings, P. (1998) Long-lived mantle-plume influence on an Archean protocontinent: Geochemical evidence from the 3 Ga Lumby Lake greenstone belt, Ontario, Canada. Geology, 26, 719-722.

Xiong, S. (2006) Trace element evidence for growth of early continental crust by melting of rutile-bearing hydrous eclogite. Geology, 34, 945-948.

Zegers, T.E. (2004) Granite formation and emplacement as indicators of Archaean tectonic processes. Eriksson, P.G., Altermann, W., Nelson, D.R., Mueller, W.U., Catuneanu, O. (Eds.) The Precambrian Earth: Temos and Events. Developments in Precambrian Geology, v. 12, p.103-118.

Zegers, T.E., and van Keken, P.E. (2001) Middle Archean continental formation by crustal delamination. Geology 29, 1083-1086.

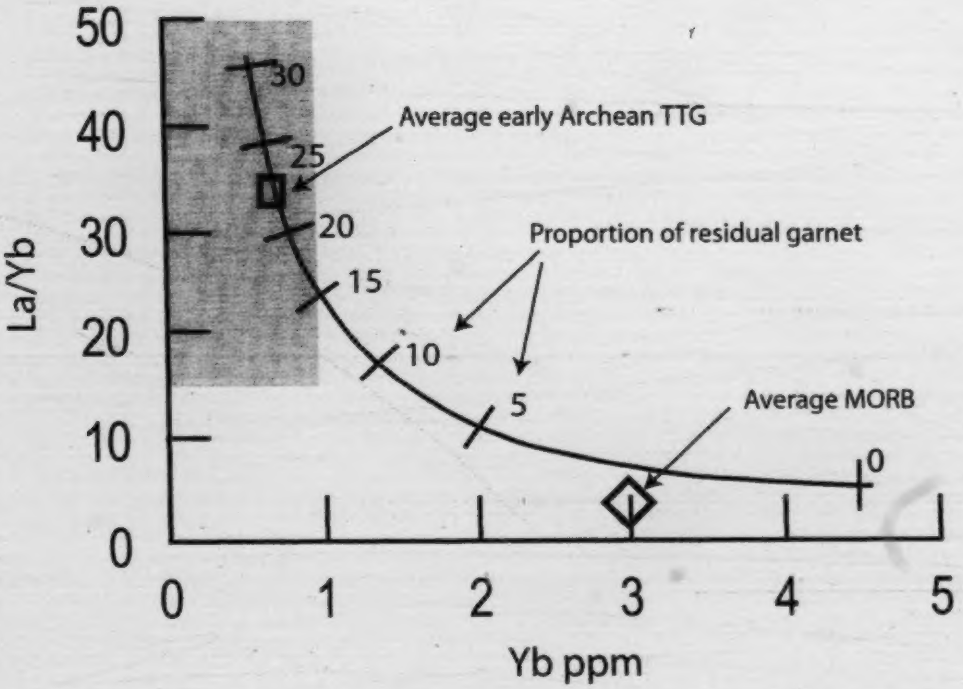

Figure 4.1: Variation in Yb and La/Yb ratio in experimental melts during dehydration melting of amphibolite as a function of garnet mode (wt.%) in the residue. The curve is drawn for a melt fraction of 0.2. Average early Archean TTG from Martin et al. (2005) and average MORB from PETDB database. Shaded region represents Yb contents and the lower range of La/Yb ratios observed in Archean TTGs.

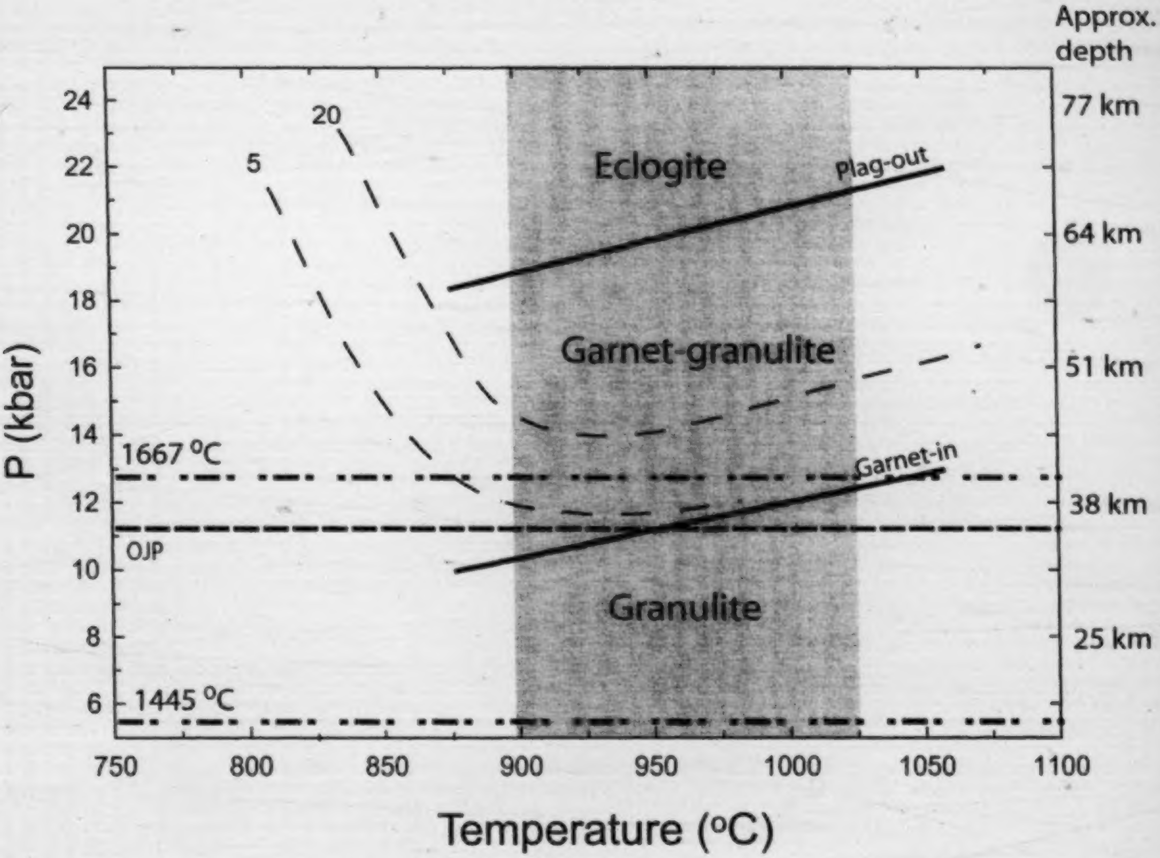

Figure 4.2: P-Tdiagram showing garnet proportion contours (5 and 20 wt.%) in th residue of metabasalt melting. Also shown are the garnet-in and plagioclase-out curves representing the transition from intermediate granulite-high pressure granulite and high pressure granulite-eclogite facies, respectively, in MORB compositions. The horizontal lines (dash-dot) represent the thickness of oceanic crust as a function of different mantle potential temperatures (Vlaar and van den Berg, 1991). Thickness of the Cretaceous Ontong Java plateau shown for comparison (dashed line). Shaded area represents minimum temperature conditions during amphibolite dehydration melting interval where melt proportions reach 20% or more.

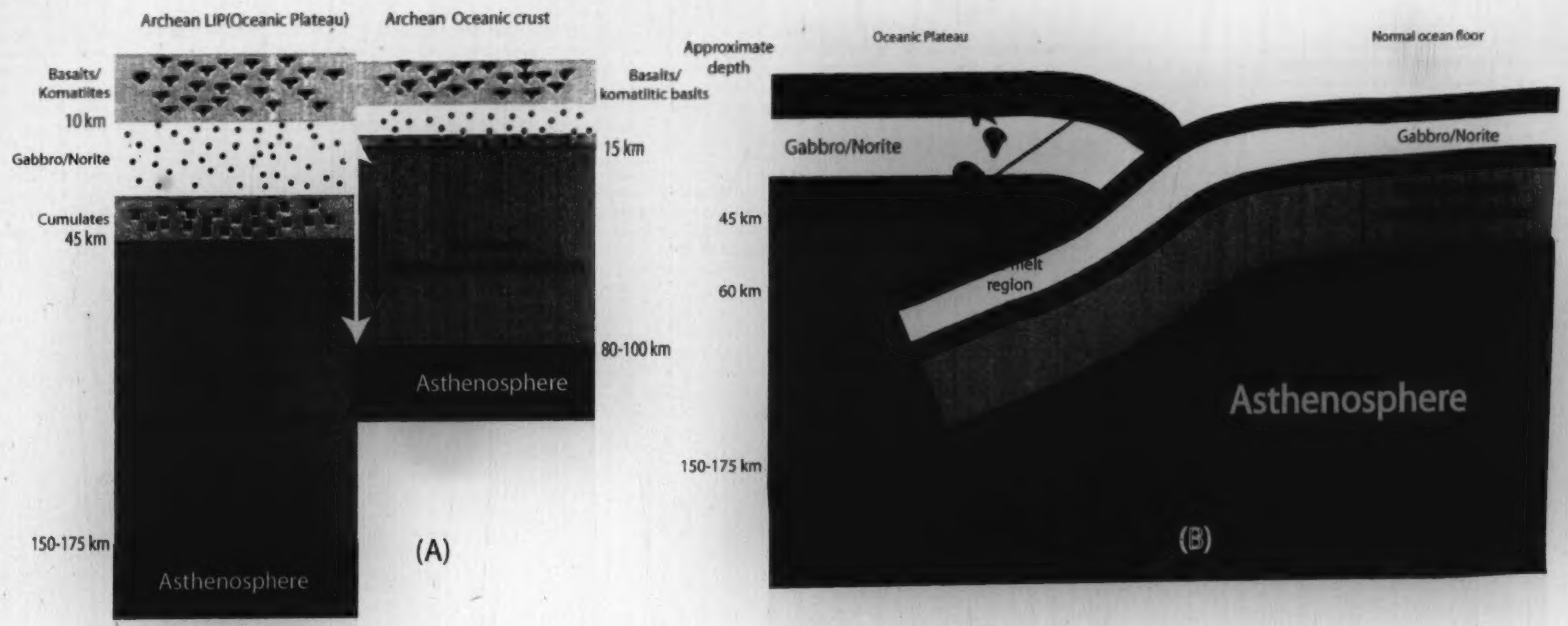
Archean LIP(Oceanic Plateau)
Archean Oceanic crust
Basalts/ Komatiites
10 km
Gabbro/Norite
Cumulates
45 km
150-175 km
Asthenosphere
Basalts/ komatiitic basits
15 km
80-100 km
Asthenosphere
(A)
Approximate depth
45 km
60 km
150-175 km
Oceanic Plateau
Normal ocean floor
Gabbro/Norite
Gabbro/Norite
melt region
Asthenosphere
(B)

Figure 4.3: Model of Archean subduction and formation of TTGs. (A) Hypothetical Structure of an Archean oceanic crust and oceanic plateau. Normal Archean oceanic crust thickness shown for a mantle potential temperature of 1445 °C. Sub-crustal sections of oceanic crust and oceanic plateau (labelled proto-mantle lithosphere, PML) represent the underplated mantle melt residua. PML of plateau owing to the higher degree of melt extraction is leass dense relative to the asthenospheric mantle and the PML of normal oceanic crust. Yellow double headed arrow indicate region where gravitational differences between plateau and normal oceanic lithospher is maximum. (B) Subduction initiation during oceanic plateau-oceanic lithospher convergence in Archean. Subduction of the oceanic lithosphere occurs along a zone of weakness developed within the PML of the oceanic plateau. Melts of subducted slabs are TTGs and are emplaced in the plateau crust.

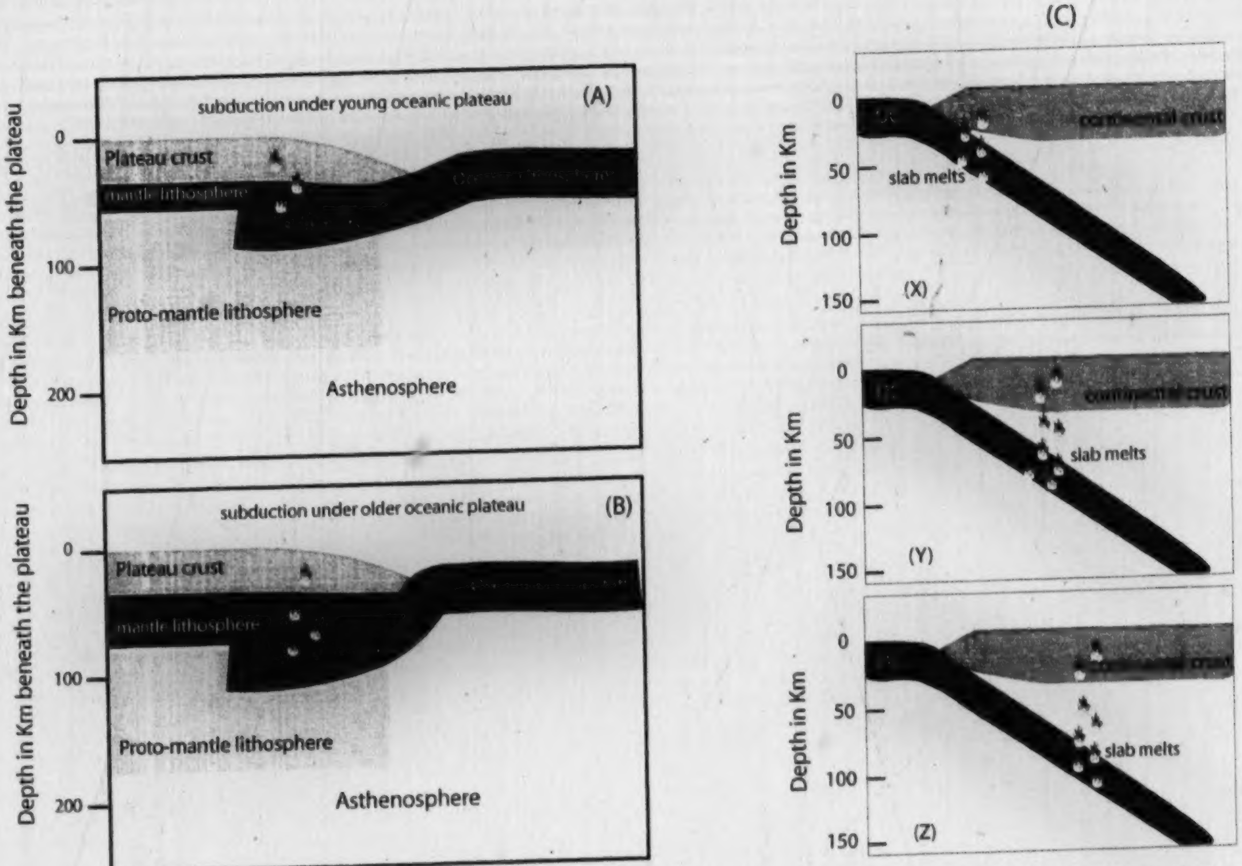
(A)
subduction under young oceanic plateau
Depth in Km beneath the plateau
0
100
200
Plateau crust
mantle lithosphere
Proto-mantle lithosphere
Asthenosphere
(B)
subduction under older oceanic plateau
Depth in Km beneath the plateau
0
100
200
Plateau crust
mantle lithosphere
Proto-mantle lithosphere
Asthenosphere
(C)
Depth in Km
0
50
100
150
slab melts
continental crust
(X)
Depth in Km
0
50
100
150
slab melts
continental crust
(Y)
Depth in Km
0
50
100
150
slab melts
continental crust
(Z)

(after Martin and Moyen, 2002)

Figure 4.4: Cartoon illustrating subduction of oceanic lithosphere under oceanic plateau in Archean during oceanic crust convergence upon a (A) young oceanic plateau and, (B) older oceanic plateau. Note the difference in thickness of the lithospheric mantle wedge that slab melts have to pass through in each case. (C) Model of Martin and Moyen (2002) showing interaction of slab melts with different thickness of mantle wedge as a function of the depth of melting. (X) High geothermal gradient (Early Archean):(Y) medium geothermal gradient (mid-Archean); (Z) lower-geothermal gradient (late-Archean); OC- oceanic crust.

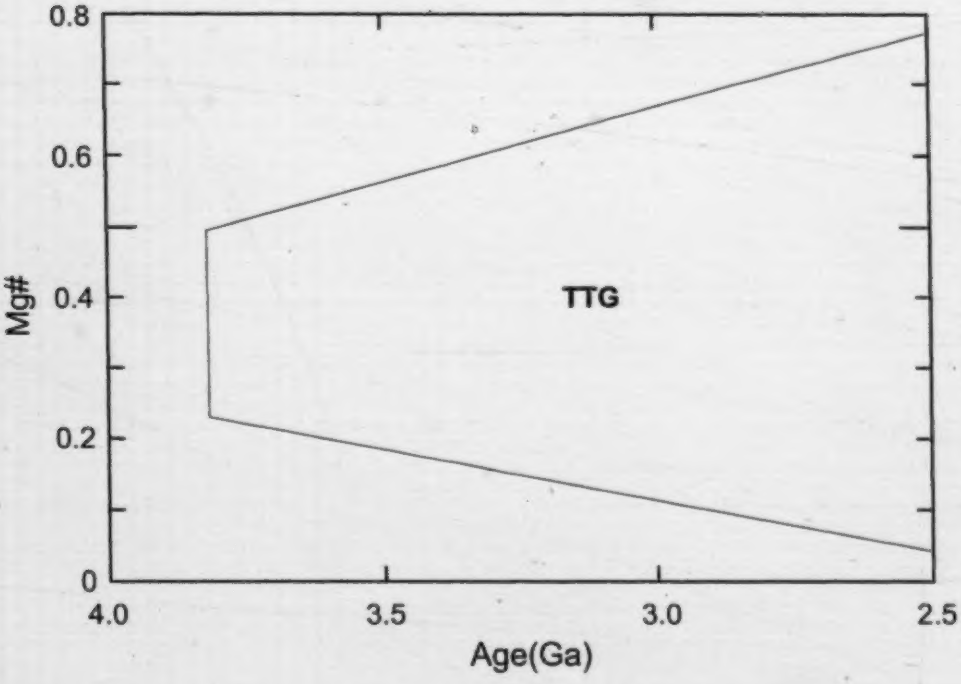

Figure 4.5: Variation of Mg # of Archean TTGs as a function of age (after Martin and Moyen, 2002). The upper and lower bounds of the TTG field in the figure are asymptotes to data points of Martin and Moyen (2002) TTG magmas with maximum and minimum Mg #, respectively. A secular trend towards increasing Mg# towards the end of the Archean is noticeable. Note also the spread of Mg # for TTGs of similar age.

Chapter 5: Conclusions and scope for future research

Dehydration melting equilibria of high-grade amphibolitic rocks of MORB-type bulk compositions determined in this study provide important insights into many unresolved aspects of metabasalt melting and crustal recycling processes involving metabasalts. The main findings of the study and its petrological applications are discussed below.

Dehydration melting of MORB-derived amphibolites

In the pressure range 7-22.5 kbar, the onset of dehydration melting in MORB-type metabasalts is represented by two peritectic melting reactions whose relative positions are pressure dependent. At lower P (<10 kbar), the solidus reaction is Hornblende + Plagioclase + Quartz = Clinopyroxene ± Orthopyroxene + Melt. In the relatively Fe-rich KAP composition, orthopyroxene is a product phase and occurs at temperatures higher than the first appearance of clinopyroxene. In the 3VG composition, orthopyroxene is stable at the dehydration melting solidus at pressures <10 kbar.

At higher P (>10 kbar), the solidus reaction is

Hornblende + Plagioclase + Quartz = Garnet + Clinopyroxene + Melt.

The higher P solidus reaction has a negative dP/dT from about 7 kbar to at least 15 kbar. The slope of the lower P (below 10 kbar) reaction was not constrained in this study, but the combination of my results and those of previous studies (Wolf and Wyllie, 1994; Lopez and Castro, 2001) suggest a steep positive slope. The location of the solidus at 7 kbar is closer to that of Lopez and Castro (2001) than that reported by

Wolf and Wyllie (1994). The present results indicate that dehydration melting of MORB-type amphibolites occurs at temperatures well above the water-saturated basalt solidus between 7 and 10 kbar. Due to the negative P-T slope of the dehydration melting solidus in the garnet stability field, metabasaltic lithologies undergo melting at relatively lower temperatures at P >10 kbar. However, the maximum temperature difference between onset of melting at high pressures (in the garnet stability field) and at low pressures (garnet unstable) is likely less than that suggested by some early studies (e.g. Wolf and Wyllie, 1994).

Melting of MORB-derived amphibolites is an important crustal recycling process that may have contributed to the evolution of continental crust. Results of the present experiments indicate that dehydration melting of MORB-type amphibolites can occur at a range of crustal pressures if temperatures reach or exceed 800 °C. A variety of settings such as collisional orogens and subduction zones may be conducive to this mode of crustal differentiation. The process would have been more important in the Archean when geothermal gradients were higher and deeply buried metabasic rocks or subducted oceanic crust could routinely undergo melting.

Metamorphic facies transitions in MORB-derived metabasalts

At intermediate pressures, the coexistence of orthopyroxene and clinopyroxene is diagnostic of granulite-facies metamorphism in metabasalts. The stability of this assemblage is widely attributed to dehydration melting of amphibolitic rocks and subsequent removal of a felsic melt phase resulting in a granulite residue. The results of this study indicate that in typical MORB-type metabasalts this assemblage is stabilized during dehydration melting at $P < 10$ kbar and at temperatures above 850 °C. Stabilization of granulite-facies assemblages occurred at temperatures above the dehydration melting solidus for both bulk compositions studied.

At high pressures, orthopyroxene-free garnet-clinopyroxene-plagioclase assemblages are indicative of granulite-facies conditions (Pattison, 2003; O'Brien and Rotzler, 2003). Such assemblages are important in understanding the limits of crustal metamorphism (Indares and Martignole, 2003). In particular, these assemblage forms a paragenetic link between the intermediate- pressure two-pyroxene granulites discussed above and high-pressure eclogite-facies assemblages in metabasaltic bulk compositions (e.g. Green and Ringwood, 1967; Pattison, 2003). Relative to intermediate-pressure granulites the high-pressure granulite assemblages are rare, although recently there has been increasing documentation of their occurrence worldwide (e.g. O'Brien and Rotzler, 2003; Indares, 2003). The present results indicate that a temperature of at least ~ 825 °C is required to stabilize garnet + cpx assemblages through dehydration melting in typical MORB-type compositions. This delimits the amphibolite – high-pressure granulite transition in similar metabasaltic compositions to $T > 825$ °C. This low temperature constraint is at significantly higher temperature than that deduced by Wolf and Wyllie (1994). Importantly, this new constraint is consistent with P-T determinations from high-pressure granulite assemblages which indicate temperatures > 750 °C (e.g. O'Brien and Rotzler, 2003; Indares, 2003). The slightly lower temperatures recorded in natural assemblages may again be due to down-temperature re-equilibration of the Fe-Mg exchange reactions used in geothermometric calculations. Alternatively, some of these temperature estimates may be from terranes where the grt + cpx assemblage develops at lower T by the breakdown of more actinolitic hornblende. The results of the present study indicate that pressures greater than 10 kbar are required to stabilize the high-pressure granulite assemblages at temperatures > 775 °C. This result is consistent with the findings of previous experimental studies (e.g. Wolf and Wyllie, 1994; Lopez and Castro, 2001). The formation of high-pressure granulite assemblages, therefore, requires attainment of metamorphic conditions with pressures exceeding that at the base of normal thickness continental crust (>35 km). In situ formation of garnet-granulites of mafic composition may therefore be restricted to the base of thickened continental crust or mature arc crust. Alternatively, tectonic burial of metabasaltic protoliths to depths >35 km may most commonly occur through subduction processes.

At higher pressures, the disappearance of plagioclase from garnet granulite leads to the development of an eclogite-facies assemblage (Carswell, 1990). My experiments indicate that the transition to eclogite assemblages require P >17.5 kbar at conditions exceeding the dehydration melting solidus, which in turn suggests that metabasaltic rocks at the base of normal or even moderately thickened continental crust (<45 km) will not transform to eclogite. This is contrary to the widely held notion that eclogite is the stable form of dry basaltic rocks within the crust (e.g. Green and Ringwood, 1967). The new results indicate that tectonic burial of basaltic rocks to mantle depths are required to stabilize eclogite. This calls into question the viability of many petrological/tectonic models that invoke eclogite formation at the base of oceanic plateau curst or moderately thick continental crust (Zegers and van Keken, 2001; Bedard, 2006).

Generation of Archean TTG magmas

The major-element compositions of melts produced in the present experiments are comparable to those of Archean TTG. In general, the melts have SiO_2 >60 wt. %, Na_2O/K_2O >1, TiO_2 < 1 wt. %, Al_2O_3 >15 wt. %, and geochemical signatures that overlap with Archean TTGs. The major-element compositions of the melts are similar to the high-Al TTG group rocks defined by Barker and Arth (1976). The Al_2O_3 content of the melts at pressures >15kbar appear to be controlled by the amount of residual garnet and clinopyroxene and not just by the amount of residual plagioclase and amphibole as previously thought. The lowest Al_2O_3 content measured in this study are for melts generated above 15 kbar where the residue is dominated by garnet and clinopyroxene.

There are some differences in the composition of melts produced in the present experiments and those produced in previous dehydration melting experiments on amphibolites. In general, the melts produced in this study have lower Na_2O/K_2O ratios than those in previous studies. I attribute this to the higher K_2O content of the present starting materials and the highly incompatible nature of K during dehydration melting of amphibolites. The K_2O content of the melts ranges from 1.1 to 4.4 wt. %, the upper range being slightly higher than the observed K_2O content in Archean TTGs. The Mg-number of the experimental melts while showing a significant overlap is generally lower than the Archean TTGs.

The results show that TTG-type magmas can be produced during the dehydration melting of MORB-derived amphibolites. TTGs may be produced at a range of depths if temperature exceeds the dehydration melting solidus. In general, significant melt production requires temperatures >900 °C. The major-element composition of the melts is influenced by the bulk composition of the protolith and the residual assemblage in equilibrium with the melt. The low TiO_2 compositions used in the present study yield melts with TiO_2 contents that are similar to natural TTGs. In contrast, the high K content of the starting materials of this study resulted in the production of relatively K-rich melts. Moderately potassic granodiorites or granites may, therefore, be directly produced by dehydration melting of K-rich MORB-derived amphibolites. It is not necessary to invoke interaction of mafic magmas with a tonalitic crust to account for the generation of some K-rich granodiorites in the Archean as envisaged by Lopez et al. (2005). Formation of true granites with $K_2O/Na_2O > 1$ require metabasalts with more K than present in the starting amphibolite used in this study. The low Mg# of the experimental melts compared to some TTGs suggests that the MgO content of these magmas are modified during ascent.

A characteristic signature of early Archean TTGs is their highly fractionated REE pattern ($(La/Yb)_N > 15$ and depletion in HREE (Yb average 0.78 ppm) (e.g. Barker and Arth, 1976; Martin et. al., 2005). This is commonly attributed to the presence of residual garnet or hornblende in the residue of partial melting (Barker and Arth, 1976; Martin, 1987). Calculated variations in the La/Yb ratio and Yb content of melts derived from MORB-type basalt indicate that at least 20 wt % garnet is required in the residue to replicate the HREE depletion observed in early Archean TTGs. Experimentally determined phase proportions in this study also show that this requirement is met only if melting occurs at pressures >15 kbar (T>900 °C). True Archean TTG melts can be produced by melting MORB—type bulk compositions at garnet-granulite or eclogite-facies conditions. Although seemingly semantic, this is an important point. Many previous studies attribute TTG formation to melting of garnet-amphibolite (Rapp et al., 1991; Foley et al., 2002; Foley et al., 2003). At the conditions required for generating TTG-type melts, the residual assemblage is either a garnet granulite or an eclogite.

Tectonic setting of early Archean TTGs and origin of continental nuclei

Modelling of REE composition of experimental melts suggests that the production of early Archean TTG-type melts requires magma generation to occur at P >15 kbar. This fundamental requirement should be satisfied by any proposed mechanism for the origin of early Archean TTGs. I argue that this requirement is not met in many lower crustal melting models proposed for the origin of Archean TTGs (e.g. Zegers and van Keken, 2001; Bedard, 2006). Specifically, these models envisage melt generation at conditions much shallower than that required to stabilize enough garnet in the residue to produce the characteristic HREE depletion in early Archean TTGs. Subduction zone processes on the other hand can transport source rocks to P >15 kbar where conditions are appropriate for TTG genesis with HREE depeletion. I, therefore, favor a subduction model for the origin of early Archean TTG and by implication that of the continental crust.

The operation of subduction zone processes in the early Archean is not universally accepted (Hamilton, 1998; Zegers and van Keken, 2001; Bedard 2006). In particular, there is the question of how subduction could have initiated in a hotter Archean Earth. A new tectonic model is presented here that outlines how subduction might have initiated in the early Archean. I propose that Archean subduction process initiated due to gravitational instabilities arising from chemical differences between a converging oceanic plateau and a normal thickness oceanic lithosphere. The chemical differences and the consequent gravitational instability between a plateau and oceanic crust is the result of different degrees of mantle melting involved in the generation of oceanic plateaus and normal oceanic crust. The residual mantle from plateau derivation is less dense than that from oceanic crust generation due to the larger degree of melting involved in the derivation of a plateau crust. In this model, the residuum of mantle melting is envisaged forming a low-density chemical layer (proto-mantle lithosphere) that underplates the plateau. This proto-mantle lithosphere subsequently cools (from top to bottom) to become part of the mantle lithosphere underneath the plateau. Juxtaposition or development of an oceanic plateau near or within an oceanic lithosphere results in the development of deformation zones near the base of the plateau crust and causes the subduction of denser oceanic lithosphere through the proto-mantle lithosphere of the plateau. Owing to high geothermal gradients in Archean, subducted oceanic crust melts resulting in the formation of TTG type magmas.

The proposed model has many implications regarding early Earth processes, including the development of first subduction zones, origin of modern-style plate tectonics, origin and growth of continental nuclei, granite-greenstone relations in Archean cratons, formation and evolution of sub-continental lithospheric mantle etc. I argue that in early Archean times, buoyant oceanic plateaus served as the backstop for subduction initiation and kick-started plate tectonics. The higher geothermal gradient in the Archean resulted in the melting of the subducted oceanic crust beneath the plateau and the formation of TTG magmas which were emplaced in the plateau crust, there by stabilizing a nucleus of continental crust. Addition to this and other similar nucleii by tectonic processes including terrain accretion results in the growth of continental crust. I interpret the spatial and temporal relationships observed in Archean cratons between tholeiitic to komatiiic volcanic rocks and TTGs as reflecting the operation of many linked processes as envisaged in the proposed model. I argue that oceanic plateaus served as the nuclei for TTG formation in the early Archean and for the formation of cratons. Archean cratons as we see them today are, therefore, ancient oceanic plateaus modified by subsequent magmatic and tectonic processes. Detailed geophysical, geochemical, isotopic, petrological and rheological studies of components of granite-greenstone terrains should be used to test the predictions of this model.

Future Work

While many aspects of amphibolite dehydration melting have been addressed in the present study, there are a number of questions regarding melting of metabasaltic rocks and their role in crustal evolution that still remains unclear. I identify some of these questions in the following paragraphs.

In my opinion, a major draw-back of the present and many previous experimental studies has been the inability to do in situ trace-element analysis of the melt compositions due to the small size of the quenched melt pockets. As a result, the trace-element composition of the experimental melts were determined by combining modal estimates of the abundance of restite phases in the experimental charges with mineral/melt partition coefficient data from the literature. While this is a reasonable approach, it is not ideal. In particular it is unclear, how uncertainties in the estimated mode and partition coefficient data propagate to uncertainties in trace-element concentrations. Melt traps using vitreous carbon spheres and diamond aggregates were successfully employed previously to generate melt pools that are sufficiently large for major- and trace-element analysis (Baker and Stolper, 1994; Hirose and Kushiro, 1992; Schwab and Johnston, 2001). These peridotite melting experimental studies claim that these melt traps help avoid quench modification of melt composition (Baker and Stolper, 1994; Schwab and Johnston, 2001). In the present study, attempts to obtain larger melt pockets using vitreous carbon spheres to create pore spaces for melt accumulation were not successful. It is unclear if the success of the melt trap technique depends critically on the viscosity of melts produced during experiments. Further studies are required to assess the viability of this technique in basalt dehydration-melting experiments, which produces melts with higher viscosity than produced in peridotite melting experiments. In situ analysis of trace-element concentrations in quenched melts is critically important to our understanding of magmatic processes within the crust. Improvements in the spatial resolution of ion probe analyses and in ion probe optics may make analysis of small melt pools feasible in future.

The present study provides constraints on the dehydration melting behavior of MORB-type amphibolites. Tholeiitic basalts of MORB composition is found in the geological record and, therefore, may have represented the crust of open oceans throughout much of Earth's history. However, basaltic lavas with higher Mg-number than average MORB are found in the Archean rock record. Although relatively rare compared to tholeiitic basalts, these high Mg-number komatiitic-basalts and basaltic-komatiites represent protolith compositions that may have contributed to crustal recycling processes in the Archean. Some petrologists argue that the early Archean oceanic crust would have been Mg-rich because of the higher heat production and therefore larger degree of melting undergone by Archean mantle (Bickle et al., 1994; Foley et al., 2003). To the best of my knowledge, phase relations in high-MgO metabasalts have not been investigated to date. Foley et al. (2003) conducted a few experiments on Gorgona komatiites and showed that the phase relations during melting high MgO basalts significantly deviate from MORB-type metabasalts. Although the effect of high Mg-number on the phase relations during melting can be qualitatively predicted by comparing the phase relations obtained from basalt melting experiments with those from the komatiite melting experiments of Foley et al. (2003), accurate knowledge of phase relations of high-MgO metabasalts through targeted experiments would significantly advance our understanding of crustal evolutionary processes in the Archean.

I believe that the experimental constraints obtained in this study have improved our understanding of the evolution of mafic composition rocks during metamorphism and anatexis. However, the origin of garnet-clinopyroxene amphibolites that presumably equilibrated at temperatures significantly lower than the temperatures at which the garnet-clinopyroxene assemblage was stable in the present experiments is puzzling. I hypothesized in Chapter 2 that the occurrence of these assemblages at low temperatures might be related to the bulk composition of the basaltic protolith and specifically to the composition of hornblende in the protolith. Based on the composition of metamorphic phases observed in these low temperature garnet-amphibolite assemblages, I speculate that these assemblages might have developed through breakdown reactions involving a ferroactinolitic-hornblende. As far as I know, there are no experimental data available on the stability of ferroactinolite-bearing metabasalts. An experimental study of ferroactinolite stability in metabasalts may provide useful information to answer this unresolved issue.

In Chapter 3, I drew attention to the high TiO_2 content of garnet produced in dehydration melting experiments and its possible role in sequestering Ti and HFSE during melting of metabasalts. A systematic study of garnet/tonalite melt partitioning of Ti may provide important information regarding the magmas that are generated in equilibrium with it. It is also of interest to investigate the Ti substitution mechanisms in garnet and the effect of bulk rock TiO_2 content on Ti concentration in garnet. This may lead to a better understanding of the observed mass imbalance in Ti between continental crust and depleted mantle (e.g. Rudnick et al., 2000).

The proposed subduction model for early Archean TTG genesis has many geologic implications that can be evaluated through further research. Initiation of subduction is a fundamental problem in geodynamics, especially in the Archean. Further development of the proposed subduction initiation model requires a better understanding of the deformation mechanisms involved in the nucleation of subduction zones. In particular, we need to better understand the formation and evolution of mantle lithosphere under the normal oceanic crust and oceanic plateaus. Although the cooling and evolution of oceanic lithosphere has been described through infinite half-space cooling models (Sclater and Parsons, 1981), the evolution of lithosphere under plateau crust is not clearly understood. Knowledge of the cooling history of oceanic crust and oceanic plateaus, viscosities of the depleted mantle under these crustal entities and, how these parameters influence deformation processes during oceanic crust-plateau convergence is fundamental to a better understanding of subduction initiation mechanisms. My model provides possible explanations for many aspects of the Archean rock record including TTG magmatism, TTG-mafic/ultramafic magma association, the formation of sub-continental lithospheric mantle, spatial association of rocks of plume and arc signatures etc. These aspects of crust/lithosphere evolution are the focus of debate today and further research, perhaps triggered by the subduction initiation hypothesis presented here, would help us better understand the geological history of the early Earth.

References:

Baker, M.B. and Stolper, E.M. (1994) Determining the composition of high-pressure mantle melts using diamond aggregates. Geochimica et Cosmochimica Acta, 58, 2811-2827.

Barker, F. and Arth, J.G. (1976) Generation of trondhjemitic-tonalitic liquids and Archean bimodal trondhjemite-basalt suites. Geology, 4, 596-600.

Bedard, J.H. (2006) A catalytic delamination-driven model for coupled genesis of Archean crust and sub-continental lithospheric mantle. Geochimica et Cosmochimica Acta, 70, 1188-1214.

Bickle, M.J. (1994) Implications of melting for stabilization of the lithosphere and heat loss in the Archean. Earth and Planetary Science Letters, 80, 314-324.

Carswell, D.A. (1990) Eclogites and the eclogite facies: definitions and classification. In: Eclogites Facies Rocks (ed. Carswell, D.A.), Chapman and Hall, New York, pp. 1-13.

Foley, S.F., Tiepolo, M. and Vannucci, R. (2002) Growth of early continental crust controlled by melting of amphibolite in subduction zones. Nature, 417, 837-840.

Foley, S.F., Buhre, S. and Jacob, D.E. (2003) Evolution of the Archean crust by delamination and shallow subduction. Nature, 421, 249-252.

Frost, C.D., Frost, B.R., Kirkwood, R. and Chamberlain, K.R. (2006) The tonalite-trondhjemite-granodiorite (TTG) to granodiorite-granite (GC) transition in the late Archean plutonic rocks of the central Wyoming Province. Canadian Journal of Earth Sciences, 43, 1419-1444.

Green, D.H. and Ringwood, A.E. (1967) An experimental investigation of the gabbro to eclogite transformation and its petrological applications. Geochimica et Cosmochimica Acta, 31, 767-833.

Hamilton, W.B. (1998) Archean magmatism and deformation were not products of plate tectonics. Precambrian Research, 91, 143-179.

Hirose, K. and Kushiro, I. (1993) Partial melting of dry peridotites at high pressures: determination of compositions of melts segregated from peridotite using aggregates of diamond. Earth and Planetary Science Letters, 114, 477-489.

Indares, A.D. (2003) Metamorphic textures and P-T evolution of high-P granulites from the Lelukuau terrane, NE Grenville Province. Journal of Metamorphic Geology, 21, 35-48.

Indares, A.D. and Martignole, J. (2003) Towards the upper limits of granulite facies. Journal of Metamorphic Geology, 21, 1-2.

Lopez, S. & Castro, A. (2001) Determination of the fluid-absent solidus and supersolidus phase relationships of MORB-derived amphibolites in the range 4-14 kbar. American Mineralogist, 86, 1396-1403.

Lopez, S., Castro, A. and Garcia-Casco, A. (2005) Production of granodiorite melt by interaction between hydrous mafic magma and tonalitic crust. Experimental constraints and implications for the generation of Archaean TTG complexes. Lithos, 79, 229-250.

Martin, H. (1987) Petrogenesis of Archean trondhjemites, tonalites and granodiorites from eastern Finland: major and trace element geochemistry. Journal of Petrology, 28, 921-953.

Martin, H., Smithies, R.H., Rapp, R., Moyen, J.-F and Champion, D. (2005) An overview of adakite, tonalite-trondhjemite-granodiorite (TTG), and sanukitoid: relationships and some implications for crustal evolution. Lithos, 79, 1-24.

O'Brien, P.J. and Rotzler, J. (2003) High-pressure granulites: formation, recovery of peak conditions and implications for tectonics. Journal of Metamorphic Geology, 21, 3-20.

/

Pattison, D.R.M. (2003) Petrogenetic significance of orthopyroxene-free garnet + clinopyroxene + plagioclase-bearing metabasites with respect to the amphibolite and granulite facies. Journal of Metamorphic Geology, 21, 21-31.

Rapp, R.P., Watson, E.B., and Miller, C.F. (1991) Partial melting of amphibolite/eclogite and the origin of Archean trondhjemites and tonalites. Precambrian Research, 51, 1-25.

Rudnick, R.L., Barth, M., Horn, I. and McDonough, W.F. (2000) Rutile-bearing refractory eclogites: missing link between continents and depleted mantle. Science, 287, 278-281.

Schwab, B.E. and Johnston, A.D. (2001) Melting systematics of modally variable, compositionally intermediate peridotites and the effects of mineral fertility. Journal of Petrology, 42, 1789-1811.

Sclater, J.G. and Parsons, B. (1981) Oceans and continents: similarities and differences in the mechanisms of heat loss. Journal of Geophysical Research, 86, 11535-11552.

Wolf, M.B. and Wyllie, P.J. (1994) Dehydration-melting of amphibolite at 10 kbar: the effects of temperature and time. Contributions to Mineralogy and Petrology, 44, 151-179.

Zegers, T.E. and van Keken, P.E. (2001) Middle Archean continental formation by crustal delamination. Geology, 29, 1083-1086.

APPENDIX A- Electron Microprobe Analyses of Experimental Phases

Hornblende Compositions

SiO_2	TiO_2	Al_2O_3	Cr_2O_3	FeO	MnO	MgO	CaO	Na_2O	K_2O	F	Cl	Total	Sample
43.96	1.46	12.98	0.02	15.60	0.22	10.05	11.46	1.48	1.27	n.a.	n.a.	98.49	3VG12-1
44.01	1.52	12.78	0	15.15	0.25	10.34	11.28	1.60	1.25	n.a.	n.a.	98.18	3VG12-2
43.71	1.45	13.24	0	15.65	0.20	10.14	11.33	1.47	1.31	n.a.	n.a.	98.49	3VG12-3
43.32	1.51	12.99	0.01	15.50	0.22	9.78	11.27	1.53	1.31	n.a.	n.a.	97.43	3VG12-4
43.48	1.84	12.82	0.02	15.41	0.19	10.56	11.25	1.62	1.27	n.a.	n.a.	98.14	3VG12-5
44.16	1.57	12.88	0.03	15.86	0.21	10.16	11.40	1.40	1.23	n.a.	n.a.	98.70	3VG12-6
44.00	1.57	12.90	0.02	15.62	0.25	10.33	11.39	1.59	1.27	n.a.	n.a.	98.70	3VG12-7
44.47	1.61	12.86	0.01	15.42	0.20	10.09	11.17	1.52	1.23	n.a.	n.a.	98.37	3VG12-8
43.57	1.54	13.30	0.01	15.88	0.20	9.83	11.30	1.54	1.28	n.a.	n.a.	98.44	3VG12-9
43.68	1.58	12.79	0.01	15.87	0.21	9.94	11.33	1.54	1.30	n.a.	n.a.	98.24	3VG12-10
43.16	1.38	12.85	0.01	16.31	0.28	9.96	11.48	1.44	1.30	n.a.	n.a.	97.92	3VG12-11
46.67	1.41	14.15	0.02	14.14	0.20	9.93	11.04	1.99	1.15	n.a.	n.a.	100.69	3VG12-12
43.26	1.48	12.71	0.03	15.82	0.21	10.12	11.57	1.40	1.32	n.a.	n.a.	97.92	3VG12-13
43.53	1.60	13.27	0	15.72	0.24	9.85	11.44	1.52	1.33	n.a.	n.a.	98.49	3VG12-14
43.66	1.48	13.02	0	16.07	0.20	9.90	11.32	1.46	1.31	n.a.	n.a.	98.41	3VG12-15
43.91	1.51	12.98	0.01	15.60	0.22	10.06	11.33	1.54	1.28	n.d.	n.d.	98.44	Average
0.84	0.07	0.40	0.01	0.49	0.02	0.22	0.13	0.14	0.05	n.d.	n.d.		Std.Dev.
42.86	1.45	12.61	0	16.21	0.21	9.91	10.92	1.44	1.37	n.a	0.05	97.01	3VG1-1
42.85	1.46	12.69	0	16.16	0.19	10.06	11.24	1.36	1.33	n.a	0.06	97.38	3VG1-2
42.44	1.52	12.31	0.01	16.57	0.22	9.93	11.04	1.51	1.42	n.a	0.09	97.03	3VG1-3
43.06	1.35	12.11	0.02	16.27	0.20	10.54	11.08	1.47	1.38	n.a	0.07	97.62	3VG1-4
43.00	1.53	12.30	0.05	15.99	0.18	10.38	10.92	1.43	1.39	n.a	0.05	97.20	3VG1-5
43.11	1.45	12.21	0.02	16.15	0.23	10.41	11.21	1.40	1.33	n.a	0.05	97.56	3VG1-6
43.26	1.41	12.28	0	16.17	0.21	10.26	10.85	1.41	1.39	n.a	0.06	97.28	3VG1-7
42.82	1.61	11.77	0.02	16.43	0.17	10.36	11.28	1.31	1.41	n.a	0.05	97.22	3VG1-8
43.02	1.33	12.81	0	15.90	0.17	10.42	10.91	1.44	1.44	n.a	0.05	97.27	3VG1-9
42.96	1.62	12.00	0	16.36	0.18	10.42	11.21	1.34	1.35	n.a	0.06	97.49	3VG1-10
43.22	1.37	12.25	0	16.31	0.19	10.50	10.88	1.38	1.30	n.a	0.05	97.44	3VG1-11
43.00	1.42	12.62	0.04	16.22	0.19	10.30	10.88	1.41	1.35	n.a	0.07	97.39	3VG1-12
42.97	1.44	12.48	0	16.34	0.23	10.12	10.75	1.56	1.33	n.a	0.06	97.26	3VG1-13
43.02	1.49	12.44	0.01	16.39	0.24	10.01	10.82	1.53	1.37	n.a	0.06	97.35	3VG1-14
43.47	1.41	11.93	0	16.42	0.19	10.74	10.80	1.50	1.21	n.a	0.06	97.71	3VG1-15
42.95	1.38	12.80	0.01	16.71	0.22	10.04	10.82	1.43	1.38	n.a	0.03	97.46	3VG1-16
42.84	1.76	11.88	0.01	15.83	0.19	10.65	11.19	1.39	1.27	n.a	0.09	97.06	3VG1-17
43.10	1.48	12.61	0	16.12	0.18	10.53	11.05	1.47	1.36	n.a	0.06	97.91	3VG1-18
42.51	1.53	12.64	0.02	16.27	0.24	10.22	10.88	1.51	1.35	n.a	0.07	97.21	3VG1-19
42.94	1.44	12.82	0	16.15	0.22	10.33	10.98	1.42	1.30	n.a	0.07	97.33	3VG1-20
42.74	1.43	12.79	0.02	16.26	0.21	10.28	10.93	1.53	1.35	n.a	0.05	97.58	3VG1-21
42.93	1.47	12.58	0.02	16.00	0.16	10.29	11.01	1.48	1.37	n.a	0.07	97.35	3VG1-22
43.12	1.36	12.86	0.02	16.04	0.19	10.40	10.91	1.41	1.28	n.a	0.07	97.44	3VG1-23
42.77	1.41	12.78	0.01	16.57	0.25	10.15	11.06	1.42	1.32	n.a	0.07	97.75	3VG1-24
42.89	1.43	12.62	0.01	15.96	0.19	10.12	11.00	1.42	1.33	n.a	0.06	97.01	3VG1-25
42.98	1.46	12.41	0.01	16.23	0.20	10.29	10.98	1.44	1.35	n.d.	0.06	97.38	Average
0.23	0.10	0.30	0.01	0.22	0.02	0.20	0.15	0.06	0.05	n.d.	0.01		Std. Dev.
43.09	1.56	12.89	0	16.34	0.27	10.51	10.63	1.76	1.29	n.a.	n.a.	98.93	3VG27-1
44.83	1.14	10.79	0	15.78	0.21	10.89	11.19	2.71	1.04	n.a.	n.a.	99.27	3VG27-2
43.35	1.64	12.43	0	15.87	0.19	10.40	10.61	3.13	1.27	n.a.	n.a.	98.87	3VG27-3
43.48	1.54	12.98	0.01	15.75	0.23	10.46	10.99	2.66	1.33	n.a.	n.a.	99.39	3VG27-4
43.24	1.57	12.83	0	15.74	0.22	10.20	10.55	3.37	1.20	n.a.	n.a.	98.91	3VG27-5
44.12	2.07	10.25	0	16.49	0.21	10.92	10.02	3.85	0.81	n.a.	n.a.	98.75	3VG27-6
43.40	1.51	12.81	0	15.82	0.22	10.71	10.84	2.37	1.29	n.a.	n.a.	98.95	3VG27-7
43.49	1.47	12.23	0	15.55	0.17	10.27	10.85	3.34	1.25	n.a.	n.a.	98.41	3VG27-8
43.25	1.52	12.80	0.01	15.45	0.18	10.08	11.12	2.86	1.34	n.a.	n.a.	98.41	3VG27-9
43.19	1.54	12.94	0	16.19	0.17	10.03	11.04	1.92	1.33	n.a.	n.a.	98.34	3VG27-10
44.05	1.50	11.88	0	15.49	0.19	10.47	11.33	3.08	1.11	n.a.	n.a.	98.88	3VG27-11
43.47	1.42	12.86	0.01	16.20	0.21	10.54	11.14	1.81	1.31	n.a.	n.a.	98.67	3VG27-12
43.60	1.65	12.71	0	15.67	0.20	10.28	11.06	2.88	1.32	n.a.	n.a.	99.37	3VG27-13
43.66	1.49	12.84	0	15.42	0.18	10.33	11.12	3.10	1.35	n.a.	n.a.	99.47	3VG27-14
43.40	1.82	10.99	0.01	15.57	0.23	11.13	10.21	3.83	1.17	n.a.	n.a.	98.06	3VG27-15
44.16	1.38	11.32	0.03	15.59	0.23	10.59	11.48	1.91	1.17	n.a.	n.a.	97.84	3VG27-16
43.63	1.53	12.19	0.00	15.81	0.21	10.49	10.87	2.77	1.22	-	-	98.72	Average
0.39	0.19	0.89	0.01	0.33	0.03	0.31	0.40	0.68	0.14	-	-		Std. Dev.
43.20	1.43	12.70	0.01	16.27	0.20	10.67	11.01	1.42	1.34	n.a.	0.06	98.28	3VG3-1
42.77	1.55	12.53	0	16.19	0.16	10.78	10.60	1.68	1.27	n.a.	0.05	97.56	3VG3-2
43.00	1.48	13.12	0	16.22	0.21	10.34	10.83	1.45	1.37	n.a.	0.07	98.04	3VG3-3
43.05	1.38	12.98	0.01	15.90	0.20	10.42	10.86	1.46	1.36	n.a.	0.05	97.67	3VG3-4
43.36	1.49	12.77	0	16.16	0.22	10.82	10.81	1.55	1.28	n.a.	0.07	98.51	3VG3-5
42.83	1.36	13.24	0	16.34	0.22	10.28	10.85	1.42	1.34	n.a.	0.06	97.94	3VG3-6
42.89	1.83	12.93	0.02	16.40	0.22	10.50	10.88	1.47	1.32	n.a.	0.04	98.17	3VG3-7
42.72	1.41	13.16	0	16.30	0.21	10.23	10.90	1.44	1.37	n.a.	0.04	97.77	3VG3-8

SiO_2	TiO_2	Al_2O_3	Cr_2O_3	FeO	MnO	MgO	CaO	Na_2O	K_2O	F	Cl	Total	Sample
42.82	1.53	13.20	0.01	16.34	0.20	10.30	10.92	1.42	1.36	n.a.	0.05	98.14	3VG3-9
43.01	1.38	13.06	0	15.93	0.20	10.53	11.09	1.51	1.37	n.a.	0.05	98.10	3VG3-10
42.92	1.45	13.00	0	16.46	0.21	10.35	10.87	1.47	1.33	n.a.	0.06	98.09	3VG3-11
43.21	1.40	13.01	0	16.19	0.19	10.56	10.87	1.55	1.30	n.a.	0.03	98.32	3VG3-12
42.89	1.44	13.04	0	16.31	0.22	10.26	10.86	1.47	1.30	n.a.	0.07	97.86	3VG3-13
42.49	1.55	12.80	0	16.33	0.20	10.31	11.24	1.50	1.36	n.a.	0.06	97.81	3VG3-14
43.24	1.34	12.33	0	16.33	0.21	10.84	11.20	1.50	1.34	n.a.	0.06	98.37	3VG3-15
43.26	1.50	12.57	0.01	15.67	0.18	10.80	10.89	1.47	1.31	n.a.	0.07	97.32	3VG3-16
42.96	1.60	12.72	0.02	15.51	0.19	10.66	10.48	1.64	1.34	n.a.	0.06	97.19	3VG3-17
42.80	1.50	12.31	0.01	16.11	0.21	10.51	11.01	1.52	1.30	n.a.	0.05	97.32	3VG3-18
43.11	1.51	13.28	0	15.93	0.21	10.96	10.71	1.49	1.37	n.a.	0.06	98.20	3VG3-19
42.71	1.41	12.89	0.02	16.07	0.28	10.12	10.67	1.44	1.37	n.a.	0.07	97.00	3VG3-20
42.95	1.39	12.72	0.02	15.78	0.21	10.40	11.05	1.57	1.37	n.a.	0.05	97.80	3VG3-21
42.98	1.46	12.87	0.01	16.13	0.21	10.49	10.88	1.50	1.34	-	0.06	97.88	Average
0.22	0.07	0.28	0.01	0.25	0.02	0.20	0.19	0.07	0.03	-	0.01		Std. Dev.
41.88	2.25	14.05	0	14.96	0.22	9.96	11.19	3.38	1.19	n.a.	n.a.	99.08	3VG2-1
43.73	1.58	11.76	0	15.09	0.22	10.43	11.73	3.12	1.06	n.a.	n.a.	98.89	3VG2-2
43.25	1.80	12.72	0.03	15.07	0.20	10.58	11.11	3.47	1.18	n.a.	n.a.	99.50	3VG2-3
43.17	1.72	12.21	0	14.78	0.18	10.67	11.28	3.30	1.24	n.a.	n.a.	98.55	3VG2-4
42.86	3.29	12.37	0.03	13.27	0.14	11.27	10.76	3.67	0.67	n.a.	n.a.	98.33	3VG2-5
43.63	1.99	12.75	0.02	15.84	0.24	10.19	11.06	2.35	1.28	n.a.	n.a.	98.92	3VG2-6
43.05	2.87	12.16	0.02	14.10	0.19	11.20	10.84	3.82	0.81	n.a.	n.a.	98.76	3VG2-7
43.11	2.52	12.61	0.01	14.82	0.22	10.44	10.76	3.80	0.87	n.a.	n.a.	99.25	3VG2-8
43.30	2.22	12.35	0.04	14.40	0.19	10.86	10.76	3.72	0.96	n.a.	n.a.	98.82	3VG2-9
43.19	1.82	12.84	0	15.16	0.22	10.36	10.87	3.13	1.24	n.a.	n.a.	98.75	3VG2-10
43.21	1.42	12.28	0.04	15.44	0.17	10.47	11.22	3.09	1.31	n.a.	n.a.	98.94	3VG2-11
42.57	1.59	12.51	0.01	15.12	0.25	10.09	10.96	3.30	1.21	n.a.	n.a.	97.62	3VG2-12
43.02	2.66	12.30	0	14.56	0.19	11.05	10.30	3.92	0.78	n.a.	n.a.	98.87	3VG2-13
43.47	2.38	12.06	0.02	13.96	0.18	11.24	10.91	3.93	0.91	n.a.	n.a.	98.65	3VG2-14
43.17	1.61	12.88	0.03	15.43	0.21	10.27	11.26	3.12	1.28	n.a.	n.a.	98.83	3VG2-15
43.11	2.09	12.60	0.01	14.80	0.20	10.61	10.99	3.39	1.05	n.d.	n.d.	98.75	Average
0.44	0.56	0.52	0.01	0.65	0.03	0.43	0.33	0.42	0.23	n.d.	n.d.		Std.Dev.
43.71	1.41	12.14	0.01	15.80	0.20	10.88	11.95	1.24	1.20	0	0.05	98.25	3VG11-1
42.35	1.44	12.72	0.02	16.29	0.24	10.20	11.56	1.49	1.28	0	0.06	97.61	3VG11-2
42.63	1.52	12.85	0.02	16.34	0.22	10.03	11.45	1.40	1.26	0	0.07	97.76	3VG11-3
43.56	1.48	12.80	0.02	15.91	0.21	10.10	11.32	1.40	1.25	0	0.03	98.08	3VG11-4
42.85	1.62	12.69	0.01	15.93	0.20	10.04	11.74	1.41	1.32	0	0.06	97.85	3VG11-5
43.07	1.44	13.05	0.03	15.89	0.25	10.11	11.32	1.62	1.20	0	0.06	97.91	3VG11-6
42.83	1.96	12.53	0	15.58	0.19	10.37	11.60	1.32	1.27	0	0.05	97.28	3VG11-7
43.50	1.30	11.86	0.03	16.58	0.28	10.48	11.81	1.42	1.19	0	0.05	98.27	3VG11-8
42.87	1.71	12.68	0	15.90	0.20	10.48	11.84	1.48	1.23	0	0.06	98.44	3VG11-9
42.58	1.39	12.58	0.01	15.87	0.25	10.64	11.38	1.49	1.33	0	0.05	97.56	3VG11-10
42.78	1.48	12.73	0.01	15.86	0.21	10.36	11.55	1.50	1.39	0	0.06	97.93	3VG11-11
42.84	1.60	12.89	0	16.07	0.19	10.28	11.56	1.27	1.27	0	0.06	97.61	3VG11-12
43.14	1.58	12.41	0	15.95	0.19	10.34	11.70	1.46	1.28	0	0.07	98.11	3VG11-13
42.68	1.60	12.40	0.01	16.17	0.23	10.31	11.77	1.40	1.36	0	0.06	97.96	3VG11-14
42.68	1.55	12.85	0	15.84	0.21	10.36	11.22	1.42	1.33	0	0.07	97.52	3VG11-15
42.87	1.43	11.88	0	16.21	0.22	10.24	11.29	1.44	1.28	0	0.06	96.88	3VG11-16
43.06	1.73	12.91	0	15.59	0.16	10.49	11.43	1.47	1.33	0	0.06	98.23	3VG11-17
44.84	1.24	10.33	0.01	15.77	0.25	11.34	11.92	1.23	0.93	0	0.04	97.89	3VG11-18
43.52	1.30	12.67	0.02	15.79	0.21	10.11	11.82	1.43	1.17	0	0.07	98.09	3VG11-19
42.97	1.50	12.79	0.02	16.10	0.21	10.20	11.36	1.44	1.35	0	0.04	98.00	3VG11-20
47.10	0.37	8.53	0.02	17.28	0.27	11.11	12.80	0.95	0.06	0	0.09	98.14	3VG11-21
42.87	1.58	12.92	0.01	15.81	0.18	10.38	11.39	1.40	1.33	0	0.07	97.94	3VG11-22
42.92	1.56	13.08	0	16.20	0.23	10.28	11.48	1.45	1.32	0	0.07	98.56	3VG11-23
43.14	1.69	12.59	0.02	15.54	0.18	10.30	11.80	1.44	1.26	0	0.09	97.72	3VG11-24
43.28	1.63	12.86	0.02	16.12	0.28	10.25	11.35	1.47	1.30	0	0.06	98.58	3VG11-25
43.22	1.46	12.38	0.01	16.00	0.22	10.39	11.59	1.40	1.22	0.00	0.06	97.94	Average
0.95	0.26	0.96	0.01	0.37	0.03	0.32	0.28	0.12	0.26	0.00	0.02		Std. Dev.
43.18	1.63	12.98	0.01	15.76	0.23	10.25	11.35	1.45	1.30	0	0.05	98.17	3VG-10-1
40.73	1.79	14.93	0	16.80	0.17	9.14	11.98	1.64	1.39	0	0.11	98.46	3VG-10-2
44.32	1.38	12.21	0	16.05	0.24	10.25	11.13	1.53	1.06	0	0.05	98.17	3VG-10-3
43.13	1.49	12.89	0.02	16.07	0.20	10.29	11.33	1.54	1.36	0	0.06	98.16	3VG-10-4
43.15	1.52	12.92	0.01	16.06	0.18	10.46	11.42	1.43	1.33	0	0.06	98.53	3VG-10-5
42.96	1.88	12.94	0	16.22	0.26	10.29	11.47	1.58	1.39	0	0.06	98.98	3VG-10-6
43.07	1.26	12.31	0	16.54	0.22	10.32	11.43	1.65	1.21	0	0.07	98.06	3VG-10-7
42.49	1.50	12.88	0.01	15.99	0.19	10.31	11.30	1.66	1.33	0	0.05	97.39	3VG-10-8
43.20	1.62	12.83	0.02	15.90	0.18	10.46	11.32	1.58	1.20	0	0.06	98.17	3VG-10-9
42.82	1.82	11.67	0.03	16.09	0.23	10.23	11.78	1.27	1.27	0	0.05	97.25	3VG-10-10
43.83	1.36	11.83	0.03	16.11	0.20	10.86	11.45	1.29	1.17	0	0.04	98.16	3VG-10-11
43.01	1.59	12.69	0	16.19	0.24	10.25	11.51	1.53	1.32	0	0.05	98.34	3VG-10-12
42.61	1.55	13.03	0	15.84	0.23	10.04	11.33	1.52	1.36	0	0.09	97.58	3VG-10-13
42.89	1.56	12.79	0.02	16.25	0.21	10.33	11.45	1.52	1.28	0	0.06	98.36	3VG-10-14
43.83	1.77	11.62	0.03	15.66	0.19	10.54	11.64	1.46	1.22	0	0.10	98.03	3VG-10-15
42.93	1.62	12.77	0.01	16.20	0.21	10.25	11.35	1.53	1.32	0	0.06	98.23	3VG-10-16
42.86	1.53	12.82	0.02	16.32	0.24	10.30	11.49	1.61	1.37	0	0.07	98.90	3VG-10-17

SiO_2	TiO_2	Al_2O_3	Cr_2O_3	FeO	MnO	MgO	CaO	Na_2O	K_2O	F	Cl	Total	Sample
42.76	1.58	12.70	0.02	16.15	0.18	10.37	11.53	1.41	1.28	0	0.08	98.04	3VG-10-18
42.97	1.53	12.76	0.01	16.04	0.19	10.36	11.23	1.44	1.28	0	0.06	97.86	3VG-10-19
42.82	1.84	12.80	0.03	16.36	0.22	10.29	11.60	1.44	1.38	0	0.04	98.62	3VG-10-20
43.06	1.45	13.06	0	15.99	0.24	10.17	11.32	1.50	1.31	0	0.07	98.16	3VG-10-21
42.82	1.34	12.46	0.02	16.28	0.21	10.44	11.44	1.42	1.28	0	0.04	97.94	3VG-10-22
42.96	1.60	12.92	0.01	15.96	0.21	10.22	11.24	1.44	1.26	0	0.06	97.85	3VG-10-23
42.87	1.56	12.71	0.01	16.11	0.21	10.28	11.44	1.49	1.29	0.00	0.06	98.14	Average
0.64	0.13	0.84	0.01	0.23	0.02	0.39	0.19	0.09	0.08	0.00	0.02		Std. Dev.
42.90	1.49	12.74	0.01	16.41	0.23	10.43	11.66	1.49	1.31	0	0.06	98.80	3VG6-1
42.85	1.60	12.75	0.01	16.35	0.22	10.29	11.32	1.52	1.28	0	0.08	98.33	3VG6-2
42.62	1.44	13.02	0.02	16.22	0.22	10.17	11.11	1.47	1.32	0	0.07	97.87	3VG6-3
44.10	1.38	11.30	0.01	15.68	0.20	10.73	11.70	1.34	1.14	0	0.07	97.72	3VG6-4
42.49	1.48	12.86	0.01	15.82	0.20	10.23	11.53	1.47	1.29	0	0.05	97.43	3VG6-5
43.37	1.65	12.61	0.03	16.27	0.22	10.20	11.26	1.59	1.13	0	0.04	98.30	3VG6-6
43.03	1.65	12.75	0.02	16.14	0.21	10.25	10.96	1.48	1.15	0	0.07	98.11	3VG6-7
42.67	1.59	12.90	0.02	16.44	0.22	10.33	11.10	1.42	1.25	0	0.06	97.74	3VG6-8
42.79	1.60	12.76	0.02	15.85	0.22	10.19	11.40	1.48	1.35	0	0.08	97.70	3VG6-9
42.98	1.59	12.62	0	16.34	0.19	10.34	11.59	1.42	1.23	0	0.08	98.31	3VG6-10
43.04	1.83	12.43	0	15.93	0.20	10.54	11.36	1.51	1.22	0	0.06	97.82	3VG6-11
43.12	1.82	12.68	0	16.01	0.19	10.46	11.40	1.37	1.33	0	0.09	98.22	3VG6-12
42.43	1.73	12.08	0	15.86	0.22	10.23	11.40	1.50	1.30	0	0.08	97.52	3VG6-13
42.73	1.42	12.82	0	16.27	0.19	10.20	11.79	1.38	1.30	0	0.08	98.13	3VG6-14
42.88	1.83	12.36	0.02	16.69	0.23	10.42	10.90	1.83	0.97	0	0.07	97.88	3VG6-15
42.80	1.87	12.76	0.01	16.04	0.17	10.28	11.14	1.54	1.27	0	0.08	97.48	3VG6-16
42.82	1.60	12.95	0.02	16.22	0.20	10.30	11.67	1.49	1.33	0	0.08	98.02	3VG6-17
42.81	1.56	12.95	0	16.14	0.22	10.32	11.33	1.59	1.29	0	0.08	98.05	3VG6-18
42.65	1.66	12.87	0.01	16.11	0.24	10.07	11.22	1.60	1.40	0	0.06	97.82	3VG6-19
42.76	1.49	12.63	0	16.10	0.19	10.40	11.58	1.43	1.31	0	0.08	97.92	3VG6-20
42.52	1.49	12.38	0	16.36	0.20	10.19	11.51	1.40	1.30	0	0.08	97.42	3VG6-21
42.84	1.50	13.07	0.03	16.03	0.21	10.33	11.34	1.51	1.27	0	0.07	98.18	3VG6-22
42.46	1.64	12.98	0	16.23	0.22	10.16	11.32	1.47	1.35	0	0.07	97.89	3VG6-23
42.81	1.62	12.83	0.02	15.89	0.18	10.57	11.30	1.51	1.29	0	0.09	97.87	3VG6-24
42.67	1.60	12.70	0	16.51	0.20	10.20	11.56	1.42	1.38	0	0.08	98.42	3VG6-25
42.85	1.56	12.69	0.01	16.16	0.21	10.30	11.36	1.48	1.27	0.00	0.07	97.98	Average
0.38	0.08	0.30	0.01	0.24	0.02	0.16	0.20	0.07	0.09	0.00	0.01		Std. Dev.
43.23	1.44	12.71	0	16.09	0.20	10.03	10.86	1.40	1.42	0	0.07	97.96	3VG5-1
43.38	1.45	12.90	0	16.06	0.19	10.37	10.92	1.46	1.39	0	0.06	98.16	3VG5-2
42.84	1.60	12.84	0	16.37	0.19	10.21	10.97	1.46	1.30	0	0.07	97.70	3VG5-3
43.03	1.31	12.69	0	16.42	0.23	10.16	10.89	1.40	1.32	0	0.06	97.51	3VG5-4
43.12	1.30	12.44	0	16.20	0.22	10.32	11.24	1.43	1.29	0	0.08	97.62	3VG5-5
42.87	1.56	12.86	0	15.87	0.19	10.38	10.80	1.43	1.38	0	0.06	97.46	3VG5-6
42.96	1.58	13.10	0	16.12	0.18	10.25	10.71	1.46	1.27	0	0.06	97.65	3VG5-7
43.27	1.59	12.84	0	16.14	0.16	10.54	10.75	1.46	1.24	0	0.07	98.06	3VG5-8
43.10	1.28	12.37	0	16.20	0.18	10.43	11.13	1.38	1.34	0	0.08	97.42	3VG5-9
43.18	1.28	12.38	0	16.53	0.19	10.33	11.31	1.41	1.32	0	0.08	97.95	3VG5-10
43.23	1.34	12.43	0	16.20	0.17	10.48	11.22	1.39	1.31	0	0.07	97.93	3VG5-11
43.11	1.46	12.60	0	16.09	0.21	10.43	11.28	1.34	1.32	0	0.04	97.87	3VG5-12
43.19	1.43	12.45	0	16.38	0.19	10.33	10.82	1.40	1.28	0	0.06	97.51	3VG5-13
43.21	1.30	12.63	0	16.25	0.19	10.31	11.19	1.44	1.37	0	0.07	97.98	3VG5-14
42.93	1.46	13.13	0.01	16.18	0.19	10.23	10.86	1.44	1.34	0	0.07	97.85	3VG5-15
42.95	1.45	13.04	0	15.87	0.19	10.32	10.84	1.58	1.29	0	0.07	97.58	3VG5-16
43.16	1.40	13.02	0	16.10	0.22	10.22	11.09	1.49	1.29	0	0.07	98.04	3VG5-17
43.11	1.45	13.29	0	15.94	0.19	10.24	10.95	1.50	1.36	0	0.07	98.09	3VG5-18
42.54	1.64	12.28	0	16.10	0.19	10.31	11.24	1.45	1.38	0	0.07	97.16	3VG5-19
42.86	1.56	12.90	0	16.11	0.18	10.26	11.09	1.47	1.32	0	0.05	97.40	3VG5-20
43.12	1.38	12.86	0	16.00	0.15	10.86	10.80	1.44	1.37	0	0.10	97.87	3VG5-21
43.13	1.49	13.11	0.02	16.34	0.22	10.20	10.73	1.45	1.34	0	0.07	98.08	3VG5-22
42.99	1.49	13.06	0.02	16.28	0.21	10.29	10.76	1.46	1.27	0	0.08	97.87	3VG5-23
43.11	1.42	12.90	0.02	16.09	0.19	10.95	11.16	1.51	1.33	0	0.05	98.41	3VG5-24
42.72	1.87	12.82	0	16.54	0.17	10.44	10.87	1.83	1.19	0	0.08	97.83	3VG5-25
42.66	1.74	12.81	0.02	16.71	0.19	10.30	10.87	1.47	1.21	0	0.08	97.74	3VG5-26
43.54	1.85	13.16	0.03	15.36	0.16	10.19	10.87	1.46	1.17	0	0.08	97.88	3VG5-27
42.59	1.54	12.85	0.01	15.81	0.19	10.32	11.07	1.37	1.30	0	0.08	96.79	3VG5-28
43.30	1.48	12.65	0	16.12	0.18	10.54	11.12	1.83	1.34	0	0.07	98.28	3VG5-29
43.07	1.45	12.78	0	15.90	0.21	10.26	10.95	1.39	1.36	0	0.06	97.41	3VG5-30
42.98	1.51	12.80	0.02	15.87	0.24	10.37	10.88	1.47	1.34	0	0.07	97.53	3VG5-31
43.62	1.48	12.72	0	15.83	0.19	10.84	10.88	1.44	1.20	0	0.09	97.88	3VG5-32
42.77	1.35	12.73	0.01	16.20	0.30	10.33	11.21	1.46	1.37	0	0.10	97.71	3VG5-33
42.74	1.51	12.76	0	16.02	0.16	10.18	10.90	1.46	1.28	0	0.09	97.18	3VG5-34
43.35	1.39	12.54	0	15.40	0.18	10.48	11.04	1.37	1.26	0	0.08	97.05	3VG5-35
43.06	1.39	12.71	0.01	15.74	0.17	10.89	10.86	1.43	1.23	0	0.06	97.15	3VG5-36
43.53	1.90	11.58	0.01	15.51	0.15	10.81	11.03	1.41	1.18	0	0.10	97.10	3VG5-37
42.44	1.58	13.07	0.02	15.87	0.13	10.25	10.84	1.42	1.31	0	0.06	96.99	3VG5-38
43.43	1.48	12.86	0	15.19	0.18	10.46	10.89	1.42	1.30	0	0.07	97.31	3VG5-39
43.09	1.74	12.43	0.02	16.03	0.17	10.41	11.06	1.52	1.17	0	0.08	97.73	3VG5-40
43.04	1.63	12.20	0.01	16.11	0.16	10.24	10.86	1.54	1.17	0	0.07	96.82	3VG5-41
43.09	1.56	12.97	0.02	16.13	0.17	10.34	10.89	1.43	1.27	0	0.08	97.71	3VG5-42
43.06	1.49	12.72	0.01	16.08	0.18	10.37	10.96	1.46	1.30	0.00	0.07	97.65	Average

SiO$_2$	TiO$_2$	Al$_2$O$_3$	Cr$_2$O$_3$	FeO	MnO	MgO	CaO	Na$_2$O	K$_2$O	F	Cl	Total	Sample
0.27	0.14	0.32	0.01	0.33	0.02	0.15	0.20	0.05	0.07	0.00	0.01		Std. Dev.
43.22	1.44	12.92	0.01	16.36	0.16	10.37	10.73	1.47	1.31	0	0.06	98.06	3VG4-1
43.14	1.38	12.84	0.01	16.43	0.17	10.59	10.71	1.49	1.28	0	0.06	98.13	3VG4-2
42.73	1.35	12.98	0	16.76	0.19	10.54	10.86	1.37	1.36	0	0.09	98.20	3VG4-3
42.62	1.43	12.93	0.01	16.64	0.21	10.40	10.86	1.41	1.31	0	0.06	97.88	3VG4-4
43.31	1.88	12.62	0.02	16.52	0.16	10.39	10.40	2.31	1.21	0	0.08	98.27	3VG4-5
42.70	1.34	12.83	0.02	16.95	0.19	10.29	11.14	1.69	1.26	0	0.06	97.84	3VG4-6
42.09	1.53	12.74	0.02	16.17	0.15	10.40	10.89	2.39	1.34	0	0.06	97.47	3VG4-7
42.19	1.65	12.81	0.01	16.38	0.17	10.51	10.70	1.82	1.20	0	0.04	97.48	3VG4-8
43.09	1.36	12.87	0.02	16.39	0.19	10.48	10.88	1.61	1.29	0	0.08	98.22	3VG4-9
43.03	1.54	12.78	0.01	16.30	0.17	10.66	10.84	1.90	1.25	0	0.06	98.54	3VG4-10
43.03	1.51	12.17	0.03	16.13	0.20	10.80	10.99	2.02	1.26	0	0.05	97.97	3VG4-11
42.64	1.39	13.02	0	16.38	0.23	10.43	10.68	1.87	1.34	0	0.06	98.02	3VG4-12
42.82	1.39	12.94	0.04	16.29	0.19	10.59	11.08	1.46	1.31	0	0.05	98.12	3VG4-13
42.90	1.33	12.93	0	16.51	0.18	10.49	10.86	1.46	1.37	0	0.07	98.08	3VG4-14
42.70	1.41	12.60	0.02	16.66	0.20	10.61	10.91	1.71	1.36	0	0.06	98.10	3VG4-15
43.32	1.43	13.12	0.01	16.57	0.22	10.80	10.84	1.47	1.34	0	0.06	98.96	3VG4-16
42.99	1.46	12.99	0.02	16.56	0.16	10.40	10.76	1.46	1.30	0	0.06	98.24	3VG4-17
43.16	1.42	13.08	0.03	16.38	0.23	10.36	10.74	1.59	1.33	0	0.07	98.27	3VG4-18
42.94	1.41	13.17	0.01	16.41	0.22	10.40	10.89	1.49	1.32	0	0.05	98.29	3VG4-19
42.76	1.42	13.00	0.02	16.88	0.19	10.49	10.60	1.62	1.32	0	0.05	98.31	3VG4-20
42.92	1.39	12.43	0	16.79	0.21	10.45	10.96	1.41	1.31	0	0.08	97.92	3VG4-21
42.98	1.49	13.17	0	16.32	0.16	10.38	10.86	1.47	1.34	0	0.08	98.23	3VG4-22
44.56	1.20	11.10	0.01	16.18	0.19	11.22	11.41	1.36	1.14	0	0.08	98.41	3VG4-23
43.01	1.51	12.99	0	16.14	0.16	10.02	11.06	1.52	1.40	0	0.07	98.48	3VG4-24
42.98	1.47	13.03	0	16.30	0.21	10.52	10.71	1.40	1.36	0	0.07	98.03	3VG4-25
43.04	1.01	12.81	0	16.81	0.18	10.82	11.07	1.49	1.38	0	0.09	98.46	3VG4-26
43.46	1.29	13.01	0.01	16.19	0.16	10.62	11.02	1.42	1.34	0	0.07	98.98	3VG4-27
43.33	1.51	13.04	0.01	16.25	0.17	10.53	10.72	1.46	1.33	0	0.08	98.41	3VG4-28
42.79	1.45	12.73	0	16.47	0.17	10.47	11.03	1.47	1.42	0	0.09	98.08	3VG4-29
43.26	1.48	12.48	0.02	16.35	0.14	10.78	11.21	1.49	1.35	0	0.06	98.58	3VG4-30
43.66	1.33	12.02	0.01	16.03	0.14	10.68	11.29	1.86	1.19	0	0.05	98.23	3VG4-31
42.91	1.44	12.87	0.02	16.41	0.19	10.38	10.77	1.50	1.33	0	0.08	97.88	3VG4-32
41.86	1.51	13.70	0.03	17.00	0.16	9.92	11.11	1.70	1.20	0	0.10	98.25	3VG4-33
42.94	1.43	12.30	0.01	16.96	0.17	10.87	10.71	1.91	1.29	0	0.05	97.34	3VG4-34
43.64	1.44	12.16	0	16.31	0.17	10.94	10.72	2.10	1.22	0	0.08	98.46	3VG4-35
42.96	1.43	12.77	0.01	16.42	0.16	10.51	10.88	1.64	1.30	0	0.07	98.16	Average
0.48	0.13	0.44	0.01	0.24	0.02	0.19	0.21	0.27	0.06	0	0.01		Std. Dev.
43.68	1.43	12.33	0.04	15.78	0.26	10.60	11.47	1.82	0.19	0	0.10	97.68	3VG22-1
43.04	1.50	13.06	0.02	15.65	0.17	10.46	11.25	2.03	0.20	0	0.06	97.44	3VG22-2
43.33	1.37	12.82	0.04	15.74	0.18	10.52	11.67	1.83	0.21	0	0.11	97.89	3VG22-3
43.12	1.42	13.18	0	15.90	0.19	10.29	11.47	1.42	0.18	0	0.08	97.33	3VG22-4
43.80	1.37	12.67	0.02	15.71	0.17	10.84	11.52	1.73	0.21	0	0.06	97.96	3VG22-5
43.24	1.55	12.84	0	15.61	0.18	10.36	11.58	1.52	0.22	0	0.04	97.31	3VG22-6
43.13	1.57	12.95	0.02	16.31	0.24	10.36	11.33	1.61	0.19	0	0.11	97.79	3VG22-7
42.76	1.47	13.07	0.01	15.99	0.21	10.11	11.41	1.62	0.22	0	0.06	96.94	3VG22-8
41.76	1.45	12.64	0.01	15.89	0.21	10.06	11.17	1.61	0.20	0	0.03	96.02	3VG22-9
42.69	1.50	12.81	0	16.13	0.24	10.14	11.74	1.73	0.18	0	0.11	97.23	3VG22-10
43.17	1.53	13.03	0.03	16.11	0.22	10.14	11.40	1.51	0.16	0	0.09	97.48	3VG22-11
43.04	1.56	13.26	0.02	16.00	0.18	10.32	11.38	1.58	0.20	0	0.03	97.56	3VG22-12
42.86	1.43	13.20	0.03	16.01	0.20	10.17	11.57	1.46	0.20	0	0.06	97.16	3VG22-13
43.12	1.49	12.75	0	16.45	0.16	10.34	11.41	1.56	0.16	0	0.10	97.53	3VG22-14
42.73	1.56	12.76	0.01	16.12	0.20	10.38	11.47	1.96	0.20	0	0.09	97.05	3VG22-15
43.45	1.50	12.88	0.01	15.48	0.17	10.42	10.83	2.07	0.18	0	0.09	97.04	3VG22-16
43.25	1.53	12.57	0.02	16.33	0.17	10.35	11.49	1.65	0.17	0	0.10	97.89	3VG22-17
43.13	1.79	12.49	0	16.05	0.18	10.47	11.73	1.60	0.16	0	0.07	97.67	3VG22-18
42.00	1.54	13.22	0	16.43	0.20	10.22	11.60	1.87	0.21	0	0.09	97.35	3VG22-19
42.83	1.61	13.08	0	15.83	0.21	10.30	11.41	1.77	0.17	0	0.08	97.28	3VG22-20
43.58	1.47	12.31	0	15.84	0.19	10.60	11.78	2.19	0.17	0	0.09	98.17	3VG22-21
43.10	1.37	12.72	0	16.25	0.20	10.45	11.64	1.77	0.22	0	0.11	97.80	3VG22-22
42.72	1.62	12.99	0.01	16.03	0.19	10.83	11.44	1.61	0.19	0	0.08	97.39	3VG22-23
42.80	1.47	13.09	0.01	15.84	0.19	10.16	11.30	2.20	0.16	0	0.08	97.00	3VG22-24
43.16	1.43	13.08	0	16.13	0.19	10.23	11.48	1.72	0.18	0	0.02	97.64	3VG22-25
43.02	1.50	12.87	0.01	15.99	0.20	10.28	11.46	1.71	0.19	0.00	0.08	97.38	Average
0.44	0.09	0.27	0.01	0.26	0.02	0.18	0.20	0.21	0.02	0.00	0.03		Std. Dev.
43.69	1.09	12.91	0	15.27	0.22	10.02	11.23	1.43	1.29	n.a.	n.a.	97.64	3VG19-1
43.56	1.54	13.01	0.02	15.80	0.22	10.13	11.33	1.47	1.40	n.a.	n.a.	98.48	3VG19-2
43.51	1.63	13.15	0.02	16.01	0.23	10.14	11.37	1.42	1.30	n.a.	n.a.	97.76	3VG19-3
43.19	1.59	13.10	0.01	15.30	0.20	10.13	11.09	1.56	1.28	n.a.	n.a.	97.45	3VG19-4
43.78	1.50	12.40	0.03	16.43	0.25	10.06	11.37	1.44	1.35	n.a.	n.a.	97.82	3VG19-5
43.63	1.46	12.83	0.02	15.63	0.23	10.39	11.28	1.48	1.30	n.a.	n.a.	98.23	3VG19-6
43.36	1.60	12.87	0	15.46	0.24	10.41	11.16	1.57	1.28	n.a.	n.a.	97.96	3VG19-7
43.55	1.20	13.66	0.03	15.75	0.26	9.84	11.37	1.61	1.15	n.a.	n.a.	98.44	3VG19-8
43.61	1.46	12.99	0.02	15.73	0.21	10.30	11.25	1.50	1.32	n.a.	n.a.	98.38	3VG19-9
43.64	1.20	12.64	0.02	15.70	0.21	10.42	11.28	1.46	1.27	n.a.	n.a.	98.28	3VG19-10
43.65	1.48	12.86	0	15.49	0.23	10.05	11.16	1.43	1.28	n.a.	n.a.	97.80	3VG19-11
43.62	1.54	13.06	0.01	15.61	0.20	10.14	11.29	1.52	1.32	n.a.	n.a.	98.29	3VG19-12

SiO_2	TiO_2	Al_2O_3	Cr_2O_3	FeO	MnO	MgO	CaO	Na_2O	K_2O	F	Cl	Total	Sample
43.33	1.45	12.43	0	16.10	0.21	9.94	11.40	1.40	1.26	n.a.	n.a.	97.53	3VG19-13
43.62	1.53	12.66	0	15.78	0.19	10.04	11.30	1.44	1.31	n.a.	n.a.	97.87	3VG19-14
43.83	1.46	12.97	0.01	15.27	0.22	10.32	11.20	1.49	1.28	n.a.	n.a.	98.04	3VG19-15
43.09	1.42	13.25	0.02	15.31	0.21	10.08	11.44	1.54	1.31	n.a.	n.a.	97.66	3VG19-16
43.55	1.48	12.92	0.01	15.56	0.22	10.15	11.29	1.49	1.29	n.d.	n.d.	97.95	Average
0.21	0.11	0.31	0.01	0.28	0.02	0.17	0.10	0.06	0.05	n.d.	n.d.		Std. Dev.
42.31	1.45	12.79	0.02	17.06	0.21	9.82	11.77	1.38	0.21	0	0.11	97.11	3VG16-1
42.67	1.52	13.00	0.01	16.39	0.23	10.37	11.66	1.55	0.17	0	0.06	97.62	3VG16-2
43.48	1.38	12.77	0.01	16.01	0.22	10.50	11.56	1.54	0.19	0	0.05	97.69	3VG16-3
43.45	1.56	13.18	0	15.98	0.24	10.34	11.05	1.70	0.15	0	0.06	97.68	3VG16-4
43.25	1.36	13.30	0.01	16.08	0.23	10.26	11.38	1.39	0.16	0	0.11	97.50	3VG16-5
43.95	1.44	12.47	0.02	15.76	0.21	10.64	11.96	1.26	0.16	0	0.05	97.94	3VG16-6
43.02	1.11	12.70	0	16.36	0.18	10.53	11.87	1.50	0.15	0	0.04	97.45	3VG16-7
43.00	1.57	13.08	0	16.21	0.24	10.39	11.47	1.52	0.19	0	0.10	97.75	3VG16-8
42.90	1.58	12.90	0	16.49	0.17	10.15	12.00	1.54	0.19	0	0.09	97.97	3VG16-9
42.97	1.46	13.40	0.02	16.19	0.23	10.20	11.07	1.71	0.21	0	0.09	97.53	3VG16-10
42.67	1.55	13.47	0	16.25	0.20	10.26	11.54	1.47	0.15	0	0.06	97.60	3VG16-11
43.37	1.52	12.93	0	16.10	0.18	10.58	11.46	1.43	0.15	0	0.04	97.74	3VG16-12
42.66	1.56	13.16	0.02	15.94	0.21	10.14	11.39	1.47	0.21	0	0.08	96.81	3VG16-13
42.62	1.42	12.97	0.02	16.22	0.21	10.44	11.19	1.84	0.19	0	0.10	97.20	3VG16-14
42.73	1.59	13.34	0.01	16.12	0.21	10.30	11.22	1.52	0.16	0	0.06	97.25	3VG16-15
42.96	1.52	12.88	0.01	15.74	0.20	10.41	11.69	1.52	0.19	0	0.06	97.16	3VG16-16
43.53	1.36	12.49	0.01	16.38	0.23	10.58	11.74	1.55	0.18	0	0.09	98.12	3VG16-17
43.16	1.61	12.68	0.02	16.22	0.21	10.39	11.63	1.57	0.17	0	0.05	97.69	3VG16-18
43.07	1.57	12.49	0.01	15.75	0.21	10.58	11.74	1.58	0.19	0	0.09	97.26	3VG16-19
43.33	1.63	13.00	0	15.99	0.21	10.33	11.35	1.47	0.16	0	0.07	97.52	3VG16-20
43.05	1.49	12.95	0.01	16.16	0.21	10.36	11.54	1.53	0.18	0	0.07	97.55	Average
0.39	0.12	0.30	0.01	0.30	0.02	0.19	0.28	0.12	0.02	0	0.02		Std. Dev.
43.94	1.77	12.67	0.01	15.45	0.21	10.33	10.53	2.91	0.99	n.a.	n.a.	98.82	3VG15-1
43.09	1.68	13.05	0	15.93	0.22	10.07	10.93	1.76	1.28	n.a.	n.a.	98.02	3VG15-2
43.08	1.50	12.66	0.02	17.03	0.20	10.25	11.18	1.50	1.31	n.a.	n.a.	98.73	3VG15-3
42.93	1.92	12.39	0.02	15.55	0.19	10.32	10.77	2.94	1.15	n.a.	n.a.	98.17	3VG15-4
43.50	1.51	12.97	0.01	16.26	0.19	10.23	10.81	2.60	1.26	n.a.	n.a.	99.32	3VG15-5
43.35	1.60	13.02	0	16.12	0.21	10.22	10.67	2.53	1.23	n.a.	n.a.	98.96	3VG15-6
43.31	1.66	12.80	0.01	16.06	0.20	10.23	10.82	2.37	1.20	n.d.	n.d.	98.67	Average
0.37	0.16	0.26	0.01	0.57	0.01	0.09	0.22	0.60	0.12	n.d.	n.d.		Std. Dev.
42.66	1.99	12.96	0	15.87	0.17	10.36	10.91	2.14	0.16	0	0.05	97.26	3VG20-1
42.96	1.37	13.11	0	15.81	0.18	10.43	11.34	1.77	0.18	0	0.07	97.20	3VG20-2
43.04	1.66	12.79	0.01	15.31	0.13	10.73	11.09	2.10	0.17	0	0.10	97.12	3VG20-3
43.50	1.53	12.40	0	16.20	0.14	10.61	11.81	1.83	0.19	0	0.04	98.24	3VG20-4
43.32	1.32	12.66	0	16.06	0.15	10.51	11.47	1.85	0.19	0	0.09	97.60	3VG20-5
43.07	1.51	13.07	0.03	15.35	0.15	10.56	11.43	1.85	0.16	0	0.08	97.25	3VG20-6
42.77	1.80	13.38	0.03	15.81	0.18	10.33	11.26	1.88	0.14	0	0.05	97.60	3VG20-7
43.39	1.37	12.98	0	15.82	0.18	10.85	11.44	1.99	0.16	0	0.07	98.25	3VG20-8
42.97	1.54	13.23	0.01	15.77	0.20	10.30	11.33	2.02	0.17	0	0.10	97.59	3VG20-9
43.50	1.52	13.22	0.03	15.66	0.16	10.66	11.39	1.97	0.17	0	0.05	98.32	3VG20-10
42.46	1.58	13.18	0	15.62	0.19	10.41	11.41	1.87	0.22	0	0.04	96.97	3VG20-11
42.61	2.04	12.78	0.02	16.03	0.17	10.63	10.92	2.36	0.16	0	0.06	97.76	3VG20-12
43.31	1.54	13.08	0.03	15.83	0.18	10.52	11.29	1.95	0.16	0	0.05	97.95	3VG20-13
43.38	1.48	13.21	0.01	15.84	0.22	10.45	11.33	1.56	0.17	0	0.07	97.70	3VG20-14
42.50	1.92	13.03	0.02	15.78	0.16	10.49	10.87	2.13	0.18	0	0.06	97.12	3VG20-15
42.87	1.93	13.25	0.03	15.80	0.21	10.38	11.04	2.05	0.17	0	0.07	97.77	3VG20-16
42.87	1.97	13.22	0.01	15.72	0.15	10.42	10.92	2.10	0.16	0	0.08	97.60	3VG20-17
43.79	1.12	12.54	0.01	15.97	0.20	10.60	11.67	1.50	0.14	0	0.07	97.58	3VG20-18
43.15	1.53	13.28	0.02	15.80	0.18	10.46	11.52	1.71	0.16	0	0.08	97.87	3VG20-19
43.01	1.43	13.01	0.02	16.13	0.25	10.20	11.47	1.48	0.17	0	0.08	97.22	3VG20-20
42.54	2.04	13.39	0.06	16.27	0.18	10.20	10.51	2.39	0.14	0	0.03	97.74	3VG20-21
43.15	1.54	12.77	0.02	16.45	0.21	10.41	11.65	1.48	0.17	0	0.09	97.92	3VG20-22
43.04	1.62	13.02	0.02	15.86	0.18	10.48	11.28	1.91	0.17	0	0.07	97.63	Average
0.36	0.26	0.27	0.01	0.27	0.03	0.16	0.31	0.26	0.02	0	0.02		Std. Dev.
42.30	1.43	12.89	0	15.89	0.21	10.43	11.21	1.64	0.14	0	0.11	96.23	3VG18-1
42.44	1.59	13.06	0	15.93	0.19	10.57	11.20	1.66	0.13	0	0.06	96.82	3VG18-2
42.23	1.51	12.75	0	15.32	0.19	10.70	11.36	1.74	0.18	0	0.06	96.02	3VG18-3
41.90	1.60	12.39	0	15.46	0.16	10.63	11.65	1.47	0.18	0	0.07	95.48	3VG18-4
41.41	2.03	13.36	0.02	15.54	0.13	10.34	11.31	1.96	0.15	0	0.07	96.31	3VG18-5
42.08	1.62	12.86	0	15.69	0.20	10.41	11.50	1.82	0.15	0	0.08	96.38	3VG18-6
41.10	1.67	12.72	0	15.02	0.18	10.46	11.38	1.73	0.20	0	0.07	94.52	3VG18-7
42.39	1.66	12.64	0.02	15.61	0.14	10.56	11.64	1.73	0.18	0	0.07	96.61	3VG18-8
42.05	1.52	12.38	0.02	15.36	0.16	10.79	11.52	1.55	0.19	0	0.06	95.57	3VG18-9
42.11	1.51	12.72	0.01	15.66	0.17	10.42	11.47	1.82	0.16	0	0.08	96.13	3VG18-10
40.16	3.60	13.62	0	15.14	0.10	10.44	10.24	2.65	0.11	0	0.09	96.13	3VG18-11
42.66	1.65	12.84	0	16.18	0.21	10.17	11.22	1.49	0.13	0	0.09	96.60	3VG18-12
42.93	1.56	13.14	0.01	16.07	0.16	10.40	11.50	1.52	0.14	0	0.08	97.48	3VG18-13
42.23	1.63	12.86	0	16.10	0.18	10.46	11.17	1.54	0.13	0	0.10	96.39	3VG18-14

SiO_2	TiO_2	Al_2O_3	Cr_2O_3	FeO	MnO	MgO	CaO	Na_2O	K_2O	F	Cl	Total	Sample
42.00	1.75	12.87	0.01	15.64	0.17	10.48	11.31	1.74	0.15	0	0.08	96.21	Average
0.70	0.55	0.34	0.01	0.36	0.03	0.15	0.35	0.30	0.03	0	0.02		Std. Dev.
43.11	1.55	13.19	0.05	15.74	0.26	9.74	11.14	1.52	1.27	n.a.	n.a.	97.55	3VG21-1
43.40	1.40	12.51	0.01	16.29	0.19	9.98	11.37	1.55	1.31	n.a.	n.a.	98.01	3VG21-2
43.28	1.42	13.13	0	15.47	0.22	10.06	11.04	1.68	1.30	n.a.	n.a.	97.60	3VG21-3
43.74	1.17	12.52	0.02	15.07	0.23	9.96	12.09	1.70	1.10	n.a.	n.a.	97.59	3VG21-4
43.58	1.68	12.74	0.01	15.47	0.23	9.97	10.98	1.54	1.27	n.a.	n.a.	97.47	3VG21-5
43.10	1.58	12.41	0.03	15.96	0.20	10.23	11.25	1.46	1.28	n.a.	n.a.	97.49	3VG21-6
42.82	1.20	14.14	0	15.28	0.21	9.36	11.13	1.81	1.28	n.a.	n.a.	97.24	3VG21-7
43.22	1.75	12.39	0.03	16.38	0.21	9.94	11.39	1.63	1.35	n.a.	n.a.	98.29	3VG21-8
43.20	1.73	12.56	0	16.17	0.21	9.90	11.23	1.52	1.34	n.a.	n.a.	97.85	3VG21-9
43.38	1.54	12.33	0	15.56	0.17	10.01	11.47	1.45	1.25	n.a.	n.a.	97.13	3VG21-10
43.09	1.42	12.64	0.01	16.15	0.21	9.95	11.06	1.52	1.35	n.a.	n.a.	97.40	3VG21-11
43.26	1.49	12.78	0.02	15.78	0.21	9.92	11.29	1.58	1.28	n.d.	n.d.	97.60	Average
0.25	0.20	0.53	0.02	0.44	0.02	0.22	0.31	0.11	0.07	n.d.	n.d.		Std. Dev.
42.91	1.54	13.07	0.02	15.87	0.19	10.42	11.33	1.47	0.20	0	0.07	97.06	3VG28-1
43.10	1.56	13.25	0.01	16.23	0.18	10.54	11.22	1.55	0.17	0	0.06	97.85	3VG28-2
42.93	1.33	13.00	0	16.37	0.21	10.40	11.32	1.50	0.18	0	0.06	97.29	3VG28-3
43.49	1.52	13.15	0.03	16.04	0.22	10.16	11.37	1.62	0.19	0	0.10	97.86	3VG28-4
43.37	1.37	12.62	0.04	16.05	0.22	10.48	11.34	1.45	0.18	0	0.09	97.20	3VG28-5
43.53	1.60	13.45	0.01	15.91	0.18	10.44	11.20	1.51	0.15	0	0.06	98.01	3VG28-6
42.78	1.12	15.49	0	15.13	0.25	9.37	11.31	1.71	0.10	0	0.09	97.32	3VG28-7
43.01	1.49	12.96	0.01	16.04	0.22	10.34	11.55	1.46	0.23	0	0.06	97.34	3VG28-8
43.02	1.52	13.15	0.01	16.08	0.23	10.34	11.36	1.47	0.16	0	0.11	97.41	3VG28-9
42.70	1.71	12.81	0	15.91	0.22	10.33	11.69	1.48	0.20	0	0.10	96.93	3VG28-10
43.01	1.49	12.45	0.01	16.27	0.21	10.36	11.61	1.50	0.16	0	0.05	97.11	3VG28-11
42.83	1.63	12.69	0	16.07	0.18	10.28	11.89	1.51	0.20	0	0.05	97.32	3VG28-12
42.98	1.44	13.06	0.01	16.14	0.22	10.46	11.31	1.49	0.20	0	0.08	97.37	3VG28-13
42.95	1.17	12.73	0.02	16.12	0.16	10.67	11.81	1.49	0.19	0	0.08	97.36	3VG28-14
42.49	1.51	13.25	0.05	16.06	0.20	10.21	11.81	1.53	0.17	0	0.06	97.32	3VG28-15
42.54	1.53	13.23	0.01	15.95	0.22	10.46	11.58	1.48	0.16	0	0.07	97.21	3VG28-16
42.33	1.59	13.48	0.04	16.04	0.19	10.29	11.56	1.46	0.19	0	0.10	97.27	3VG28-17
42.58	1.49	13.19	0	16.36	0.19	10.49	11.48	1.52	0.22	0	0.07	97.56	3VG28-18
42.92	1.48	13.16	0.01	16.03	0.20	10.33	11.48	1.51	0.18	0	0.06	97.36	Average
0.33	0.15	0.65	0.01	0.27	0.02	0.27	0.21	0.06	0.03	0	0.02		Std. Dev.
43.88	1.17	12.51	0.01	15.94	0.24	10.49	11.44	1.60	1.04	n.a.	n.a.	98.32	3VG29-1
43.25	1.64	13.27	0	15.78	0.23	9.89	11.13	1.58	1.32	n.a.	n.a.	98.08	3VG29-2
43.62	1.38	13.68	0.01	15.11	0.18	10.02	10.98	1.81	1.22	n.a.	n.a.	98.00	3VG29-3
43.12	1.55	13.01	0	15.56	0.21	9.99	11.22	1.51	1.35	n.a.	n.a.	97.53	3VG29-4
42.94	1.72	12.89	0.03	15.65	0.16	10.14	11.40	1.54	1.36	n.a.	n.a.	97.82	3VG29-5
43.19	1.58	12.89	0.04	16.01	0.24	10.07	11.18	1.55	1.27	n.a.	n.a.	98.00	3VG29-6
43.29	1.13	13.53	0	15.57	0.19	10.06	11.18	1.60	1.17	n.a.	n.a.	97.73	3VG29-7
43.26	1.58	13.04	0.01	15.78	0.20	9.95	11.09	1.74	1.29	n.a.	n.a.	97.94	3VG29-8
43.54	1.51	13.14	0	15.50	0.20	9.94	10.92	1.63	1.20	n.a.	n.a.	97.58	3VG29-9
43.55	1.44	13.01	0	15.61	0.20	9.88	11.02	1.64	1.17	n.a.	n.a.	97.52	3VG29-10
43.65	1.44	12.80	0.01	15.80	0.23	10.23	11.34	1.68	1.33	n.a.	n.a.	98.50	3VG29-11
43.55	1.26	12.97	0	15.64	0.25	10.08	10.87	1.53	1.15	n.a.	n.a.	97.29	3VG29-12
43.36	1.55	13.31	0.01	15.59	0.20	9.79	10.95	1.68	1.24	n.a.	n.a.	97.67	3VG29-13
43.62	1.47	13.28	0.02	15.52	0.16	9.85	11.09	1.60	1.21	n.a.	n.a.	97.71	3VG29-14
42.99	1.45	13.06	0.02	15.63	0.21	9.74	11.04	1.57	1.32	n.a.	n.a.	97.03	3VG29-15
43.26	1.50	12.81	0.02	15.26	0.18	10.08	11.30	1.41	1.33	n.a.	n.a.	97.14	3VG29-16
43.08	1.51	12.94	0.02	15.86	0.18	9.84	11.18	1.42	1.35	n.a.	n.a.	97.40	3VG29-17
43.13	1.90	12.43	0.02	15.84	0.22	10.12	11.38	1.45	1.32	n.a.	n.a.	97.82	3VG29-18
43.35	1.49	13.03	0.01	15.65	0.20	10.01	11.15	1.58	1.26	n.d.	n.d.	97.73	Average
0.26	0.18	0.31	0.01	0.22	0.03	0.18	0.17	0.11	0.09	n.d.	n.d.		Std. Dev.
46.60	1.41	8.95	0	13.16	0.10	11.99	14.94	1.78	0.91	0	0.05	99.88	3VG8-1
42.69	1.40	12.50	0	15.80	0.16	10.31	11.31	1.84	1.29	0	0.06	97.36	3VG8-2
42.12	1.59	12.74	0	16.03	0.19	9.88	11.14	1.63	1.27	0	0.06	96.66	3VG8-3
42.56	1.66	12.13	0	15.72	0.18	10.37	11.56	1.53	1.31	0	0.06	97.07	3VG8-4
42.11	1.73	12.60	0.01	16.17	0.18	10.36	11.55	1.55	1.34	0	0.10	97.77	3VG8-5
42.49	1.54	13.04	0.02	15.83	0.19	10.03	11.13	1.71	1.27	0	0.09	97.31	3VG8-6
42.35	1.62	12.63	0.01	15.88	0.18	10.16	11.16	1.66	1.23	0	0.07	96.84	3VG8-7
42.77	1.62	12.95	0	15.63	0.19	10.14	11.17	1.65	1.28	0	0.07	97.44	3VG8-8
42.06	1.56	12.96	0.03	15.47	0.17	9.94	10.81	1.70	1.25	0	0.07	96.03	3VG8-9
43.16	1.73	13.19	0	14.84	0.13	10.93	11.04	2.00	1.19	0	0.08	98.25	3VG8-10
42.81	1.53	12.86	0	15.98	0.19	10.41	11.16	1.73	1.27	0	0.07	98.02	3VG8-11
42.39	1.62	12.90	0.01	15.44	0.20	10.33	11.39	1.66	1.34	0	0.07	97.34	3VG8-12
42.27	1.63	13.35	0	15.51	0.22	10.13	11.16	1.81	1.35	0	0.06	97.48	3VG8-13
42.53	1.44	12.60	0	16.04	0.20	10.25	11.59	1.42	1.28	0	0.03	97.37	3VG8-14
43.00	1.53	12.61	0	15.29	0.15	10.45	11.32	1.77	1.19	0	0.03	97.32	3VG8-15
42.36	1.52	12.65	0.01	15.95	0.19	10.20	11.48	1.48	1.41	0	0.05	97.31	3VG8-16
42.17	1.60	12.72	0	15.54	0.18	10.18	11.13	1.72	1.27	0	0.06	96.55	3VG8-17
42.29	1.61	12.79	0.01	15.57	0.19	10.03	11.44	1.65	1.39	0	0.05	97.00	3VG8-18
42.27	1.72	12.13	0.02	15.91	0.20	10.27	11.72	1.41	1.30	0	0.05	96.97	3VG8-19
42.19	1.64	12.88	0	15.58	0.21	10.00	11.09	1.78	1.32	0	0.04	96.73	3VG8-20

SiO_2	TiO_2	Al_2O_3	Cr_2O_3	FeO	MnO	MgO	CaO	Na_2O	K_2O	F	Cl	Total	Sample
42.48	1.60	12.81	0.01	15.86	0.21	10.18	11.25	1.56	1.27	0	0.08	97.30	3VG8-21
42.14	1.64	12.57	0	15.99	0.24	10.07	11.21	1.42	1.27	0	0.08	96.60	3VG8-22
43.03	1.66	12.69	0	15.26	0.16	10.71	11.65	1.84	1.25	0	0.07	98.20	3VG8-23
42.65	1.59	12.58	0.01	15.58	0.18	10.32	11.45	1.68	1.27	0	0.08	97.36	Average
0.82	0.09	0.84	0.01	0.61	0.03	0.43	0.79	0.15	0.10	0	0.02		Std. Dev.
43.45	1.38	12.95	0.02	16.47	0.22	10.48	11.86	1.59	0.17	0	0.08	98.64	3VG7-1
43.04	1.38	13.00	0	16.15	0.22	10.46	11.56	1.56	0.18	0	0.10	97.62	3VG7-2
43.26	1.66	13.14	0.03	15.97	0.22	10.41	11.50	1.70	0.16	0	0.03	98.08	3VG7-3
43.25	1.47	13.03	0.01	16.20	0.22	10.45	11.64	1.62	0.17	0	0.07	98.13	Average
0.21	0.16	0.10	0.01	0.26	0.00	0.04	0.19	0.08	0.01	0	0.04		Std. Dev.
43.92	1.49	12.66	0.02	16.17	0.21	9.36	11.56	1.61	1.29	n.a.	n.a.	98.30	3VG34-1
43.92	1.56	12.61	0.03	16.53	0.19	9.51	11.56	1.77	1.12	n.a.	n.a.	98.80	3VG34-2
43.85	1.51	12.34	0.01	16.63	0.20	9.58	11.56	1.80	1.20	n.a.	n.a.	98.66	3VG34-3
43.90	1.52	12.54	0.02	16.44	0.20	9.48	11.56	1.73	1.20	n.d.	n.d.	98.58	Average
0.04	0.03	0.17	0.01	0.24	0.01	0.11	0.00	0.10	0.08	n.d.	n.d.		Std. Dev.
41.36	1.90	12.61	0.04	18.32	0.28	8.68	11.67	1.61	1.10	0	0.05	97.52	KAP1-1
42.14	1.92	12.46	0.02	17.79	0.25	9.21	11.56	1.63	1.08	0	0.02	98.09	KAP1-2
40.90	2.03	13.14	0.02	18.68	0.30	8.30	11.57	1.81	1.10	0	0.00	97.83	KAP1-3
41.34	1.88	12.72	0.04	18.35	0.24	8.64	11.69	1.60	1.21	0	0.00	97.70	KAP1-4
41.49	1.96	12.46	0.06	18.37	0.26	8.60	11.69	1.61	1.10	0	0.02	97.63	KAP1-5
41.61	1.73	12.62	0.02	18.21	0.25	8.70	11.52	1.50	1.28	0	0.06	97.68	KAP1-6
41.69	1.98	12.30	0.05	18.39	0.28	8.80	11.53	1.66	1.09	0	0.05	97.81	KAP1-7
41.22	1.91	12.72	0.01	18.42	0.29	8.39	11.65	1.68	1.08	0	0.01	97.36	KAP1-8
41.68	2.06	12.42	0.03	18.72	0.19	8.56	11.57	1.64	1.15	0	0.03	98.04	KAP1-9
41.50	1.79	13.29	0.04	18.05	0.27	8.43	11.74	1.63	1.21	0	0.03	97.96	KAP1-10
41.18	1.93	12.45	0.03	18.34	0.29	8.50	11.88	1.63	1.09	0	0.04	97.42	KAP1-11
41.96	1.94	12.40	0.03	17.83	0.27	9.00	11.86	1.51	1.11	0	0.03	97.91	KAP1-12
41.56	2.17	13.27	0.05	18.25	0.25	8.42	11.80	1.67	1.14	0	0.04	98.60	KAP1-13
41.22	1.82	13.39	0.03	17.66	0.28	8.39	11.72	1.46	1.18	0	0.05	97.17	KAP1-14
41.67	2.03	12.42	0.04	18.32	0.32	8.95	11.64	1.60	1.11	0	0.01	98.12	KAP1-15
41.16	2.03	12.46	0.02	17.67	0.27	8.88	11.52	1.70	1.08	0	0.01	96.79	KAP1-16
41.79	1.95	12.53	0.02	18.22	0.25	8.38	11.69	1.57	1.11	0	0.00	97.51	KAP1-17
41.34	1.88	12.72	0.03	18.78	0.23	8.66	11.75	1.67	1.13	0	0.04	98.22	KAP1-18
41.51	1.98	13.19	0.02	17.79	0.22	8.77	11.83	1.62	1.16	0	0.02	98.09	KAP1-19
41.93	2.06	12.68	0.02	17.78	0.26	9.04	11.78	1.60	1.04	0	0.02	98.23	KAP1-20
41.81	2.30	12.72	0.05	17.50	0.20	8.94	11.86	1.65	1.09	0	0.01	98.18	KAP1-21
42.63	1.86	11.99	0.04	17.19	0.28	9.65	11.73	1.46	1.06	0	0.03	97.89	KAP1-22
41.67	2.02	12.52	0.02	18.53	0.27	8.58	11.56	1.74	1.10	0	0.03	98.02	KAP1-23
40.55	1.83	13.33	0.04	18.96	0.24	8.18	11.80	1.85	1.10	0	0.02	97.89	KAP1-24
41.57	2.08	12.73	0.02	18.64	0.25	8.35	11.83	1.78	1.14	0	0.04	98.39	KAP1-25
41.55	1.96	12.70	0.03	18.19	0.26	8.69	11.68	1.63	1.12	0	0.03	97.85	Average
0.42	0.12	0.36	0.01	0.44	0.03	0.33	0.11	0.09	0.05	0	0.02		Std. Dev.
41.65	1.86	12.78	0.06	18.23	0.22	8.81	11.86	2.79	0.15	0	0.02	98.42	KAP27-1
41.81	1.87	13.11	0.06	17.94	0.27	8.63	11.86	2.98	0.14	0	0.02	98.69	KAP27-2
42.12	1.70	12.65	0.04	18.13	0.28	8.85	11.77	2.96	0.15	0	0.06	98.68	KAP27-3
41.79	1.86	12.85	0.06	18.06	0.26	8.68	11.41	3.29	0.13	0	0.02	98.44	KAP27-4
42.45	1.69	12.61	0.06	17.99	0.26	9.06	11.78	2.23	0.18	0	0.00	98.70	KAP27-5
42.86	1.68	12.57	0.05	16.93	0.29	9.23	11.88	2.52	0.14	0	0.00	98.13	KAP27-6
41.65	2.00	12.93	0.05	18.67	0.28	8.66	11.64	1.75	0.12	0	0.04	97.80	KAP27-7
42.05	1.47	13.65	0.04	18.95	0.31	8.84	11.75	2.01	0.19	0	0.05	99.26	KAP27-8
42.53	1.62	13.22	0.07	17.80	0.27	9.13	11.72	1.61	0.14	0	0.04	98.35	KAP27-9
41.62	1.54	13.88	0.03	19.12	0.23	8.39	11.71	1.72	0.16	0	0.03	98.42	KAP27-10
42.00	1.81	12.88	0.04	17.20	0.30	9.15	11.56	3.31	0.17	0	0.03	98.44	KAP27-11
41.93	1.90	13.23	0.06	18.38	0.22	8.35	11.75	2.54	0.17	0	0.00	98.53	KAP27-12
39.67	1.66	15.46	0.05	18.51	0.19	7.54	12.06	2.58	0.23	0	0.07	97.99	KAP27-13
41.79	2.03	13.04	0.08	18.69	0.24	8.82	11.69	1.99	0.14	0	0.02	98.51	KAP27-14
41.85	1.79	13.22	0.05	18.19	0.26	8.73	11.75	2.45	0.16	0	0.03	98.46	Average
0.73	0.16	0.74	0.01	0.61	0.03	0.43	0.15	0.57	0.03	0	0.02		Std. Dev.
40.95	2.18	13.36	0.05	17.09	0.23	9.62	11.61	1.88	1.19	0	0.04	97.97	KAP3-1
41.64	1.85	12.56	0.04	18.63	0.22	8.89	11.64	1.67	1.15	0	0.02	98.18	KAP3-2
42.15	1.70	12.93	0.03	18.13	0.23	9.06	11.57	1.74	1.03	0	0.04	98.59	KAP3-3
42.14	2.39	12.08	0.05	16.85	0.26	10.37	10.94	2.07	0.83	0	0.03	98.00	KAP3-4
41.50	2.01	12.80	0.04	18.02	0.23	9.09	11.88	1.73	1.10	0	0.04	98.19	KAP3-5
41.62	2.04	12.73	0.04	18.46	0.25	8.86	11.73	1.60	1.09	0	0.03	98.45	KAP3-6
41.66	1.94	12.60	0.04	17.62	0.26	9.44	11.45	1.64	1.07	0	0.01	97.72	KAP3-7
41.81	1.89	12.59	0.02	17.34	0.26	9.70	11.86	1.74	1.03	0	0.03	98.05	KAP3-8
42.97	1.66	11.96	0.04	17.78	0.23	9.27	11.42	1.54	1.05	0	0.01	98.14	KAP3-9
41.74	1.71	13.06	0.03	17.32	0.25	9.65	11.48	1.86	1.13	0	0.03	98.25	KAP3-10
42.36	1.84	12.33	0.03	17.22	0.28	9.65	11.72	1.77	1.02	0	0.03	98.42	KAP3-11
42.21	2.03	12.49	0.02	17.28	0.28	9.59	11.58	1.76	1.09	0	0.03	98.34	KAP3-12
41.51	1.87	12.55	0.04	18.77	0.27	8.72	11.78	1.70	1.09	0	0.01	98.31	KAP3-13
42.03	1.61	12.30	0.03	17.86	0.18	9.35	12.07	1.59	1.02	0	0.02	98.65	KAP3-14

SiO_2	TiO_2	Al_2O_3	Cr_2O_3	FeO	MnO	MgO	CaO	Na_2O	K_2O	F	Cl	Total	Sample
41.85	1.98	12.58	0.03	17.71	0.27	9.38	11.43	1.76	1.10	0	0.01	96.09	KAP3-15
42.06	1.97	12.33	0.02	17.11	0.31	9.78	11.68	1.81	1.05	0	0.01	98.11	KAP3-16
42.07	2.04	12.22	0.04	17.47	0.26	9.76	11.58	1.94	1.00	0	0.01	98.39	KAP3-17
42.08	1.96	12.65	0.03	17.73	0.26	9.11	11.21	1.96	1.12	0	0.04	98.12	KAP3-18
41.80	2.03	12.88	0.04	17.20	0.26	9.93	11.34	1.95	1.13	0	0.02	98.35	KAP3-19
41.21	1.72	13.39	0.01	18.62	0.23	8.66	11.79	1.70	1.08	0	0.04	98.45	KAP3-20
41.97	2.03	12.37	0.06	17.20	0.24	9.75	11.70	1.81	1.11	0	0.04	98.27	KAP3-21
42.50	2.00	12.61	0.05	17.27	0.26	9.56	11.41	1.85	1.03	0	0.02	98.54	KAP3-22
41.80	2.04	12.42	0.03	18.66	0.24	8.89	11.73	1.58	1.10	0	0.02	98.50	KAP3-23
42.11	1.91	12.52	0.04	17.00	0.28	9.98	11.42	1.80	1.05	0	0.01	98.13	KAP3-24
41.92	1.94	12.60	0.03	17.69	0.25	9.41	11.56	1.77	1.07	0	0.02	98.26	Average
0.45	0.16	0.35	0.01	0.61	0.03	0.46	0.22	0.13	0.07	0	0.01		Std. Dev.
41.38	1.97	12.39	0.05	17.25	0.24	9.07	11.27	3.25	1.06	0	0.02	97.93	KAP2-1
41.43	1.98	12.60	0.03	17.79	0.26	8.63	11.62	3.35	1.00	0	0.02	98.67	KAP2-2
41.21	2.02	12.62	0.07	17.78	0.16	9.01	11.66	2.53	1.07	0	0.04	98.18	KAP2-3
41.07	2.04	12.45	0.05	18.23	0.30	8.64	11.43	2.66	1.06	0	0.02	97.93	KAP2-4
40.94	1.96	12.57	0.03	17.89	0.27	8.87	11.40	2.67	1.00	0	0.04	97.63	KAP2-5
41.89	1.86	13.14	0.04	16.87	0.22	8.56	11.41	2.80	1.04	0	0.02	97.86	KAP2-6
40.92	2.95	12.17	0.04	17.36	0.27	9.02	10.95	3.48	0.70	0	0.04	97.89	KAP2-7
40.99	2.11	12.56	0.04	17.27	0.18	8.90	11.61	3.03	1.07	0	0.03	97.78	KAP2-8
40.97	1.58	12.62	0.05	17.66	0.30	9.37	11.58	2.40	1.13	0	0.02	97.68	KAP2-9
41.01	1.91	12.48	0.02	18.43	0.25	8.62	11.63	2.37	1.06	0	0.03	97.82	KAP2-10
40.77	1.97	12.41	0.04	17.36	0.30	8.98	11.54	2.91	1.03	0	0.03	97.34	KAP2-11
41.40	2.39	12.35	0.04	16.69	0.25	9.31	11.20	3.31	0.99	0	0.02	97.94	KAP2-12
41.66	2.00	12.41	0.04	16.70	0.24	9.42	11.48	3.32	0.97	0	0.02	98.25	KAP2-13
40.14	1.64	13.91	0.06	19.04	0.21	8.10	11.80	1.93	1.28	0	0.04	98.13	KAP2-14
40.03	3.22	12.87	0.07	16.93	0.22	8.76	10.92	3.25	0.88	0	0.01	97.14	KAP2-15
40.30	3.33	12.65	0.06	17.17	0.24	9.02	10.63	3.61	0.73	0	0.02	97.74	KAP2-16
38.73	1.88	15.42	0.02	19.62	0.23	7.13	11.51	2.00	1.44	0	0.05	97.71	KAP2-17
41.08	1.91	12.47	0.04	18.71	0.27	8.75	11.66	2.08	1.15	0	0.02	98.12	KAP2-18
41.10	1.97	12.84	0.03	17.66	0.27	8.67	11.70	2.96	1.15	0	0.00	98.34	KAP2-19
40.90	1.65	12.56	0.05	18.16	0.22	9.09	11.53	2.31	1.19	0	0.01	97.66	KAP2-20
42.24	1.91	11.77	0.02	17.09	0.27	9.17	12.12	2.67	0.89	0	0.01	98.16	KAP2-21
40.90	2.07	12.51	0.05	18.23	0.20	8.60	11.61	2.41	1.05	0	0.03	97.64	KAP2-22
40.88	2.11	12.65	0.04	19.06	0.28	8.60	11.60	1.79	1.14	0	0.03	98.16	KAP2-23
41.35	2.33	12.38	0.05	17.11	0.25	8.95	11.82	2.71	1.01	0	0.01	97.96	KAP2-24
40.86	1.92	12.87	0.04	17.39	0.18	8.63	11.82	2.65	1.26	0	0.03	97.65	KAP2-25
40.96	2.09	12.71	0.04	17.74	0.24	8.79	11.50	2.75	1.05	0	0.02	97.90	Average
0.66	0.45	0.68	0.01	0.78	0.04	0.46	0.32	0.51	0.16	0	0.01		Std. Dev.
40.92	2.27	12.94	0.02	18.28	0.37	8.41	11.90	1.51	1.17	0	0.03	97.81	KAP11-1
41.30	2.02	13.36	0.06	18.26	0.29	8.17	11.60	1.63	1.26	0	0.01	97.94	KAP11-2
41.36	1.83	12.27	0.02	18.41	0.24	8.63	11.59	1.60	1.13	0	0.02	97.10	KAP11-3
41.31	1.87	12.84	0.05	18.89	0.31	8.30	11.71	1.77	1.06	0	0.04	98.13	KAP11-4
41.33	1.97	12.79	0.02	18.57	0.23	8.26	11.65	1.66	1.13	0	0.04	97.64	KAP11-5
41.60	1.90	12.36	0.02	18.52	0.30	8.47	11.58	1.60	1.10	0	0.05	97.50	KAP11-6
41.91	1.24	12.89	0	18.51	0.12	8.21	11.98	1.19	1.36	0	0.05	97.44	KAP11-7
41.67	1.36	13.03	0	18.23	0.18	8.20	12.21	1.26	1.24	0	0.02	97.40	KAP11-8
41.77	2.31	12.47	0.06	17.74	0.21	8.69	11.66	1.64	1.18	0	0.04	97.76	KAP11-9
41.84	2.34	12.39	0.04	17.83	0.20	8.85	11.92	1.65	1.19	0	0	98.24	KAP11-10
41.01	1.99	12.63	0.01	18.52	0.22	8.34	11.84	1.71	1.08	0	0.01	97.36	KAP11-11
41.40	2.16	12.60	0.02	17.90	0.28	8.85	11.67	1.65	1.13	0	0.01	97.63	KAP11-12
41.43	1.94	12.54	0.02	18.50	0.27	8.57	11.67	1.74	1.16	0	0.03	97.84	KAP11-13
41.34	1.96	12.63	0.02	18.56	0.28	8.52	11.75	1.65	1.09	0	0.02	97.81	KAP11-14
41.41	2.05	13.28	0.03	18.29	0.27	8.21	11.75	1.60	1.23	0	0.03	98.15	KAP11-15
41.70	1.80	12.67	0.02	18.97	0.21	8.32	11.73	1.79	1.08	0	0.01	98.30	KAP11-16
41.77	1.77	12.89	0.03	17.97	0.27	8.80	11.67	1.65	1.14	0	0.01	97.95	KAP11-17
41.56	1.97	12.58	0.04	18.48	0.21	8.51	11.52	1.76	1.07	0	0.03	97.72	KAP11-18
41.42	1.65	12.92	0.05	18.22	0.23	8.74	11.98	1.56	1.19	0	0	97.97	KAP11-19
41.73	1.80	12.47	0.04	17.55	0.27	9.03	11.71	1.60	1.07	0	0.04	97.31	KAP11-20
42.40	1.96	12.65	0.02	16.73	0.27	9.16	11.74	1.58	1.11	0	0.03	97.64	KAP11-21
41.66	2.27	12.49	0.07	17.60	0.20	8.66	11.71	1.52	1.14	0	0.03	97.34	KAP11-22
40.92	1.76	12.28	0.04	18.31	0.25	8.47	11.70	1.49	1.10	0	0.03	96.33	KAP11-23
41.66	1.65	12.64	0.04	18.41	0.29	8.73	11.55	1.67	1.11	0	0.02	97.98	KAP11-24
41.29	1.36	14.31	0.05	18.56	0.21	8.09	11.75	1.44	1.32	0	0.02	98.41	KAP11-25
41.51	1.90	12.76	0.03	18.23	0.25	8.53	11.74	1.60	1.15	0	0.02	97.71	Average
0.33	0.28	0.43	0.02	0.48	0.06	0.28	0.16	0.14	0.08	0	0.01		Std. Dev.
40.99	2.10	12.95	0.07	18.33	0.26	8.27	11.55	1.66	1.09	0	0.02	97.28	KAP10-1
40.69	1.77	12.71	0.02	19.06	0.22	8.19	11.69	1.64	1.09	0	0.02	97.09	KAP10-2
41.43	1.74	12.18	0.02	18.11	0.29	8.72	11.48	1.64	1.01	0	0.05	96.65	KAP10-3
41.10	2.02	11.99	0.05	19.38	0.23	8.50	11.76	1.61	1.19	0	0.01	97.82	KAP10-4
40.96	1.97	12.59	0.04	18.81	0.23	8.34	11.72	1.70	1.07	0	0.03	97.46	KAP10-5
41.67	1.39	12.42	0.01	18.17	0.26	8.89	11.60	1.56	1.04	0	0.04	97.05	KAP10-6
41.31	1.84	12.30	0.04	18.07	0.31	8.65	11.51	1.64	1.02	0	0.02	96.89	KAP10-7
40.83	1.99	12.11	0.03	18.45	0.29	8.62	11.59	1.68	1.11	0	0.03	96.71	KAP10-8
41.07	1.79	12.18	0	18.37	0.20	8.74	11.80	1.61	1.17	0	0.04	96.95	KAP10-9
40.98	1.89	12.81	0.05	17.67	0.25	8.88	11.54	1.67	1.07	0	0.05	96.84	KAP10-10

SiO_2	TiO_2	Al_2O_3	Cr_2O_3	FeO	MnO	MgO	CaO	Na_2O	K_2O	F	Cl	Total	Sample
41.73	1.85	12.80	0.05	18.38	0.23	8.60	11.53	1.61	1.06	0	0.02	97.87	KAP10-11
41.64	1.80	12.22	0.04	17.77	0.27	8.93	11.67	1.84	1.12	0	0.00	97.11	KAP10-12
41.27	1.88	12.19	0.02	18.41	0.27	9.10	11.73	1.83	1.10	0	0.06	97.81	KAP10-13
41.24	1.53	12.39	0.03	18.70	0.29	9.00	11.57	1.69	1.11	0	0.03	97.57	KAP10-14
41.19	1.56	11.92	0.03	18.54	0.23	8.70	12.05	1.46	1.23	0	0.02	96.91	KAP10-15
40.67	1.96	12.40	0.04	18.18	0.29	8.65	11.72	1.68	1.09	0	0.05	96.70	KAP10-16
43.17	1.43	10.72	0.03	17.56	0.23	9.76	12.14	1.28	0.92	0	0.02	97.24	KAP10-17
41.10	2.00	12.67	0.06	18.28	0.26	8.84	11.65	1.56	1.05	0	0.03	97.49	KAP10-18
40.86	1.84	12.31	0.03	18.77	0.20	8.66	11.54	1.65	1.12	0	0.04	97.00	KAP10-19
41.42	1.99	12.32	0.04	18.22	0.27	8.64	11.74	1.86	1.14	0	0.02	97.45	KAP10-20
40.27	2.02	14.14	0.03	17.87	0.21	8.04	11.56	1.57	1.19	0	0.03	96.93	KAP10-21
40.84	2.05	12.48	0.03	18.36	0.24	8.68	11.57	1.65	1.07	0	0.01	96.96	KAP10-22
41.20	1.84	12.40	0.03	18.34	0.25	8.71	11.67	1.61	1.09	0	0.03	97.17	Average
0.56	0.20	0.59	0.02	0.44	0.03	0.35	0.17	0.09	0.07	0	0.01		Std. Dev.
42.18	1.60	8.85	0.04	18.76	0.19	13.01	11.21	1.61	1.19	0	0.04	98.67	KAP6-1
44.73	1.43	10.66	0.03	16.22	0.26	11.12	11.58	1.33	0.82	0	0.03	98.19	KAP6-2
42.22	1.70	8.74	0.04	18.61	0.22	12.94	11.22	1.80	1.17	0	0.01	98.67	KAP6-3
42.40	1.96	9.22	0.06	18.01	0.22	12.50	11.29	1.64	1.09	0	0.01	98.39	KAP6-4
42.22	1.94	9.36	0.04	17.93	0.25	12.57	11.49	1.69	1.12	0	0.03	98.63	KAP6-5
42.10	1.86	8.88	0.04	18.56	0.21	12.93	11.12	1.73	1.15	0	0.02	98.57	KAP6-6
42.80	1.80	9.25	0.05	16.04	0.24	12.03	11.42	1.71	0.95	0	0.02	98.32	KAP6-7
42.67	1.79	9.24	0.05	17.99	0.24	12.70	11.16	1.69	1.06	0	0.02	98.61	KAP6-8
42.14	1.93	8.70	0.03	18.65	0.26	12.56	11.25	1.66	1.10	0	0.03	98.30	KAP6-9
42.35	1.94	8.96	0.04	18.66	0.28	12.63	10.90	1.72	1.12	0	0.03	98.62	KAP6-10
41.12	1.83	8.11	0.06	18.95	0.21	14.56	11.14	1.65	1.42	0	0.04	99.06	KAP6-11
41.98	1.91	8.82	0.04	18.27	0.21	12.92	11.16	1.62	1.22	0	0.02	98.16	KAP6-12
42.10	1.80	9.07	0.04	18.72	0.24	12.85	11.29	1.66	1.11	0	0.02	98.86	KAP6-13
42.38	1.81	9.15	0.04	18.53	0.25	12.81	11.14	1.75	1.06	0	0.02	98.96	KAP6-14
42.23	1.70	9.01	0.04	18.41	0.21	12.62	11.43	1.57	1.12	0	0.02	98.35	KAP6-15
42.53	1.61	8.91	0.05	18.60	0.21	12.69	11.37	1.69	1.09	0	0.03	98.76	KAP6-16
42.75	1.68	9.07	0.03	18.41	0.22	12.63	11.12	1.69	1.10	0	0.01	98.69	KAP6-17
42.90	1.75	9.10	0.03	18.56	0.19	12.52	10.77	1.66	0.99	0	0.04	98.50	KAP6-18
42.01	1.62	8.92	0.04	18.90	0.18	12.82	11.23	1.65	1.15	0	0.02	98.54	KAP6-19
42.59	1.82	9.31	0.03	18.49	0.24	12.24	10.67	1.78	1.00	0	0.03	98.19	KAP6-20
43.21	1.86	9.31	0.05	18.20	0.24	11.99	11.16	1.65	1.05	0	0.02	98.53	KAP6-21
42.86	1.72	9.07	0.07	17.51	0.23	12.55	11.73	1.54	1.03	0	0.03	98.33	KAP6-22
42.58	1.66	9.28	0.08	17.97	0.26	12.40	10.99	1.62	1.03	0	0.01	97.88	KAP6-23
42.76	1.59	9.34	0.06	17.79	0.22	12.38	10.85	1.64	0.94	0	0.03	97.59	KAP6-24
42.69	2.00	9.16	0.06	18.49	0.26	12.14	10.43	1.86	0.95	0	0.04	98.07	KAP6-25
43.61	1.91	9.33	0.09	18.28	0.27	11.44	10.80	1.71	0.83	0	0.03	98.29	KAP6-26
41.95	1.85	8.42	0.07	18.92	0.23	12.82	11.09	1.70	1.11	0	0.03	98.18	KAP6-27
41.68	1.77	8.23	0.07	19.15	0.21	12.67	11.08	1.67	1.18	0	0.04	97.73	KAP6-28
41.99	1.81	8.39	0.07	19.00	0.20	12.74	11.14	1.84	1.14	0	0.03	98.15	KAP6-29
41.85	1.88	8.73	0.09	19.08	0.23	12.26	11.26	1.72	1.06	0	0.03	98.22	KAP6-30
42.23	1.53	8.56	0.05	18.80	0.24	12.98	11.11	1.57	1.10	0	0.02	98.17	KAP6-31
40.73	2.23	8.17	0.06	18.29	0.23	13.83	11.20	1.73	1.28	0	0.04	97.76	KAP6-32
40.72	2.13	8.30	0.12	18.57	0.22	13.84	11.21	1.76	1.26	0	0.03	98.16	KAP6-33
42.24	1.69	8.90	0.08	18.28	0.20	12.87	11.13	1.67	1.09	0	0.04	98.19	KAP6-34
42.20	1.71	8.73	0.06	18.37	0.23	12.96	11.13	1.65	1.20	0	0.02	98.25	KAP6-35
42.07	1.67	8.67	0.08	18:46	0.20	12.90	11.08	1.56	1.18	0	0.04	97.89	KAP6-36
42.13	1.73	8.89	0.06	18.15	0.22	12.46	11.27	1.71	1.02	0	0.03	97.66	KAP6-37
42.51	1.82	9.13	0.07	18.13	0.21	12.34	10.73	1.78	0.98	0	0.04	97.72	KAP6-38
43.40	1.74	9.40	0.05	17.51	0.25	12.51	10.86	1.84	0.93	0	0.03	98.52	KAP6-39
43.67	1.56	9.73	0.12	16.31	0.29	12.61	11.40	1.41	1.01	0	0.01	98.09	KAP6-40
41.56	1.96	8.68	0.07	17.69	0.21	13.42	11.06	1.71	1.12	0	0.04	97.40	KAP6-41
42.15	1.64	9.18	0.04	18.30	0.22	11.95	11.24	1.58	1.07	0	0.02	97.38	KAP6-42
42.48	1.81	9.01	0.06	18.04	0.22	12.90	11.05	1.66	1.06	0	0.03	98.31	KAP6-43
42.66	1.85	9.07	0.06	17.97	0.22	12.80	10.90	1.82	1.16	0	0.03	98.52	KAP6-44
43.02	1.65	9.19	0.04	17.70	0.27	13.05	11.00	1.72	1.07	0	0.02	98.73	KAP6-45
42.20	1.94	8.78	0.05	18.07	0.23	12.65	10.69	1.74	1.10	0	0.02	97.47	KAP6-46
42.47	1.76	9.23	0.05	18.15	0.22	12.41	11.24	1.71	1.02	0	0.02	98.27	KAP6-47
42.51	1.50	9.13	0.04	17.73	0.27	13.00	11.28	1.65	1.10	0	0.01	98.20	KAP6-48
42.34	1.78	8.93	0.08	17.76	0.24	12.85	11.15	1.74	1.06	0	0.03	97.94	KAP6-49
41.77	1.76	8.85	0.06	18.09	0.22	12.92	11.37	1.81	1.09	0	0.00	97.94	KAP6-50
42.02	1.77	8.95	0.05	18.08	0.26	12.70	11.23	1.73	1.08	0	0.01	97.89	KAP6-51
43.21	1.72	9.54	0.03	17.32	0.24	12.14	11.08	1.72	1.08	0	0.01	98.09	KAP6-52
40.64	1.96	8.27	0.05	18.25	0.22	13.79	11.34	1.79	1.13	0	0.01	97.46	KAP6-53
43.23	1.60	9.04	0.05	17.99	0.27	12.28	11.09	1.72	1.00	0	0.01	98.28	KAP6-54
42.58	1.77	9.03	0.06	17.87	0.22	12.78	11.10	1.80	1.12	0	0.04	98.37	KAP6-55
42.37	1.77	8.98	0.06	18.21	0.23	12.69	11.13	1.68	1.08	0	0.02	98.24	Average
0.71	0.15	0.42	0.02	0.57	0.02	0.55	0.23	0.09	0.10	0	0.01		Std. Dev.
41.41	1.53	8.30	0.04	18.81	0.22	13.55	11.43	1.68	1.27	0	0.04	98.27	KAP5-1
39.84	1.27	7.64	0.02	18.52	0.23	15.95	11.45	1.61	1.67	0	0.03	98.21	KAP5-2
40.14	1.29	7.94	0.05	18.56	0.19	15.19	11.05	1.59	1.53	0	0.04	97.55	KAP5-3
43.03	1.50	9.40	0.06	17.89	0.21	12.11	11.47	1.57	1.08	0	0.04	98.34	KAP5-4
41.37	1.85	8.64	0.09	18.54	0.14	13.87	11.31	1.73	1.25	0	0.02	98.81	KAP5-5
41.94	1.86	8.74	0.04	18.45	0.19	12.63	11.07	1.72	1.16	0	0.04	97.84	KAP5-6
41.95	1.93	8.80	0.08	18.94	0.20	12.84	11.02	1.74	1.15	0	0.04	98.46	KAP5-7

SiO_2	TiO_2	Al_2O_3	Cr_2O_3	FeO	MnO	MgO	CaO	Na_2O	K_2O	F	Cl	Total	Sample
41.90	1.90	8.76	0.09	18.65	0.24	12.58	11.04	1.81	1.11	0	0.04	98.11	KAP5-8
42.57	1.61	9.08	0.08	18.35	0.18	12.15	11.50	1.50	1.24	0	0.04	98.28	KAP5-9
42.12	1.60	8.98	0.07	18.60	0.18	13.07	11.10	1.75	1.17	0	0.04	98.68	KAP5-10
41.70	1.89	9.20	0.05	17.89	0.14	13.42	10.88	1.80	1.12	0	0.03	98.11	KAP5-11
42.17	1.50	8.72	0.04	17.92	0.16	13.38	11.54	1.61	1.29	0	0.04	98.26	KAP5-12
42.23	1.56	8.71	0.07	18.38	0.18	13.52	11.51	1.40	1.26	0	0.04	98.91	KAP5-13
42.34	1.71	9.03	0.09	18.09	0.17	12.81	11.37	1.64	1.16	0	0.04	98.44	KAP5-14
42.19	1.80	9.33	0.06	18.44	0.24	12.38	11.26	1.67	1.14	0	0.05	98.51	KAP5-15
42.17	1.95	8.77	0.17	17.83	0.19	13.53	11.29	1.61	1.29	0	0.04	98.62	KAP5-16
42.58	1.73	9.18	0.05	18.42	0.20	12.48	11.14	1.83	1.08	0	0.04	98.69	KAP5-17
42.54	1.70	9.21	0.08	18.38	0.23	12.45	11.16	1.74	1.04	0	0.04	98.53	KAP5-18
41.92	1.74	8.71	0.06	18.82	0.24	12.99	11.37	1.69	1.15	0	0.03	98.72	KAP5-19
42.02	1.65	8.67	0.08	18.28	0.24	13.02	11.25	1.72	1.16	0	0.05	98.30	KAP5-20
42.56	1.73	9.50	0.03	17.48	0.22	13.17	11.16	1.71	1.07	0	0.03	98.62	KAP5-21
40.48	1.06	7.57	0.01	19.26	0.19	15.60	11.41	1.52	1.59	0	0.05	98.73	KAP5-22
40.06	1.03	7.65	0.05	19.65	0.20	15.10	11.29	1.53	1.53	0	0.04	98.70	KAP5-23
41.47	1.35	8.56	0.03	18.69	0.18	14.05	11.42	1.56	1.28	0	0.03	98.62	KAP5-24
42.64	1.92	9.49	0.05	16.90	0.27	12.74	11.39	1.57	1.11	0	0.02	98.07	KAP5-25
41.73	1.94	9.32	0.06	17.75	0.21	13.07	10.92	1.86	1.07	0	0.02	97.94	KAP5-26
42.99	1.70	9.66	0.08	17.54	0.27	12.80	11.18	1.62	1.12	0	0.00	98.74	KAP5-27
41.73	1.64	9.38	0.06	18.17	0.28	12.91	11.12	1.62	1.09	0	0.01	97.98	KAP5-28
41.98	1.69	9.17	0.05	18.13	0.28	12.71	11.07	1.70	1.07	0	0.01	97.86	KAP5-29
42.02	1.51	9.47	0.04	18.39	0.22	12.44	11.16	1.72	0.89	0	0.00	97.86	KAP5-30
41.89	1.88	9.34	0.04	18.14	0.25	12.98	11.28	1.76	1.13	0	0.01	98.35	KAP5-31
42.63	1.50	9.33	0.05	17.94	0.25	12.61	11.22	1.56	1.06	0	0.02	98.23	KAP5-32
41.92	1.81	9.09	0.01	17.80	0.27	13.30	11.42	1.60	1.12	0	0.00	98.34	KAP5-33
41.41	1.50	8.72	0.06	18.44	0.22	13.14	11.15	1.74	1.19	0	0.00	97.57	KAP5-34
41.57	1.66	8.58	0.07	18.79	0.23	13.08	11.07	1.71	1.18	0	0.01	97.94	KAP5-35
40.44	1.65	8.78	0.02	18.26	0.21	14.50	11.02	1.80	1.33	0	0.01	98.00	KAP5-36
42.73	1.62	9.42	0.05	18.33	0.22	11.74	11.13	1.68	1.08	0	0.03	98.03	KAP5-37
41.53	1.74	9.11	0.05	18.05	0.25	13.17	11.22	1.75	1.13	0	0.00	98.00	KAP5-38
39.90	1.08	8.28	0.00	18.77	0.13	15.42	11.35	1.43	1.67	0	0.02	98.05	KAP5-39
41.69	2.04	8.96	0.06	18.22	0.22	12.98	11.17	1.79	1.13	0	0.01	98.27	KAP5-40
42.17	1.74	9.30	0.07	18.14	0.32	12.63	11.21	1.73	1.00	0	0.02	98.42	KAP5-41
41.81	1.65	8.86	0.06	18.30	0.22	13.26	11.23	1.67	1.20	0	0.03	98.30	Average
0.79	0.25	0.52	0.03	0.50	0.04	0.96	0.17	0.10	0.17	0	0.01		Std. Dev.
41.19	1.60	8.31	0.06	18.20	0.19	13.49	11.15	2.45	1.30	0	0.02	97.94	KAP4-1
41.18	1.81	8.60	0.06	18.57	0.25	13.16	11.09	2.32	1.11	0	0.01	98.14	KAP4-2
41.77	1.40	8.93	0.02	17.76	0.22	12.58	11.05	2.88	1.14	0	0.02	97.57	KAP4-3
42.11	1.52	8.85	0.05	18.05	0.24	12.94	11.14	2.21	1.06	0	0.02	98.19	KAP4-4
41.62	1.48	8.49	0.07	18.66	0.16	13.62	11.25	1.68	1.19	0	0.02	98.23	KAP4-5
42.18	1.64	8.97	0.08	18.23	0.26	12.87	11.24	1.75	1.12	0	0.01	98.35	KAP4-6
41.74	1.08	8.73	0.08	18.50	0.20	12.72	11.32	2.33	1.15	0	0.02	98.46	KAP4-7
41.66	1.71	8.89	0.07	18.96	0.20	12.80	11.00	1.85	1.19	0	0.00	98.32	KAP4-8
41.60	1.70	8.93	0.07	18.79	0.15	12.65	11.03	1.84	1.16	0	0.01	97.92	KAP4-9
41.55	1.39	8.71	0.06	18.36	0.16	12.69	11.31	2.45	1.15	0	0.02	98.05	KAP4-10
40.94	1.28	7.97	0.05	18.90	0.20	13.91	11.09	2.04	1.31	0	0.03	97.81	KAP4-11
41.41	1.75	8.79	0.04	18.46	0.25	12.64	11.05	2.43	1.10	0	0.03	97.94	KAP4-12
41.18	1.91	8.68	0.05	18.60	0.24	13.00	11.26	1.82	1.21	0	0.02	97.97	KAP4-13
41.32	1.95	8.75	0.08	18.76	0.23	12.87	11.15	1.75	1.21	0	0.03	98.00	KAP4-14
41.40	1.94	8.74	0.07	18.43	0.24	12.87	11.00	1.99	1.19	0	0.02	97.88	KAP4-15
41.90	1.98	8.86	0.04	18.47	0.24	12.31	11.03	1.68	1.28	0	0.02	97.79	KAP4-16
41.73	1.83	9.03	0.03	18.13	0.22	12.32	10.74	2.16	1.23	0	0.04	97.43	KAP4-17
41.97	1.74	8.64	0.06	19.57	0.21	12.59	11.03	1.73	1.13	0	0.02	98.69	KAP4-18
41.49	1.79	8.44	0.05	18.97	0.19	12.54	11.10	2.16	1.10	0	0.03	97.84	KAP4-19
41.21	1.66	8.40	0.08	18.50	0.23	13.23	10.90	2.09	1.13	0	0.03	97.61	KAP4-20
41.97	1.67	8.82	0.07	18.01	0.23	12.56	10.77	2.30	1.07	0	0.00	97.46	KAP4-21
41.31	1.87	8.44	0.04	18.33	0.24	13.27	11.09	1.97	1.17	0	0.02	97.75	KAP4-22
41.50	2.12	8.63	0.06	18.42	0.22	12.90	10.38	2.68	0.98	0	0.03	97.91	KAP4-23
41.41	2.16	8.91	0.03	17.92	0.21	12.92	10.43	2.30	0.97	0	0.02	97.27	KAP4-24
41.94	1.58	9.20	0.04	17.83	0.15	12.38	11.07	1.40	1.19	0	0.02	96.82	KAP4-25
41.84	1.74	9.25	0.05	18.10	0.28	12.48	10.98	1.62	1.06	0	0.02	97.32	KAP4-26
39.92	1.26	7.36	0.07	18.09	0.22	15.10	11.08	2.24	1.38	0	0.03	96.77	KAP4-27
41.27	1.86	8.04	0.05	18.21	0.25	12.56	10.72	2.51	1.10	0	0.02	96.58	KAP4-28
40.02	2.01	7.71	0.08	18.14	0.27	13.07	9.82	2.84	0.84	0	0.03	96.73	KAP4-29
40.95	2.12	8.26	0.09	18.06	0.23	12.47	10.63	2.52	1.03	0	0.04	96.60	KAP4-30
40.67	2.33	7.98	0.07	18.27	0.25	12.42	9.91	2.90	0.92	0	0.06	95.83	KAP4-31
42.66	1.78	8.75	0.07	16.99	0.23	11.54	10.74	2.56	1.13	0	0.02	96.47	KAP4-32
41.48	1.64	8.69	0.07	17.64	0.27	12.16	10.41	2.60	1.03	0	0.02	95.96	KAP4-33
41.56	1.65	8.15	0.06	17.92	0.21	12.51	10.36	2.71	1.08	0	0.02	96.21	KAP4-34
41.85	1.73	8.49	0.05	18.13	0.22	11.94	10.44	2.82	1.05	0	0.00	96.53	KAP4-35
41.67	1.51	8.51	0.11	17.90	0.24	12.83	11.24	1.63	1.14	0	0.03	96.80	KAP4-36
40.08	2.23	7.81	0.08	18.27	0.22	13.84	10.80	2.46	1.15	0	0.04	96.77	KAP4-37
40.51	1.67	8.04	0.08	17.32	0.22	12.59	10.61	2.20	1.12	0	0.03	94.36	KAP4-38
41.66	1.60	8.17	0.09	16.59	0.20	13.42	10.97	2.27	1.09	0	0.03	96.08	KAP4-39
41.74	1.84	7.68	0.06	17.29	0.23	13.59	10.44	2.50	0.98	0	0.02	96.44	KAP4-40
41.09	1.82	8.12	0.05	17.95	0.25	12.71	10.93	2.39	1.22	0	0.01	96.54	KAP4-41
41.26	1.53	8.17	0.05	17.76	0.22	12.82	10.94	2.45	1.20	0	0.03	96.46	KAP4-42
41.13	1.62	8.00	0.10	18.08	0.20	13.29	10.79	2.29	1.45	0	0.04	96.96	KAP4-43

SiO_2	TiO_2	Al_2O_3	Cr_2O_3	FeO	MnO	MgO	CaO	Na_2O	K_2O	F	Cl	Total	Sample
41.41	1.77	8.48	0.06	18.21	0.22	12.86	10.86	2.22	1.13	0	0.02	97.28	Average
0.56	0.29	0.43	0.02	0.56	0.03	0.59	0.35	0.38	0.11	0	0.01		Std. Dev.
41.20	2.31	13.11	0.02	18.56	0.25	8.71	11.78	1.91	0.16	0	0.01	98.01	KAP22-1
42.44	1.44	13.32	0.05	17.56	0.24	9.19	11.83	1.90	0.15	0	0.04	97.73	KAP22-2
41.69	1.75	12.75	0.06	18.40	0.27	8.82	11.77	1.81	0.14	0	0.07	97.50	KAP22-3
39.82	1.16	16.67	0.00	17.46	0.22	8.54	11.50	1.88	0.20	0	0.04	97.50	KAP22-4
41.90	1.84	12.80	0.04	17.81	0.25	9.28	11.60	1.85	0.15	0	0.03	97.84	KAP22-5
40.27	3.30	14.28	0.07	18.02	0.23	9.53	9.99	2.44	0.10	0	0.02	98.24	KAP22-6
41.98	1.65	12.11	0.05	18.49	0.18	9.13	11.92	1.75	0.18	0	0.01	97.44	KAP22-7
40.52	2.68	14.40	0.03	18.02	0.21	9.30	10.46	2.41	0.14	0	0.04	98.19	KAP22-8
41.62	1.80	12.85	0.00	18.28	0.25	9.08	11.46	1.96	0.13	0	0.00	97.50	KAP22-9
41.20	2.07	13.25	0.05	17.97	0.29	9.09	11.68	1.94	0.16	0	0.02	97.70	KAP22-10
41.32	2.10	13.23	0.04	17.32	0.20	9.38	11.37	1.97	0.14	0	0.00	97.08	KAP22-11
39.92	3.17	13.83	0.08	17.91	0.26	8.88	10.42	2.37	0.11	0	0.00	96.95	KAP22-12
41.99	2.17	12.53	0.02	17.00	0.17	9.89	11.50	1.95	0.12	0	0.02	97.36	KAP22-13
40.43	3.17	13.98	0.04	17.27	0.25	10.04	10.35	2.44	0.12	0	0.09	98.14	KAP22-14
41.64	1.91	12.78	0.04	17.72	0.19	9.20	11.68	1.96	0.17	0	0.01	97.28	KAP22-15
40.97	2.47	13.22	0.06	17.19	0.22	9.57	10.98	2.22	0.12	0	0.02	97.01	KAP22-16
41.59	1.81	12.75	0.06	18.16	0.28	9.17	11.57	1.83	0.12	0	0.05	97.39	KAP22-17
41.37	1.82	12.98	0.06	18.76	0.23	8.72	11.60	1.98	0.16	0	0.01	97.09	KAP22-18
41.25	1.78	12.75	0.02	18.52	0.26	8.97	11.60	1.82	0.18	0	0.00	97.15	KAP22-19
41.22	2.13	13.30	0.05	17.92	0.23	9.18	11.32	1.98	0.14	0	0.03	97.53	Average
0.73	0.59	1.01	0.02	0.82	0.03	0.39	0.58	0.27	0.03	0	0.02		Std. Dev.
42.64	1.90	12.69	0.04	18.43	0.22	8.77	11.58	1.66	1.13	n.a.	n.a.	99.07	KAP19-1
42.43	1.75	13.16	0.04	17.94	0.21	8.67	11.43	1.68	1.09	n.a.	n.a.	98.37	KAP19-2
41.41	1.76	13.55	0.04	18.19	0.23	8.16	11.55	1.73	1.41	n.a.	n.a.	98.02	KAP19-3
42.77	1.59	12.42	0.06	17.39	0.31	8.97	11.65	1.66	1.06	n.a.	n.a.	97.88	KAP19-4
42.25	1.82	12.88	0.02	18.14	0.21	8.44	11.32	1.90	1.08	n.a.	n.a.	98.06	KAP19-5
42.54	1.76	12.50	0.04	17.61	0.24	9.05	11.28	1.87	1.01	n.a.	n.a.	97.89	KAP19-6
42.23	1.80	12.78	0.05	17.97	0.20	8.71	11.24	1.82	1.19	n.a.	n.a.	97.99	KAP19-7
41.85	1.19	13.63	0.06	18.05	0.18	8.34	11.68	1.53	1.30	n.a.	n.a.	97.79	KAP19-8
42.49	1.80	12.75	0.05	18.16	0.25	9.01	11.46	1.70	1.07	n.a.	n.a.	98.73	KAP19-9
43.05	1.76	13.01	0.03	17.63	0.24	8.84	11.30	1.79	1.11	n.a.	n.a.	98.76	KAP19-10
42.32	1.76	12.91	0.03	18.61	0.23	8.53	11.26	1.75	1.07	n.a.	n.a.	98.45	KAP19-11
42.30	1.91	12.33	0.01	17.72	0.25	8.89	11.39	1.80	1.03	n.a.	n.a.	97.64	KAP19-12
42.35	1.73	12.88	0.04	17.99	0.23	8.70	11.43	1.74	1.13	n.d.	n.d.	98.22	Average
0.42	0.19	0.41	0.01	0.36	0.03	0.28	0.16	0.10	0.12	n.d.	n.d.		Std. Dev.
39.39	1.82	16.31	0.04	18.75	0.25	7.29	11.76	1.62	0.16	0	0.03	97.10	KAP16-1
41.29	1.83	12.56	0.01	18.13	0.25	8.93	11.74	1.80	0.13	0	0.04	96.71	KAP16-2
41.83	1.86	12.67	0.08	17.92	0.26	9.08	11.92	1.70	0.14	0	0.03	97.48	KAP16-3
40.95	1.75	14.22	0.09	17.20	0.27	8.52	12.03	1.56	0.12	0	0.02	96.73	KAP16-4
41.66	1.76	12.72	0.08	17.96	0.20	8.94	11.77	1.70	0.10	0	0.06	96.92	KAP16-5
41.45	1.99	12.72	0.04	17.91	0.24	9.00	11.92	1.74	0.14	0	0.02	97.16	KAP16-6
40.94	1.75	12.94	0.04	18.89	0.20	8.51	11.84	1.62	0.13	0	0.00	96.86	KAP16-7
41.03	1.70	12.91	0.03	19.04	0.22	8.47	11.95	1.71	0.13	0	0.08	97.33	KAP16-8
41.13	2.06	13.02	0.08	17.99	0.27	8.87	11.96	1.70	0.13	0	0.07	97.28	KAP16-9
40.97	1.86	12.69	0.04	18.63	0.27	8.77	11.74	1.72	0.16	0	0.07	96.91	KAP16-10
40.68	1.92	12.87	0.05	18.32	0.22	8.69	11.84	1.71	0.15	0	0.03	96.48	KAP16-11
41.42	2.13	12.32	0.06	17.65	0.26	9.36	11.70	1.63	0.16	0	0.02	96.71	KAP16-12
41.09	1.77	12.66	0.04	18.64	0.23	8.57	11.81	1.77	0.16	0	0.01	96.78	KAP16-13
41.17	1.93	13.19	0.00	18.39	0.22	8.47	11.84	1.69	0.11	0	0.06	97.04	KAP16-14
41.33	1.84	13.26	0.06	18.22	0.26	8.77	11.45	1.93	0.14	0	0.06	97.29	KAP16-15
41.99	1.93	12.75	0.05	17.46	0.25	9.10	11.66	1.72	0.12	0	0.00	97.01	KAP16-16
40.74	1.86	14.08	0.05	18.54	0.18	7.99	11.89	1.63	0.21	0	0.01	96.97	KAP16-17
41.26	1.99	12.83	0.06	18.49	0.22	8.83	11.78	1.69	0.12	0	0.02	97.27	KAP16-18
41.60	1.79	13.24	0.05	18.04	0.16	8.75	11.86	1.83	0.12	0	0.01	97.50	KAP16-19
41.16	1.85	13.16	0.05	18.22	0.24	8.68	11.81	1.71	0.14	0	0.03	97.03	Average
0.55	0.14	0.90	0.02	0.49	0.03	0.45	0.13	0.08	0.03	0	0.02		Std. Dev.
42.34	1.52	13.28	0.06	17.86	0.19	9.25	11.76	1.87	0.18	0	0.05	98.33	KAP15-1
41.96	1.90	12.60	0.07	18.37	0.23	8.80	11.95	1.91	0.16	0	0.00	97.96	KAP15-2
42.23	2.21	13.31	0.07	18.96	0.17	8.86	11.31	2.30	0.15	0	0.06	98.29	KAP15-3
43.27	1.49	12.01	0.00	17.75	0.13	9.29	11.64	2.00	0.16	0	0.01	98.34	KAP15-4
42.76	1.29	13.17	0.03	18.14	0.10	9.11	11.37	1.98	0.19	0	0.03	98.26	KAP15-5
41.93	1.90	12.95	0.07	18.23	0.16	8.70	11.53	2.04	0.14	0	0.02	97.66	KAP15-6
42.27	1.95	13.28	0.05	17.71	0.19	9.22	11.58	2.10	0.17	0	0.03	98.56	KAP15-7
42.43	1.68	12.23	0.03	17.50	0.22	9.23	12.09	1.79	0.14	0	0.04	97.39	KAP15-8
41.49	1.95	12.82	0.06	18.60	0.14	8.95	11.59	2.06	0.15	0	0.02	97.81	KAP15-9
42.04	1.84	12.84	0.03	17.55	0.28	9.39	11.69	2.15	0.14	0	0.02	97.96	KAP15-10
42.27	1.77	12.92	0.05	17.85	0.19	9.15	11.65	2.02	0.16	0	0.03	98.06	Average
0.49	0.27	0.35	0.02	0.47	0.04	0.26	0.24	0.15	0.02	0	0.02		Std. Dev.
40.87	1.85	12.70	0.05	17.84	0.29	8.71	11.61	1.68	0.19	0	0.04	95.81	KAP20-1
41.79	1.82	12.72	0.07	17.57	0.16	9.18	11.27	2.09	0.15	0	0.06	96.83	KAP20-2
44.12	2.08	13.07	0.06	15.53	0.14	9.11	11.01	2.34	0.15	0	0.04	97.64	KAP20-3

SiO_2	TiO_2	Al_2O_3	Cr_2O_3	FeO	MnO	MgO	CaO	Na_2O	K_2O	F	Cl	Total	Sample
41.64	2.87	13.70	0.06	16.87	0.13	9.45	10.44	2.52	0.08	0	0.02	97.87	KAP20-4
41.44	2.04	12.96	0.04	18.60	0.21	8.52	11.79	1.90	0.17	0	0.05	97.70	KAP20-5
40.63	1.71	14.55	0.05	16.88	0.14	8.74	11.95	1.83	0.19	0	0.04	96.71	KAP20-6
41.82	2.19	12.92	0.02	17.30	0.22	9.16	11.49	2.12	0.11	0	0.01	97.37	KAP20-7
41.03	2.44	13.67	0.02	17.28	0.18	8.80	11.22	2.08	0.11	0	0.06	96.94	KAP20-8
41.51	1.95	12.80	0.04	17.58	0.24	9.04	11.84	1.88	0.15	0	0.03	97.04	KAP20-9
41.34	2.35	13.06	0.04	16.80	0.17	9.56	11.28	2.29	0.12	0	0.03	97.03	KAP20-11
41.56	1.81	13.57	0.05	17.91	0.23	9.06	11.80	1.98	0.14	0	0.04	98.13	KAP20-12
41.93	1.97	12.73	0.02	17.95	0.26	8.80	11.69	1.76	0.14	0	0.02	97.28	KAP20-13
40.78	2.03	12.74	0.06	17.86	0.25	8.82	11.77	1.77	0.12	0	0.00	95.99	KAP20-14
41.49	1.98	13.11	0.03	16.17	0.17	9.59	11.52	2.02	0.12	0	0.02	96.22	KAP20-15
42.31	1.73	13.37	0.04	15.61	0.15	10.01	11.53	1.96	0.14	0	0.05	96.89	KAP20-16
41.55	2.03	12.97	0.04	17.77	0.22	9.01	11.77	1.91	0.10	0	0.07	97.42	KAP20-17
41.64	2.08	12.68	0.08	18.17	0.18	8.93	11.45	2.07	0.15	0	0.03	97.45	KAP20-18
41.61	2.05	13.14	0.04	17.26	0.19	9.00	11.50	2.02	0.14	0	0.03	[illegible]	Average
0.78	0.29	0.50	0.02	0.86	0.05	0.38	0.37	0.24	0.03	0	0.02		Std. Dev.
41.61	2.05	13.06	0.04	18.06	0.23	8.91	11.74	2.13	0.13	0	0.00	97.87	KAP18-1
41.45	2.34	13.27	0.05	17.34	0.16	9.18	11.03	2.33	0.12	0	0.04	97.30	KAP18-2
40.60	2.80	14.26	0.06	17.07	0.16	9.77	10.62	2.91	0.10	0	0.05	98.39	KAP18-3
41.24	2.42	13.16	0.06	17.18	0.19	9.25	11.53	2.35	0.15	0	0.03	97.55	KAP18-4
40.23	3.56	14.28	0.05	16.99	0.15	9.23	10.95	2.67	0.09	0	0.02	98.22	KAP18-5
42.01	1.92	12.28	0.06	17.51	0.22	9.36	11.71	2.14	0.15	0	0.00	97.35	KAP18-6
41.34	2.23	12.94	0.05	17.03	0.14	9.81	11.55	2.52	0.12	0	0.02	97.74	KAP18-7
40.53	2.36	14.05	0.03	17.58	0.14	8.96	11.74	2.28	0.17	0	0.00	97.86	KAP18-8
40.87	1.76	13.71	0.07	17.98	0.17	8.75	12.00	2.18	0.15	0	0.04	97.66	KAP18-9
41.70	1.86	12.72	0.06	17.70	0.27	9.31	12.09	2.10	0.14	0	0.02	97.98	KAP18-10
41.92	1.84	13.29	0.08	17.20	0.17	9.14	11.87	1.97	0.13	0	0.01	97.61	KAP18-11
41.79	2.01	12.72	0.01	18.50	0.23	9.00	11.74	1.75	0.13	0	0.03	97.80	KAP18-12
40.87	3.16	13.34	0.02	17.19	0.21	9.20	11.51	2.66	0.08	0	0.03	98.26	KAP18-13
41.88	2.16	12.79	0.05	17.58	0.22	8.90	11.94	2.09	0.13	0	0.00	97.73	KAP18-14
43.20	1.98	11.20	0.09	15.79	0.18	9.73	13.79	1.93	0.08	0	0.01	97.93	KAP18-15
41.34	2.34	13.51	0.09	17.23	0.18	9.34	10.97	2.50	0.13	0	0.05	97.66	KAP18-16
42.02	1.68	11.81	0.03	19.02	0.19	9.05	12.10	1.86	0.12	0	0.05	97.92	KAP18-17
41.54	2.24	13.32	0.09	17.68	0.21	9.04	11.24	2.33	0.12	0	0.05	97.83	KAP18-18
41.50	2.49	13.04	0.06	17.11	0.21	9.48	11.21	2.66	0.16	0	0.05	97.95	KAP18-19
41.91	2.21	12.86	0.06	16.96	0.21	9.53	11.51	2.32	0.16	0	0.00	97.72	KAP18-20
41.86	1.93	12.76	0.05	17.78	0.17	9.36	11.57	2.30	0.14	0	0.04	97.94	KAP18-21
41.49	2.25	13.06	0.05	17.45	0.19	9.25	11.64	2.28	0.13	0	0.03	97.83	Average
0.65	0.46	0.74	0.02	0.65	0.03	0.29	0.64	0.30	0.03	0	0.02		Std. Dev.
42.14	1.82	13.04	0.05	18.32	0.25	8.67	11.79	1.67	0.15	0	0.02	97.91	KAP21-1
42.04	1.85	13.36	0.04	17.85	0.21	8.51	12.00	1.81	0.15	0	0.00	97.82	KAP21-2
42.51	1.78	13.07	0.05	17.14	0.29	9.03	11.83	1.83	0.12	0	0.04	97.68	KAP21-3
43.53	1.84	12.03	0.02	16.77	0.27	9.02	12.75	1.85	0.12	0	0.06	98.04	KAP21-4
41.84	1.85	12.95	0.07	18.26	0.26	8.74	11.93	1.80	0.16	0	0.03	97.44	KAP21-5
40.81	1.76	13.76	0.03	18.03	0.22	8.23	11.98	1.88	0.16	0	0.00	96.67	KAP21-6
42.68	2.01	12.91	0.06	17.69	0.26	8.80	11.87	1.74	0.14	0	0.07	98.23	KAP21-7
42.32	1.83	13.12	0.05	18.38	0.24	8.54	11.80	1.56	0.17	0	0.00	97.81	KAP21-8
42.07	1.81	13.21	0.07	17.35	0.17	8.86	11.81	1.71	0.16	0	0.00	97.23	KAP21-9
42.21	2.22	13.35	0.10	16.93	0.23	8.98	11.69	1.77	0.18	0	0.02	97.68	KAP21-10
41.94	1.86	13.22	0.08	18.29	0.23	8.57	11.88	1.67	0.17	0	0.07	97.95	KAP21-11
42.68	1.86	12.37	0.05	17.74	0.28	8.90	11.98	1.73	0.14	0	0.05	97.77	KAP21-12
42.25	1.90	12.93	0.06	18.44	0.24	8.40	11.95	1.60	0.16	0	0.02	97.93	KAP21-13
42.30	1.80	12.80	0.02	18.19	0.25	8.97	11.81	1.69	0.13	0	0.05	98.20	KAP21-14
42.41	1.80	12.97	0.08	17.91	0.27	9.11	11.80	1.76	0.14	0	0.02	98.25	KAP21-15
41.09	1.60	15.42	0.02	17.86	0.22	8.03	12.19	1.54	0.16	0	0.02	98.16	KAP21-16
42.18	1.81	13.16	0.05	17.82	0.24	8.71	11.94	1.72	0.15	0	0.03	97.80	Average
0.62	0.16	0.72	0.02	0.53	0.03	0.31	0.25	0.10	0.02	0	0.02		Std. Dev.
41.65	2.02	13.41	0.10	18.72	0.20	8.23	11.90	1.56	0.19	0	0.02	97.99	KAP28-1
41.88	1.80	13.72	0.03	17.97	0.25	8.79	11.64	1.93	0.12	0	0.06	98.18	KAP28-2
42.28	1.76	13.30	0.06	18.13	0.21	8.63	11.86	1.73	0.18	0	0.03	98.17	KAP28-3
42.21	1.99	13.00	0.09	18.54	0.18	8.67	11.90	1.74	0.22	0	0.02	98.56	KAP28-4
42.65	1.97	12.83	0.04	18.45	0.24	8.85	12.00	1.81	0.15	0	0.00	98.97	KAP28-5
41.96	1.80	13.03	0.04	18.63	0.20	8.58	11.82	1.74	0.20	0	0.01	97.99	KAP28-6
42.89	1.62	13.97	0.03	17.27	0.24	8.97	11.59	1.93	0.13	0	0.00	98.62	KAP28-7
42.05	2.15	13.06	0.07	18.44	0.17	8.68	11.78	1.78	0.16	0	0.00	98.29	KAP28-8
42.51	1.67	12.88	0.05	18.24	0.28	9.15	11.93	1.71	0.12	0	0.04	98.55	KAP28-9
42.22	1.93	12.90	0.02	18.33	0.26	8.73	11.62	1.77	0.13	0	0.02	97.92	KAP28-10
42.77	1.27	13.27	0.08	17.53	0.15	9.06	12.02	1.60	0.15	0	0.03	97.92	KAP28-11
41.77	1.38	14.15	0.08	16.81	0.24	9.19	12.09	1.42	0.16	0	0.02	97.31	KAP28-12
40.93	2.01	14.70	0.08	18.42	0.22	7.80	11.91	1.67	0.18	0	0.02	97.93	KAP28-13
42.29	1.88	12.96	0.06	18.11	0.19	8.64	11.70	1.88	0.14	0	0.04	97.87	KAP28-14
41.30	2.02	13.60	0.07	17.94	0.17	8.63	12.08	1.83	0.15	0	0.01	97.80	KAP28-15
42.58	1.74	13.00	0.03	17.73	0.28	9.29	11.83	1.84	0.18	0	0.03	98.32	KAP28-16
42.52	2.18	12.70	0.03	16.58	0.25	9.39	12.05	1.84	0.14	0	0.00	97.67	KAP28-17
42.76	1.77	12.10	0.00	18.03	0.26	9.14	11.91	1.71	0.12	0	0.00	97.89	KAP28-18
41.84	2.01	13.44	0.06	17.39	0.20	8.78	11.86	1.65	0.15	0	0.00	97.39	KAP28-19

SiO_2	TiO_2	Al_2O_3	Cr_2O_3	FeO	MnO	MgO	CaO	Na_2O	K_2O	F	Cl	Total	Sample
41.29	1.98	13.01	0.06	18.35	0.23	8.55	11.74	1.82	0.17	0	0.02	97.03	KAP28-20
42.12	1.85	13.25	0.06	17.98	0.22	8.79	11.86	1.73	0.16	0	0.02	98.02	Average
0.54	0.23	0.57	0.02	0.59	0.04	0.37	0.15	0.13	0.03	0	0.02		Std.Dev.
43.51	1.78	12.10	0.05	16.67	0.17	9.59	11.26	1.89	0.97	n.a.	n.a.	97.98	KAP29-1
41.97	1.78	12.85	0.03	17.81	0.23	8.71	11.66	1.84	1.20	n.a.	n.a.	98.07	KAP29-2
42.13	1.58	13.52	0.06	17.59	0.13	8.77	11.56	1.98	1.21	n.a.	n.a.	98.52	KAP29-3
42.28	2.05	12.67	0.06	16.74	0.13	9.21	11.16	2.05	1.10	n.a.	n.a.	97.44	KAP29-4
42.17	1.82	13.00	0.05	17.57	0.13	8.72	11.25	1.96	1.06	n.a.	n.a.	97.70	KAP29-5
42.45	1.90	12.76	0.05	17.38	0.24	9.23	11.46	1.91	0.99	n.a.	n.a.	98.38	KAP29-6
42.17	1.91	12.55	0.08	17.79	0.24	9.10	11.47	1.90	1.05	n.a.	n.a.	98.23	KAP29-7
42.55	1.91	12.25	0.05	17.57	0.24	8.85	11.50	1.74	1.06	n.a.	n.a.	97.72	KAP29-8
43.27	1.88	13.07	0.04	15.99	0.10	9.32	11.15	2.06	1.02	n.a.	n.a.	97.98	KAP29-9
42.91	2.00	12.51	0.08	16.85	0.15	9.44	11.08	2.00	1.01	n.a.	n.a.	98.01	KAP29-10
42.24	1.74	12.94	0.03	18.59	0.25	8.71	11.56	1.85	1.20	n.a.	n.a.	98.10	KAP29-11
42.12	1.95	12.38	0.08	17.72	0.21	8.94	11.47	2.13	1.14	n.a.	n.a.	98.12	KAP29-12
42.48	1.86	12.72	0.06	17.36	0.19	9.06	11.38	1.94	1.08	n.d.	n.d.	98.10	Average
0.49	0.13	0.39	0.01	0.68	0.05	0.31	0.19	0.11	0.08	n.d.	n.d.		Std. Dev.
41.84	1.83	12.42	0.03	17.15	0.27	9.10	11.83	1.93	1.08	0	0.02	97.08	KAP8-1
41.12	1.72	12.09	0.04	19.12	0.23	8.57	11.41	1.79	1.09	0	0.03	97.20	KAP8-2
41.54	1.77	12.29	0.03	17.34	0.25	9.22	11.42	1.87	1.08	0	0.02	96.84	KAP8-3
41.52	1.90	12.58	0.06	17.48	0.28	8.89	11.68	1.91	1.06	0	0.02	97.36	KAP8-4
40.75	1.87	13.19	0.03	18.45	0.17	8.24	11.70	2.16	1.15	0	0.02	97.72	KAP8-5
41.29	1.71	13.08	0.02	17.14	0.17	8.73	11.09	2.40	1.10	0	0.00	96.72	KAP8-6
41.36	1.85	12.47	0.05	17.69	0.23	8.50	11.50	1.92	1.07	0	0.02	96.65	KAP8-7
40.61	2.11	13.50	0.03	16.93	0.21	8.44	11.21	2.05	1.07	0	0.02	96.17	KAP8-8
41.27	2.04	12.61	0.03	17.54	0.23	8.74	11.53	2.14	1.14	0	0.03	97.29	KAP8-9
41.01	1.88	12.53	0.03	17.76	0.21	8.74	11.34	1.73	1.08	0	0.01	96.31	KAP8-10
41.00	1.92	12.87	0.03	18.27	0.20	8.33	11.70	1.82	1.08	0	0.00	97.01	KAP8-11
40.59	1.67	13.88	0.03	17.84	0.25	8.21	11.68	1.77	1.32	0	0.02	97.14	KAP8-12
41.16	1.84	12.87	0.05	17.85	0.23	8.47	11.63	1.82	1.11	0	0.02	97.04	KAP8-13
41.75	1.74	12.94	0.06	18.21	0.30	8.06	11.73	1.78	1.09	0	0.03	98.29	KAP8-14
42.86	1.98	11.67	0.05	16.66	0.28	9.79	11.96	1.71	0.97	0	0.04	97.12	KAP8-15
41.30	1.81	12.73	0.04	17.60	0.23	8.71	11.53	1.91	1.10	0	0.02	97.07	Average
0.56	0.16	0.55	0.01	0.64	0.04	0.42	0.21	0.21	0.07	0	0.01		Std. Dev.
41.77	2.02	9.19	0.06	17.23	0.21	12.96	11.26	2.33	1.06	0.02	0.21	98.19	KAP7-1
40.99	2.98	9.36	0.06	16.58	0.12	13.39	11.32	2.49	1.17	0.05	0.20	98.29	KAP7-2
42.06	1.84	9.37	0.03	17.14	0.20	12.75	11.79	2.18	1.10	0.01	0.24	98.59	KAP7-3
41.47	2.57	9.41	0.05	16.75	0.15	13.67	10.96	2.59	1.13	0.02	0.24	98.89	KAP7-4
41.09	2.78	9.35	0.07	16.94	0.14	13.70	11.05	2.64	1.10	0.02	0.19	98.97	KAP7-5
42.13	1.90	9.47	0.08	17.00	0.22	12.89	11.83	2.28	1.16	0.03	0.23	98.97	KAP7-6
41.28	2.98	9.38	0.04	16.71	0.15	13.32	11.27	2.38	1.11	0.03	0.19	98.35	KAP7-7
40.92	2.22	9.01	0.08	17.58	0.18	13.04	11.39	2.25	1.17	0.03	0.22	98.09	KAP7-8
41.41	2.43	9.47	0.08	16.86	0.19	13.15	11.24	2.84	1.06	0.04	0.20	98.98	KAP7-9
41.48	2.34	9.33	0.06	16.99	0.17	13.21	11.32	2.41	1.12	0.03	0.21	98.94	Average
0.45	0.34	0.15	0.02	0.33	0.03	0.34	0.26	0.18	0.04	0.01	0.02		Std. Dev.
42.60	1.65	12.92	0.06	17.99	0.19	8.64	11.49	2.11	1.21	n.a.	n.a.	98.76	KAP39-1
42.67	1.80	13.10	0.08	18.24	0.28	8.13	11.75	1.83	1.18	n.a.	n.a.	98.81	KAP39-2
41.78	1.77	13.31	0.06	18.43	0.18	7.87	11.93	1.80	1.30	n.a.	n.a.	98.22	KAP39-3
42.57	1.69	13.00	0.05	19.37	0.28	7.09	11.67	1.82	1.08	n.a.	n.a.	99.19	KAP39-4
42.92	1.93	12.15	0.03	17.46	0.31	8.87	11.80	1.84	1.08	n.a.	n.a.	98.38	KAP39-5
43.09	1.79	13.03	0.08	17.00	0.13	9.00	11.22	2.43	1.11	n.a.	n.a.	98.85	KAP39-6
42.52	1.89	13.02	0.04	16.90	0.19	8.71	11.86	2.04	1.20	n.a.	n.a.	98.36	KAP39-7
42.43	1.90	12.80	0.03	18.55	0.23	7.96	11.75	1.80	1.12	n.a.	n.a.	98.66	KAP39-8
42.67	2.10	13.00	0.05	17.04	0.19	8.77	11.56	2.09	1.13	n.a.	n.a.	98.61	KAP39-9
42.44	2.08	12.96	0.03	17.41	0.23	8.24	11.88	2.08	1.14	n.a.	n.a.	98.16	KAP39-10
42.57	1.87	12.93	0.05	17.94	0.22	8.38	11.68	1.94	1.15	n.d.	n.d.	98.60	Average
0.35	0.15	0.30	0.01	0.81	0.06	0.48	0.21	0.25	0.07	n.d.	n.d.		Std. Dev.

Clinopyroxene Compositions

SiO_2	TiO_2	Al_2O_3	Cr_2O_3	FeO	MnO	MgO	CaO	Na_2O	K_2O	Total	Sample
52.87	0.05	0.53	0	9.93	0.33	11.61	24.14	0.22	0.02	99.70	3VG12-1
52.46	0.10	1.84	0	11.61	0.36	12.14	21.66	0.52	0.01	100.71	3VG12-2
52.52	0.12	1.75	0	11.43	0.34	12.25	21.86	0.46	0.03	100.74	3VG12-3
52.27	0.17	2.14	0	11.37	0.36	12.01	21.65	0.47	0.02	100.46	3VG12-4
52.20	0.09	2.15	0.01	11.38	0.36	11.93	21.64	0.46	0.03	100.24	3VG12-5
52.35	0.09	1.90	0.01	11.60	0.36	12.05	21.56	0.46	0	100.37	3VG12-6
51.82	0.19	2.31	0.01	11.73	0.32	11.80	21.26	0.50	0.03	99.96	3VG12-7
52.42	0.15	1.88	0.01	9.97	0.22	12.72	22.57	0.43	0.01	100.35	3VG12-8
52.15	0.14	2.06	0.02	11.11	0.27	12.15	21.83	0.45	0.02	100.20	3VG12-9
51.99	0.15	2.04	0	11.09	0.35	11.87	21.76	0.38	0.06	99.68	3VG12-10
52.30	0.13	1.86	0.01	11.12	0.33	12.05	21.99	0.43	0.02	100.24	Average
0.29	0.04	0.50	0.01	0.65	0.05	0.30	0.83	0.09	0.01		Std. Dev.
52.19	0.12	1.81	0	11.23	0.27	12.55	21.45	0.42	0.03	100.06	3VG1-1
51.35	0.21	2.26	0	12.23	0.34	12.21	20.27	0.41	0.04	99.32	3VG1-2
52.60	0.07	1.15	0	10.75	0.35	12.89	21.78	0.22	0.05	99.86	3VG1-3
51.92	0.14	1.48	0	11.08	0.33	12.66	21.34	0.28	0.04	99.27	3VG1-4
51.76	0.16	2.26	0	11.57	0.35	12.26	20.90	0.44	0.04	99.82	3VG1-5
51.61	0.19	2.33	0.01	11.45	0.30	12.05	20.65	0.45	0.06	99.09	3VG1-6
51.89	0.19	2.03	0	10.84	0.31	12.54	21.47	0.34	0.03	99.63	3VG1-7
51.90	0.15	1.86	0.01	10.97	0.35	12.49	21.86	0.30	0.02	100.03	3VG1-8
51.99	0.14	2.12	0	11.30	0.31	12.16	20.94	0.44	0.03	99.44	3VG1-9
52.24	0.14	1.81	0.01	10.67	0.32	12.48	21.67	0.38	0.04	99.76	3VG1-10
52.07	0.19	1.95	0	11.61	0.32	12.46	20.92	0.43	0.05	99.99	3VG1-11
51.88	0.15	2.21	0	11.48	0.35	12.35	21.08	0.46	0.02	99.99	3VG1-12
51.96	0.10	1.96	0	11.21	0.30	12.59	21.19	0.35	0.04	99.70	3VG1-13
51.79	0.15	2.16	0.01	11.40	0.31	12.48	21.21	0.44	0.03	99.94	3VG1-14
51.93	0.11	1.94	0.02	11.13	0.36	12.37	21.25	0.41	0.03	99.54	3VG1-15
51.94	0.15	1.96	0	11.26	0.32	12.43	21.21	0.38	0.04	99.69	Average
0.28	0.04	0.32	0	0.39	0.03	0.21	0.43	0.07	0.01		Std. Dev.
52.05	0.09	1.79	0.13	11.31	0.33	12.38	21.54	0.32	0.05	100.00	3VG27-1
51.86	0.10	2.01	0.03	12.09	0.33	12.25	20.82	0.46	0.04	100.00	3VG27-2
52.50	0.02	1.23	0.03	11.07	0.28	12.56	22.00	0.26	0.04	100.00	3VG27-3
52.22	0.04	1.59	0	11.11	0.26	12.62	21.73	0.41	0.02	100.00	3VG27-4
51.89	0.13	2.26	0	11.73	0.32	11.99	21.16	0.50	0.03	100.00	3VG27-5
52.14	0.10	1.88	0.09	11.40	0.31	12.20	21.39	0.44	0.06	100.00	3VG27-6
51.92	0.09	2.16	0.08	12.03	0.33	12.09	20.86	0.42	0.03	100.00	3VG27-7
51.98	0.07	2.01	0.02	11.81	0.32	12.23	21.06	0.45	0.05	100.00	3VG27-8
51.90	0.12	2.27	0.22	11.75	0.32	12.01	20.87	0.52	0.04	100.00	3VG27-9
51.80	0.10	2.32	0.09	12.12	0.27	11.90	20.84	0.42	0.05	100.00	3VG27-10
52.05	0.06	1.70	0.09	11.15	0.32	12.44	21.69	0.46	0.06	100.00	3VG27-11
51.65	0.00	2.06	0	11.47	0.34	12.31	21.64	0.41	0.03	100.00	3VG27-12
51.62	0.04	2.26	0.01	12.61	0.34	12.27	20.31	0.51	0.02	100.00	3VG27-13
51.59	0.11	2.25	0	11.97	0.32	11.96	21.23	0.56	0.04	100.00	3VG27-14
51.94	0.08	1.98	0.06	11.69	0.31	12.24	21.22	0.44	0.04	100.00	Average
0.26	0.03	0.32	0.06	0.46	0.03	0.22	0.46	0.08	0.01		Std. Dev.
51.78	0.20	2.15	0	12.06	0.33	12.04	20.99	0.44	0.02	100.00	3VG26-1
51.49	0.18	2.27	0	11.99	0.31	12.15	21.13	0.47	0.02	100.00	3VG26-2
51.78	0.22	2.14	0.02	11.92	0.32	12.13	20.96	0.46	0.02	100.00	3VG26-3
51.66	0.15	2.14	0.02	12.21	0.33	12.16	20.89	0.43	0.03	100.00	3VG26-4
52.32	0.12	1.54	0	11.20	0.30	12.48	21.70	0.34	0.02	100.00	3VG26-5
51.83	0.19	1.97	0	11.85	0.32	12.32	21.13	0.37	0.02	100.00	3VG26-6
51.96	0.13	1.73	0	11.34	0.32	12.36	21.78	0.36	0.01	100.00	3VG26-7
51.90	0.16	2.07	0.13	11.58	0.31	12.54	20.90	0.38	0.02	100.00	3VG26-8
50.64	0.46	3.38	0	14.38	0.32	12.90	17.33	0.58	0.02	100.00	3VG26-9
51.88	0.19	2.35	0.08	12.02	0.33	11.82	20.83	0.47	0.05	100.00	3VG26-10
51.74	0.19	2.18	0	11.92	0.33	11.98	21.21	0.43	0.03	100.00	3VG26-11
51.99	0.16	2.01	0	11.66	0.33	12.16	21.23	0.43	0.03	100.00	3VG26-12
51.84	0.15	1.84	0	11.59	0.31	12.27	21.56	0.41	0.04	100.00	3VG26-13
51.80	0.13	1.94	0	11.25	0.27	12.30	22.11	0.38	0	100.00	3VG26-14
51.92	0.19	2.09	0.01	11.86	0.32	11.90	21.17	0.42	0.04	100.00	3VG26-15
51.76	0.19	2.12	0.02	11.93	0.32	12.23	21.00	0.42	0.02	100.00	Average

SiO_2	TiO_2	Al_2O_3	Cr_2O_3	FeO	MnO	MgO	CaO	Na_2O	K_2O	Total	Sample
0.36	0.08	0.41	0.04	0.74	0.02	0.27	1.08	0.06	0.01		Std. Dev.
50.45	0.55	4.25	0.03	11.85	0.32	13.90	18.41	0.54	0.02	100.31	3VG14-1
50.83	0.52	3.71	0.02	13.07	0.29	12.92	18.24	0.41	0.03	100.05	3VG14-2
50.14	0.91	4.96	0.01	13.69	0.23	13.18	16.70	0.42	0.04	100.27	3VG14-3
52.33	0.12	2.45	0.01	11.18	0.30	11.84	21.90	0.45	0.02	100.61	3VG14-4
50.33	0.68	4.29	0.02	12.38	0.28	13.60	17.95	0.47	0.02	100.11	3VG14-5
52.12	0.12	2.22	0.02	11.57	0.33	11.96	21.64	0.47	0.02	100.48	3VG14-6
51.38	0.32	3.01	0	11.51	0.27	12.96	20.40	0.45	0.02	100.33	3VG14-7
50.62	0.58	3.98	0.04	12.74	0.31	14.07	17.30	0.45	0.01	100.09	3VG14-8
49.84	0.68	4.35	0.03	14.31	0.32	14.06	15.88	0.43	0.01	99.91	3VG14-9
50.69	0.56	4.00	0	12.18	0.29	13.24	18.97	0.52	0.01	100.48	3VG14-10
50.87	0.50	3.72	0.02	12.45	0.30	13.18	18.74	0.46	0.02	100.26	Average
0.82	0.25	0.88	0.01	1.01	0.03	0.80	2.02	0.04	0.01		Std. Dev.
51.93	0.11	2.27	0	11.34	0.28	11.72	21.08	0.45	0	99.18	3VG11-1
52.23	0.17	2.25	0.01	11.31	0.28	11.70	20.96	0.49	0.01	99.40	3VG11-2
51.61	0.16	2.71	0	11.44	0.33	11.79	20.77	0.50	0	99.30	3VG11-3
52.11	0.15	2.27	0.01	11.57	0.29	11.79	21.04	0.53	0.01	99.76	3VG11-4
52.37	0.18	2.38	0	11.67	0.35	11.59	21.30	0.53	0.02	100.38	3VG11-5
52.26	0.18	2.28	0.01	11.46	0.29	11.73	21.35	0.42	0.01	100.00	3VG11-6
52.32	0.15	2.24	0	11.32	0.29	11.64	21.07	0.45	0.01	99.50	3VG11-7
52.12	0.16	2.34	0	11.44	0.30	11.71	21.08	0.48	0.01	99.64	Average
0.27	0.03	0.17	0	0.14	0.03	0.07	0.20	0.04	0.01		Std. Dev.
52.98	0.06	0.57	0	9.99	0.39	12.55	24.17	0.11	0.03	100.86	3VG10-1
52.81	0.13	2.31	0.01	11.34	0.34	12.01	20.56	0.44	0.04	99.99	3VG10-2
50.98	0.18	2.54	0	11.72	0.34	11.88	20.05	0.49	0.12	98.30	3VG10-3
51.60	0.10	2.17	0	11.40	0.33	12.14	21.07	0.42	0.03	99.26	3VG10-4
51.88	0.11	2.03	0	11.51	0.33	12.46	20.79	0.49	0.03	99.60	3VG10-5
51.57	0.10	2.04	0	11.45	0.33	12.23	21.16	0.41	0.04	99.32	3VG10-6
51.97	0.11	1.94	0	11.23	0.34	12.21	21.30	0.39	0.05	99.55	Average
0.77	0.04	0.70	0	0.62	0.02	0.26	1.46	0.14	0.04		Std. Dev.
51.82	0.15	2.23	0.01	11.43	0.31	12.40	21.00	0.38	0.04	99.77	3VG6-1
51.94	0.10	1.98	0.01	11.02	0.33	12.52	21.25	0.49	0.05	99.68	3VG6-2
52.00	0.14	1.91	0.04	10.98	0.31	12.48	21.33	0.47	0.02	99.70	3VG6-3
51.92	0.13	2.04	0.02	11.14	0.32	12.47	21.19	0.45	0.04	99.72	Average
0.10	0.03	0.17	0.02	0.25	0.01	0.06	0.17	0.06	0.01		Std. Dev.
51.91	0.14	2.44	0	11.90	0.32	12.18	20.26	0.51	0.04	99.898	3VG5-1
50.97	0.37	3.49	0.02	13.36	0.28	11.51	18.54	0.45	0.09	99.075	3VG5-2
52.03	0.25	2.11	0.02	12.71	0.29	12.43	19.44	0.33	0.05	99.639	3VG5-3
52.18	0.14	2.20	0	11.46	0.31	12.49	21.02	0.39	0.04	100.219	3VG5-4
52.20	0.12	2.58	0	12.26	0.30	12.16	20.09	0.51	0.04	100.264	3VG5-5
52.48	0.18	2.64	0.01	12.51	0.31	12.34	19.95	0.44	0.03	100.904	3VG5-6
52.76	0.15	2.24	0	11.52	0.35	12.30	20.68	0.49	0.03	100.553	3VG5-7
51.83	0.26	2.98	0.02	12.83	0.31	12.10	19.11	0.53	0.06	100.061	3VG5-8
52.21	0.11	2.05	0	11.03	0.29	12.33	21.14	0.37	0.02	99.557	3VG5-9
51.78	0.16	2.14	0	11.37	0.31	12.17	20.72	0.36	0.01	99.021	3VG5-10
51.96	0.12	1.86	0	10.87	0.31	12.34	21.47	0.34	0.02	99.263	3VG5-11
51.79	0.18	2.34	0.01	11.82	0.27	12.24	20.48	0.37	0.02	99.519	3VG5-12
51.50	0.35	3.45	0.01	13.56	0.31	11.90	17.87	0.47	0.09	99.514	3VG5-13
51.01	0.37	3.35	0.01	13.88	0.33	11.78	18.50	0.46	0.05	99.761	3VG5-14
51.90	0.21	2.56	0.01	12.22	0.31	12.16	19.95	0.43	0.04	99.79	Average
0.50	0.10	0.56	0.01	0.95	0.02	0.27	1.10	0.07	0.03		Std. Dev.
51.68	0.25	2.86	0.02	13.85	0.33	12.03	18.77	0.64	0.07	100.49	3VG4-1
51.44	0.24	2.44	0	12.25	0.36	12.11	20.52	0.53	0.04	99.93	3VG4-2
51.76	0.11	2.27	0	11.99	0.35	11.99	20.86	0.45	0.02	99.81	3VG4-3
52.07	0.08	1.21	0	10.74	0.29	12.58	22.15	0.32	0.03	99.44	3VG4-4
51.39	0.12	2.21	0	11.48	0.31	12.04	21.17	0.47	0.02	99.20	3VG4-5
51.60	0.07	1.70	0.02	11.04	0.34	12.31	21.90	0.40	0.03	99.38	3VG4-6
51.84	0.07	1.27	0	11.11	0.28	12.32	22.32	0.30	0.01	99.51	3VG4-7
51.46	0.06	1.94	0.04	11.19	0.33	12.23	21.41	0.48	0.01	99.15	3VG4-8

SiO_2	TiO_2	Al_2O_3	Cr_2O_3	FeO	MnO	MgO	CaO	Na_2O	K_2O	Total	Sample
51.52	0.17	1.78	0	11.09	0.34	12.32	21.80	0.39	0.05	99.45	3VG4-9
51.64	0.13	1.96	0.01	11.64	0.33	12.21	21.21	0.44	0.03	99.60	Average
0.22	0.08	0.54	0.01	0.96	0.02	0.19	1.09	0.11	0.02		Std. Dev.
52.252	0.112	2.489	0.031	11.776	0.304	12.025	20.801	0.495	0.029	100.314	3VG19-1
52.551	0.108	2.332	0.018	11.79	0.352	12.190	20.971	0.482	0.009	100.822	3VG19-2
52.40	0.11	2.41	0.02	11.78	0.33	12.11	20.89	0.49	0.02		Average
0.21	0.00	0.11	0.01	0.01	0.03	0.12	0.12	0.00	0.01		Std. Dev.
51.87	0.14	2.32	0	11.94	0.31	12.52	20.71	0.50	0.04	100.35	3VG16-1
51.72	0.13	2.51	0	12.00	0.36	12.13	20.69	0.50	0.03	100.06	3VG16-2
51.72	0.18	2.09	0	11.26	0.36	12.48	21.25	0.40	0.04	99.86	3VG16-3
52.04	0.14	2.19	0.01	11.51	0.35	12.26	20.87	0.41	0.04	99.82	3VG16-4
51.69	0.17	2.46	0.02	11.53	0.39	12.09	20.56	0.48	0.05	99.46	3VG16-5
51.83	0.14	2.09	0.02	11.19	0.32	12.39	21.30	0.37	0.04	99.66	3VG16-6
50.87	0.28	4.43	0.01	12.68	0.32	11.34	19.00	0.77	0.03	99.90	3VG16-7
51.94	0.13	2.13	0.01	11.25	0.35	12.38	20.78	0.46	0.05	99.48	3VG16-8
52.21	0.17	2.25	0	11.57	0.35	12.42	20.64	0.44	0.04	100.10	3VG16-9
52.22	0.16	2.23	0.01	11.14	0.33	12.46	21.48	0.41	0.04	100.47	3VG16-10
51.89	0.18	2.10	0	10.95	0.31	12.58	22.42	0.38	0.04	100.84	3VG16-11
51.98	0.18	2.23	0.01	12.25	0.36	12.30	21.14	0.46	0.03	100.92	3VG16-12
51.96	0.18	2.19	0.01	11.88	0.36	12.39	21.90	0.38	0.02	100.97	3VG16-13
51.86	0.17	2.35	0.02	11.57	0.33	12.28	21.64	0.41	0.04	100.45	3VG16-14
52.18	0.14	2.08	0.02	11.12	0.36	12.28	22.63	0.39	0.04	101.24	3VG16-15
51.85	0.16	2.38	0.01	11.58	0.34	12.29	21.13	0.46	0.04	100.24	Average
0.33	0.03	0.58	0.01	0.51	0.02	0.29	0.87	0.10	0.01		Std. Dev.
51.48	0.13	2.27	0	12.11	0.33	12.19	20.51	0.43	0.09	99.54	3VG15-1
51.57	0.15	2.16	0	11.57	0.36	12.21	21.03	0.50	0.04	99.59	3VG15-2
51.75	0.14	2.19	0	11.70	0.34	12.30	20.85	0.45	0.03	99.74	3VG15-3
51.39	0.12	2.26	0	11.76	0.35	12.07	20.67	0.43	0.04	99.08	3VG15-4
52.53	0.00	0.28	0	9.25	0.46	12.39	24.23	0.11	0.03	99.28	3VG15-5
51.84	0.15	2.28	0	11.37	0.33	12.36	21.02	0.48	0.03	99.87	3VG15-6
52.04	0.12	1.79	0	11.05	0.31	12.60	21.72	[illegible]	0.02	100.00	3VG15-7
51.79	0.12	2.08	0	11.27	0.36	12.48	21.31	[illegible]	0.03	99.83	3VG15-8
52.41	0.09	1.34	0	10.36	0.30	12.72	21.95	0.33	0.03	99.54	3VG15-9
51.96	0.09	1.28	0.02	10.36	0.31	12.90	22.00	0.33	0.04	99.29	3VG15-10
51.24	0.32	3.93	0	12.80	0.27	11.84	18.74	0.91	0.04	99.88	3VG15-11
51.82	0.11	1.95	0.02	11.43	0.35	12.38	20.98	0.45	0.03	99.54	3VG15-12
51.81	0.14	2.00	0.01	11.21	0.34	12.38	21.42	0.46	0.03	99.79	3VG15-13
51.91	0.09	1.54	0	10.84	0.34	12.68	21.75	0.35	0.02	99.52	3VG15-14
52.03	0.08	1.75	0.02	11.14	0.35	12.43	21.73	0.37	0.04	99.92	3VG15-15
51.84	0.12	1.94	0	11.21	0.34	12.38	21.33	0.42	0.04	99.63	Average
0.35	0.07	0.77	0.01	0.83	0.04	0.30	1.14	0.17	0.02		Std. Dev.
48.36	0.85	7.12	0.03	13.88	0.21	11.84	16.15	0.83	0.06	99.33	3VG18-1
48.28	0.91	7.16	0.01	12.36	0.16	11.86	17.38	1.13	0.06	99.02	3VG18-2
48.99	0.72	6.28	0.02	12.71	0.14	11.84	17.21	1.08	0.06	99.03	3VG18-3
48.45	0.85	6.95	0	12.55	0.13	11.63	17.38	1.06	0.06	99.06	3VG18-4
49.60	0.69	5.40	0.01	12.22	0.15	12.16	17.78	0.96	0.04	99.03	3VG18-5
48.76	0.74	6.76	0	13.80	0.21	11.86	16.31	0.89	0.06	99.37	3VG18-6
49.63	0.72	6.07	0.01	12.87	0.17	11.75	17.60	1.01	0.04	99.87	3VG18-7
49.39	0.73	6.66	0	14.11	0.21	11.58	16.13	0.97	0.04	99.83	3VG18-8
49.94	0.69	6.20	0	12.32	0.14	12.00	17.44	1.04	0.06	99.83	3VG18-9
48.98	0.80	6.65	0	13.06	0.18	11.77	16.88	0.92	0.05	99.29	3VG18-10
49.29	0.68	6.48	0	13.44	0.20	11.64	16.93	0.85	0.04	99.56	3VG18-11
48.38	0.87	7.02	0.01	13.31	0.16	11.44	17.01	1.03	0.04	99.28	3VG18-12
49.72	0.55	6.11	0.05	16.80	0.25	12.88	12.82	0.79	0.04	100.01	3VG18-13
52.23	0.16	2.32	0.01	11.07	0.25	12.51	20.94	0.44	0.02	99.96	3VG18-14
50.20	0.44	4.95	0	13.19	0.23	12.27	17.80	0.76	0.02	99.87	3VG18-15
51.34	0.14	2.14	0.02	12.18	0.43	12.36	20.27	0.32	0.03	99.24	3VG18-16
52.04	0.12	1.89	0.03	11.01	0.31	12.30	21.51	0.35	0.03	99.58	3VG18-17
51.91	0.13	2.33	0.02	11.77	0.33	12.18	20.80	0.41	0.03	99.89	3VG18-18
52.25	0.09	2.20	0.01	11.69	0.36	12.16	21.12	0.43	0.04	100.34	3VG18-19
48.45	0.82	7.56	0.06	14.96	0.22	11.68	14.72	0.91	0.08	99.44	3VG18-20
50.95	0.15	2.59	0.02	12.36	0.32	12.09	19.94	0.51	0.04	98.96	3VG18-21

SiO_2	TiO_2	Al_2O_3	Cr_2O_3	FeO	MnO	MgO	CaO	Na_2O	K_2O	Total	Sample
48.48	0.63	7.29	0.01	15.16	0.28	11.98	14.96	0.74	0.03	99.56	3VG18-22
52.13	0.20	2.59	0.02	11.67	0.29	11.84	20.96	0.49	0.04	100.22	3VG18-23
47.91	0.89	6.95	0	13.84	0.21	12.10	16.14	0.91	0.02	98.77	3VG18-24
49.05	0.58	6.01	0.01	14.08	0.21	12.53	15.67	0.79	0.01	98.93	3VG18-25
49.88	0.47	4.81	0	13.01	0.20	11.70	17.93	0.79	0.02	98.91	3VG18-26
49.79	0.55	5.33	0.01	13.06	0.23	11.99	17.68	0.76	0.04	99.47	Average
1.41	0.28	1.99	0.01	1.32	0.07	0.35	2.23	0.25	0.01		Std. Dev.
51.87	0.14	2.32	0.02	11.42	0.32	11.99	21.05	0.50	0	99.62	3VG29-1
52.50	0.12	2.30	0	11.56	0.37	12.15	21.33	0.43	0.02	100.78	3VG29-2
52.29	0.14	2.50	0	11.13	0.33	12.07	21.30	0.46	0.02	100.23	3VG29-3
52.25	0.13	2.01	0.01	11.41	0.36	12.41	21.43	0.40	0	100.43	3VG29-4
52.57	0.07	0.97	0	10.22	0.35	13.19	22.59	0.31	0.03	100.30	3VG29-5
52.30	0.12	2.02	0.01	11.14	0.36	12.36	21.54	0.42	0.01	100.27	Average
0.28	0.03	0.61	0.01	0.54	0.02	0.49	0.61	0.07	0.01		Std. Dev.
51.85	0.12	2.14	0	11.70	0.37	12.24	20.96	0.42	0.04	99.83	3VG8-1
51.86	0.16	2.27	0.03	11.24	0.28	12.27	20.99	0.44	0.04	99.57	3VG8-2
51.77	0.12	1.76	0	10.97	0.32	12.44	21.74	0.38	0.04	99.53	3VG8-3
51.79	0.13	2.22	0	11.97	0.35	12.15	20.56	0.43	0.03	99.62	3VG8-4
52.26	0.09	1.92	0.04	10.88	0.33	12.46	21.58	0.42	0.04	100.00	3VG8-5
52.26	0.11	1.73	0	10.51	0.30	12.62	21.54	0.37	0.04	99.48	3VG8-6
51.39	0.27	3.43	0.04	11.82	0.29	11.99	19.75	0.61	0.06	99.61	3VG8-7
51.88	0.14	2.21	0.02	11.30	0.32	12.31	21.02	0.44	0.04	99.66	Average
0.30	0.06	0.58	0.02	0.55	0.03	0.21	0.70	0.08	0.01		Std. Dev.
50.82	0.75	5.96	0.01	9.82	0.10	11.82	18.65	1.31	0.04	99.29	3VG7-1
51.41	0.63	5.33	0	10.37	0.12	12.27	18.24	1.30	0.02	99.71	3VG7-2
51.68	0.62	4.78	0	10.24	0.12	12.64	18.46	1.17	0.03	99.74	3VG7-3
51.04	0.65	6.02	0	9.96	0.12	12.33	18.86	1.22	0.06	99.36	3VG7-4
50.90	0.69	5.55	0	10.09	0.11	12.12	18.54	1.37	0.03	99.40	3VG7-5
51.06	0.86	6.22	0.01	10.73	0.14	12.03	17.69	1.23	0.06	99.61	3VG7-6
51.43	0.47	4.35	0.01	11.37	0.24	12.23	19.35	0.80	0.04	100.31	3VG7-7
51.56	0.76	5.89	0	10.02	0.12	12.29	18.01	1.24	0.06	99.96	3VG7-8
52.12	0.26	3.04	0	11.03	0.27	12.45	20.98	0.57	0.05	100.78	3VG7-9
51.04	0.79	6.38	0.03	9.91	0.12	11.81	18.43	1.49	0.03	100.04	3VG7-10
50.62	0.93	7.69	0	10.37	0.12	11.44	17.82	1.31	0.06	100.38	3VG7-11
52.20	0.58	4.74	0	10.28	0.11	12.80	18.62	1.13	0.05	100.51	3VG7-12
51.72	0.71	6.08	0	10.04	0.11	12.10	18.42	1.44	0.09	100.73	3VG7-13
50.89	1.11	7.27	0	9.91	0.12	11.64	18.38	1.46	0.06	100.84	3VG7-14
51.33	0.84	6.51	0	9.93	0.12	11.59	18.62	1.36	0.02	100.33	3VG7-15
51.32	0.70	5.65	0	10.27	0.14	12.10	18.61	1.22	0.05	100.08	Average
0.47	0.20	1.17	0.01	0.46	0.05	0.39	0.77	0.25	0.02		Std. Dev.
50.16	0.55	6.92	0.01	10.47	0.14	12.38	17.74	1.09	0.03	99.44	3VG9-1
49.44	0.83	8.04	0	10.98	0.15	11.32	16.42	1.19	0.19	98.36	3VG9-2
50.49	0.45	6.11	0.02	11.85	0.17	12.49	17.16	1.03	0.06	99.85	3VG9-3
49.06	0.82	8.82	0.01	11.77	0.20	11.58	16.38	1.15	0.03	99.76	3VG9-4
49.78	0.66	7.47	0	11.10	0.15	11.81	17.68	1.14	0.06	99.85	3VG9-5
50.29	0.60	7.40	0	10.28	0.14	11.75	18.68	1.24	0.05	100.41	3VG9-6
49.63	0.65	8.06	0.01	10.82	0.13	11.83	17.67	1.06	0.04	99.89	3VG9-7
50.68	0.48	5.82	0.01	11.33	0.23	12.01	19.18	0.86	0.08	100.68	3VG9-8
49.38	0.73	8.83	0.01	10.86	0.14	11.46	17.40	1.24	0.07	100.12	3VG9-9
50.43	0.42	5.70	0.01	10.82	0.16	12.05	19.20	0.92	0.06	99.78	3VG9-10
49.18	0.69	8.94	0.02	11.43	0.15	11.69	16.81	0.95	0.05	99.90	3VG9-11
49.80	0.79	8.04	0.02	10.90	0.14	11.31	18.41	1.19	0.06	100.26	3VG9-12
49.62	0.74	8.06	0.01	10.28	0.13	11.36	17.82	1.27	0.11	100.00	3VG9-13
50.93	0.39	5.08	0.02	10.67	0.18	12.22	19.45	0.79	0.07	99.81	3VG9-14
49.83	0.96	7.97	0.01	13.60	0.21	12.41	14.06	1.16	0.08	100.00	3VG9-15
49.55	0.65	8.01	0.02	10.86	0.16	11.85	17.25	1.23	0.03	99.40	3VG9-16
49.44	0.79	8.11	0.01	10.21	0.13	11.98	18.31	1.12	0.06	99.73	3VG9-17
49.97	0.86	7.28	0.03	10.17	0.12	11.77	18.56	1.18	0.05	99.81	3VG9-18
49.25	0.67	8.64	0.01	11.66	0.18	11.56	16.59	1.07	0.04	99.67	3VG9-19
48.30	0.77	9.27	0.02	13.86	0.21	12.04	14.45	0.99	0.02	99.96	3VG9-20
51.14	0.28	4.07	0	11.07	0.21	12.42	19.45	0.84	0.06	99.34	3VG9-21
50.17	0.88	8.01	0.04	10.84	0.14	11.86	17.05	1.23	0.08	100.08	3VG9-22

SiO_2	TiO_2	Al_2O_3	Cr_2O_3	FeO	MnO	MgO	CaO	Na_2O	K_2O	Total	Sample
50.47	0.61	7.04	0.02	10.63	0.12	12.29	17.75	1.04	0.03	100.02	3VG9-23
49.87	0.63	7.49	0.01	11.13	0.16	11.86	17.84	1.07	0.06	99.83	Average
0.86	0.14	1.34	0.01	0.85	0.03	0.37	1.40	0.16	0.03		Std. Dev.
51.86	0.51	9.13	0.03	9.75	0.11	10.72	16.80	2.23	n.d.	101.16	3VG34-1
52.33	0.60	8.31	0.01	8.71	0.07	10.68	17.43	2.74	n.d.	100.87	3VG34-2
52.26	0.62	8.03	0.02	8.56	0.06	10.44	17.33	2.70	n.d.	100.06	3VG34-3
51.39	0.61	8.42	0.01	9.16	0.09	10.44	16.68	2.63	n.d.	99.83	3VG34-4
51.45	0.69	8.56	0.02	9.70	0.11	10.52	16.66	2.46	n.d.	100.13	3VG34-5
49.54	0.56	10.61	0.02	10.64	0.14	9.99	16.40	2.03	n.d.	99.95	3VG34-6
51.39	0.57	7.87	0.01	9.07	0.06	10.67	16.56	2.43	n.d.	98.62	3VG34-7
51.73	0.64	7.88	0.02	9.52	0.05	10.85	16.80	2.36	n.d.	99.84	3VG34-8
50.33	0.54	7.19	0.01	10.86	0.10	10.56	16.98	1.89	n.d.	98.43	3VG34-9
51.92	0.59	8.33	0.06	9.45	0.11	10.46	16.38	2.70	n.d.	100.02	3VG34-10
51.42	0.62	8.43	0.02	9.54	0.09	10.53	16.82	2.42	-	99.89	Average
0.87	0.06	0.92	0.01	0.75	0.03	0.23	0.35	0.29	-		Std. Dev.
51.61	0.76	7.95	0.03	8.86	0.07	10.57	18.74	2.44	0.01	100.73	3VG35-1
50.78	0.68	8.38	0	9.87	0.12	10.74	17.36	2.20	0.02	100.15	3VG35-2
51.58	0.70	8.25	0.02	8.42	0.09	10.36	18.54	2.54	0.02	100.52	3VG35-3
49.76	0.79	9.90	0.01	10.59	0.14	10.18	17.03	2.02	0.02	100.44	3VG35-4
51.42	0.77	7.90	0.00	8.92	0.08	10.60	18.52	2.19	0.01	100.48	3VG35-5
50.06	1.11	9.75	0.02	8.79	0.10	10.21	18.06	2.38	0.02	100.47	3VG35-6
50.64	0.86	8.84	0.01	9.22	0.10	10.66	17.82	2.28	0	100.43	3VG35-7
51.96	0.76	9.21	0.02	8.10	0.08	9.94	17.73	2.66	0.17	100.62	3VG35-8
49.90	0.94	9.77	0	9.79	0.11	10.30	17.50	2.10	0.02	100.61	3VG35-9
51.28	0.65	7.54	0.03	8.88	0.06	10.79	18.96	2.12	0.03	99.93	3VG35-10
50.91	0.80	8.75	0.01	9.11	0.09	10.44	17.90	2.29	0.03	100.44	Average
0.79	0.14	0.87	0.01	0.76	0.02	0.26	0.56	0.21	0.05		Std. Dev.
50.31	0.99	12.91	0.03	7.84	0.08	9.36	14.14	3.97	0.37	100.01	3VG44-1
52.63	0.76	11.67	0.02	7.26	0.06	8.95	15.16	4.18	0.04	100.74	3VG44-2
51.51	0.58	11.46	0	8.60	0.13	8.94	15.90	3.32	0.03	100.69	3VG44-3
52.35	0.71	11.50	0.01	7.19	0.05	9.22	15.33	4.20	0.01	100.57	3VG44-4
52.13	0.69	10.98	0.01	7.45	0.08	9.17	15.39	3.87	0.06	99.82	3VG44-5
51.02	0.57	11.82	0.01	8.38	0.11	8.83	15.77	3.29	0.07	99.87	3VG44-6
52.23	0.60	10.00	0.03	7.89	0.06	9.90	15.62	3.72	0.02	100.07	3VG44-7
51.27	0.81	11.82	0	7.73	0.07	8.99	15.23	3.76	0.02	99.71	3VG44-8
52.56	0.68	12.27	0.03	7.12	0.08	8.48	15.17	3.69	0.14	100.23	3VG44-9
51.07	0.78	11.88	0.03	8.13	0.06	9.31	15.00	3.59	0.19	100.05	3VG44-10
51.88	0.71	11.94	0.02	7.90	0.10	9.27	15.14	3.80	0.15	100.90	3VG44-11
51.57	0.81	11.81	0.03	7.87	0.07	9.16	15.32	3.81	0.10	100.54	3VG44-12
51.79	0.80	11.78	0.02	7.81	0.07	9.03	15.18	4.00	0.02	100.50	3VG44-13
52.40	0.62	11.14	0.02	7.61	0.09	9.44	15.46	3.91	0.06	100.76	3VG44-14
52.48	0.70	11.28	0.04	7.61	0.12	9.28	15.57	3.94	0.03	101.04	3VG44-15
51.81	0.72	11.62	0.02	7.77	0.08	9.16	15.29	3.80	0.09	100.37	3VG44-16
51.81	0.72	11.62	0.02	7.77	0.08	9.16	15.29	3.80	0.09	100.37	Average
0.66	0.11	0.62	0.01	0.43	0.02	0.31	0.39	0.25	0.09		Std. Dev.
52.72	0.66	9.86	0.02	8.15	0.10	9.96	17.18	3.30	0.01	101.97	3VG41-1
52.10	0.87	10.59	0	7.87	0.06	9.82	17.13	3.45	-0.01	101.92	3VG41-2
51.11	1.17	10.78	0.02	8.57	0.12	9.76	16.45	3.10	0.03	101.11	3VG41-3
51.83	0.66	9.86	0.01	8.14	0.12	10.09	17.07	3.28	0.02	101.07	3VG41-4
52.32	0.65	9.25	0.04	8.04	0.08	10.06	17.07	3.18	0.01	100.68	3VG41-5
51.70	0.78	10.02	0	8.11	0.09	10.27	17.00	3.13	0.02	101.10	3VG41-6
52.51	0.77	10.54	0.01	7.66	0.11	9.61	16.95	3.69	0.01	101.85	3VG41-7
51.99	0.71	10.12	0.01	7.67	0.08	9.98	17.31	3.29	0.01	101.18	3VG41-8
50.69	1.15	11.52	0	8.70	0.09	9.86	15.60	3.03	0.06	100.50	3VG41-9
51.89	0.82	10.28	0.01	8.10	0.10	9.91	16.86	3.27	0.02	101.26	Average
0.65	0.20	0.68	0.01	0.36	0.02	0.22	0.53	0.20	0.02		Std. Dev.
52.82	0.47	10.47	0	6.86	0.06	9.09	16.00	4.58	0.02	100.37	3VG43-1
52.87	0.52	11.43	0.01	7.42	0.10	8.70	15.66	4.21	0.01	100.93	3VG43-2
52.52	0.57	11.67	0.03	6.81	0.07	8.71	15.61	4.59	0.01	100.58	3VG43-3
51.94	0.64	12.20	0	7.72	0.06	8.23	15.41	4.21	0.06	100.35	3VG43-4

SiO_2	TiO_2	Al_2O_3	Cr_2O_3	FeO	MnO	MgO	CaO	Na_2O	K_2O	Total	Sample
52.40	0.48	10.33	0.01	7.45	0.07	9.19	15.92	4.19	0.03	100.07	3VG43-5
53.00	0.33	9.66	0.01	6.45	0.05	9.59	16.41	4.37	0.03	99.89	3VG43-6
52.80	0.49	11.01	0	6.98	0.07	9.09	15.96	4.34	0	100.74	3VG43-7
52.79	0.50	9.96	0.03	7.27	0.07	9.53	16.49	4.01	0	100.66	3VG43-8
52.55	0.49	12.27	0.01	7.08	0.07	8.41	15.36	4.55	0.02	100.80	3VG43-9
53.54	0.34	9.61	0.02	6.77	0.02	9.22	16.40	4.78	0.03	100.73	3VG43-10
52.78	0.32	10.89	0	7.02	0.13	8.69	16.16	4.41	0.01	100.40	3VG43-11
53.64	0.31	8.74	0.03	6.82	0.07	9.95	16.81	4.15	0.04	100.55	3VG43-12
53.80	0.48	10.76	0.01	7.30	0.05	8.80	15.64	4.35	0.02	101.20	3VG43-13
53.55	0.32	10.92	0.01	7.06	0.05	8.81	15.65	4.81	0.01	101.19	3VG43-14
52.22	0.34	12.02	0.01	7.91	0.17	8.02	16.17	4.05	0.03	100.94	3VG43-15
52.88	0.43	10.79	0.01	7.13	0.07	8.94	15.98	4.37	0.02	100.63	Average
0.54	0.09	1.03	0.01	0.39	0.04	0.52	0.43	0.25	0.01		Std. Dev.
53.02	0.55	11.80	0	7.36	0.06	8.71	13.56	4.34	n.a.	99.40	3VG38-1
53.68	0.43	10.88	0	7.26	0.12	9.53	15.22	3.81	n.a.	100.94	3VG38-2
53.15	0.52	10.32	0.02	7.52	0.06	9.08	14.26	4.02	n.a.	98.95	3VG38-3
53.19	0.57	10.13	0	7.25	0.10	9.76	14.32	4.17	n.a.	99.48	3VG38-4
53.16	0.74	11.26	0	7.10	0.09	9.53	14.08	4.05	n.a.	100.01	3VG38-5
54.12	0.43	9.41	0	7.03	0.08	9.57	15.88	3.82	n.a.	100.32	3VG38-6
53.17	0.48	10.07	0	6.78	0.12	9.30	15.68	4.00	n.a.	99.60	3VG38-7
50.97	0.51	15.02	0.02	7.77	0.12	7.39	13.45	3.79	n.a.	99.04	3VG38-8
52.37	0.46	12.23	0.01	7.25	0.13	7.85	14.02	3.81	n.a.	98.13	3VG38-9
52.98	0.52	11.24	0.01	7.26	0.10	8.97	14.50	3.98	n.d.	99.54	Average
0.89	0.10	1.68	0.01	0.28	0.03	0.83	0.89	0.19	n.d.		Std. Dev.
53.50	0.47	9.45	0.03	7.66	0.10	9.64	16.56	3.42	0.01	100.83	3VG45-1
53.15	0.63	10.23	0	7.27	0.12	9.25	16.50	3.64	0.01	100.80	3VG45-2
51.62	0.96	11.68	0.03	8.59	0.12	8.91	14.79	3.48	0.02	100.20	3VG45-3
53.02	0.52	9.75	0.02	7.17	0.08	9.38	16.79	3.54	0.02	100.30	3VG45-4
53.28	0.66	10.81	0	7.49	0.09	9.10	16.05	3.77	0	101.25	3VG45-5
53.38	0.44	8.61	0.02	7.37	0.07	9.69	17.30	3.48	0.01	100.38	3VG45-6
53.49	0.39	8.67	0.02	7.52	0.10	9.69	16.95	3.31	0.02	100.15	3VG45-7
52.84	0.65	9.99	0.02	7.13	0.10	8.89	16.46	3.71	0.05	99.82	3VG45-8
52.62	0.49	9.53	0.01	7.67	0.10	9.46	16.19	3.41	0.04	99.51	3VG45-9
52.51	0.41	9.49	0	7.69	0.08	9.26	16.53	3.45	0.03	99.44	3VG45-10
53.25	0.46	9.17	0	7.26	0.08	9.36	16.63	3.53	0.02	99.75	3VG45-11
51.99	0.68	10.59	0.06	8.08	0.09	9.32	15.91	3.52	0.05	100.28	3VG45-12
52.76	0.50	9.08	0	7.38	0.10	9.56	17.01	3.56	0.02	99.98	3VG45-13
52.84	0.65	11.06	0	6.98	0.07	8.95	16.05	3.93	0.03	100.55	3VG45-14
52.75	0.61	9.56	0.01	7.22	0.08	9.31	16.80	3.57	0.01	99.92	3VG45-15
53.22	0.47	9.15	0.02	7.30	0.07	9.67	16.96	3.43	0.04	100.32	3VG45-16
53.23	0.48	9.00	0.02	7.44	0.10	9.94	17.03	3.49	0.02	100.74	3VG45-17
53.43	0.46	9.06	0.01	7.26	0.09	9.56	17.07	3.55	0.03	100.52	3VG45-18
52.72	0.59	11.54	0.01	8.06	0.08	8.89	15.34	3.74	0.02	100.99	3VG45-19
52.93	0.55	9.81	0.01	7.50	0.09	9.36	16.47	3.55	0.02	100.30	Average
0.50	0.13	0.93	0.01	0.39	0.02	0.31	0.63	0.15	0.01		Std. Dev.
51.32	0.70	10.16	0	8.89	0.10	10.01	16.30	2.98	0.04	100.49	3VG46-1
51.54	0.78	10.91	0	8.82	0.10	9.86	16.19	3.00	0.05	101.24	3VG46-2
52.63	0.53	9.15	0.04	8.24	0.12	10.24	16.94	2.80	0.03	100.72	3VG46-3
51.30	0.78	9.64	0	8.60	0.15	10.19	16.80	2.89	0.04	100.38	3VG46-4
51.85	0.60	9.29	0.01	8.34	0.10	10.27	17.36	2.69	0.03	100.52	3VG46-5
51.98	0.56	9.49	0.02	8.39	0.13	10.25	16.83	2.81	0.03	100.48	3VG46-6
51.96	0.55	9.35	0.01	8.06	0.12	10.22	16.84	2.97	0.01	100.08	3VG46-7
51.48	0.75	10.71	0	8.73	0.13	9.79	16.26	2.96	0.04	100.86	3VG46-8
52.82	0.62	9.54	0.02	7.80	0.10	10.07	17.05	3.16	0.02	101.19	3VG46-9
52.45	0.56	8.41	0	8.46	0.12	10.68	17.36	2.73	0.02	100.78	3VG46-10
52.64	0.54	8.48	0	8.33	0.14	10.70	17.52	2.71	0.02	101.07	3VG46-11
52.00	0.63	9.56	0.01	8.42	0.12	10.21	16.86	2.88	0.03	100.71	Average
0.56	0.10	0.79	0.01	0.33	0.02	0.29	0.46	0.15	0.01		Std. Dev.
51.30	0.26	2.57	0.01	12.01	0.28	11.23	21.94	0.71	0	100.31	KAP12-1
50.37	0.57	3.17	0.05	11.91	0.39	10.88	19.67	2.12	0.02	99.16	KAP12-2
52.04	0.19	1.97	0.02	11.56	0.42	11.53	21.89	0.71	0.02	100.34	KAP12-3

SiO_2	TiO_2	Al_2O_3	Cr_2O_3	FeO	MnO	MgO	CaO	Na_2O	K_2O	Total	Sample
51.24	0.34	2.57	0.03	11.82	0.36	11.21	21.16	1.18	0.01	99.93	Average
0.84	0.21	0.60	0.02	0.23	0.07	0.33	1.29	0.81	0.01		Std. Dev.
50.15	0.35	3.26	0.05	12.82	0.35	10.16	21.36	0.75	0.01	99.25	KAP1-1
50.47	0.23	2.60	0.06	12.07	0.30	10.57	22.08	0.64	0.02	99.03	KAP1-2
51.09	0.31	2.93	0.04	12.87	0.35	10.37	20.70	0.71	0.02	99.40	KAP1-3
51.36	0.29	2.51	0.06	11.48	0.29	10.82	21.68	0.64	0.01	99.13	KAP1-4
50.46	0.27	2.82	0.06	12.37	0.31	10.29	22.07	0.75	0.02	99.42	KAP1-5
50.85	0.23	2.50	0.04	12.21	0.33	10.57	22.25	0.61	0	99.59	KAP1-6
51.23	0.22	2.61	0.03	12.25	0.34	10.62	21.89	0.63	0	99.81	KAP1-7
51.29	0.26	2.89	0.02	12.14	0.28	10.40	21.74	0.75	0	99.76	KAP1-8
50.95	0.29	2.69	0.02	12.07	0.35	10.51	21.95	0.65	0.01	99.49	KAP1-9
50.91	0.26	2.70	0.00	12.08	0.38	10.69	21.71	0.66	0.01	99.42	KAP1-10
50.88	0.27	2.75	0.04	12.24	0.33	10.50	21.74	0.68	0.01	99.43	Average
0.40	0.04	0.23	0.02	0.40	0.03	0.20	0.44	0.06	0.01		Std. Dev.
50.95	0.33	3.23	0.08	13.15	0.35	10.96	19.86	1.04	0.06	100.00	KAP27-1
52.14	0.23	1.78	0.18	13.28	0.51	12.46	18.45	0.94	0.03	100.00	KAP27-2
51.36	0.13	2.67	0.08	11.71	0.41	11.10	21.96	0.57	0.02	100.00	KAP27-3
52.40	0.00	0.87	0.01	11.12	0.41	12.22	22.48	0.45	0.04	100.00	KAP27-4
52.94	0.00	0.83	0.12	10.95	0.36	12.00	22.31	0.46	0.04	100.00	KAP27-5
51.28	0.16	2.58	0.12	11.99	0.31	10.85	22.02	0.66	0.04	100.00	KAP27-6
51.34	0.45	3.28	0.14	13.24	0.33	10.15	18.72	2.32	0.04	100.00	KAP27-7
51.23	0.20	2.63	0.13	12.28	0.33	10.62	21.79	0.76	0.04	100.00	KAP27-8
51.88	0.07	2.10	0	11.92	0.32	11.24	21.66	0.76	0.04	100.00	KAP27-9
51.04	0.16	2.75	0.14	12.67	0.35	10.69	21.44	0.71	0.03	100.00	KAP27-10
51.45	0.14	2.19	0.09	12.04	0.28	11.22	21.93	0.63	0.03	100.00	KAP27-11
52.00	0.07	1.88	0	11.41	0.28	11.59	22.19	0.54	0.05	100.00	KAP27-12
51.59	0.20	2.48	0.07	11.59	0.23	11.19	21.96	0.65	0.04	100.00	KAP27-13
51.29	0.16	2.46	0.00	12.07	0.32	11.01	21.94	0.72	0.04	100.00	KAP27-14
51.57	0.15	2.13	0.19	11.60	0.32	11.14	22.29	0.56	0.04	100.00	KAP27-15
51.69	0.14	2.13	0	11.73	0.32	11.25	22.13	0.56	0.05	100.00	KAP27-16
52.10	0.16	2.15	0.04	11.27	0.24	11.54	21.80	0.66	0.03	100.00	KAP27-17
51.80	0.17	1.90	0	11.69	0.28	11.52	21.93	0.68	0.04	100.00	KAP27-18
51.67	0.16	2.22	0.08	11.98	0.33	11.26	21.49	0.76	0.04	100.00	Average
0.51	0.10	0.65	0.07	0.70	0.07	0.57	1.20	0.42	0.01		Std. Dev.
50.33	0.45	3.74	0	13.52	0.37	11.70	18.78	1.05	0.05	100.00	KAP26-1
51.16	0.22	2.54	0.19	12.35	0.32	10.93	21.59	0.68	0.02	100.00	KAP26-2
51.37	0.22	2.49	0	11.65	0.38	11.31	21.84	0.71	0.04	100.00	KAP26-3
50.56	0.43	3.27	0.16	14.32	0.49	12.62	17.28	0.82	0.04	100.00	KAP26-4
50.64	0.30	2.91	0.11	12.71	0.35	10.51	21.72	0.72	0.03	100.00	KAP26-5
51.03	0.32	3.24	0.08	12.47	0.31	10.98	20.65	0.85	0.07	100.00	KAP26-6
51.36	0.18	2.27	0.14	11.58	0.31	11.22	22.24	0.65	0.05	100.00	KAP26-7
50.80	0.25	2.65	0.43	12.34	0.33	11.13	21.39	0.64	0.05	100.00	KAP26-8
51.08	0.26	2.48	0.18	12.00	0.24	11.22	21.87	0.66	0.03	100.00	KAP26-9
50.96	0.30	2.99	0.02	12.74	0.36	11.21	20.29	1.10	0.02	100.00	KAP26-10
51.25	0.18	2.25	0	12.18	0.35	11.83	21.28	0.64	0.03	100.00	KAP26-11
50.85	0.38	3.87	0	13.51	0.40	11.63	18.09	1.17	0.10	100.00	KAP26-12
50.86	0.18	2.71	0.01	12.84	0.33	10.71	21.69	0.65	0.03	100.00	KAP26-13
51.08	0.20	2.56	0	12.41	0.34	11.06	21.59	0.72	0.02	100.00	KAP26-14
50.74	0.27	2.82	0	12.73	0.40	11.12	21.22	0.67	0.04	100.00	KAP26-15
51.59	0.22	2.41	0.05	12.04	0.27	11.70	21.09	0.60	0.02	100.00	KAP26-16
50.57	0.30	3.18	0.05	12.84	0.38	11.38	20.56	0.72	0.02	100.00	KAP26-17
51.54	0.07	1.85	0	11.77	0.34	11.66	22.24	0.51	0.02	100.00	KAP26-18
51.17	0.18	2.49	0.07	11.88	0.33	11.25	21.95	0.68	0.02	100.00	KAP26-19
50.94	0.27	3.21	0	12.47	0.39	11.23	20.71	0.77	0.03	100.00	KAP26-20
50.53	0.42	3.46	0.04	13.74	0.45	12.32	18.31	0.70	0.04	100.00	KAP26-21
51.03	0.14	2.39	0.04	12.16	0.33	11.13	22.09	0.69	0.01	100.00	KAP26-22
50.97	0.26	2.81	0.07	12.56	0.35	11.36	20.84	0.74	0.04	100.00	Average
0.34	0.10	0.51	0.10	0.71	0.05	0.48	1.44	0.16	0.02		Std. Dev.
51.05	0.53	3.88	0	13.17	0.40	11.37	19.78	0.53	0.03	100.73	KAP14-1
50.67	0.60	4.13	0.01	13.88	0.42	12.89	17.45	0.51	0.01	100.56	KAP14-2
50.47	0.63	4.65	0.01	12.34	0.40	13.14	18.21	0.49	0.02	100.34	KAP14-3
50.46	0.68	4.75	0.02	12.37	0.42	13.12	17.63	0.46	0.04	99.95	KAP14-4
49.92	0.72	5.05	0.01	13.09	0.40	12.78	18.06	0.56	0.05	100.63	KAP14-5

SiO_2	TiO_2	Al_2O_3	Cr_2O_3	FeO	MnO	MgO	CaO	Na_2O	K_2O	Total	Sample
50.59	0.60	4.02	0.03	13.09	0.44	13.03	17.85	0.56	0.03	100.14	KAP14-6
50.22	0.62	4.58	0.02	13.13	0.45	13.27	17.28	0.50	0.04	100.10	KAP14-7
50.03	0.72	4.77	0.05	13.10	0.42	12.41	18.10	0.53	0.01	100.14	KAP14-8
50.84	0.54	3.79	0.02	13.26	0.45	13.22	17.09	0.45	0.02	99.69	KAP14-9
50.49	0.67	4.57	0.03	12.92	0.39	12.57	18.13	0.49	0.03	100.29	KAP14-10
50.47	0.62	4.42	0.02	13.03	0.42	12.78	17.96	0.51	0.03	100.26	Average
0.35	0.08	0.43	0.01	0.44	0.02	0.57	0.75	0.04	0.01		Std. Dev.
51.66	0.23	2.12	0.02	10.47	0.35	11.53	21.94	0.61	0	98.93	KAP10-1
51.26	0.25	2.65	0.02	11.60	0.29	10.62	22.01	0.60	0	99.28	KAP10-2
50.93	0.26	2.76	0.03	11.98	0.34	10.28	21.85	0.64	0	99.06	KAP10-3
51.04	0.28	2.80	0.02	12.16	0.33	10.32	21.68	0.67	0	99.30	KAP10-4
50.94	0.29	3.14	0.03	13.01	0.46	12.49	18.26	0.47	0.01	99.10	KAP10-5
50.94	0.35	3.12	0.04	12.40	0.34	10.19	21.52	0.68	0	99.58	KAP10-6
52.44	0.08	1.25	0	11.04	0.38	11.47	22.30	0.52	0	99.49	KAP10-7
51.54	0.23	2.23	0.02	11.59	0.33	10.80	22.06	0.62	0	99.41	KAP10-8
51.56	0.21	2.31	0.03	11.53	0.28	10.87	21.97	0.60	0.01	99.35	KAP10-9
52.66	0.07	1.03	0.02	10.64	0.36	11.72	22.38	0.41	0	99.30	KAP10-10
51.14	0.28	2.91	0.03	11.78	0.35	10.35	21.91	0.74	0	99.47	KAP10-11
51.07	0.29	2.74	0.03	11.89	0.33	10.53	21.62	0.71	0.01	99.21	KAP10-12
51.02	0.28	2.73	0.03	11.85	0.32	10.34	21.91	0.68	0	99.16	KAP10-13
50.43	0.27	2.87	0.03	12.19	0.34	10.40	21.86	0.62	0	99.01	KAP10-14
51.38	0.30	2.66	0.03	11.72	0.39	10.65	21.94	0.66	0	99.73	KAP10-15
51.91	0.22	2.34	0.02	11.49	0.31	10.87	22.29	0.55	0	99.99	KAP10-16
51.65	0.18	2.21	0.01	11.42	0.30	10.77	22.08	0.65	0	99.27	KAP10-17
51.57	0.23	2.35	0.01	11.40	0.37	10.85	21.84	0.57	0	99.19	KAP10-18
51.61	0.26	2.61	0.05	11.65	0.26	10.71	22.10	0.59	0.01	99.84	KAP10-19
51.22	0.29	2.68	0.04	11.75	0.27	10.64	21.92	0.57	0	99.37	KAP10-20
51.69	0.26	2.25	0.03	11.23	0.35	10.92	22.07	0.55	0.01	99.38	KAP10-21
51.41	0.24	2.46	0.02	11.66	0.33	10.82	21.79	0.61	0	99.35	Average
0.52	0.07	0.53	0.01	0.56	0.05	0.56	0.84	0.08	0		Std. Dev.
52.32	0.02	1.06	0.04	11.00	0.30	11.76	22.91	0.49	0.00	99.90	KAP6-1
50.50	0.24	2.91	0.03	12.56	0.33	10.23	21.65	0.67	0.00	99.11	KAP6-2
50.82	0.25	2.90	0.04	12.58	0.32	10.30	21.62	0.66	0.00	99.47	KAP6-3
51.40	0.21	2.23	0.03	11.47	0.37	10.96	22.25	0.68	0.00	99.58	KAP6-4
51.31	0.23	2.33	0.01	11.40	0.32	10.76	22.39	0.63	0.01	99.39	KAP6-5
51.26	0.25	2.41	0.03	11.55	0.31	10.65	22.15	0.65	0.00	99.26	KAP6-6
51.26	0.18	2.36	0.03	12.05	0.27	10.69	22.09	0.62	0.00	99.56	KAP6-7
51.47	0.09	2.74	0.02	11.55	0.33	10.68	21.63	0.88	0.00	99.39	KAP6-8
51.59	0.13	2.87	0.04	11.76	0.33	10.69	21.33	0.83	0.00	99.55	KAP6-9
50.91	0.31	2.75	0.01	12.41	0.30	10.42	22.02	0.64	0.01	99.77	KAP6-10
51.37	0.15	2.04	0.03	11.03	0.28	11.19	22.82	0.60	0.00	99.51	KAP6-11
51.49	0.17	2.29	0.01	11.68	0.38	11.05	22.11	0.67	0.00	99.86	KAP6-12
51.19	0.18	2.57	0.01	11.86	0.36	10.80	21.88	0.76	0.00	99.61	KAP6-13
50.66	0.29	3.15	0.02	12.51	0.31	10.19	21.88	0.69	0.00	99.68	KAP6-14
50.88	0.23	2.84	0.04	12.19	0.32	10.57	21.80	0.70	0.01	99.58	KAP6-15
51.36	0.16	2.08	0.03	11.56	0.28	10.92	22.32	0.64	0.01	99.36	KAP6-16
51.41	0.20	2.35	0.01	11.67	0.30	10.67	22.22	0.64	0.02	99.47	KAP6-17
51.07	0.24	2.48	0.04	11.85	0.36	10.64	21.94	0.67	0.02	99.30	KAP6-18
51.37	0.20	2.62	0.04	11.65	0.39	10.77	21.77	0.66	0.01	99.47	KAP6-19
51.45	0.14	1.65	0.01	10.52	0.32	11.62	22.99	0.48	0.01	99.17	KAP6-20
50.86	0.29	2.88	0.02	12.43	0.30	10.31	21.86	0.71	0.01	99.67	KAP6-21
51.24	0.16	2.57	0.02	12.39	0.30	10.47	21.55	0.63	0.00	99.32	KAP6-22
51.24	0.20	2.46	0.03	11.80	0.32	10.74	22.05	0.66	0.00	99.50	Average
0.38	0.07	0.47	0.01	0.55	0.03	0.40	0.44	0.09	0.01		Std. Dev.
51.29	0.22	2.43	0.04	11.91	0.36	10.80	22.79	0.65	0.02	100.51	KAP19-1
51.14	0.28	2.63	0.03	11.70	0.25	10.84	22.16	0.57	0	99.60	KAP19-2
52.34	0.16	1.83	0	11.27	0.26	11.41	22.42	0.58	0	100.28	KAP19-3
52.05	0.19	1.82	0.02	11.13	0.30	11.56	22.54	0.59	0.01	100.20	KAP19-4
51.71	0.21	2.18	0.02	11.50	0.29	11.15	22.48	0.60	0.01	100.15	Average
0.58	0.05	0.41	0.02	0.36	0.05	0.39	0.26	0.04	0.01		Std. Dev.
51.19	0.25	2.38	0.01	11.57	0.39	11.23	22.09	0.51	0.04	99.67	KAP16-1
51.40	0.14	1.77	0.02	10.78	0.39	11.84	21.66	0.45	0.08	98.53	KAP16-2

SiO_2	TiO_2	Al_2O_3	Cr_2O_3	FeO	MnO	MgO	CaO	Na_2O	K_2O	Total	Sample
51.57	0.21	2.32	0.01	11.79	0.28	11.20	21.80	0.61	0.04	99.83	KAP16-3
52.01	0.12	1.51	0	10.80	0.38	11.91	22.27	0.58	0.02	99.58	KAP16-4
50.07	0.39	6.17	0.03	12.10	0.28	9.67	18.69	1.02	0.09	98.49	KAP16-5
49.47	0.32	3.11	0.01	12.08	0.33	10.27	21.29	0.74	0.06	97.68	KAP16-6
50.87	0.29	2.77	0.03	12.25	0.39	10.79	21.79	0.61	0.03	99.81	KAP16-7
50.54	0.35	3.96	0.03	12.65	0.33	10.57	20.58	0.71	0.04	99.75	KAP16-8
51.04	0.25	2.60	0.03	11.99	0.36	11.16	21.91	0.67	0.03	100.03	KAP16-9
50.26	0.28	2.81	0.02	12.12	0.31	10.79	21.53	0.69	0.05	98.86	KAP16-10
51.32	0.25	2.32	0	11.42	0.29	11.22	22.36	0.58	0.03	99.80	KAP16-11
50.85	0.30	2.72	0.03	10.84	0.28	11.59	22.68	0.53	0.04	99.85	KAP16-12
50.76	0.27	3.06	0.03	12.33	0.34	10.72	21.46	0.67	0.04	99.68	KAP16-13
51.30	0.21	2.25	0.02	11.37	0.38	11.32	22.26	0.56	0.04	99.70	KAP16-14
51.81	0.16	1.78	0.01	11.25	0.30	11.77	22.34	0.48	0.05	99.94	KAP16-15
50.96	0.25	2.77	0.02	11.69	0.34	11.07	21.65	0.63	0.04	99.41	Average
0.68	0.08	1.12	0.01	0.60	0.04	0.62	0.97	0.14	0.02		Std. Dev.
50.09	0.39	3.71	0.01	12.45	0.29	11.01	20.48	0.63	0.05	99.09	KAP15-1
51.66	0.23	2.41	0.03	11.75	0.26	11.54	21.67	0.63	0.06	100.24	KAP15-2
50.00	0.71	5.46	0.05	12.34	0.11	10.88	19.27	0.92	0.02	99.76	KAP15-3
50.90	0.24	2.54	0.01	11.82	0.32	11.19	21.87	0.68	0.02	99.58	KAP15-4
51.04	0.20	2.74	0	12.15	0.35	11.05	21.56	0.65	0.02	99.76	KAP15-5
51.36	0.23	2.67	0.03	11.72	0.29	11.37	21.65	0.63	0.03	99.97	KAP15-6
51.40	0.23	2.32	0.03	11.25	0.22	11.58	22.33	0.64	0.02	100.01	KAP15-7
51.20	0.27	2.68	0.02	11.88	0.39	11.29	22.35	0.64	0.04	100.74	KAP15-8
51.05	0.42	3.61	0.03	13.65	0.21	12.02	18.74	0.65	0.03	100.40	KAP15-9
51.90	0.20	2.21	0.02	10.36	0.26	12.23	22.54	0.55	0.04	100.30	KAP15-10
52.49	0.11	1.40	0.02	10.81	0.39	12.28	22.17	0.50	0.04	100.21	KAP15-11
51.23	0.39	3.05	0.02	11.69	0.30	11.45	22.24	0.62	0.06	101.04	KAP15-12
50.75	0.30	3.25	0.03	12.47	0.34	10.88	21.88	0.64	0.04	100.57	KAP15-13
50.87	0.26	2.67	0.01	12.22	0.39	11.16	22.61	0.57	0.02	100.79	KAP15-14
51.14	0.30	2.91	0.02	11.90	0.29	11.42	21.53	0.64	0.04	100.18	Average
0.65	0.15	0.94	0.01	0.79	0.08	0.47	1.20	0.09	0.01		Std. Dev.
47.80	0.98	8.56	0.06	14.12	0.23	9.62	17.48	1.17	0.04	100.06	KAP18-1
50.01	0.41	3.87	0.05	12.92	0.32	10.78	20.23	0.80	0.02	99.39	KAP18-2
51.52	0.32	2.82	0.01	12.04	0.39	10.65	21.64	0.72	0.02	100.12	KAP18-3
51.46	0.22	2.38	0.02	11.72	0.32	10.93	22.06	0.60	0.02	99.72	KAP18-4
47.94	0.85	7.17	0.02	14.11	0.32	10.03	18.51	0.91	0.03	99.89	KAP18-5
47.88	0.96	7.46	0.04	13.54	0.18	10.09	18.17	1.17	0.02	99.51	KAP18-6
49.37	0.46	5.16	0.04	12.94	0.24	10.19	19.72	0.93	0.04	99.10	KAP18-7
51.55	0.30	3.11	0.01	11.62	0.36	10.88	21.95	0.66	0.04	100.47	KAP18-8
50.88	0.28	2.70	0.02	11.95	0.34	10.70	21.96	0.65	0.01	99.49	KAP18-9
51.37	0.20	2.20	0.04	11.39	0.34	11.25	22.40	0.55	0.02	99.77	KAP18-10
51.58	0.18	2.39	0.02	11.36	0.33	11.49	22.09	0.75	0.03	100.23	KAP18-11
49.05	0.82	6.62	0.04	13.65	0.26	10.03	18.17	1.32	0.07	100.03	KAP18-12
48.39	0.92	7.68	0.05	13.47	0.25	10.29	17.89	1.18	0.05	100.18	KAP18-13
49.33	0.86	6.34	0.04	13.05	0.26	10.21	18.92	1.16	0.03	100.19	KAP18-14
48.71	0.91	7.29	0.04	13.13	0.21	10.39	18.40	1.17	0.07	100.31	KAP18-15
51.05	0.24	2.90	0.03	12.17	0.38	10.66	21.89	0.69	0.03	100.04	KAP18-16
49.46	0.73	6.22	0.04	12.84	0.19	10.99	18.49	1.05	0.02	100.03	KAP18-17
47.03	1.88	7.85	0.06	14.26	0.24	10.11	17.53	1.21	0.04	100.19	KAP18-18
49.11	0.81	7.00	0.08	13.23	0.18	10.77	17.82	1.23	0.05	100.28	KAP18-19
47.15	0.98	8.37	0.03	14.36	0.26	9.98	17.28	1.15	0.04	99.58	KAP18-20
49.53	0.67	5.40	0.04	12.89	0.28	10.50	19.63	0.95	0.03	99.93	Average
1.56	0.42	2.33	0.02	0.98	0.07	0.48	1.91	0.25	0.01		Std. Dev.
51.26	0.20	3.03	0	12.80	0.32	10.49	21.19	0.71	0.01	100.00	KAP28-1
51.07	0.24	2.81	0	12.80	0.33	10.46	21.58	0.68	0.04	100.00	KAP28-2
51.58	0.18	2.58	0	12.23	0.25	10.80	21.69	0.67	0.03	100.00	KAP28-3
51.92	0.11	2.10	0	11.44	0.38	11.54	21.96	0.52	0.03	100.00	KAP28-4
51.55	0.16	2.62	0	12.12	0.26	11.02	21.63	0.63	0.02	100.00	KAP28-5
51.42	0.19	2.62	0	12.33	0.32	10.96	21.49	0.62	0.05	100.00	KAP28-6
51.36	0.25	2.83	0	12.62	0.28	10.67	21.30	0.65	0.05	100.00	KAP28-7
51.27	0.29	2.94	0	13.03	0.34	10.37	21.05	0.69	0.02	100.00	KAP28-8
51.49	0.15	2.14	0	12.20	0.33	11.21	21.65	0.60	0.04	100.00	KAP28-9
51.44	0.20	2.63	0	12.40	0.31	10.83	21.53	0.64	0.03	100.00	Average

SiO_2	TiO_2	Al_2O_3	Cr_2O_3	FeO	MnO	MgO	CaO	Na_2O	K_2O	Total	Sample
0.24	0.06	0.33	0	0.48	0.04	0.39	0.30	0.06	0.01		Std. Dev.
51.52	0.24	2.18	0.04	10.83	0.31	11.53	22.80	0.56	0.03	100.03	KAP29-1
50.77	0.45	4.56	0.04	11.75	0.18	10.12	20.18	1.03	0.08	99.15	KAP29-2
51.02	0.23	2.82	0.02	11.68	0.30	10.61	21.97	0.60	0.03	99.28	KAP29-3
50.62	0.41	3.73	0.03	12.33	0.37	10.34	21.64	0.80	0.01	100.29	KAP29-4
51.32	0.26	2.45	0.02	11.34	0.37	11.15	22.16	0.67	0	99.73	KAP29-5
51.85	0.15	1.91	0.01	11.25	0.32	11.46	22.47	0.62	0.04	100.08	KAP29-6
49.00	0.71	6.40	0.02	12.75	0.23	9.73	19.49	1.26	0.17	99.75	KAP29-7
50.87	0.35	3.44	0.02	11.70	0.30	10.71	21.53	0.79	0.05	99.76	Average
0.93	0.19	1.60	0.01	0.66	0.07	0.69	1.23	0.26	0.06		Std. Dev.
50.01	0.65	6.03	0.04	10.85	0.12	10.44	19.53	1.63	0.04	99.34	KAP8-1
49.98	0.73	6.46	0.04	10.68	0.08	10.75	19.28	1.45	0.04	99.49	KAP8-2
50.34	0.60	5.72	0.05	11.41	0.12	11.17	19.00	1.36	0.04	99.79	KAP8-3
50.24	0.53	5.79	0.04	10.43	0.11	11.18	19.69	1.52	0.04	99.58	KAP8-4
50.05	0.77	6.46	0.07	11.71	0.11	10.51	18.98	1.40	0.01	100.07	KAP8-5
50.37	0.55	5.55	0.05	10.77	0.10	11.13	19.18	1.55	0.11	99.35	KAP8-6
51.04	0.60	5.27	0.04	11.25	0.12	11.13	19.25	1.62	0.03	100.35	KAP8-7
50.83	0.64	5.74	0.05	10.91	0.11	10.94	19.01	1.67	0.04	99.93	KAP8-8
50.23	0.63	6.17	0.04	11.08	0.10	10.89	18.86	1.55	0.03	99.57	KAP8-9
50.34	0.63	5.91	0.05	11.01	0.11	10.90	19.20	1.53	0.04	99.72	Average
0.37	0.08	0.40	0.01	0.40	0.01	0.28	0:27	0.11	0.03		Std. Dev.
50.48	1.05	7.20	0.04	10.58	0.09	10.59	18.93	1.58	0.02	100.56	KAP7-1
50.17	1.10	7.84	0.04	10.82	0.12	10.13	18.51	1.71	0.04	100.48	KAP7-2
49.54	1.00	7.23	0.01	10.62	0.10	10.53	18.74	1.52	0.03	99.33	KAP7-3
49.64	0.98	8.29	0.06	10.36	0.10	10.18	18.75	1.58	0.06	99.99	KAP7-4
49.81	0.93	7.35	0.03	11.22	0.10	10.58	18.61	1.49	0.04	100.17	KAP7-5
50.03	0.72	6.55	0.04	11.13	0.11	10.86	18.21	1.45	0.02	99.15	KAP7-6
49.70	0.74	6.02	0.05	11.64	0.10	10.79	18.80	1.50	0.02	99.37	KAP7-7
49.51	0.98	7.82	0	10.79	0.08	10.21	18.67	1.58	0.03	99.67	KAP7-8
49.86	0.80	6.97	0.03	10.81	0.10	10.41	18.84	1.76	0.04	99.62	KAP7-9
48.38	1.35	8.40	0.04	11.20	0.11	9.99	18.77	1.50	0.03	99.76	KAP7-10
49.63	0.98	7.14	0.05	10.42	0.09	10.46	19.10	1.37	0.03	99.27	KAP7-11
49.87	0.93	6.61	0.02	10.73	0.11	10.31	19.04	1.52	0.04	99.15	KAP7-12
49.72	0.96	7.28	0.03	10.86	0.10	10.42	18.75	1.55	0.03	99.71	Average
0.51	0.17	0.71	0.02	0.37	0.01	0.27	0.24	0.11	0.01		Std. Dev.
46.26	1.42	10.38	0.07	12.28	0.15	9.35	17.63	1.51	0.03	99.08	KAP9-1
47.71	1.41	9.44	0.05	11.06	0.14	9.68	18.79	1.41	0.03	99.74	KAP9-2
47.77	1.15	8.38	0.04	11.44	0.15	10.16	18.63	1.33	0.02	99.07	KAP9-3
45.75	1.29	10.85	0.04	13.89	0.23	9.60	16.37	1.13	0.03	99.20	KAP9-4
46.91	1.19	9.88	0.07	13.02	0.20	9.79	16.99	1.30	0.04	99.40	KAP9-5
47.52	1.28	9.35	0.05	11.99	0.14	9.81	17.99	1.43	0.02	99.58	KAP9-6
46.63	1.18	9.56	0.03	13.52	0.20	10.09	16.67	1.32	0.05	99.26	KAP9-7
46.60	1.15	9.74	0.06	13.00	0.18	9.78	17.33	1.18	0.02	99.03	KAP9-8
48.66	1.09	8.36	0.03	11.70	0.16	10.57	18.12	1.44	0.04	100.17	KAP9-9
48.12	1.22	8.85	0.04	11.40	0.14	10.04	18.17	1.38	0.06	99.42	KAP9-10
46.42	1.53	10.78	0.02	12.28	0.15	9.33	17.53	1.43	0.05	99.53	KAP9-11
47.69	1.11	9.52	0.04	13.04	0.18	9.99	16.79	1.21	0.04	99.60	KAP9-12
47.17	1.25	9.59	0.04	12.39	0.17	9.85	17.58	1.34	0.04	99.42	Average
0.87	0.14	0.82	0.01	0.90	0.03	0.35	0.78	0.12	0.01		Std. Dev.
51.06	0.91	8.40	0.02	9.76	0.13	9.20	18.40	2.52	0.07	100.46	KAP35-1
48.96	1.45	9.82	0.05	11.87	0.16	9.30	16.15	2.32	0.42	100.48	KAP35-2
50.71	0.86	8.50	0.04	10.23	0.10	9.30	18.35	2.55	0.05	100.69	KAP35-3
50.32	0.80	7.50	0.02	11.07	0.17	9.35	18.87	2.04	0.04	100.17	KAP35-4
49.88	0.93	8.44	0.03	12.16	0.13	9.26	17.17	2.12	0.01	100.14	KAP35-5
51.59	0.87	8.28	0.03	10.23	0.11	9.27	17.98	2.34	0.04	100.73	KAP35-6
51.77	0.80	7.72	0.06	10.41	0.13	9.73	18.11	2.51	0.03	101.25	KAP35-7
50.73	0.85	8.20	0.04	11.04	0.17	9.39	17.98	2.31	0.05	100.75	KAP35-8
49.76	1.07	9.31	0.02	11.32	0.11	9.15	17.73	2.21	0.04	100.71	KAP35-9
51.56	0.80	7.87	0.04	9.84	0.14	9.51	18.84	2.36	0.03	100.98	KAP35-10
51.05	0.79	7.58	0.01	10.66	0.11	9.23	18.72	2.14	0.06	100.34	KAP35-11
50.56	0.90	8.42	0.02	10.48	0.11	9.24	18.17	2.36	0	100.25	KAP35-12

SiO_2	TiO_2	Al_2O_3	Cr_2O_3	FeO	MnO	MgO	CaO	Na_2O	K_2O	Total	Sample
50.91	0.74	8.32	0	10.58	0.10	8.75	17.71	2.22	0.14	99.48	KAP35-13
49.92	1.12	9.46	0.03	10.52	0.16	8.51	18.14	2.35	0.03	100.24	KAP35-14
49.99	0.93	8.77	0.02	11.81	0.17	8.92	17.49	2.01	0.02	100.13	KAP35-15
50.34	1.16	9.46	0.05	10.49	0.13	8.87	17.88	2.60	0.02	100.98	KAP35-16
49.96	1.10	9.32	0.07	10.74	0.13	8.92	17.85	2.65	0.03	100.76	KAP35-17
50.89	0.81	7.48	0.04	10.33	0.10	9.56	18.26	2.36	0.04	99.85	KAP35-18
50.55	0.94	8.49	0.03	10.75	0.13	9.19	17.99	2.33	0.06	100.47	Average
0.73	0.18	0.73	0.02	0.67	0.03	0.30	0.64	0.18	0.09		Std. Dev.
53.27	0.38	9.12	0.05	7.88	0.07	9.05	16.54	4.33	0.04	100.72	KAP36-1
52.98	0.60	10.37	0.04	8.02	0.02	8.29	15.43	4.27	0.17	100.19	KAP36-2
52.54	0.57	9.96	0.07	8.19	0.07	8.42	15.78	4.10	0.09	99.79	KAP36-3
52.52	0.67	9.86	0.03	8.30	0.06	8.56	16.08	4.36	0.02	100.46	KAP36-4
51.35	0.56	11.05	0.01	9.13	0.06	7.88	16.51	3.77	0.03	100.34	KAP36-5
53.14	0.60	10.31	0.05	8.05	0.05	8.42	15.27	4.53	0.13	100.55	KAP36-6
53.10	0.50	9.61	0.02	7.96	0.05	9.01	16.18	4.30	0.07	100.80	KAP36-7
51.18	0.74	11.04	0.03	8.23	0.08	8.61	16.11	4.12	0.06	100.20	KAP36-8
52.66	0.70	11.12	0.03	8.28	0.06	8.29	15.75	4.19	0.12	101.20	KAP36-9
53.92	0.46	10.51	0	7.79	0.08	8.46	15.71	4.72	0.04	101.08	KAP36-10
51.09	0.69	10.52	0.04	9.14	0.10	8.34	16.88	3.73	0.05	100.58	KAP36-11
49.78	0.85	10.99	0.04	10.14	0.12	8.58	14.70	4.11	0.33	99.64	KAP36-12
51.33	0.69	10.45	0.04	9.08	0.11	8.37	16.55	3.63	0.06	100.30	KAP36-13
52.40	0.60	8.93	0.06	8.79	0.07	9.10	15.94	3.96	0.20	100.05	KAP36-14
51.13	0.57	11.02	0.03	9.85	0.06	8.52	15.58	3.73	0.01	100.50	KAP36-15
52.48	0.59	9.39	0.08	8.41	0.07	8.86	15.82	4.16	0.10	99.96	KAP36-16
52.29	0.56	9.61	0.04	8.17	0.03	8.77	15.83	4.30	0.05	99.65	KAP36-17
53.42	0.36	8.00	0.03	8.55	0.08	9.45	16.81	3.74	0.04	100.48	KAP36-18
52.46	0.60	9.94	0.06	8.19	0.07	8.42	15.86	4.41	0.03	100.02	KAP36-19
52.71	0.52	9.32	0.07	8.08	0.10	8.84	16.34	4.13	0.02	100.13	KAP36-20
52.26	0.59	10.06	0.04	8.51	0.07	8.61	15.98	4.13	0.08	100.33	Average
0.97	0.12	0.84	0.02	0.65	0.02	0.36	0.54	0.29	0.08		Std. Dev.
51.10	0.68	11.61	0.04	9.63	0.07	8.21	15.45	3.52	0.02	100.34	KAP44-1
50.61	0.71	10.86	0.03	10.22	0.11	8.98	16.43	2.86	0.04	100.84	KAP44-2
51.91	0.84	12.53	0.02	7.74	0.08	7.86	15.98	4.26	0.03	101.24	KAP44-3
51.09	0.86	10.44	0.07	9.44	0.09	8.97	15.50	3.69	0.13	100.28	KAP44-4
51.24	0.69	10.76	0.05	8.85	0.09	8.94	14.85	3.89	0.03	99.38	KAP44-5
51.58	0.78	10.64	0.04	9.50	0.08	8.90	15.74	3.83	0.04	101.12	KAP44-6
50.33	0.98	12.61	0.03	9.21	0.06	8.08	15.80	3.49	0.09	100.68	KAP44-7
51.78	0.70	10.81	0.03	8.85	0.06	8.83	16.12	3.70	0.02	100.89	KAP44-8
51.78	0.73	11.41	0.02	8.74	0.10	8.48	15.39	4.21	0.05	100.91	KAP44-9
51.84	0.78	11.76	0.04	9.01	0.09	8.10	15.24	4.15	0.01	101.02	KAP44-10
52.65	0.49	9.79	0.00	9.93	0.07	9.20	15.22	3.90	0.01	101.25	KAP44-11
51.46	0.65	11.74	0.01	9.34	0.10	8.01	15.33	3.95	0.02	100.60	KAP44-12
52.20	0.60	9.21	0.01	9.12	0.07	9.13	17.14	3.56	0.02	101.05	KAP44-13
51.50	0.73	11.09	0.03	9.20	0.08	8.59	15.71	3.77	0.04	100.74	Average
0.63	0.12	0.99	0.02	0.62	0.01	0.48	0.60	0.37	0.03		Std. Dev.
50.22	0.89	10.30	0.03	8.96	0.09	8.68	17.41	3.33	0.03	99.93	KAP41-1
50.29	0.84	10.12	0.03	9.27	0.08	8.75	17.36	3.21	0.01	99.94	KAP41-2
50.38	0.76	10.31	0.03	9.02	0.12	8.82	17.15	3.25	0.01	99.84	KAP41-3
51.14	0.90	10.60	0.05	8.86	0.12	8.28	16.67	3.41	0.10	100.13	KAP41-4
50.51	0.84	10.33	0.03	9.03	0.10	8.63	17.15	3.30	0.04	99.96	Average
0.43	0.06	0.20	0.01	0.18	0.02	0.24	0.34	0.09	0.04		Std. Dev.
53.12	0.51	11.96	0.04	7.59	0.03	7.39	14.76	5.21	0.15	100.75	KAP43-1
52.23	0.70	13.28	0.04	7.53	0.04	6.74	14.05	5.48	0.01	100.09	KAP43-2
52.11	0.80	14.84	0	7.66	0.07	6.27	13.77	5.38	0.08	100.97	KAP43-3
51.91	0.57	11.37	0.02	8.09	0.06	8.12	15.10	4.85	0.02	100.12	KAP43-4
51.91	0.82	13.89	0.04	7.26	0.03	6.80	14.22	5.26	0.05	100.27	KAP43-5
53.13	0.53	13.34	0.03	6.60	0.07	7.09	14.55	5.49	0.02	100.85	KAP43-6
52.26	0.91	13.04	0.05	7.82	0.05	7.00	14.45	5.33	0.02	100.92	KAP43-7
53.14	0.41	11.34	0	7.15	0.04	7.94	15.75	4.99	0.01	100.77	KAP43-8
52.75	0.84	14.06	0.01	7.08	0.06	6.80	14.11	5.49	0.03	101.22	KAP43-9
51.04	0.59	13.87	0.02	8.69	0.11	6.55	15.26	4.56	0.03	100.72	KAP43-10

SiO_2	TiO_2	Al_2O_3	Cr_2O_3	FeO	MnO	MgO	CaO	Na_2O	K_2O	Total	Sample
52.36	0.67	13.10	0.02	7.56	0.06	7.07	14.60	5.20	0.04	100.67	Average
0.68	0.17	1.19	0.02	0.58	0.02	0.56	0.62	0.31	0.04		Std. Dev.
49.95	0.86	14.26	0.02	8.65	0.14	6.48	14.64	4.17	n.a.	99.16	KAP38-1
51.55	0.62	12.33	0.05	8.70	0.02	7.60	15.12	4.46	n.a.	100.45	KAP38-2
52.09	0.78	13.75	0.01	7.72	0.08	6.95	14.47	4.77	n.a.	100.61	KAP38-3
50.87	2.16	11.94	0.07	7.85	0.07	7.44	15.65	4.39	n.a.	100.43	KAP38-4
51.62	0.88	13.23	0	9.04	0.08	6.52	13.72	4.49	n.a.	99.56	KAP38-5
51.22	1.06	13.10	0.03	8.39	0.08	7.00	14.72	4.45	n.d.	100.04	Average
0.83	0.62	0.96	0.03	0.57	0.04	0.51	0.73	0.22	n.d.		Std. Dev.
53.26	0.52	10.60	0.02	7.89	0.09	7.96	16.48	4.04	0.01	100.87	KAP45-1
52.17	0.66	11.43	0.05	7.85	0.07	7.56	16.18	4.08	0.01	100.06	KAP45-2
52.20	0.67	12.59	0.03	7.55	0.05	7.08	15.79	4.44	0.01	100.39	KAP45-3
50.68	1.15	13.93	0.07	9.04	0.09	6.48	14.66	4.22	0.06	100.36	KAP45-4
52.96	0.54	9.57	0.02	8.17	0.05	8.22	16.64	3.91	0.01	100.08	KAP45-5
51.70	0.81	12.47	0.05	8.56	0.08	7.28	15.39	4.06	0.01	100.41	KAP45-6
50.38	1.23	13.96	0.03	9.01	0.08	6.56	14.62	4.20	0.03	100.11	KAP45-7
51.55	0.72	12.60	0.05	7.64	0.08	7.24	15.80	4.45	0.03	100.15	KAP45-8
52.53	0.58	12.31	0.02	7.35	0.10	7.69	15.82	4.37	0.01	100.78	KAP45-9
52.84	0.60	10.41	0.01	7.94	0.13	8.16	16.58	4.05	0	100.73	KAP45-10
51.70	0.82	11.95	0.05	7.79	0.07	7.62	15.96	4.35	0.03	100.32	KAP45-11
50.99	0.88	13.27	0.07	8.18	0.15	7.05	15.36	4.30	0	100.26	KAP45-12
52.75	0.64	11.73	0.04	7.32	0.08	7.81	16.10	4.21	0.02	100.69	KAP45-13
51.72	0.87	13.08	0.04	7.59	0.08	7.14	15.70	4.39	0.03	100.63	KAP45-14
51.96	0.76	12.14	0.04	7.99	0.09	7.42	15.79	4.22	0.02	100.42	Average
0.87	0.22	1.30	0.02	0.55	0.03	0.54	0.63	0.17	0.01		Std. Dev.
51.75	0.75	10.19	0.03	8.47	0.07	9.16	16.87	3.50	0.02	100.82	KAP46-1
50.37	0.99	10.92	0.05	9.14	0.11	8.85	16.78	3.21	0.02	100.44	KAP46-2
50.69	1.07	12.20	0.07	8.93	0.10	8.27	16.16	3.71	0.01	101.19	KAP46-3
49.69	1.32	12.25	0.06	9.85	0.12	8.14	16.06	3.15	0.04	100.67	KAP46-4
49.12	1.43	13.42	0.02	10.98	0.12	7.99	14.02	3.73	0.08	100.90	KAP46-5
51.81	0.85	12.35	0.03	7.60	0.04	7.77	15.82	4.56	0	100.86	KAP46-6
50.83	0.94	12.15	0.02	8.24	0.08	8.03	16.82	3.61	0.01	100.72	KAP46-7
50.92	1.08	10.59	0.04	8.74	0.09	8.79	17.17	3.42	0.02	100.87	KAP46-8
49.49	1.37	13.20	0.04	10.06	0.11	7.87	14.35	3.47	0.05	100.00	KAP46-9
50.62	1.05	11.16	0.02	8.70	0.11	8.56	17.05	3.30	0.02	100.58	KAP46-10
51.00	0.93	12.97	0.04	9.05	0.11	7.71	15.10	3.55	0.16	100.60	KAP46-11
49.08	1.41	13.03	0.06	11.03	0.18	7.76	15.00	3.34	0.01	100.89	KAP46-12
51.67	0.78	10.31	0.03	8.67	0.09	8.86	16.93	3.42	0.01	100.76	KAP46-13
50.80	1.11	10.86	0.04	8.73	0.11	8.46	17.05	3.28	0.02	100.45	KAP46-14
52.04	0.86	12.14	0.07	7.78	0.08	7.64	15.80	4.46	0	100.87	KAP46-15
51.12	0.84	11.10	0.01	8.83	0.07	8.50	16.88	3.55	0	100.88	KAP46-16
51.05	1.07	10.23	0.07	9.06	0.10	8.92	17.30	3.36	0.01	101.16	KAP46-17
50.16	0.87	12.02	0.04	9.61	0.11	8.28	15.77	3.27	0.03	100.16	KAP46-18
50.68	1.04	11.73	0.04	9.08	0.10	8.31	16.16	3.55	0.03	100.71	Average
0.89	0.22	1.07	0.02	0.93	0.03	0.48	1.00	0.39	0.04		Std. Dev.

Orthopyroxene Compositions

SiO_2	TiO_2	Al_2O_3	Cr_2O_3	FeO	MnO	MgO	CaO	Na_2O	K_2O	Total	Sample
49.45	0.09	2.24	0.01	26.32	0.56	16.83	3.43	n.a.	n.a.	98.94	3VG1-1
49.92	0.14	2.58	0	25.90	0.57	16.82	2.48	n.a.	n.a.	98.41	3VG1-2
49.22	0.18	2.58	0	27.71	0.63	17.36	1.47	n.a.	n.a.	99.15	3VG1-3
49.06	0.12	2.44	0.01	27.46	0.61	17.58	1.64	n.a.	n.a.	98.93	3VG1-4
49.51	0.11	2.82	0.02	27.88	0.56	17.40	1.30	n.a.	n.a.	99.61	3VG1-5
49.56	0.19	2.18	0.03	28.26	0.54	17.19	1.70	n.a.	n.a.	99.65	3VG1-6
49.71	0.28	1.68	0.02	28.02	0.45	16.90	1.97	n.a.	n.a.	99.02	3VG1-7
49.50	0.24	1.75	0	28.17	0.51	16.44	2.13	n.a.	n.a.	98.74	3VG1-8
49.35	0.11	2.54	0.01	27.93	0.55	17.29	1.45	n.a.	n.a.	99.23	3VG1-9
49.72	0.15	2.04	0	28.81	0.52	16.37	1.46	n.a.	n.a.	99.06	3VG1-10
49.50	0.16	2.28	0.01	27.65	0.55	17.02	1.90	n.d.	n.d.	99.07	Average
0.25	0.06	0.38	0.01	0.89	0.05	0.41	0.65	n.d.	n.d.		Std. Dev
50.01	0.33	2.89	0	25.24	0.43	19.09	1.59	n.a.	n.a.	99.57	3VG3-1
49.54	0.21	2.73	0	26.29	0.41	18.38	1.78	n.a.	n.a.	99.32	3VG3-2
49.53	0.35	3.32	0	26.04	0.43	18.10	2.02	n.a.	n.a.	99.78	3VG3-3
49.57	0.32	3.24	0.05	24.50	0.38	17.91	3.56	n.a.	n.a.	99.54	3VG3-4
49.27	0.24	3.41	0	26.86	0.38	17.18	1.88	n.a.	n.a.	99.23	3VG3-5
49.18	0.14	3.57	0.02	25.75	0.39	18.61	1.62	n.a.	n.a.	99.28	3VG3-6
49.43	0.31	3.41	0.02	25.81	0.43	18.12	1.97	n.a.	n.a.	99.51	3VG3-7
49.56	0.32	2.93	0	26.76	0.42	17.01	2.72	n.a.	n.a.	99.71	3VG3-8
49.38	0.31	2.88	0.03	27.23	0.45	17.25	2.16	n.a.	n.a.	99.69	3VG3-9
49.19	0.30	3.49	0.01	26.90	0.38	17.43	1.59	n.a.	n.a.	99.28	3VG3-10
48.45	0.87	3.24	0.01	27.33	0.39	17.62	1.52	n.a.	n.a.	99.44	3VG3-11
49.38	0.23	3.07	0.02	25.28	0.45	18.36	2.00	n.a.	n.a.	98.78	3VG3-12
48.83	0.25	3.64	0	26.15	0.39	17.88	1.53	n.a.	n.a.	98.68	3VG3-13
49.40	0.20	3.36	0.04	25.34	0.41	18.53	1.55	n.a.	n.a.	98.83	3VG3-14
48.75	0.23	3.78	0.03	26.04	0.41	18.06	1.65	n.a.	n.a.	98.94	3VG3-15
49.61	0.17	2.94	0	25.06	0.40	19.31	1.55	n.a.	n.a.	99.04	3VG3-16
49.50	0.26	3.08	0.03	24.75	0.43	19.25	1.58	n.a.	n.a.	98.88	3VG3-17
49.33	0.30	3.23	0.02	25.96	0.41	18.12	1.90	n.d.	n.d.	99.26	Average
0.37	0.16	0.30	0.02	0.86	0.02	0.70	0.53	n.d.	n.d.		Std. Dev
50.32	0.12	3.39	0	25.67	0.47	18.12	1.80	0.07	0.04	100.00	3VG26-1
50.14	0.20	3.40	0.02	25.76	0.47	18.15	1.75	0.07	0.04	100.00	3VG26-2
50.54	0.26	3.09	0.10	25.57	0.44	17.79	2.12	0.05	0.05	100.00	3VG26-3
51.64	0.18	2.34	0	24.15	0.39	19.39	1.80	0.06	0.04	100.00	3VG26-4
50.15	0.19	3.52	0	26.30	0.44	17.64	1.71	0.06	0.00	100.00	3VG26-5
50.73	0.15	2.84	0	25.92	0.46	17.77	2.09	0.04	0.01	100.00	3VG26-6
50.50	0.12	3.47	0.05	25.80	0.42	17.93	1.62	0.06	0.02	100.00	3VG26-7
50.19	0.21	3.29	0.00	25.92	0.41	18.14	1.76	0.08	0.00	100.00	3VG26-8
49.96	0.25	3.84	0.15	25.87	0.41	17.92	1.52	0.04	0.04	100.00	3VG26-9
49.88	0.31	3.44	0.08	26.18	0.44	17.58	1.96	0.13	0.01	100.00	3VG26-10
50.36	0.16	3.07	0	26.14	0.43	17.97	1.75	0.09	0.03	100.00	3VG26-11
50.52	0.22	2.96	0	25.73	0.40	17.87	2.21	0.06	0.03	100.00	3VG26-12
50.00	0.16	4.03	0	25.75	0.45	17.89	1.65	0.06	0.01	100.00	3VG26-13
50.79	0.15	2.89	0	24.97	0.43	18.75	1.98	0.05	0.00	100.00	3VG26-14
50.31	0.27	3.42	0	25.66	0.41	18.29	1.55	0.08	0.02	100.00	3VG26-15
50.50	0.29	3.15	0	25.57	0.43	17.77	2.20	0.09	0.00	100.00	3VG26-16
50.92	0.34	3.08	0	24.42	0.44	18.61	2.12	0.06	0.01	100.00	3VG26-17
51.92	0.25	3.66	0	23.91	0.34	17.32	2.14	0.18	0.29	100.00	3VG26-18
50.81	0.24	3.04	0	24.81	0.45	18.30	2.25	0.08	0.02	100.00	3VG26-19
50.63	0.19	2.95	0	25.54	0.45	18.21	1.97	0.06	0.02	100.00	3VG26-20
50.65	0.24	3.06	0	25.23	0.46	18.25	2.05	0.06	0.03	100.00	3VG26-21
50.63	0.26	3.10	0	25.36	0.43	18.00	2.08	0.07	0.07	100.00	3VG26-22
50.13	0.20	3.84	0.01	25.33	0.41	18.43	1.53	0.07	0.04	100.00	3VG26-23
50.71	0.26	2.95	0.02	25.30	0.42	17.96	2.26	0.08	0.03	100.00	3VG26-24
51.00	0.22	3.57	0.07	24.36	0.41	18.52	1.67	0.13	0.06	100.00	3VG26-25
50.14	0.13	3.91	0.01	25.13	0.41	18.61	1.51	0.10	0.05	100.00	3VG26-26
50.54	0.21	3.28	0.02	25.40	0.43	18.12	1.89	0.08	0.04	99.96	Average
0.48	0.06	0.39	0.04	0.63	0.03	0.43	0.25	0.03	0.06		Std. Dev
49.46	0.39	5.80	0	22.36	0.33	19.27	2.10	n.a.	n.a.	99.70	3VG14-1
49.43	0.46	4.60	0.02	23.53	0.34	19.53	1.98	n.a.	n.a.	99.88	3VG14-2
49.25	0.40	4.72	0.01	23.63	0.35	19.37	2.20	n.a.	n.a.	99.91	3VG14-3

SiO_2	TiO_2	Al_2O_3	Cr_2O_3	FeO	MnO	MgO	CaO	Na_2O	K_2O	Total	Sample
49.65	0.36	4.57	0.01	23.15	0.33	19.66	2.00	n.a.	n.a.	99.72	3VG14-4
49.57	0.41	4.53	0.03	23.42	0.32	19.61	1.89	n.a.	n.a.	99.77	3VG14-5
50.05	0.36	3.82	0	21.46	0.36	19.32	4.55	n.a.	n.a.	99.91	3VG14-6
49.57	0.40	3.80	0	23.60	0.28	19.42	2.52	n.a.	n.a.	99.50	3VG14-7
49.72	0.40	3.79	0	23.09	0.35	19.96	2.05	n.a.	n.a.	99.35	3VG14-8
49.44	0.42	4.45	0.04	23.30	0.33	19.86	1.88	n.a.	n.a.	99.71	3VG14-9
49.42	0.47	4.67	0.01	23.67	0.36	19.80	1.80	n.a.	n.a.	100.19	3VG14-10
49.11	0.42	4.79	0	23.52	0.32	19.49	1.87	n.a.	n.a.	99.53	3VG14-11
49.28	0.41	4.33	0	22.99	0.33	19.63	2.27	n.a.	n.a.	99.25	3VG14-12
49.67	0.43	3.92	0.01	23.08	0.35	19.53	2.61	n.a.	n.a.	99.61	3VG14-13
50.04	0.39	4.02	0	23.24	0.38	19.62	2.28	n.a.	n.a.	99.97	3VG14-14
49.55	0.41	4.41	0.01	23.15	0.34	19.57	2.28	n.d.	n.d.	99.72	Average
0.27	0.03	0.54	0.01	0.60	0.02	0.20	0.70	n.d.	n.d.		Std. Dev
50.34	0.20	3.36	0.01	28.87	0.58	15.75	1.66	0.11	0.05	100.87	3VG6-1
50.85	0.14	4.08	0.01	26.93	0.57	15.22	2.50	0.37	0.09	100.66	3VG6-2
49.98	0.23	3.17	0.02	27.19	0.62	16.21	2.41	0.16	0.13	100.00	3VG6-3
50.72	0.06	3.18	0	28.96	0.55	16.07	1.35	0.02	0.02	100.92	3VG6-4
51.64	0.05	1.09	0.02	29.58	0.76	17.07	0.81	0.02	0.03	101.03	3VG6-5
51.72	0.05	1.10	0	28.31	0.75	17.11	1.22	0.07	0.03	100.34	3VG6-6
51.68	0.04	0.86	0	29.15	0.75	17.32	0.77	0.01	0.03	100.57	3VG6-7
50.74	0.13	2.54	0.01	28.58	0.66	16.15	1.87	0.04	0.01	100.72	3VG6-8
50.96	0.11	2.42	0.01	28.45	0.65	16.36	1.57	0.10	0.06	100.69	Average
0.66	0.07	1.24	0.01	0.94	0.09	0.74	0.66	0.12	0.04		Std. Dev
50.43	0.26	3.03	0	28.07	0.49	16.71	1.66	0.06	0.02	100.72	3VG5-1
50.57	0.19	2.69	0.02	27.92	0.43	16.86	1.59	0.04	0.02	100.34	3VG5-2
50.12	0.22	3.56	0	28.22	0.44	16.48	1.51	0.07	0.06	100.68	3VG5-3
50.03	0.20	3.83	0.01	27.39	0.46	16.35	1.65	0.13	0.04	100.09	3VG5-4
49.74	0.29	3.79	0.02	27.43	0.45	16.73	1.77	0.08	0.10	100.40	3VG5-5
50.08	0.22	3.20	0.01	27.76	0.48	16.96	1.49	0.02	0.05	100.27	3VG5-6
50.41	0.26	3.19	0.01	26.80	0.46	16.25	2.89	0.10	0.04	100.40	3VG5-7
49.86	0.23	4.01	0.04	28.22	0.43	16.68	1.30	0.07	0.02	100.85	3VG5-8
50.59	0.24	3.43	0.04	28.36	0.48	16.84	1.56	0.05	0.03	101.63	3VG5-9
50.45	0.18	3.08	0.01	27.70	0.44	16.97	1.50	0.02	0.02	100.37	3VG5-10
49.96	0.22	4.27	0.01	28.20	0.46	16.49	1.34	0.05	0.02	101.03	3VG5-11
51.02	0.23	3.20	0.02	27.66	0.44	16.72	1.48	0.08	0.06	100.90	3VG5-12
51.22	0.16	2.18	0	27.83	0.48	17.48	1.33	0.05	0.03	100.77	3VG5-13
50.28	0.15	3.56	0	27.66	0.44	16.74	1.39	0.06	0.03	100.30	3VG5-14
50.05	0.26	3.63	0.02	28.03	0.41	16.59	1.57	0.04	0.03	100.63	3VG5-15
50.86	0.19	3.04	0.03	27.50	0.43	16.80	2.01	0.08	0.03	100.96	3VG5-16
50.68	0.14	3.01	0.02	28.14	0.44	16.95	1.29	0.06	0.03	100.75	3VG5-17
50.39	0.29	3.70	0.01	27.61	0.48	16.77	1.81	0.16	0.06	101.28	3VG5-18
49.72	0.26	4.31	0.02	27.95	0.39	16.46	1.40	0.01	0.03	100.54	3VG5-19
50.19	0.23	3.68	0	28.20	0.46	16.41	1.57	0.06	0.01	100.81	3VG5-20
50.43	0.23	3.21	0	28.42	0.47	16.41	1.71	0.04	0.03	100.95	3VG5-21
50.54	0.26	3.17	0	27.52	0.47	16.61	1.71	0.05	0.03	100.36	3VG5-22
50.37	0.22	3.29	0.02	28.00	0.44	16.56	1.49	0.06	0.06	100.52	3VG5-23
51.00	0.22	2.62	0	28.15	0.51	16.98	1.58	0.06	0.02	101.12	3VG5-24
50.81	0.20	3.23	0	27.33	0.43	16.38	2.52	0.06	0.09	101.06	3VG5-25
50.23	0.25	3.66	0	27.92	0.43	16.70	1.36	0.01	0.03	100.61	3VG5-26
50.65	0.23	3.17	0.04	27.97	0.50	16.38	1.91	0.04	0.03	100.92	3VG5-27
50.33	0.28	3.28	0.02	28.10	0.46	16.52	1.86	0.05	0.03	100.90	3VG5-28
49.90	0.22	3.28	0.03	28.30	0.46	16.40	1.75	0.04	0.02	100.40	3VG5-29
49.78	0.32	3.67	0	27.53	0.41	16.39	2.16	0.08	0.06	100.41	3VG5-30
49.83	0.25	3.65	0.02	28.53	0.45	16.45	1.42	0.03	0.01	100.65	3VG5-31
50.33	0.18	3.08	0.01	28.11	0.49	16.67	1.56	0.03	0.04	100.48	3VG5-32
50.34	0.23	3.36	0.01	27.89	0.45	16.65	1.66	0.06	0.04	100.69	Average
0.39	0.04	0.45	0.01	0.38	0.03	0.26	0.35	0.03	0.02		Std. Dev
50.05	0.21	2.44	0.04	27.49	0.41	16.49	2.22	n.a.	n.a.	99.33	3VG4-1
49.07	0.26	3.83	0.01	27.65	0.40	16.46	1.75	n.a.	n.a.	99.43	3VG4-2
49.36	0.17	3.97	0	27.35	0.42	16.43	1.86	n.a.	n.a.	99.56	3VG4-3
48.48	0.23	4.66	0.02	27.62	0.43	16.48	1.55	n.a.	n.a.	99.47	3VG4-4
48.36	0.27	3.41	0	27.95	0.46	16.45	1.40	n.a.	n.a.	98.30	3VG4-5
49.09	0.24	3.84	0	27.61	0.42	16.64	1.72	n.a.	n.a.	99.56	3VG4-6
48.57	0.28	4.61	0	27.69	0.37	16.52	1.57	n.a.	n.a.	99.61	3VG4-7

SiO_2	TiO_2	Al_2O_3	Cr_2O_3	FeO	MnO	MgO	CaO	Na_2O	K_2O	Total	Sample
49.44	0.26	3.09	0	27.78	0.42	16.00	2.08	n.a.	n.a.	99.06	3VG4-8
49.56	0.28	3.76	0	25.98	0.36	15.56	3.59	n.a.	n.a.	99.09	3VG4-9
48.56	0.32	4.42	0	27.75	0.41	16.40	1.92	n.a.	n.a.	99.79	3VG4-10
49.12	0.31	3.53	0.01	27.81	0.45	16.11	2.50	n.a.	n.a.	99.83	3VG4-11
48.38	0.25	3.90	0.06	28.36	0.41	16.28	1.72	n.a.	n.a.	99.34	3VG4-12
49.00	0.26	3.79	0.01	27.59	0.41	16.32	1.99	n.d.	n.d.	99.36	Average
0.54	0.04	0.63	0.02	0.57	0.03	0.30	0.59	n.d.	n.d.		Std. Dev
49.95	0.22	5.15	0	25.78	0.35	16.60	1.83	0.09	0.03	100.00	3VG23-1
50.89	0.17	4.36	0.13	24.78	0.30	17.45	1.85	0.08	0.01	100.00	3VG23-2
49.31	0.23	5.81	0	25.58	0.37	17.14	1.41	0.12	0.03	100.00	3VG23-3
51.21	0.13	3.69	0	25.10	0.28	18.01	1.42	0.13	0.04	100.00	3VG23-4
50.60	0.23	3.98	0	25.57	0.33	17.50	1.64	0.09	0.06	100.00	3VG23-5
50.22	0.26	4.35	0	26.04	0.39	16.87	1.78	0.06	0.03	100.00	3VG23-6
49.86	0.29	5.24	0	25.50	0.33	17.08	1.63	0.06	0.02	100.00	3VG23-7
51.02	0.27	3.88	0	25.27	0.39	17.40	1.65	0.08	0.03	100.00	3VG23-8
50.86	0.25	4.26	0	24.96	0.34	17.66	1.63	0.03	0.02	100.00	3VG23-9
50.15	0.23	5.45	0	24.92	0.39	17.14	1.62	0.11	0.01	100.00	3VG23-10
49.90	0.22	4.63	0	25.92	0.37	16.78	2.07	0.07	0.03	100.00	3VG23-11
49.97	0.27	4.64	0	25.79	0.40	17.00	1.83	0.10	0.02	100.00	3VG23-12
50.77	0.18	3.53	0.04	25.49	0.37	17.79	1.69	0.09	0.06	100.00	3VG23-13
50.41	0.24	4.50	0.04	25.46	0.34	16.76	2.07	0.15	0.06	100.00	3VG23-14
49.68	0.18	4.96	0.17	25.85	0.34	17.11	1.63	0.06	0.03	100.00	3VG23-15
50.31	0.20	4.79	0	25.24	0.37	17.26	1.68	0.12	0.06	100.00	3VG23-16
49.57	0.23	5.59	0.04	25.35	0.37	16.94	1.73	0.13	0.06	100.00	3VG23-17
50.27	0.22	4.63	0.02	25.45	0.35	17.20	1.72	0.09	0.03	100.00	Average
0.55	0.04	0.67	0.05	0.37	0.03	0.39	0.18	0.03	0.02		Std. Dev
49.30	0.36	5.61	0.03	25.06	0.34	17.46	1.86	0.15	0.01	100.00	3VG22-1
49.30	0.32	6.87	0.09	23.86	0.33	16.88	2.09	0.22	0.08	100.00	3VG22-2
49.34	0.35	5.58	0	24.77	0.34	17.54	1.92	0.13	0.02	100.00	3VG22-3
50.38	0.34	3.90	0	24.92	0.36	18.06	1.93	0.09	0.04	100.00	3VG22-4
49.73	0.25	5.42	0.02	24.60	0.36	17.60	1.84	0.11	0.06	100.00	3VG22-5
49.44	0.30	5.34	0	25.04	0.37	17.38	2.01	0.12	0.01	100.00	3VG22-6
49.71	0.35	5.14	0.20	24.67	0.33	17.63	1.90	0.06	0.02	100.00	3VG22-7
49.03	0.32	6.06	0.06	24.74	0.34	17.56	1.82	0.08	0.02	100.00	3VG22-8
49.69	0.39	5.36	0.11	24.66	0.37	17.38	1.96	0.06	0.06	100.00	3VG22-9
49.68	0.37	5.19	0	24.83	0.38	17.47	1.95	0.08	0.04	100.00	3VG22-10
49.55	0.35	5.45	0	24.98	0.36	17.64	1.58	0.07	0.04	100.00	3VG22-11
49.77	0.37	5.37	0	24.79	0.34	17.43	1.86	0.05	0.02	100.00	3VG22-12
49.88	0.38	4.71	0	24.87	0.36	17.63	2.08	0.06	0.04	100.00	3VG22-13
49.64	0.42	5.46	0	24.26	0.30	17.18	2.59	0.07	0.08	100.00	3VG22-14
49.68	0.36	4.95	0	24.70	0.32	17.27	2.63	0.08	0.02	100.00	3VG22-15
49.32	0.39	5.64	0.03	24.82	0.33	17.76	1.62	0.06	0.04	100.00	3VG22-16
49.63	0.28	5.24	0	24.81	0.36	17.66	1.93	0.06	0.04	100.00	3VG22-17
49.03	0.46	6.26	0	24.95	0.34	17.30	1.57	0.07	0.03	100.00	3VG22-18
50.04	0.26	4.67	0	24.89	0.36	18.06	1.76	0.06	0.02	100.00	3VG22-19
49.30	0.37	5.70	0	24.79	0.33	17.44	1.94	0.12	0.01	100.00	3VG22-20
50.06	0.31	4.68	0	24.90	0.37	17.50	2.03	0.12	0.02	100.00	3VG22-21
49.95	0.29	4.79	0.01	25.04	0.41	17.76	1.67	0.06	0.02	100.00	3VG22-22
49.79	0.34	4.80	0.14	24.83	0.32	18.17	1.54	0.06	0.01	100.00	3VG22-23
50.06	0.36	4.56	0.04	24.57	0.35	17.46	2.46	0.10	0.06	100.00	3VG22-24
50.48	0.28	3.96	0	25.17	0.33	17.93	1.76	0.07	0.02	100.00	3VG22-25
50.06	0.36	5.05	0.10	23.80	0.33	16.75	3.30	0.20	0.04	100.00	3VG22-26
49.69	0.34	5.22	0.03	24.74	0.35	17.53	1.98	0.09	0.03	99.97	Average
0.37	0.05	0.65	0.05	0.33	0.02	0.32	0.39	0.04	0.02		Std. Dev
49.72	0.24	5.16	0	25.96	0.36	16.73	1.71	0.09	0.02	100.00	3VG20-1
49.56	0.28	4.99	0.02	26.01	0.39	16.53	2.08	0.11	0.04	100.00	3VG20-2
49.41	0.29	4.98	0	26.05	0.40	16.73	2.09	0.06	0.01	100.00	3VG20-3
49.61	0.27	4.45	0.09	26.00	0.39	16.86	2.37	0.11	0.05	100.00	3VG20-4
50.13	0.20	4.05	0	26.33	0.42	17.26	1.52	0.05	0.06	100.00	3VG20-5
49.50	0.25	4.55	0.12	26.26	0.42	17.24	1.56	0.09	0.03	100.00	3VG20-6
49.48	0.23	4.66	0	26.59	0.43	16.72	1.77	0.09	0.02	100.00	3VG20-7
49.40	0.30	5.13	0	26.32	0.40	16.54	1.73	0.15	0.04	100.00	3VG20-8
50.07	0.19	4.37	0.06	25.83	0.39	16.95	2.03	0.09	0.03	100.00	3VG20-9
50.35	0.31	4.41	0	24.28	0.36	15.73	4.29	0.26	0.01	100.00	3VG20-10

SiO_2	TiO_2	Al_2O_3	Cr_2O_3	FeO	MnO	MgO	CaO	Na_2O	K_2O	Total	Sample
49.31	0.22	5.10	0	26.37	0.37	16.97	1.55	0.11	0.03	100.00	3VG20-11
49.06	0.25	5.86	0.05	26.32	0.42	16.77	1.47	0.08	0.01	100.00	3VG20-12
49.11	0.31	5.64	0	26.27	0.35	16.72	1.51	0.06	0.03	100.00	3VG20-13
49.59	0.26	4.88	0.03	26.04	0.39	16.73	1.97	0.10	0.03	100.00	Average
0.39	0.04	0.48	0.04	0.57	0.03	0.38	0.75	0.05	0.02		Std. Dev
48.91	0.35	4.95	0.03	24.17	0.24	18.58	1.71	n.a.	n.a.	98.94	3VG18-2
48.22	0.33	6.51	0	24.25	0.25	18.06	1.79	n.a.	n.a.	99.42	3VG18-3
48.21	0.40	6.60	0.01	24.25	0.27	18.13	1.52	n.a.	n.a.	99.39	3VG18-4
48.61	0.25	5.90	0	24.31	0.27	18.56	1.66	n.a.	n.a.	99.53	3VG18-5
47.17	0.40	6.39	0	24.06	0.22	17.61	1.82	n.a.	n.a.	97.67	3VG18-6
48.22	0.35	6.07	0.01	24.21	0.25	18.19	1.70	n.d.	n.d.	98.99	Average
0.66	0.06	0.68	0.01	0.09	0.02	0.40	0.12	n.d.	n.d.		Std. Dev
48.36	0.88	5.67	0	23.00	0.57	18.40	4.46	0.52	0.36	100.21	KAP3-1
50.42	0.42	4.03	0.03	23.76	0.62	18.08	2.20	0.21	0.20	99.98	KAP3-2
51.34	0.32	3.72	0.01	23.85	0.72	17.66	2.01	0.22	0.18	100.01	KAP3-3
51.17	0.22	3.01	0.01	24.42	0.72	19.00	1.39	0.09	0.03	100.06	KAP3-4
51.39	0.26	3.29	0.01	24.58	0.72	18.79	1.57	0.09	0.06	100.73	KAP3-5
50.96	0.30	3.04	0.01	24.30	0.66	19.24	1.38	0.03	0.03	99.93	KAP3-6
51.46	0.24	3.23	0.01	24.05	0.62	19.18	1.85	0.06	0.03	100.75	KAP3-7
50.50	0.25	3.31	0.04	24.62	0.66	19.18	1.42	0.07	0.02	100.16	KAP3-8
49.96	0.22	3.86	0.02	24.46	0.70	18.86	1.52	0.11	0.01	99.77	KAP3-9
50.40	0.29	3.21	0.01	24.58	0.68	18.98	1.48	0.05	0.03	99.72	KAP3-10
50.72	0.27	3.27	0	24.65	0.61	18.96	1.52	0.09	0.02	100.10	KAP3-11
50.34	0.30	3.56	0	24.65	0.67	18.83	1.60	0.03	0.02	99.97	KAP3-12
50.52	0.28	3.26	0	24.60	0.69	18.74	2.00	0.07	0.01	100.17	KAP3-13
50.91	0.29	3.20	0.02	24.54	0.64	18.91	1.90	0.03	0.05	100.47	KAP3-14
50.84	0.29	3.31	0.02	24.17	0.69	19.00	2.02	0.05	0.01	100.20	KAP3-15
50.29	0.29	3.27	0.03	23.94	0.59	18.38	2.63	0.08	0.02	99.52	KAP3-16
50.74	0.36	2.84	0	21.12	0.56	17.13	6.40	0.10	0.04	99.28	KAP3-17
50.63	0.28	3.67	0.02	24.21	0.63	19.19	1.52	0.03	0.02	100.20	KAP3-18
50.72	0.32	3.14	0.01	24.10	0.60	19.11	1.72	0.02	0.03	99.76	KAP3-19
51.06	0.21	2.39	0.01	24.28	0.67	19.18	1.62	0.03	0.02	99.47	KAP3-20
50.39	0.25	3.66	0.03	24.14	0.66	18.88	1.65	0.07	0.02	99.75	KAP3-21
50.75	0.24	3.70	0.02	23.91	0.69	18.14	1.92	0.18	0.06	99.59	KAP3-22
49.77	0.33	3.82	0.02	24.25	0.67	18.49	1.79	0.10	0.06	99.27	KAP3-23
50.59	0.31	3.45	0.01	24.09	0.65	18.62	2.07	0.10	0.06	99.96	Average
0.64	0.13	0.61	0.01	0.75	0.05	0.72	1.14	0.11	0.08		Std. Dev
51.54	0.38	4.00	0.01	0.57	20.77	21.44	1.85	0.04	0.03	100.63	KAP14-1
52.32	0.29	3.32	0.01	0.57	21.24	20.96	1.95	0.09	0.03	100.78	KAP14-2
50.31	0.45	4.21	0.01	0.59	20.62	21.68	1.63	0.02	0.03	99.54	KAP14-3
51.66	0.31	3.70	0.00	0.60	21.17	20.71	1.82	0.06	0.00	100.03	KAP14-4
51.29	0.34	3.65	0.01	0.58	20.36	20.75	2.06	0.11	0.02	99.17	KAP14-5
52.42	0.33	3.40	0.01	0.59	21.47	20.82	1.82	0.04	0.00	100.90	KAP14-6
52.30	0.29	3.51	0.01	0.60	22.40	19.29	1.66	0.08	0.00	100.14	KAP14-7
51.29	0.32	4.13	0.01	0.59	21.19	21.77	1.81	0.07	0.00	101.20	KAP14-8
51.64	0.34	3.74	0.01	0.59	21.15	20.93	1.83	0.06	0.01	100.30	Average
0.71	0.06	0.34	0	0.01	0.62	0.78	0.14	0.03	0.01		Std. Dev
48.90	0.30	5.43	0	24.62	0.51	16.86	3.25	0.12	0.02	100.00	KAP22-1
49.14	0.32	5.47	0.08	26.01	0.52	16.71	1.59	0.14	0.03	100.00	KAP22-2
49.07	0.37	5.73	0	25.71	0.55	16.73	1.74	0.07	0.04	100.00	KAP22-3
49.09	0.32	5.76	0.12	25.83	0.46	16.69	1.68	0.04	0.02	100.00	KAP22-4
49.05	0.33	5.60	0.05	25.54	0.51	16.75	2.06	0.09	0.03	100.00	Average
0.10	0.03	0.17	0.06	0.63	0.04	0.07	0.79	0.04	0.01		Std. Dev

Garnet Compositions

SiO_2	TiO_2	Al_2O_3	Cr_2O_3	FeO	MnO	MgO	CaO	Na_2O	Total	Sample
38.88	0.71	21.40	0	24.98	1.40	5.29	8.36	0.06	101.12	3VG16-1
38.44	0.67	21.51	0	24.62	1.42	5.09	8.78	0.03	100.56	3VG16-2
38.79	0.86	21.54	0	24.72	1.41	4.95	9.12	0.06	101.23	3VG16-3
38.29	0.86	21.28	0	25.36	1.36	4.70	8.87	0.02	100.80	3VG16-4
38.38	0.84	21.31	0	25.06	1.46	5.01	8.32	0.09	100.24	3VG16-5
39.42	0.81	20.81	0	23.98	1.31	5.49	8.99	0.07	100.46	3VG16-6
39.14	0.90	20.79	0	24.74	1.29	5.77	7.98	0.06	100.26	3VG16-7
38.76	0.84	21.20	n.d.	24.78	1.38	5.19	8.64	0.06	100.83	Average
0.43	0.07	0.36	n.d.	0.43	0.06	0.36	0.41	0.03		Std. Dev.
38.56	0.95	21.36	n.a.	24.33	0.74	6.29	8.00	n.a.	100.25	3VG15-1
38.69	1.19	21.08	n.a.	24.89	0.70	6.61	7.90	n.a.	100.37	3VG15-2
38.76	1.03	21.34	n.a.	24.01	0.83	6.66	7.67	n.a.	100.29	3VG15-3
39.15	1.23	21.15	n.a.	23.92	0.72	6.75	7.93	n.a.	100.86	3VG15-4
38.79	1.10	21.23	n.d.	24.21	0.70	6.57	7.83	n.d.	100.44	Average
0.25	0.13	0.14	n.d.	0.31	0.05	0.20	0.23	n.d.		Std. Dev.
38.94	0.81	21.49	n.a.	24.93	0.88	7.24	6.84	0.07	100.88	3VG20-1
39.38	0.82	20.04	n.a.	24.92	0.80	7.51	7.03	0.08	100.38	3VG20-2
39.33	0.89	20.60	n.a.	25.12	0.87	7.40	7.04	0.09	101.03	3VG20-3
38.73	0.82	21.32	n.a.	25.11	0.88	7.10	7.27	0.01	100.93	3VG20-4
38.41	1.00	21.16	n.a.	24.96	0.79	6.90	7.81	0.06	101.08	3VG20-5
38.47	1.28	20.82	n.a.	24.29	0.78	6.70	7.80	0.02	100.16	3VG20-6
38.14	0.80	21.31	n.a.	24.82	0.77	6.67	7.81	0.08	100.31	3VG20-7
38.21	1.11	20.97	n.a.	24.51	0.88	6.67	7.88	0.10	100.80	3VG20-8
38.47	1.06	20.97	n.a.	24.26	0.82	6.98	8.39	0.09	100.54	3VG20-9
38.68	0.85	20.96	n.d.	24.75	0.83	7.08	7.58	0.06	100.68	Average
0.45	0.28	0.44	n.d.	0.30	0.04	0.33	0.50	0.04		Std. Dev.
38.47	1.18	21.24	n.a.	22.73	0.48	8.47	7.62	0.06	100.22	3VG19-1
38.47	0.94	21.49	n.a.	22.47	0.44	8.43	7.89	0.01	100.14	3VG19-2
38.52	1.21	21.26	n.a.	22.83	0.50	8.31	7.63	0.02	100.29	3VG19-3
38.53	1.03	21.33	n.a.	22.59	0.46	8.51	7.53	0.08	100.06	3VG19-4
38.14	1.06	21.45	n.a.	22.82	0.54	8.09	7.52	0.08	99.47	3VG19-5
38.24	1.10	21.52	n.a.	22.73	0.50	8.13	8.13	0.04	100.37	3VG19-6
38.07	1.12	21.39	n.a.	22.58	0.46	8.69	7.33	0.04	99.61	3VG19-7
38.19	0.97	21.48	n.a.	22.74	0.46	8.91	7.13	0.03	99.93	3VG19-8
38.27	1.36	21.25	n.a.	23.02	0.53	8.41	7.86	0.06	100.63	3VG19-9
38.26	1.06	21.39	n.a.	22.41	0.41	8.68	7.29	0.06	99.86	3VG19-10
38.32	1.10	21.38	n.d.	22.67	0.48	8.45	7.57	0.04	100.02	Average
0.17	0.12	0.10	n.d.	0.18	0.04	0.26	0.29	0.02		Std. Dev.
38.60	0.71	21.06	n.a.	23.42	1.57	4.28	11.16	0.09	101.28	3VG29-1
38.51	0.73	21.21	n.a.	23.06	1.41	4.49	10.98	0.08	100.46	3VG29-2
38.21	0.64	21.44	n.a.	23.78	1.37	4.28	10.19	0.06	99.80	3VG29-3
37.80	0.83	21.07	n.a.	23.76	1.53	3.98	10.21	0.23	99.00	3VG29-4
38.40	0.56	21.81	n.a.	24.25	1.44	4.20	10.29	0.05	100.81	3VG29-5
38.38	0.76	21.47	n.a.	22.95	1.59	4.01	11.27	0.01	100.45	3VG29-6
38.25	0.50	21.76	n.a.	23.58	1.61	4.08	10.43	0.03	100.24	3VG29-7
38.29	0.62	21.33	n.a.	22.84	1.36	4.05	11.26	0.02	99.77	3VG29-8
38.60	0.54	21.86	n.a.	23.40	1.53	4.16	10.78	0.05	100.91	3VG29-9
38.04	0.74	21.43	n.a.	23.08	1.63	4.02	11.17	0.08	100.16	3VG29-10
38.38	0.40	21.70	n.a.	23.54	1.53	4.18	11.00	0.02	100.74	3VG29-11
38.45	0.66	21.45	n.a.	23.21	1.58	3.96	11.10	0.06	100.95	3VG29-12
38.31	0.62	21.49	n.d.	23.41	1.51	4.14	10.83	0.06	100.38	Average
0.28	0.11	0.23	n.d.	0.41	0.09	0.15	0.43	0.06		
38.23	1.21	20.81	0.01	23.86	0.88	6.15	8.66	0.06	99.49	3VG8-1
38.56	0.96	20.85	0	23.82	0.57	6.01	8.68	0.06	99.52	3VG8-2
38.41	1.21	20.61	0	23.73	0.80	6.72	8.21	0.06	99.74	3VG8-3
38.78	1.15	20.89	0.01	23.26	0.44	7.31	7.81	0.09	99.73	3VG8-4
38.50	1.13	20.74	0	23.67	0.62	6.30	8.09	0.07	99.62	Average
0.23	0.12	0.15	0	0.28	0.18	0.70	0.38	0.01		
39.28	1.58	20.86	0	22.21	0.42	7.94	8.10	0.11	100.50	3VG7-1
38.58	1.64	20.72	0.01	23.32	0.52	7.25	8.03	0.10	100.16	3VG7-2
39.77	1.32	19.89	0.01	21.17	0.40	8.06	9.29	0.15	100.06	3VG7-3
39.10	1.31	20.91	0.02	22.98	0.39	7.80	7.86	0.10	99.72	3VG7-4
38.80	1.27	20.90	0.01	23.31	0.61	7.05	8.18	0.06	99.96	3VG7-5
39.19	1.57	20.27	0.02	22.58	0.47	7.58	8.30	0.09	100.06	3VG7-6
39.21	1.51	20.98	0.01	22.26	0.41	8.10	7.80	0.15	100.43	3VG7-7
39.31	1.46	21.07	0.02	22.07	0.41	7.98	7.93	0.13	100.36	3VG7-8
38.55	1.77	20.77	0.02	23.10	0.59	7.11	8.13	0.08	100.11	3VG7-9
39.48	1.44	20.59	0.03	22.42	0.46	8.07	7.79	0.15	100.43	3VG7-10
39.07	1.55	20.88	0.01	22.19	0.43	7.86	7.98	0.14	100.10	3VG7-11
38.84	1.82	20.81	0.00	22.56	0.48	7.76	7.88	0.12	100.09	3VG7-12

SiO_2	TiO_2	Al_2O_3	Cr_2O_3	FeO	MnO	MgO	CaO	Na_2O	Total	Sample
39.11	1.10	21.17	0.00	23.30	0.56	6.79	6.38	0.06	100.81	3VG7-13
38.76	1.73	20.74	0	22.82	0.50	7.48	7.96	0.12	99.91	3VG7-14
38.89	1.81	20.84	0	22.18	0.43	7.87	7.97	0.14	99.80	3VG7-15
38.47	1.77	20.44	0.02	23.21	0.60	6.95	7.89	0.06	99.40	3VG7-16
38.54	1.66	20.44	0.03	23.29	0.60	7.01	7.80	0.06	99.37	3VG7-17
38.77	1.35	20.84	0	22.91	0.49	7.24	7.87	0.08	99.63	3VG7-18
39.14	1.49	20.94	0.01	22.61	0.41	7.66	7.36	0.08	100.06	3VG7-19
39.05	1.30	21.22	0.02	22.64	0.42	7.43	8.06	0.10	100.25	3VG7-20
38.84	1.81	20.72	0	22.28	0.46	7.80	7.90	0.12	99.69	3VG7-21
39.04	1.11	21.22	0	22.48	0.40	7.75	7.99	0.07	100.04	3VG7-22
39.09	1.52	20.88	0.01	22.57	0.48	7.49	7.98	0.06	100.04	3VG7-23
38.94	1.66	20.56	0.04	22.54	0.43	7.87	7.55	0.11	99.66	3VG7-24
39.09	1.82	20.80	0.00	22.15	0.41	7.66	8.21	0.09	100.06	3VG7-25
39.08	1.70	20.53	0	22.44	0.46	7.71	7.92	0.09	99.87	3VG7-26
38.76	1.89	20.58	0	22.90	0.50	7.51	8.10	0.06	100.12	3VG7-27
39.08	1.51	20.76	0.05	21.92	0.40	7.83	8.24	0.09	99.90	3VG7-28
38.86	1.66	20.63	0.03	22.42	0.35	7.67	7.86	0.09	99.58	3VG7-29
39.51	1.46	19.89	0.02	22.18	0.41	8.20	7.86	0.12	99.57	3VG7-30
39.00	1.51	20.73	0.01	22.56	0.46	7.60	8.00	0.10	99.96	Average
0.31	0.16	0.32	0.01	0.46	0.07	0.36	0.32	0.03		Std. Dev.
38.31	1.97	20.40	0.03	21.06	0.46	8.21	7.98	0.05	99.12	3VG8-1
38.86	1.24	20.86	0.00	20.46	0.42	8.20	8.94	0.07	99.12	3VG8-2
38.72	1.08	21.43	0.03	20.49	0.41	8.25	8.90	0.06	99.37	3VG8-3
38.37	1.69	20.75	0	20.77	0.40	8.16	8.79	0.06	99.08	3VG8-4
38.89	0.89	21.81	0	20.71	0.47	8.90	8.27	0.05	99.17	3VG8-5
38.56	1.55	20.82	0.03	20.87	0.37	8.37	8.83	0.06	99.10	3VG8-6
38.95	1.47	20.87	0.01	20.89	0.41	8.37	8.77	0.03	99.37	3VG8-7
38.93	0.81	21.45	0	20.27	0.44	8.83	8.79	0.06	99.28	3VG8-8
38.65	1.29	21.03	0.02	20.77	0.42	8.34	8.63	0.06	99.20	Average
0.24	0.47	0.42	0.01	0.43	0.03	0.16	0.35	0.01		Std. Dev.
38.53	0.71	21.06	n.a.	21.71	0.72	5.24	12.06	0.06	100.70	3VG39-1
38.10	0.67	21.36	n.a.	21.81	0.73	5.60	11.40	0.04	99.73	3VG39-2
38.82	0.79	21.50	n.a.	21.71	0.64	5.78	11.26	0.08	100.56	3VG39-3
38.56	0.70	21.67	n.a.	22.12	0.67	5.76	11.11	0.06	100.76	3VG39-4
38.33	0.90	21.12	n.a.	22.06	0.75	5.29	11.55	0.11	100.13	3VG39-5
38.20	0.80	21.16	n.a.	21.96	0.83	5.22	11.77	0.06	100.05	3VG39-6
38.20	0.86	21.50	n.a.	22.06	0.61	5.37	11.46	0.05	100.13	3VG39-7
38.74	0.67	21.73	n.a.	22.82	0.69	5.36	10.43	0.07	100.66	3VG39-8
39.13	0.61	21.00	n.a.	22.32	0.71	5.90	11.11	0.06	100.89	3VG39-9
38.33	0.53	21.46	n.a.	22.03	0.71	5.62	11.06	0.06	99.77	3VG39-10
38.49	0.71	21.42	n.d.	22.07	0.75	5.62	11.32	0.07	100.34	Average
0.33	0.11	0.24	n.d.	0.33	0.06	0.26	0.46	0.02		Std. Dev.
38.47	1.07	21.39	n.a.	21.43	0.30	8.30	8.39	n.a.	99.25	3VG34-1
38.89	0.89	22.01	n.a.	22.24	0.37	7.73	8.28	n.a.	100.10	3VG34-2
38.65	1.28	21.41	n.a.	21.81	0.32	8.25	8.02	n.a.	99.74	3VG34-3
38.66	0.84	21.86	n.a.	21.87	0.36	7.95	7.99	n.a.	99.20	3VG34-4
37.31	1.20	21.35	n.a.	22.25	0.31	7.90	7.94	n.a.	97.87	3VG34-5
38.71	1.05	21.56	n.a.	21.84	0.32	8.32	8.07	n.a.	98.98	3VG34-6
38.73	1.11	20.89	n.a.	21.59	0.30	8.17	7.88	n.a.	98.66	3VG34-7
38.81	1.60	21.34	n.a.	21.30	0.31	8.04	8.60	n.a.	100.20	3VG34-8
38.96	1.41	21.28	n.a.	22.11	0.32	7.83	8.63	n.a.	100.22	3VG34-9
38.72	1.20	21.44	n.a.	21.02	0.27	8.33	8.61	n.a.	99.59	3VG34-10
38.82	0.71	21.71	n.a.	22.01	0.28	8.10	8.63	n.a.	100.25	3VG34-11
38.84	1.33	20.96	n.a.	22.35	0.31	8.00	7.98	n.a.	99.64	3VG34-12
38.56	1.51	20.81	n.a.	22.17	0.33	7.90	8.09	n.a.	99.39	3VG34-13
39.04	1.20	21.14	n.a.	22.10	0.35	8.39	7.84	n.a.	100.06	3VG34-14
38.93	1.44	20.92	n.a.	21.66	0.35	7.82	8.66	n.a.	99.44	3VG34-15
39.14	1.04	21.25	n.a.	21.59	0.36	8.34	8.25	n.a.	99.96	3VG34-16
38.90	1.46	20.88	n.a.	21.72	0.34	7.46	9.16	n.a.	99.61	3VG34-17
38.57	1.23	21.23	n.a.	21.87	0.32	8.47	7.76	n.a.	99.47	3VG34-18
38.78	1.36	21.08	n.a.	21.27	0.30	8.21	8.46	n.a.	99.43	3VG34-19
39.09	0.95	21.82	n.a.	22.08	0.36	8.43	7.72	n.a.	100.13	3VG34-20
38.67	1.16	21.29	n.d.	21.82	0.32	8.09	8.24	n.d.	99.61	Average
0.37	0.26	0.31	n.d.	0.37	0.03	0.27	0.42	n.d.		Std. Dev.
37.82	1.49	20.96	n.a.	22.36	0.41	7.40	8.35	n.a.	98.76	3VG36-1
37.86	1.66	20.66	n.a.	22.97	0.46	6.74	8.95	n.a.	98.99	3VG36-2
38.23	0.86	21.58	n.a.	22.92	0.40	6.94	8.49	n.a.	99.39	3VG36-3
38.00	1.65	21.03	n.a.	22.84	0.36	7.76	7.64	n.a.	98.97	3VG36-4
38.06	1.48	20.70	n.a.	22.41	0.38	7.29	8.56	n.a.	98.87	3VG36-5
37.45	1.79	20.62	n.a.	22.89	0.46	7.41	7.95	n.a.	98.57	3VG36-6
38.20	1.62	20.84	n.a.	21.89	0.35	7.89	8.33	n.a.	99.13	3VG36-7
38.14	1.53	20.96	n.a.	21.99	0.36	8.03	8.06	n.a.	99.07	3VG36-8
38.23	1.29	21.29	n.a.	21.59	0.40	8.37	7.86	n.a.	98.83	3VG36-9
37.86	1.29	21.10	n.a.	22.04	0.40	7.89	7.86	n.a.	98.23	3VG36-10
37.70	1.35	21.10	n.a.	22.22	0.36	7.95	7.67	n.a.	98.95	3VG36-11

SiO_2	TiO_2	Al_2O_3	Cr_2O_3	FeO	MnO	MgO	CaO	Na_2O	Total	Sample
37.88	1.33	21.16	n.a.	22.14	0.36	7.82	8.05	n.a.	98.73	3VG35-12
37.63	1.36	20.91	n.a.	21.80	0.36	8.18	7.77	n.a.	98.00	3VG35-13
38.13	1.59	20.28	n.a.	21.94	0.36	7.86	8.09	n.a.	98.28	3VG35-14
38.18	0.96	21.27	n.a.	21.84	0.39	7.69	8.02	n.a.	98.34	3VG35-15
38.08	1.10	21.48	n.a.	21.52	0.34	8.18	7.91	n.a.	98.62	3VG35-16
37.77	1.31	21.01	n.a.	21.94	0.35	8.08	7.50	n.a.	97.94	3VG35-17
38.32	1.39	20.24	n.a.	21.50	0.39	8.05	8.36	n.a.	98.24	3VG35-18
37.85	1.19	21.10	n.a.	22.11	0.33	8.41	7.53	n.a.	98.51	3VG35-19
38.05	1.42	21.04	n.a.	22.01	0.39	7.60	7.87	n.a.	98.94	3VG35-20
38.16	1.12	21.47	n.a.	21.80	0.37	8.17	7.98	n.a.	99.08	3VG35-21
38.16	1.63	21.02	n.a.	21.56	0.33	7.93	8.47	n.a.	99.10	3VG35-22
37.95	1.59	20.94	n.a.	22.09	0.36	8.12	7.83	n.a.	98.88	3VG35-23
38.12	1.38	21.30	n.a.	21.80	0.35	8.24	7.80	n.a.	98.99	3VG35-24
38.45	1.46	21.03	n.a.	21.79	0.35	8.26	7.84	n.a.	99.15	3VG35-25
37.99	1.38	21.00	n.d.	22.08	0.37	7.86	8.05	n.d.	98.72	Average
0.26	0.22	0.33	n.d.	0.45	0.03	0.42	0.37	n.d.		Std. Dev.
38.498	1.566	21.447	n.a.	22.814	0.369	7.693	8.013	0.129	100.526	3VG40-1
38.849	1.480	21.776	n.a.	21.701	0.373	8.169	7.932	0.111	100.39	3VG40-2
38.771	1.627	21.601	n.a.	22.044	0.325	7.902	8.060	0.08	100.419	3VG40-3
38.783	1.726	20.41	n.a.	22.77	0.432	7.46	8.46	0.166	100.207	3VG40-4
38.409	1.516	21.712	n.a.	22.28	0.417	8.049	7.744	0.146	100.286	3VG40-5
38.873	1.698	21.433	n.a.	22.377	0.366	8.062	7.964	0.152	100.915	3VG40-6
38.399	1.583	21.795	n.a.	22.433	0.371	7.783	8.131	0.083	100.478	3VG40-7
38.677	1.437	21.316	n.a.	21.941	0.346	7.803	8.324	0.136	100	3VG40-8
39.086	1.717	21.469	n.a.	21.442	0.387	7.757	8.742	0.13	100.73	3VG40-9
39.011	1.456	21.739	n.a.	22.343	0.346	8.201	7.723	0.129	100.95	3VG40-10
38.73	1.58	21.47	n.d.	22.20	0.37	7.89	8.12	0.13	100.49	Average
0.24	0.11	0.40	n.d.	0.44	0.03	0.23	0.33	0.04		Std. Dev.
38.13	0.69	21.90	n.a.	21.74	0.39	5.94	10.88	0.13	99.81	3VG36-1
38.67	0.75	21.82	n.a.	21.96	0.63	5.82	10.49	0.10	100.32	3VG36-2
38.62	0.74	22.08	n.a.	22.00	0.41	6.04	9.43	0.12	100.00	3VG36-3
38.24	0.68	21.92	n.a.	21.72	0.39	6.13	10.71	0.09	99.87	3VG36-4
39.01	0.50	22.28	n.a.	21.96	0.39	6.09	10.83	0.09	101.12	3VG36-5
39.03	0.75	21.89	n.a.	22.34	0.52	5.82	10.06	0.13	100.46	3VG36-6
38.40	0.93	21.72	n.a.	22.16	0.54	5.99	10.71	0.16	100.58	3VG36-7
38.47	0.97	21.39	n.a.	21.94	0.46	6.12	10.67	0.13	100.17	3VG36-8
38.73	0.83	21.72	n.a.	21.86	0.34	6.06	9.87	0.10	100.20	3VG36-9
38.44	0.94	21.64	n.a.	22.20	0.44	5.88	10.56	0.14	100.27	3VG36-10
38.57	0.78	21.79	n.d.	22.08	0.46	6.09	10.43	0.13	100.26	Average
0.30	0.14	0.26	n.d.	0.27	0.09	0.34	0.46	0.03		Std. Dev.
38.05	1.03	21.83	n.a.	21.13	0.29	8.09	8.01	n.a.	98.43	3VG31-1
39.67	1.13	21.67	n.a.	20.57	0.31	8.30	8.80	n.a.	100.44	3VG31-2
38.77	1.09	21.13	n.a.	21.77	0.29	7.09	9.01	n.a.	99.14	3VG31-3
38.44	1.30	21.22	n.a.	21.44	0.29	7.50	9.02	n.a.	99.20	3VG31-4
38.53	1.31	21.25	n.a.	21.28	0.28	8.31	8.00	n.a.	98.94	3VG31-5
38.62	1.04	21.58	n.a.	21.41	0.28	7.32	8.11	n.a.	98.37	3VG31-6
38.08	1.29	21.44	n.a.	21.74	0.29	7.50	8.63	n.a.	98.94	3VG31-7
37.99	1.40	21.29	n.a.	21.50	0.31	7.47	8.89	n.a.	98.86	3VG31-8
38.40	1.30	21.36	n.a.	20.96	0.28	8.21	8.40	n.a.	99.05	3VG31-9
38.28	0.92	21.66	n.a.	21.58	0.23	7.87	8.22	n.a.	98.74	3VG31-10
38.81	1.04	22.14	n.a.	21.20	0.28	8.42	8.02	n.a.	99.90	3VG31-11
38.54	1.07	21.81	n.a.	21.56	0.29	8.37	7.77	n.a.	99.40	3VG31-12
38.72	1.23	21.33	n.a.	21.31	0.29	8.50	7.84	n.a.	99.22	3VG31-13
37.98	1.20	21.21	n.a.	21.78	0.37	6.96	9.38	n.a.	98.88	3VG31-14
38.72	1.23	20.68	n.a.	21.20	0.32	8.65	7.85	n.a.	98.64	3VG31-15
38.27	1.36	21.23	n.a.	21.98	0.30	7.03	8.96	n.a.	99.32	3VG31-16
38.53	1.18	21.42	n.d.	21.37	0.29	7.89	8.53	n.d.	99.22	Average
0.39	0.15	0.35	n.d.	0.32	0.03	0.53	0.53	n.d.		Std. Dev.
38.91	1.19	0.28	n.a.	21.77	21.28	8.14	8.21	0.21	99.94	3VG44-1
38.82	1.15	0.44	n.a.	22.40	21.10	6.68	9.60	0.13	100.31	3VG44-2
39.43	1.15	0.29	n.a.	21.98	21.49	8.73	7.43	0.19	100.70	3VG44-3
38.97	1.33	0.34	n.a.	21.40	21.10	8.01	8.67	0.28	100.10	3VG44-4
39.26	1.44	0.30	n.a.	21.40	21.23	8.86	8.10	0.31	100.86	3VG44-5
39.08	1.22	0.33	n.a.	21.60	21.20	8.07	8.40	0.20	100.09	3VG44-6
39.20	1.30	0.29	n.a.	21.73	21.31	7.65	8.81	0.12	100.81	3VG44-7
39.11	1.34	0.33	n.a.	21.98	21.20	7.29	8.94	0.19	100.47	3VG44-8
38.84	1.03	0.67	n.a.	22.20	21.04	5.74	10.87	0.18	100.18	3VG44-9
39.15	0.93	0.31	n.a.	21.80	21.46	7.58	8.79	0.15	100.17	3VG44-10
38.86	0.88	0.44	n.a.	21.72	21.57	6.06	10.70	0.01	100.11	3VG44-11
39.18	1.22	0.30	n.a.	21.77	21.22	7.71	8.64	0.10	100.08	3VG44-12
39.30	0.84	0.31	n.a.	21.77	21.64	6.82	9.40	0.19	100.46	3VG44-13
39.29	1.09	0.30	n.a.	21.75	21.28	7.18	9.22	0.09	100.29	3VG44-14
39.38	1.10	0.29	n.a.	21.54	21.29	7.84	8.67	0.14	100.31	3VG44-15
39.35	0.98	0.24	n.a.	21.42	21.59	8.72	7.90	0.16	100.36	3VG44-16
42.33	0.88	0.28	n.a.	18.86	18.29	8.30	10.14	0.80	99.86	3VG44-17
39.34	1.07	0.33	n.a.	22.94	21.37	6.63	9.02	0.19	100.89	3VG44-18

SiO_2	TiO_2	Al_2O_3	Cr_2O_3	FeO	MnO	MgO	CaO	Na_2O	Total	Sample
39.40	1.30	0.30	n.a.	21.46	20.76	8.06	8.53	0.24	100.04	3VG44-19
39.48	1.07	0.28	n.a.	21.75	21.51	8.62	7.67	0.19	100.57	3VG44-20
39.35	1.47	0.32	n.a.	21.24	21.18	7.86	8.86	0.16	100.42	3VG44-21
39.32	1.14	0.33	n.d.	21.62	21.15	7.65	8.88	0.20	100.29	Average
0.73	0.20	0.08	n.d.	0.71	0.69	0.83	0.89	0.15		Std. Dev.
38.58	1.36	21.21	n.a.	21.36	0.32	7.96	8.93	0.12	99.84	3VG41-1
38.58	1.36	21.21	n.a.	21.36	0.32	7.96	8.93	0.12	99.84	3VG41-2
38.50	1.04	21.85	n.a.	21.14	0.36	8.49	8.14	0.14	99.66	3VG41-3
39.25	1.39	21.58	n.a.	21.21	0.32	8.35	8.63	0.22	100.94	3VG41-4
39.16	1.21	21.90	n.a.	21.24	0.33	8.10	8.88	0.07	100.89	3VG41-5
38.65	1.46	21.65	n.a.	21.66	0.33	8.20	8.24	0.19	100.37	3VG41-6
39.36	1.25	21.87	n.a.	21.40	0.32	7.94	8.60	0.13	100.86	3VG41-7
38.42	1.05	21.63	n.a.	20.76	0.31	7.71	9.81	0.05	99.74	3VG41-8
38.88	1.30	21.66	n.a.	21.85	0.34	8.13	8.18	0.15	100.49	3VG41-9
38.81	1.27	21.78	n.a.	21.60	0.33	7.46	9.41	0.05	100.71	3VG41-10
39.05	1.01	21.91	n.a.	21.40	0.37	8.24	8.38	0.10	100.44	3VG41-11
38.92	0.92	22.17	n.a.	21.83	0.37	7.58	8.85	0.05	100.69	3VG41-12
38.69	1.31	21.56	n.a.	21.83	0.36	8.12	7.84	0.12	99.85	3VG41-13
38.92	1.29	21.90	n.a.	20.51	0.37	7.74	9.59	0.16	100.46	3VG41-14
39.02	1.52	21.65	n.a.	21.01	0.33	7.79	9.25	0.12	100.69	3VG41-15
39.05	1.29	21.89	n.a.	20.71	0.34	8.16	9.18	0.15	100.77	3VG41-16
38.98	1.48	21.40	n.a.	21.53	0.34	7.67	9.14	0.11	100.64	3VG41-17
38.87	1.26	21.70	n.d.	21.32	0.34	7.98	8.82	0.12	100.40	Average
0.27	0.17	0.26	n.d.	0.40	0.02	0.29	0.55	0.05		Std. Dev.
39.01	1.04	21.79	n.a.	22.14	0.35	6.83	9.82	0.17	101.14	3VG43-1
39.29	1.00	21.80	n.a.	21.40	0.32	7.96	9.32	0.14	101.24	3VG43-2
38.50	1.28	21.39	n.a.	22.50	0.40	6.18	10.17	0.15	100.56	3VG43-3
39.22	0.88	22.03	n.a.	21.89	0.28	6.94	9.49	0.04	100.76	3VG43-4
38.86	0.80	22.11	n.a.	23.98	0.59	6.15	8.99	0.21	101.68	3VG43-5
38.92	0.93	21.83	n.a.	22.27	0.37	6.56	9.55	0.12	100.55	3VG43-6
39.42	1.06	21.88	n.a.	21.64	0.29	7.67	9.44	0.13	101.52	3VG43-7
39.37	0.97	21.92	n.a.	21.90	0.35	7.56	9.21	0.10	101.37	3VG43-8
39.04	0.91	21.73	n.a.	21.45	0.27	7.85	9.15	0.15	100.56	3VG43-9
39.46	1.00	21.84	n.a.	21.73	0.24	8.02	9.12	0.12	101.53	3VG43-10
39.12	0.74	22.15	n.a.	22.25	0.32	7.61	8.91	0.12	101.21	3VG43-11
39.11	0.96	21.86	n.d.	22.10	0.34	7.21	9.38	0.13	101.10	Average
0.29	0.14	0.21	n.d.	0.71	0.09	0.71	0.37	0.04		Std. Dev.
39.14	1.46	21.78	n.a.	21.96	0.33	7.16	9.02	0.11	100.95	3VG38-1
38.90	1.28	21.87	n.a.	21.12	0.24	8.67	8.05	0.17	100.29	3VG38-2
37.95	1.46	21.12	n.a.	21.54	0.31	7.57	8.86	0.16	98.96	3VG38-3
38.48	1.54	21.42	n.a.	21.30	0.24	8.17	8.71	0.15	100.01	3VG38-4
39.00	1.10	22.13	n.a.	21.14	0.27	8.06	8.98	0.15	100.83	3VG38-5
38.80	1.34	21.46	n.a.	21.02	0.25	8.69	8.38	0.18	100.12	3VG35-6
38.65	1.18	21.93	n.a.	20.51	0.26	8.60	8.24	0.13	99.49	3VG38-7
38.69	1.42	21.70	n.a.	21.09	0.26	8.50	8.59	0.13	100.39	3VG38-8
38.33	1.33	21.70	n.a.	21.69	0.26	7.40	9.24	0.16	100.12	3VG38-9
38.63	1.41	21.66	n.a.	22.08	0.33	6.55	9.57	0.13	100.37	3VG38-10
38.54	1.35	21.72	n.a.	22.27	0.35	6.33	9.73	0.10	100.38	3VG38-11
38.65	1.35	21.68	n.d.	21.43	0.28	7.79	8.85	0.14	100.17	Average
0.33	0.13	0.27	n.d.	0.53	0.04	0.85	0.53	0.02		Std. Dev.
38.46	1.22	0.34	n.a.	21.66	21.57	6.80	9.84	0.11	99.99	3VG45-1
38.59	1.20	0.37	n.a.	22.24	21.35	6.50	9.95	0.13	100.33	3VG45-2
38.57	1.32	0.35	n.a.	22.37	21.53	6.98	9.30	0.16	100.57	3VG45-3
38.79	1.36	0.34	n.a.	20.84	21.47	8.03	8.94	0.15	99.92	3VG45-4
39.03	1.45	0.28	n.a.	21.16	21.38	7.70	9.11	0.22	100.32	3VG45-5
38.81	1.21	0.28	n.a.	20.64	21.65	7.15	10.03	0.22	100.00	3VG45-6
38.82	1.44	0.28	n.a.	20.57	21.11	7.68	9.32	0.14	99.36	3VG45-7
38.91	1.36	0.29	n.a.	21.02	21.48	7.64	9.38	0.15	100.23	3VG45-8
37.95	1.20	0.33	n.a.	22.06	21.57	7.05	9.05	0.04	99.25	3VG45-9
38.45	1.04	0.30	n.a.	21.87	21.11	6.63	9.79	0.04	99.23	3VG45-10
38.71	1.44	0.35	n.a.	21.61	21.12	6.68	10.03	0.11	100.06	3VG45-11
39.11	1.19	0.30	n.a.	20.41	21.55	7.15	10.46	0.16	100.34	3VG45-12
38.70	1.44	0.32	n.a.	21.60	21.51	8.11	8.08	0.21	99.97	3VG45-13
38.64	1.13	0.31	n.a.	20.89	21.72	7.29	9.62	0.14	99.73	3VG45-14
39.19	1.44	0.34	n.a.	22.13	21.17	7.59	8.37	0.14	100.36	3VG45-15
39.10	1.24	0.37	n.a.	21.30	21.16	8.03	8.53	0.25	99.97	3VG45-16
38.46	1.33	0.35	n.a.	21.97	21.59	6.98	9.27	0.15	100.10	3VG45-17
38.72	1.26	0.31	n.a.	22.01	21.47	6.97	9.15	0.16	100.05	3VG45-18
38.42	1.39	0.32	n.a.	22.09	21.36	6.84	9.53	0.11	100.07	3VG45-19
38.80	0.98	0.33	n.a.	20.77	21.65	6.87	10.10	0.18	99.69	3VG45-20
38.71	1.28	0.32	n.d.	21.46	21.43	7.23	9.39	0.15	99.98	Average
0.29	0.14	0.03	n.d.	0.63	0.20	0.50	0.62	0.05		Std. Dev.
39.29	1.27	0.37	n.a.	21.33	21.56	7.47	9.54	0.11	100.93	3VG46-1
39.12	1.36	0.37	n.a.	21.44	21.00	8.12	8.40	0.13	99.92	3VG46-2

SiO_2	TiO_2	Al_2O_3	Cr_2O_3	FeO	MnO	MgO	CaO	Na_2O	Total	Sample
39.00	1.43	0.36	n.a.	21.27	21.16	7.74	9.06	0.16	100.17	3VG46-3
39.22	1.09	0.30	n.a.	21.01	21.61	8.46	8.80	0.10	100.58	3VG46-4
38.68	1.47	0.33	n.a.	19.83	21.05	7.46	10.30	0.11	99.22	3VG46-5
39.19	1.25	0.40	n.a.	22.01	21.27	8.03	7.99	0.24	100.36	3VG46-6
39.05	1.32	0.35	n.a.	21.35	21.17	7.46	9.28	0.14	100.12	3VG46-7
38.47	1.63	0.34	n.a.	22.02	20.80	7.32	9.02	0.21	99.82	3VG46-8
38.28	1.34	0.36	n.a.	21.78	21.31	7.14	9.40	0.10	99.71	3VG46-9
39.04	1.28	0.34	n.a.	21.61	21.07	8.22	8.43	0.20	100.17	3VG46-10
39.05	1.23	0.32	n.a.	21.18	21.37	7.54	9.50	0.13	100.30	3VG46-11
39.06	1.29	0.38	n.a.	21.34	21.23	8.13	8.57	0.18	100.17	3VG46-12
38.61	1.35	0.34	n.a.	21.47	20.84	7.63	9.10	0.10	99.63	3VG46-13
38.98	1.18	0.40	n.a.	21.32	20.92	8.13	8.21	0.16	99.31	3VG46-14
38.88	1.31	0.32	n.a.	21.39	21.36	8.18	8.35	0.13	99.92	3VG46-15
39.12	1.16	0.41	n.a.	21.95	21.14	8.14	7.86	0.21	99.98	3VG46-16
39.16	1.28	0.38	n.a.	22.34	21.28	8.48	7.36	0.16	100.45	3VG46-17
39.21	1.13	0.45	n.a.	21.30	21.31	8.16	8.46	0.14	100.17	3VG46-18
38.75	1.31	0.31	n.a.	21.48	21.21	7.74	9.20	0.14	100.14	3VG46-19
39.13	1.32	0.39	n.a.	21.39	20.79	7.86	8.43	0.21	99.53	3VG46-20
38.97	1.30	0.36	n.d.	21.44	21.17	7.87	8.76	0.15	100.03	Average
0.26	0.12	0.04	n.d.	0.50	0.23	0.39	0.69	0.04		Std. Dev.
39.11	0.69	21.07	n.a.	26.03	1.30	5.19	8.09	0.04	101.50	KAP5-1
39.40	0.43	21.34	n.a.	26.00	1.41	5.01	7.95	0.02	101.55	KAP5-2
38.89	0.62	21.11	n.a.	25.94	1.42	4.94	8.13	0.07	101.12	KAP5-3
38.94	0.69	20.92	n.a.	25.72	1.30	5.09	8.08	0.02	100.76	KAP5-4
38.67	0.42	21.33	n.a.	25.18	1.69	4.27	9.27	0.05	100.88	KAP5-5
39.03	0.80	21.13	n.a.	25.93	1.20	5.27	8.20	0.07	101.63	KAP5-6
38.95	0.93	21.10	n.a.	26.22	1.20	5.12	7.89	0.06	101.46	KAP5-7
39.00	0.65	21.14	n.d.	25.86	1.36	4.98	8.23	0.05	101.27	Average
0.22	0.18	0.15	n.d.	0.33	0.17	0.33	0.47	0.02		Std. Dev.
36.84	0.65	20.10	0.09	24.43	1.50	4.08	9.38	0.01	97.07	KAP16-1
38.27	1.05	20.63	0.04	24.15	0.99	4.29	9.19	0.20	98.81	KAP16-2
36.92	1.15	20.03	0.06	24.02	1.11	4.08	9.73	0.02	97.12	KAP16-3
37.53	1.14	20.48	0.07	24.63	0.99	4.35	8.95	0.04	98.18	KAP16-4
36.96	1.02	19.06	0.04	23.67	1.36	4.08	10.38	0.02	96.58	KAP16-5
36.83	1.06	20.34	0	24.67	1.01	4.42	8.76	0.05	97.14	KAP16-6
36.92	0.97	19.85	0.04	24.35	1.31	4.18	9.28	0.03	96.92	KAP16-7
37.59	0.98	19.69	0.05	24.13	0.84	4.16	8.84	0.11	96.39	KAP16-8
36.93	0.53	19.87	0.04	24.25	1.98	3.74	9.71	0.03	97.08	KAP16-9
36.67	1.01	19.90	0.03	24.67	1.20	4.39	9.10	0.06	97.03	KAP16-10
37.08	1.15	19.56	0.02	24.33	1.27	4.19	9.73	0.07	97.39	KAP16-11
37.06	0.71	20.05	0.02	24.57	1.69	4.00	9.48	0.11	97.68	KAP16-12
36.80	0.89	20.42	0.05	24.63	1.19	4.20	8.88	0.06	97.13	KAP16-13
36.75	0.93	19.69	0.02	24.86	1.49	4.08	9.31	0.05	97.17	KAP16-14
37.35	0.90	19.95	0.03	24.50	1.00	4.35	8.28	0.17	96.53	KAP16-15
37.10	0.94	19.97	0.04	24.39	1.26	4.17	9.27	0.07	97.21	Average
0.42	0.18	0.40	0.02	0.31	0.31	0.18	0.51	0.06		Std. Dev.
37.74	1.07	20.49	0.02	24.46	0.68	5.14	7.93	0.08	97.61	KAP15-1
37.26	1.24	19.91	0.05	24.91	0.82	5.05	7.85	0.08	97.17	KAP15-2
37.89	1.43	20.07	0.03	24.65	0.68	5.18	7.75	0.08	97.77	KAP15-3
37.90	1.08	20.53	0.01	24.65	0.68	5.33	7.40	0.06	97.63	KAP15-4
37.36	1.13	19.78	0.01	25.24	0.97	5.21	7.51	0.09	97.29	KAP15-5
37.87	1.28	20.47	0.05	24.78	0.70	5.11	7.83	0.13	98.22	KAP15-6
37.80	1.04	19.89	0.05	25.37	1.09	5.01	8.79	0.07	99.10	KAP15-7
37.70	1.13	20.05	0.03	25.14	1.03	5.06	8.73	0.06	98.92	KAP15-8
37.49	1.09	19.91	0.07	25.18	1.06	5.34	8.50	0.09	98.73	KAP15-9
37.70	1.16	20.39	0.07	25.19	0.74	5.45	8.04	0.10	98.84	KAP15-10
37.67	1.16	20.15	0.04	24.96	0.84	5.19	8.03	0.09	98.13	Average
0.23	0.12	0.29	0.02	0.31	0.17	0.14	0.49	0.02		Std. Dev.
38.05	0.91	20.67	n.a.	24.56	0.93	6.37	8.33	0.07	99.88	KAP20-1
38.03	0.82	21.03	n.a.	24.79	0.87	6.25	8.36	0.05	100.19	KAP20-2
38.16	0.91	20.99	n.a.	24.75	0.78	6.55	8.22	0.08	100.44	KAP20-3
37.86	0.78	21.05	n.a.	24.83	0.92	6.51	7.84	0.08	99.86	KAP20-4
38.54	0.85	21.43	n.a.	24.55	0.66	7.09	7.23	0.00	100.34	KAP20-5
38.30	0.76	20.83	n.a.	24.43	0.91	6.31	8.25	0.04	99.84	KAP20-6
38.32	0.74	21.19	n.a.	24.50	0.65	6.47	8.51	0.05	100.43	KAP20-7
37.64	0.78	20.69	n.a.	24.74	0.95	6.28	8.33	0.03	99.44	KAP20-8
38.32	1.01	20.95	n.a.	24.63	0.76	6.22	8.68	0.02	100.58	KAP20-9
38.01	0.88	20.75	n.a.	25.04	0.79	6.18	8.32	0.09	100.05	KAP20-10
38.70	0.70	21.62	n.a.	24.40	0.64	6.67	8.06	0.06	100.85	KAP20-11
38.36	0.78	21.14	n.a.	25.20	0.95	6.32	8.16	0.04	100.94	KAP20-12
38.53	0.70	20.55	n.a.	24.84	0.85	6.19	8.74	0.05	100.45	KAP20-13
38.61	0.79	20.91	n.a.	24.85	0.89	6.12	8.38	0.25	100.79	KAP20-14
38.24	0.81	20.99	n.d.	24.72	0.83	6.39	8.24	0.06	100.29	Average
0.30	0.09	0.30	n.d.	0.23	0.11	0.25	0.37	0.06		Std. Dev.

SiO_2	TIO_2	Al_2O_3	Cr_2O_3	FeO	MnO	MgO	CaO	Na_2O	Total	Sample
37.62	1.27	19.56	0.04	23.78	0.70	6.83	8.01	0.03	97.83	KAP18-1
37.32	1.47	19.37	0.04	24.04	0.70	6.92	7.67	0.05	97.58	KAP18-2
37.89	1.07	19.75	0.02	23.56	0.64	7.18	7.91	0.07	98.07	KAP18-3
37.34	1.18	19.57	0.03	24.14	0.67	7.03	7.85	0.05	97.87	KAP18-4
37.64	1.20	19.55	0.04	23.86	0.65	7.16	7.71	0.07	97.88	KAP18-5
38.11	0.95	19.78	0.06	23.47	0.60	7.31	7.63	0.08	97.99	KAP18-6
38.17	0.90	19.68	0.07	23.93	0.74	6.67	7.79	0.10	98.05	KAP18-7
37.47	0.82	19.97	0.04	23.36	0.87	6.96	7.87	0.03	97.40	KAP18-8
37.84	1.15	19.32	0.04	23.55	0.83	7.14	7.29	0.04	97.19	KAP18-9
37.37	1.10	19.30	0.06	23.81	0.74	7.06	7.54	0.03	97.03	KAP18-10
37.56	1.09	19.53	0.06	23.02	0.76	7.42	8.15	0.02	97.61	KAP18-11
37.58	0.96	19.53	0.01	23.56	0.74	7.04	8.20	0.06	97.68	KAP18-12
39.20	0.08	22.18	0	22.93	0.52	10.69	4.01	0.01	99.62	KAP18-13
38.03	1.01	19.85	0.03	23.87	0.89	6.83	7.77	0.06	98.34	KAP18-14
38.11	0.99	19.41	0.04	23.53	0.83	7.06	8.05	0.05	98.08	KAP18-15
38.02	1.08	19.74	0	23.95	0.73	7.18	7.57	0.03	98.31	KAP18-16
37.63	1.26	19.61	0.03	23.76	0.76	7.20	7.52	0.04	97.81	KAP18-17
38.36	1.01	19.26	0	23.36	0.70	7.10	8.05	0.08	97.92	KAP18-18
38.11	1.03	19.96	0.02	23.93	0.82	6.71	8.09	0.08	98.74	KAP18-19
37.79	0.89	20.42	0.07	23.79	0.77	7.10	7.63	0.01	98.27	KAP18-20
37.74	1.11	19.70	0.05	23.75	0.75	7.07	7.73	0.05	97.95	KAP18-21
37.61	1.24	19.46	0.08	24.14	0.71	7.15	7.69	0.02	98.10	KAP18-22
37.88	1.16	19.98	0.08	23.96	0.72	7.23	7.50	0.02	98.54	KAP18-23
37.48	1.42	19.38	0.07	23.62	0.78	7.35	7.77	0.03	97.89	KAP18-24
37.73	0.96	20.00	0.08	24.00	0.75	6.92	7.54	0.02	98.00	KAP18-25
37.66	1.16	19.45	0.04	23.85	0.86	7.23	7.62	0.06	97.93	KAP18-26
37.84	1.12	19.13	0.08	23.62	0.86	6.98	8.31	0.08	98.00	KAP18-27
37.52	1.34	19.63	0.08	23.69	0.72	7.04	7.97	0.02	98.01	KAP18-28
37.10	1.38	19.28	0.07	23.95	0.79	7.01	7.79	0.03	97.40	KAP18-29
37.76	1.01	20.17	0.08	23.72	0.61	7.19	7.87	0.09	98.49	KAP18-30
37.56	1.27	19.52	0.07	24.08	0.70	6.92	7.80	0.06	97.97	KAP18-31
37.49	1.37	19.95	0.07	23.66	0.61	7.32	7.55	0.09	98.09	KAP18-32
37.77	1.09	19.72	0.05	23.73	0.73	7.19	7.67	0.05	97.99	Average
0.39	0.26	0.53	0.03	0.29	0.09	0.66	0.71	0.02		Std. Dev.
38.06	1.28	19.96	0.04	23.76	0.66	5.95	8.75	0.09	98.54	KAP8-1
38.00	1.23	20.26	0.06	23.91	0.88	5.53	9.13	0.07	99.06	KAP8-2
38.10	1.22	20.21	0.08	23.86	0.74	5.76	8.98	0.10	99.05	KAP8-3
38.34	1.29	20.30	0.07	23.71	0.45	6.34	8.53	0.13	99.17	KAP8-4
38.12	1.25	20.18	0.07	23.81	0.68	5.89	8.85	0.10	98.98	Average
0.15	0.03	0.16	0.02	0.09	0.18	0.34	0.26	0.02		Std. Dev.
38.35	1.49	20.10	0.05	23.88	0.59	6.46	8.92	0.11	99.95	KAP7-1
38.53	1.39	20.23	0.04	23.45	0.60	6.45	9.21	0.10	100.00	KAP7-2
38.68	1.25	20.16	0.07	23.49	0.61	6.72	8.53	0.07	99.57	KAP7-3
38.26	1.39	19.86	0.03	23.95	0.75	6.48	8.84	0.08	99.63	KAP7-4
38.29	1.46	19.94	0.03	24.00	0.69	6.53	8.67	0.09	99.70	KAP7-5
38.41	1.52	20.05	0.07	23.46	0.60	6.33	9.29	0.10	99.82	KAP7-6
38.53	1.03	20.34	0.02	23.69	0.64	6.32	8.84	0.05	99.45	KAP7-7
38.29	1.53	20.02	0.05	24.12	0.61	6.16	9.16	0.06	99.99	KAP7-8
38.62	1.33	20.31	0.05	23.76	0.58	6.71	8.31	0.13	99.80	KAP7-9
38.29	1.62	19.89	0.05	23.87	0.68	6.56	9.08	0.04	100.09	KAP7-10
38.72	1.75	19.78	0.01	23.42	0.67	6.60	9.22	0.07	100.24	KAP7-11
38.62	1.67	19.42	0.04	23.16	0.58	6.46	9.61	0.10	99.65	KAP7-12
38.74	1.50	20.04	0.01	24.05	0.67	6.45	8.63	0.07	100.17	KAP7-13
38.79	1.33	20.32	0	24.41	0.67	6.70	8.26	0.06	100.54	KAP7-14
38.38	1.42	20.43	0.04	23.02	0.51	6.39	9.30	0.08	99.57	KAP7-15
38.65	1.46	20.43	0	23.17	0.51	6.51	9.15	0.08	99.96	KAP7-16
38.43	1.64	20.02	0.06	23.45	0.62	6.51	9.40	0.07	100.19	KAP7-17
38.56	1.25	20.62	0	23.69	0.56	6.44	9.02	0.08	100.21	KAP7-18
38.18	1.56	19.69	0.05	24.28	0.66	6.27	8.61	0.07	99.36	KAP7-19
38.35	1.44	20.11	0.02	23.67	0.57	6.32	9.10	0.10	99.67	KAP7-20
38.48	1.45	20.09	0.03	23.70	0.62	6.47	8.96	0.08	99.88	Average
0.18	0.17	0.28	0.02	0.38	0.06	0.15	0.36	0.02		Std. Dev.
37.83	1.59	20.18	0.04	22.74	0.53	7.19	8.51	0.11	98.73	KAP9-1
37.88	1.50	20.03	0.04	22.57	0.55	7.53	8.60	0.12	98.82	KAP9-2
37.47	1.53	19.87	0.03	22.06	0.59	7.53	8.59	0.24	97.89	KAP9-3
37.31	1.36	19.93	0.08	22.09	0.51	7.15	8.65	0.25	97.33	KAP9-4
37.54	1.43	20.14	0.03	22.35	0.52	7.29	8.73	0.26	98.27	KAP9-5
37.51	1.42	19.86	0.02	21.96	0.51	7.38	8.73	0.27	97.63	KAP9-6
37.64	1.29	20.19	0.07	22.24	0.49	7.56	8.34	0.17	98.01	KAP9-7
37.53	1.61	19.89	0.09	22.88	0.52	7.29	8.73	0.12	98.64	KAP9-8
37.74	1.23	19.94	0.03	22.91	0.58	7.02	8.70	0.10	98.23	KAP9-9
38.11	1.37	18.96	0.04	21.93	0.56	7.45	9.34	0.14	97.91	KAP9-10
38.07	1.39	20.15	0.02	22.85	0.55	7.60	8.41	0.09	99.11	KAP9-11
38.13	1.12	20.59	0.05	22.34	0.50	7.27	8.68	0.10	98.78	KAP9-12
38.09	1.47	19.87	0.02	22.82	0.60	7.70	8.41	0.17	99.16	KAP9-13
38.02	1.24	20.27	0.02	22.91	0.59	7.73	8.19	0.13	99.10	KAP9-14
38.36	0.70	20.61	0	22.68	0.55	8.01	7.73	0.04	98.68	KAP9-15
37.92	1.34	19.94	0.03	23.26	0.62	7.90	7.88	0.13	99.01	KAP9-16

SiO_2	TiO_2	Al_2O_3	Cr_2O_3	FeO	MnO	MgO	CaO	Na_2O	Total	Sample
38.54	1.16	19.15	0.05	21.53	0.48	7.51	9.31	0.25	97.96	KAP9-17
37.70	1.32	19.91	0.03	22.44	0.50	7.39	8.34	0.14	97.77	KAP9-18
38.54	1.16	20.15	0.07	22.26	0.54	7.76	8.25	0.13	98.86	KAP9-19
38.42	1.12	20.79	0.07	22.11	0.52	7.53	8.34	0.09	98.98	KAP9-20
37.88	1.34	20.27	0.05	22.58	0.54	7.53	8.50	0.06	98.75	KAP9-21
38.16	0.74	21.04	0.04	22.49	0.60	8.10	7.66	0.06	98.88	KAP9-22
37.51	1.69	20.06	0.08	22.73	0.50	7.82	8.14	0.08	98.60	KAP9-23
37.53	1.75	19.64	0.06	22.82	0.62	7.62	8.64	0.08	98.77	KAP9-24
37.23	1.66	19.65	0.05	22.77	0.53	7.58	8.47	0.08	98.04	KAP9-25
37.87	1.34	20.04	0.04	22.49	0.54	7.54	8.47	0.14	98.48	Average
0.37	0.26	0.45	0.02	0.40	0.04	0.26	0.39	0.07		Std. Dev.
38.51	1.56	20.77	n.a.	23.96	0.79	5.97	9.62	0.11	101.28	KAP34-1
38.90	1.26	20.94	n.a.	23.44	0.43	6.62	8.94	0.24	100.78	KAP34-2
38.25	1.50	20.51	n.a.	23.27	0.77	6.36	9.46	0.11	100.22	KAP34-3
38.28	1.22	20.88	n.a.	24.07	0.61	6.08	9.22	0.14	100.49	KAP34-4
38.34	1.66	20.40	n.a.	23.34	0.42	6.32	9.76	0.14	100.38	KAP34-5
38.69	1.41	20.63	n.a.	23.20	0.39	6.83	8.85	0.26	100.27	KAP34-6
38.75	1.17	21.18	n.a.	23.57	0.43	6.42	9.21	0.13	100.86	KAP34-7
38.04	1.37	20.63	n.a.	23.50	0.73	5.86	9.81	0.14	100.07	KAP34-8
38.79	1.32	20.57	n.a.	23.57	0.72	6.24	9.49	0.19	100.88	KAP34-9
38.70	1.44	20.58	n.a.	23.90	0.54	6.55	8.80	0.18	100.70	KAP34-10
38.52	1.39	20.71	n.d.	23.58	0.58	6.33	9.32	0.16	100.59	Average
0.29	0.16	0.23	n.d.	0.30	0.16	0.30	0.37	0.05		Std. Dev.
37.92	1.50	20.00	n.a.	24.09	0.61	6.47	8.43	n.d.	99.03	KAP35-1
37.50	1.92	19.90	n.a.	23.77	0.48	6.71	8.57	n.d.	98.86	KAP35-2
37.99	1.48	20.38	n.a.	22.63	0.39	6.67	9.39	n.d.	98.94	KAP35-3
37.76	1.74	19.99	n.a.	23.63	0.43	6.15	9.11	n.d.	98.81	KAP35-4
37.93	1.37	20.27	n.a.	23.57	0.46	6.69	8.84	n.d.	99.13	KAP35-5
38.25	0.94	21.29	n.a.	23.70	0.43	6.60	8.62	n.d.	99.84	KAP35-6
38.08	1.44	20.42	n.a.	23.83	0.50	6.72	8.40	n.d.	99.38	KAP35-7
37.92	1.53	20.32	n.a.	23.24	0.41	6.86	8.56	n.d.	98.83	KAP35-8
38.02	1.58	20.03	n.a.	23.98	0.51	6.53	8.73	n.d.	99.38	KAP35-9
38.30	1.38	20.39	n.a.	23.64	0.50	6.39	9.34	n.d.	99.94	KAP35-10
37.86	2.02	19.03	n.a.	23.21	0.63	6.64	9.64	n.d.	99.03	KAP35-11
37.57	1.56	20.07	n.a.	23.07	0.45	6.48	9.12	n.d.	98.35	KAP35-12
37.66	1.82	20.04	n.a.	23.40	0.46	6.29	9.52	n.d.	99.17	KAP35-13
37.91	1.56	20.16	n.d.	23.52	0.48	6.55	8.94		99.13	Average
0.24	0.28	0.49	n.d.	0.40	0.07	0.20	0.43			Std. Dev.
38.95	1.35	20.46	n.a.	23.81	0.43	6.85	9.01	0.11	100.96	KAP40-1
39.05	1.57	20.08	n.a.	22.99	0.64	7.26	9.05	0.13	100.76	KAP40-2
39.21	1.40	20.58	n.a.	23.56	0.44	6.89	8.84	0.15	101.07	KAP40-3
38.57	1.51	20.03	n.a.	23.93	0.58	7.10	8.70	0.14	100.55	KAP40-4
38.79	1.79	19.72	n.a.	23.80	0.62	6.81	8.95	0.12	100.60	KAP40-5
38.94	1.45	20.48	n.a.	23.99	0.49	6.85	8.47	0.13	100.80	KAP40-6
38.85	1.28	20.45	n.a.	23.61	0.63	6.75	9.16	0.06	100.80	KAP40-7
38.66	1.57	20.13	n.a.	24.19	0.59	7.03	8.22	0.14	100.52	KAP40-8
38.43	1.35	20.47	n.a.	24.15	0.64	7.37	7.73	0.07	100.21	KAP40-9
38.59	1.50	20.05	n.a.	23.86	0.83	6.59	9.07	0.12	100.60	KAP40-10
38.66	1.37	20.45	n.a.	23.82	0.60	6.79	8.97	0.08	100.74	KAP40-11
38.79	1.47	20.26	n.d.	23.79	0.59	6.93	8.74	0.11	100.69	Average
0.23	0.14	0.27	n.d.	0.33	0.11	0.23	0.44	0.03		Std. Dev.
39.25	1.03	21.12	n.a.	22.38	0.58	7.29	9.23	0.07	100.93	KAP42-1
38.71	1.50	20.49	n.a.	23.00	0.59	7.39	8.94	0.12	100.73	KAP42-2
38.69	1.31	20.86	n.a.	22.59	0.59	7.37	8.99	0.12	100.51	KAP42-3
38.63	1.24	20.87	n.a.	23.14	0.61	7.59	8.53	0.12	100.73	KAP42-4
38.66	1.26	20.94	n.a.	22.50	0.61	7.12	9.64	0.08	100.81	KAP42-5
39.07	1.78	20.09	n.a.	23.68	0.61	7.56	8.64	0.10	101.53	KAP42-6
39.79	1.05	21.38	n.a.	22.13	0.62	7.14	9.33	0.10	101.53	KAP42-7
39.23	1.29	20.69	n.a.	23.16	0.56	7.25	9.12	0.04	101.34	KAP42-8
39.40	1.15	20.89	n.a.	22.55	0.56	7.57	8.88	0.07	101.07	KAP42-9
38.93	1.46	20.73	n.a.	22.66	0.61	7.28	9.15	0.07	100.88	KAP42-10
38.58	1.60	20.14	n.a.	23.20	0.63	7.27	8.88	0.09	100.40	KAP42-11
38.99	1.33	20.74	n.d.	22.82	0.60	7.35	9.03	0.09	100.95	Average
0.39	0.23	0.39	n.d.	0.45	0.02	0.16	0.31	0.03		Std. Dev.
38.72	1.22	21.18	n.a.	23.46	0.42	5.34	10.24	0.19	100.76	KAP36-1
38.53	1.27	20.95	n.a.	23.05	0.39	5.56	10.84	0.21	100.79	KAP36-2
38.21	1.06	20.90	n.a.	22.14	0.75	4.54	11.82	0.12	99.54	KAP36-3
38.33	1.01	21.14	n.a.	23.11	0.52	5.06	10.84	0.15	100.16	KAP36-4
38.36	1.08	21.16	n.a.	23.53	0.51	5.34	10.01	0.15	100.12	KAP36-5
39.29	1.00	20.91	n.a.	23.25	0.47	5.27	10.49	0.16	100.84	KAP36-6
38.96	0.62	21.34	n.a.	22.09	0.91	4.51	12.30	0.07	100.82	KAP36-7
39.13	1.00	21.24	n.a.	23.73	0.49	5.46	9.78	0.15	100.97	KAP36-8
38.97	1.07	21.07	n.a.	23.25	0.41	5.55	10.16	0.18	100.66	KAP36-9
38.88	1.09	20.98	n.a.	23.44	0.65	4.81	10.88	0.15	100.87	KAP36-10

SiO_2	TiO_2	Al_2O_3	Cr_2O_3	FeO	MnO	MgO	CaO	Na_2O	Total	Sample
38.74	1.04	21.09	n.d.	23.10	0.55	5.14	10.73	0.15	100.55	Average
0.37	0.17	0.15	n.d.	0.56	0.17	0.40	0.80	0.04		Std. Dev.
39.32	1.09	1.25	n.a.	22.91	19.96	4.95	10.53	0.20	100.20	KAP44-1
38.61	1.21	0.59	n.a.	23.61	20.48	5.99	9.44	0.15	100.08	KAP44-2
38.00	1.15	0.79	n.a.	23.18	20.28	5.38	10.33	0.15	99.26	KAP44-3
38.26	1.46	0.49	n.a.	23.03	19.86	6.12	9.69	0.24	99.14	KAP44-4
38.38	1.24	0.50	n.a.	22.77	20.62	5.86	10.34	0.05	99.74	KAP44-5
38.94	1.15	0.61	n.a.	22.35	19.57	5.94	10.56	0.32	99.43	KAP44-6
38.54	1.29	0.45	n.a.	23.28	20.50	6.65	9.20	0.27	100.17	KAP44-7
38.57	1.14	0.59	n.a.	23.13	20.32	6.12	9.70	0.22	99.77	KAP44-8
38.13	1.15	0.93	n.a.	23.10	20.20	5.31	10.36	0.10	99.26	KAP44-9
38.01	1.47	0.55	n.a.	22.90	19.97	5.95	10.29	0.14	99.27	KAP44-10
41.93	0.87	0.30	n.a.	20.85	20.68	6.01	8.75	0.54	99.92	KAP44-11
38.37	1.33	0.54	n.a.	23.32	20.41	6.46	9.02	0.22	99.67	KAP44-12
38.88	1.20	0.62	n.a.	23.86	20.41	6.06	9.14	0.18	100.34	KAP44-13
38.47	1.32	0.46	n.a.	23.09	20.21	6.65	9.10	0.26	99.54	KAP44-14
38.49	1.27	0.68	n.a.	23.30	20.38	5.84	9.63	0.14	99.73	KAP44-15
39.05	1.29	0.36	n.a.	22.66	20.39	6.83	8.98	0.24	99.81	KAP44-16
39.64	1.20	0.37	n.a.	22.32	20.56	7.02	8.81	0.24	100.15	KAP44-17
38.29	1.31	0.49	n.a.	23.28	20.76	6.29	9.38	0.20	99.99	KAP44-18
38.61	1.23	0.32	n.a.	22.22	20.82	7.21	9.28	0.35	100.03	KAP44-19
38.76	1.23	0.57	n.d.	22.90	20.33	6.14	9.61	0.22	99.78	Average
0.88	0.13	0.23	n.d.	0.65	0.32	0.58	0.61	0.11		Std. Dev.
38.52	1.65	20.04	n.a.	23.67	0.58	6.40	9.69	0.06	100.61	KAP41-1
39.18	1.79	19.39	n.a.	23.36	0.57	6.72	9.17	0.17	100.34	KAP41-2
38.86	1.54	20.57	n.a.	23.81	0.47	6.83	8.49	0.16	100.72	KAP41-3
38.60	1.44	20.89	n.a.	23.01	0.39	6.55	9.81	0.11	100.82	KAP41-4
38.87	1.71	20.36	n.a.	23.38	0.47	7.06	8.17	0.08	100.11	KAP41-5
38.71	1.66	20.72	n.a.	23.81	0.52	7.26	7.91	0.11	100.70	KAP41-6
38.77	1.53	20.79	n.a.	23.46	0.51	6.95	8.67	0.11	100.77	KAP41-7
38.92	1.62	20.56	n.a.	23.29	0.44	7.07	9.02	0.16	101.08	KAP41-8
38.86	1.20	21.21	n.a.	23.38	0.44	6.63	9.01	0.11	100.85	KAP41-9
39.15	1.53	20.83	n.a.	23.45	0.45	6.95	8.66	0.12	101.14	KAP41-10
38.84	1.57	20.54	n.d.	23.46	0.48	6.84	8.86	0.12	100.71	Average
0.21	0.16	0.51	n.d.	0.25	0.06	0.27	0.61	0.03		Std. Dev.
39.19	0.94	21.58	n.a.	23.35	0.38	6.00	9.55	0.20	101.18	KAP43-1
39.11	1.08	21.39	n.a.	22.99	0.41	5.62	10.39	0.17	101.15	KAP43-2
38.73	1.14	21.20	n.a.	23.04	0.68	4.95	11.06	0.06	100.85	KAP43-3
38.87	1.26	21.00	n.a.	22.43	0.54	5.08	11.24	0.14	100.56	KAP43-4
39.06	1.07	21.25	n.a.	21.86	0.36	5.89	10.62	0.16	100.26	KAP43-5
38.92	1.18	21.25	n.a.	20.81	0.71	5.02	13.19	0.08	101.15	KAP43-6
38.71	1.10	21.07	n.a.	22.47	0.77	5.07	11.34	0.11	100.64	KAP43-7
39.05	1.04	21.39	n.a.	22.85	0.56	5.51	10.63	0.22	101.28	KAP43-8
38.70	1.07	21.18	n.a.	23.24	0.62	5.49	10.27	0.16	100.73	KAP43-9
39.29	0.80	21.48	n.a.	22.80	0.34	5.97	10.04	0.13	100.85	KAP43-10
39.80	0.87	21.44	n.a.	22.57	0.33	6.14	10.00	0.20	101.34	KAP43-11
39.04	1.05	21.29	n.d.	22.58	0.52	5.52	10.76	0.15	100.91	Average
0.32	0.14	0.18	n.d.	0.72	0.16	0.44	0.98	0.05		Std. Dev.
38.49	1.40	20.85	n.a.	22.70	0.59	5.80	10.49	0.18	100.50	KAP38-1
38.46	1.32	21.22	n.a.	22.67	0.40	6.75	9.49	0.19	100.50	KAP38-2
38.21	1.32	20.45	n.a.	23.03	0.73	5.95	10.28	0.08	100.05	KAP38-3
38.66	1.24	21.03	n.a.	22.78	0.78	5.53	10.36	0.09	100.46	KAP38-4
38.94	1.09	21.75	n.a.	22.41	0.38	7.03	9.12	0.14	100.84	KAP38-5
38.75	1.41	21.29	n.a.	22.75	0.38	6.59	9.47	0.14	100.78	KAP38-6
38.31	1.10	21.12	n.a.	22.32	0.43	6.12	10.48	0.06	99.95	KAP38-7
38.53	1.26	20.99	n.a.	22.74	0.62	5.98	9.84	0.18	100.14	KAP38-8
38.44	1.46	21.03	n.a.	22.46	0.45	6.12	10.31	0.16	100.43	KAP38-9
38.53	1.29	21.08	n.d.	22.65	0.53	6.21	9.98	0.13	100.41	Average
0.22	0.13	0.35	n.d.	0.22	0.16	0.48	0.51	0.05		Std. Dev.
38.85	1.01	0.42	n.a.	22.01	21.02	6.24	10.38	0.07	99.99	KAP45-1
38.80	1.52	0.42	n.a.	22.67	20.77	6.73	9.49	0.20	100.59	KAP45-2
38.49	1.61	0.46	n.a.	22.66	20.48	6.95	9.23	0.14	100.01	KAP45-3
39.09	1.10	0.40	n.a.	22.30	20.87	6.41	9.47	0.20	99.84	KAP45-4
38.62	1.36	0.48	n.a.	22.57	20.63	6.56	9.75	0.20	100.16	KAP45-5
39.57	0.73	0.50	n.a.	20.56	21.25	5.87	11.41	0.19	100.06	KAP45-6
38.53	1.24	0.63	n.a.	22.15	20.60	6.17	10.15	0.15	99.62	KAP45-7
38.46	1.28	0.39	n.a.	22.57	20.81	6.79	8.80	0.16	99.27	KAP45-8
38.77	1.54	0.42	n.a.	22.00	20.26	6.81	10.07	0.26	100.12	KAP45-9
38.18	1.58	0.41	n.a.	22.06	20.55	6.88	9.20	0.27	99.12	KAP45-10
38.73	1.25	0.46	n.a.	22.42	21.01	6.48	10.17	0.17	100.68	KAP45-11
39.07	0.83	0.38	n.a.	21.43	21.28	6.33	10.70	0.17	100.19	KAP45-12
38.90	0.91	0.47	n.a.	22.58	21.20	6.22	9.76	0.11	100.15	KAP45-13
39.10	1.59	0.40	n.a.	21.72	20.22	6.64	10.34	0.14	100.15	KAP45-14
38.80	1.25	0.44	n.d.	22.12	20.78	6.51	9.92	0.17	100.00	Average

SiO_2	TiO_2	Al_2O_3	Cr_2O_3	FeO	MnO	MgO	CaO	Na_2O	Total	Sample
0.35	0.30	0.07	n.d.	0.58	0.34	0.31	0.68	0.05		Std. Dev.
39.07	0.99	0.38	n.a.	22.80	21.28	6.06	9.90	0.16	100.62	KAP46-1
38.86	1.06	0.40	n.a.	21.73	20.97	5.96	10.90	0.19	100.05	KAP46-2
41.09	1.04	0.47	n.a.	21.59	20.53	5.97	8.90	0.47	100.04	KAP46-3
39.02	1.33	0.29	n.a.	21.37	21.00	6.55	10.37	0.20	100.13	KAP46-4
38.75	1.57	0.54	n.a.	23.33	20.39	5.74	9.33	0.14	99.79	KAP46-5
38.68	1.25	0.40	n.a.	22.87	20.88	6.34	9.18	0.27	99.87	KAP46-6
38.70	2.10	0.46	n.a.	22.00	19.81	6.67	9.24	0.28	99.26	KAP46-7
38.48	2.02	0.35	n.a.	23.13	20.44	6.37	8.95	0.24	99.99	KAP46-8
38.97	1.24	0.36	n.a.	22.15	20.96	6.32	10.11	0.11	100.21	KAP46-9
39.01	1.18	0.39	n.a.	20.88	21.00	5.82	11.55	0.13	99.96	KAP46-10
39.24	0.96	0.46	n.a.	21.05	21.26	6.30	10.81	0.21	100.29	KAP46-11
38.76	1.13	0.38	n.a.	21.94	20.84	6.26	10.29	0.15	99.74	KAP46-12
38.69	1.19	0.45	n.a.	21.51	20.92	6.01	10.70	0.31	99.78	KAP46-13
38.19	1.55	0.42	n.a.	22.54	20.67	6.36	9.86	0.12	99.70	KAP46-14
38.74	1.10	0.37	n.a.	21.68	20.63	6.35	10.45	0.24	99.56	KAP46-15
38.21	1.24	0.42	n.a.	21.81	20.37	5.92	10.62	0.32	98.91	KAP46-16
38.69	1.07	0.34	n.a.	22.90	20.97	5.94	9.83	0.14	99.87	KAP46-17
38.89	1.29	0.40	n.d.	22.07	20.76	6.17	10.06	0.22	99.87	Average
0.63	0.34	0.06	n.d.	0.73	0.37	0.27	0.76	0.09		Std. Dev.

Plagioclase Compositions

SiO_2	TiO_2	Al_2O_3	FeO	MnO	MgO	CaO	Na_2O	K_2O	Total	Sample
57.05	0.01	27.62	0.52	0.01	n.a.	9.55	6.00	0.59	101.33	3VG12-1
57.09	0	27.12	0.48	0	n.a.	9.10	6.12	0.65	100.55	3VG12-2
56.53	0	27.55	0.46	0.01	n.a.	9.63	5.98	0.53	100.68	3VG12-3
56.44	0	27.71	0.53	0.04	n.a.	9.46	5.71	0.79	100.68	3VG12-4
56.82	0	27.41	0.48	0.02	n.a.	9.42	5.91	0.54	100.59	3VG12-5
56.33	0	27.30	0.51	0	n.a.	9.59	5.64	0.75	100.12	3VG12-6
56.39	0	27.05	0.72	0	n.a.	9.59	5.79	0.64	100.16	3VG12-7
56.78	0	27.52	0.50	0.02	n.a.	9.45	5.98	0.59	100.81	3VG12-8
56.40	0	27.61	0.49	0.02	n.a.	9.52	5.89	0.48	100.41	3VG12-9
56.73	0.02	27.69	0.54	0	n.a.	9.66	5.71	0.60	100.96	3VG12-10
56.77	0	27.49	0.51	0	n.a.	9.46	5.70	0.75	100.68	3VG12-11
56.87	0.01	26.98	0.55	0	n.a.	9.63	5.74	0.78	100.56	3VG12-12
56.08	0.06	27.39	0.56	0.03	n.a.	10.01	5.42	0.65	100.19	3VG12-13
56.93	0	27.49	0.49	0.02	n.a.	9.51	5.92	0.59	100.94	3VG12-14
56.99	0.06	27.49	0.50	0.02	n.a.	9.46	5.92	0.73	101.18	3VG12-15
56.54	0	27.45	0.52	0.01	n.a.	9.74	5.77	0.69	100.71	3VG12-16
56.76	0.03	27.69	0.46	0	n.a.	9.69	5.75	0.68	101.05	3VG12-17
56.17	0	27.70	0.45	0	n.a.	9.76	5.74	0.74	100.56	3VG12-18
56.71	0.07	27.39	0.56	0.04	n.a.	9.33	5.56	0.88	100.53	3VG12-19
56.64	0	27.39	0.56	0	n.a.	9.51	5.73	0.79	100.63	3VG12-20
56.65	0.01	27.45	0.52	0.01	n.d.	9.55	5.80	0.67	100.67	Average
0.28	0.02	0.21	0.06	0.01	n.d.	0.19	0.17	0.10		Std. Dev.
56.33	0	26.07	0.68	0.02	n.a.	10.19	5.46	0.51	99.46	3VG1-1
57.27	0	26.59	0.61	0	n.a.	9.28	5.41	0.77	99.93	3VG1-2
56.12	0	27.26	0.51	0.02	n.a.	9.82	5.44	0.56	99.72	3VG1-3
54.81	0.02	27.52	0.82	0.01	n.a.	10.31	5.31	0.50	99.30	3VG1-4
57.02	0.03	26.77	0.59	0.01	n.a.	9.29	5.76	0.60	100.07	3VG1-5
57.09	0	27.12	0.55	0.02	n.a.	9.30	5.94	0.55	100.56	3VG1-6
56.70	0.01	27.30	0.56	0	n.a.	9.53	5.68	0.54	100.31	3VG1-7
56.99	0	27.13	0.47	0.02	n.a.	9.35	5.91	0.53	100.41	3VG1-8
57.10	0	27.44	0.49	0.01	n.a.	9.43	5.82	0.50	100.79	3VG1-9
56.81	0	27.49	0.51	0.01	n.a.	9.25	5.73	0.54	100.34	3VG1-10
55.61	0	28.10	0.72	0.03	n.a.	10.26	5.28	0.53	100.52	3VG1-11
56.83	0	27.45	0.45	0	n.a.	9.46	5.91	0.51	100.62	3VG1-12
56.60	0	27.26	0.47	0.01	n.a.	9.55	5.52	0.65	100.05	3VG1-13
56.78	0	27.29	0.70	0.01	n.a.	9.32	5.64	0.69	100.42	3VG1-14
56.69	0	27.77	0.46	0.00	n.a.	9.86	5.59	0.42	100.80	3VG1-15
56.64	0	27.14	0.58	0.01	n.a.	9.55	5.78	0.69	100.39	3VG1-16
56.66	0.04	27.55	0.63	0	n.a.	9.66	5.76	0.53	100.83	3VG1-17
57.38	0	27.60	0.52	0	n.a.	9.39	5.79	0.45	101.14	3VG1-18
56.64	0.01	27.27	0.58	0.01	n.d.	9.60	5.65	0.56	100.31	Average
0.62	0.01	0.45	0.12	0.01	n.d.	0.35	0.21	0.09		Std. Dev.
56.69	0.04	27.59	0.55	0.01	n.a.	9.31	6.21	0.42	100.81	3VG27-1
56.96	0	27.13	0.48	0.01	n.a.	9.28	6.27	0.40	100.53	3VG27-2
56.80	0	27.36	0.59	0.01	n.a.	9.49	6.10	0.42	100.76	3VG27-3
57.07	0	27.14	0.50	0	n.a.	9.27	6.49	0.40	100.86	3VG27-4
57.02	0	27.36	0.54	0.03	n.a.	8.97	6.34	0.40	100.66	3VG27-5
57.52	0.03	27.22	0.50	0	n.a.	8.78	6.30	0.44	100.78	3VG27-6
56.88	0.02	27.15	0.48	0.02	n.a.	9.07	6.19	0.41	100.20	3VG27-7
57.51	0.02	26.94	0.51	0.02	n.a.	8.93	6.39	0.34	100.66	3VG27-8
56.74	0.0	27.53	0.46	0	n.a.	9.34	6.05	0.41	100.55	3VG27-9
57.31	0.02	27.37	0.50	0.02	n.a.	9.14	6.37	0.42	101.16	3VG27-10
57.15	0	27.35	0.55	0	n.a.	9.08	6.12	0.38	100.63	3VG27-11
56.81	0	27.50	0.49	0.04	n.a.	9.23	6.28	0.36	100.70	3VG27-12
57.37	0	27.19	0.56	0	n.a.	8.97	6.41	0.39	100.90	3VG27-13
57.28	0	27.21	0.52	0.03	n.a.	8.80	6.51	0.41	100.77	3VG27-14
56.85	0	27.34	0.49	0	n.a.	8.92	6.33	0.37	100.30	3VG27-15
57.91	0	26.84	0.49	0.02	n.a.	8.76	6.43	0.39	100.84	3VG27-16
57.28	0	27.16	0.60	0	n.a.	9.05	6.41	0.43	100.92	3VG27-17
57.25	0	27.38	0.56	0.01	n.a.	9.18	6.14	0.43	100.94	3VG27-18
57.19	0.07	27.52	0.48	0.02	n.a.	9.17	6.15	0.40	101.00	3VG27-19
57.65	0.03	27.11	0.49	0	n.a.	8.87	6.47	0.41	101.02	3VG27-20
57.16	0.01	27.27	0.52	0.01	n.d.	9.08	6.30	0.40	100.75	Average

SiO_2	TiO_2	Al_2O_3	FeO	MnO	MgO	CaO	Na_2O	K_2O	Total	Sample
0.33	0.02	0.20	0.04	0.01	n.d.	0.20	0.14	0.02		Std. Dev.
56.83	0.02	27.14	0.42	0.03	0	9.15	5.79	0.44	99.81	3VG3-1
57.15	0.04	27.07	0.41	0.01	0	9.05	6.04	0.46	100.23	3VG3-2
57.29	0.01	27.17	0.46	0	0	8.94	5.96	0.48	100.30	3VG3-3
57.34	0.03	27.05	0.46	0.02	0	9.01	5.98	0.43	100.31	3VG3-4
57.08	0.04	27.21	0.47	0	0	9.31	6.05	0.46	100.63	3VG3-5
56.88	0.01	27.11	0.56	0	0	9.19	6.06	0.47	100.26	3VG3-6
56.68	0.02	27.49	0.46	0.01	0	9.54	5.77	0.48	100.45	3VG3-7
57.04	0	27.45	0.45	0.01	0	9.57	5.91	0.45	100.88	3VG3-8
57.07	0.02	27.25	0.40	0	0	9.39	5.79	0.43	100.35	3VG3-9
57.00	0	27.24	0.45	0.01	0.01	9.11	5.74	0.52	100.06	3VG3-10
56.10	0	26.59	0.74	0.01	0.05	9.14	5.48	0.64	98.74	3VG3-11
55.97	0	27.16	0.43	0.01	0.01	9.35	5.66	0.42	99.02	3VG3-12
56.34	0	27.04	0.55	0.01	0.01	9.23	5.71	0.56	99.45	3VG3-13
55.23	0	27.67	0.60	0.01	0.01	9.83	5.33	0.46	99.14	3VG3-14
55.55	0	27.54	0.51	0.01	0.01	9.78	5.46	0.45	99.30	3VG3-15
54.52	0	28.09	0.67	0.01	0.01	10.31	5.11	0.41	99.13	3VG3-16
56.16	0	26.98	0.57	0	0.01	9.55	5.65	0.51	99.43	3VG3-17
55.31	0.03	27.87	0.61	0.01	0.01	10.01	5.39	0.44	99.69	3VG3-18
55.44	0.00	26.50	0.67	0.01	0.02	9.15	5.61	0.59	97.99	3VG3-19
57.31	0.03	26.85	0.46	0	0.01	8.83	6.06	0.55	100.10	3VG3-20
57.70	0.01	26.75	0.46	0	0	9.11	5.75	0.51	100.30	3VG3-21
56.63	0.02	26.42	0.46	0	0	8.91	6.01	0.50	98.94	3VG3-22
57.26	0.01	26.78	0.68	0.02	0.03	8.97	5.90	0.58	100.23	3VG3-23
56.42	0	27.22	0.56	0.01	0.01	9.36	5.98	0.48	100.04	3VG3-24
57.00	0.03	27.05	0.46	0	0	9.48	5.78	0.47	100.26	3VG3-25
56.53	0.01	27.15	0.52	0.01	0.01	9.33	5.76	0.49	99.80	Average
0.81	0.01	0.40	0.10	0.01	0.01	0.36	0.25	0.06		Std. Dev.
56.55	0.02	27.37	0.48	0	n.a.	9.24	6.15	0.38	100.18	3VG26-1
56.49	0	27.55	0.43	0	n.a.	9.36	5.99	0.40	100.24	3VG26-2
57.24	0.01	27.17	0.52	0.01	n.a.	8.86	6.28	0.45	100.53	3VG26-3
57.19	0.01	27.14	0.50	0	n.a.	8.81	6.00	0.38	100,03	3VG26-4
56.88	0	27.32	0.45	0.01	n.a.	8.99	6.17	0.42	100.25	3VG26-5
56.76	0	27.33	0.57	0.01	n.a.	8.94	6.23	0.42	100.26	3VG26-6
56.08	0	27.56	0.53	0.01	n.a.	9.41	6.01	0.36	99.95	3VG26-7
56.33	0	27.83	0.49	0	n.a.	9.66	5.77	0.37	100.45	3VG26-8
54.40	0.01	28.90	0.77	0	n.a.	10.90	5.26	0.28	100.52	3VG26-9
53.71	0	28.99	0.71	0.01	n.a.	11.09	5.07	0.29	99.87	3VG26-10
56.60	0	27.30	0.48	0	n.a.	9.02	6.29	0.40	100.08	3VG26-11
56.39	0	27.40	0.52	0.02	n.a.	9.07	6.17	0.39	99.96	3VG26-12
57.20	0	27.28	0.46	0	n.a.	9.15	6.32	0.41	100.81	3VG26-13
56.15	0.05	27.49	0.56	0.01	n.a.	9.43	5.99	0.37	100.05	3VG26-14
56.35	0.05	27.32	0.51	0	n.a.	9.20	6.04	0.48	99.96	3VG26-15
54.21	0.04	28.79	0.66	0.02	n.a.	10.94	5.00	0.30	99.96	3VG26-16
55.71	0	27.81	0.47	0.01	n.a.	9.63	5.75	0.38	99.76	3VG26-17
56.64	0	27.62	0.46	0.06	n.a.	9.31	6.12	0.38	100.59	3VG26-18
56.69	0	27.64	0.54	0.01	n.a.	9.48	6.22	0.38	100.95	3VG26-19
56.93	0	27.38	0.44	0	n.a.	9.05	6.32	0.39	100.51	3VG26-20
56.22	0.01	27.66	0.53	0.01	n.d.	9.48	5.96	0.38	100.24	Average
1.00	0.02	0.56	0,09	0.01	n.d.	0.69	0.40	0.05		Std. Dev.
54.41	0.07	27.89	1.08	0.01	n.a.	11.46	4.17	0.59	99.69	3VG14-1
53.47	0	29.27	0.65	0	n.a.	12.33	4.60	0.29	100.62	3VG14-2
53.50	0	29.62	0.83	0.02	n.a.	12.32	4.29	0.30	100.88	3VG14-3
52.79	0.02	29.74	0.80	0.01	n.a.	12.73	4.22	0.30	100.60	3VG14-4
53.46	0.06	29.93	0.64	0.01	n.a.	12.56	4.30	0.25	101.22	3VG14-5
53.05	0	29.71	0.66	0.01	n.a.	12.39	4.36	0.25	100.43	3VG14-6
53.16	0.07	29.51	0.87	0.03	n.a.	12.65	4.30	0.26	100.85	3VG14-7
53.01	0.02	29.76	0.69	0	n.a.	12.60	4.30	0.27	100.65	3VG14-8
53.21	0	29.86	0.77	0.02	n.a.	12.53	4.34	0.30	101.03	3VG14-9
53.07	0	29.86	0.75	0.03	n.a.	12.66	4.32	0.25	100.93	3VG14-10
53.59	0	29.85	0.73	0.03	n.a.	12.47	4.41	0.26	101.35	3VG14-11
53.98	0	29.21	0.75	0.02	n.a.	12.13	4.63	0.28	100.99	3VG14-12
54.14	0	28.83	0.73	0.01	n.a.	11.70	4.79	0.33	100.53	3VG14-13
53.45	0.02	29.46	0.77	0.02	n.d.	12.35	4.39	0.30	100.75	Average
0.48	0.03	0.57	0.12	0.01	n.d.	0.38	0.18	0.09		Std. Dev.

SiO_2	TiO_2	Al_2O_3	FeO	MnO	MgO	CaO	Na_2O	K_2O	Total	Sample
56.55	0.01	27.62	0.46	0.02	n.a.	9.63	5.79	0.37	100.45	3VG11-1
57.20	0	27.28	0.50	0.01	n.a.	9.45	5.85	0.54	100.82	3VG11-2
57.45	0	27.17	0.51	0.02	n.a.	9.40	5.83	0.47	100.84	3VG11-3
57.41	0	27.31	0.44	0	n.a.	9.56	5.75	0.38	100.85	3VG11-4
56.83	0	27.18	0.49	0.01	n.a.	9.66	5.68	0.50	100.35	3VG11-5
56.60	0	27.44	0.46	0.01	n.a.	9.80	5.78	0.45	100.53	3VG11-6
56.97	0	27.29	0.56	0.03	n.a.	9.53	5.84	0.52	100.73	3VG11-7
56.95	0	27.38	0.46	0.01	n.a.	9.67	5.85	0.39	100.69	3VG11-8
57.09	0	27.02	0.53	0.01	n.a.	9.46	5.92	0.52	100.55	3VG11-9
57.35	0	27.03	0.47	0	n.a.	9.38	6.03	0.49	100.75	3VG11-10
56.95	0	26.61	0.53	0.02	n.a.	9.44	5.93	0.43	99.90	3VG11-11
57.17	0	26.99	0.48	0.01	n.a.	9.48	6.26	0.38	100.77	3VG11-12
57.07	0	27.10	0.49	0	n.a.	9.46	5.87	0.45	100.44	3VG11-13
58.56	0.05	26.20	0.60	0.05	n.a.	9.03	6.00	0.61	101.12	3VG11-14
56.49	0	27.13	0.69	0.01	n.a.	9.85	5.59	0.46	100.21	3VG11-15
57.47	0	27.26	0.49	0	n.a.	9.61	5.97	0.41	101.19	3VG11-16
55.73	0.01	26.61	0.64	0.02	n.a.	9.71	5.72	0.46	98.86	3VG11-17
57.06	0	27.18	0.50	0	n.a.	9.44	6.15	0.42	100.76	3VG11-18
57.05	0	27.10	0.52	0.01	n.d.	9.53	5.88	0.46	100.55	Average
0.57	0.01	0.34	0.07	0.01	n.d.	0.19	0.16	0.06		Std. Dev.
56.65	0	27.62	0.52	0.02	n.a.	9.63	5.86	0.34	100.63	3VG10-1
57.68	0.03	27.25	0.52	0.02	n.a.	8.98	6.39	0.35	101.22	3VG10-2
56.96	0	27.32	0.46	0.02	n.a.	9.29	5.95	0.35	100.35	3VG10-3
56.89	0	26.47	0.65	0	n.a.	9.57	5.85	0.43	99.85	3VG10-4
57.12	0	26.95	0.46	0	n.a.	9.01	5.99	0.43	99.95	3VG10-5
57.13	0	27.03	0.50	0	n.a.	9.25	5.87	0.41	100.19	3VG10-6
56.90	0	27.34	0.47	0.02	n.a.	9.34	5.86	0.40	100.31	3VG10-7
57.33	0.02	27.15	0.54	0	n.a.	9.23	5.76	0.46	100.48	3VG10-8
57.54	0.04	26.91	0.54	0.01	n.a.	8.77	6.19	0.50	100.50	3VG10-9
57.47	0	26.80	0.58	0.03	n.a.	9.11	5.90	0.62	100.50	3VG10-10
56.99	0	27.30	0.51	0.02	n.a.	9.64	5.72	0.42	100.60	3VG10-11
56.85	0	27.23	0.51	0	n.a.	9.52	5.82	0.43	100.36	3VG10-12
57.46	0	26.77	0.50	0.01	n.a.	9.11	6.05	0.58	100.47	3VG10-13
56.72	0	27.35	0.50	0	n.a.	9.60	6.01	0.45	100.62	3VG10-14
57.03	0.01	27.37	0.50	0	n.a.	9.68	5.85	0.47	100.92	3VG10-15
57.08	0	27.09	0.56	0.01	n.a.	9.52	5.81	0.55	100.62	3VG10-16
57.11	0.01	27.12	0.52	0.01	n.d.	9.33	5.93	0.45	100.47	Average
0.30	0.01	0.29	0.05	0.01	n.d.	0.28	0.17	0.08		Std. Dev.
56.83	0	27.43	0.51	0	0	9.39	5.87	0.42	100.44	3VG6-1
57.35	0	26.88	0.55	0.01	0.01	9.03	5.70	0.78	100.31	3VG6-2
56.60	0.04	26.14	1.17	0.01	0.58	9.13	5.71	0.65	100.03	3VG6-3
57.21	0	27.09	0.41	0	0	9.10	5.77	0.48	100.05	3VG6-4
56.44	0	26.81	0.37	0	0.01	8.96	5.91	0.50	99.00	3VG6-5
57.67	0.02	26.82	0.48	0.02	0.02	8.91	5.93	0.58	100.44	3VG6-6
57.16	0	27.05	0.53	0	0.06	9.38	5.66	0.61	100.44	3VG6-7
56.53	0.04	27.38	0.50	0.02	0.02	9.65	5.64	0.42	100.19	3VG6-8
57.38	0.01	27.09	0.46	0	0.04	8.99	5.78	0.53	100.28	3VG6-9
57.34	0	27.07	0.59	0.01	0.01	9.02	6.03	0.57	100.64	3VG6-10
57.08	0	27.48	0.48	0.03	0.02	9.52	5.62	0.48	100.71	3VG6-11
57.60	0.02	27.26	0.43	0.02	0.02	9.06	5.95	0.54	100.91	3VG6-12
56.93	0.01	27.32	0.44	0	0.01	9.43	5.64	0.55	100.32	3VG6-13
56.66	0	27.56	0.45	0.01	0.02	9.71	5.68	0.44	100.53	3VG6-14
57.05	0	27.10	0.43	0	0	9.35	5.59	0.49	100.01	3VG6-15
57.36	0	26.98	0.41	0	0.02	9.10	5.83	0.44	100.14	3VG6-16
57.17	0.05	27.09	0.46	0	0	9.25	5.60	0.59	100.20	3VG6-17
57.62	0.01	26.98	0.41	0	0	8.95	5.73	0.47	100.16	3VG6-18
56.76	0.01	27.59	0.51	0.01	0.01	9.74	5.69	0.51	100.83	3VG6-19
57.35	0	26.91	0.44	0.02	0.01	9.02	5.93	0.50	100.17	3VG6-20
57.81	0	26.89	0.60	0	0.02	9.01	5.77	0.81	100.90	3VG6-21
57.36	0	27.42	0.45	0.02	0.02	9.42	5.78	0.59	101.06	3VG6-22
57.06	0	27.15	0.52	0.03	0.03	9.19	5.64	0.59	100.20	3VG6-23
57.26	0	27.02	0.50	0	0.05	9.12	5.80	0.58	100.33	3VG6-24
57.36	0	27.10	0.47	0	0.03	9.38	5.92	0.61	100.86	3VG6-25
57.39	0	26.93	0.58	0.02	0.12	9.10	5.88	0.68	100.69	3VG6-26
57.01	0.04	25.35	1.12	0.03	0.49	8.85	5.23	1.05	99.16	3VG6-27
57.62	0	26.83	0.53	0.01	0.02	9.11	5.65	0.72	100.48	3VG6-28
57.42	0	26.18	0.68	0.02	0.15	8.81	5.78	0.83	99.67	3VG6-29

SiO_2	TiO_2	Al_2O_3	FeO	MnO	MgO	CaO	Na_2O	K_2O	Total	Sample
57.18	0.01	27.15	0.60	0.03	0.02	9.21	5.59	0.67	100.45	3VG6-30
57.40	0.01	26.75	0.57	0	0.02	9.19	5.69	0.69	100.33	3VG6-31
57.21	0.01	27.36	0.55	0.01	0	9.58	5.66	0.45	100.83	3VG6-32
57.31	0	27.30	0.51	0.01	0.02	9.23	5.90	0.48	100.75	3VG6-33
57.38	0.01	26.82	0.53	0.04	0.02	8.95	5.71	0.80	100.24	3VG6-34
56.87	0.02	26.87	0.51	0.02	0.02	9.15	5.72	0.52	99.70	3VG6-35
57.46	0.02	27.10	0.44	0.01	0.02	9.07	5.67	0.55	100.35	3VG6-36
56.81	0.05	26.75	0.61	0.04	0.14	9.48	5.80	0.69	100.36	3VG6-37
57.29	0.06	27.04	0.44	0.02	0.02	9.24	5.84	0.51	100.46	3VG6-38
57.19	0.01	27.00	0.53	0.01	0.05	9.20	5.74	0.59	100.34	Average
0.33	0.02	0.41	0.16	0.01	0.12	0.24	0.14	0.14		Std. Dev.
56.95	0	27.35	0.46	0	0	9.32	5.84	0.44	100.38	3VG5-1
56.87	0.02	27.17	0.48	0	0.01	8.98	5.83	0.43	99.79	3VG5-2
56.64	0	27.11	0.38	0	0	9.28	5.90	0.42	99.73	3VG5-3
56.29	0.01	27.03	0.43	0	0	9.12	5.76	0.43	99.06	3VG5-4
56.91	0.01	27.36	0.44	0	0	9.40	5.85	0.40	100.35	3VG5-5
56.46	0	27.20	0.52	0	0.01	9.31	5.71	0.48	99.69	3VG5-6
56.08	0.02	27.35	0.39	0	0	9.50	5.62	0.39	99.35	3VG5-7
56.90	0	27.01	0.45	0	0	9.35	5.80	0.44	99.96	3VG5-8
56.32	0.04	26.51	0.85	0.01	0.33	9.85	5.63	0.42	99.95	3VG5-9
57.11	0.02	26.82	0.48	0	0	8.99	5.96	0.50	99.88	3VG5-10
56.67	0.06	27.09	0.44	0	0.01	9.12	5.91	0.45	99.76	3VG5-11
56.33	0.02	27.03	0.48	0	0.02	9.19	5.93	0.43	99.44	3VG5-12
56.00	0	26.93	0.44	0	0.01	9.27	5.98	0.42	99.05	3VG5-13
56.52	0.02	26.90	0.50	0	0.03	9.20	6.09	0.48	99.74	3VG5-14
56.52	0.03	27.14	0.48	0	0.01	9.24	5.91	0.47	99.79	3VG5-15
56.30	0.03	27.23	0.49	0	0.01	9.32	5.82	0.53	99.72	3VG5-16
56.11	0.04	27.02	0.52	0	0.03	9.10	5.77	0.50	99.08	3VG5-17
56.92	0.05	27.31	0.46	0	0.02	9.14	5.79	0.45	100.12	3VG5-18
56.87	0.04	27.20	0.50	0.01	0.02	9.08	5.90	0.44	100.05	3VG5-19
56.95	0.03	26.35	0.45	0	0.02	8.75	6.36	0.43	99.36	3VG5-20
56.90	0	27.34	0.53	0.02	0	9.28	5.93	0.48	100.48	3VG5-21
56.98	0	27.31	0.48	0	0.01	9.25	5.83	0.45	100.31	3VG5-22
56.94	0	27.28	0.48	0.03	0	9.31	5.84	0.43	100.31	3VG5-23
57.07	0	27.39	0.44	0.03	0	9.12	6.03	0.44	100.52	3VG5-24
57.19	0	27.12	0.52	0.02	0.01	9.19	6.13	0.45	100.62	3VG5-25
57.32	0	27.11	0.46	0.01	0.01	8.95	6.08	0.45	100.38	3VG5-26
57.67	0	26.99	0.49	0.01	0.02	8.80	6.02	0.52	100.52	3VG5-27
56.62	0.02	27.75	0.50	0	0.02	10.00	5.69	0.46	101.06	3VG5-28
56.80	0.02	27.04	0.63	0.01	0.05	9.23	5.88	0.52	100.18	3VG5-29
56.47	0	27.08	0.81	0	0.14	9.69	5.71	0.45	100.35	3VG5-30
55.94	0.02	27.40	0.60	0.01	0.07	9.95	5.40	0.47	99.86	3VG5-31
56.04	0	27.59	0.58	0.01	0.03	9.93	5.73	0.47	100.39	3VG5-32
56.64	0.03	27.22	0.77	0.02	0.18	9.83	5.67	0.48	100.82	3VG5-33
55.63	0.05	27.76	0.58	0	0.02	10.12	5.52	0.42	100.08	3VG5-34
55.78	0.02	27.91	0.68	0.01	0.04	10.18	5.43	0.42	100.47	3VG5-35
56.62	0.02	27.18	0.52	0.01	0.03	9.35	5.83	0.46	100.02	Average
0.46	0.02	0.31	0.11	0.01	0.06	0.37	0.19	0.03		Std. Dev.
56.97	0.03	26.85	0.54	0.02	0	8.77	6.32	0.45	99.96	3VG4-1
56.48	0.02	26.73	0.52	0.00	0	8.75	6.66	0.52	99.68	3VG4-2
57.41	0.05	26.74	0.53	0	0.01	8.60	6.38	0.46	100.17	3VG4-3
57.47	0	26.85	0.54	0	0	8.50	6.44	0.45	100.24	3VG4-4
57.52	0.04	26.76	0.50	0.02	0	8.52	6.41	0.47	100.22	3VG4-5
57.37	0.03	26.73	0.68	0.01	0	8.44	6.57	0.55	100.38	3VG4-6
56.83	0.02	26.62	0.48	0.01	0	8.43	6.54	0.47	99.40	3VG4-7
56.46	0.01	26.71	0.50	0	0	8.78	6.48	0.49	99.44	3VG4-8
56.77	0.02	26.86	0.42	0	0	8.73	6.42	0.32	99.54	3VG4-9
57.19	0	26.90	0.53	0.01	0	8.58	6.44	0.56	100.21	3VG4-10
57.58	0.02	27.13	0.53	0.02	0.03	8.69	6.34	0.48	100.81	3VG4-11
56.92	0	27.20	0.42	0.00	0.02	8.81	6.21	0.41	99.97	3VG4-12
57.44	0	27.31	0.47	0.01	0.03	8.64	6.44	0.40	100.75	3VG4-13
56.99	0.05	27.36	0.53	0.02	0.02	8.81	6.17	0.47	100.40	3VG4-14
57.92	0	27.02	0.47	0.01	0.02	8.36	6.35	0.47	100.62	3VG4-15
57.00	0.01	27.26	0.57	0.02	0.02	8.81	6.17	0.44	100.30	3VG4-16
57.36	0.03	27.40	0.47	0.03	0.03	8.61	6.27	0.42	100.62	3VG4-17
57.32	0.02	26.79	0.56	0	0.02	8.65	6.33	0.52	100.21	3VG4-18
57.41	0	26.92	0.60	0.02	0.02	8.71	6.31	0.50	100.48	3VG4-19

SiO_2	TiO_2	Al_2O_3	FeO	MnO	MgO	CaO	Na_2O	K_2O	Total	Sample
57.39	0.03	27.14	0.42	0	0	8.62	5.99	0.46	100.05	3VG4-20
57.17	0.03	27.33	0.40	0	0.01	8.68	6.01	0.41	100.03	3VG4-21
57.49	0.02	27.24	0.47	0	0	8.61	6.11	0.42	100.35	3VG4-22
57.30	0	27.69	0.52	0.01	0.01	9.32	6.23	0.42	101.50	3VG4-23
57.50	0.03	27.55	0.48	0	0	8.93	6.62	0.50	101.61	3VG4-24
57.62	0.05	27.32	0.55	0.01	0	8.58	6.53	0.51	101.17	3VG4-25
57.81	0.00	27.38	0.50	0.03	0	8.76	6.45	0.43	101.36	3VG4-26
57.38	0.02	27.02	0.63	0.01	0.01	8.73	6.46	0.53	100.78	3VG4-27
56.96	0.02	27.38	0.55	0.00	0	9.03	6.27	0.48	100.69	3VG4-28
57.25	0.02	27.08	0.51	0.01	0.01	8.69	6.35	0.46	100.39	Average
0.36	0.02	0.29	0.06	0.01	0.01	0.19	0.17	0.05		Std. Dev.
57.58	0.02	27.52	0.55	0	n.a.	9.51	5.98	0.49	101.65	3VG22-1
54.84	0.02	28.81	0.63	0.02	n.a.	11.38	5.10	0.32	101.13	3VG22-2
57.09	0.01	27.31	0.52	0	n.a.	9.59	5.87	0.52	100.90	3VG22-3
57.09	0	27.53	0.59	0	n.a.	9.76	5.78	0.51	101.26	3VG22-4
56.01	0	28.42	0.62	0.01	n.a.	10.69	5.31	0.43	101.47	3VG22-5
57.46	0	27.47	0.43	0	n.a.	9.26	6.08	0.39	101.09	3VG22-6
56.79	0	27.66	0.49	0.01	n.a.	9.80	5.73	0.42	100.89	3VG22-7
57.47	0	27.44	0.53	0	n.a.	9.65	5.88	0.46	101.42	3VG22-8
57.25	0	27.71	0.49	0.01	n.a.	9.77	6.10	0.29	101.60	3VG22-9
57.50	0.06	27.61	0.52	0	n.a.	9.39	5.83	0.49	101.42	3VG22-10
56.81	0	27.73	0.52	0.02	n.a.	9.79	5.95	0.48	101.29	3VG22-11
57.36	0	27.59	0.48	0.01	n.a.	9.34	5.90	0.46	101.14	3VG22-12
54.91	0	29.45	0.63	0	n.a.	11.46	4.95	0.32	101.72	3VG22-13
56.92	0.08	27.62	0.51	0	n.a.	9.54	6.02	0.52	101.21	3VG22-14
57.02	0	28.13	0.57	0.02	n.a.	9.91	5.86	0.41	101.94	3VG22-15
57.10	0	27.62	0.60	0.01	n.a.	9.67	5.78	0.46	101.22	3VG22-16
57.72	0.13	27.34	0.71	0.01	n.a.	9.33	5.97	0.52	101.72	3VG22-17
55.35	0	28.70	0.62	0.02	n.a.	10.93	5.19	0.35	101.16	3VG22-18
57.41	0.03	27.20	0.44	0	n.a.	9.07	5.88	0.52	100.54	3VG22-19
55.33	0.10	28.93	0.65	0.04	n.a.	11.08	5.19	0.36	101.68	3VG22-20
54.89	0.03	28.97	0.62	0.02	n.a.	11.30	5.02	0.37	101.22	3VG22-21
56.66	0.02	27.94	0.56	0.01	n.d.	10.01	5.68	0.43	101.32	Average
0.99	0.04	0.66	0.07	0.01	n.d.	0.77	0.38	0.07		Std. Dev.
57.39	0	26.90	0.53	0.01	n.a.	9.23	6.08	0.38	100.52	3VG19-1
58.25	0	26.06	0.57	0	n.a.	8.72	6.06	0.47	100.13	3VG19-2
57.06	0	27.13	0.46	0	n.a.	9.45	5.65	0.36	100.12	3VG19-3
57.40	0.04	27.09	0.46	0	n.a.	9.47	6.00	0.43	100.89	3VG19-4
57.24	0	26.66	0.56	0.01	n.a.	9.36	6.04	0.42	100.28	3VG19-5
57.12	0	26.90	0.45	0	n.a.	9.42	6.09	0.44	100.42	3VG19-6
57.18	0	26.96	0.44	0	n.a.	9.41	6.09	0.45	100.52	3VG19-7
56.86	0	27.14	0.53	0	n.a.	9.64	5.86	0.41	100.43	3VG19-8
56.99	0	26.70	0.62	0.01	n.a.	9.27	6.05	0.46	100.10	3VG19-9
57.00	0	26.83	0.55	0	n.a.	9.25	5.93	0.37	99.92	3VG19-10
55.92	0	27.00	0.62	0.01	n.a.	9.70	5.69	0.38	99.31	3VG19-11
56.83	0.02	27.47	0.50	0	n.a.	9.49	5.90	0.38	100.58	3VG19-12
56.94	0.02	27.27	0.47	0	n.a.	9.20	6.12	0.38	100.39	3VG19-13
57.04	0	27.37	0.52	0.01	n.a.	9.45	6.01	0.39	100.79	3VG19-14
56.78	0.07	27.07	0.53	0	n.a.	9.56	5.80	0.39	100.20	3VG19-15
57.80	0.01	26.06	0.59	0	n.a.	8.25	6.05	0.55	99.30	3VG19-16
56.44	0.06	27.07	0.46	0	n.a.	9.41	5.73	0.37	99.54	3VG19-17
57.07	0.01	26.92	0.52	0	n.d.	9.31	5.95	0.41	100.20	Average
0.51	0.02	0.39	0.06	0	n.d.	0.35	0.15	0.05		Std. Dev.
57.52	0	27.27	0.43	0	n.a.	9.25	6.00	0.42	100.89	3VG16-1
57.80	0	26.86	0.52	0.03	n.a.	9.03	5.86	0.53	100.62	3VG16-2
57.28	0	27.59	0.44	0	n.a.	9.58	5.85	0.38	101.12	3VG16-3
57.38	0.04	27.65	0.44	0	n.a.	9.51	5.89	0.43	101.34	3VG16-4
56.99	0.02	27.18	0.55	0.03	n.a.	9.37	5.94	0.43	100.50	3VG16-5
57.32	0.04	27.26	0.47	0.01	n.a.	9.34	5.99	0.42	100.84	3VG16-6
57.02	0	27.49	0.48	0	n.a.	9.60	5.94	0.45	100.98	3VG16-7
56.99	0	27.48	0.46	0.02	n.a.	9.53	5.87	0.47	100.82	3VG16-8
57.47	0.05	26.57	0.66	0.01	n.a.	9.19	5.91	0.45	100.31	3VG16-9
56.69	0	27.27	0.52	0.01	n.a.	9.57	5.84	0.38	100.28	3VG16-10
57.46	0.07	27.18	0.48	0.03	n.a.	9.26	6.19	0.42	101.09	3VG16-11

SiO_2	TiO_2	Al_2O_3	FeO	MnO	MgO	CaO	Na_2O	K_2O	Total	Sample
57.26	0.02	27.25	0.50	0.01	n.d.	9.38	5.93	0.43	100.80	Average
0.31	0.03	0.32	0.07	0.01	n.d.	0.19	0.10	0.04		Std. Dev.
56.89	0	26.50	0.92	0.02	n.a.	9.42	5.86	0.46	100.07	3VG29-1
57.66	0.01	26.96	0.49	0	n.a.	9.11	6.13	0.39	100.74	3VG29-2
57.30	0	27.34	0.53	0	n.a.	9.52	6.03	0.38	101.10	3VG29-3
57.79	0	26.58	0.50	0	n.a.	8.97	6.24	0.29	100.36	3VG29-4
58.37	0	26.92	0.47	0.01	n.a.	9.01	6.27	0.34	101.40	3VG29-5
58.62	0	26.12	0.56	0.02	n.a.	8.22	6.44	0.49	100.46	3VG29-6
58.02	0	27.04	0.52	0.01	n.a.	9.08	6.15	0.38	101.20	3VG29-7
57.81	0	27.06	0.42	0	n.a.	9.18	6.15	0.43	101.06	3VG29-8
57.50	0	27.50	0.46	0	n.a.	9.36	5.97	0.38	101.18	3VG29-9
58.42	0	26.64	0.61	0.04	n.a.	8.80	6.29	0.45	101.24	3VG29-10
57.71	0	27.24	0.43	0.01	n.a.	9.12	6.22	0.28	101.00	3VG29-11
57.66	0	26.74	0.46	0	n.a.	9.09	6.17	0.45	100.57	3VG29-12
57.38	0	26.94	0.48	0	n.a.	8.98	5.99	0.39	100.16	3VG29-13
57.28	0.01	27.04	0.45	0	n.a.	9.24	6.07	0.35	100.43	3VG29-14
57.70	0.01	27.33	0.36	0.01	n.a.	9.30	5.86	0.39	100.97	3VG29-15
57.50	0.04	27.05	0.48	0	n.a.	9.16	5.89	0.41	100.53	3VG29-16
57.86	0	27.37	0.54	0	n.a.	9.01	6.16	0.37	101.31	3VG29-17
57.42	0.02	27.13	0.46	0.01	n.a.	9.21	5.95	0.42	100.64	3VG29-18
57.49	0.01	26.92	0.48	0.03	n.a.	9.00	6.16	0.30	100.38	3VG29-19
57.70	0.01	26.97	0.51	0.01	n.d.	9.09	6.11	0.39	100.78	Average
0.42	0.01	0.34	0.11	0.01	n.d.	0.27	0.16	0.06		Std. Dev.
57.02	0	27.84	0.51	0	n.a.	9.18	6.27	0.40	101.21	3VG8-1
56.89	0.01	27.56	0.48	0.02	n.a.	9.12	6.37	0.38	100.81	3VG8-2
56.97	0	27.71	0.41	0.02	n.a.	9.18	6.43	0.38	101.10	3VG8-3
56.66	0	27.90	0.54	0	n.a.	9.36	5.94	0.36	100.75	3VG8-4
57.89	0	26.47	0.52	0.01	n.a.	8.26	6.71	0.44	100.31	3VG8-5
57.17	0	27.59	0.45	0	n.a.	8.64	6.74	0.40	100.99	3VG8-6
56.19	0.02	27.81	0.54	0.03	n.a.	9.07	6.29	0.41	100.34	3VG8-7
57.49	0	27.58	0.51	0	n.a.	8.98	6.37	0.40	101.31	3VG8-8
57.27	0.04	27.63	0.44	0	n.a.	9.01	6.27	0.41	101.05	3VG8-9
56.62	0	27.71	0.48	0	n.a.	9.01	6.34	0.40	100.56	3VG8-10
57.88	0	26.41	0.51	0	n.a.	8.10	6.57	0.54	100.02	3VG8-11
57.05	0	27.74	0.46	0.02	n.a.	8.86	6.36	0.42	100.92	3VG8-12
57.34	0	27.60	0.45	0	n.a.	8.92	6.42	0.29	101.02	3VG8-13
56.86	0	27.57	0.39	0.01	n.a.	9.00	6.32	0.44	100.59	3VG8-14
57.14	0.01	27.51	0.47	0	n.a.	8.85	6.47	0.41	100.85	3VG8-15
57.25	0.08	27.46	0.53	0	n.a.	8.90	6.39	0.42	101.04	3VG8-16
57.11	0.01	27.51	0.48	0.01	n.d.	8.90	6.39	0.41	100.80	Average
0.44	0.02	0.43	0.05	0.01	n.d.	0.33	0.19	0.05		Std. Dev.
57.98	0.01	26.11	0.63	0	0.25	8.43	6.29	0.51	100.21	3VG7-1
56.78	0.03	27.54	0.37	0	0.01	9.26	5.91	0.26	100.15	3VG7-2
57.31	0.01	27.27	0.45	0	0.02	8.95	6.10	0.40	100.50	3VG7-3
57.19	0	27.57	0.40	0	0.01	9.06	5.99	0.38	100.60	3VG7-4
56.66	0	27.56	0.39	0	0.02	9.18	5.94	0.30	100.05	3VG7-5
57.61	0.04	27.29	0.42	0.03	0.01	9.07	6.01	0.34	100.80	3VG7-6
57.50	0.03	26.27	0.46	0.03	0.11	8.55	6.24	0.42	99.60	3VG7-7
57.51	0.03	27.02	0.40	0.02	0	8.88	6.14	0.40	100.39	3VG7-8
57.53	0.04	27.37	0.36	0.01	0.01	8.97	6.20	0.41	100.89	3VG7-9
57.01	0	27.21	0.39	0	0.01	9.26	5.87	0.38	100.12	3VG7-10
57.25	0	27.50	0.47	0.02	0.01	8.98	6.14	0.34	100.71	3VG7-11
57.50	0.03	27.33	0.44	0.02	0.01	8.97	6.09	0.41	100.80	3VG7-12
57.63	0	27.07	0.43	0	0.02	8.85	6.17	0.40	100.56	3VG7-13
56.76	0	27.98	0.39	0.01	0.02	9.54	5.80	0.39	100.88	3VG7-14
57.08	0	27.37	0.39	0.02	0.02	9.06	6.11	0.42	100.46	3VG7-15
56.97	0	27.40	0.39	0.01	0.02	9.21	6.06	0.42	100.46	3VG7-16
57.14	0	27.19	0.49	0.02	0.03	8.98	6.13	0.43	100.40	3VG7-17
57.48	0	27.22	0.43	0.01	0.03	8.80	6.09	0.40	100.47	3VG7-18
57.56	0	26.97	0.43	0	0.02	8.91	6.24	0.44	100.56	3VG7-19
56.65	0.01	27.49	0.43	0	0.02	9.15	5.86	0.41	100.04	3VG7-20
57.09	0.01	27.50	0.41	0	0	8.92	6.08	0.42	100.42	3VG7-21
56.87	0.03	27.55	0.51	0	0.02	8.97	6.11	0.44	100.50	3VG7-22
57.12	0	27.34	0.41	0	0.00	9.13	5.91	0.41	100.32	3VG7-23
57.31	0	26.96	0.49	0.03	0.02	8.93	6.08	0.46	100.27	3VG7-24
57.23	0.04	27.40	0.50	0.01	0.02	9.00	6.17	0.44	100.80	3VG7-25

SiO_2	TiO_2	Al_2O_3	FeO	MnO	MgO	CaO	Na_2O	K_2O	Total	Sample
57.65	0.03	27.31	0.47	0	0.02	8.87	6.23	0.43	101.02	3VG7-26
57.66	0	27.31	0.43	0	0.02	8.92	6.20	0.42	100.97	3VG7-27
57.42	0	27.53	0.49	0	0.02	8.96	6.20	0.38	100.99	3VG7-28
57.10	0.03	27.26	0.45	0	0.01	9.02	6.03	0.42	100.33	3VG7-29
57.56	0.03	27.13	0.48	0.01	0.03	8.91	6.12	0.45	100.72	3VG7-30
57.29	0.01	27.47	0.48	0	0.01	9.05	6.20	0.41	100.91	3VG7-31
56.53	0.03	27.54	0.47	0	0.02	9.21	5.96	0.37	100.12	3VG7-32
57.69	0.02	27.12	0.43	0	0	8.86	6.31	0.44	100.87	3VG7-33
57.05	0.01	27.65	0.46	0.02	0.02	9.47	5.89	0.42	100.98	3VG7-34
57.21	0.03	27.46	0.42	0.01	0.01	9.05	6.24	0.43	100.86	3VG7-35
57.34	0.01	27.27	0.41	0.00	0.01	9.05	6.32	0.40	100.81	3VG7-36
57.30	0.02	27.49	0.44	0.01	0.01	9.05	5.98	0.40	100.69	3VG7-37
57.26	0.01	27.30	0.44	0.01	0.02	9.01	6.09	0.40	100.55	Average
0.33	0.01	0.34	0.05	0.01	0.04	0.20	0.13	0.04		Std. Dev.
57.04	0.03	27.04	0.43	0	0.04	8.87	5.86	0.35	99.66	3VG9-1
58.40	0.05	25.92	0.68	0.01	0.09	7.55	6.74	0.47	99.92	3VG9-2
56.33	0.02	27.80	0.55	0.02	0.07	9.27	5.77	0.34	100.16	3VG9-3
56.98	0	27.34	0.42	0.03	0.04	8.73	6.13	0.37	100.02	3VG9-4
56.84	0.01	27.34	0.53	0.01	0.03	8.84	5.96	0.35	99.90	3VG9-5
56.43	0.01	27.56	0.43	0.03	0.04	8.96	5.68	0.35	99.50	3VG9-6
56.85	0.03	27.49	0.44	0.02	0.05	8.97	5.86	0.37	100.06	3VG9-7
55.46	0.03	28.07	0.50	0	0.06	9.76	5.43	0.30	99.60	3VG9-8
58.28	0.04	25.84	0.56	0	0.10	7.72	6.27	0.49	99.31	3VG9-9
57.33	0	27.05	0.43	0	0.08	8.68	6.00	0.40	99.97	3VG9-10
57.04	0.01	27.32	0.45	0	0.06	8.95	5.95	0.36	100.14	3VG9-11
58.73	0.05	24.58	0.88	0	0.58	7.61	6.69	0.45	99.57	3VG9-12
56.59	0.02	27.57	0.47	0.01	0.07	9.13	5.67	0.38	99.90	3VG9-13
56.80	0.04	27.20	0.45	0	0.03	8.68	5.97	0.41	99.58	3VG9-14
58.37	0.11	25.60	0.66	0.01	0.10	7.64	6.33	0.53	99.33	3VG9-15
58.16	0.04	26.31	0.55	0	0.06	7.83	6.38	0.42	99.77	3VG9-16
57.36	0.03	26.86	0.47	0	0.04	8.49	5.99	0.40	99.65	3VG9-17
56.87	0	27.36	0.49	0.01	0.06	9.06	5.86	0.33	100.02	3VG9-18
56.94	0.04	27.31	0.46	0	0.05	8.91	5.90	0.36	99.97	3VG9-19
57.20	0.03	26.92	0.52	0.01	0.09	8.61	6.02	0.39	99.79	Average
0.84	0.02	0.88	0.11	0.01	0.12	0.64	0.34	0.06		Std. Dev.
57.33	0	27.25	0.40	0.01	n.a.	8.95	6.17	0.37	100.47	3VG35-1
57.21	0	27.55	0.43	0.01	n.a.	9.12	6.42	0.33	101.07	3VG35-2
57.25	0	27.51	0.36	0	n.a.	9.16	6.46	0.40	101.14	3VG35-3
56.66	0.05	27.59	0.42	0.02	n.a.	9.49	6.09	0.34	100.66	3VG35-4
56.69	0	27.68	0.44	0	n.a.	9.46	6.23	0.38	100.88	3VG35-5
57.05	0.02	27.70	0.42	0.01	n.a.	9.22	6.31	0.30	101.02	3VG35-6
56.92	0	27.57	0.45	0.03	n.a.	9.21	6.23	0.34	100.74	3VG35-7
57.12	0	27.77	0.40	0.02	n.a.	9.33	6.22	0.38	101.24	3VG35-8
56.74	0.01	27.57	0.36	0	n.a.	9.07	6.40	0.35	100.49	3VG35-9
56.69	0	27.69	0.44	0.03	n.a.	9.42	6.06	0.39	100.72	3VG35-10
57.32	0	27.16	0.39	0.01	n.a.	8.99	6.48	0.41	100.75	3VG35-11
56.78	0	27.58	0.36	0	n.a.	9.29	6.22	0.35	100.59	3VG35-12
57.20	0	27.40	0.29	0	n.a.	9.04	6.17	0.37	100.47	3VG35-13
57.11	0	27.64	0.41	0.02	n.a.	9.26	6.18	0.35	100.95	3VG35-14
56.66	0	27.82	0.46	0.01	n.a.	9.61	6.16	0.33	101.06	3VG35-15
56.81	0	27.76	0.40	0	n.a.	9.27	6.43	0.37	101.05	3VG35-16
57.14	0	27.44	0.43	0	n.a.	9.07	6.53	0.32	100.92	3VG35-17
57.08	0	27.57	0.44	0.03	n.a.	9.00	6.37	0.40	100.89	3VG35-18
57.02	0.02	27.43	0.46	0.03	n.a.	9.12	6.32	0.31	100.69	3VG35-19
56.99	0.01	27.56	0.41	0.01	n.d.	9.21	6.29	0.36	100.83	Average
0.23	0.01	0.17	0.04	0.01	n.d.	0.18	0.14	0.03		Std. Dev.
58.04	0	27.49	0.34	0	n.a.	9.09	6.51	0.41	101.88	3VG41-1
59.14	0	26.65	0.43	0	n.a.	8.65	6.05	0.56	101.48	3VG41-2
57.81	0	27.68	0.33	0.01	n.a.	9.22	6.33	0.35	101.73	3VG41-3
58.43	0	27.55	0.35	0.01	n.a.	8.87	6.35	0.41	101.96	3VG41-4
58.25	0.01	27.46	0.33	0.03	n.a.	9.40	6.14	0.41	102.03	3VG41-5
57.86	0	27.46	0.42	0	n.a.	9.19	6.31	0.40	101.64	3VG41-6
57.25	0	27.80	0.42	0	n.a.	9.33	6.38	0.43	101.60	3VG41-7
56.78	0	27.74	0.36	0.02	n.a.	9.11	6.31	0.40	100.71	3VG41-8
57.27	0	27.47	0.35	0	n.a.	8.89	6.29	0.34	100.60	3VG41-9

SiO_2	TiO_2	Al_2O_3	FeO	MnO	MgO	CaO	Na_2O	K_2O	Total	Sample
57.11	0	27.49	0.37	0	n.a.	9.14	6.26	0.41	100.77	3VG41-10
57.40	0	27.94	0.38	0.02	n.a.	9.10	6.39	0.36	101.59	3VG41-11
57.76	0	27.52	0.37	0.01	n.d.	9.09	6.30	0.41	101.45	Average
0.69	0	0.33	0.04	0.01	n.d.	0.22	0.12	0.06		Std. Dev.
58.50	0	26.36	0.55	0	n.a.	7.75	7.12	0.39	100.67	KAP12-1
58.82	0	26.33	0.46	0	n.a.	7.96	7.01	0.36	100.99	KAP12-2
58.54	0	26.24	0.50	0	n.a.	7.75	7.11	0.40	100.53	KAP12-3
58.30	0	26.38	0.43	0.01	n.a.	7.88	6.76	0.33	100.10	KAP12-4
58.52	0.02	26.55	0.46	0	n.a.	7.90	6.89	0.33	100.67	KAP12-5
58.84	0	26.53	0.41	0.01	n.a.	7.97	6.74	0.34	100.83	KAP12-6
58.45	0.01	26.47	0.45	0.03	n.a.	7.85	7.00	0.36	100.62	KAP12-7
58.42	0	26.52	0.42	0	n.a.	7.96	6.94	0.30	100.56	KAP12-8
58.64	0	26.46	0.45	0.01	n.a.	7.81	7.01	0.33	100.71	KAP12-9
58.40	0.04	26.53	0.46	0.02	n.a.	8.03	6.90	0.32	100.69	KAP12-10
58.61	0	26.66	0.46	0.03	n.a.	7.75	7.01	0.33	100.86	KAP12-11
60.11	0	24.52	0.53	0.02	n.a.	6.31	7.56	0.43	99.48	KAP12-12
57.94	0	26.34	0.62	0.02	n.a.	7.68	7.10	0.31	100.01	KAP12-13
58.61	0.02	26.62	0.50	0.01	n.a.	7.91	7.12	0.33	101.14	KAP12-14
58.69	0	26.32	0.44	0.03	n.a.	7.78	7.10	0.29	100.65	KAP12-15
58.36	0	26.33	0.63	0.04	n.a.	7.97	6.92	0.34	100.58	KAP12-16
58.56	0.10	26.07	0.58	0	n.a.	7.83	6.70	0.28	100.12	KAP12-17
58.65	0	26.29	0.52	0.01	n.a.	7.82	6.92	0.30	100.51	KAP12-18
58.93	0	26.45	0.53	0.02	n.a.	7.78	6.92	0.30	100.92	KAP12-19
59.78	0.03	25.62	0.48	0	n.a.	7.04	7.21	0.51	100.66	KAP12-20
58.59	0	26.39	0.49	0	n.a.	7.78	6.93	0.34	100.51	KAP12-21
58.65	0	26.60	0.46	0.03	n.a.	7.83	7.12	0.33	101.02	KAP12-22
58.31	0	26.34	0.54	0	n.a.	7.85	7.21	0.32	100.57	KAP12-23
58.60	0.04	26.06	0.53	0.01	n.a.	7.88	6.98	0.31	100.41	KAP12-24
58.21	0.04	25.36	0.86	0	n.a.	7.63	7.18	0.42	99.69	KAP12-25
58.98	0	26.04	0.59	0.01	n.a.	7.52	7.22	0.39	100.74	KAP12-26
58.65	0.01	26.25	0.51	0.01	n.d.	7.74	7.03	0.35	100.55	Average
0.44	0.02	0.46	0.09	0.01	n.d.	0.35	0.16	0.05		Std. Dev.
59.16	0	26.43	0.35	0.01	0.01	8.25	6.76	0.46	101.45	KAP1-1
59.18	0	26.68	0.45	0	0.01	8.20	6.82	0.26	101.60	KAP1-2
59.20	0	26.38	0.47	0	0.01	8.15	6.72	0.25	101.17	KAP1-3
59.29	0.01	26.53	0.47	0	0.01	8.22	6.67	0.30	101.50	KAP1-4
59.23	0.01	26.50	0.47	0.01	0.02	8.19	6.49	0.60	101.50	KAP1-5
59.29	0.01	26.62	0.42	0.01	0.01	8.22	6.76	0.40	101.74	KAP1-6
58.58	0.02	26.58	0.47	0.00	0.02	8.23	6.37	0.42	100.69	KAP1-7
59.13	0	26.46	0.44	0.02	0.01	8.08	6.69	0.43	101.27	KAP1-8
59.08	0	26.59	0.44	0.03	0.02	8.25	6.79	0.33	101.51	KAP1-9
59.03	0	26.64	0.43	0.00	0.02	8.22	6.69	0.27	101.30	KAP1-10
59.06	0.02	26.55	0.38	0.01	0	8.28	6.80	0.27	101.36	KAP1-11
59.27	0.02	26.25	0.37	0.00	0	8.20	6.84	0.40	101.36	KAP1-12
58.11	0.10	25.82	0.73	0.02	0.29	8.46	6.47	0.56	100.56	KAP1-13
58.91	0.04	26.24	0.39	0.02	0.00	8.19	7.00	0.24	101.01	KAP1-14
59.27	0.03	26.16	0.40	0.01	0.01	8.25	7.05	0.27	101.46	KAP1-15
58.91	0	26.02	0.43	0.02	0.00	8.16	6.74	0.24	100.51	KAP1-16
59.14	0	26.27	0.41	0.02	0	8.19	6.70	0.43	101.15	KAP1-17
59.19	0	26.25	0.38	0.01	0	8.11	6.78	0.42	101.12	KAP1-18
59.05	0.01	25.80	0.42	0.01	0.01	8.20	6.82	0.28	100.60	KAP1-19
58.89	0.01	25.96	0.39	0.01	0.02	8.43	6.59	0.46	100.76	KAP1-20
59.22	0.08	26.68	0.42	0.02	0.01	8.35	6.61	0.52	101.91	KAP1-21
58.75	0.03	26.51	0.41	0.03	0.02	8.09	6.59	0.49	100.91	KAP1-22
59.02	0.03	26.72	0.37	0.03	0	8.12	6.83	0.21	101.32	KAP1-23
58.96	0.01	26.88	0.49	0.02	0	8.25	6.75	0.37	101.72	KAP1-24
58.95	0.04	26.66	0.47	0.01	0	8.06	6.56	0.38	101.12	KAP1-25
59.53	0.06	26.04	0.56	0.01	0.01	7.87	6.43	0.79	101.29	KAP1-26
58.93	0.04	26.54	0.52	0.03	0	8.25	6.56	0.41	101.28	KAP1-27
58.87	0.02	26.74	0.46	0.04	0	8.24	6.44	0.53	101.34	KAP1-28
57.58	0	26.12	0.41	0.02	0	8.12	6.43	0.23	98.91	KAP1-29
58.99	0.02	26.40	0.44	0.01	0.02	8.20	6.68	0.39	101.15	Average
0.38	0.03	0.29	0.07	0.01	0.05	0.11	0.17	0.13		Std. Dev.
58.63	0.00	26.16	0.46	0.00	n.a.	8.02	6.91	0.31	100.50	KAP27-1
58.69	0.03	26.33	0.38	0.05	n.a.	7.94	6.90	0.35	100.66	KAP27-2

SiO_2	TiO_2	Al_2O_3	FeO	MnO	MgO	CaO	Na_2O	K_2O	Total	Sample
59.01	0	26.47	0.44	0.02	n.a.	7.90	7.08	0.34	101.26	KAP27-3
58.65	0	26.39	0.46	0	n.a.	8.02	6.95	0.26	100.72	KAP27-4
58.00	0.10	26.46	0.74	0.04	n.a.	8.25	6.84	0.28	100.71	KAP27-5
58.24	0	26.29	0.54	0.01	n.a.	7.83	7.26	0.31	100.49	KAP27-6
59.82	0	25.51	0.52	0	n.a.	7.12	7.37	0.31	100.65	KAP27-7
58.81	0	26.52	0.46	0.01	n.a.	7.99	7.08	0.18	101.05	KAP27-8
58.93	0	26.49	0.44	0.02	n.a.	7.89	7.13	0.22	101.12	KAP27-9
58.74	0.02	26.45	0.43	0	n.a.	7.98	7.02	0.23	100.86	KAP27-10
58.86	0.01	26.51	0.45	0.02	n.a.	7.79	7.11	0.23	100.98	KAP27-11
58.93	0	26.37	0.58	0	n.a.	7.64	7.17	0.24	100.93	KAP27-12
58.34	0.07	24.88	1.49	0.05	n.a.	8.99	6.94	0.24	101.00	KAP27-13
59.25	0	26.49	0.53	0	n.a.	7.65	7.14	0.22	101.27	KAP27-14
58.78	0.02	26.24	0.57	0.02	n.d.	7.93	7.06	0.26	100.87	Average
0.44	0.03	0.47	0.28	0.02	n.d.	0.40	0.15	0.05		Std. Dev.
58.14	0.04	26.20	0.43	0	0.01	8.23	6.50	0.39	99.93	KAP3-1
58.02	0.02	26.07	0.51	0	0.01	8.15	6.50	0.47	99.75	KAP3-2
57.68	0.02	26.23	0.48	0	0.02	8.39	6.43	0.47	99.71	KAP3-3
58.18	0.04	25.79	0.48	0	0.02	8.04	6.46	0.48	99.49	KAP3-4
58.20	0	26.18	0.51	0	0.03	8.16	6.58	0.43	100.09	KAP3-5
58.04	0.01	25.97	0.40	0.01	0	8.27	6.41	0.48	99.59	KAP3-6
56.05	0.05	26.66	0.78	0.00	0.04	9.49	5.52	0.48	99.07	KAP3-7
58.05	0.01	26.21	0.42	0.00	0.01	8.26	6.71	0.47	100.14	KAP3-8
58.17	0	26.44	0.44	0.01	0.01	7.87	6.56	0.44	99.94	KAP3-9
58.15	0.01	26.32	0.41	0	0.02	7.82	6.61	0.45	99.78	KAP3-10
58.42	0	26.35	0.44	0	0.01	7.80	6.61	0.47	100.10	KAP3-11
58.02	0	26.58	0.49	0	0.01	7.96	6.58	0.43	100.07	KAP3-12
58.18	0	26.28	0.42	0.01	0.03	7.96	6.52	0.32	99.73	KAP3-13
57.99	0.02	26.44	0.40	0	0	7.97	6.73	0.37	99.91	KAP3-14
57.94	0	26.27	0.42	0.03	0.01	7.94	6.69	0.46	99.77	KAP3-15
57.86	0	26.34	0.44	0.02	0.02	7.88	6.61	0.49	99.64	KAP3-16
57.82	0	26.28	0.53	0.01	0.02	7.98	6.63	0.46	99.73	KAP3-17
58.21	0	26.17	0.46	0	0	7.73	6.58	0.42	99.58	KAP3-18
57.86	0.04	26.46	0.65	0.01	0.02	8.37	6.65	0.49	100.56	KAP3-19
57.83	0.01	26.45	0.56	0.03	0.01	8.19	6.63	0.50	100.19	KAP3-20
57.88	0.01	26.40	0.47	0.01	0	8.21	6.59	0.44	100.01	KAP3-21
57.98	0.01	26.47	0.47	0.01	0.02	8.25	6.41	0.49	100.08	KAP3-22
57.87	0	26.18	0.51	0	0	8.33	6.71	0.47	100.06	KAP3-23
58.38	0.01	26.26	0.49	0	0.02	8.15	6.61	0.46	100.38	KAP3-24
57.45	0.02	26.10	0.49	0.02	0	8.18	6.36	0.46	99.07	KAP3-25
55.32	0	26.86	0.82	0.03	0.04	9.73	5.91	0.42	99.11	KAP3-26
56.92	0.05	26.20	0.54	0.02	0.02	8.60	6.27	0.44	99.04	KAP3-27
56.82	0.03	26.35	0.61	0.03	0.04	8.53	6.31	0.45	99.18	KAP3-28
57.70	0.01	25.95	0.52	0.01	0	8.28	6.59	0.49	99.55	KAP3-29
58.94	0.01	26.24	0.47	0	0.01	8.06	6.14	0.50	100.39	KAP3-30
56.28	0.01	27.03	0.76	0.01	0.03	9.21	5.64	0.39	99.37	KAP3-31
57.49	0.02	26.44	0.70	0.02	0.03	8.65	6.08	0.50	99.92	KAP3-32
58.25	0.02	26.03	0.70	0.01	0.03	8.33	6.30	0.51	100.17	KAP3-33
56.01	0	27.56	0.71	0.02	0.01	9.68	5.70	0.36	100.05	KAP3-34
58.06	0.01	25.99	0.47	0	0.02	7.96	6.35	0.51	99.36	KAP3-35
58.33	0	26.12	0.48	0.01	0.02	8.00	6.59	0.47	100.01	KAP3-36
58.20	0	26.25	0.48	0	0.01	8.09	6.53	0.47	100.02	KAP3-37
57.40	0	26.87	0.62	0.03	0.03	8.46	6.02	0.44	99.86	KAP3-38
58.44	0.01	26.08	0.59	0	0.02	8.03	6.46	0.51	100.13	KAP3-39
57.76	0.01	26.33	0.53	0.01	0.02	8.29	6.41	0.45	99.81	Average
0.75	0.01	0.32	0.11	0.01	0.01	0.48	0.30	0.04		Std. Dev.
58.01	0.02	26.13	0.50	0.03	0	7.70	7.04	0.22	99.66	KAP2-1
57.71	0.01	26.19	0.44	0.04	0.01	7.81	6.99	0.25	99.45	KAP2-2
57.55	0	26.44	0.46	0.01	0.02	7.74	6.99	0.22	99.42	KAP2-3
58.32	0.02	26.04	0.40	0.02	0	7.62	7.19	0.24	99.84	KAP2-4
57.82	0.02	26.23	0.44	0.01	0.01	7.72	7.23	0.22	99.70	KAP2-5
57.90	0	26.28	0.44	0	0	7.62	7.00	0.22	99.47	KAP2-6
58.17	0.02	26.24	0.45	0.04	0.02	7.66	7.17	0.24	99.99	KAP2-7
57.78	0.05	26.17	0.57	0.02	0.03	7.64	7.16	0.25	99.67	KAP2-8
57.98	0.01	26.23	0.47	0	0	7.55	7.10	0.26	99.62	KAP2-9
58.28	0	25.97	0.40	0.01	0.01	7.51	7.10	0.26	99.55	KAP2-10
57.81	0	26.31	0.38	0.01	0	7.90	6.92	0.20	99.53	KAP2-11
57.98	0.01	25.77	0.39	0	0	7.73	7.10	0.26	99.23	KAP2-12

SiO_2	TiO_2	Al_2O_3	FeO	MnO	MgO	CaO	Na_2O	K_2O	Total	Sample
58.45	0.03	26.04	0.40	0	0	7.78	7.18	0.24	100.12	KAP2-13
57.77	0.04	25.99	0.48	0	0	7.67	7.07	0.26	99.26	KAP2-14
57.60	0.04	26.28	0.59	0	0	7.84	7.04	0.34	99.72	KAP2-15
57.85	0.02	25.79	0.46	0	0	7.49	7.06	0.28	98.95	KAP2-16
57.59	0.06	26.14	0.43	0	0	7.63	7.14	0.25	99.25	KAP2-17
57.33	0.03	26.29	0.33	0	0	7.89	7.11	0.22	99.20	KAP2-18
56.82	0.01	26.62	0.51	0	0	8.79	6.53	0.22	99.51	KAP2-19
57.99	0.05	26.16	0.40	0.01	0.01	7.70	7.07	0.27	99.65	KAP2-20
58.24	0	26.40	0.32	0	0.01	7.78	7.24	0.25	100.23	KAP2-21
58.25	0.02	26.38	0.38	0	0.02	7.88	6.99	0.23	100.16	KAP2-22
58.52	0.02	26.27	0.40	0	0.02	7.79	7.10	0.26	100.36	KAP2-23
58.27	0.01	26.13	0.48	0.01	0.02	7.73	7.12	0.25	100.01	KAP2-24
58.65	0	26.13	0.37	0	0	7.55	7.13	0.27	100.10	KAP2-25
58.63	0.01	26.26	0.39	0	0	7.62	7.27	0.23	100.41	KAP2-26
59.44	0.02	26.01	0.44	0	0	7.83	6.65	0.25	100.65	KAP2-27
58.79	0	26.28	0.42	0.01	0	7.76	7.04	0.26	100.55	KAP2-28
59.16	0	25.91	0.42	0.01	0	7.57	7.27	0.28	100.62	KAP2-29
58.73	0	26.10	0.41	0.01	0	7.72	7.07	0.26	100.30	KAP2-30
58.97	0.01	26.21	0.49	0	0	7.63	7.36	0.27	100.94	KAP2-31
58.15	0.02	26.46	0.51	0	0.03	7.95	7.12	0.25	100.48	KAP2-32
58.69	0.02	26.24	0.48	0	0	7.78	7.14	0.25	100.59	KAP2-33
58.16	0.02	26.18	0.44	0.01	0.01	7.74	7.08	0.25	99.88	Average
0.55	0.02	0.18	0.06	0.01	0.01	0.22	0.16	0.03		Std. Dev.
58.11	0	26.92	0.52	0	n.a.	8.53	6.60	0.43	101.11	KAP14-1
58.40	0	26.91	0.42	0	n.a.	8.50	6.65	0.39	101.26	KAP14-2
56.29	0.21	26.29	1.61	0.02	n.a.	9.69	5.15	0.65	99.91	KAP14-3
58.17	0	26.64	0.40	0	n.a.	8.37	6.58	0.39	100.55	KAP14-4
58.29	0.06	27.06	0.50	0.01	n.a.	8.40	6.57	0.50	101.39	KAP14-5
58.64	0.01	26.69	0.44	0	n.a.	8.50	6.53	0.46	101.27	KAP14-6
57.70	0	27.12	0.47	0.02	n.a.	8.59	6.51	0.45	100.86	KAP14-7
58.08	0	26.94	0.41	0.01	n.a.	8.38	6.63	0.27	100.73	KAP14-8
57.84	0	26.79	0.47	0	n.a.	8.37	6.49	0.34	100.30	KAP14-9
58.23	0.01	26.85	0.40	0.01	n.a.	8.53	6.46	0.47	100.97	KAP14-10
58.18	0.03	26.86	0.42	0.02	n.a.	8.54	6.65	0.46	101.17	KAP14-11
58.17	0	26.89	0.42	0	n.a.	8.45	6.53	0.32	100.78	KAP14-12
57.91	0	26.84	0.43	0	n.a.	8.34	6.71	0.32	100.54	KAP14-13
53.89	0.02	29.57	0.74	0.01	n.a.	11.68	4.87	0.27	101.05	KAP14-14
57.86	0.01	26.84	0.43	0	n.a.	8.37	6.50	0.36	100.37	KAP14-15
58.42	0	26.85	0.45	0.01	n.a.	8.28	6.59	0.41	101.00	KAP14-16
58.01	0	26.87	0.47	0	n.a.	8.41	6.67	0.45	100.88	KAP14-17
57.78	0.02	27.00	0.53	0.01	n.d.	8.70	6.39	0.41	100.83	Average
1.12	0.05	0.69	0.29	0.01	n.d.	0.83	0.53	0.10		Std. Dev.
58.39	0	26.52	0.58	0.01	n.a.	8.61	6.20	0.47	100.78	KAP11-1
59.45	0.01	25.84	0.66	0	n.a.	7.92	6.48	0.69	101.04	KAP11-2
58.31	0	26.64	0.45	0	n.a.	8.53	6.63	0.26	100.81	KAP11-3
58.09	0	26.56	0.45	0.02	n.a.	8.47	6.59	0.28	100.46	KAP11-4
58.32	0.03	26.55	0.57	0.02	n.a.	8.39	6.57	0.32	100.76	KAP11-5
58.54	0.01	26.49	0.67	0.02	n.a.	8.18	6.75	0.57	101.21	KAP11-6
58.58	0	26.65	0.49	0	n.a.	8.78	6.28	0.41	101.19	KAP11-7
58.53	0	26.76	0.50	0.05	n.a.	8.43	6.54	0.44	101.24	KAP11-8
58.07	0	26.48	0.55	0.03	n.a.	8.55	6.37	0.43	100.48	KAP11-9
58.85	0.01	26.47	0.37	0.02	n.a.	8.33	6.64	0.32	101.01	KAP11-10
58.43	0	26.64	0.43	0.01	n.a.	8.47	6.59	0.44	101.00	KAP11-11
58.50	0	26.54	0.35	0.01	n.a.	8.23	6.41	0.45	100.48	KAP11-12
58.80	0	26.33	0.41	0.01	n.a.	8.34	6.56	0.50	100.94	KAP11-13
59.22	0	25.95	0.47	0.02	n.a.	7.57	6.97	0.54	100.75	KAP11-14
58.58	0	26.46	0.50	0.01	n.d.	8.34	6.54	0.44	100.87	Average
0.39	0.01	0.26	0.10	0.01	n.d.	0.30	0.19	0.12		Std. Dev.
58.62	0	26.86	0.50	0	n.a.	8.38	6.76	0.33	101.44	KAP10-1
58.20	0.03	26.84	0.50	0.01	n.a.	8.40	6.71	0.36	101.05	KAP10-2
58.25	0	26.80	0.56	0.02	n.a.	8.23	6.64	0.39	100.89	KAP10-3
58.21	0.05	26.79	0.50	0.03	n.a.	8.41	6.69	0.24	100.92	KAP10-4
58.28	0	26.94	0.47	0	n.a.	8.39	6.67	0.32	101.07	KAP10-5
57.96	0	26.64	0.55	0	n.a.	8.20	6.57	0.45	100.37	KAP10-6
58.21	0	26.81	0.53	0	n.a.	8.29	6.64	0.41	100.87	KAP10-7

SiO_2	TiO_2	Al_2O_3	FeO	MnO	MgO	CaO	Na_2O	K_2O	Total	Sample
58.04	0.02	26.61	0.53	0.02	n.a.	8.27	6.54	0.43	100.46	KAP10-8
57.98	0	26.98	0.53	0.01	n.a.	8.42	6.79	0.34	101.05	KAP10-9
57.81	0	26.68	0.63	0.01	n.a.	8.43	6.57	0.50	100.62	KAP10-10
58.13	0	26.70	0.62	0.01	n.a.	8.30	6.65	0.36	100.76	KAP10-11
58.06	0.03	26.81	0.47	0.03	n.a.	8.33	6.68	0.36	100.78	KAP10-12
58.27	0.06	26.65	0.52	0.03	n.a.	8.30	6.50	0.41	100.74	KAP10-13
58.62	0	26.61	0.48	0.02	n.a.	8.16	6.71	0.43	101.03	KAP10-14
58.35	0	26.73	0.50	0	n.a.	8.22	6.73	0.40	100.92	KAP10-15
58.25	0.01	26.90	0.51	0.03	n.a.	8.24	6.72	0.37	101.03	KAP10-16
60.86	0.02	24.37	0.50	0	n.a.	7.54	6.33	0.40	100.02	KAP10-17
57.89	0	26.76	0.43	0.02	n.a.	8.36	6.81	0.28	100.54	KAP10-18
58.33	0.01	26.64	0.52	0.01	n.d.	8.27	6.65	0.38	100.81	Average
0.67	0.02	0.58	0.05	0.01	n.d.	0.20	0.12	0.06		Std. Dev.
58.70	0.02	26.48	0.42	0.02	0.02	8.24	6.54	0.34	100.77	KAP6-1
58.17	0	26.52	0.42	0	0.01	8.20	6.72	0.23	100.26	KAP6-2
58.32	0	26.43	0.44	0.01	0.02	8.20	6.68	0.32	100.44	KAP6-3
58.04	0.03	26.36	0.42	0.02	0	8.03	6.78	0.16	99.84	KAP6-4
58.02	0.02	26.66	0.39	0.01	0	8.04	7.08	0.18	100.40	KAP6-5
57.35	0	26.54	0.39	0.01	0.01	8.12	6.71	0.19	99.30	KAP6-6
57.85	0	26.50	0.40	0	0.01	8.06	6.95	0.19	99.96	KAP6-7
57.82	0	26.11	0.72	0.03	0.09	8.50	6.53	0.46	100.26	KAP6-8
56.81	0	25.95	0.64	0	0.06	8.39	6.28	0.45	98.58	KAP6-9
57.03	0	25.85	0.74	0	0.16	8.33	6.32	0.44	98.86	KAP6-10
58.56	0	26.45	0.46	0.01	0.01	8.19	6.56	0.38	100.64	KAP6-11
58.68	0	26.56	0.45	0	0	8.21	6.74	0.30	100.94	KAP6-12
58.58	0	26.48	0.49	0	0	8.13	6.80	0.35	100.82	KAP6-13
58.66	0	26.44	0.41	0.02	0.01	8.01	6.70	0.30	100.53	KAP6-14
58.10	0	26.33	0.50	0	0.01	8.12	6.46	0.42	99.95	KAP6-15
58.13	0	26.43	0.41	0.02	0	8.11	6.68	0.14	99.92	KAP6-16
58.19	0	26.46	0.49	0.00	0.01	8.21	6.78	0.36	100.48	KAP6-17
58.27	0	26.56	0.42	0.02	0	8.17	6.91	0.25	100.60	KAP6-18
58.84	0	26.42	0.46	0	0.01	8.06	6.81	0.34	100.93	KAP6-19
58.57	0	26.17	0.80	0	0.01	7.79	6.75	0.52	100.61	KAP6-20
58.67	0.01	26.56	0.42	0	0.01	8.00	6.97	0.18	100.82	KAP6-21
58.40	0.05	26.40	0.47	0.02	0.01	8.18	6.55	0.39	100.46	KAP6-22
58.86	0.01	26.28	0.44	0.01	0	8.20	6.65	0.30	100.76	KAP6-23
58.82	0.04	26.45	0.54	0	0.01	8.14	6.66	0.45	101.11	KAP6-24
58.38	0.01	26.05	0.59	0.02	0.09	8.27	6.66	0.42	100.49	KAP6-25
58.42	0.01	26.03	0.63	0.01	0.03	8.34	6.35	0.47	100.29	KAP6-26
58.81	0.03	26.16	0.63	0	0.04	8.10	6.53	0.47	100.78	KAP6-27
58.00	0.05	26.21	0.53	0	0.03	8.26	6.51	0.45	100.04	KAP6-28
58.25	0.01	26.35	0.50	0.01	0.02	8.16	6.67	0.34	100.32	Average
0.52	0.02	0.21	0.12	0.01	0.04	0.14	0.19	0.11		Std. Dev.
57.85	0.02	26.49	0.51	0.03	0.01	8.22	6.47	0.41	100.01	KAP5-1
58.06	0.03	26.56	0.47	0.02	0	8.24	6.46	0.38	100.20	KAP5-2
58.16	0.01	26.49	0.47	0.03	0	8.20	6.54	0.37	100.28	KAP5-3
57.94	0.02	26.53	0.47	0.01	0	8.13	6.63	0.33	100.07	KAP5-4
58.03	0.02	26.68	0.50	0.03	0.01	8.54	6.51	0.42	100.73	KAP5-5
58.52	0	26.43	0.50	0.05	0.02	8.16	6.52	0.43	100.61	KAP5-6
58.88	0.01	26.04	0.38	0.02	0	8.07	6.94	0.19	100.52	KAP5-7
59.07	0	26.14	0.42	0.03	0	8.02	6.98	0.20	100.86	KAP5-8
59.02	0.05	26.30	0.39	0.01	0	8.11	6.71	0.24	100.84	KAP5-9
58.77	0	25.83	0.44	0	0.01	8.10	6.69	0.35	100.20	KAP5-10
58.45	0.02	26.39	0.48	0.02	0	8.28	6.45	0.38	100.47	KAP5-11
58.39	0	26.12	0.48	0.02	0	7.98	6.66	0.41	100.07	KAP5-12
58.56	0.02	26.06	0.45	0.02	0	8.05	6.64	0.37	100.17	KAP5-13
58.03	0.06	26.03	0.49	0.03	0.03	8.15	6.42	0.41	99.66	KAP5-14
58.74	0	26.37	0.44	0.03	0.01	8.17	5.96	0.37	100.08	KAP5-15
58.07	0.01	26.64	0.67	0.02	0.01	8.42	5.88	0.41	100.13	KAP5-16
58.69	0.01	26.39	0.50	0.00	0	7.94	6.05	0.37	99.95	KAP5-17
58.58	0.04	26.27	0.55	0.01	0.04	8.11	6.10	0.43	100.11	KAP5-18
58.75	0.01	26.30	0.44	0.01	0	7.92	5.92	0.39	99.75	KAP5-19
58.36	0.04	26.54	0.47	0.02	0	8.03	6.05	0.40	99.90	KAP5-20
58.32	0.02	26.48	0.48	0.01	0	8.00	6.08	0.38	99.77	KAP5-21
59.08	0.01	26.29	0.49	0.01	0	7.77	6.27	0.45	100.36	KAP5-22
58.60	0.01	26.54	0.44	0.01	0	8.10	5.92	0.37	99.98	KAP5-23
59.81	0	26.57	0.59	0.03	0.03	8.29	6.38	0.38	102.08	KAP5-24

SiO_2	TiO_2	Al_2O_3	FeO	MnO	MgO	CaO	Na_2O	K_2O	Total	Sample
58.53	0	26.23	0.54	0.03	0.02	8.21	6.51	0.42	100.49	KAP5-25
57.03	0	26.93	0.66	0.02	0.03	9.06	6.09	0.38	100.20	KAP5-26
58.30	0	26.54	0.58	0.02	0.02	8.35	6.43	0.39	100.64	KAP5-27
58.32	0	26.41	0.54	0.03	0.02	7.99	6.42	0.40	100.13	KAP5-28
58.81	0	26.31	0.50	0.03	0.02	8.10	6.67	0.41	100.84	KAP5-29
56.63	0	27.39	0.68	0.03	0.05	9.62	5.78	0.29	100.47	KAP5-30
58.18	0	26.52	0.61	0.02	0.08	8.42	6.52	0.40	100.76	KAP5-31
58.40	0.01	26.41	0.50	0.02	0.01	8.22	6.38	0.37	100.33	Average
0.59	0.02	0.29	0.08	0.01	0.02	0.35	0.32	0.06		Std. Dev.
58.57	0.01	26.24	0.52	0	0	7.65	7.20	0.46	100.65	KAP4-1
58.29	0.01	26.39	0.44	0.01	0	7.82	7.21	0.22	100.37	KAP4-2
58.41	0.04	26.23	0.39	0	0	7.57	7.28	0.28	100.19	KAP4-3
58.20	0.01	26.26	0.42	0.01	0	7.82	7.15	0.26	100.12	KAP4-4
58.01	0.03	26.37	0.48	0.01	0.01	7.83	7.07	0.43	100.22	KAP4-5
58.25	0.02	26.23	0.44	0	0.01	7.87	6.93	0.38	100.14	KAP4-6
58.12	0.03	26.44	0.43	0	0	7.76	7.18	0.31	100.26	KAP4-7
58.29	0.01	26.48	0.44	0	0	7.87	7.07	0.22	100.39	KAP4-8
58.28	0.01	26.34	0.44	0	0	7.89	7.16	0.20	100.32	KAP4-9
58.16	0.01	26.38	0.40	0	0	8.03	7.19	0.19	100.37	KAP4-10
57.90	0.01	26.16	0.41	0.03	0.01	7.77	6.79	0.21	99.29	KAP4-11
58.33	0	26.34	0.51	0.03	0.01	7.49	6.97	0.43	100.10	KAP4-12
57.74	0.02	26.33	0.57	0.04	0.01	7.49	6.63	0.38	99.21	KAP4-13
58.68	0	26.05	0.58	0.02	0.02	7.28	7.09	0.44	100.15	KAP4-14
58.32	0	26.37	0.63	0.01	0.04	7.48	6.70	0.44	99.99	KAP4-15
58.55	0	26.23	0.43	0.03	0.01	7.52	6.83	0.35	99.94	KAP4-16
58.41	0	26.32	0.38	0.02	0.01	7.34	6.83	0.34	99.64	KAP4-17
58.60	0	26.21	0.43	0.02	0.02	7.39	7.04	0.40	100.10	KAP4-18
57.72	0	26.57	0.43	0.03	0.01	8.13	6.62	0.36	99.86	KAP4-19
58.49	0	26.16	0.48	0	0	7.49	6.84	0.40	99.86	KAP4-20
58.64	0	26.45	0.42	0.04	0	7.80	6.80	0.24	100.39	KAP4-21
58.64	0	25.94	0.41	0.02	0	7.61	6.77	0.28	99.66	KAP4-22
58.22	0.01	26.54	0.47	0.03	0	7.79	6.52	0.45	100.04	KAP4-23
58.03	0	26.05	0.40	0.02	0	7.81	6.75	0.28	99.34	KAP4-24
58.77	0	26.34	0.51	0	0	7.59	6.68	0.42	100.30	KAP4-25
58.48	0	26.31	0.54	0.01	0	7.43	7.08	0.48	100.34	KAP4-26
57.96	0.02	26.19	0.63	0	0.04	7.68	6.82	0.49	99.82	KAP4-27
58.86	0	25.71	0.53	0	0	7.06	7.06	0.51	99.73	KAP4-28
57.94	0.01	26.56	0.59	0	0	7.91	6.68	0.46	100.17	KAP4-29
58.36	0.02	25.99	0.71	0.02	0.12	7.61	6.72	0.45	100.01	KAP4-30
58.62	0	26.39	0.49	0.01	0	7.47	7.02	0.43	100.42	KAP4-31
58.56	0	26.44	0.54	0.01	0	7.48	6.95	0.42	100.39	KAP4-32
58.32	0.01	26.28	0.48	0.01	0.01	7.65	6.93	0.36	100.05	Average
0.29	0.01	0.19	0.08	0.01	0.02	0.23	0.21	0.10		Std. Dev.
58.15	0.01	26.39	0.50	0.01	n.a.	8.35	6.53	0.29	100.23	KAP19-1
58.26	0	26.21	0.44	0.02	n.a.	8.27	6.48	0.39	100.08	KAP19-2
58.22	0	26.45	0.52	0.01	n.a.	8.30	6.72	0.31	100.54	KAP19-3
57.98	0	26.25	0.53	0.01	n.a.	8.27	6.59	0.30	99.94	KAP19-4
59.53	0	25.49	0.54	0	n.a.	7.20	7.00	0.52	100.29	KAP19-5
57.97	0	26.48	0.50	0.02	n.a.	8.28	6.67	0.28	100.19	KAP19-6
58.11	0	26.42	0.51	0.01	n.a.	8.31	6.64	0.34	100.33	KAP19-7
58.18	0	26.43	0.51	0.02	n.a.	8.36	6.61	0.27	100.38	KAP19-8
58.54	0	26.54	0.43	0	n.a.	8.30	6.57	0.31	100.68	KAP19-9
58.43	0	26.40	0.48	0	n.a.	8.34	6.59	0.34	100.56	KAP19-10
58.29	0	26.60	0.48	0.01	n.a.	8.30	6.71	0.38	100.76	KAP19-11
58.10	0	26.40	0.57	0	n.a.	8.29	6.54	0.41	100.30	KAP19-12
58.33	0	26.38	0.45	0.03	n.a.	8.31	6.47	0.31	100.27	KAP19-13
58.13	0	26.27	0.55	0.02	n.a.	8.01	6.67	0.41	100.06	KAP19-14
57.78	0.04	26.23	0.50	0	n.a.	8.23	6.40	0.38	99.56	KAP19-15
58.24	0.01	25.98	0.46	0.01	n.a.	7.84	6.43	0.41	99.38	KAP19-16
58.15	0.04	26.20	0.50	0.02	n.a.	8.28	6.57	0.32	100.09	KAP19-17
58.55	0	26.62	0.46	0.02	n.a.	8.26	6.48	0.36	100.75	KAP19-18
58.27	0.01	26.32	0.50	0.01	n.d.	8.19	6.59	0.35	100.24	Average
0.37	0.01	0.26	0.04	0.01	n.d.	0.28	0.14	0.06		Std. Dev.
58.02	0.08	26.24	0.49	0.04	n.a.	8.15	6.58	0.32	99.91	KAP16-1
58.44	0	25.95	0.54	0	n.a.	7.86	6.65	0.35	99.79	KAP16-2

SiO_2	TiO_2	Al_2O_3	FeO	MnO	MgO	CaO	Na_2O	K_2O	Total	Sample
58.23	0	26.11	0.43	0.03	n.a.	7.92	6.68	0.28	99.68	KAP16-3
58.32	0	26.36	0.54	0.02	n.a.	8.14	6.52	0.31	100.21	KAP16-4
57.89	0	25.91	0.53	0	n.a.	8.16	6.55	0.30	99.34	KAP16-5
58.14	0	26.15	0.49	0	n.a.	8.18	6.85	0.31	100.12	KAP16-6
57.76	0	26.09	0.50	0.01	n.a.	8.33	6.54	0.34	99.57	KAP16-7
58.43	0.01	26.18	0.48	0	n.a.	8.23	6.65	0.28	100.25	KAP16-8
57.94	0.01	26.29	0.53	0.01	n.a.	8.21	6.35	0.33	99.67	KAP16-9
58.02	0.03	26.06	0.55	0.04	n.a.	8.16	6.44	0.37	99.66	KAP16-10
57.79	0	26.22	0.52	0.03	n.a.	8.37	6.55	0.36	99.83	KAP16-11
57.95	0.01	26.01	0.63	0.01	n.a.	8.20	6.47	0.38	99.64	KAP16-12
57.71	0	26.05	0.57	0.03	n.a.	8.10	6.57	0.29	99.32	KAP16-13
57.87	0	26.28	0.52	0.02	n.a.	8.28	6.53	0.27	99.77	KAP16-14
57.90	0	26.22	0.58	0.01	n.a.	8.50	6.35	0.33	99.88	KAP16-15
57.89	0	25.92	0.45	0.01	n.a.	8.40	6.55	0.28	99.51	KAP16-16
58.13	0	26.16	0.55	0	n.a.	8.39	6.24	0.34	99.82	KAP16-17
59.29	0	25.23	0.55	0.02	n.a.	7.33	6.80	0.47	99.68	KAP16-18
58.89	0.01	25.61	0.58	0.02	n.a.	7.64	6.70	0.37	99.81	KAP16-19
58.14	0.01	26.05	0.53	0.02	n.d.	8.13	6.56	0.33	99.76	Average
0.40	0.02	0.26	0.05	0.01	n.d.	0.28	0.15	0.05		Std. Dev.
57.20	0.03	26.50	0.75	0.04	n.a.	8.37	6.30	0.41	99.59	KAP18-1
57.57	0	26.18	0.54	0.01	n.a.	7.99	6.33	0.40	99.03	KAP18-2
57.81	0	26.22	0.51	0.02	n.a.	8.05	6.41	0.35	99.34	KAP18-3
57.37	0	26.45	0.69	0.02	n.a.	8.37	6.46	0.33	99.69	KAP18-4
57.80	0	26.09	0.46	0.02	n.a.	8.10	6.61	0.38	99.45	KAP18-5
57.51	0.02	26.33	0.63	0.01	n.a.	8.64	6.49	0.36	99.98	KAP18-6
57.65	0.02	26.09	0.53	0.04	n.a.	8.14	6.55	0.38	99.40	KAP18-7
57.88	0.06	26.17	0.60	0.01	n.a.	8.33	6.47	0.38	99.89	KAP18-8
57.62	0.00	25.86	0.48	0.02	n.a.	8.33	6.35	0.40	99.06	KAP18-9
57.40	0.04	25.62	0.77	0	n.a.	8.67	6.35	0.34	99.20	KAP18-10
57.92	0	25.82	0.49	0.04	n.a.	8.15	6.63	0.36	99.41	KAP18-11
57.77	0	25.99	0.43	0	n.a.	8.36	6.61	0.32	99.47	KAP18-12
57.08	0	26.23	0.70	0	n.a.	8.51	6.27	0.35	99.14	KAP18-13
57.90	0	26.05	0.67	0.02	n.a.	8.05	6.59	0.38	99.66	KAP18-14
58.01	0	26.29	0.57	0.01	n.a.	8.04	6.60	0.37	99.88	KAP18-15
56.51	0.01	26.44	0.66	0.03	n.a.	8.82	6.22	0.33	99.02	KAP18-16
57.56	0.01	26.14	0.59	0.02	n.d.	8.31	6.45	0.36	99.45	Average
0.39	0.02	0.24	0.11	0.01	n.d.	0.25	0.14	0.03		Std. Dev.
58.25	0.07	26.58	0.49	0	n.a.	8.42	6.85	0.22	100.88	KAP28-1
57.88	0	26.53	0.51	0.03	n.a.	8.51	6.71	0.17	100.34	KAP28-2
58.18	0	26.19	0.62	0.01	n.a.	8.13	6.87	0.31	100.30	KAP28-3
58.99	0	26.28	0.42	0.01	n.a.	7.94	7.13	0.18	100.94	KAP28-4
58.30	0	26.75	0.44	0	n.a.	8.33	6.85	0.22	100.88	KAP28-5
58.53	0	26.66	0.43	0.01	n.a.	8.32	6.89	0.23	101.05	KAP28-6
59.05	0	26.13	0.45	0.02	n.a.	7.91	6.98	0.27	100.81	KAP28-7
58.26	0	26.76	0.48	0.06	n.a.	8.45	6.83	0.21	101.04	KAP28-8
58.21	0	26.49	0.49	0.01	n.a.	8.44	6.86	0.25	100.73	KAP28-9
58.50	0.03	26.44	0.51	0	n.a.	8.34	6.82	0.19	100.82	KAP28-10
59.10	0	25.92	0.56	0	n.a.	7.64	7.22	0.23	100.67	KAP28-11
58.08	0	26.53	0.48	0.01	n.a.	8.30	6.99	0.16	100.54	KAP28-12
58.53	0	26.33	0.41	0.02	n.a.	8.30	6.65	0.15	100.39	KAP28-13
58.67	0.04	26.24	0.45	0	n.a.	7.90	6.89	0.29	100.47	KAP28-14
58.28	0	26.53	0.44	0	n.a.	8.17	6.65	0.27	100.34	KAP28-15
58.11	0	26.48	0.54	0.02	n.a.	8.27	6.74	0.30	100.45	KAP28-16
58.39	0.05	26.54	0.49	0.01	n.a.	8.20	6.70	0.22	100.59	KAP28-17
58.37	0	26.86	0.44	0	n.a.	8.25	6.92	0.13	100.96	KAP28-18
58.73	0	26.69	0.48	0	n.a.	8.30	6.93	0.19	101.30	KAP28-19
58.62	0	26.69	0.40	0	n.a.	8.24	6.71	0.18	100.86	KAP28-20
58.45	0.01	26.48	0.48	0.01	n.d.	8.22	6.86	0.22	100.72	Average
0.33	0.02	0.24	0.05	0.01	n.d.	0.22	0.15	0.05		Std. Dev.
58.04	0	26.20	0.49	0	n.a.	8.00	6.59	0.37	99.70	KAP29-1
58.21	0	26.29	0.44	0	n.a.	8.15	6.61	0.27	99.98	KAP29-2
57.93	0	26.16	0.47	0.02	n.a.	7.99	6.63	0.32	99.50	KAP29-3
58.12	0.02	26.41	0.49	0	n.a.	8.17	6.87	0.34	100.41	KAP29-4
59.14	0	26.20	0.49	0	n.a.	7.66	6.90	0.38	100.76	KAP29-5
58.37	0.03	26.06	0.44	0.03	n.a.	8.00	6.64	0.32	99.89	KAP29-6

SiO_2	TiO_2	Al_2O_3	FeO	MnO	MgO	CaO	Na_2O	K_2O	Total	Sample
58.97	0.01	25.74	0.59	0	n.a.	7.25	6.99	0.40	99.94	KAP29-7
57.63	0.04	26.18	0.51	0.02	n.a.	7.85	6.61	0.35	99.19	KAP29-8
57.78	0.01	26.35	0.47	0	n.a.	8.23	6.53	0.28	99.63	KAP29-9
57.81	0	25.99	0.49	0	n.a.	8.22	6.67	0.30	99.47	KAP29-10
58.56	0	25.37	0.50	0.01	n.a.	7.83	6.90	0.38	99.56	KAP29-11
57.73	0	26.37	0.47	0	n.a.	8.20	6.76	0.35	99.87	KAP29-12
57.68	0	26.04	0.49	0.04	n.a.	8.04	6.56	0.30	99.15	KAP29-13
58.02	0	25.84	0.48	0.01	n.a.	7.93	6.67	0.34	99.29	KAP29-14
57.93	0.03	25.93	0.48	0	n.a.	8.26	6.66	0.31	99.60	KAP29-15
57.08	0.05	24.39	1.31	0.02	n.a.	7.83	6.21	0.47	97.36	KAP29-16
58.07	0.05	25.51	0.56	0.03	n.a.	7.67	6.74	0.39	99.02	KAP29-17
57.71	0.04	26.06	0.52	0.02	n.a.	8.06	6.56	0.30	99.28	KAP29-18
58.04	0.02	25.95	0.54	0.01	n.d.	7.96	6.67	0.34	99.53	Average
0.49	0.02	0.48	0.20	0.01	n.d.	0.26	0.18	0.05		Std. Dev.
58.56	0.02	26.04	0.56	0.01	n.a.	8.21	6.41	0.39	100.19	KAP8-1
58.65	0.02	26.13	0.49	0	n.a.	8.23	6.62	0.37	100.51	KAP8-2
58.89	0	26.26	0.57	0.01	n.a.	8.03	6.59	0.35	100.71	KAP8-3
58.10	0.03	26.16	0.51	0.02	n.a.	8.30	6.48	0.40	99.99	KAP8-4
58.60	0.01	26.51	0.47	0.05	n.a.	8.21	6.67	0.34	100.86	KAP8-5
58.33	0	26.34	0.47	0.01	n.a.	8.29	6.60	0.38	100.41	KAP8-6
58.51	0	26.59	0.47	0.03	n.a.	8.32	6.54	0.36	100.81	KAP8-7
58.38	0.01	26.50	0.57	0	n.a.	8.17	6.63	0.36	100.61	KAP8-8
58.65	0	26.53	0.48	0.01	n.a.	7.88	6.58	0.37	100.50	KAP8-9
59.08	0	25.91	0.43	0	n.a.	7.43	7.06	0.37	100.28	KAP8-10
57.99	0	26.39	0.58	0.02	n.a.	8.20	6.52	0.33	100.03	KAP8-11
58.10	0	26.50	0.48	0.01	n.a.	8.05	6.68	0.33	100.16	KAP8-12
58.67	0	26.32	0.45	0	n.a.	7.77	6.91	0.38	100.48	KAP8-13
58.18	0.03	26.69	0.42	0.02	n.a.	8.10	6.66	0.35	100.45	KAP8-14
57.97	0.04	26.47	0.49	0.03	n.a.	8.14	6.53	0.29	99.95	KAP8-15
57.44	0.05	26.03	0.76	0.02	n.a.	8.01	6.56	0.40	99.27	KAP8-16
57.91	0	26.40	0.47	0.00	n.a.	8.05	6.63	0.37	99.82	KAP8-17
58.39	0.05	26.04	0.50	0.02	n.a.	7.67	7.00	0.43	100.09	KAP8-18
58.36	0.01	26.32	0.51	0.01	n.d.	8.06	6.65	0.36	100.28	Average
0.40	0.02	0.23	0.08	0.01	n.d.	0.24	0.17	0.03		Std. Dev.
56.31	0	26.54	0.44	0	0.03	8.30	6.47	0.44	98.51	KAP7-1
56.25	0.03	26.56	0.50	0	0.01	8.18	6.57	0.41	98.52	KAP7-2
57.76	0.00	25.57	0.55	0.01	0.02	7.31	7.20	0.45	98.87	KAP7-3
57.62	0.01	25.94	0.48	0	0.01	7.38	6.98	0.48	98.90	KAP7-4
56.38	0	26.57	0.42	0.01	0.03	8.17	6.77	0.40	98.74	KAP7-5
57.07	0	26.65	0.40	0	0.01	8.48	6.75	0.25	99.61	KAP7-6
57.42	0	26.78	0.37	0	0.02	8.17	6.93	0.38	100.07	KAP7-7
56.97	0	26.87	0.44	0.03	0.01	8.29	6.85	0.35	99.81	KAP7-8
59.31	0.08	23.60	0.82	0.02	0.30	6.20	7.31	0.68	98.29	KAP7-9
56.21	0	26.48	0.46	0.02	0.03	8.03	6.83	0.37	98.45	KAP7-10
56.47	0	26.74	0.43	0.04	0.01	8.22	6.87	0.28	99.05	KAP7-11
56.70	0	26.66	0.42	0.01	0.02	8.19	6.84	0.33	99.15	KAP7-12
56.10	0.03	26.54	0.41	0.01	0.02	8.19	6.88	0.32	98.50	KAP7-13
56.46	0	26.71	0.45	0.02	0.01	8.20	6.76	0.34	98.94	KAP7-14
56.28	0.01	26.54	0.49	0.03	0.01	8.17	6.72	0.44	98.69	KAP7-15
56.10	0.01	27.24	0.52	0.02	0.01	8.89	6.48	0.36	99.61	KAP7-16
56.74	0.01	26.66	0.55	0	0.06	8.36	6.75	0.38	99.51	KAP7-17
57.96	0	25.44	0.52	0.01	0.03	7.15	7.32	0.52	98.96	KAP7-18
57.25	0.01	26.67	0.47	0	0.04	8.16	6.75	0.38	99.71	KAP7-19
56.97	0	26.32	0.51	0.01	0.04	7.90	6.84	0.41	99.01	KAP7-20
56.73	0.08	26.23	0.74	0	0.17	7.91	6.89	0.43	99.17	KAP7-21
56.69	0	26.02	0.51	0.01	0.08	8.27	6.70	0.38	98.65	KAP7-22
56.60	0	26.72	0.45	0	0.03	8.09	6.70	0.44	99.02	KAP7-23
56.79	0.02	26.50	0.44	0.02	0.03	8.17	6.73	0.38	99.09	KAP7-24
56.95	0.02	26.21	0.53	0.01	0.11	8.08	6.76	0.36	99.01	KAP7-25
56.14	0.04	26.49	0.47	0	0	8.08	6.73	0.38	98.33	KAP7-26
56.38	0	26.42	0.51	0	0	8.29	6.63	0.37	98.60	KAP7-27
56.90	0.02	26.56	0.61	0	0.01	8.03	6.46	0.39	99.00	KAP7-28
57.42	0.03	26.63	0.56	0.02	0.04	7.99	6.69	0.37	99.74	KAP7-29
56.76	0.03	26.33	0.46	0.01	0.01	8.28	6.79	0.42	99.09	KAP7-30
56.78	0.02	26.49	0.49	0.01	0.01	8.02	6.84	0.38	99.03	KAP7-31
56.72	0.04	26.44	0.52	0	0.02	8.24	6.92	0.38	99.27	KAP7-32
56.54	0.03	26.46	0.53	0	0.01	8.21	6.82	0.36	98.96	KAP7-33

SiO_2	TiO_2	Al_2O_3	FeO	MnO	MgO	CaO	Na_2O	K_2O	Total	Sample
59.69	0.03	25.12	0.54	0.00	0.01	6.15	7.72	0.57	99.82	KAP7-34
56.92	0.02	26.34	0.50	0.01	0.04	7.99	6.83	0.40	99.05	Average
0.81	0.02	0.63	0.09	0.01	0.06	0.56	0.25	0.08		Std. Dev.
58.63	0.01	25.93	0.53	0	0.04	7.48	6.55	0.43	99.60	KAP9-1
58.22	0.02	25.93	0.67	0.02	0.04	7.62	6.65	0.43	99.61	KAP9-2
58.19	0.02	26.50	0.52	0	0.03	7.94	6.37	0.38	99.94	KAP9-3
57.64	0.05	26.49	0.71	0.01	0.05	8.04	6.21	0.40	99.59	KAP9-4
57.85	0.09	25.92	0.71	0.01	0.07	7.54	6.41	0.50	99.10	KAP9-5
57.78	0.00	26.22	0.55	0.01	0.03	7.85	6.55	0.44	99.42	KAP9-6
58.29	0.10	24.82	0.87	0.02	0.33	7.36	6.73	0.47	98.98	KAP9-7
57.92	0.04	26.27	0.53	0	0.03	7.97	6.56	0.39	99.72	KAP9-8
58.21	0.05	25.83	0.58	0	0.04	7.32	6.99	0.42	99.44	KAP9-9
57.93	0.02	26.11	0.58	0.02	0.03	7.74	6.64	0.42	99.48	KAP9-10
57.96	0.02	26.17	0.51	0	0.04	7.75	6.50	0.44	99.37	KAP9-11
58.40	0.02	25.75	0.56	0.01	0.02	7.30	6.64	0.43	99.13	KAP9-12
58.07	0.04	26.28	0.49	0	0.03	7.82	6.50	0.38	99.60	KAP9-13
58.15	0.02	26.23	0.47	0.01	0.04	7.63	6.72	0.39	99.66	KAP9-14
58.27	0.01	26.33	0.45	0.01	0.04	7.70	6.49	0.42	99.71	KAP9-15
58.09	0	26.24	0.46	0	0.04	7.67	6.60	0.40	99.50	KAP9-16
57.33	0	26.11	0.49	0	0.04	7.66	6.48	0.41	98.52	KAP9-17
57.14	0.01	26.04	0.53	0.01	0.04	7.71	6.44	0.36	98.27	KAP9-18
57.76	0.02	26.20	0.50	0	0.04	7.86	6.57	0.42	99.37	KAP9-19
57.84	0.02	26.30	0.57	0.02	0.04	7.76	6.71	0.44	99.69	KAP9-20
58.05	0.02	25.90	0.60	0.02	0.07	7.53	6.80	0.37	99.36	KAP9-21
58.22	0.01	26.49	0.51	0.01	0.05	7.69	6.76	0.43	100.17	KAP9-22
58.35	0	25.92	0.59	0.01	0.06	7.42	6.76	0.42	99.52	KAP9-23
58.24	0.03	26.20	0.59	0.02	0.04	7.77	6.78	0.39	100.05	KAP9-24
57.89	0.04	26.38	0.57	0.02	0.05	7.76	6.33	0.38	99.42	KAP9-25
57.07	0	26.97	0.77	0.01	0.06	8.78	6.08	0.40	100.14	KAP9-26
57.74	0	26.61	0.60	0	0.04	7.92	6.50	0.39	99.80	KAP9-27
57.88	0	26.15	0.56	0	0.04	7.56	6.47	0.37	99.03	KAP9-28
58.22	0	26.25	0.55	0.03	0.05	7.63	6.66	0.37	99.78	KAP9-29
57.72	0	26.16	0.59	0	0.03	7.78	6.42	0.42	99.13	KAP9-30
57.81	0	26.22	0.62	0	0.12	7.72	6.38	0.43	99.29	KAP9-31
58.13	0	26.46	0.51	0	0.04	7.72	6.65	0.36	99.88	KAP9-32
58.23	0	26.17	0.48	0	0.03	7.76	6.54	0.38	99.58	KAP9-33
58.19	0.01	26.35	0.49	0	0.03	7.62	6.84	0.37	99.89	KAP9-34
58.07	0.03	26.22	0.46	0	0.03	7.52	6.54	0.38	99.26	KAP9-35
57.79	0	26.40	0.51	0.02	0.05	7.72	6.42	0.36	99.26	KAP9-36
58.16	0.01	26.40	0.55	0	0.04	7.78	6.73	0.42	100.10	KAP9-37
58.39	0.00	26.11	0.50	0	0.05	7.37	6.85	0.44	99.70	KAP9-38
57.27	0.04	26.76	0.64	0	0.05	8.13	6.32	0.38	99.59	KAP9-39
59.97	0	24.88	0.58	0.03	0.04	6.29	7.54	0.56	99.89	KAP9-40
59.70	0.02	25.43	0.52	0	0.05	6.70	6.83	0.41	99.65	KAP9-41
58.07	0.02	26.15	0.56	0.01	0.05	7.66	6.60	0.41	99.52	Average
0.53	0.02	0.40	0.09	0.01	0.05	0.37	0.24	0.04		Std. Dev.
58.74	0.05	25.77	0.49	0.02	n.a.	7.69	6.56	0.39	99.69	KAP40-1
58.04	0	26.20	0.50	0.01	n.a.	8.03	6.64	0.35	99.77	KAP40-2
58.29	0	26.26	0.52	0.04	n.a.	8.12	6.43	0.37	100.03	KAP40-3
57.87	0	25.95	0.42	0.01	n.a.	8.07	6.62	0.38	99.30	KAP40-4
60.63	0.05	24.43	0.49	0.01	n.a.	6.24	7.60	0.51	99.96	KAP40-5
57.97	0.00	25.96	0.49	0.02	n.a.	8.09	6.61	0.37	99.51	KAP40-6
58.54	0.01	25.66	0.51	0	n.a.	7.72	7.03	0.37	99.82	KAP40-7
58.21	0	25.81	0.38	0.02	n.a.	8.21	6.61	0.33	99.57	KAP40-8
60.81	0	23.82	0.50	0.03	n.a.	5.92	7.81	0.51	99.41	KAP40-9
57.93	0.01	26.28	0.43	0	n.a.	8.12	6.80	0.34	99.89	KAP40-10
58.23	0.01	26.30	0.43	0.01	n.a.	8.01	6.71	0.26	99.95	KAP40-11
57.85	0.06	26.20	0.48	0	n.a.	7.96	6.67	0.35	99.59	KAP40-12
58.06	0	26.46	0.39	0.02	n.a.	8.01	6.74	0.30	99.96	KAP40-13
58.23	0	26.08	0.46	0.01	n.a.	7.69	6.69	0.38	99.53	KAP40-14
57.83	0.02	26.36	0.44	0.02	n.a.	8.05	6.76	0.36	99.84	KAP40-15
57.93	0.02	26.24	0.45	0	n.a.	8.07	6.45	0.35	99.52	KAP40-16
58.41	0	26.23	0.50	0.02	n.a.	7.87	6.50	0.40	99.93	KAP40-17
57.72	0	26.36	0.48	0.02	n.a.	8.05	6.56	0.34	99.54	KAP40-18
57.90	0	26.25	0.47	0.02	n.a.	8.02	6.69	0.34	99.66	KAP40-19
58.12	0.02	26.26	0.38	0	n.a.	7.84	6.65	0.39	99.65	KAP40-20

SiO_2	TiO_2	Al_2O_3	FeO	MnO	MgO	CaO	Na_2O	K_2O	Total	Sample
58.36	0.01	25.94	0.46	0.01	n.d.	7.79	6.76	0.37	99.71	Average
0.84	0.02	0.66	0.04	0.01	n.d.	0.60	0.35	0.06		Std. Dev.
58.70	0.01	26.37	0.51	0.01	n.a.	7.82	6.61	0.44	100.45	KAP44-1
58.37	0	26.38	0.50	0	n.a.	7.91	6.87	0.44	100.47	KAP44-2
58.04	0	26.44	0.49	0.01	n.a.	7.83	6.97	0.50	100.27	KAP44-3
58.30	0.02	27.05	0.51	0.02	n.a.	7.54	7.23	0.25	100.91	KAP44-4
58.79	0	26.49	0.43	0.03	n.a.	7.61	6.92	0.47	100.74	KAP44-5
57.97	0	26.59	0.48	0	n.a.	8.11	6.70	0.26	100.11	KAP44-6
58.21	0.05	26.69	0.43	0	n.a.	7.99	6.90	0.22	100.49	KAP44-7
58.16	0.03	26.58	0.49	0	n.a.	8.07	6.89	0.24	100.46	KAP44-8
58.54	0.02	26.42	0.48	0	n.a.	7.32	7.15	0.51	100.44	KAP44-9
57.96	0	26.76	0.47	0.01	n.a.	8.12	6.92	0.27	100.50	KAP44-10
58.29	0	26.44	0.54	0	n.a.	7.90	7.00	0.44	100.60	KAP44-11
57.90	0	26.82	0.50	0	n.a.	8.03	7.05	0.22	100.51	KAP44-12
57.85	0.01	26.87	0.43	0.02	n.a.	7.96	7.05	0.19	100.36	KAP44-13
58.55	0	26.79	0.49	0.01	n.a.	8.04	7.05	0.19	101.11	KAP44-14
58.05	0.05	26.81	0.41	0.01	n.a.	8.06	7.02	0.21	100.62	KAP44-15
58.16	0	26.82	0.37	0	n.a.	8.04	6.97	0.23	100.59	KAP44-16
58.08	0	26.61	0.45	0	n.a.	7.90	7.02	0.12	100.18	KAP44-17
57.95	0	26.90	0.45	0.01	n.a.	8.19	6.94	0.20	100.64	KAP44-18
58.22	0.01	26.66	0.47	0.01	n.d.	7.91	6.96	0.30	100.52	Average
0.28	0.02	0.20	0.04	0.01	n.d.	0.22	0.15	0.13		Std. Dev.
58.57	0.02	26.54	0.39	0.01	n.a.	8.27	6.77	0.32	100.89	KAP46-1
58.99	0.01	26.46	0.39	0.04	n.a.	8.02	6.90	0.43	101.24	KAP46-2
58.50	0.01	26.76	0.31	0.01	n.a.	8.20	6.89	0.22	100.91	KAP46-3
58.14	0.01	26.37	0.40	0.01	n.a.	8.10	6.84	0.25	100.12	KAP46-4
58.35	0	26.58	0.37	0.02	n.a.	8.01	6.89	0.24	100.45	KAP46-5
58.31	0	26.61	0.38	0.02	n.a.	8.23	6.79	0.34	100.66	KAP46-6
58.32	0	26.76	0.43	0	n.a.	8.20	6.65	0.48	100.84	KAP46-7
58.45	0.06	26.75	0.48	0	n.a.	8.22	6.85	0.29	101.10	KAP46-8
58.45	0.01	26.60	0.39	0.01	n.d.	8.16	6.82	0.32	100.78	Average
0.25	0.02	0.15	0.05	0.01	n.d.	0.10	0.08	0.09		Std. Dev.

Melt Compositions†

†SiO_2	TiO_2	Al_2O_3	FeO	MnO	MgO	CaO	† Na_2O	K_2O	Cl	Total*	Sample	Beam Diameter
61.83	0.35	16.56	4.68	0.11	0.72	1.93	3.60	2.28	0.16	92.22	3VG26-1	2µm
60.94	0.35	18.22	4.54	0.06	0.66	2.74	3.59	1.83	0.16	93.09	3VG26-2	2µm
62.03	0.40	16.55	4.80	0.09	0.73	1.81	3.23	2.06	0.13	91.83	3VG26-3	2µm
62.08	0.43	16.35	5.10	0.13	0.78	1.95	4.03	1.90	0.21	92.95	3VG26-4	2µm
62.00	0.51	16.90	4.72	0.09	0.85	2.08	3.13	1.90	0.16	92.33	3VG26-5	2µm
63.15	0.30	17.00	4.65	0.02	0.81	1.97	3.37	2.07	0.13	93.46	3VG26-6	2µm
0.70	0.08	0.68	0.19	0.04	0.07	0.33	0.32	0.16	0.03		Std. dev.	
59.86	0.73	16.82	5.07	0.12	1.43	4.41	5.04	2.55	0.11	96.15	3VG14-1	focussed
57.75	0.54	19.16	4.78	0.14	1.29	6.15	5.90	2.07	0.10	97.51	3VG14-2	focussed
59.46	0.75	18.49	4.82	0.12	1.25	5.30	5.21	2.24	0.08	97.66	3VG14-3	focussed
59.93	0.81	16.39	5.01	0.07	1.36	3.94	4.82	2.65	0.09	95.16	3VG14-4	focussed
58.08	0.65	14.40	5.42	0.14	3.07	7.11	4.28	2.14	0.10	95.62	3VG14-5	focussed
60.52	0.67	16.74	4.99	0.09	1.45	4.42	5.01	2.60	0.15	96.69	3VG14-6	focussed
1.11	0.09	1.68	0.23	0.03	0.71	1.21	0.53	0.25	0.02		Std. dev.	
69.17	0.18	13.91	1.99	0.03	0.31	3.33	2.03	2.08	0.08	93.11	3VG5-1	1µm
68.79	0.26	13.68	1.91	0.06	0.37	3.34	2.06	2.23	0.13	93.03	3VG5-2	1µm
73.91	0.16	12.79	1.89	0.08	0.25	3.03	2.22	1.98	0.11	96.43	3VG5-3	1µm
70.11	0.13	14.28	1.95	0.10	0.32	3.35	1.85	2.35	0.09	94.52	3VG5-4	1µm
2.34	0.05	0.64	0.04	0.03	0.05	0.16	0.15	0.16	0.02		Std. dev.	
64.86	0.22	16.00	2.74	0.00	0.35	4.21	5.17	1.34	0.10	94.98	3VG4-2	10µm
64.37	0.25	16.11	2.57	0.00	0.31	4.24	4.75	1.34	0.14	94.08	3VG4-3	10µm
64.60	0.28	16.83	2.51	0.03	0.33	3.80	5.12	1.99	0.14	95.63	3VG4-4	10µm
65.17	0.35	15.92	2.70	0.08	0.44	4.28	4.99	1.29	0.12	95.33	3VG4-5	10µm
64.81	0.27	16.02	2.64	0.05	0.27	4.18	5.05	1.25	0.13	94.67	3VG4-6	10µm
64.73	0.26	15.84	2.55	0.05	0.31	4.30	4.89	1.18	0.12	94.23	3VG4-7	10µm
64.89	0.30	15.83	2.63	0.07	0.33	4.18	4.86	1.21	0.10	94.39	3VG4-8	10µm
65.29	0.21	16.18	2.56	0.03	0.38	4.13	5.15	1.22	0.11	95.25	3VG4-9	10µm
0.29	0.05	0.32	0.08	0.03	0.05	0.16	0.15	0.26	0.02		Std. dev.	
57.60	0.60	21.28	4.07	0.04	0.44	6.25	4.53	1.86	0.07	96.75	3VG22-1	focussed
58.66	0.83	16.62	6.09	0.10	1.15	4.40	3.00	2.77	0.09	93.71	3VG22-2	focussed
58.00	0.82	17.09	5.58	0.04	0.56	3.99	3.04	2.97	0.12	92.21	3VG22-3	focussed
57.51	0.78	15.94	4.67	0.11	1.57	6.00	4.21	2.25	0.10	93.13	3VG22-4	focussed
0.52	0.10	2.41	0.90	0.04	0.52	1.13	0.79	0.50	0.02		Std. dev.	
60.63	0.16	18.39	2.34	0.05	0.24	0.60	5.32	4.38	0.09	92.21	3VG15-1	focussed
60.20	0.12	17.80	2.31	0.04	0.19	0.50	4.64	4.11	0.13	90.04	3VG15-2	focussed
60.38	0.15	18.25	2.67	0.06	0.23	0.59	3.44	3.68	0.16	89.62	3VG15-3	focussed
58.99	0.08	17.71	2.77	0.03	0.31	0.65	2.92	3.40	0.16	87.02	3VG15-4	focussed
0.73	0.04	0.33	0.23	0.02	0.05	0.06	1.10	0.44	0.04		Std. dev.	
64.99	0.23	16.09	2.62	0.00	0.34	3.46	3.97	2.28	0.06	96.03	3VG20-1	focussed
65.67	0.37	15.27	2.94	0.06	0.49	2.48	2.49	2.92	0.10	92.78	3VG20-2	focussed
65.45	0.30	15.83	2.80	0.05	0.30	2.18	2.98	2.84	0.13	92.86	3VG20-3	focussed
65.42	0.33	15.86	2.82	0.05	0.31	2.22	2.63	2.69	0.13	92.45	3VG20-4	focussed
65.63	0.30	15.84	3.21	0.05	0.35	2.14	2.86	2.96	0.13	93.47	3VG20-5	focussed
65.96	0.25	15.93	3.25	0.00	0.57	2.38	2.99	2.67	0.08	94.08	3VG20-6	focussed
65.58	0.35	15.70	3.03	0.10	0.57	2.24	3.08	2.77	0.12	93.53	3VG20-7	focussed
66.29	0.26	16.15	2.82	0.00	0.38	2.26	2.90	2.82	0.12	93.99	3VG20-8	focussed
0.38	0.05	0.85	0.22	0.04	0.11	0.43	0.44	0.21	0.03		Std. dev.	
62.15	0.78	16.70	4.36	0.12	0.76	2.89	3.90	2.72	0.08	94.46	3VG18-1	focussed
62.06	0.62	16.41	4.42	0.03	0.88	3.20	3.83	2.75	0.09	94.28	3VG18-2	focussed
61.90	0.65	16.64	4.50	0.05	0.82	3.09	3.76	2.84	0.11	94.36	3VG18-3	focussed
62.18	0.69	16.70	4.39	0.01	0.88	3.07	3.74	2.67	0.10	94.43	3VG18-4	focussed
62.33	0.70	16.74	4.34	0.00	1.00	3.20	3.99	2.80	0.08	95.18	3VG18-5	focussed
62.75	0.80	16.85	4.21	0.03	0.83	3.21	3.67	2.70	0.11	95.16	3VG18-6	focussed
62.10	0.83	16.68	4.26	0.05	0.89	3.21	3.95	2.74	0.09	94.80	3VG18-7	focussed
62.50	0.80	16.85	4.43	0.01	0.89	3.25	4.19	2.71	0.11	95.74	3VG18-8	focussed
61.80	0.71	16.45	4.29	0.00	0.95	3.17	3.56	2.83	0.12	93.88	3VG18-9	focussed
62.19	0.80	16.61	4.42	0.06	0.72	2.81	3.65	2.76	0.10	94.12	3VG18-10	focussed

†SiO_2	TiO_2	Al_2O_3	FeO	MnO	MgO	CaO	† Na_2O	K_2O	Cl	Total*	Sample	Beam Diameter
0.28	0.07	0.15	0.09	0.04	0.08	0.15	0.19	0.06	0.02		Std. dev.	
63.72	0.75	14.34	3.44	0.03	1.83	3.02	3.67	2.99	0.11	93.89	3VG8-1	5µm
68.66	0.23	14.50	1.46	0.02	0.28	3.46	3.63	1.33	0.16	93.72	3VG8-2	5µm
68.67	0.23	14.61	1.37	0.03	0.25	3.56	3.60	1.35	0.10	93.75	3VG8-3	5µm
68.36	0.26	14.20	1.35	0.02	0.27	3.60	3.50	1.42	0.07	93.05	3VG8-4	5µm
67.28	0.26	14.00	1.60	0.03	0.51	3.33	3.36	1.70	0.14	92.21	3VG8-5	5µm
67.86	0.27	14.21	1.54	0.03	0.44	3.41	3.44	1.54	0.13	92.86	3VG8-6	5µm
64.72	0.55	14.18	2.54	0.02	1.74	3.18	3.54	2.90	0.12	93.49	3VG8-7	5µm
66.89	0.22	17.03	1.36	0.07	0.30	2.68	4.41	2.60	0.12	95.68	3VG8-8	5µm
1.86	0.19	0.99	0.76	0.02	0.67	0.31	0.33	0.72	0.03		Std. dev.	
67.14	0.44	15.62	1.91	0.03	0.29	1.83	3.10	2.96	0.13	93.48	3VG7-1	focussed
66.63	0.44	15.69	2.02	0.04	0.37	1.74	3.24	3.10	0.16	93.43	3VG7-2	focussed
66.72	0.41	15.56	2.10	0.05	0.36	1.77	2.85	2.97	0.17	92.98	3VG7-3	focussed
66.19	0.39	15.30	1.98	0.06	0.59	1.80	3.01	3.07	0.13	92.51	3VG7-4	focussed
66.66	0.42	15.29	2.05	0.08	0.45	1.81	3.25	3.06	0.12	93.18	3VG7-5	focussed
67.55	0.41	16.64	1.89	0.03	0.32	2.27	4.04	2.74	0.15	96.04	3VG7-6	focussed
0.47	0.02	0.50	0.08	0.02	0.11	0.20	0.42	0.13	0.02		Std. dev.	
63.15	0.66	17.37	4.43	0.07	0.93	3.46	3.65	2.05	0.10	95.87	3VG9-1	focussed
63.25	0.73	17.35	4.36	0.06	0.78	3.34	3.73	2.09	0.03	95.73	3VG9-2	focussed
63.64	0.65	17.59	3.85	0.07	0.66	3.16	4.00	2.27	0.09	95.98	3VG9-3	focussed
63.71	0.74	17.11	4.19	0.09	0.81	3.30	3.70	2.11	0.11	95.87	3VG9-4	focussed
63.39	0.84	17.12	4.31	0.00	0.91	3.52	3.98	2.15	0.08	96.10	3VG9-5	focussed
63.55	0.76	17.56	4.23	0.03	0.66	3.11	3.62	2.12	0.06	95.71	3VG9-6	focussed
0.22	0.06	0.21	0.21	0.03	0.12	0.16	0.17	0.08	0.03		Std. dev.	
68.48	0.30	15.05	1.38	0.00	0.18	3.80	3.80	1.31	0.20	94.50	3VG34-1	5µm
68.00	0.31	15.05	1.41	0.02	0.18	3.76	3.89	1.35	0.06	94.02	3VG34-2	5µm
68.04	0.31	15.17	1.37	0.01	0.26	3.85	3.96	1.37	0.13	94.47	3VG34-3	5µm
67.37	0.30	15.16	1.38	0.00	0.31	3.83	3.90	1.31	0.14	93.70	3VG34-4	5µm
67.24	0.30	14.55	1.40	0.00	0.26	3.88	3.60	1.40	0.13	92.75	3VG34-5	5µm
67.57	0.31	14.96	1.57	0.07	0.28	3.76	3.76	1.40	0.17	93.85	3VG34-6	5µm
68.94	0.28	14.90	1.55	0.04	0.27	3.18	2.99	1.34	0.14	93.63	3VG34-7	5µm
68.75	0.25	14.93	1.54	0.03	0.32	3.19	2.83	1.50	0.16	93.50	3VG34-8	5µm
68.81	0.29	15.46	1.58	0.00	0.30	3.29	2.97	1.29	0.18	94.17	3VG34-9	5µm
69.22	0.30	15.26	1.33	0.02	0.27	3.21	3.02	1.30	0.18	94.11	3VG34-10	5µm
69.26	0.27	15.08	1.49	0.02	0.22	3.14	2.79	1.24	0.19	93.70	3VG34-11	5µm
0.73	0.02	0.23	0.09	0.02	0.05	0.32	0.48	0.07	0.04		Std. dev.	
67.78	0.38	15.80	1.80	0.05	0.30	1.62	3.48	2.95	0.16	94.31	3VG35-1	focussed
67.66	0.36	15.64	1.79	0.06	0.32	1.59	3.66	3.00	0.15	94.23	3VG35-2	focussed
67.53	0.43	15.60	1.76	0.02	0.37	1.73	3.45	2.92	0.13	93.95	3VG35-3	focussed
68.23	0.49	15.90	1.69	0.04	0.28	1.63	3.44	3.17	0.11	94.98	3VG35-4	focussed
66.22	0.42	14.78	2.31	0.02	1.48	3.95	3.46	2.77	0.10	95.51	3VG35-5	focussed
67.79	0.41	15.70	1.73	0.00	0.33	1.68	3.28	3.02	0.13	94.08	3VG35-6	focussed
0.69	0.04	0.40	0.23	0.02	0.48	0.94	0.12	0.13	0.02		Std. dev.	
67.54	0.41	15.50	2.20	0.04	0.33	3.01	3.07	1.67	0.12	93.89	3VG40-1	1µm
67.80	0.40	15.75	1.85	0.06	0.31	2.92	3.33	1.77	0.23	94.40	3VG40-2	1µm
67.75	0.42	15.52	2.03	0.00	0.25	2.97	3.39	1.56	0.19	94.08	3VG40-3	1µm
68.14	0.39	15.41	2.00	0.02	0.28	2.95	3.32	1.64	0.26	94.42	3VG40-4	1µm
68.07	0.36	15.47	1.93	0.00	0.28	2.86	3.45	1.66	0.18	94.28	3VG40-5	1µm
67.91	0.41	15.67	1.86	0.03	0.37	2.96	3.40	1.67	0.18	94.45	3VG40-6	1µm
67.85	0.41	15.36	1.69	0.00	0.35	2.96	3.48	1.76	0.18	94.04	3VG40-7	1µm
68.19	0.38	15.40	1.79	0.06	0.34	2.90	3.53	1.59	0.19	94.39	3VG40-8	1µm
67.92	0.44	15.63	2.08	0.03	0.41	2.82	3.28	1.70	0.19	94.50	3VG40-9	1µm
67.75	0.38	15.41	1.83	0.00	0.31	2.92	3.24	1.66	0.24	93.74	3VG40-10	1µm
0.20	0.02	0.13	0.15	0.03	0.05	0.06	0.13	0.07	0.04		Std. dev.	
65.22	0.67	16.19	3.18	0.00	0.61	2.64	3.13	1.57	0.12	93.34	3VG42-1	2µm
64.70	0.66	16.44	3.30	0.03	0.73	2.84	3.07	1.55	0.15	93.47	3VG42-2	2µm
64.76	0.52	16.19	3.47	0.07	0.78	2.72	2.89	1.56	0.14	93.09	3VG42-3	2µm
65.08	0.73	16.19	3.51	0.02	0.73	2.75	3.25	1.51	0.17	93.94	3VG42-4	2µm
64.66	0.67	16.12	3.46	0.04	0.70	2.81	3.04	1.53	0.17	93.20	3VG42-5	2µm
64.86	0.60	16.12	3.40	0.04	0.73	2.80	3.25	1.49	0.11	93.40	3VG42-6	2µm
64.53	0.52	16.31	3.59	0.00	0.74	2.88	2.98	1.51	0.14	93.20	3VG42-7	2µm

†SiO_2	TiO_2	Al_2O_3	FeO	MnO	MgO	CaO	† Na_2O	K_2O	Cl	Total*	Sample	Beam Diameter
65.09	0.63	16.33	3.31	0.04	0.57	2.59	3.08	1.58	0.21	93.43	3VG42-8	2µm
65.31	0.59	16.25	3.41	0.05	0.81	2.84	2.94	1.51	0.13	93.83	3VG42-9	2µm
65.05	0.66	16.19	3.55	0.00	0.81	2.79	2.95	1.57	0.16	93.73	3VG42-10	2µm
65.67	0.66	16.15	3.16	0.02	0.60	2.68	3.14	1.59	0.12	93.78	3VG42-11	2µm
65.78	0.60	16.55	3.19	0.05	0.53	2.56	3.16	1.58	0.17	94.17	3VG42-12	2µm
65.45	0.59	16.41	3.60	0.04	0.79	2.86	2.97	1.52	0.14	94.38	3VG42-13	2µm
65.58	0.62	16.34	3.41	0.00	0.73	2.60	2.92	1.50	0.19	93.89	3VG42-14	2µm
65.53	0.63	16.41	3.53	0.02	0.63	2.68	3.11	1.55	0.12	94.22	3VG42-15	2µm
64.96	0.67	16.36	3.40	0.00	0.67	2.65	2.95	1.51	0.18	93.35	3VG42-16	2µm
0.39	0.06	0.13	0.14	0.02	0.09	0.10	0.11	0.03	0.03		Std. dev.	
67.40	0.25	14.51	1.16	0.05	0.53	1.78	3.30	3.51	0.15	92.63	3VG31-1	focussed
67.12	0.27	14.56	1.16	0.03	0.20	1.01	3.36	3.43	0.12	91.25	3VG31-2	focussed
67.08	0.29	14.35	1.18	0.00	0.22	0.96	3.71	3.54	0.12	91.45	3VG31-3	focussed
67.34	0.33	14.59	1.15	0.03	0.24	0.99	3.58	3.55	0.14	91.93	3VG31-4	focussed
67.10	0.31	14.35	1.09	0.00	0.20	1.09	3.35	3.73	0.13	91.35	3VG31-5	focussed
67.93	0.27	14.45	1.13	0.05	0.21	1.06	3.38	3.70	0.09	92.26	3VG31-6	focussed
67.56	0.25	14.31	1.05	0.02	0.17	0.92	3.64	3.48	0.11	91.50	3VG31-7	focussed
67.58	0.26	14.44	1.07	0.00	0.24	1.05	3.50	3.57	0.12	91.83	3VG31-8	focussed
67.67	0.30	14.65	1.03	0.05	0.22	1.00	3.39	3.64	0.15	92.10	3VG31-9	focussed
67.45	0.26	14.29	1.02	0.00	0.19	1.04	3.68	3.56	0.10	91.59	3VG31-10	focussed
0.28	0.03	0.12	0.06	0.02	0.10	0.25	0.15	0.09	0.02		Std. dev.	
68.16	0.19	14.93	1.18	0.00	0.23	1.03	2.84	2.86	0.17	91.59	3VG44-1	2µm
68.68	0.21	14.53	1.16	0.04	0.26	1.01	2.55	2.79	0.23	91.45	3VG44-2	2µm
0.37	0.01	0.28	0.01	0.03	0.02	0.01	0.21	0.05	0.04		Std. dev.	
68.47	0.23	14.12	0.90	0.02	0.23	0.97	2.47	2.40	0.16	89.99	3VG44-3	3µm
67.53	0.26	13.94	1.11	0.00	0.25	1.12	2.37	2.46	0.19	89.25	3VG44-4	3µm
67.56	0.20	14.09	1.13	0.00	0.24	1.00	2.55	2.52	0.18	89.48	3VG44-5	3µm
68.06	0.20	14.37	1.06	0.01	0.22	0.99	2.54	2.37	0.23	90.05	3VG44-6	3µm
67.66	0.26	14.50	1.22	0.01	0.26	1.05	2.51	2.53	0.19	90.21	3VG44-7	3µm
68.33	0.16	14.36	1.22	0.00	0.24	1.01	2.50	2.56	0.21	90.57	3VG44-8	3µm
67.87	0.23	14.02	1.13	0.00	0.29	0.97	2.53	2.43	0.23	89.71	3VG44-9	3µm
67.45	0.25	14.06	1.18	0.00	0.24	1.09	2.41	2.40	0.18	89.25	3VG44-10	3µm
67.02	0.21	13.70	0.99	0.05	0.21	0.97	2.22	2.50	0.14	88.01	3VG44-11	3µm
0.46	0.04	0.25	0.11	0.02	0.03	0.06	0.11	0.07	0.03		Std. dev.	
67.94	0.36	14.95	1.25	0.07	0.25	1.24	3.50	3.50	0.15	93.19	3VG41-1	focussed
68.57	0.31	14.77	1.31	0.00	0.24	1.17	3.25	3.63	0.18	93.43	3VG41-2	focussed
67.96	0.26	14.58	1.28	0.00	0.23	1.21	3.74	3.63	0.15	93.04	3VG41-3	focussed
67.75	0.26	14.63	1.19	0.02	0.25	1.27	3.44	3.59	0.16	92.54	3VG41-4	focussed
67.71	0.28	14.80	1.35	0.00	0.22	1.29	3.74	3.58	0.18	93.14	3VG41-5	focussed
67.96	0.30	14.81	1.33	0.07	0.30	1.42	3.63	3.64	0.20	93.64	3VG41-6	focussed
67.50	0.28	14.64	1.27	0.02	0.20	1.25	3.52	3.65	0.15	92.49	3VG41-7	focussed
68.03	0.33	14.65	1.24	0.00	0.27	1.29	3.57	3.46	0.15	92.99	3VG41-8	focussed
68.07	0.36	14.57	1.39	0.00	0.28	1.27	3.76	3.67	0.15	93.52	3VG41-9	focussed
68.13	0.31	14.68	1.29	0.05	0.27	1.27	3.70	3.78	0.14	93.62	3VG41-10	focussed
67.96	0.33	14.95	1.39	0.02	0.26	1.21	3.61	3.73	0.16	93.61	3VG41-11	focussed
0.27	0.04	0.14	0.06	0.03	0.03	0.06	0.15	0.09	0.02		Std. dev.	
66.13	0.23	13.96	0.99	0.05	0.18	5.12	3.68	0.87	0.33	91.54	3VG38-1	8µm
66.33	0.22	13.89	1.00	0.03	0.22	4.93	3.59	0.86	0.34	91.39	3VG38-2	8µm
65.60	0.19	14.19	1.05	0.03	0.45	4.82	3.92	1.42	0.30	91.96	3VG38-3	8µm
65.89	0.17	14.00	0.99	0.04	0.18	4.97	3.85	0.88	0.34	91.31	3VG38-4	8µm
65.38	0.49	14.04	1.10	0.01	0.21	4.95	3.75	0.97	0.28	91.18	3VG38-5	8µm
66.38	0.17	14.28	0.97	0.00	0.19	5.02	3.77	0.95	0.36	92.08	3VG38-6	8µm
66.27	0.16	14.17	1.01	0.03	0.19	4.96	3.86	0.97	0.39	91.99	3VG38-7	8µm
66.46	0.30	14.22	1.07	0.01	0.11	4.94	3.52	0.93	0.29	91.84	3VG38-8	8µm
65.77	0.27	14.04	0.97	0.04	0.20	4.81	3.47	0.91	0.35	90.82	3VG38-9	8µm
65.12	0.19	13.95	0.99	0.03	0.20	4.97	3.47	0.99	0.38	90.30	3VG38-10	8µm
65.02	0.20	14.14	1.10	0.00	0.19	4.89	3.36	0.98	0.25	90.12	3VG38-11	8µm
65.17	0.14	14.05	0.81	0.00	0.18	5.07	3.09	0.92	0.29	90.31	3VG38-12	8µm
0.49	0.10	0.12	0.08	0.02	0.08	0.09	0.24	0.15	0.04		Std. dev.	
69.14	0.32	14.34	1.35	0.09	0.23	1.24	3.77	3.44	0.19	92.78	3VG45-1	focussed
69.34	0.35	14.14	1.26	0.04	0.28	1.25	3.96	3.73	0.24	93.18	3VG45-2	focussed
69.03	0.34	14.21	1.34	0.00	0.18	1.17	4.13	3.87	0.21	93.01	3VG45-3	focussed
68.58	0.32	14.02	1.35	0.01	0.25	1.20	4.36	3.62	0.18	92.35	3VG45-4	focussed

†SiO_2	TiO_2	Al_2O_3	FeO	MnO	MgO	CaO	† Na_2O	K_2O	Cl	Total*	Sample	Beam Diameter
68.22	0.33	14.14	1.19	0.01	0.18	1.15	3.94	3.58	0.21	91.56	3VG45-5	focussed
67.94	0.32	14.20	1.49	0.00	0.23	1.34	4.08	3.79	0.18	92.11	3VG45-6	focussed
68.28	0.36	14.28	1.29	0.03	0.28	1.25	4.16	3.73	0.18	92.32	3VG45-7	focussed
68.65	0.25	14.28	1.43	0.03	0.30	1.30	4.16	3.73	0.18	92.84	3VG45-8	focussed
0.49	0.03	0.10	0.10	0.03	0.04	0.08	0.18	0.13	0.02		Std. dev.	
69.51	0.55	14.55	1.52	0.01	0.25	2.62	3.24	1.29	0.13	93.66	3VG46-1	1μm
69.70	0.49	14.42	1.61	0.03	0.31	2.77	3.33	1.32	0.22	94.20	3VG46-2	2μm
69.49	0.41	14.75	1.52	0.04	0.32	3.05	3.68	1.36	0.18	94.82	3VG46-3	3μm
68.75	0.39	14.66	1.63	0.01	0.33	3.26	4.31	1.42	0.17	94.94	3VG46-4	5μm
67.67	0.44	14.60	1.54	0.01	0.28	3.38	4.88	1.47	0.07	94.34	3VG46-5	8μm
67.85	0.53	14.23	1.55	0.00	0.27	3.26	4.71	1.39	0.12	93.92	3VG46-6	10μm
67.39	0.43	14.44	1.62	0.06	0.28	3.22	4.99	1.44	0.21	94.07	3VG46-7	12μm
67.51	0.63	14.23	1.68	0.02	0.48	3.30	4.56	1.65	0.16	94.40	3VG46-8	15μm
56.79	0.25	21.96	4.78	0.09	0.46	2.62	7.57	1.71	0.04	96.27	KAP2-1	1μm
56.52	0.30	21.75	4.92	0.18	0.42	2.59	7.89	1.73	0.06	96.35	KAP2-2	1μm
56.75	0.22	22.08	4.75	0.16	0.34	2.58	7.28	1.54	0.06	95.75	KAP2-3	1μm
56.54	0.29	22.12	5.09	0.14	0.52	2.56	7.20	1.63	0.06	96.14	KAP2-4	1μm
56.53	0.25	22.12	5.31	0.10	0.45	2.44	7.60	1.47	0.14	96.40	KAP2-5	1μm
56.39	0.35	22.30	4.96	0.16	0.45	2.61	7.97	1.52	0.05	96.78	KAP2-6	1μm
0.15	0.05	0.19	0.21	0.04	0.06	0.07	0.31	0.11	0.04		Std. dev.	
60.60	0.89	16.59	4.70	0.10	1.51	2.71	3.33	4.24	0.13	94.89	KAP14-1	1μm
60.55	0.94	16.79	4.83	0.16	1.32	2.87	4.08	4.00	0.14	95.68	KAP14-2	1μm
60.90	0.87	16.61	5.21	0.17	1.62	2.59	3.27	4.58	0.14	95.96	KAP14-3	1μm
60.45	0.90	17.33	4.59	0.16	1.59	2.48	3.18	5.54	0.11	96.33	KAP14-4	1μm
60.47	0.81	16.62	5.13	0.12	1.59	2.75	3.20	4.53	0.11	95.33	KAP14-5	1μm
0.18	0.05	0.31	0.26	0.03	0.12	0.15	0.38	0.59	0.02		Std. dev.	
68.28	0.23	13.98	2.26	0.06	0.29	2.26	2.36	3.06	0.05	92.84	KAP5-1	focussed
68.35	0.17	13.73	2.03	0.04	0.34	2.21	2.15	2.89	0.03	91.94	KAP5-2	focussed
67.98	0.21	13.67	2.00	0.00	0.32	2.18	2.40	2.95	0.02	91.74	KAP5-3	focussed
68.31	0.19	13.65	2.16	0.00	0.29	2.16	2.47	3.00	0.02	92.25	KAP5-4	focussed
69.47	0.18	13.62	2.08	0.11	0.25	2.16	2.42	3.04	0.04	93.36	KAP5-5	focussed
69.07	0.20	13.60	1.81	0.07	0.29	2.15	2.74	3.00	0.01	92.95	KAP5-6	focussed
68.87	0.26	13.41	2.03	0.03	0.31	2.23	2.32	3.05	0.03	92.54	KAP5-7	focussed
67.27	0.19	12.84	1.82	0.05	0.27	2.09	2.78	2.89	0.06	90.27	KAP5-8	focussed
70.19	0.21	13.61	1.95	0.08	0.30	2.23	2.62	3.12	0.01	94.32	KAP5-9	focussed
70.28	0.21	13.82	1.80	0.04	0.32	2.27	2.56	3.00	0.03	94.32	KAP5-10	focussed
0.96	0.03	0.30	0.15	0.03	0.03	0.06	0.19	0.07	0.02		Std. dev.	
59.46	0.32	19.34	3.80	0.10	0.33	3.96	5.85	1.24	0.11	94.51	KAP4-1	1μm
59.68	0.31	19.57	3.57	0.09	0.30	4.05	5.97	1.21	0.06	94.81	KAP4-2	1μm
59.64	0.29	19.39	3.50	0.10	0.31	3.97	6.40	1.21	0.00	94.82	KAP4-3	1μm
59.32	0.31	19.58	3.61	0.06	0.31	4.08	6.40	1.26	0.07	95.00	KAP4-4	1μm
59.23	0.30	19.57	3.51	0.00	0.33	3.99	6.00	1.33	0.06	94.32	KAP4-5	1μm
0.20	0.01	0.12	0.12	0.04	0.01	0.05	0.26	0.05	0.04		Std. dev.	
58.28	0.25	19.52	3.52	0.07	0.32	4.39	7.11	1.39	0.01	94.86	KAP4-6	3μm
58.92	0.25	20.02	3.61	0.12	0.34	4.52	7.13	1.31	0.07	96.30	KAP4-7	3μm
0.45	0.00	0.35	0.06	0.04	0.01	0.09	0.01	0.05	0.04		Std. dev.	
58.77	0.86	17.40	6.61	0.14	0.74	5.04	2.31	1.74	0.06	93.66	KAP22-1	focussed
58.44	0.72	17.99	5.59	0.06	0.41	4.41	2.80	2.06	0.03	92.51	KAP22-2	focussed
56.12	0.93	16.84	7.71	0.19	1.19	5.21	2.75	1.82	0.03	92.79	KAP22-3	focussed
56.22	0.94	16.87	7.83	0.16	1.19	5.30	2.71	1.80	0.03	93.05	KAP22-4	focussed
56.38	0.96	17.16	7.60	0.15	1.12	5.09	2.37	1.83	0.03	92.69	KAP22-5	focussed
55.66	0.84	17.02	8.26	0.11	1.28	5.53	2.66	1.77	0.01	93.14	KAP22-6	focussed
57.86	0.94	18.34	6.70	0.15	0.88	5.58	3.56	1.52	0.07	95.40	KAP22-7	focussed
1.26	0.09	0.58	0.92	0.04	0.33	0.39	0.41	0.16	0.02		Std. dev.	
64.44	0.38	15.19	2.34	0.04	0.40	2.48	3.11	2.69	0.03	91.10	KAP15-1	focussed
63.49	0.37	14.98	1.98	0.00	0.29	2.45	3.04	2.60	0.05	89.23	KAP15-2	focussed
62.75	0.37	14.81	2.04	0.06	0.31	2.44	3.30	2.69	0.02	88.78	KAP15-3	focussed
62.65	0.33	14.87	2.17	0.01	0.39	2.48	3.27	2.64	0.05	88.86	KAP15-4	focussed
62.81	0.28	14.66	2.02	0.00	0.41	2.56	3.17	2.61	0.02	88.56	KAP15-5	focussed
62.89	0.31	14.72	2.15	0.00	0.38	2.60	3.00	2.70	0.02	88.77	KAP15-6	focussed

†SiO_2	TiO_2	Al_2O_3	FeO	MnO	MgO	CaO	† Na_2O	K_2O	Cl	Total*	Sample	Beam Diameter
64.47	0.28	14.81	2.04	0.08	0.48	2.57	3.12	2.63	0.02	90.48	KAP15-7	focused
65.22	0.32	15.67	1.88	0.00	0.40	2.48	3.14	2.80	0.06	91.76	KAP15-8	focused
65.14	0.38	15.45	2.10	0.05	0.33	2.50	2.87	2.58	0.05	91.46	KAP15-9	focused
64.93	0.35	15.38	2.02	0.05	0.40	2.51	2.89	2.62	0.05	91.20	KAP15-10	focused
1.07	0.04	0.34	0.13	0.03	0.05	0.05	0.14	0.04	0.02		Std. dev.	
65.03	0.48	15.65	3.14	0.04	0.61	3.12	1.70	1.99	0.05	91.81	KAP20-1	focused
64.13	0.47	15.29	2.90	-0.00	0.43	2.67	2.32	2.15	0.04	90.40	KAP20-2	focused
64.45	0.44	15.69	3.31	0.11	0.52	3.07	2.58	2.27	0.06	92.49	KAP20-3	focused
64.63	0.43	15.73	3.01	0.00	0.38	2.57	2.02	2.32	0.06	91.14	KAP20-4	focused
64.14	0.41	15.67	2.99	0.05	0.61	3.14	2.80	2.38	0.06	92.25	KAP20-5	focused
63.17	0.45	15.75	3.06	0.03	0.48	2.92	2.27	2.15	0.05	90.32	KAP20-6	focused
0.63	0.02	0.17	0.14	0.04	0.09	0.24	0.39	0.14	0.01		Std. dev.	
60.92	0.57	16.97	5.39	0.10	0.61	2.72	3.88	2.40	0.10	93.67	KAP18-1	focused
61.20	0.67	17.88	4.73	0.11	0.47	2.36	4.13	2.57	0.10	94.21	KAP18-2	focused
60.70	0.72	17.37	5.40	0.09	0.82	2.45	4.28	2.98	0.00	94.82	KAP18-3	focused
61.73	0.67	17.86	4.99	0.07	0.54	2.44	4.46	2.47	0.07	95.30	KAP18-4	focused
60.82	0.63	17.28	5.40	0.07	0.80	2.15	4.89	3.10	0.08	95.20	KAP18-5	focused
60.52	0.64	17.62	5.60	0.17	1.00	1.99	4.16	3.24	0.04	94.98	KAP18-6	focused
61.17	0.58	17.54	5.29	0.08	0.65	2.38	4.54	2.79	0.03	95.05	KAP18-7	focused
61.03	0.60	17.50	5.31	0.09	0.78	2.28	4.22	2.89	0.00	94.79	KAP18-8	focused
0.37	0.05	0.30	0.27	0.03	0.17	0.22	0.31	0.30	0.04		Std. dev.	
65.04	0.29	14.92	1.73	0.03	0.25	1.70	3.31	3.34	0.06	90.67	KAP8-1	focused
63.68	0.50	15.01	2.11	0.04	0.83	2.45	3.18	3.15	0.07	91.03	KAP8-2	focused
59.65	1.08	14.42	5.11	0.08	2.57	4.92	3.45	2.75	0.06	94.09	KAP8-3	focused
65.16	0.33	15.46	1.62	0.07	0.25	1.66	3.27	3.32	0.08	91.22	KAP8-4	focused
2.58	0.37	0.43	1.66	0.02	1.10	1.54	0.11	0.27	0.01		Std. dev.	
58.19	0.93	17.63	5.15	0.02	0.63	2.75	4.39	2.71	0.06	92.45	KAP9-1	focused
57.99	1.17	17.12	5.39	0.01	0.83	3.51	4.64	2.24	0.09	92.99	KAP9-2	focused
57.63	1.08	16.90	5.71	0.14	0.95	3.77	3.91	2.04	0.04	92.27	KAP9-3	focused
57.31	1.14	16.94	5.74	0.00	0.85	3.38	4.47	2.34	0.07	92.25	KAP9-4	focused
58.22	1.01	17.12	5.38	0.01	0.75	3.32	4.48	2.43	0.06	92.76	KAP9-5	focused
59.16	1.22	17.52	5.05	0.03	0.50	2.98	4.72	2.70	0.05	93.92	KAP9-6	focused
59.32	1.04	17.41	5.76	0.03	0.82	3.28	4.84	2.40	0.03	94.94	KAP9-7	focused
59.05	1.14	17.63	5.48	0.04	0.66	3.16	4.69	2.57	0.05	94.47	KAP9-8	focused
58.50	1.09	17.31	5.41	0.07	0.76	3.28	4.95	2.61	0.07	94.05	KAP9-9	focused
58.90	1.05	17.74	5.18	0.09	0.57	2.69	4.62	2.85	0.06	93.84	KAP9-10	focused
0.68	0.08	0.29	0.25	0.04	0.14	0.33	0.29	0.25	0.02		Std. dev.	
69.26	0.23	15.03	1.38	0.07	0.20	2.98	2.95	1.51	0.11	93.72	KAP34-1	1μm
68.40	0.24	14.78	1.48	0.00	0.29	2.79	2.55	1.72	0.11	92.36	KAP34-2	1μm
66.82	0.39	14.36	1.94	0.00	0.95	2.62	2.69	3.92	0.07	93.76	KAP34-3	1μm
68.79	0.31	14.88	1.44	0.04	0.29	2.98	2.86	1.69	0.06	93.12	KAP34-4	1μm
68.69	0.29	14.66	1.47	0.07	0.20	2.86	2.61	1.47	0.05	92.37	KAP34-5	1μm
68.75	0.28	14.75	1.37	0.02	0.16	3.06	2.77	1.36	0.08	92.61	KAP34-6	1μm
69.25	0.21	14.78	1.37	0.04	0.18	2.97	2.70	1.47	0.09	93.06	KAP34-7	1μm
68.76	0.26	14.32	1.26	0.04	0.19	2.99	2.80	1.39	0.11	92.11	KAP34-8	1μm
68.40	0.25	14.22	1.21	0.03	0.21	3.02	2.99	1.40	0.13	91.85	KAP34-9	1μm
0.72	0.05	0.28	0.21	0.02	0.25	0.14	0.15	0.82	0.03		Std. dev.	
67.73	0.41	15.64	1.78	0.06	0.26	2.79	3.08	1.56	0.04	93.35	KAP35-1	1μm
68.05	0.40	15.24	1.86	0.04	0.25	2.67	3.17	1.71	0.08	93.47	KAP35-2	1μm
66.64	0.47	14.79	2.13	0.06	0.90	2.50	3.19	3.37	0.14	94.20	KAP35-3	1μm
66.72	0.48	15.92	2.96	0.08	0.71	2.47	3.11	2.54	0.09	95.07	KAP35-4	1μm
67.76	0.38	15.13	1.94	0.00	0.29	2.50	3.19	2.11	0.08	93.47	KAP35-5	1μm
68.35	0.39	15.56	1.86	0.04	0.24	2.80	3.31	1.54	0.04	94.13	KAP35-6	1μm
0.70	0.04	0.40	0.44	0.03	0.29	0.14	0.08	0.71	0.04		Std. dev.	
64.38	0.49	16.22	1.98	0.00	0.41	2.98	4.88	2.27	0.06	93.47	KAP40-1	5μm
64.19	0.54	16.51	2.13	0.01	0.46	2.93	5.08	2.27	0.05	94.18	KAP40-2	5μm
64.64	0.45	16.05	1.96	0.01	0.34	2.96	4.82	2.31	0.11	93.64	KAP40-3	5μm
64.57	0.51	16.03	1.82	0.05	0.34	3.01	5.00	2.29	0.04	93.65	KAP40-4	5μm
65.96	0.40	16.01	1.63	0.01	0.22	2.51	3.46	1.86	0.03	92.08	KAP40-5	1μm
66.05	0.56	16.16	1.91	0.07	0.25	2.46	2.83	1.91	0.07	92.27	KAP40-6	1μm

†SiO$_2$	TiO$_2$	Al$_2$O$_3$	FeO	MnO	MgO	CaO	† Na$_2$O	K$_2$O	Cl	Total*	Sample	Beam Diameter
66.63	0.38	15.90	2.05	0.05	0.29	2.55	2.72	1.84	0.10	92.51	KAP40-7	1µm
67.34	0.48	15.46	1.89	0.00	0.23	2.67	3.07	1.73	0.13	93.00	KAP40-8	1µm
67.84	0.38	15.17	1.85	0.00	0.21	2.54	3.16	1.56	0.14	92.85	KAP40-9	1µm
68.37	0.43	15.59	1.72	0.00	0.23	2.56	3.29	1.63	0.10	93.91	KAP40-10	1µm
67.00	0.37	15.61	1.67	0.00	0.27	3.08	4.49	1.82	0.07	94.37	KAP40-11	5µm
66.50	0.35	15.60	1.77	0.00	0.26	2.97	4.14	1.85	0.09	93.53	KAP40-12	5µm
63.10	0.42	13.91	2.50	0.04	1.57	2.21	3.23	4.94	0.07	91.99	KAP40-13	2µm
65.24	0.41	14.47	2.48	0.01	1.51	2.35	3.48	5.34	0.08	95.38	KAP40-14	2µm
66.36	0.35	15.26	1.71	0.04	0.42	2.65	2.85	2.11	0.11	91.85	KAP40-15	2µm
66.49	0.34	15.71	1.69	0.01	0.26	2.90	3.22	1.96	0.11	92.70	KAP40-16	2µm
1.45	0.07	0.67	0.26	0.02	0.43	0.27	0.84	1.11	0.03		Std. dev.	
64.28	1.04	17.06	4.72	0.08	0.67	2.30	4.26	3.29	0.05	97.75	KAP42-1	1µm
63.96	1.04	17.44	4.42	0.03	0.48	2.35	4.04	2.76	0.04	96.55	KAP42-2	1µm
64.51	0.97	17.46	4.26	0.00	0.52	2.39	4.19	2.76	0.07	97.13	KAP42-3	1µm
63.67	0.95	16.96	4.28	0.08	0.59	2.33	3.97	2.70	0.15	95.66	KAP42-4	1µm
63.49	1.02	17.32	4.56	0.05	0.60	2.38	4.06	3.08	0.10	96.69	KAP42-5	1µm
63.42	0.96	17.19	4.33	0.09	0.54	2.46	4.08	2.79	0.06	95.92	KAP42-6	1µm
63.61	0.85	17.48	4.12	0.03	0.51	2.36	4.61	2.77	0.05	96.40	KAP42-7	1µm
63.77	1.05	16.96	4.45	0.09	0.47	2.31	4.07	2.70	0.09	95.96	KAP42-8	1µm
62.76	0.92	16.01	4.40	0.11	1.27	2.01	4.23	5.70	0.02	97.43	KAP42-9	1µm
0.51	0.07	0.46	0.18	0.04	0.25	0.13	0.19	0.97	0.04		Std. dev.	
68.00	0.15	14.68	0.86	0.02	0.13	3.52	2.22	1.09	0.18	90.85	KAP36-1	1µm
68.36	0.16	14.79	0.86	0.00	0.11	3.50	2.69	1.17	0.09	91.74	KAP36-2	1µm
68.54	0.19	14.72	0.91	0.05	0.16	3.48	2.42	1.17	0.12	91.76	KAP36-3	1µm
68.26	0.17	14.51	0.91	0.01	0.17	3.57	2.30	1.17	0.12	91.18	KAP36-4	1µm
68.11	0.15	14.45	0.90	0.03	0.13	3.56	2.52	1.18	0.14	91.18	KAP36-5	1µm
68.00	0.17	14.29	1.02	0.03	0.24	3.43	2.48	1.36	0.12	91.16	KAP36-6	1µm
67.93	0.20	14.64	0.94	0.02	0.15	3.63	2.62	1.10	0.13	91.36	KAP36-7	1µm
0.23	0.02	0.17	0.06	0.02	0.04	0.07	0.17	0.10	0.03		Std. dev.	
67.38	0.31	15.21	1.24	0.03	0.17	2.77	2.77	1.22	0.04	91.15	KAP31-1	1µm
67.41	0.31	15.25	1.25	0.00	0.15	2.79	2.98	1.31	0.10	91.56	KAP31-2	1µm
68.02	0.30	15.48	1.18	0.07	0.14	2.82	3.05	0.93	0.06	92.05	KAP31-3	1µm
67.57	0.25	15.03	1.16	0.00	0.18	2.63	3.07	1.32	0.04	91.25	KAP31-4	1µm
67.40	0.31	15.18	1.31	0.01	0.16	2.79	3.18	1.24	0.08	91.67	KAP31-5	1µm
67.61	0.26	14.97	1.24	0.08	0.14	2.84	3.07	1.15	0.06	91.41	KAP31-6	1µm
67.15	0.38	14.97	1.17	0.00	0.19	2.88	3.30	1.28	0.10	91.42	KAP31-7	1µm
67.30	0.31	15.02	1.17	0.04	0.17	2.73	3.11	1.14	0.08	91.05	KAP31-8	1µm
67.74	0.29	15.35	1.16	0.00	0.14	2.51	3.72	1.35	0.09	92.34	KAP31-9	1µm
68.17	0.28	15.01	1.27	0.07	0.25	2.73	2.45	1.46	0.06	91.75	KAP31-10	1µm
0.32	0.04	0.18	0.05	0.03	0.03	0.11	0.33	0.14	0.02		Std. dev.	
68.86	0.22	14.93	1.16	0.06	0.19	3.22	1.67	1.63	0.10	92.04	KAP44-1	1µm
68.99	0.22	14.83	0.97	0.00	0.11	3.25	2.81	1.41	0.15	92.74	KAP44-2	1µm
68.77	0.23	14.92	1.07	0.04	0.31	3.20	2.50	1.97	0.07	93.06	KAP44-3	1µm
69.12	0.27	14.86	1.04	0.06	0.24	3.14	2.75	1.77	0.08	93.33	KAP44-4	1µm
69.75	0.26	15.10	1.14	0.00	0.14	3.30	2.68	1.32	0.04	93.73	KAP44-5	1µm
68.65	0.27	14.56	1.00	0.01	0.16	3.33	2.64	1.34	0.08	92.04	KAP44-6	1µm
69.47	0.22	14.97	1.06	0.00	0.12	3.22	2.41	1.36	0.16	92.99	KAP44-7	1µm
0.40	0.02	0.17	0.07	0.03	0.07	0.06	0.39	0.25	0.04		Std. dev.	
68.94	0.36	15.13	1.51	0.03	0.17	2.67	2.82	1.52	0.03	93.17	KAP41-1	1µm
69.07	0.35	14.79	1.48	0.00	0.19	2.54	3.01	1.69	0.06	93.17	KAP41-2	1µm
69.15	0.37	14.79	1.48	0.00	0.25	2.67	2.91	1.53	0.06	93.22	KAP41-3	1µm
68.71	0.33	14.61	1.46	0.02	0.14	2.70	3.08	1.65	0.08	92.78	KAP41-4	1µm
67.22	0.41	14.26	1.49	0.08	0.22	2.62	3.20	1.81	0.05	91.15	KAP41-5	1µm
69.22	0.24	14.82	1.40	0.00	0.21	2.83	3.34	1.58	0.09	93.71	KAP41-6	1µm
68.36	0.30	14.81	1.47	0.02	0.16	2.68	3.42	1.55	0.08	92.85	KAP41-7	1µm
69.70	0.31	15.58	1.34	0.00	0.19	2.70	3.00	1.58	0.14	94.54	KAP41-8	1µm
69.42	0.42	15.22	1.30	0.05	0.20	2.72	3.26	1.59	0.04	94.31	KAP41-9	1µm
69.40	0.41	15.22	1.34	0.01	0.14	2.68	3.38	1.64	0.10	94.33	KAP41-10	1µm
0.71	0.06	0.37	0.06	0.03	0.04	0.07	0.21	0.06	0.03		Std. dev.	
66.29	0.13	14.00	0.82	0.00	0.12	2.58	2.63	1.20	0.29	88.06	KAP43-1	focussed
65.93	0.10	14.05	1.00	0.00	0.35	2.47	2.66	1.76	0.18	88.50	KAP43-2	focussed
66.45	0.09	13.91	0.97	0.02	0.25	2.63	2.07	1.52	0.20	88.11	KAP43-3	focussed

†SiO_2	TiO_2	Al_2O_3	FeO	MnO	MgO	CaO	† Na_2O	K_2O	Cl	Total*	Sample	Beam Diameter
66.77	0.14	13.79	0.90	0.00	0.22	2.68	1.87	1.54	0.24	88.15	KAP43-4	focussed
67.44	0.10	14.15	0.85	0.00	0.12	2.52	1.65	1.27	0.14	88.24	KAP43-5	focussed
0.57	0.02	0.14	0.08	0.01	0.10	0.08	0.45	0.23	0.06		Std. dev.	
66.60	0.21	14.64	0.93	0.00	0.10	1.27	2.99	4.09	0.11	90.94	KAP38-1	focussed
67.36	0.21	14.73	0.90	0.00	0.16	1.18	3.01	4.00	0.10	91.65	KAP38-2	focussed
66.92	0.17	14.82	0.98	0.03	0.13	1.22	3.01	3.83	0.08	91.19	KAP38-3	focussed
67.28	0.26	14.77	0.91	0.00	0.16	1.18	3.17	3.76	0.09	91.57	KAP38-4	focussed
67.24	0.26	14.71	0.96	0.03	0.12	1.29	3.02	3.93	0.09	91.65	KAP38-5	focussed
67.12	0.24	14.79	1.00	0.01	0.13	1.30	3.09	3.87	0.08	91.63	KAP38-6	focussed
66.61	0.28	14.31	0.99	0.02	0.13	1.28	3.12	4.00	0.12	90.85	KAP38-7	focussed
66.68	0.26	14.23	0.88	0.04	0.21	1.38	3.07	3.86	0.11	90.72	KAP38-8	focussed
66.46	0.26	14.39	0.96	0.00	0.16	1.23	3.12	3.88	0.10	90.55	KAP38-9	focussed
64.45	0.33	14.06	1.39	0.02	1.14	3.69	3.59	3.23	0.09	91.99	KAP38-10	focussed
0.84	0.04	0.27	0.15	0.02	0.32	0.77	0.18	0.24	0.01		Std. dev.	
69.20	0.33	14.85	1.25	0.00	0.12	3.06	2.27	1.39	0.05	92.52	KAP45-1	1µm
69.04	0.34	14.56	1.33	0.04	0.13	3.01	2.63	1.38	0.06	92.53	KAP45-2	1µm
69.76	0.28	14.25	1.40	0.00	0.12	3.13	2.77	1.40	0.08	93.18	KAP45-3	1µm
69.80	0.25	15.03	1.28	0.01	0.18	3.09	2.83	1.43	0.07	93.97	KAP45-4	1µm
69.30	0.31	14.80	1.22	0.00	0.19	3.00	3.04	1.53	0.11	93.51	KAP45-5	1µm
68.88	0.37	14.62	1.22	0.05	0.17	3.16	2.67	1.47	0.10	92.72	KAP45-6	1µm
69.07	0.32	14.42	1.22	0.03	0.18	3.11	2.85	1.41	0.09	92.70	KAP45-7	1µm
69.28	0.33	14.70	1.17	0.04	0.13	2.97	2.32	1.36	0.08	92.37	KAP45-8	1µm
69.79	0.29	14.40	1.33	0.00	0.21	3.03	2.53	1.47	0.05	93.10	KAP45-9	1µm
0.35	0.04	0.25	0.07	0.02	0.03	0.06	0.25	0.05	0.02		Std. dev.	
67.84	0.48	14.95	1.54	0.01	0.25	3.23	4.78	1.69	0.12	94.88	KAP46-1	8µm
68.17	0.41	14.61	1.36	0.00	0.27	3.37	3.67	1.73	0.08	93.66	KAP46-2	8µm
68.38	0.46	14.70	1.47	0.00	0.28	3.24	3.14	1.71	0.09	93.46	KAP46-3	8µm
67.90	0.47	14.72	1.55	0.02	0.23	3.30	5.06	1.71	0.04	95.00	KAP46-4	8µm
68.23	0.48	14.79	1.68	0.06	0.25	3.07	5.00	1.78	0.06	95.40	KAP46-5	8µm
68.35	0.43	14.81	1.46	0.05	0.28	3.19	4.93	1.73	0.04	95.27	KAP46-6	8µm
0.23	0.03	0.12	0.11	0.03	0.02	0.10	0.82	0.03	0.03		Std. dev.	
68.44	0.50	14.75	1.57	0.04	0.24	3.26	4.54	1.70	0.07	95.10	KAP46-7	5µm
69.17	0.52	14.88	1.50	0.04	0.18	3.22	4.70	1.73	0.08	96.02	KAP46-8	5µm
66.55	0.49	14.54	1.99	0.04	1.17	2.79	4.92	4.14	0.09	96.72	KAP46-9	5µm
69.03	0.41	14.92	1.58	0.00	0.24	3.26	5.01	1.78	0.06	96.29	KAP46-10	5µm
1.21	0.05	0.17	0.22	0.02	0.48	0.23	0.21	1.20	0.01		Std. dev.	
69.86	0.45	15.12	1.59	0.03	0.22	2.93	3.79	1.81	0.04	95.84	KAP46-11	2µm
69.94	0.43	14.93	1.54	0.00	0.23	2.98	3.48	1.63	0.00	95.16	KAP46-12	2µm
70.08	0.55	15.16	1.49	0.05	0.26	3.04	3.62	1.68	0.08	96.01	KAP46-13	2µm
69.46	0.39	15.14	1.45	0.04	0.17	2.99	3.88	1.57	0.06	95.15	KAP46-14	2µm
0.27	0.07	0.11	0.06	0.02	0.04	0.05	0.18	0.10	0.04		Std. dev.	
69.82	0.49	15.08	1.59	0.00	0.22	2.76	3.39	1.55	0.12	95.01	KAP46-15	1µm
69.36	0.41	15.06	1.55	0.02	0.19	2.86	3.61	1.64	0.12	94.82	KAP46-16	1µm
70.08	0.51	15.23	1.54	0.00	0.23	2.82	3.85	1.63	0.05	95.94	KAP46-17	1µm
69.86	0.49	14.89	1.68	0.00	0.23	2.73	3.41	1.61	0.09	94.98	KAP46-18	1µm
70.29	0.50	15.13	1.54	0.07	0.20	2.79	3.70	1.59	0.09	95.89	KAP46-19	1µm
0.35	0.04	0.12	0.06	0.03	0.02	0.05	0.20	0.04	0.03		Std. dev.	

†-uncorrected melt compositions; *- analytical total.

Magnetite Compositions

SiO_2	TiO_2	Al_2O_3	Cr_2O_3	FeO	MnO	MgO	CaO	Total	Sample
3.94	2.36	2.19	0.00	81.99	0.25	2.18	0.82	93.72	3VG27-1
3.21	3.17	1.90	0.00	81.97	0.28	1.66	0.47	92.65	3VG27-2
1.09	2.88	1.74	0.04	84.19	0.32	1.27	0.52	92.05	3VG27-3
0.35	4.94	2.06	0.02	83.45	0.31	1.13	0.31	92.60	3VG27-4
0.33	10.23	1.81	0.00	78.75	0.48	1.46	0.32	93.38	3VG27-5
1.65	3.10	2.95	0.01	83.42	0.29	1.17	0.47	93.05	3VG27-6
0.26	5.60	2.22	0.00	82.91	0.40	1.18	0.31	92.88	3VG27-7
3.41	3.10	2.97	0.03	81.15	0.37	1.43	0.58	93.03	3VG27-8
0.29	14.10	1.61	0.02	76.27	0.69	1.66	0.34	94.96	3VG27-9
0.76	12.26	1.55	0.03	76.95	0.42	1.51	0.52	93.99	3VG27-10
1.53	6.17	2.10	0.01	81.11	0.38	1.46	0.47	93.23	Average
1.45	4.37	0.51	0.01	2.82	0.13	0.32	0.16		Std. Dev.
0.39	10.63	3.84	0.05	76.24	0.27	1.50	0.31	93.23	3VG3-1
0.93	10.48	3.65	0.05	76.18	0.24	1.65	0.36	93.55	3VG3-2
3.31	10.02	3.49	0.09	73.60	0.27	2.55	0.47	93.80	3VG3-3
1.79	10.52	3.70	0.07	75.12	0.27	2.07	0.28	93.81	3VG3-4
1.94	10.55	4.44	0.09	74.67	0.26	1.61	0.47	94.03	3VG3-5
2.27	10.32	3.63	0.09	74.83	0.28	2.32	0.40	94.12	3VG3-6
1.75	10.60	3.58	0.05	75.15	0.28	1.88	0.34	93.63	3VG3-7
0.39	10.81	3.74	0.07	76.51	0.26	1.53	0.25	93.55	3VG3-8
0.26	10.69	3.63	0.06	76.75	0.26	1.54	0.27	93.46	3VG3-9
0.39	10.70	3.66	0.07	76.57	0.25	1.57	0.29	93.51	3VG3-10
0.34	10.74	3.62	0.07	76.25	0.23	1.52	0.28	93.05	3VG3-11
0.19	10.74	3.58	0.06	76.67	0.23	1.50	0.22	93.19	3VG3-12
0.49	10.48	3.91	0.05	76.23	0.25	1.56	0.30	93.25	3VG3-13
0.56	10.65	3.64	0.07	76.17	0.24	1.57	0.35	93.25	3VG3-14
0.60	10.57	3.70	0.07	76.62	0.24	1.59	0.45	93.86	3VG3-15
0.24	10.82	3.58	0.09	77.05	0.27	1.51	0.30	93.84	3VG3-16
0.19	11.17	3.66	0.39	76.15	0.26	1.56	0.17	93.55	3VG3-17
0.94	10.62	3.71	0.09	75.93	0.26	1.71	0.32	93.57	Average
0.92	0.24	0.21	0.08	0.92	0.02	0.31	0.09		Std. Dev.
3.41	7.16	3.90	0.03	75.26	0.26	2.50	1.36	93.89	3VG26-1
0.29	7.66	4.16	0.05	78.94	0.24	1.90	0.26	93.50	3VG26-2
0.62	7.56	4.02	0.04	78.30	0.22	2.00	0.27	93.03	3VG26-3
0.26	7.58	4.07	0.07	78.51	0.28	1.93	0.28	92.97	3VG26-4
0.41	7.43	4.12	0.04	78.33	0.26	1.76	0.34	92.68	3VG26-5
0.22	7.41	3.98	0.06	78.60	0.22	1.75	0.18	92.41	3VG26-6
0.17	7.38	4.08	0.01	79.23	0.25	1.81	0.24	93.16	3VG26-7
0.62	7.38	4.18	0.02	78.15	0.23	1.84	0.30	92.72	3VG26-8
2.93	7.49	5.67	0.04	74.92	0.21	1.69	0.49	93.44	3VG26-9
0.41	8.17	4.35	0.05	77.60	0.24	1.88	0.26	92.95	3VG26-10
0.19	9.15	4.05	0.04	78.20	0.25	1.98	0.18	94.03	3VG26-11
0.23	8.41	4.00	0.01	78.96	0.21	1.84	0.17	93.83	3VG26-12
0.26	8.20	4.30	0.04	78.10	0.24	1.78	0.22	93.12	3VG26-13
0.31	7.97	4.37	0.02	78.37	0.26	1.89	0.25	93.43	3VG26-14
1.66	7.87	5.02	0.04	76.59	0.25	1.83	0.62	93.88	3VG26-15
0.47	7.81	4.07	0.04	78.31	0.28	1.98	0.24	93.22	3VG26-16
0.32	8.02	4.27	0.03	78.68	0.25	1.89	0.21	93.67	3VG26-17
1.81	7.56	4.17	0.01	76.92	0.26	2.33	0.25	93.30	3VG26-18
0.81	7.79	4.26	0.03	77.89	0.24	1.92	0.34	93.29	Average
0.98	0.48	0.43	0.02	1.21	0.02	0.20	0.28		Std. Dev.
3.77	12.45	7.73	0.53	67.06	0.30	2.07	0.76	94.68	KAP22-1
6.05	11.94	7.76	0.58	65.73	0.28	2.27	1.04	95.64	KAP22-2
5.27	12.10	8.77	0.57	66.51	0.30	1.86	0.78	96.15	KAP22-3
9.26	10.96	8.51	0.48	59.35	0.30	2.63	2.60	94.09	KAP22-4
0.74	13.07	7.22	0.60	69.38	0.28	1.88	0.35	93.53	KAP22-5
1.04	13.18	7.43	0.69	69.60	0.26	1.96	0.42	94.59	KAP22-6
0.95	13.46	6.96	0.68	69.55	0.35	2.03	0.36	94.33	KAP22-7
2.23	12.51	7.07	0.53	68.94	0.31	2.13	0.64	94.35	KAP22-8
3.65	12.22	7.88	0.53	68.35	0.26	1.93	0.49	95.30	KAP22-9
3.66	12.43	7.70	0.58	67.17	0.29	2.08	0.82	94.74	Average
2.84	0.76	0.62	0.07	3.25	0.03	0.24	0.70		Std. Dev.

APPENDIX B

Melt Correction Procedure

The migration of alkali metals (Na and K) out of the excitation volume during electron microprobe (EMP) analysis of hydrous alkali glasses is known to be a problem (Nielson and Sigurdson, 1981; Morgan and London, 1996) and is particularly severe for analysis using high beam currents, long counting times, smaller beam diameters and focused beam. It has also been shown that migration of Na results in 'grow-in' of immobile elements (e.g. Si and Al) during EMP analysis (Morgan and London, 1996). Thus during routine analysis of alkali-bearing hydrous silicate glasses steps are taken to reduce alkali migration and immobile element grow-in is employed. The analytical protocols employed include using a defocused beam, large beam diameters, low beam current, and short counting time for alkali elements. However, the resulting analytical data may still suffer from Na-loss and a correction has to be applied to the measured compositions.

Alkali migration during EMP analysis is particularly relevant to experimental melting studies in which the small size of the quenched melt pockets requires use of small beam diameters during analysis. A common approach to account for Na migration during analyses of quenched experimental melts is to correct for Na-loss by establishing a Na X-ray counts versus time curve and extrapolating this curve to zero time (start of the analyses) (e.g Patino Douce and Beard, 1995; Sen and Dunn, 1994). I monitored the decay of Na-counts as a function of time in 3VG46, an experiment that produced a relatively large proportion of melt. Considerable decay of Na counts were noticed in about 60s with relatively low Na-count decay in the first 10s. It was also noticed that the decay of Na-counts was accompanied by an increase in the count rate of Si. Therefore, during glass analyses Na-loss is accompanied by a gain of Si, a phenomenon that has been reported before (Morgan and London, 1996). The decay of Na and grow-in of Si was found to be a function of the beam size used in the analyses with the effect being pronounced for beam diameters <8μm. During glass analyses peak measurements for Na was done for 10s duration and Na was measured before measuring other elements on one of the spectrometers equipped with a TAP diffracting crystal in order to minimize the Na-loss. Despite these precautionary measures considerable Na-loss did occur during melt analyses. Therefore, the measured Na_2O contents were corrected using the procedure outlined below.

Melt pockets in 3VG46 was analyzed using beam diameters varying from 1 to 15 μm. The measured Na_2O and SiO_2 content could be linearly correlated with the beam diameter up to 8μm. Specifically, the measured Na_2O content decreases and SiO_2 content increases linearly with a decrease in beam diameter (Figure A.1). A correction factor was determined for Na_2O and SiO_2 content of the melt as a function of beam diameter for analyses using beam diameters <8μm (Figure A.2). For Na_2O, this correction factor ranged from 0% at beam diameter ≥8μm to ~40% for a focused beam. For SiO_2, the corresponding correction factors vary from 0% at beam diameters ≥8μm to ~3.5% for a focused beam.

References:

Morgan, G.B. and London, D. (1996) Optimizing the electron microprobe analysis of hydrous aluminosilicate glasses. American Mineralogist, 81, 1176-1185.

Nielsen, C.H. and Sigurdsson, H. (1981) Quantitative methods for electron microprobe analysis of sodium in natural and synthetic glasses. American Mineralogist, 66, 547-552.

Patino Douce, A.E. and Beard, J.S. (1995) Dehydration-melting of biotite gneiss and quartz amphibolite from 3 to 15 kbar. Journal of Petrology, 36, 707-738.

Sen,C. and Dunn, T. (1994) Dehydration melting of a basaltic composition amphibolite at 1.5 and 2.0 GPa: implications for the origin of adakites. Contributions to Mineralogy and Petrology, 117, 394-409.

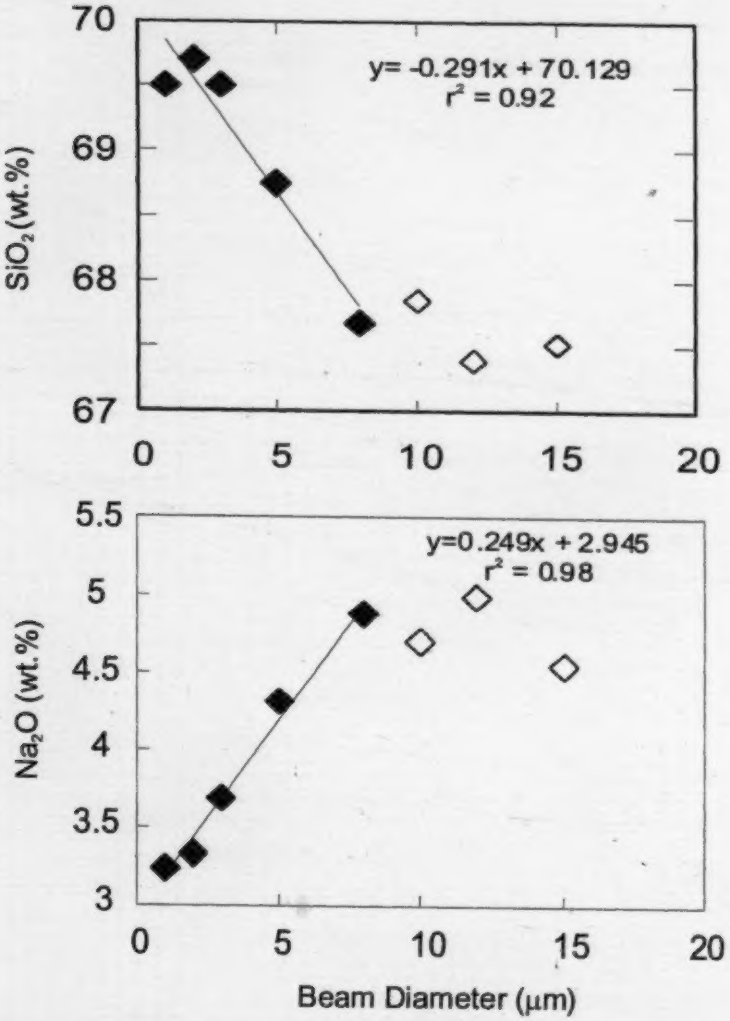

Figure A.1: Variation of SiO_2 and Na_2O content of melt in 3VG 46 as a function of beam diameter. SiO_2 and Na_2O content show a linear correlation with beam diameter for values of beam diameterfrom 1-8μm. Open symbols represent melt analyses using beam diameters >10μm and were not used in the regression.

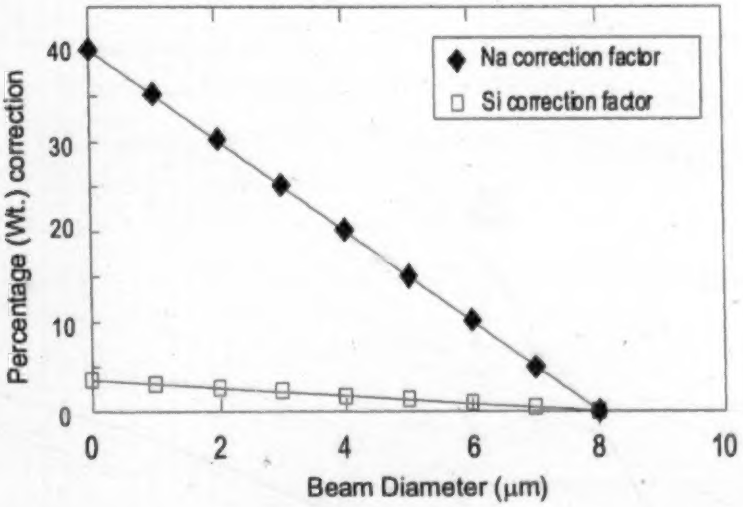

Figure A.2: Relative (wt. %) correction applied to melt analyses as a function of beam diameter. No correction was applied for melt analyses that used beam diameters ≥8 μm.

APPENDIX C

MASS BALANCE USING SINGULAR VALUE DECOMPOSITION

Matrix analyses techniques of mass balancing have the advantage over graphical and regression methods in that they can deal more efficiently with multicomponent systems. In this respect, they are useful in analyzing compositional spaces of metamorphic assemblages. A matix analysis method of Singular Value Decomposition (SVD) was used to for mass balance analysis in this study. SVD is a linear algebraic technique of analyzing compositional spaces (Fisher, 1989).

Theory

Compositional space of any given mineral assemblage may be represented by a m x n matrix A, where m represents the components and n represents the phases (m>n). Matrix A can then be written as,

$$\mathbf{A = UWV^T}$$

where U is a m x n column-orthogonal matrix , W is an n x n diagonal matrix, and V is an n x n orthogonal matrix. The number of non-zero diagonal elements of W (called singular values) gives the rank of matrix A. The number of zero elements of W gives the number of independent reactions in the compositions space. For each diagonal element in W, the corresponding column in V is an orthonormal basis vector for the null space and any linear combination between them represent a set of stoichiometric coefficients. Alternatively, if no elements of the diagonal matrix W are non-zero, assigning the lowest singular value to be zero enables one to formulate a matrix A' which is model for matrix A. If matrix A' is a satisfactory model of matrix A (which can be evaluated by the analytical uncertainties in the compositional space of A), then a univariant reaction can be mapped in the null space.

Example calculation

The software C-space (Torres-Roldan et al., 2000) was used for SVD analyses in this paper. Mass balance analyses were done in the chemical system Si-Ti-Al-Fe-Mg-Mn-Ca-Na-K which accounts for over 98 % of the oxygen-free composition of the rock. All the components were given equal weights in the SVD analyses. The mineral phases considered for mass balance are hornblende, plagioclase, orthopyroxene, clinopyroxene, garnet, quartz and quenched melt. Together these phases account for >98 % of the experimental run products. Measured oxide compositions of the phases were recast into cations, normalized to the total oxygen in one formula unit of the phase. The calculate cation proportions were used to formulate the input matrix. For the melt phase, compositions were recast assuming 10 oxygens per formula unit. Quartz was assumed to be pure. Hornblende and plagioclase compositions were from the starting materials. This was done to examine the mass balance between the starting assemblage and the product phases.

Here, I show an example of SVD analysis on the run product 3VG08 (7 kbar, 900 °C). Matrix A below is composed of cation proportions in each phase recalculated on the basis of number of oxygens present in the phase as discussed above.

Matrix A

	Qtz	Cpx	Plag	Grt	Hbl	Melt
Si	1.000	1.959	2.548	2.993	6.426	3.899
Ti	0.000	0.004	0.000	0.066	0.243	0.015
Al	0.000	0.102	1.446	1.900	2.156	1.017
Fe	0.000	0.368	0.003	1.539	1.838	0.090
Mn	0.000	0.010	0.000	0.041	0.015	0.001
Mg	0.000	0.695	0.000	0.730	2.445	0.062
Ca	0.000	0.830	0.454	0.715	1.773	0.125
Na	0.000	0.034	0.542	0.011	0.433	0.490
K	0.000	0.000	0.014	0.000	0.281	0.246

Matrix A can then be written as the product of matrices U, W and V below

Matrix U

0.8706	0.3440	-0.2632	0.2093	-0.0642	-0.0807
-0.0216	-0.0533	-0.0131	-0.0081	-0.2131	0.1970
-0.3170	0.0487	0.8257	-0.3385	-0.1385	0.1672
-0.2094	-0.5606	0.3460	0.5372	0.3092	-0.1121
-0.0030	-0.0084	0.0157	0.0219	0.0520	-0.0397
-0.2303	-0.6215	-0.3191	-0.2127	-0.2704	0.5386
-0.1967	-0.3533	-0.1434	-0.5733	0.2642	-0.6137
-0.0677	0.2228	-0.0108	-0.4148	0.4032	0.3179
-0.0310	0.0368	-0.0788	0.0809	0.7262	0.3805

Matrix W

10.0230	0.0000	0.0000	0.0000	0.0000	0.0000
0.0000	1.9183	0.0000	0.0000	0.0000	0.0000
0.0000	0.0000	1.344	0.0000	0.0000	0.0000
0.0000	0.0000	0.0000	0.6084	0.0000	0.0000
0.0000	0.0000	0.0000	0.0000	0.0737	0.0000
0.0000	0.0000	0.0000	0.0000	0.0000	0.3848

Matrix V

-0.0868	0.1793	-0.1957	0.3441	-0.8716	-0.2097
-0.2135	-0.1279	-0.4796	-0.1058	0.2524	-0.7957
-0.2796	0.4724	0.3364	-0.7205	-0.1941	-0.1695
-0.3831	-0.2336	0.7271	0.3958	0.0627	-0.3307
-0.7597	-0.3997	-0.2522	-0.1516	-0.1075	0.4061
-0.3805	0.7169	-0.1619	0.4143	0.3514	0.1409

Singluar values of matrix A are the number of non-zero elements in the diagonal matrix W. These are 10.0273, 1.9183, 1.344, 0.6084, 0.0737, 0.3848.

The matrix A has a rank of 6 as there as six non-zero singular values. This means that the assemblage is at least divariant in this system. By setting the smallest singular value to zero yields a rank deficient model matrix can be set up. This model matrix of rank 5 is:

Model Matrix (A')

	Qtz	Cpx	Plag	Grt	Hbl	Melt
Si	0.9959	1.9602	2.5471	2.9933	6.4255	3.9007
Ti	-0.0137	0.008	-0.003	0.067	0.2413	0.0205
Al	-0.0089	0.1046	1.444	1.9006	2.1549	1.0206
Fe	0.0199	0.3622	0.0074	1.5376	1.8405	0.082
Mn	0.0033	0.0090	0.0007	0.0408	0.0154	-0.0003
Mg	-0.0174	0.7000	-0.0039	0.7312	2.4429	0.069
Ca	0.017	0.8251	0.4578	0.7138	1.7751	0.1182
Na	0.0259	0.0265	0.5478	0.0091	0.4362	0.4796
K	0.0466	-0.0135	0.0244	-0.0034	0.2868	0.2272

The rank deficient matrix has a null space with reaction relationship which can be examined provided the model matrix A' is a satisfactory model for Matrix A. This can be evaluated by seeing if matrix A is within the tolerance limit of matrix A. For matrix A, tolerance (uncertainty) limits were set by constructing another m x n matrix with 2-sigma uncertainties in the electron microprobe data. For quartz, uncertainties for all elements excluding Si were assigned a value of 0.001. For Si a value of 0.03 was set as the tolerance limit in accordance with the uncertainty estimates for major elements in other phases. Any values less than 0.001 was assigned 0.001.

The tolerance matrix B is

	Qtz	Cpx	Plag	Grt	Hbl	Mlt
Si	0.030	0.020	0.014	0.015	0.033	0.178
Ti	0.001	0.003	0.001	0.014	0.068	0.018
Al	0.001	0.051	0.012	0.019	0.130	0.115
Fe	0.001	0.035	0.003	0.050	0.138	0.077
Mn	0.001	0.002	0.001	0.021	0.007	0.002
Mg	0.001	0.024	0.001	0.155	0.131	0.120
Ca	0.001	0.056	0.015	0.101	0.064	0.092
Na	0.001	0.012	0.011	0.004	0.019	0.066
K	0.001	0.001	0.003	0.001	0.031	0.047

A matrix of residuals given by subtracting Matrix A-A' can be used to evaluate the adequacy of Matrix A' in modelling matrix A. The residual matrix C is

	Qtz	Cpx	Plag	Grt	Hbl	Mlt
Si	-0.0041	0.0012	-0.0009	0.0003	-0.0005	0.0017
Ti	-0.0137	0.0040	-0.0030	0.0010	-0.0017	0.0055
Al	-0.0089	0.0026	-0.0020	0.0006	-0.0011	0.0036
Fe	0.0199	-0.0058	0.0044	-0.0014	0.0025	-0.0080
Mn	0.0033	-0.0010	0.0007	-0.0002	0.0004	-0.0013
Mg	-0.0174	0.0050	-0.0039	0.0012	-0.0021	0.0070
Ca	0.0170	-0.0049	0.0038	-0.0012	0.0021	-0.0068
Na	0.0259	-0.0075	0.0058	-0.0019	0.0032	-0.0104
K	0.0466	-0.0135	0.0104	-0.0034	0.0058	-0.0188

A matrix of residual/tolerance ratios is a criteria to evaluate the effectiveness of matrix A' as a model of matrix A.

The matrix of residual/tolerance ratio, D is

	Qtz	Cpx	Plag	Grt	Hbl	Mlt
Si	-0.1375	0.0597	-0.0656	0.0198	-0.0154	0.0093
Ti	**-13.6911**	1.3215	**-3.0491**	0.0704	-0.0248	0.3067
Al	**-8.8944**	0.0505	-0.1651	0.0337	-0.0084	0.0312
Fe	**19.8643**	-0.1643	1.4747	-0.0286	0.0178	-0.1040
Mn	**3.3408**	-0.4837	0.7440	-0.0114	0.0589	-0.6736
Mg	**-17.3693**	0.2096	**-3.8683**	0.0081	-0.0164	0.0584
Ca	**16.9726**	-0.0878	0.2520	-0.0121	0.0327	-0.0744
Na	**25.8989**	-0.6250	0.5244	-0.4658	0.1682	-0.1582
K	**46.6495**	**-13.5083**	**3.4631**	**-3.3559**	0.1856	-0.4002

Several residuals have greater than three times the estimated 2-sigma analytical precisions. These elements are, therefore, poorly modelled by the model matrix A'. Quartz is poorly modelled primarily because the analytical uncertainties for the minor elements were assigned were the lowest (0.001). Thus, one may argue that model matrix A' is not a valid model for matrix A. However, if one examines the matrix carefully, the large residual/tolerance ratios are only for elements with low abundance in a particular phase. If the poor fit to these minor elements can be ignored, the matrix A' obviously become a satisfactory model for matrix A. The null space can then be investigated for univariant mass balance which yielded the following mass balance:

0.8716 Qtz + 0.1941 Plag + 0.1075 Hbl = 0.2524 Cpx + 0.0627 Grt + 0.3514 Melt

This univariant reaction relates the starting assemblage to the product assemblage in 3VG08.

References:

Fisher, G.W. (1989) Matrix analysis of metamorphic mineral assemblages and reactions. Contributions to Mineralogy and Petrology, 102, 69-77.

Torres-Roldan, R.L., Garcia-Casco, A. and Garcia-Sanchez, P.A. (2000) CSpace: An integrated workplace for the graphical and algebraic analysis of phase assemblages on 32-bit Wintel platforms. Computers and Geosciences, 26, 779-793.

****

3VG INPUT MATRICES

sample	Component	Si	Ti	Al	Fe	Mn	Mg	Ca	Na	K
7 kbar	Phase									
	Qtz	1.000	0	0	0	0	0	0	0	0
	Cpx	1.954	0.005	0.094	0.377	0.010	0.688	0.849	0.031	0.001
	Opx	1.898	0.009	0.146	0.835	0.013	1.039	0.078	0.000	0
	Plag	2.548	0.000	1.446	0.003	0.000	0.000	0.454	0.542	0.014
	Grt	0	0	0	0	0	0	0	0	0
	Hbl	6.426	0.243	2.156	1.838	0.015	2.445	1.773	0.433	0.281
	Mlt	3.666	0.018	1.209	0.241	0.004	0.069	0.131	0.588	0.161

sample	Component	Si	Ti	Al	Fe	Mn	Mg	Ca	Na	K
10 kbar	Phase									
	Qtz	1.000	0	0	0	0	0	0	0	0
	Cpx	1.958	0.006	0.114	0.385	0.010	0.684	0.806	0.031	0.002
	Opx	1.920	0.007	0.151	0.889	0.015	0.947	0.068	0.004	0.002
	Plag	2.548	0.000	1.446	0.003	0.000	0.000	0.454	0.542	0.014
	Grt	0	0	0	0	0	0	0	0	0
	Hbl	6.426	0.243	2.156	1.838	0.015	2.445	1.773	0.433	0.281
	Mlt	4.003	0.008	0.945	0.094	0.003	0.028	0.135	0.357	0.244

sample	Component	Si	Ti	Al	Fe	Mn	Mg	Ca	Na	K
12.5 kbar	Phase									
	Qtz	1.000	0	0	0	0	0	0	0	0
	Cpx	1.960	0.003	0.086	0.354	0.011	0.698	0.864	0.031	0.000
	Opx	0	0	0	0	0	0	0	0	0
	Plag	2.548	0.000	1.446	0.003	0.000	0.000	0.454	0.542	0.014
	Grt	2.988	0.064	1.927	1.559	0.046	0.754	0.646	0	0
	Hbl	6.426	0.243	2.156	1.838	0.015	2.445	1.773	0.433	0.281
	Mlt	3.635	0.006	1.325	0.131	0.002	0.023	0.039	0.762	0.310

sample	Component	Si	Ti	Al	Fe	Mn	Mg	Ca	Na	K
15 kbar	Phase									
	Qtz	1.000	0	0	0	0	0	0	0	0
	Cpx	1.959	0.004	0.102	0.368	0.010	0.695	0.830	0.034	0.000
	Opx	0	0	0	0	0	0	0	0	0
	Plag	2.548	0.000	1.446	0.003	0.000	0.000	0.454	0.542	0.014
	Grt	2.993	0.066	1.900	1.539	0.041	0.730	0.715	0.011	0
	Hbl	6.426	0.243	2.156	1.838	0.015	2.445	1.773	0.433	0.281
	Mlt	3.899	0.015	1.017	0.09	0.001	0.062	0.125	0.49	0.246

sample	Component	Si	Ti	Al	Fe	Mn	Mg	Ca	Na	K
17.5 kbar	Phase									
	Qtz	1.000	0	0	0	0	0	0	0	0
	Cpx	1.895	0.017	0.366	0.294	0.003	0.579	0.664	0.173	0
	Opx	0	0	0	0	0	0	0	0	0
	Plag	2.548	0.000	1.446	0.003	0.000	0.000	0.454	0.542	0.014
	Grt	2.972	0.068	1.928	1.402	0.021	0.927	0.678	0.000	0.000
	Hbl	6.426	0.243	2.156	1.838	0.015	2.445	1.773	0.433	0.281
	Mlt	3.924	0.013	1.041	0.071	0.001	0.023	0.084	0.511	0.262

sample	Component	Si	Ti	Al	Fe	Mn	Mg	Ca	Na	K
20 kbar	Phase									
	Qtz	1.000	0	0	0	0	0	0	0	0
	Cpx	1.878	0.020	0.496	0.236	0.003	0.495	0.594	0.267	0.004
	Opx	0	0	0	0	0	0	0	0	0
	Plag	2.548	0.000	1.446	0.003	0.000	0.000	0.454	0.542	0.014
	Grt	3.006	0.065	1.900	1.376	0.021	0.864	0.733	0.030	0.000
	Hbl	6.426	0.243	2.156	1.838	0.015	2.445	1.773	0.433	0.281
	Mlt	3.997	0.010	1.022	0.057	0.001	0.022	0.066	0.416	0.203

sample	Component	Si	Ti	Al	Fe	Mn	Mg	Ca	Na	K
22.5 kbar	Phase									
	Qtz	1.000	0	0	0	0	0	0	0	0
	Cpx	1.920	0.014	0.480	0.220	0.003	0.485	0.563	0.280	0.000
	Opx	0	0	0	0	0	0	0	0	0
	Plag	2.548	0.000	1.446	0.003	0.000	0.000	0.454	0.542	0.014
	Grt	2.952	0.077	1.954	1.366	0.018	0.887	0.730	0.021	0
	Hbl	6.426	0.243	2.156	1.838	0.015	2.445	1.773	0.433	0.281
	Mlt	3.971	0.01	1.001	0.051	0.001	0.019	0.062	0.423	0.381

TOLERANCE MATRICES

3VG	2-sigma									
sample	Component	Si	Ti	Al	Fe	Mn	Mg	Ca	Na	K
7 kbar	Phase									
	Qtz	0.030	0.001	0.001	0.001	0.001	0.001	0.001	0.001	0.001
	Cpx	0.014	0.002	0.028	0.030	0.002	0.023	0.036	0.011	0.001
	Opx	0.026	0.003	0.035	0.046	0.002	0.045	0.020	0.004	0.005
	Plag	0.014	0.000	0.012	0.003	0.001	0.001	0.015	0.011	0.003
	Hbl	0.033	0.068	0.130	0.138	0.007	0.131	0.064	0.019	0.031
	Mlt	0.074	0.007	0.090	0.020	0.004	0.012	0.043	0.076	0.026

sample	Component	Si	Ti	Al	Fe	Mn	Mg	Ca	Na	K
10 kbar	Phase									
	Qtz	0.030	0.001	0.001	0.001	0.001	0.001	0.001	0.001	0.001
	Cpx	0.022	0.006	0.049	0.062	0.001	0.026	0.087	0.010	0.002
	Opx	0.024	0.002	0.041	0.025	0.002	0.028	0.028	0.005	0.002
	Plag	0.014	0.000	0.012	0.003	0.001	0.001	0.015	0.011	0.003
	Hbl	0.033	0.068	0.130	0.138	0.007	0.131	0.064	0.019	0.031
	Mlt	0.076	0.003	0.077	0.010	0.002	0.005	0.038	0.037	0.030

sample	Component	Si	Ti	Al	Fe	Mn	Mg	Ca	Na	K
12.5 kbar	Phase									
	Qtz	0.030	0.001	0.001	0.001	0.001	0.001	0.001	0.001	0.001
	Cpx	0.026	0.004	0.068	0.052	0.003	0.034	0.093	0.024	0.002
	Plag	0.014	0.000	0.012	0.003	0.001	0.001	0.015	0.011	0.003
	Grt	0.015	0.015	0.034	0.050	0.006	0.042	0.038	0.001	0.001
	Hbl	0.033	0.068	0.130	0.138	0.007	0.131	0.064	0.019	0.031
	Mlt	0.075	0.003	0.034	0.029	0.002	0.010	0.009	0.381	0.058

sample	Component	Si	Ti	Al	Fe	Mn	Mg	Ca	Na	K
15 kbar	Phase									
	Qtz	0.030	0.001	0.001	0.001	0.001	0.001	0.001	0.001	0.001
	Cpx	0.020	0.003	0.051	0.035	0.002	0.024	0.056	0.012	0.001
	Plag	0.014	0.000	0.012	0.003	0.001	0.001	0.015	0.011	0.003
	Grt	0.015	0.014	0.019	0.050	0.021	0.155	0.101	0.004	0.001
	Hbl	0.033	0.068	0.130	0.138	0.007	0.131	0.064	0.019	0.031
	Mlt	0.178	0.018	0.115	0.077	0.002	0.120	0.092	0.066	0.047

sample	Component	Si	Ti	Al	Fe	Mn	Mg	Ca	Na	K
17.5 kbar	Phase									
	Qtz	0.030	0.001	0.001	0.001	0.001	0.001	0.001	0.001	0.001
	Cpx	0.048	0.005	0.078	0.050	0.002	0.027	0.028	0.040	0.001
	Plag	0.014	0.000	0.012	0.003	0.001	0.001	0.015	0.011	0.003
	Grt	0.029	0.031	0.053	0.053	0.004	0.058	0.067	0.001	0.001
	Hbl	0.033	0.068	0.130	0.138	0.007	0.131	0.064	0.019	0.031
	Mlt	0.022	0.000	0.022	0.008	0.003	0.009	0.006	0.025	0.010

sample	Component	Si	Ti	Al	Fe	Mn	Mg	Ca	Na	K
20 kbar	Phase									
	Qtz	0.030	0.001	0.001	0.001	0.001	0.001	0.001	0.001	0.001
	Cpx	0.035	0.006	0.054	0.028	0.001	0.034	0.031	0.034	0.009
	Plag	0.014	0.000	0.012	0.003	0.001	0.001	0.015	0.011	0.003
	Grt	0.097	0.023	0.128	0.098	0.010	0.183	0.151	0.045	0.001
	Hbl	0.033	0.068	0.130	0.138	0.007	0.131	0.064	0.019	0.031
	Mlt	0.025	0.003	0.023	0.010	0.002	0.005	0.007	0.022	0.011

sample	Component	Si	Ti	Al	Fe	Mn	Mg	Ca	Na	K
22.5 kbar	Phase									
	Qtz	0.030	0.001	0.001	0.001	0.001	0.001	0.001	0.001	0.001
	Cpx	0.055	0.005	0.146	0.018	0.002	0.086	0.066	0.027	0.001
	Plag	0.014	0.000	0.012	0.003	0.001	0.001	0.015	0.011	0.003
	Grt	0.018	0.015	0.034	0.076	0.005	0.189	0.091	0.007	0.001
	Hbl	0.033	0.068	0.130	0.138	0.007	0.131	0.064	0.019	0.031
	Mlt	0.029	0.009	0.016	0.008	0.002	0.014	0.019	0.053	0.015

KAP INPUT MATRICES

sample	Component	Si	Ti	Al	Fe	Mn	Mg	Ca	Na	K
7 kbar	Phase									
	Qtz	1.000	0	0	0	0	0	0	0	0
	Cpx	1.945	0.007	0.110	0.386	0.011	0.617	0.878	0.052	0
	Opx	1.915	0.009	0.154	0.762	0.021	1.051	0.084	0.007	0.003
	Plag	2.612	0	1.386	0.001	0	0	0.384	0.609	0.014
	Grt	0	0	0	0	0	0	0	0	0
	Hbl	6.403	0.206	2.236	2.257	0.036	2.084	1.777	0.329	0.216
	Mlt	3.525	0.040	1.186	0.246	0.007	0.136	0.294	0.613	0.205

sample	Component	Si	Ti	Al	Fe	Mn	Mg	Ca	Na	K
10 kbar	Phase									
	Qtz	1.000	0	0	0	0	0	0	0	0
	Cpx	1.961	0.007	0.111	0.359	0.011	0.623	0.883	0.047	0.000
	Opx	0	0	0	0	0	0	0	0	0
	Plag	2.612	0	1.386	0.001	0	0	0.384	0.609	0.014
	Grt	3.011	0.038	1.924	1.669	0.088	0.573	0.681	0.007	0.000
	Hbl	6.403	0.206	2.236	2.257	0.036	2.084	1.777	0.329	0.216
	Mlt	3.974	0.009	0.953	0.099	0.002	0.026	0.140	0.442	0.228

sample	Component	Si	Ti	Al	Fe	Mn	Mg	Ca	Na	K
12.5 kbar	Phase									
	Qtz	1.000	0	0	0	0	0	0	0	0
	Cpx	1.932	0.009	0.130	0.376	0.009	0.643	0.872	0.047	0.000
	Opx	0	0	0	0	0	0	0	0	0
	Plag	2.612	0	1.386	0.001	0	0	0.384	0.609	0.014
	Grt	2.995	0.068	1.887	1.666	0.060	0.618	0.690	0.013	0.000
	Hbl	6.403	0.206	2.236	2.257	0.036	2.084	1.777	0.329	0.216
	Mlt	3.817	0.015	1.093	0.107	0.001	0.035	0.165	0.570	0.207

sample	Component	Si	Ti	Al	Fe	Mn	Mg	Ca	Na	K
15 kbar	Phase									
	Qtz	1.000	0	0	0	0	0	0	0	0
	Cpx	1.891	0.018	0.262	0.346	0.003	0.611	0.773	0.111	0.002
	Opx	0	0	0	0	0	0	0	0	0
	Plag	2.612	0	1.386	0.001	0	0	0.384	0.609	0.014
	Grt	2.995	0.074	1.869	1.564	0.045	0.690	0.745	0.015	0.000
	Hbl	6.403	0.206	2.236	2.257	0.036	2.084	1.777	0.329	0.216
	Mlt	3.754	0.025	1.076	0.135	0.003	0.089	0.176	0.604	0.244

sample	Component	Si	Ti	Al	Fe	Mn	Mg	Ca	Na	K
17.5 kbar	Phase									
	Qtz	1.000	0	0	0	0	0	0	0	0
	Cpx	1.893	0.018	0.349	0.286	0.002	0.544	0.734	0.179	0.000
	Opx	0	0	0	0	0	0	0	0	0
	Plag	2.612	0	1.386	0.001	0	0	0.384	0.609	0.014
	Grt	2.972	0.081	1.883	1.521	0.038	0.728	0.770	0.024	0.000
	Hbl	6.403	0.206	2.236	2.257	0.036	2.084	1.777	0.329	0.216
	Mlt	3.940	0.012	1.021	0.071	0.002	0.026	0.112	0.485	0.220

sample	Component	Si	Ti	Al	Fe	Mn	Mg	Ca	Na	K
20 kbar	Phase									
	Qtz	1.000	0	0	0	0	0	0	0	0
	Cpx	1.876	0.020	0.476	0.260	0.002	0.466	0.613	0.266	0.000
	Opx	0	0	0	0	0	0	0	0	0
	Plag	2.612	0	1.386	0.001	0	0	0.384	0.609	0.014
	Grt	3.008	0.072	1.860	1.486	0.037	0.710	0.799	0.033	0.000
	Hbl	6.403	0.206	2.236	2.257	0.036	2.084	1.777	0.329	0.216
	Mlt	3.955	0.011	1.033	0.061	0.001	0.016	0.096	0.463	0.244

sample	Component	Si	Ti	Al	Fe	Mn	Mg	Ca	Na	K
22.5 kbar	Phase									
	Qtz	1.000	0	0	0	0	0	0	0	0
	Cpx	1.865	0.029	0.562	0.255	0.002	0.380	0.574	0.314	0.000
	Opx	0	0	0	0	0	0	0	0	0
	Plag	2.612	0	1.386	0.001	0	0	0.384	0.609	0.014
	Grt	2.969	0.075	1.914	1.459	0.035	0.713	0.824	0.019	0.000
	Hbl	6.403	0.206	2.236	2.257	0.036	2.084	1.777	0.329	0.216
	Mlt	3.911	0.011	1.036	0.050	0.001	0.022	0.097	0.564	0.296

TOLERANCE MATRICES

KAP sample 7 kbar	2-sigma Component Phase	Si	Ti	Al	Fe	Mn	Mg	Ca	Na	K
	Qtz	0.030	0.001	0.001	0.001	0.001	0.001	0.001	0.001	0.001
	Cpx	0.029	0.006	0.048	0.097	0.004	0.049	0.113	0.015	0.001
	Opx	0.040	0.008	0.055	0.046	0.003	0.078	0.093	0.016	0.008
	Plag	0.031	0.000	0.042	0.001	0.001	0.000	0.020	0.022	0.016
	Hbl	0.083	0.038	0.121	0.083	0.004	0.085	0.128	0.071	0.023
	Mlt	0.041	0.004	0.035	0.026	0.003	0.021	0.072	0.088	0.024

sample 10 kbar	Component Phase	Si	Ti	Al	Fe	Mn	Mg	Ca	Na	K
	Qtz	0.030	0.001	0.001	0.001	0.001	0.001	0.001	0.001	0.001
	Cpx	0.014	0.002	0.031	0.040	0.003	0.035	0.042	0.011	0.001
	Plag	0.031	0.000	0.042	0.001	0.001	0.000	0.020	0.022	0.016
	Grt	0.020	0.021	0.029	0.034	0.023	0.074	0.082	0.006	0.001
	Hbl	0.083	0.038	0.121	0.083	0.004	0.085	0.128	0.071	0.023
	Mlt	0.024	0.002	0.034	0.016	0.003	0.005	0.005	0.071	0.008

sample 12.5 kbar	Component Phase	Si	Ti	Al	Fe	Mn	Mg	Ca	Na	K
	Qtz	0.030	0.001	0.001	0.001	0.001	0.001	0.001	0.001	0.001
	Cpx	0.041	0.008	0.084	0.051	0.005	0.048	0.096	0.014	0.001
	Plag	0.031	0.000	0.042	0.001	0.001	0.000	0.020	0.022	0.016
	Grt	0.026	0.014	0.048	0.044	0.023	0.033	0.079	0.006	0.001
	Hbl	0.083	0.038	0.121	0.083	0.004	0.085	0.128	0.071	0.023
	Mlt	0.019	0.004	0.024	0.014	0.003	0.010	0.009	0.064	0.011

sample 15 kbar	Component Phase	Si	Ti	Al	Fe	Mn	Mg	Ca	Na	K
	Qtz	0.030	0.001	0.001	0.001	0.001	0.001	0.001	0.001	0.001
	Cpx	0.020	0.004	0.036	0.024	0.001	0.031	0.024	0.015	0.003
	Plag	0.031	0.000	0.042	0.001	0.001	0.000	0.020	0.022	0.016
	Grt	0.011	0.004	0.019	0.020	0.024	0.077	0.047	0.007	0.001
	Hbl	0.083	0.038	0.121	0.083	0.004	0.085	0.128	0.071	0.023
	Mlt	0.284	0.034	0.053	0.170	0.003	0.200	0.202	0.043	0.041

sample 17.5 kbar	Component Phase	Si	Ti	Al	Fe	Mn	Mg	Ca	Na	K
	Qtz	0.030	0.001	0.001	0.001	0.001	0.001	0.001	0.001	0.001
	Cpx	0.026	0.004	0.083	0.013	0.001	0.062	0.026	0.031	0.001
	Plag	0.031	0.000	0.042	0.001	0.001	0.000	0.020	0.022	0.016
	Grt	0.022	0.018	0.036	0.039	0.021	0.066	0.065	0.016	0.001
	Hbl	0.083	0.038	0.121	0.083	0.004	0.085	0.128	0.071	0.023
	Mlt	0.074	0.005	0.028	0.021	0.002	0.044	0.102	0.034	0.021

sample 20 kbar	Component Phase	Si	Ti	Al	Fe	Mn	Mg	Ca	Na	K
	Qtz	0.030	0.001	0.001	0.001	0.001	0.001	0.001	0.001	0.001
	Cpx	0.038	0.007	0.083	0.039	0.001	0.055	0.047	0.051	0.003
	Plag	0.031	0.000	0.042	0.001	0.001	0.000	0.020	0.022	0.016
	Grt	0.094	0.016	0.047	0.101	0.030	0.129	0.112	0.031	0.001
	Hbl	0.083	0.038	0.121	0.083	0.004	0.085	0.128	0.071	0.023
	Mlt	0.024	0.002	0.013	0.005	0.003	0.014	0.034	0.034	0.011

sample 22.5 kbar	Component Phase	Si	Ti	Al	Fe	Mn	Mg	Ca	Na	K
	Qtz	0.030	0.001	0.001	0.001	0.001	0.001	0.001	0.001	0.001
	Cpx	0.040	0.034	0.085	0.038	0.003	0.054	0.056	0.026	0.001
	Plag	0.031	0.000	0.042	0.001	0.001	0.000	0.020	0.022	0.016
	Grt	0.016	0.015	0.044	0.038	0.021	0.105	0.092	0.014	0.001
	Hbl	0.083	0.038	0.121	0.083	0.004	0.085	0.128	0.071	0.023
	Mlt	0.080	0.004	0.031	0.015	0.002	0.057	0.101	0.066	0.036

APPENDIX D

Role of oceanic plateaus in the initiation of subduction and origin of continental crust

Rajeev Nair
Thomas Chacko
Department of Earth and Atmospheric Sciences, University of Alberta, Edmonton T6G 2E3, Canada

ABSTRACT

Archean tonalite-trondhjemite-granodiorite (TTG) magmatic suites represent the oldest coherent pieces of felsic continental crust. We present results of long-duration dehydration-melting experiments on amphibolites to show that melting depths of >48 km are required to have sufficient garnet in the residuum for generating the degree of heavy rare earth element (REE) depletion documented in Early Archean TTG. This depth constraint is inconsistent with early crust evolution models that posit melting at the base of oceanic plateaus or oceanic crust to explain the origin of Early Archean continental crust. Alternative explanations for this early crust, e.g., subduction models, are problematic in that they do not readily provide a mechanism for initiation of subduction in a hotter Archean Earth. We hypothesize that intraoceanic subduction systems in the Archean originated due to gravitational instabilities produced by compositional and density contrasts between converging oceanic plateau and normal oceanic lithosphere. Our model differs from earlier models of subduction initiation in that subduction of oceanic lithosphere occurs through the 'hot' mantle residuum (protomantle lithosphere) at the base of newly formed oceanic plateau crust. Under a high Archean geothermal gradient, subducted oceanic crust would melt to produce TTG. This model explains the origin of subduction systems, TTG, TTG–mafic and/or ultramafic magma association, stabilization of continental crust, and the broadly coeval formation of cratons and their lithospheric roots.

Keywords: tonalite-trondhjemite-granodiorite, continental crust, dehydration melting, garnet stability, subduction initiation.

INTRODUCTION

Tonalite-trondhjemite-granodiorite (TTG) and tholeiitic to komatiitic lavas form the dominant magmatic suites in Archean cratons. Experimental and theoretical studies support the origin of TTG through the partial melting of hydrated metabasaltic rocks (e.g., Rapp et al., 1991; Martin et al., 2005). Highly fractionated rare earth element (REE) patterns $[(La/Yb)_N = 15–100]$ and depletion in heavy REEs ($Yb < 1$ ppm) of TTG require generation of these magmas at depths where garnet and/or amphibole are present in the residue (Martin, 1986). Tectonic models proposed to satisfy this requirement include melting of subducted oceanic crust (Martin, 1986), melting in the root zones of oceanic plateaus (Zegers and van Keken, 2001), or thick oceanic crust followed by repeated delamination of eclogitized lower crust (Bedard, 2006). Magmas with TTG-like major element compositions can be generated in all of these tectonic settings, making interpretations of the specific setting of early continental crust formation equivocal. Here we consider some fundamental characteristics of Archean TTG, including their spatial relationship in granite-greenstone terrains, heavy REE depletion, and oxygen isotope systematics, and present new experimental data to argue that conditions envisaged in lower crustal melting models are inadequate in explaining Early Archean TTG formation. We propose a modified subduction model for the origin of TTG that formed the first continental nuclei.

CONSTRAINTS ON TTG FORMATION

Any model of TTG formation should (1) account for the high proportion of TTG (to >60%) in many Archean cratons, (2) address the conditions required for generating the observed heavy REE depletion in Early Archean TTG, (3) satisfy the requirement that hydrated basaltic rocks be present in the source region of TTG to produce significant quantities of melt at reasonable crustal temperatures (<1100 °C), and (4) explain the high $\delta^{18}O$ values measured in zircons from Archean TTGs (Bindeman et al., 2005).

Experimental studies have produced TTG-type melts by ~20% partial melting of metabasaltic protoliths at temperatures >900 °C (e.g., Rapp et al., 1991). The high proportion of TTG in many Archean cratons requires a large volume of mafic rocks in the source region. The heavy REE depletion in TTG is generally attributed to the presence of garnet in the residue of TTG source rocks (Martin, 1986). The amount of residual garnet needed to produce the observed heavy REE depletion in Early Archean TTG was assessed by combining modal abundance data from experiments with published mineral/melt partition coefficients for REEs (Springer and Seck, 1997; Klein et al., 1997; 2000). Our calculations, using Yb as a representative heavy REE, indicate that for 20% partial melting of a mid-oceanic ridge basalt (MORB) composition source rock, at least 20 wt% garnet is required in the melt residue to generate the observed Yb depletion in average Early Archean TTG (Fig. 1). Because garnet abundance in metabasaltic rocks can be correlated with equilibration pressure, we can use experimental data to evaluate the depth of TTG magma generation.

EXPERIMENTAL INVESTIGATION AND DISCUSSION

We conducted 40 dehydration-melting experiments (see Nair and Chacko, 2002, for methodology) using a piston cylinder at 7–22.5 kbar, 775–1050 °C on a natural high-grade amphibolite sample (see Table DR1 in the GSA Data Repository[1]), similar in composition to MORB. Experimental duration varied from 2 days at temperatures >1000 °C to as long as 6 weeks at temperatures <1000 °C. Phases were characterized using a JEOL 8900 electron microprobe and phase proportions were determined using a combination of grayscale thresholding of backscattered electron images and whole-rock mass-balance constraints.

Experimental Constraints

At temperatures above the dehydration-melting solidus, residual minerals coexisted with melts of TTG composition. In metabasaltic rocks, the stability of garnet is in part controlled by the bulk composition of the protolith (Green and Ringwood, 1967). The composition of Archean oceanic crust, the presumed protolith of TTG, is not precisely known. Available evidence from Archean basaltic lavas in greenstone belts and a recent report of an Early Archean ophiolite (Furnes et al., 2007) suggest that the composition of Archean oceanic crust may have been similar to modern-day MORB. Our experimental data on a MORB-type amphibolite show that garnet becomes stable at ~10 kbar, consistent with the results of previous experimental studies. Pressures of >15 kbar (>48 km) are required to stabilize 20 wt% garnet in the melt residue (see Table DR2) (Fig. 2). We consider this to be the minimum depth of melting to produce the strong heavy REE depletion characteristic of Early Archean TTG. This is consistent with the depth of TTG magma generation suggested

---

[1] GSA Data Repository item 2008137, Table DR1 (run table showing experimental conditions and run products) and Table DR2 (showing modal proportion of residual phases), is available online at www.geosociety.org/pubs/ft2008.htm, or on request from editing@geosociety.org or Documents Secretary, GSA, P.O. Box 9140, Boulder, CO 80301, USA.

© 2008 The Geological Society of America. For permission to copy, contact Copyright Permissions, GSA, or editing@geosociety.org.
Geology, July 2008; v. 36; no. 7; p. 583–586; doi: 10.1130/G24773A.1; 3 figures; Data Repository item 2008137.

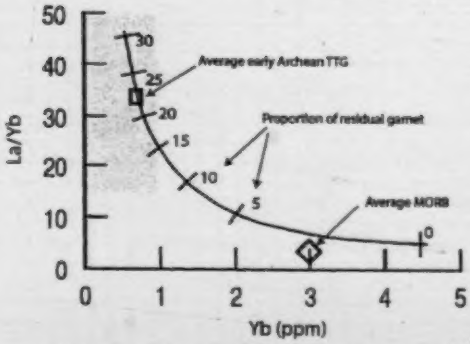

Figure 1. Variation in Yb and La/Yb ratio in 20% melt fraction during dehydration melting of amphibolite as function of garnet mode (wt%) in residue. Average Early Archean tonalite-trondhjemite-granodiorite (TTG) is from Martin et al. (2005) and average mid-oceanic ridge basalt (MORB) is from Petrologic Data Base of the Ocean Floor (2006). Shaded region represents Yb contents and the lower range of La/Yb ratios observed in Archean TTGs.

from REE modeling of experimental melts in recent studies (Xiong, 2006; Moyen and Stevens, 2006). If Archean oceanic crust had higher MgO content than MORB, as argued by some petrologists (e.g., Bickle et al., 1994; Foley et al., 2003), the depth required for generating sufficient garnet would further increase because of the dependence of garnet stability on the Mg-number [Mg/(Mg + Fe)] of the protolith (Green and Ringwood, 1967). Our results also indicate that pressures of >18 kbar (58 km) are needed to form a plagioclase-free eclogite assemblage (Fig. 2).

Implications for Tectonic Models

The requirement of melt generation at depths >48–58 km has implications for models of Early Archean TTG formation. Delamination models (Zegers and van Keken, 2001; Bedard, 2006) are problematic due to the large crustal thickness necessary to transform mafic rocks to eclogite. Eclogite formation is critical to these models in that it is the density increase associated with this facies transition that induces delamination. Parameterized modeling of mantle melting indicates that even with a mantle potential temperature of 1500 °C, the resulting oceanic crust is unlikely to have been >20 km thick (Vlaar and van den Berg, 1991). The base of such crust would not be in the eclogite stability field, or in the garnet stability field (~35 km or 10 kbar). As a consequence, melts generated in the lower parts of this crust would not have the heavy REE depletion observed in Early Archean TTG. Thickening of crust through repeated underplating of basaltic magmas (Zegers, 2004) may help attain the depth requirement for generating strongly heavy REE–depleted TTG magmas. However, melt production in this case would occur in rocks that had never interacted with surface fluids. This is inconsistent with the oxygen isotope compositions of zircons crystallized from TTG magmas that suggest derivation from rocks that had a prior history of surface fluid-rock interaction (Bindeman et al., 2005). Models invoking melting in the root zones of oceanic plateaus are also inadequate in that oceanic plateaus thicker than 35 km are not known in the geologic record. The root zones of oceanic plateaus are, therefore, not at sufficient depth to stabilize the required amount of garnet for generating heavy REE–depleted TTG. Moreover, these plateau root zones are likely dominated by low-Si, high-Mg anhydrous cumulates, which would not be conducive to generating TTG magmas at reasonable temperatures (<1100 °C). Advocates of delamination and lower crustal melting models have recognized the problem of low melt productivity and had to invoke repeated delamination events (Bedard, 2006), unusually thick oceanic plateaus, or crustal thickening postdating TTG production (Zegers, 2004) in order to explain the large volume of TTG in Archean cratons.

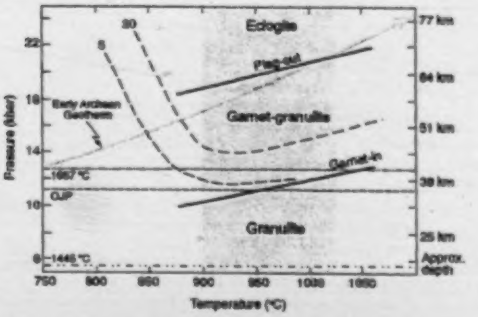

Figure 2. Pressure-temperature diagram showing garnet proportion contours (5 and 20 wt%) in the residue of metabasalt melting. Also shown are garnet-in and plagioclase-out curves representing the transition from intermediate granulite–high-pressure granulite and high-pressure granulite-eclogite facies, respectively, in mid-oceanic ridge basalt compositions. Horizontal lines (dash-dot) represent thickness of oceanic crust as function of different mantle potential temperatures (Vlaar and van den Berg, 1991); thickness of Cretaceous Ontong Java plateau is shown for comparison (dashed line). Shaded area represents minimum temperature conditions during amphibolite dehydration melting interval where melt proportions reach 20% or more; geotherm is from Martin and Moyen (2002).

Models involving melting of subducted oceanic crust (Martin, 1986) are more consistent with the depth requirements for generating TTG. However, the role of subduction processes in the Archean has been disputed on physical grounds that plates did not attain the negative buoyancy to initiate the subduction process (e.g., Davies, 1992). We present a modified subduction model that addresses these concerns.

Modified Subduction Model

Existing Archean subduction models invoke subduction of young oceanic lithosphere along a steep geothermal gradient (e.g., Martin, 1986). It seems intuitive that early subduction must have been intraoceanic, but how and why subduction would initiate remain uncertain. Here we present a model that hypothesizes subduction initiation and resultant TTG magmatism in the Archean.

There is general consensus that the Archean Earth was hotter than at present, although the magnitude of the temperature difference is a matter of debate. Today, Earth's heat-loss mechanisms involve cooling of the mantle through the production of plates and intermittent plume activity (Davies, 1993). It is likely that the Archean Earth also supported both of these cooling mechanisms. Early Archean oceanic crust would therefore have comprised two entities, normal oceanic crust produced by mantle upwelling at divergent margins, and oceanic plateaus produced by upwelling mantle plumes (Fig. 3). Both of these entities would have been positively buoyant relative to modern-day oceanic crust because of their large crustal thickness. However, a slight buoyancy contrast is established due to the greater thickness and slightly more Mg-rich nature of plateau crust, making it buoyant relative to normal oceanic crust of the same age. A relatively larger buoyancy/density contrast exists between the plateau lithosphere and normal oceanic lithosphere owing to differences in the

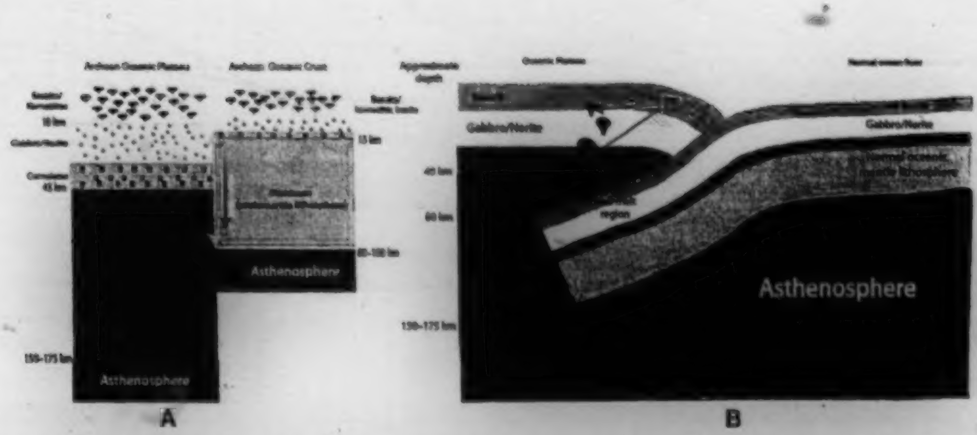

Figure 3. Model of Archean subduction and formation of tonalite-trondhjemite-granodiorites (TTGs). A: Hypothetical structure of Archean oceanic crust (for mantle potential temperature of 1445 °C) and oceanic plateau. Protomantle lithosphere (PML) represents underplated mantle melt residua. PML of plateau is less dense relative to asthenospheric mantle and PML of normal oceanic crust. Yellow double-headed arrow indicates region where gravitational differences between plateau and normal oceanic lithosphere is maximum. B: Subduction initiation during oceanic plateau-crust convergence in Archean. Subduction of oceanic lithosphere occurs along zone of weakness developed within PML of the oceanic plateau. Subducted slab melts at depth >50 km, producing TTG magmas, which are emplaced in plateau crust. MORB—mid-oceanic ridge basalt.

compositions of their respective mantle lithospheres. Normal oceanic mantle lithosphere is less depleted than plateau lithosphere because of the smaller degree of mantle melting needed to produce standard oceanic crust. The mantle source region of a plateau is highly depleted because of extraction of large volumes of tholeiitic and komatiitic magmas that form the plateau sequences. Density differences between the mantle residue after normal oceanic crust and oceanic plateau formation were calculated based on the residual mineral modes and compositions from peridotite melting experiments of Walter (1998). We calculated a minimum density contrast of 0.6% based on melt residuum data at 30 kbar for melt fractions of 14% and 37% (Walter, 1998), corresponding well with a 0.7% density contrast calculated based on the differences in the composition of highly depleted forearc and less depleted abyssal peridotites (Niu et al., 2003). The effect of oceanic plateau creation is a less dense residual mantle that rises buoyantly and underplates the plateau crust. Once underplated, this strongly depleted mantle (which we term protomantle lithosphere) cools conductively to eventually become the plateau lithosphere. Cooling of the protomantle lithosphere occurs at a slower rate compared to oceanic mantle lithosphere because of its larger thickness. The slower cooling of the protomantle lithosphere is also affected by a decrease in thermal diffusivity due to the high initial temperature of the residuum.

The net result of these compositional, thermal, and density differences between normal oceanic and oceanic plateau lithosphere is that a gravitational instability develops when the two are juxtaposed. This gravitational instability is enhanced if the formation age of the oceanic plateau is younger than the oceanic lithosphere. This facilitates the subduction of relatively dense normal oceanic lithosphere under the plateau crust, through the depleted residuum (Fig. 3). A similar model for initiation of subduction was proposed for the Solomon arc (Niu et al., 2003). Our model differs from this previous model in the location of the subducting plate. The Benioff plane in our model is located within the mantle residuum (protomantle lithosphere) of the oceanic plateau rather than below this layer (Fig. 3B). This is consistent with seismic profiles showing shallow dipping reflectors within the mantle beneath some Archean cratons (Calvert et al., 1995). Analogue models of subduction zones stress the importance of lateral density contrasts in the initiation of the subduction (Mart et al., 2005). It is interesting that these models also suggest that, given appropriate boundary conditions, the downgoing plate can subduct at a relatively shallow angle into the ductile lithospheric layer of the overriding plate (Mart et al., 2005). We propose that the depth at which protomantle lithosphere of the oceanic plateau supports ductile deformation determines the top of the subduction plane. This depth is a function of the cooling history of the melt residuum after oceanic plateau extraction and is determined by the time interval between formation of the plateau and the initiation of subduction. Specifically, a short time interval leads to a hotter protomantle lithosphere and in turn a shallower subduction plane. Variations in the age of plateaus at the onset of subduction, therefore, determine the thickness of lithospheric mantle wedge. The zone of weakness for subduction initiation develops as ductile fault or shear zone arising from compressive stresses sustained between protomantle lithosphere and the converging oceanic lithosphere. Despite the high initial viscosity of the protomantle lithosphere, ductile deformation and slab penetration may be enabled by shear localization near the boundaries of subducting lithosphere by viscous energy dissipation caused by shear heating (Costa and Macedonio, 2003; Kaus and Podladchikov, 2006) and viscosity reduction by dewatering (Hirth and Kohlstedt, 1996) of sediments at the top of the slab. Dewatering of sediments may also cause melting near the top of the descending lithosphere, which in turn may partition strain into these melt-rich zones (Holtzman et al., 2005). A higher Archean geothermal gradient, combined with the relatively young age of oceanic crust and, shear heating during subduction, would cause the hydrothermally altered portions of the subducting crust to melt and produce TTG. Because of a thicker pillow lava section in Archean relative to present-day oceanic crust (Bickle et al., 1994; Kent et al., 1996) (Fig. 3A), a larger thickness of Archean oceanic crust likely underwent hydration through interaction with seawater. In turn, this thick, hydrated pillow lava section would be capable of producing a larger volume of TTG magma than is possible by slab melting today. It is important that melting of the subducted slab under thick plateau crust would enable melting to occur at sufficient depth to generate >20 wt% garnet in the residue and strong heavy REE depletion in the TTG magma.

The variable but generally higher Mg-number of TTG relative to experimental melts from metabasalts has been attributed to differing degrees of slab melt–mantle wedge interactions (Martin and Moyen, 2002). In our model, these differences in the degree of interaction are caused by variations in the age of oceanic plateau at the onset of subduction, as this determines the thickness of the lithospheric wedge through which TTG melts must travel to be emplaced in the crust.

CONCLUSIONS

We have shown that melting of metabasalts at a depth >48 km was required to generate Early Archean TTG, which is inconsistent with the depth of source regions envisaged in lower crustal melting models. Our experimental data also suggest that delamination of oceanic plateau lower crust may not have been a viable crustal recycling mechanism in the Archean due to lack of sufficiently thick oceanic crust.

Our experimental constraints favor a model of TTG formation by melting of subducted oceanic crust. We propose that subduction zones initiated in the Archean from gravitational instability of the oceanic lithosphere arising from chemical differences between converging oceanic plateau and normal oceanic lithosphere. In the Archean, buoyant oceanic plateau lithosphere may have provided the boundary conditions for nucleating subduction zones. In our model, the spatial and temporal association in Archean cratons of tholeiitic to komatiitic volcanics, thick lithospheric mantle roots, and TTG-composition magmatic rocks is the result of separate but linked processes, the formation of an oceanic plateau and its associated mantle root followed by initiation of subduction beneath the plateau and the generation of TTG by melting of subducting oceanic crust. Oceanic plateaus served as the nuclei for Archean cratons because they represent the substrate on which TTG composition magmas were emplaced.

ACKNOWLEDGMENTS

This research was supported by a Geological Society of America research grant to Nair and a Natural Sciences and Engineering Research Council grant to Chacko. We thank D. Pattison for the starting material, R. Luth for discussions and access to experimental facilities, T. Stachel and K. Muehlenbachs for reviews of an early draft, and H. Martin, G. Sen, and M. Sun for constructive journal reviews.

REFERENCES CITED

Bédard, J.H., 2006, A catalytic delamination-driven model for coupled genesis of Archean crust and sub-continental lithospheric mantle: Geochimica et Cosmochimica Acta, v. 70, p. 1188–1214, doi: 10.1016/j.gca.2005.11.008.

Bickle, M.J., Nisbet, E.G., and Martin, A., 1994, Archean greenstone belts are not oceanic crust: Journal of Geology, v. 102, p. 121–138.

Bindeman, I.N., Eiler, J.M., Yogodzinski, G.M., Tatsumi, Y., Stern, C.R., Grove, T.L., Portnyagin, M., Hoernle, K., and Danyushevsky, L.V., 2005, Oxygen isotope evidence for slab melting in modern and ancient subduction zones: Earth and Planetary Science Letters, v. 235, p. 480–496, doi: 10.1016/j.epsl.2005.04.014.

Calvert, A.J., Sawyer, E.W., Davis, W.J., and Ludden, J.N., 1995, Archaean subduction inferred from seismic images of a mantle suture in the Superior Province: Nature, v. 375, p. 670–674, doi: 10.1038/375670a0.

Costa, A., and Macedonio, G., 2003, Viscous heating in fluids with temperature dependent viscosity: Implications for magma flows: Nonlinear Processes in Geophysics, v. 10, p. 101–111.

Davies, G.F., 1992, On the emergence of plate tectonics: Geology, v. 20, p. 963–966.

Davies, G.F., 1993, Conjectures on the thermal and tectonic evolution of the Earth: Lithos, v. 30, p. 281–289, doi: 10.1016/0024–4937(93)90041-A.

Foley, S.F., Buhre, S., and Jacob, D.E., 2003, Evolution of the Archaean crust by delamination and shallow subduction: Nature, v. 421, p. 249–252.

Furnes, H., de Wit, M., Staudigel, H., Rosing, M., and Muehlenbachs, K., 2007, A vestige of Earth's oldest ophiolite: Science, v. 315, p. 1704–1707.

Green, D.H., and Ringwood, A.E., 1967, An experimental investigation of the gabbro to eclogite transformation and its petrological applications: Geochimica et Cosmochimica Acta, v. 31, p. 767–833.

Hirth, G., and Kohlstedt, D.L., 1996, Water in the oceanic upper mantle: Implications for rheology, melt extraction and evolution of the lithosphere: Earth and Planetary Science Letters, v. 144, p. 93–108, doi: 10.1016/0012–821X(96)00154–9.

Holtzman, B.K., Kohlstedt, D.L., and Morgan, J.P., 2005, Viscous energy dissipation and strain partitioning in partially molten rocks: Journal of Petrology, v. 46, p. 2569–2592, doi: 10.1093/petrology/egi065.

Kaus, B.J.P., and Podladchikov, Y.Y., 2006, Initiation of localized shear zones in viscoelastoplastic rocks: Journal of Geophysical Research, v. 111, B04412, doi: 10.1029/2005JB003652.

Kent, R.W., Hardarson, B.S., Saunders, A.D., and Storey, M., 1996, Plateaux ancient and modern: Geochemical and sedimentological perspectives on Archean oceanic magmatism: Lithos, v. 37, p. 129–142, doi: 10.1016/0024–4937(95)00033-X.

Klein, M., Stosch, H.-G., and Seck, A., 1997, Partitioning of high field-strength and rare-earth elements between amphibole and quartz dioritic to tonalitic melts: An experimental study: Chemical Geology, v. 138, p. 257–271, doi: 10.1016/S0009–2541(97)00019–3.

Klein, M., Stosch, H.-G., Seck, A., and Shimizu, N., 2000, Experimental partitioning of high field strength and rare earth elements between clinopyroxene and garnet in andesitic to tonalitic systems: Geochimica et Cosmochimica Acta, v. 64, p. 99–115, doi: 10.1016/S0016–7037(99)00178–7.

Mart, Y., Aharonov, E., Mulugeta, G., Ryan, W., Tentler, T., and Goren, L., 2005, Analogue modelling of the initiation of subduction: Geophysical Journal International, v. 160, p. 1081–1091, doi: 10.1111/j.1365–246X.2005.02544.x.

Martin, H., 1986, Effect of steeper Archean geothermal gradient on geochemistry of subduction-zone magmas: Geology, v. 14, p. 753–756, doi: 10.1130/0091–7613(1986)14<753:EOSAGG>2.0.CO;2.

Martin, H., and Moyen, J.-F., 2002, Secular changes in tonalite-trondhjemite-granodiorite composition as markers of progressive cooling of the Earth: Geology, v. 30, p. 319–322, doi: 10.1130/0091–7613(2002)030<0319:SCITTG>2.0.CO;2.

Martin, H., Smithies, R.H., Rapp, R., Moyen, J.-F., and Champion, D., 2005, An overview of adakite, tonalite-trondhjemite-granodiorite (TTG), and sanukitoid: Relationships and some implications for crustal evolution: Lithos, v. 79, p. 1–24, doi: 10.1016/j.lithos.2004.04.048.

Moyen, J.-F., and Stevens, G., 2006, Experimental constraints on TTG petrogenesis: Implications for Archean geodynamics, *in* Benn, K., et al., eds., Archean geodynamics and environments: American Geophysical Union Geophysical Monograph 164, p.149–175.

Nair, R., and Chacko, T., 2002, Fluid-absent melting of high-grade semi-pelites: P-T constraints on orthopyroxene formation and implications for granulite genesis: Journal of Petrology, v. 43, p. 2121–2142, doi: 10.1093/petrology/43.11.2121.

Niu, Y., O'Hara, M.J., and Pearce, J.A., 2003, Initiation of subduction zones as a consequence of lateral compositional buoyancy contrast in the lithosphere: A petrologic perspective: Journal of Petrology, v. 44, p. 851–866, doi: 10.1093/petrology/44.5.851.

Petrologic Data Base of the Ocean Floor, 2006, PetDB: Information system for geochemical data of igneous and metamorphic rocks from the ocean floor: http:www.petdb.org/ (June 2006).

Rapp, R.P., Watson, E.B., and Miller, C.F., 1991, Partial melting of amphibolite/eclogite and the origin of Archean trondhjemites and tonalites: Precambrian Research, v. 51, p. 1–25, doi: 10.1016/0301–9268(91)90092-O.

Springer, W., and Seck, H.A., 1997, Partial fusion of basic granulites at 5 to 15 kbar: Implications for the origin of TTG magmas: Contributions to Mineralogy and Petrology, v. 127, p. 30–45, doi: 10.1007/s004100050263.

Vlaar, N.J., and, van den Berg, A.P., 1991, Continental evolution and archeo-sealevels, *in* Sabadini, R., et al., eds., Glacial isostasy, sea level and mantle rheology: Dordrecht, Kluwer, 708 p.

Walter, M.J., 1998, Melting of garnet-peridotite and the origin of komatiite and depleted lithosphere: Journal of Petrology, v. 39, p. 29–60, doi: 10.1093/petrology/39.1.29.

Xiong, X., 2006, Trace element evidence for growth of early continental crust by melting of rutile-bearing hydrous eclogite: Geology, v. 34, p. 945–948, doi: 10.1130/G22711A.

Zegers, T.E., 2004, Granite formation and emplacement as indicators of Archaean tectonic processes, *in* Eriksson, P.G., et al., eds., The Precambrian Earth: Tempos and events: Developments in Precambrian Geology Volume 12: Amsterdam, Elsevier, p. 103–118.

Zegers, T.E., and van Keken, P.E., 2001, Middle Archean continental formation by crustal delamination: Geology, v. 29, p. 1083–1086, doi: 10.1130/0091–7613(2001)029<1083:MACFBC>2.0.CO;2.

Manuscript received 29 January 2008
Revised manuscript received 31 March 2008
Manuscript accepted 4 April 2008

Printed in USA